The University Of Adelaide
Department of Geology and Geophysics

The Application of High Resolution Aeromagnetic Surveys to Petroleum Exploration in the Western Otway Basin

Stephen L. Markham
B.Sc. [Flinders], B.Sc. [Hons.] [Flinders]

September 1997

A thesis submitted to the University of Adelaide
in fulfilment of the requirements for the degree of
Master of Science

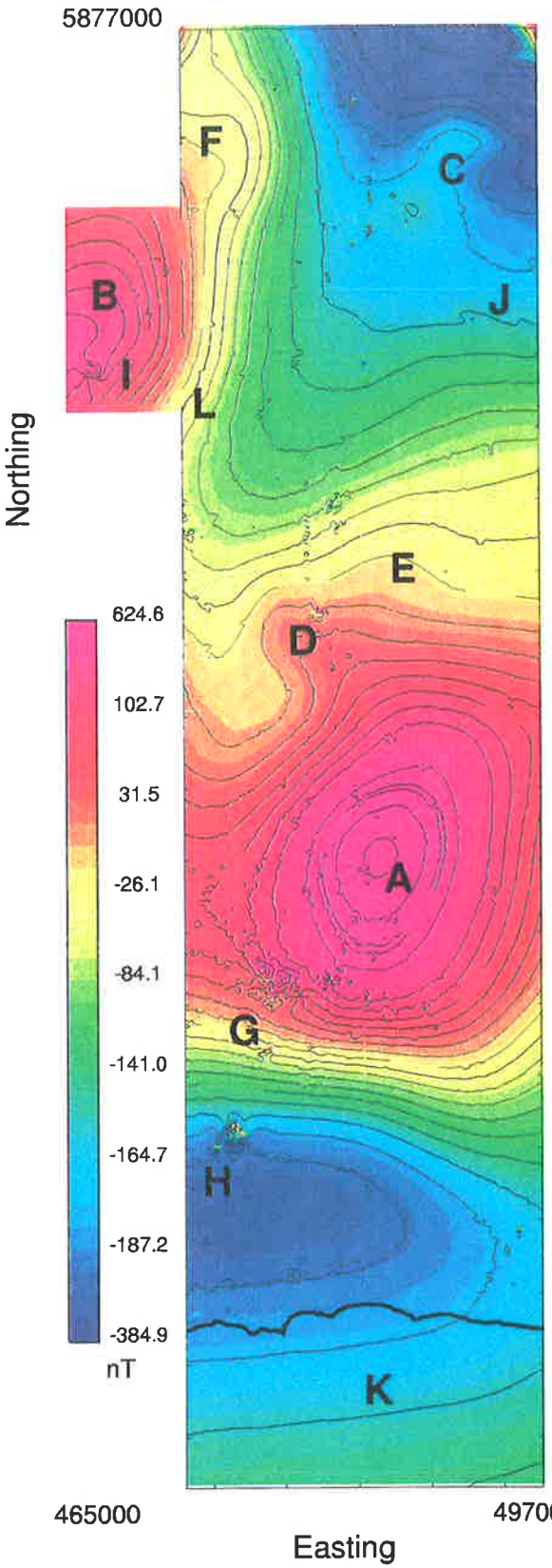

Location of most important magnetic features, A to L

A Mt Gambier Anomaly

B Western Penola Trough Anomaly

C Northeast Penola Trough Anomalies

D Kalangadoo High Anomaly

E Mid-Penola Trough Anomaly

F Northwest Penola Trough Anomaly

G Mt Gambier Volcanic Complex

H Mt Schank Volcanic Complex

I Hungerford Anomaly

J East Penola Trough Linear Anomalies

K Offshore Linear Anomalies

L Northwest Kalangadoo Linear Anomaly

Contour interval = 20 nT

Scale = 1 : 500,000

Coastline shown in black

Plate 1. P1 Area, TMI image and contours with location of anomalies discussed in thesis

Contents

Abstract

In 1993 the South Australian Department of Mines and Energy (MESA) commissioned a high resolution aeromagnetic survey over part of the Western Otway Basin (SAEI region, P1). The survey area consisted of a section along the S.A./Vic. border, approximately 25 km. wide, from north of Penola to offshore south of Mt. Gambier (-37° 15′ S to -38° 10′ S and 140° 40′ E to 141° E). The survey was intended as a test case to determine whether a high resolution survey (400 m line spacing and 60 m flight height) would permit the detection of weakly magnetic, intersedimentary horizons and allow the mapping of magnetic lineations that might correspond to faults and shear zones, thus assisting in the detection of structural traps that may contain significant reservoirs of hydrocarbons. The economic potential of the study area is demonstrated by recent gas discoveries.

The Otway Basin formed as a result of the separation of Australia and Antarctica with rifting commencing in the late Jurassic. In the northern part of the study area, the Penola Trough was the initial deposition centre which was filled by the Early Cretaceous Crayfish Group. During the Aptian/Albian, volcanogenic sediments of the Eumeralla Formation covered both the Penola Trough and adjacent basement highs. In the late Cretaceous the active spreading centre moved to the south with the result that the Sherbrook Group and overlying Tertiary sequences are much thicker in the south than in the Penola Trough. Volcanism occurred during the initial rifting stage, during the Cretaceous and early Tertiary, and during the Pleistocene/Holocene.

Theoretical studies in part of the Penola Trough between Penola 1 and the Katnook gas field were based on models developed from seismic evidence and susceptibility measurements from cores. From these studies, it was found that only faults or offset magnetic horizons within the Sherbrook Group and, especially, the Eumeralla Formation are likely to produce detectable anomalies at the flight altitude used in the survey.

The main magnetic features of the survey area result from bodies within or at the top of the Palaeozoic basement, with the exception of the Mt. Gambier and Mt. Schank volcanic cones as well as an anomaly near Hungerford 1 believed to be a shallow, blind basaltic plug. The depths to the top of the basement bodies, both within the survey area and adjacent to it, were derived using spectral analysis.

There are a number of subtle linear magnetic features in the Penola Trough and offshore that are the result of sources within the sedimentary section. In the Penola Trough, and especially southeast of Penola, there are a series of low amplitude, linear anomalies (1 to 3 nT) striking west-northwest to east-southeast which are the result of magnetic sources within the Eumeralla Formation (200-600m. deep). The offshore anomalies appear to be produced by magnetic sources located mostly within Early Tertiary sediments (500 m to 1 km deep).

Three models were created from the seismic line OK90-414 which is approximately perpendicular to the East Penola Trough linear anomalies discussed above. These models consisted of, (1) Thin igneous dykes mostly emplaced along the prominent fault planes within the Eumeralla Formation, (2) Thin horizontal layers or shallow channel fill at or near the top of the Eumeralla Formation with some layers in the overlying Sherbrook Group and Tertiary sediments, and (3) Zones of variable magnetisation associated with the major Eumeralla Formation faults. The igneous dyke model seems to be geologically less likely than the other two models. Measurements from cores have revealed a moderate vertical variation in susceptibility throughout the Eumeralla Formation but the layer and zone models require a similar lateral variation.

This study shows that an aeromagnetic survey with these specifications can distinguish the relatively small magnetisation contrasts found in sedimentary basins. Some of the magnetic lineations studied are the result of magnetic horizons being offset by faults and shear zones, but most appear to result from demagnetisation of sediments in the vicinity of fault zones. There are two examples of magnetic highs over fault zones suggesting that there may be some process generating magnetic minerals in these areas.

Statement

This thesis does not contain any material previously published or written by other people, and does not include material that has been accepted for the award of any degree or diploma in any University, except where reference has been made.

If this thesis is accepted for the award of the degree, I consent to the thesis being made available for photocopying and loan.

Stephen Markham

September 1997

Acknowledgements

I would like to thank the following people,

Peter Brooker for taking over the project and helping bring it to completion.

David Cockshell for his interest, enthusiasm and assistance in completing the project.

MESA for granting me a research scholarship and supplying the data, reports and maps required to complete the project.

Irena Kivior for assistance in the interpretation of spectral analysis results and for advice on various aspects of geophysics and geology.

Prof. Boyd for asking pertinent questions, making helpful suggestions and giving the benefit of his extensive experience.

Zhiqun Shi for demonstrating how to use Automag and assisting in the interpretation of initial results.

Andy Mitchell, John Foden and Vic Gostin for helpful discussions on aspects of seismic interpretation, igneous emplacement and sedimentology.

John Willoughby and Sam Yates for helping to solve innumerable computer problems, and Sherry Proferes for assistance in printing.

Shanti Rajagopalan for helping define the aims and direction of the project, and permitting use of her Postscript image software.

The Department of Geology and Geophysics, University of Adelaide for the use of facilities.

I dedicate this thesis to my parents who have always encouraged me to pursue my aspirations.

List of Figures

(facing page)

List of Tables

Chapter 1

Introduction

Aeromagnetic surveys have been used primarily as an initial reconnaissance method in petroleum exploration where a survey is utilised to determine the depth to basement in a previously unexplored basin and locate any intrusive bodies in the sedimentary section. Older surveys were typically flown at altitudes of 300 m or more and with flightline spacings of 1.5 km or greater, using magnetometers that had a sensitivity of one nanoTesla or worse. With these kinds of survey specifications, it was generally considered that the sediments in most petroleum exploration permit areas were nonmagnetic, that is, any magnetic response was the result of the basement or intrusives.

Improvements in technology suggest that aeromagnetic surveys should be able to detect much more subtle anomalies than the older surveys discussed above. These technological improvements include substantially more sensitive magnetometers (0.01 nT), better compensation for aircraft noise (0.2 nT noise envelope) and more accurate location methods such as GPS. This means that modern surveys can be flown at 60 to 80 m altitude with flightline spacings of 400 m or less with the result that the sample interval along the flightline can be 5 to 7 m The improvement in sensitivity allows the detection of sedimentary structures that have a very low magnetite content, in particular, sediments such as shales and sandstones with the typically low susceptibilities found in sedimentary basins.

Aims

This survey was intended as a test case to determine whether a high resolution survey with the specifications of 400 m line spacing and 60 m flight altitude would enable the detection of weakly magnetic, intersedimentary horizons and permit the mapping of magnetic lineations that could correspond to faults and shear zones. The region was selected because of a number of factors which inhibited petroleum exploration. These include the presence of volcanic eruptive centres of

Pleistocene/Recent age in the Western Otway Basin and the contamination of three petroleum wells in the study area by carbon dioxide of igneous origin. The presence of karstic terrain in the south of the study area, particularly around Mt. Gambier and between the Tartwaup Fault Zone and the coastline as well as offshore, has prevented the depth to the basement from being determined from seismic data. It was considered that a high resolution aeromagnetic survey might allow the detection of volcanic pipes, feeder dykes and other intrusive features in the sedimentary section, and could help determine depth to basement where seismic methods had failed.

Structure of the thesis

The thesis begins with a review of the geology of the Otway Basin and the study area in Chapter 2. In the first section the regional stratigraphy, igneous activity and tectonic history are discussed, concluding with a review of the exploration history of the Western Otway Basin. The second section deals with the structure and stratigraphy of the study area, the depth to the top of major formations in the petroleum wells adjacent to and in the study area, and the history of eruptions at Mt. Gambier and Mt. Schank.

Chapter 3 begins with a review of magnetic properties, in particular the acquisition of remanence, and then discusses the properties of a number of common and rare magnetic minerals. The second part of Chapter 3 first discusses magnetic minerals in igneous and metamorphic rocks. This is then followed by an extensive literature review of magnetic minerals in sediments including postulated associations with hydrocarbon accumulations. The section concludes with a discussion of mineralogical and petrological studies conducted by previous authors on samples recovered from wells in the study area. The chapter finishes with the tabulation of susceptibility measurements made by Chatfield (1992) on igneous outcrops exposed at Mt. Gambier and Mt. Schank, and susceptibility measurements made on sediment and metasediment cores recovered from several petroleum wells by MESA staff.

Previous geophysical studies of the Otway Basin are reviewed in Chapter 4. In these the authors discuss the history of rift formation, reconstruction of the direction of extension, and the timing of continental breakup based on seismic, aeromagnetic and gravity surveys as well as petroleum well logs, aeroradiometric and satellite data.

The second part of Chapter 4 reviews the two previous aeromagnetic surveys conducted over the Western Otway Basin, the first of which was undertaken in 1955 and the second in 1992 by AGSO (Reeves et al., 1993). The 1955 survey is only briefly considered, primarily in order to reproduce the depth estimates of major bodies made by the interpreters, while the 1992 AGSO survey is discussed more extensively because it uses previously acquired gravity data as well as the aeromagnetic data to interpret a number of the major features in the Western Otway Basin. The AGSO record also publishes the result of spectral analysis applied to the whole area as well as the northeast, onshore section. The chapter ends with as brief review of the Euler Deconvolution depth-to-basement results from the 1992 regional survey which were published in an article in the APEA Journal (O'Brien et al., 1994).

Chapter 5 is divided into two sections, the first is a discussion of the data processing and interpretation methods used to create the maps and profiles used in later chapters and the methods used to produce the magnetic models in Chapter 8. The second section presents the results of theoretical, simulation studies where models of a part of the Penola Trough were constructed using depth-converted seismic horizon maps. The simulation study investigates the effect of, fault offsets at the top of a formation, susceptibility contrasts between fault-bounded blocks, and non-magnetised and highly magnetised fault zones on the theoretical profiles. There is a comparison of the theoretical profiles with observed data along the north-south flightline used to construct the theoretical models. The chapter finishes with a discussion of the detectibility of anomalies revealed by the simulation and the application of this information to the modelling of the intersedimentary anomalies in section 8.2.

The depth determination studies reported in Chapter 6 were accomplished with the use of spectral analysis, Euler Deconvolution and Automag©. The first section discusses the spectral analysis results obtained from both MESA and AGSO data using software developed by former students of the University of Adelaide. The AGSO data were used because some anomalies were only partially covered by the MESA data. The second section discusses the Euler Deconvolution results obtained by Cowan Geodata Services for MESA. The results are presented as a series of maps (with all solutions within a particular depth range plotted and with colour

corresponding to depth). The final section in this chapter discusses the results obtained using Automag on selected anomalies in the P1 area.

The geophysical overview presented in Chapter 7 discusses, in the first section, the magnetic and gravity features of the Western Otway Basin and the regional structure determined from seismic data. Comparison is made between bodies apparent on gravity and magnetic maps, and the basement topography as revealed by seismic methods. The second section focuses on the study area and the relationship between the magnetic and gravity dataset and the seismic mapping.

The magnetic models of Chapter 8 are divided into two sections, the first consists of source bodies that are of likely igneous origin, and the second section presents models of bodies within the sedimentary section. The igneous bodies are located within the Palaeozoic basement with the exception of the Mt. Gambier and Schank volcanic complexes and the source of the Hungerford Anomaly. The intersedimentary bodies are all less than 1000 m deep and occur within the Penola Trough with the exception of those source bodies offshore.

Chapter 9 presents the conclusions made from the study and briefly discusses future work that would resolve the unanswered questions raised by this study.

In Appendix A, there is a brief discussion of the problem of cultural anomalies with some examples shown.

Definitions

The maps and profiles presented in this thesis use Australian Map Grid (AMG) coordinates although some maps may also have latitude and longitude coordinates marked. The AMG system specifies locations with northings and eastings which are in metres. Eastings in this study are measured from the central meridian of AMG zone 54 where 141°E longitude is equivalent to 500 000m Easting.

All quantities used in this thesis are measured in SI units and any data that were originally in other measurement systems have been converted. This means that depths are in metres, TMI anomalies are measured in nanoTesla, gravity anomalies in micrometres per second per second (1 $\mu m\ s^{-2}$ = 1 gravity unit or g.u. = 0.1 milligal), susceptibilities are given in SI units and densities in kg m^{-3} unless otherwise stated.

The IGRF reference values for the centre of the study area are, IGRF inclination = -69° 32' 36", IGRF declination = 9° 31' 59", and IGRF total field = 60896.788 nT.

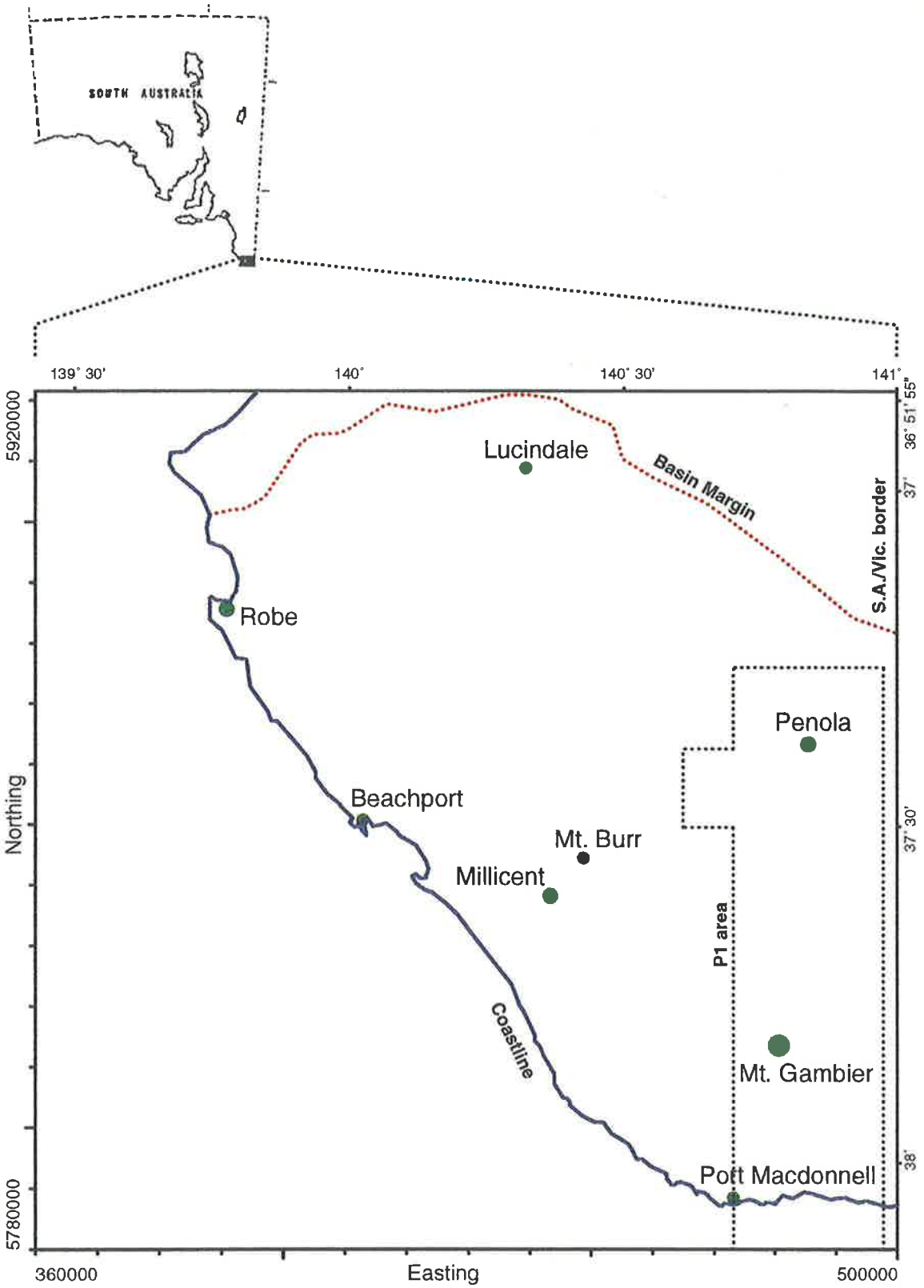

Fig. 2.1.0.1 Location map of the Western Otway Basin in South Australia Scale = 1:1,000,000, map shows major towns, coastline, basin margin and outline of P1 area (dashed)

Chapter 2

Geological Studies

Introduction

This chapter begins with a review of the stratigraphy of the Otway Basin and, in particular, the Western Otway Basin and then discusses the igneous activity with an emphasis on the eruptions in the South Australian part of the Basin. After a short section on the regional tectonic history (2.1.3), the exploration history of the Western Otway Basin up until 1995 is discussed. The second half of the chapter examines the structure and stratigraphy of the study area, discusses the depths of the major formations at the wells in the study area (2.2.3), and concludes with an outline of the eruption history of the Mt. Gambier and Mt. Schank volcanic complexes.

The Otway Basin forms part of the southern margin of the Australian continent, and is located both offshore and onshore in southeastern South Australia and southwestern Victoria. The onshore part of the basin extends approximately 500km, from the South Australian coastline between Robe and Cape Jaffa in the west, to Port Phillip Bay south of Melbourne. The offshore section extends from the Trumpet Fault on the northwestern side of the Robe Trough to the Sorell Fault, west of Tasmania (Perincek and Cockshell, 1995). The northern margin of the basin onshore is delineated by the outcrop of Palaeozoic basement and in the western basin by the northern limit of Otway Group sediments while the southern, offshore margin is marked by the limit of Early Cretaceous sediments (Cockshell, 1995). The basin has been divided into a number of sub-basins separated by basement ridges or highs. The area studied is part of the western-most sub-basin (sometimes called the Gambier Embayment), which extends from the S.A. coast south of the Padthaway Ridge to the Merino Uplift/Dartmoor Ridge in western Victoria. The project area covers the region P1 of the S.A. Exploration Initiative, and is between 37° 15' S and 38° 10' S, and 140° 40' E and 141° E with its eastern margin along the S.A./Victorian border and extending from north of Penola to approximately 10 km offshore from Port MacDonnell (Fig. 2.1.0.1). The major magnetic features of the P1 area are shown in Plate 1.

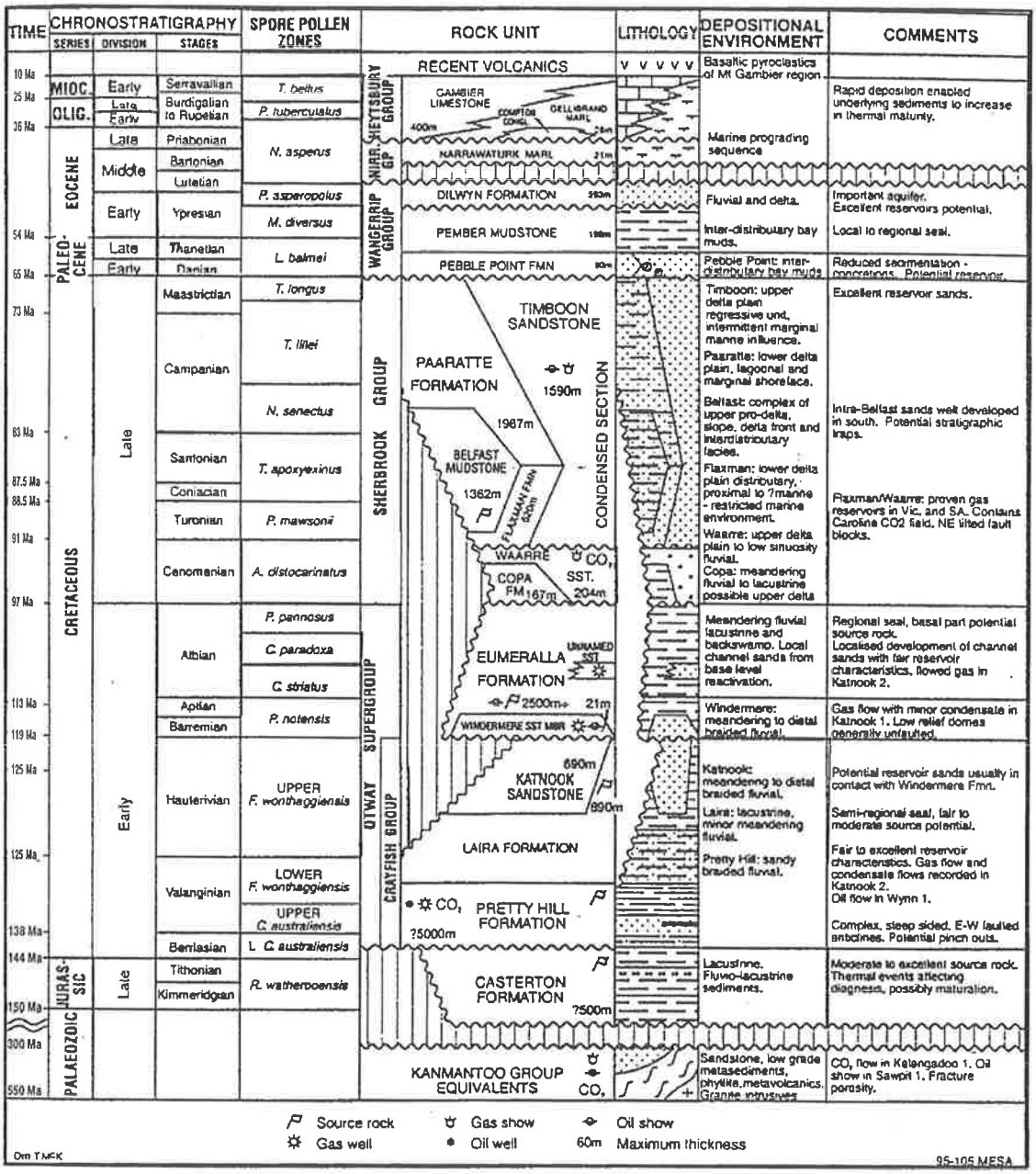

Fig. 2.1.1.1 Otway Basin stratigraphic column (After Morton et al., 1995)

2.1 The Geology of the Otway Basin

2.1.1 Regional Stratigraphy

The Otway Basin formed as a result of the breakup of east Gondwanaland into Australia and Antarctica, which began with rifting in the late Jurassic. Fig. (2.1.1.1) shows the relationships between the stratigraphic units. Basement rocks in the Otway Basin are late Proterozoic to Ordovician igneous and metamorphic rocks of the Lachlan and Delamerian Orogenies. The lithology of these rocks has been established principally from drillhole cores and the most commonly intersected rocks are metasediments such as phyllites, schists, quartzites and metamorphosed limestone, and rocks of igneous origin such as meta-basalts, meta-andesites and tuffs. Only a low-grade of metamorphism was evident. The metasediments have been interpreted as equivalents of the Kanmantoo and Normanville Groups, and the Glenelg Metamorphic Complex (Morton et al., 1995).

The late Jurassic, lacustrine *Casterton Formation* is considered to be a pre-rift or early syn-rift deposit and consists of interbedded carbonaceous shale or mudstone, with minor feldspathic sandstone and siltstones, olivine basalt volcanics and tuffs. However, the volcanic units which characterise the formation in Victoria were not intersected in the Sawpit 1 well east of Penola, which is the only South Australian occurrence of the Formation found to this date (Morton et al., 1995). The Casterton Formation only occurs in some isolated parts of the basin where it is found in the deeper parts of the half-grabens as an erosional remnant.

The fluvio-lacustrine *Otway Supergroup* was the next sedimentary sequence deposited, during the late Jurassic and early Cretaceous, and consists of the *Crayfish Group* at the base with the *Eumeralla Formation* at the top. The Crayfish Group is subdivided into, from the base, the *Pretty Hill Formation* (interbedded fine to medium grained quartz-feldspathic sandstone with carbonaceous siltstone and mudstone), the *Laira Formation* which is a lacustrine siltstone/shale with minor sandstone, and at the top, the *Katnook Sandstone* which is a light grey, fine-to-medium-grained cross bedded sandstone, interbedded with dark grey micaceous and carbonaceous siltstone.

The group was deposited in rapidly subsiding half-grabens usually oriented northwest to southeast, and consists of a system of low sinuosity channels and flood-basin deposits with occasional periods of high sinuosity fluvial deposition (Morton et al., 1994). SAGASGO staff working in the Penola Trough have informally divided the Pretty Hill Formation into a number of members. At the base of the Crayfish Group and overlying the Casterton Formation is the *McEachern Sandstone* which occurs principally in the Victorian part of the trough. This is overlain by the *Sawpit Shale*, which is locally divided into upper and lower units by a sandstone sequence called the *Sawpit Sandstone*. The uppermost member of the formation was named the *Pretty Hill Sandstone* (Lovibond et al., 1995). Morton et al., (1995) point out that this subdivision is not accepted by MESA.

The *Eumeralla Formation* (Aptian-Albian in age) is separated from the underlying Crayfish Subgroup by the basal Aptian unconformity, with the lowest unit in the sequence being the *Windermere Sandstone Member* which consists of a fine-to-medium-grained sandstone with minor siltstone and coal. The Eumeralla Formation is composed of laminated medium greenish grey, micaceous, carbonaceous silty claystone with subordinate thin coal seams, mudstone and very fine grained sandstone, all of which were deposited in low energy fluvial and lacustrine environments (Morton, 1991). The upper part of the formation in the Penola Trough area is characterised by channel sands overlying meandering fluvial/lacustrine deposits (Martin, 1992). Morton et al., (1995) report that marine microfossils have been found in the upper parts of the formation, suggesting that marine environments were nearby at the time of deposition. Duddy (1983) found that the lower Eumeralla Formation sandstones in Victoria contain between 38 and 53% volcanic lithics, less than 10% accessory minerals (red garnet, amphibole, apatite, zircon, magnetite etc.) and up to 35% diagenetic cement (chlorite, calcite/siderite, clay minerals, etc.).

Felton (1997) subdivided the Eumeralla formation in the Western Otway Basin into four informal lithostratigraphic units, based on well log analysis and studies of cores and cuttings. The *Eumeralla I* unit at the base of the formation, is a siltstone sequence with mudstone, fine-grained sandstone and coal beds interpreted to have been deposited by low-energy meandering streams with numerous shallow lakes and coal swamps (Felton, 1997). *Eumeralla II* is mostly siltstone and mudstone with many

thin, volcaniclastic, sandstone beds but with much less coal. Felton (1997) believes this unit to be mainly lacustrine in origin. *Eumeralla III* is a fine to coarse grained volcaniclastic sandstone sequence with interbedded volcaniclastic siltstone and minor conglomerate, deposited in high energy braided fluvial channels and flood plains. Felton (1997) considers that increased volcanic activity or uplift of volcanic terrains resulted in rapid erosion and redeposition of volcanogenic sands. *Eumeralla IV* is predominantly siltstone but with thin, fine volcaniclastic sandstone and coal beds. This unit is interpreted to mark the return of the low energy meandering stream, shallow lake and coal swamp environment in which Eumeralla I was deposited (Felton, 1997).

During the late Cretaceous, the deltaic-to-shallow marine *Sherbrook Group* was deposited after the basal Cenomanian unconformity. In the western Otway Basin, the Sherbrook Group has its greatest thickness south of the Tautwaup Fault zone but is undifferentiated and condensed approaching the northern margin of the basin, especially in the Robe and Penola Troughs. The first sediments of this group to be deposited (into depressions in the Otway Supergroup terrain) was the *Copa Formation*, a medium grey-brown claystone and carbonaceous siltstone. This is overlain by the deltaic *Waarre Sandstone* which is a light grey, medium to very coarse grained sandstone with subordinate grey carbonaceous siltstone and mudstone interbeds; followed by the shallow marine *Flaxman Formation*, a fine-grained sandstone interbedded with carbonaceous micaceous muddy siltstone. The overlying (or contemporaneous) *Belfast Mudstone* is a grey/black massive silty mudstone which is carbonaceous with finely disseminated pyrite; and, in turn, is overlain by the *Paaratte Formation*, a fine-to-coarse-grained quartz-rich sandstone containing siderite concretions, with minor interbeds of black carbonaceous shale and mudstone. The *Timboon Sandstone*, at the top of the sequence, is an upper delta plain regressive unit consisting of medium-to-coarse-grained, massive quartz sandstone with ferruginous cement and ooliths, along with minor fine-grained sandstone and siltstone. There are substantial interbeds of black/brown micaceous, silty mudstone (Morton, 1991).

In South Australia the Tertiary sequences have been considered to be part of the overlying Gambier Basin, while in Victoria they are included in the Otway Basin. This summary includes the Tertiary sequences in the Otway Basin. The early Tertiary (Palaeocene to Eocene) *Wangerrip Group* is subdivided into, from the base up, the

Pebble Point Formation which comprises conglomeratic and ferruginous sands, the prodelta muds and silts of the *Pember Mudstone* and at the top of the sequence, the *Dilwyn Formation* which is a series of sands and shales derived from fluvial and delta distributary channels as part of a number of transgressive/regressive cycles. The Eocene/Oligocene marine sandstone and marls of the *Nirranda Group* are overlain by the Miocene marine carbonate *Heytesbury Group*, both of which were deposited on the continental margins as Australia and Antarctica separated. The Nirranda Group is subdivided into the basal *Mepunga Formation*, a limonitic, quartz or calcareous sandstone; and the *Narrawaturk Marl*, a silty marl with calcareous mudstone and muddy limestone. The Heytesbury Group has the *Compton Conglomerate* as its basal unit, with a thick sequence of shelf deposits, the *Gellibrand Marl* and *Gambier Limestone*, overlying it (Morton et al., 1995).

This last depositional period was followed by regional uplift (Kosciusko Uplift) of the onshore parts of the basin with Pliocene/Recent sandy, carbonate and volcaniclastic surficial deposits. These surficial deposits occur only in some parts of the basin with outcrops of the Heytesbury and Wangerrip Groups in the west; and Otway Group in the northwest. The *Coomandook Formation* was deposited during a marine transgression in the Early Pleistocene while the overlying *Bridgewater Formation* forms a series of stranded coastal ridges which are composed of calcarenite. The *Padthaway Formation* was deposited between the ridges of the Bridgewater Formation during the Pleistocene, and include lacustrine and lagoonal carbonates. The *Molineaux Sands* are generally unconsolidated siliceous sands which form extensive dunefields and sheets; and which range in age from late Pliocene to Holocene (Tucker and Frears, 1995).

2.1.2 Regional Igneous Activity

Volcanic eruptions occurred in the initial rifting stage during the late Jurassic, offshore during the early Cretaceous, during the early Tertiary (Palaeocene-*Older Volcanics*) and during the late Tertiary/Quaternary (*Newer Volcanics*). The Older Volcanics (early to mid-Tertiary; 59-19 Ma) are mainly confined to the eastern part of Victoria and occur largely in the subsurface at their two locations in the Otway Basin, one of which is north of Portland in Victoria (Tyrendarra Embayment) and the other,

further to the east in the northern Otway Ranges. The western extrusives are mainly alkali olivine basalt with isolated occurrences of basanite and tholeiitic basalt (Sheard and Nicholls, 1989). The early Cretaceous volcanic activity has, in some instances, been considered separate to the late Jurassic eruptions and to the early Tertiary activity, but Day, (1989) considers that there has been a long history of almost continuous volcanism, at least from 95 Ma to 19 Ma, and perhaps back to 150 Ma (formation of the initial rift valley) with erosional episodes obscuring the record. The volcanic activity occurring in uplands adjacent to the rift, developing basin and later continental margin, would result in quantities of volcaniclastic material being deposited, either directly as lava flows, pyroclastics or ash falls, or as reworked material eroded and transported to the basin.

The Newer Volcanics are the result of a series of eruptions beginning in the Miocene and continuing through the Quaternary with the most recent eruptions at Mt. Gambier being around 4710 years before present (B.P.). These volcanic eruptions occurred at nearly 400 centres throughout southeast Australia with the earliest (6-7 Ma) in central Victoria, and the latest in the western Otway Basin. The Late Tertiary/Quaternary volcanism in the Otway Basin is believed to be the most recent episode of a sequence of volcanic activity along the eastern side of the Australian continent which is the result of the northward motion of the Australian plate over a mantle plume or 'hotspot' or , perhaps, rift upwellings (Sutherland, 1991). In the western Otway Basin surface or near surface basalt flows, pyroclastic and ash deposits occur, around Mt. Gambier and Mt. Schank, and to the northwest around Millicent and Glencoe with the Mount Burr group.

The Mount Burr group consists of fifteen centres with an age range of 2 Ma to 20000 years B.P. and includes cones and domes composed of pyroclastic fall deposits, lava flows and maars. Of the group, the centres of The Bluff, Mt. McIntyre and Mt. Watch have lavas that lack feldspar, and consist of phenocrysts of olivine in a groundmass of titanaugite prisms, olivine grains, titanomagnetite granules, apatite, and interstitial analcime; and therefore, are classified as Olivine Analcimites (Irving and Green, 1976). All these centres are partly-to-completely buried by Pleistocene dune sands of the Bridgewater Formation. The lava flows at Mt. Gambier and Mt. Schank (along with Mt. Burr) are Potassium-rich Nepheline Hawaiites consisting of olivine

phenocrysts in a groundmass of andesine laths, titanaugite prisms, olivine grains, titanomagnetite granules, thin apatite needles, and interstitial nepheline. The eruptions are characterised by scoria cones, overlapping maars with characteristic bedded surge deposits and bedded ash/lapilli deposits (Sheard and Nicholls, 1989). Irving and Green (1976) argue that these iron-rich lavas (at Mt. Schank) are low-pressure (< 5 kb) fractionation products of high-pressure magmas, indicating a crustal, rather than, mantle origin.

The major magnetic horizons within the sedimentary section occur within the Eumeralla Formation and within the Sherbrook Group, where offshore responses are associated with glauconitic facies in the Belfast Mudstone and beds of ferromagnetic minerals within the Waare, Flaxman and Paaratte Formations (Gerdes, 1987). This is due to the presence of volcanic, volcaniclastic and pyroclastic detritus in the sequences.

2.1.3 Regional Tectonic History

The Otway Basin is characterised by normal, generally down-to-the-basin faulting with the fault strikes trending north-south (basement), northeast-eastnortheast (inferred to be the earliest phase of extensional faulting) and northwest to west-northwest (believed to be breakup normal faulting). In the older, more northerly parts of the basin major faults dip towards the troughs while in the south major faults dip seaward.

Reeves et al, (1993) proposed that the rifting in the Otway Basin and other basins on the southern margin of Australia during the period 150 Ma to 120 Ma (late Jurassic to early Cretaceous) took place in rift segments oriented EW-ENE with the extension direction NNW-SSE which is disputed by other authors (section 4.1). The developing rift was filled with a thick sequence of low energy fluviatile sediments corresponding to the Casterton Formation and the Crayfish Group. Around 120 Ma the direction of stress changed and the sedimentary sequence was uplifted and eroded, and by approximately 115 Ma the extension direction had changed to NE-SW with the result that the earlier EW-ENE fault and fold trends were overprinted by a new WNW-ESE fault and fold trend. Deposition of the Eumeralla Formation in the

developing rift commenced at the same time as the establishment of the new extension direction (Reeves et al, 1993).

Williamson et al, (1990) have proposed that the original rift system was closer to the northern margin of the present basin, with the Robe, St. Clair, Penola and Ardonachie Troughs being the remanent structures of the original rift (two-phase model); but Hill and Durrand, (1993) suggest that these troughs were subsidiary to the main rift system and were formed at the same time (rift capture model). They postulate that during the Aptian, the northerly-dipping faults locked and crustal extension was confined seaward of the Tartwaup/Nautilus Fault Zone on a southerly dipping detachment. The regionally more important south-dipping system became dominant following the Barremian with the northerly dipping faults undergoing minor rejuvenation. The breakup of the rift and the beginning of seafloor spreading has usually been dated at 95 ± 5 Ma (Albian: (Veevers, 1986)). Reeves et al, (1993) suggest that breakup could have commenced earlier during the Neocomian (circa. 120 Ma), implying that the Eumeralla Formation was deposited on the developing passive continental margin which underwent subsidence as the oceanic crust was formed (section 4.1).

After breakup, a period of slow seafloor spreading followed with the probability of two phases of erosion, followed by basal marine transgressions and condensed marine successions, both topped by progradational sequences (Smith, 1988). It has been suggested that the cyclic sedimentation and erosional unconformities result from intermittent spreading after continental breakup (Hill and Durrand, 1993). During the Eocene, a period of rapid seafloor spreading began with the result that a siliclastic-starved, carbonate-prone passive margin developed (Hill and Durrand, 1993). The Oligocene unconformity is believed to be glacio-eustatic in origin rather than associated with the rapid drift phase. Regional compression and uplift since the Oligocene have resulted in the development of NE-SW and WNW-ESE folding as older structures were reactivated (Hill and Durrand, 1993).

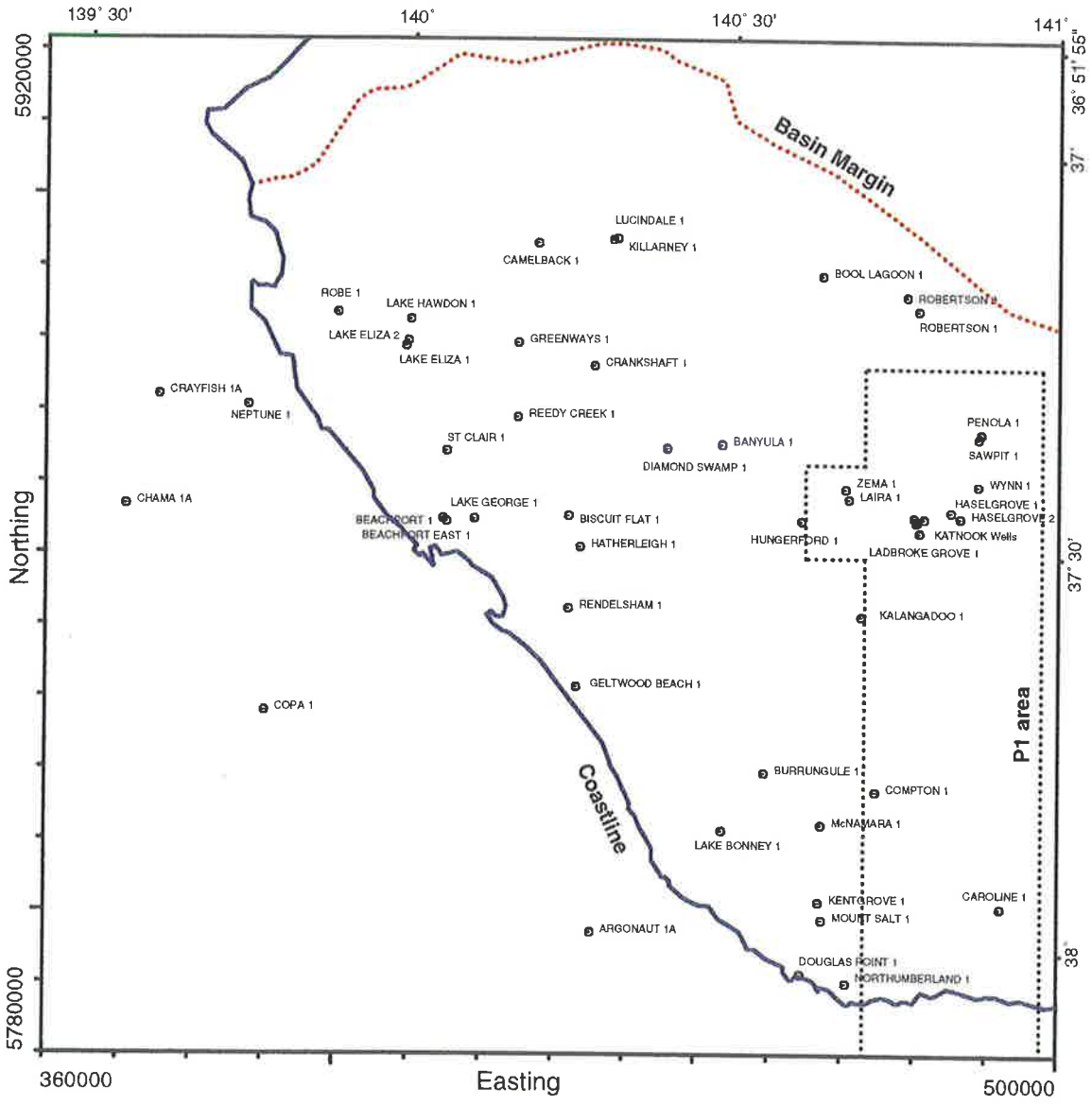

Fig. 2.1.4.1 Location of Petroleum wells: Western Otway Basin in S.A.

Scale = 1:1,000,000, outline of coastline, basin margin and P1 area shown

2.1.4 Exploration History of the Western Otway Basin

The first petroleum exploration in this part of Australia was the digging of a well in 1866 in the Coorong area, looking for the source of a rubber-like material (called coorongite) thought to result from oil seeps. It was later shown that this substance is desiccated algal material with no relation to crude oil. The first petroleum drilling in the region was undertaken in 1882 at Alfred Flat near Salt Creek, where the well was drilled to 281 m in an attempt to find the source of the purported oil seeps (Sprigg, 1986).

In 1915 Robe 1 was drilled and reached 1373 m, probably in Crayfish Group sediments, while below a depth of 917 m a flammable gas was encountered in the Eumeralla Formation sequence. Between 1918 and 1922 five wells were drilled to depths ranging from 256 to 556 m ending in Early Tertiary Wangerrip Group sediments with no hydrocarbons detected. Exploration continued with a further seven wells, mostly shallow, being drilled between 1923 and 1934, one of which was the Comaum bore that penetrated Early Cretaceous sediments.

The first use of geophysics in the region was a ground magnetic survey on the Knight Dome in 1930 and coincided with the drilling of Knight Dome 2 in the same year (Sprigg, 1986). The first aeromagnetic survey in the Otway Basin was conducted in 1948 between Cape Jaffa and Portland in Victoria, while the first gravity surveys began in 1949 with a Melbourne/Adelaide traverse and continued until 1960, defining the Robe and Penola Troughs as well as the Kalangadoo and Beachport Highs.

The first petroleum licence issued in the South Australian part of the Otway Basin was OEL 22 which was granted in 1959 and covered all of the onshore basin plus the offshore section out to the three nautical mile limit. This licence was later split up with two companies undertaking seismic surveys in 1960-61 and 1961-62 (Sprigg, 1986). In 1960 Tarpeena 1 was drilled and Penola 1 the following year. Tarpeena 1 reached 622 m (Wangerrip Group) without finding hydrocarbons while Penola 1 detected only minor gas shows in the Crayfish Group and did not penetrate the Pretty Hill Formation sandstone members. The Mt Salt 1 well was drilled in 1962 to a depth of 3061 m in the Sherbrook Group (fig. 2.1.4.1). Fig. 2.1.4.2 shows the petroleum tenements map of the Western Otway Basin.

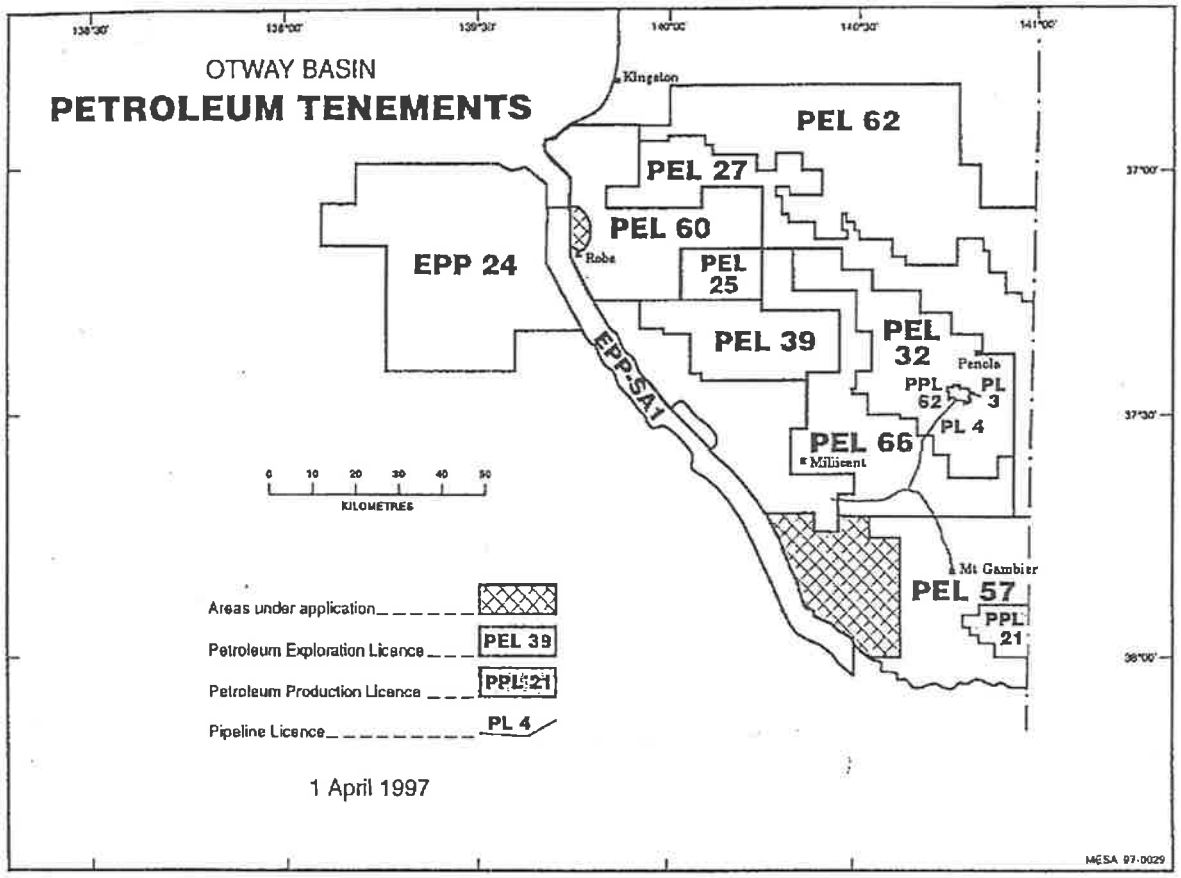

Fig. 2.1.4.2 Petroleum Tenement map of Western Otway Basin (SA)

from MESA information sheet P1: MESA 97-0029

The next well drilled in the vicinity of the study area was the Kalangadoo 1 well in 1965 which reached 2758 m in fractured basement (Palaeozoic metasediments) after cutting through thin Crayfish Group sediments. There was a flow of commercial quantities of carbon dioxide but the pressure declined indicating only a small resource. In 1967 Caroline 1 was drilled to the Late Cretaceous Waarre Sandstone (Sherbrook Group) where a commercial flow of CO_2 was detected and the well was put into production. The Robertson 1 and 2 wells were drilled in the same year to the north of the study area but both wells penetrated basement without encountering reservoir rocks (Sprigg, 1986).

It was not until 1973 that any wells were drilled close to the study area (others were drilled in the Robe Trough or on basement highs) but that year Douglas Point 1 was drilled to a depth of 1205 m in the Late Cretaceous Timboon Sandstone. This was followed in 1976 by the drilling of Kentgrove 1 which reached 991 m in the same formation but like the previous well encountered no hydrocarbons. Both these wells are close to Mt Salt 1 and are south of the Tartwaup Fault Zone which means that the Late Cretaceous and Tertiary sections are much thicker than in the north. The Breaksea Reef 1 well was drilled offshore in 1982 and reached 4468 m, detecting gas shows in the Waarre Sandstone and a possible oil reservoir in sands of the Belfast Mudstone but because of a parted drill pipe was unable to be logged or tested.

The Katnook 1 well, drilled in 1987, was the first commercial gas discovery in the Western Otway Basin and reached 2520 m in the Laira Formation but detected gas in the basal Windermere Sandstone member of the Eumeralla Formation. In the same year McNamara 1 (north of Mt Salt 1) was drilled, reached 680 m in the Paaratte Formation but encountered no hydrocarbons. Compton 1 was drilled in 1988 in order to test the Pebble Point Formation at the base of the Tertiary but was plugged and abandoned. The same year saw the drilling of Katnook 2 which recorded large gas flows (450,000 m^3/day) from the Pretty Hill Formation in the Early Cretaceous section. The Ladbroke Grove 1 well was drilled to the same part of the Pretty Hill Formation as Katnook 2 but the recovered gas had a high CO_2 content. Katnook 3 was drilled to the same target and detected sufficient reserves for the whole field to be declared commercial (Frears, 1995).

Also in 1989 the Laira 1 well, several km west of Katnook, was drilled in order to intersect the expected Pretty Hill Formation reservoir but there were only small flows from wet reservoirs. The Zema 1 well was drilled updip from Laira 1 in 1992 and detected oil and gas shows in the top of the Pretty Hill Formation but the gas flows were uneconomical with a large amount of water recovered. Another well drilled in 1992 was Sawpit 1, east of Penola, where minor oil shows were identified in the Crayfish Group and in fractured basement (andesite and mudstone). The basement interval yielded 1.5 barrels of oil (Frears, 1995).

Northumberland 1 (1993) was drilled to the base of the Tertiary and the top of the Late Cretaceous section but did not detect any hydrocarbon shows. In 1994 Wynn 1 which is located 8 km to the northeast of Katnook, found oil and gas in several Pretty Hill Formation sandstone units, with the shallowest unit yielding greater than 100 barrels of oil per day. The high water content and declining pressure implied that the reservoirs are thin, discrete and limited. The Hungerford 1 well was drilled on the Kalangadoo High west of Katnook but found that the Crayfish Group sediments were thin and lacking reservoirs. Haselgrove 1, around 4 km east of Katnook, was drilled to locate the Pretty Hill Formation reservoirs where gas was discovered at the Katnook field and found a substantial reservoir with commercial quantities of gas. Haselgrove 2 was drilled 1.5 km to the east and confirmed the extension of the gas reservoir (Frears, 1995). The Katnook 4 well was drilled on the southern side of the Katnook field to locate a trap with Windermere Sandstone and Pretty Hill Formation targets but found that the reservoirs were structurally lower than expected.

The first seismic surveys carried out in the area, beginning in 1960, used explosives as the energy source and were displayed as single fold reflection data (Frears, 1995), and because the quality of the data was fair at best it was only possible to carry out structural mapping to the base of the Tertiary section. The Bureau of Mineral Resources (BMR) experimented with vibroseis energy sources in a small survey in 1964, and the first offshore seismic surveys commenced in 1966 using explosives or aquapulse. Weight-drop energy sources were used in 1970 in an attempt to improve the seismic data quality onshore. In 1972 airgun sources were introduced and became the preferred energy source offshore while in 1973 vibroseis became the accepted onshore source.

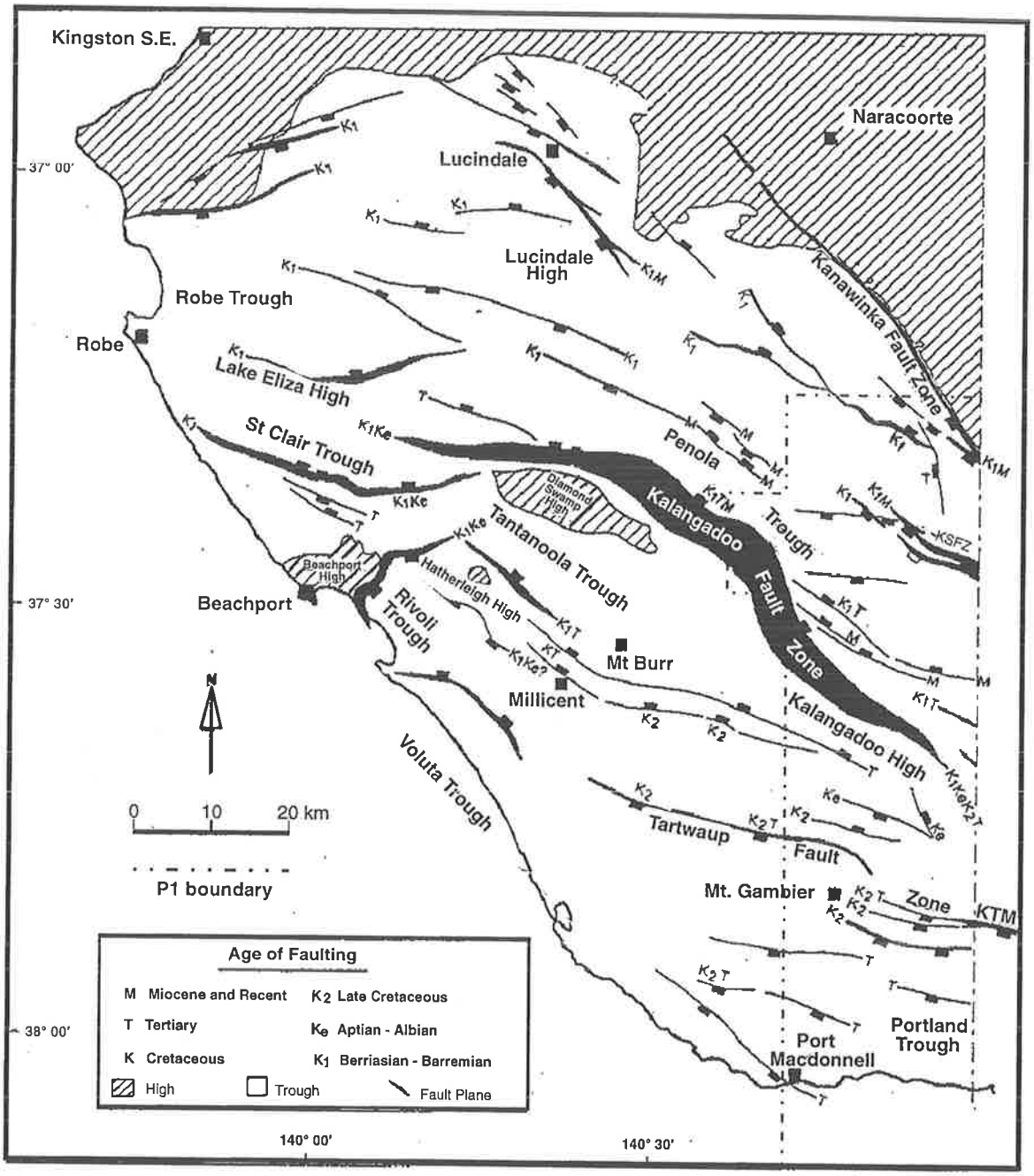

Fig. 2.2.1.1 Structural elements map of the Western Otway Basin showing age of faulting (After Cockshell, Finlayson and Perincek, 1994).

In 1983 a marine hydrocarbon detection survey was conducted along with sparker seismic and side-scan sonar surveys, which resulted in the detection of a seepage anomaly interpreted to be from an oil source. The BMR conducted seafloor dredge sampling surveys in 1985 and 1987 with heat flow measurements made during the latter survey. Geochemical studies of the samples revealed the highest hydrocarbon readings adjacent to near sea bottom faults (Frears, 1995). Geochemical surveys examining soil-gas content were conducted around the Katnook field after discovery and around Kalangadoo 1 but the anomalies could not be correlated to the known gas field.

The first 3-D seismic survey in the South Australian part of the basin was carried out over the area around Sawpit 1 in 1993 after the discovery of oil shows in the well. In the same year MESA conducted a gas sampling survey of water bores penetrating the Dilwyn Formation aquifer in order to determine the origin of any gas. Hydrocarbons which were detected are believed to be from biogenic and thermogenic sources. During 1995 a 3-D seismic survey was conducted over the area of the Katnook and Haselgrove fields, as well as adjacent prospects.

2.2 The Geology of the Study Area

2.2.1 Structure of the Study Area

The study area consists of a series of fault-bounded troughs and highs which follow the regionally dominant north-west to southeast trends (fig. 2.2.1.1). From north to south, the main structural elements are (a) the *Padthaway Ridge*, bounded by the Kanawinka Fault Zone which is the northern margin of this part of the basin, (b) the *Penola Trough*, (c) the *Kalangadoo/Beachport High*, the northern boundary of which is normal faulted towards the Penola Trough (the Kalangadoo Fault Zone or System), (d) the *Tantanoola Trough* which is bounded in the south by the Tartwaup Fault, (e) the *Portland Trough* and (f) the western *Voluta Trough* to the south of the study area and offshore.

2.2.2 The Stratigraphy of the Study Area

Only two wells within the study area have reached basement, these were Kalangadoo 1 and Sawpit 1. Drilling penetrated 693 m into basement at Kalangadoo 1 and found a sequence of turbidites and minor tuffs subjected to a low grade of metamorphism. At Sawpit 1, 189 m of steeply dipping, finely interbedded micaceous siltstone and mudstone (very low grade metamorphism) were intersected, overlain by andesite.

As discussed previously, the Casterton Formation has only been intersected in the Sawpit 1 well near Penola where the formation is 60 m thick but Morton et al., (1995) report seismic interpretations indicating a thickness of up to 500 m in the deepest parts of the Penola Trough.

The Crayfish Group is up to 5 km thick in the deepest parts of the Penola Trough (where basement is over 7 km below the surface) but is thin over the Kalangadoo High and disappears completely near the Kanawinka Fault Zone on the northern margin of the Basin. South of the Kalangadoo High, the Crayfish Group is too deep to have been intersected in wells and seismic evidence is unreliable south of the Tartwaup Fault Zone.

The Eumeralla Formation ranges in thickness, from approximately 500 m to the north of Sawpit 1, to around 1000 m over the central Penola Trough and Kalangadoo Fault zone. In the southern part of the study area, several wells have reached Eumeralla sediments but the thickness is unknown. The undifferentiated Sherbrook Group in the northern P1 area is generally around 50 m thick but the Sherbrook Group sequence thickens rapidly south of the Tartwaup Fault Zone to be around 1.8 km thick at Caroline 1 and probably much thicker offshore.

In the northern part of the area, the Tertiary sediments are very thin (approx. 100 m) and dominated by Gambier Limestone while along the coastline the Cretaceous/Tertiary boundary is around 1200 m deep. The evidence from Victorian wells suggests that the Tertiary sequences may be several kilometres thick offshore. The Holocene volcanic deposits are limited in areal extent to the vicinity of the Mt. Gambier and Mt. Schank volcanic complexes, while Holocene sand dunes crossing the area indicate palaeocoastlines.

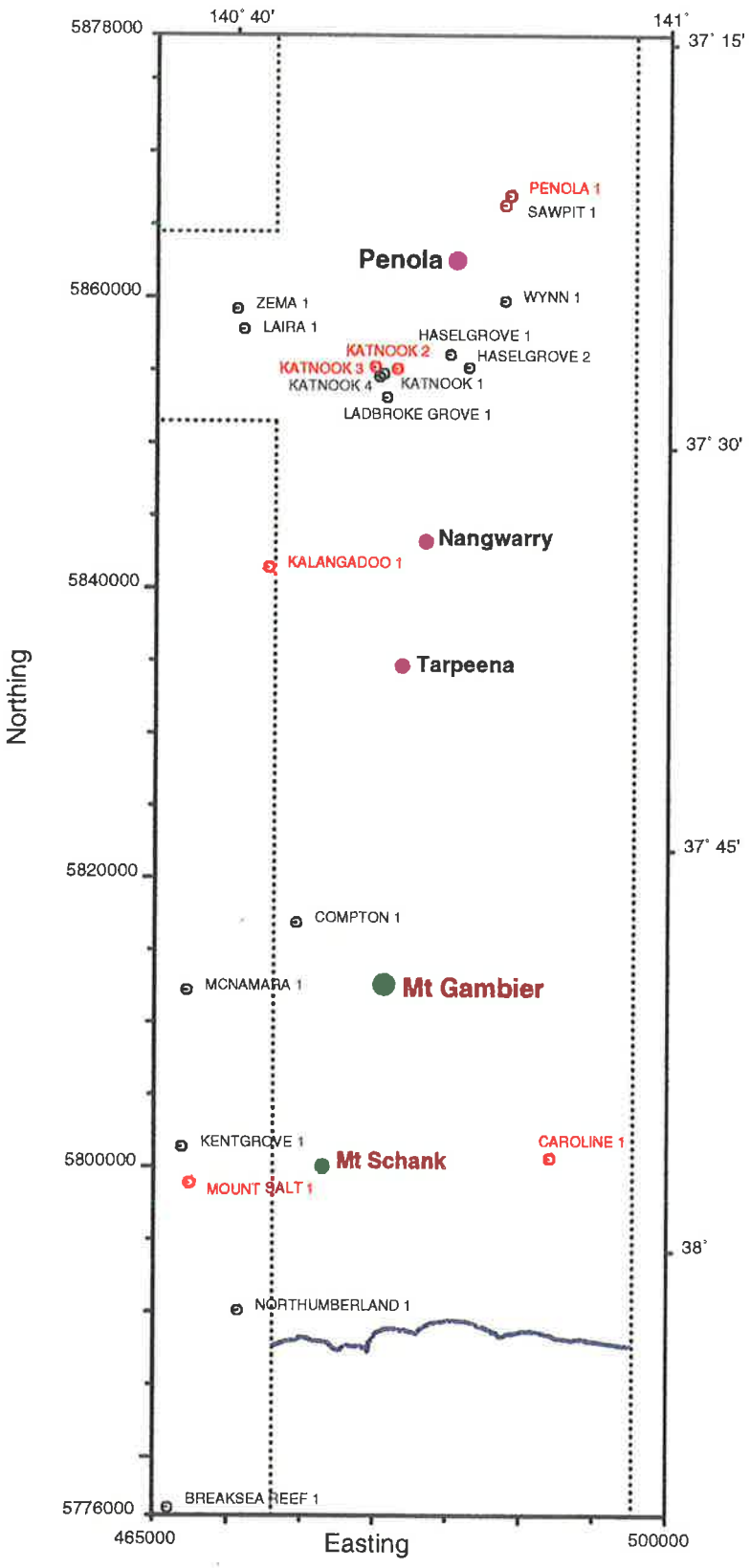

Fig. 2.2.3.1 Western Otway Basin (P1 area)

Locations of Petroleum wells

Susceptibility measurements from locations shown in red

2.2.3 Well Data

MESA has published data giving the depths to major stratigraphic unit tops (Morton and Drexel, 1995) for wells in the South Australian section of the Otway Basin. The wells in the P1 area for which data are available are, Caroline 1, Compton 1, Kalangadoo 1, Katnook 1,2 and 3, Ladbroke Grove 1, Laira 1, Penola 1, Sawpit 1 and Zema 1. Other wells which may be of significance to this study are Breaksea Reef 1 and Mt Salt 1 because both are south of the Tartwaup Hinge Zone and are close to P1.

Depths in metres below KB	Gambier Lst	Dilwyn Fm	Sher-brook Gp	Eumeralla Fm	Crayfish Gp	Caster ton Fm	Basement	Total Depth
Penola 1	2	76		317	1210			1519
Sawpit 1	26	108	291	326	1239	2466	2509	2698
Laira 1	6	195	597	793	1932			3003
Zema 1	6	206	580	757	1898			2730
Katnook 1	5	64	456	619	1892			2520
Katnook 2	18	65	461	619	1892			3478
Katnook 3	6	67	460	627	1893			3105
Ladbroke Grove 1	6	80	523	716	1835			3422
Kalangadoo 1	3	105	597	765	1887		2062	2755
Compton 1	5	60	621	1949				2200
Caroline 1	5	195	951	2892				3371
Mt Salt 1	5	167	994					3061
Breaksea Reef 1	90	510	1034					4468

Table 2.2.3.1 Depths to the top of major stratigraphic units in P1 wells

The Penola 1 and Sawpit 1 wells (fig. 2.2.3.1) are on the northern margin of the Penola Trough and the depths (table 2.2.3.1) show that the Late Cretaceous (Sherbrook Group) and Tertiary (Gambier Limestone and Dilwyn Formation) sections are thin compared with the Early Cretaceous sediments (Eumeralla Formation and

Crayfish Group). Sawpit 1 is the only well in the Western Otway Basin where the Casterton Formation was intersected and one of two wells which intersected basement. This well also did not intersect the Tertiary Gambier Limestone horizon until 26 m depth was reached, most probably because of overlying Quaternary dunes. The Late Cretaceous Sherbrook Group could not be identified in the Penola 1 well.

The Laira 1 and Zema 1 wells are in the western extension of the study area (fig. 2.2.3.1) and are in the Penola Trough close to the Kalangadoo Fault Zone. The depths of the horizons (table 2.2.3.1) indicate that all formations are thicker than on the northern margins of the trough, but with neither well reaching the Casterton Formation (if present) or basement. The Katnook wells and Ladbroke Grove 1 are in the central part of the Penola Trough in the study area with the horizon depths slightly shallower than the Laira and Zema wells. There is a general trend towards greater depths to formation tops, especially for the Tertiary, Sherbrook and Eumeralla horizons, the greater the distance from the northeastern margin of the basin a well is drilled. The Katnook gas field is around 10 km east of the Laira and Zema wells which could explain the difference in depths (table 2.2.3.1).

The principal difference between the depths of horizons for the Kalangadoo 1 well and the wells discussed in the previous paragraph, is that the Crayfish Group is extremely thin (table 2.2.3.1) with basement intersected less than 200 m below the top of the Crayfish Group. The Kalangadoo 1 well is on the shallowest part of the Kalangadoo Basement High, south of the Kalangadoo Fault Zone which is the southern boundary of the Penola Trough. The other formation depths are similar to those of wells in the Penola Trough which confirms that the later sediments were deposited over both the basement high and the sediments filling the rift.

Compton 1 is a short distance south of the Tartwaup Hingeline so the depth to the top of the Tertiary and Late Cretaceous horizons is similar to that for Kalangadoo 1 but the depth to the top of the Eumeralla Formation has increased substantially (from 765 to 1949 m, table 2.2.3.1). The top Crayfish Group horizon was not intersected in this well or any others south of the Tartwaup Fault Zone. Caroline 1 is further south than Compton 1 and over on the eastern side of P1 (fig. 2.2.3.1) and the depths are all substantially greater (except for the Gambier Limestone) with the

Dilwyn Formation and Sherbrook Group sediments much thicker. The Eumeralla Formation was only intersected near the base of the well.

Mt Salt 1 and Breaksea Reef 1 are not in the P1 area but are adjacent to it and help delineate the structural trends. Mt Salt 1 is slightly south of the latitude of Caroline 1 but is near the western margin of P1, and while the Tertiary and Late Cretaceous horizons are at similar depths, the Eumeralla Formation was not intersected despite the total depth reached (table 2.2.3.1). Breaksea Reef 1 is around 13 km offshore and to the west of the southwest corner of the P1 area (fig. 2.2.3.1). All the formation tops are now at much greater depths with the Flaxman Fm intersected near the base of the well at 4.3 km and the Gambier Limestone at 90 m.

2.2.4 Igneous Activity in the Study Area

The Mt. Gambier Volcanic Complex consists of a series of composite maars originally inferred to result from two periods of eruption which were dated at 4710 ±70 and 1410 ±90 years (?) B.P. (Sheard, 1978). However, the later date is now considered unlikely, suggesting that the eruptions were contemporaneous (Smith and Prescott, 1987). Each of the two periods of eruption are characterised by three phases of activity, with the second period being of a much larger scale and considerably more violent than the first period, resulting in fragments of pre-existing formations being torn from the sides of the vent and ejected along with the lava and ash.

The first phase of the first period of eruption began when the magma became steam-charged as a result of passing through water-saturated sediments. The explosive eruption produced maars with vents 25-100 m across and ramparts 5-10 m high, and a thin layer of locally deposited ejecta comprised of a basal conglomerate of country rock-ash origin, overlain by coarse-bedded ash and fine-laminated lapilli/ash. This phase was followed by the eruption of basaltic lava from fissures and vents, with the lava flows constrained by NW-SE trending, parallel, Pleistocene-age, aeolian sand dunes. The lava froze as a grey-blue, fine-grained basalt with medium-grained olivine phenocrysts. The third phase was more violent because of the influx of meteoric water into the system, with the construction of a small scoria cone on the western side of the eruptive centre. Steam passing through the scoria oxidised most of the material to a deep red colour.

During the time break which separated the two eruption periods, groundwater percolated down until it reached the hot magma where it may have induced remelting of the partially solidified rock (Sheard, 1978) or at least, decreased the viscosity substantially and increased the vapour pressure. New vents formed where the basalt caps of the previous eruption were blasted out of the way, with blocks of limestone and basalt up to 20 tonnes in mass being displaced. The first phase of this eruptive period produced tuff agglomerates which grade from poorly-bedded near the craters to finely-laminated ash and lapilli-tuffs away from the rims. The second phase was the most violent and produced composite or grouped maars which formed through the coalescing of numerous smaller conduits abraded by high velocity gas flow. Most of the volcanic detritus were tuff-agglomerates comprised of country rock fragments (Heytesbury and Wangerrip Groups, and basement rocks) and volcanic bombs (olivine and basalt), lapilli, cinders and ash. When the previous activity subsided, the influx of large amounts of meteoric water caused the ejection of wet ash from one crater. Continuing eruptions from the westernmost crater produced tuff-agglomerate while the eastern crater ejected vitric lapilli-tuff. The third phase concluded with a short period of lava fountaining which represents degassing of the magma. The last activity was fumarolic with four fumaroles in or adjacent to the craters and three blowholes outside the main volcanic vents which may be associated with a near surface dyke.

The eruptions at Mt. Schank, about 14 km south of Mt. Gambier, were similar in that they occurred in two phases but there is considerable uncertainty in the dates. Radiocarbon dating using charcoal fragments buried beneath tuff yielded an age of 18100 ±350 years B.P. (Polach et al, 1978). Barbetti and Sheard, (1981) employed palaeomagnetic field measurements to give dates of either greater than 7000 years or between 5000 and 1000 years B.P. Thermoluminescence dating of dune sand baked by the overlying lava flow has yielded a data of 4930 ± 540 years B.P., a date the authors (Smith and Prescott, 1987) argue is consistent with dates obtained by Blackburn et al, (1982) and the earlier date above for volcanism at Mt. Gambier. Therefore, it is not possible to determine whether the Mt. Gambier eruption predates or postdates the eruption at Mt. Schank.

The first phase of the eruption began when a northwest-trending fissure 1200 m long opened in the underlying limestone and basaltic ash was vented from the

fissure until it enlarged sufficiently to permit lava flow. Lava flowed west and south from the fissure with activity gradually contracting to the southern end of the fissure and the subsequent development of a scoria cone. Phreatic explosions created a maar 250 m south of the fissure. The second phase of activity commenced once the venting of ejecta from the phase one centres ceased. A new vent opened up between the maar and scoria cone driven by a larger magma supply, which was interacting with near-surface groundwater to create a hybrid maar/cone. This consisted of bedded tuff-agglomerate, lapilli and ash with substantial amounts of country rock fragments displaced from the conduit walls. Large amounts of ejecta partially buried the previously emplaced scoria cone with several large vent-clearing phreatic explosions creating a wide-mouthed crater. Pyroclastic material buried more than half of the scoria cones along the original fissure and blanketed the main lava flow. Steam emission during the late stages of the eruption resulted in a small explosion crater and breached the previous lava flow (phase one), along with the creation of a small blowhole away from the main vents (Sheard, 1986).

This chapter has outlined the geology of the Otway Basin and study area, and reviewed the exploration history of the South Australian part of the Western Otway Basin. The depositional and tectonic history was introduced in section 2.1.3 and this will be expanded upon in section 4.1 where there will be a greater geophysical emphasis than in this chapter.

Chapter 3

MAGNETIC MINERALS

This chapter begins by reviewing the overall properties of magnetic minerals, then discusses the major and minor ferrimagnetic minerals as well as some paramagnetic minerals that may be significant in sediments (section 3.1). Average susceptibility values for a number of ferrimagnetic and paramagnetic minerals are tabulated from several different sources. The following section (3.2) discusses the origin of magnetic minerals in various rock types, with the first part (3.2.1) dealing with igneous rocks and the effects of metamorphism on the magnetic mineral content, while the second part (3.2.2) considers the evidence for the processes of creation, destruction and alteration of magnetic minerals in sediments and the proposed association with hydrocarbons. The third part (3.2.3) reviews studies of the mineralogy of cores extracted from petroleum wells in the study area with particular emphasis on the magnetic mineral content while the fourth part (3.2.4) tabulates the inclination and declination of the palaeomagnetic field vector from the Mid-Jurassic to the present. The range and average susceptibility values for a number of different igneous, metamorphic and sedimentary rocks is tabulated in 3.2.1. Section 3.3 discusses the magnetic susceptibility measurements made on volcanic extrusions at Mts. Gambier and Schank (3.3.1) and on cores recovered from 6 petroleum wells in or adjacent to the study area (3.3.2). The range of susceptibilities for each of the main sedimentary formations from the various wells are tabulated in section 3.3.2.

3.1 Magnetic Mineral Properties

3.1.1 Introduction

Magnetic properties result from the motion of electric charges, predominantly electrons, within a material. If an external magnetic field is applied to a material where the electron shells are complete, a small magnetisation is induced in the opposite direction to the external field which disappears as soon as that field is removed. Materials that exhibit this type of behaviour are called *diamagnetic* and include common minerals such as quartz and calcite (Telford et al., 1990). *Paramagnetic* materials have incomplete electron shells with the result that a weak temporary magnetisation is induced in the same direction as an external field. The

paramagnetic transition elements, iron, nickel and cobalt, have relatively large regions called *domains* where the individual atomic magnetisations are aligned in one direction. This effect is called *ferromagnetism* and is not only much larger than diamagnetism or paramagnetism but also persists in the absence of an external inducing field. In some ferromagnetic materials the domains are divided into *subdomains* which have magnetisations that are aligned in opposite directions and so tend to substantially reduce the overall magnetisation of the material. This is called *antiferromagnetic* behaviour, of which haematite is an important example. In materials where the subdomains are oppositely aligned, it is possible for subdomains aligned in one direction to have a greater magnetisation, for there to be more of them or for the alignment to be canted such a way that they only partially cancel, with the result that the overall magnetisation of the material is relatively large. Materials exhibiting this type of behaviour are called *ferrimagnetic* and include magnetite and pyrrhotite (Telford et al., 1990).

The domain structure of the mineral grains determines the magnetic properties of ferrimagnetic minerals. The individual atomic magnetic moments within fine grains are aligned and the whole grain is magnetised in one direction, which produces single domain (SD) structure. With larger grains it is more energetically favourable to subdivide the grains into magnetic domains where the magnetisation is not in alignment with that of the neighbours and these magnetic domains are separated by domain walls in which the individual atomic moments are aligned randomly (Clark, 1983). This is called multidomain (MD) structure and the threshold size (for equidimensional grains) at which MD structure becomes energetically favourable is known as the critical SD size. Examples of this grain size are 0.06 μm for magnetite, 15.0 μm for haematite and 1.6 μm for pyrrhotite. When MD grains contain only a few domains their properties are intermediate between those of SD grains and those of true MD grains, and vary systematically with grain size. These are usually called pseudo-single domain (PSD) grains and are of significance because a relatively large proportion of the grain size distribution in magnetite-bearing rocks is in the PSD range (between approx. 0.1 to 15 μm) (Clark, 1983). The grain size of minerals is determined by factors such as the time taken for a mineral to crystallise from a melt (slow cooling produces coarse, usually MD grains), or the type of chemical processes occurring in sediments (usually SD and PSD) or under regional metamorphic conditions.

The total magnetisation of a rock or mineral is expressed as a vector quantity consisting of two components, (1) the *Induced magnetisation* which is produced by the

external (geomagnetic) field, and (2) the *Natural remanent magnetisation* (NRM) which is a permanent property of the rock independent of the external field. Remanent magnetisation contributes in both amplitude and direction to the total magnetisation of a rock and may be due to several causes, (a) *Thermoremanent magnetisation* (TRM) which is acquired when magnetic minerals cool below the Curie point in the presence of the Earth's field. This is particularly stable and is fixed in the amplitude and direction of the ambient field at the time of cooling. (b) *Detrital remanent magnetisation* (DRM) occurs with the slow settling of fine-grained particles such as clays in the presence of an external field. (c) *Chemical remanent magnetisation* (CRM) which occurs with the increase in size of magnetic minerals or change in composition as a result of chemical action at moderate temperatures. (d) *Viscous remanent magnetisation* (VRM) which is produced by long exposure to the magnetic field of the Earth. This is more characteristic of fine-grained rather than coarse-grained rocks and is quite stable. (e) *Isothermal remanent magnetisation* (IRM) is the residual left following the removal of an external field and is commonly produced in outcrops by lightning strikes (Telford et al., 1990).

Whether a ferrimagnetic mineral retains a remanent magnetisation after the inducing field is removed can depend more on the grain size rather than the composition. For example, larger single or pseudo-single domain grains can retain an IRM (from a strong inducing field) for several thousand years while MD grains only retain that magnetisation for a few decades. The IRM of small SD grains is much shorter, decaying within minutes for grains smaller than 0.05 μm and almost as soon as the inducing field is removed for grains smaller than 20 nm. The last type of behaviour is called *superparamagnetism* (SPM) but minerals exhibiting it have a much higher susceptibility than paramagnetic minerals (O'Reilly, 1984). Single domain (SD) and PSD grains have a much lower susceptibility than SPM grains but can retain a relatively intense, hard and stable remanence (Clark, 1983). Generally, plutonic rocks and metamorphic rocks where slow crystallisation/recrystallisation has produced a coarse-grained texture, have small Koenigsberger ratios which is indicative of the dominance of induced magnetisation over NRM. The low remanent magnetisation is the result of the multi-domain (MD) structure of the coarse-grained ferrimagnetic minerals produced under these conditions. Extrusive rocks on the other hand have chilled quickly, producing a fine-grained texture with the result that the Koenigsberger ratios are greater than unity (O'Reilly, 1984).

There were no studies of remanent magnetisation on core or outcrop samples (section 3.3) from the study area so the anomalies modelled in chapter 8 were initially assumed to result

from induced magnetisation only. When a geologically realistic model failed to produce an anomaly resembling that on the observed profile, remanent magnetisation was added to the model with the constraints discussed above and in section 3.2.4.

If ferrimagnetic minerals are present in amounts larger than about 0.1% by volume of the rock, then the magnetic properties of the rock will be dominated by them because of their much greater susceptibilities. However, if the volume percentage is substantially less or ferrimagnetic minerals are absent altogether, then when the paramagnetic mineral content is greater than around 1%, the magnetic properties of the paramagnetic minerals will be dominant over those of the diamagnetic minerals, once again because of the higher susceptibilities of those minerals. Generally, the three types of minerals will all contribute to some degree to the observed properties.

3.1.2 Magnetic Minerals

The main ferrimagnetic minerals are Magnetite (α-$Fe_3\ O_4$), monoclinic Pyrrhotite ($FeS_{1.14}$), Titano-magnetite, Maghaemite (γ-Fe_2O_3), Titano-haematite, Native iron or Fe-Ni-Co alloys, and some Ilmeno-haematites (Clark and Emerson, (1991); McIntyre, (1980); Grant, (1985)). Some haematites possess a large thermoremanent magnetisation (TRM) despite their generally low magnetic susceptibility. All of the most common ferrimagnetic minerals except for pyrrhotite are Fe-oxides or Fe-Ti-oxides. The spontaneous magnetisation and Curie temperature of titanium-containing ferrimagnetic minerals decreases steadily as the Ti content increases (the Curie temperature ranges from around 580^0 C for pure magnetite to about 25^0 C for a solid solution of 75% ulvospinel to 25% magnetite, with the result that the susceptibility of 75% ulvospinel is one tenth that of pure magnetite). Pyrrhotite is an iron sulphide of varying composition, only some phases of which are ferrimagnetic. In addition to pyrrhotite, there is another ferrimagnetic iron sulphide called Griegite ($Fe_3\ S_4$), which is a spinel with a similar structure to magnetite but with sulphur substituting for oxygen (Skinner et al., 1964). Griegite has a similar susceptibility to magnetite but has generally been thought to transform rapidly into pyrite and marcasite with the result that it should only be found in Recent sediments. However, Reynolds et al., (1994) report griegite in sediments of Cretaceous age while Roberts (1995) discusses occurrences ranging from Miocene to Pleistocene sediments, suggesting that the mineral may be metastable over geological time. Griegite has been found to convert to pyrite, marcasite and minor pyrrhotite above 300°C with subsequent conversion to ferric oxides at

temperatures greater than 400°C (Krs et al., 1992). The three most significant magnetic minerals for most aeromagnetic surveys, particularly in areas prospective for economic mineralisation, are magnetite, maghaemite and pyrrhotite (pyrrhotite is especially important in areas of sulphide mineralisation) because of their high susceptibilities, with the other minerals expected to contribute only to the magnetic remanence of some bodies (see Table 3.1.2.1).

Other ferrimagnetic minerals may contribute to magnetic anomalies, but because of their rarity or instability (or both) have not been considered important. These minerals can have a high susceptibility or a substantial remanence by themselves or only when in solid solution with magnetite. They include sulphide minerals such as Smythite ($[Fe, Ni]_9 S_{11}$) and Cubanite ($Cu Fe_2 S_3$), spinels such as Magnesioferrite ($Mg Fe_2 O_4$), Jacobsite ($Fe_2 Mn O_4$), Franklinite ($Zn Fe_2 O_4$), Chromite-magnetite ($Fe_2 Cr O_4$), Hercinite ($Fe Al_2 O_4$) and Magnetoplumbite ($Pb_{0.6} Fe_2 O_3$), and the oxyhydroxide Goethite (α-Fe OOH) (Clark, 1983). With the exception of Goethite, these minerals result from the substitution of other cations into the crystal lattices of pyrrhotite and magnetite. Clark (1983) also mentions that a number of silicate and ore minerals which are intrinsically non-magnetic, have been found to exhibit relatively strong magnetic properties. This can be explained by the presence of ultrafine titanomagnetite grains within the rock matrix or titanomagnetite inclusions inside non-magnetic grains (Clark, 1983; Hounslow and Maher, 1996).

Some paramagnetic sulphides are unstable in oxidising environments, in particular, marcasite and to a lesser extent, pyrite, and can alter to a range of ferrimagnetic hydrated iron sulphates which have considerably higher susceptibilities (Deer et al., 1966).

Paramagnetic minerals can have a significant effect on the magnetic properties of rocks in their own right provided the ferrimagnetic mineral content is low or because they can alter to ferrimagnetic minerals under certain environmental conditions. Important paramagnetic minerals include Ilmenite ($FeTiO_3$), Siderite ($FeCO_4$), Pyrite (FeS_2) and iron-bearing silicates such as, Chlorite, Biotite, Muscovite, Fe-Olivine (Fayalite) and iron-rich clay minerals (such as Illite), as well as, paramagnetic variants of the ferrimagnetic minerals discussed earlier. At temperatures above 300° C, Siderite (and Ankerite, $Ca Fe (CO_2)_3$) commonly breaks down to form Maghaemite (Ellwood et al., 1986) while iron-rich silicates, particularly clays, can convert to Haematite under diagenetic conditions (Tarling and Hrouda, 1993).

The process of weathering generally has the effect of increasing the oxidation state of iron in minerals (from native iron Fe, to ferrous iron Fe(II) to ferric Fe(III)) while regional and contact metamorphism tends in most cases to reduce it; however, the reaction rates are slow at low temperatures/pressures and metastable oxidation states can persist almost indefinitely. Table 3.1.2.1 lists a number of magnetic minerals, their approximate composition and average volume susceptibility.

Magnetic Mineral	Composition	Average Susceptibility (k)
Magnetite	α-Fe_3O_4	600,000
Ilmenite	$FeTiO_3$	180,000
Pyrrhotite	$FeS_{1.14}$	150,000
Franklinite	$ZnFe_2O_4$	43,000
Chromite	$FeCr_2O_4$	700
Haematite	α-Fe_2O_3	650
Limonite	$Fe_2O_3 \cdot H_2O$	250
Pyrite	FeS_2	150
Siderite	$FeCO_4$	400
Biotite	$KFe^{2+}_3 Fe^{3+} Si_3O_{10}(OH)_2$	120
Chlorite	$Fe^{2+}_{12} Si_8O_{20}(OH)_8$	36
Fayalite	Fe_2SiO_4	550
Goethite	α-FeOOH	200
Illite		43

Table 3.1.2.1 Average Magnetic Susceptibility values for various Ferrimagnetic and Paramagnetic Minerals (S.I. $\times 10^{-5}$). From Telford et al., (1990), Carmichael, (1989), Clark, (1983), and Tarling and Hrouda (1993).

3.2 Origin of Magnetic Minerals

3.2.1 Igneous Rocks and the Effects of Metamorphism

Magnetite and its variants are important constituents of igneous rocks, the amount present dependent on the differentiation path taken by the melt during cooling. Magnetite is the

most important magnetic mineral in igneous rocks and is usually the only magnetic mineral considered significant in most igneous and metamorphic terrains. When a melt is crystallising, whether the iron present will enter the silicate lattices or remain free to form oxides depends on the oxidisation ratio; too low and most Fe will enter the silicates; too high and the oxides formed will be haematite and ilmenite which are only relatively weakly magnetic. One differentiation path leads to residual fluids which are high in silica and low in iron, and is followed by basaltic magmas that have a high degree of oxygen availability (through a substantial water content) during cooling and results in iron being prevented from accumulating in the residual liquids by the separation of the Fe-Ti oxides as a primary phase. As crystallisation proceeds, the oxidisation level rises and most of the Ti crystallises out early in the sequence. This results in basic and ultrabasic rocks containing oxides with lower Fe:Ti ratios and, subsequently, weaker magnetic properties than intermediate and acidic rocks (Grant, 1985).

Where there is no external supply of oxygen, the crystallisation process results in residual liquids that are depleted in silica and rich in iron. As crystallisation proceeds the residual liquid attains a lower and lower oxidation state, with Ti remaining in solution, allowing titano-magnetites to form at a late stage; and if the melt cools slowly the exsolution of distinct phases of magnetite and ilmenite can occur, with the result that the rocks are more highly magnetic and support a stronger remanent magnetisation (Grant, 1985). The presence of other cations in the melt will influence the process previously described, in particular, a low magnesium content and/or a high aluminium content will favour the production of primary magnetite and muscovite + magnetite respectively.

Extrusive rocks of acidic and intermediate composition will contain oxides with the highest Fe:Ti ratios and, therefore, the strongest magnetisation; while basic extrusives form oxides with low Fe:Ti ratios and, thus have relatively weak susceptibilities. Rhyolites, however, tend to be less magnetic than andesitic and trachytitic rocks while trachyandesites and trachytes usually have moderate to high susceptibilities. Fresh basalts and dolerites have moderate to high susceptibilities which are reduced by subsequent hydrothermal alteration. Ultramafic rocks such as pyroxenites, hornblendites and serpentinised dunites are generally highly magnetic while mafic and intermediate rocks like gabbro, diorite and monzonites are moderately to highly magnetic (Clark and Emerson, 1991). Of the intrusive rocks, granites are similar to the acid volcanics and might be expected to contain strongly magnetic oxides while syenites and

monzonites should be similar to the basic volcanic rocks. From empirical studies it has been found that for extrusive rocks bulk magnetic susceptibility attains a maximum within the dacite compositional range while basalt and andesite are distinctly less magnetic (Clark, 1983). Among intrusive rocks, the peak of magnetic susceptibility occurs within the quartz diorite compositional range.

Magnetite that is formed as a result of crystallisation in a cooling magma is called primary magnetite. In some mafic and ultramafic rocks, there are very intense anomalies which are almost always the result of alteration processes that have occurred since primary deposition. This secondary magnetite is most often the product of the serpentinisation of the rocks, where olivine and orthopyroxene are transformed into hydrous (Fe, Mg) silicates and magnetite in a low temperature retro-metamorphic process. The amount of magnetite that can be formed during metamorphism is, naturally, dependent on the iron content of the original rocks, with shales and other argillaceous sediments containing more iron due to the tendency of the metal to become attached to clay particles during sedimentation (Grant, 1985).

Secondary magnetite is produced at all stages of progressive metamorphism but magnetite is generated in significant quantities either under relatively low grade conditions in haematite-rich rocks, or under high grade conditions where there is substantial breakdown of biotite and amphibole. There is a general tendency for iron-bearing rocks to become more magnetic with increasing metamorphic grade; a situation that applies to contact as well as regional metamorphism. At very high temperatures/pressures near the threshold of partial melting, there is a marked reduction in magnetisation because iron and titanium oxides begin to recombine in magnetite/ilmenite solid solutions.

Other factors influencing the magnetite content of metamorphic rocks are the effects of excessive aluminium which results in the alteration of iron biotite and sillimanite to muscovite and magnetite in a similar manner to the igneous reactions. Carbon can act to reduce the amount of magnetite present, with the result that there is often a complete absence of magnetite in graphitic metasediments and rocks that have undergone carbonate alteration (Grant, 1985). McIntyre (1980), however, reports that the presence of methane at less than 500^0C, and carbon monoxide and vaporised graphite at higher temperatures, causes the reduction of oxidised Fe(III) minerals with the result that Fe(II) states are promoted. Table 3.2.1.1 shows the range and average susceptibility of various rock types.

Igneous	Granite	Rhyolite	Gabbro	Basalt	Diorite	Pyroxenite	Andesite
Range	0-5000	20-3500	100-9000	20-17500	60-12000		
Average	250		7000	7000	8500	12500	16000
Metamorphic	Phyllite	Schist	Gneiss	Quartzite	Slate		
Range	25-250	30-300	10-2500		0-3500		
Average	150	140		400	600		
Sediments	Dolomite	Limestone	Sandstone	Shale			
Range	0-90	0-300	0-2000	1-1500			
Average	10	30	40	60			

Table 3.2.1.1 Magnetic Volume Susceptibility range and average values ($k \times 10^{-5}$ S.I. units) for various rock types (Telford et al., 1990; Carmichael, 1989).

3.2.2 Magnetic Minerals in Sediments

The amount of iron in sediments depends on the source rocks that the sediments are derived from. The principal sources of detrital iron in sediments are, (1) *volcanics*, where iron occurs in silicates and oxides, with magnetite a more common oxide than haematite or ilmenite, (2) *plutonic* and *metamorphic* rocks, where iron occurs in Fe-silicates, ilmenite, haematite and magnetite, (3) *sediments* previously deposited, where iron occurs in fine-grained rocks derived from clays that have absorbed the metal onto their surfaces, (4) *soils* (laterites) that are enriched in iron, which occurs as amorphous hydrous ferric oxide (Grant, 1985).

The chemical weathering and sedimentation process occurs in several stages, (1) *chemical weathering*, where attack by groundwater containing CO_2 causes the ferrous minerals in rocks to break down eventually as Fe(II) is slightly soluble in carbon-dioxide-containing water. The ferrous iron which goes into solution is usually oxidised to ferric iron (in aerobic environments) which is almost completely insoluble, so it precipitates as goethite, a hydrated ferric oxide. (2) *leaching of soils* occurs when heavy, persistent rain (as found in the tropics) attacks the constituents of the soil with the removal of the soluble components, leaving laterite deposits behind. While these deposits are rich in haematite, they sometimes contain small amounts of maghaemite. (3) *transportation of iron* in solution or suspension can result in colloidal ferric hydroxyls becoming preferentially attached to clay or silt particles which tend to be deposited in quiet, relatively deep-water environments. (4) during *compaction*, the ferric hydroxides form haematite, and during early diagenesis, most iron is incorporated into haematite (aerobic environments), pyrite (organic sulphur bacteria-rich environments) and

siderite (organic fresh-water environments) (Grant, 1985). Grant considered that magnetite would usually only be found in unmetamorphosed sediments in very small quantities because it is unstable in the low-temperature, highly-oxidising environment of chemical weathering and sedimentation. McIntyre, (1980) asserted that iron should be more commonly found in silicates, hydrous ferric oxides, haematite and siderite, with detrital magnetite being unusual and therefore only likely to occur in sediments such as beach sands and river placers that have undergone minimal chemical weathering. Grant (1985) believed that, from studies of sedimentary iron formations of all ages, magnetite does not, and has not in the past, formed in any significant quantity by chemical diagenetic processes.

There are a number of relatively recent published studies discussing various organic and inorganic mechanisms by which slightly or non-magnetic iron compounds could be converted into higher susceptibility forms in sediments, some of which may have a relationship with hydrocarbon deposits. Below the water/sediment interface conditions of low Eh and high pH such as contact between alkaline brine solutions and anaerobic sedimentary environments may result in the formation of magnetite by the reduction of haematite or the oxidisation of pyrite or siderite (Machel and Burton, 1991a, 1991b; Kilgore and Elmore, 1989; Elmore et al., 1987, Donovan et al., 1979) or in the formation of magnetic iron sulphides (Reynolds et al., 1990a; Sassen et al., 1989; Reynolds et al., 1991; Goldhaber and Reynolds, 1991; Krs et al., 1992). Reducing environments where this process has been postulated to occur by the above authors include environments caused by hydrocarbon seepage that have been called geochemical plumes (Machel and Burton, 1991b), leakage plumes or alteration haloes (Gay, 1992). They result from the escape of liquid and gaseous hydrocarbons through the top seal (caprock) of a hydrocarbon reservoir and the subsequent migration of these fluids due to buoyancy or upward advection to a shallow iron-rich environment.

Machel and Burton (1991a, 1991b) discuss the thermodynamical constraints on chemical reactions occurring in hydrocarbon seepage environments that can result in the creation and/or breakdown of magnetic minerals. The authors base their conclusions on theoretical studies and experimental evidence (e.g. Nordstrom and Munoz, 1986, and Machel, 1987, respectively) that these chemical reactions can occur under conditions of thermodynamic equilibrium but point out that 'many natural environments are in thermodynamic disequilibrium and are governed by kinetic', ,' processes which may inhibit or promote reactions under conditions different from those permissible from thermodynamic considerations'. In

environments where the pH is greater than 7, magnetite may precipitate or replace haematite while in strongly reducing environments (Eh < -0.45 V) and a pH greater than 7.8, siderite may precipitate or replace magnetite but Machel and Burton, (1991a) point out that the stability field for this reaction is very small. In conditions that are relatively sulphur-rich, and where the pH is above 6.6, an increasingly reducing environment results in the replacement of haematite by pyrite, and then the replacement of pyrite by pyrrhotite (at Eh < -0.38 V). However, the amount of total dissolved sulphur also determines the stability of pyrrhotite, with too great an amount causing replacement by pyrite and too little by siderite and magnetite. In sulphur-free conditions, the stability of magnetic minerals is also dependent on the amount of total inorganic carbon (HCO_3^-), with magnetite predominant over haematite under increasingly reducing conditions but where siderite only replaces magnetite when the total inorganic carbon content is greater than that necessary for siderite to be supersaturated (Machel and Burton, 1991a).

Gay (1992) rejects the hypothesis that magnetite can form through diagenetic/authigenic processes by advancing the alternative view that *detrital* magnetite is very common in various sediments and magnetic anomalies found in the vicinity of hydrocarbon fields are more likely to be caused by folding and/or faulting of highly magnetic beds, the presence of concentrations of volcanic material, the demagnetisation of sediments by the passage of hydrocarbon or hydrothermal fluids, or cultural artifacts. Gay points out that magnetite from highly magnetic formations may be transported into channels and other concentrations by normal fluvial, lacustrine or marine processes which can produce anomalies that may appear to be caused by diagenetic magnetic minerals. Gay (1992) believes there is a possibility that migrating hydrocarbons may generate small amounts of sulphide minerals (principally pyrite and marcasite but occasionally pyrrhotite and griegite) which could subsequently be oxidised to magnetic iron oxides and hydroxides (probably maghemite) above the water table but believes that such accumulations of magnetic minerals are unlikely to be magnetic enough or thick enough, despite their very shallow depth, to be distinguishable in an aeromagnetic survey. Gay (1992) concludes that, to his knowledge, there has been no published study that proves a link between 'magnetic minerals in leakage plumes or alteration haloes above oil fields to a corresponding measured aeromagnetic anomaly'.

A combined aeromagnetic, groundmagnetic and core sample survey was conducted over the Formby oil field, Lancashire, U.K. in order to determine whether any diagenetic magnetic minerals were formed in the shallow seepage environment above the field. Busby et

al., (1991) found a circular positive anomaly about 300 m in diameter with an amplitude of 8 nT over the oil field, which is approximately the size and amplitude of an anomaly expected from diagenetic magnetic minerals. Busby et al., (1991) report that a detailed groundmagnetic survey was subsequently undertaken over the oil field to investigate the anomaly, and concluded that the positive anomaly was the result of well casings from the 22 wells in the field. The mineralogical analysis of the core material showed that there was a substantial amount of contamination from steel particles and rust introduced during drilling. These contaminants were similar to those found in cuttings from the Cement oil field, Oklahoma, where Donovan et al., (1979) postulated the formation of diagenetic magnetite in association with hydrocarbon seepage. Fragments of igneous rock were very common and there were varying amounts of coarse-grained magnetite, ilmenite, haematite and pyrrhotite present, all of which the authors believe to be detrital in origin. They found a small proportion of the fine-grained, iron-rich particles could not be identified with certainty but considered that their varying composition pointed to more contaminants. They concluded from this study that any diagenetic magnetic minerals present are probably in such small quantities as to be undetectable.

In research on the magnetic properties of soils, Maher and Taylor, (1988) report the presence of pure, ultra-fine grained magnetite in British soils that have no apparent external source of the mineral. The authors selected the particular soils in order to eliminate the possibility of any substantial detrital content by choosing soils with weakly magnetic source material (slates and limestones) and where there is no glacial drift. The susceptibility values increase from the base of the soil up towards the surface with the maximum values found at around 10 cm deep. Various rock magnetic methods were used to identify the magnetic phase present, with the conclusion that the measured parameters were caused by sub-micron diameter grains, particularly those in the superparamagnetic (SP) to single domain size (SD) or the range 10 to 30 nm, which had Curie temperatures of 580 to 600° C. This and the other properties all suggested that magnetite was the ferrimagnetic mineral present, and X-ray diffraction experiments found that iron was often the only metal detected although trace amounts of manganese and zinc were reported. Transmission electron microscope images showed octagonal or hexagonal crystals with sizes in the range of less than 10 to 100 nm. Maher and Taylor, (1988) believe the magnetite is of authigenic origin because the crystals are quite different from other ultra-fine grained magnetites which occur as titanium-substituted,

elongated inclusions in silicates. The burning of the surface soil can transform goethite into ferrimagnetic minerals but goethites found in soils are usually substituted with aluminium which means that the product ferrimagnetic minerals are as well (Maher and Taylor, 1988). Taylor et al., (1987) discuss laboratory experiments where pure, ultra-fine grained magnetite closely resembling the soil minerals in purity, grain-size and magnetic properties was easily synthesised by controlled oxidation of ferrous solutions at 25° C and near-neutral pH which the authors believe are realistic approximations of the soil environment.

In a study of deep sea sediments obtained through the Ocean Drilling Program, Lu and Banerjee, (1994), found that the dissolution of magnetite occurred in zones at depths of around 675 m to 1243 m below the sea floor. The authors concluded that, because of the increase in temperature with depth, organic matter will break down (catagenesis) into light hydrocarbons and CO_2 with an accompanying reduction of Fe^{3+}, Mn^{4+} or SO_4^{2-}. This process is believed to cause the dissolution of pre-existing magnetite through the reduction of the Fe(III) cations in magnetite to Fe(II). The temperature range at which catagenesis occurs is between about 60° and 200° C, of which at least the minimum value was reached in the wells studied (Lu and Banerjee, 1994). Similarly, Canfield and Berner, (1987) investigated the dissolution and replacement of magnetite by pyrite in anoxic marine sediments, and found that degree of dissolution of magnetite is dependent on the surface area of the magnetite particles, the concentration of dissolved sulphide, and the time in which the magnetite is in contact with sulphide-rich pore waters. Extensive bioturbation lowers the dissolved sulphide pore-fluid concentration resulting in a slow rate of magnetite dissolution while the absence of bioturbation allows the build-up of high levels of sulphide which causes the formation of a pyrite coating on magnetite grains. If the pyrite coating completely covers the magnetite grain then any further reaction with dissolved sulphide is prevented and magnetite preservation is enhanced. Preservation is also enhanced, by rapid sedimentation because this limits the time magnetite is in contact with dissolved sulphide, and if there is a high level of reactive iron minerals such as goethite or other iron oxy-hydroxides, then the other iron minerals react with the dissolved sulphides removing them from solution with the result that magnetite is protected from dissolution..

Brothers et al., (1996) report geochemical experiments designed to simulate the alteration of pyrite grains to magnetite in organic matter-rich carbonate formations in

Colorado, U.S.A. The pyrite grains were found to have magnetite rims which formed as a replacement of existing pyrite rather than as an overgrowth. In their experiments, the authors found that aqueous solutions of ferric-organic complexes and pyrite which were initially kept at a temperature of 60°C with very little oxygen, yielded a ferrous hydroxide precipitate when the pH was increased. The precipitate subsequently converted to magnetite when the temperature was increased to 90°C. The degree of dissolution of pyrite was dependent on the presence of Fe(III) because the ferric-organic complexes yielded much more Fe(II) in solution than the organic compounds by themselves. The presence of clays such as bentonite or strongly-reducing organic ligands was found to be able to prevent pyrite dissolution and interfere with the crystallisation of magnetite. Brothers et al., (1996) suggest that in near-surface environments, the availability of molecular oxygen would result in the formation of haematite, while at greater depths or where porosity was restricted, the process would stop at magnetite.

Yeremin et al., (1986) report studies from the Timan-Pechora and western Bashkiria regions of Russia where the susceptibility of hydrocarbon-bearing formations was compared with that of the same formation outside but adjacent to the reservoir, and at some distance from it. The background values for the formations were taken from wells between 4 and 30 km away from the hydrocarbon deposits, with the range for the sandstone and siltstone members found to be $\chi = 0$ to 6×10^{-5} SI units while the overall range for the argillaceous sequences was $\chi = 6$ to 65×10^{-5} S.I. units, with the most common range being $\chi = 10$ to 33×10^{-5} S.I. units. The authors found that the susceptibilities of oil saturated rocks were very similar to that of the background values but in the argillaceous layers, especially in the regional caprocks, the range increases to $\chi = 0$ to 260×10^{-5} S.I. units, with the average being $\chi = 26$ to 90×10^{-5} S.I. units. The authors found that the magnetisation of the caprocks over anticlinal traps showed a substantial increase in the central parts of the trap but declined quickly towards the edges. There were two types of vertical distribution of magnetisation, the first has the greatest magnetisation in the caprock member directly above the hydrocarbon pool with a gradual decline to the background level as the depth decreases, while the second type has the greatest magnetisation not only above the hydrocarbons but directly beneath the trap as well. Generally, it was observed that those sequences with relatively high magnetisations surround the hydrocarbon deposits with only weakly magnetised rocks away from them (Yeremin et al., 1986).

The most widespread epigenetic minerals of iron in that region are siderite and ankerite, but their petrographic observations (Yeremin et al., 1986) indicated no support for the hypothesis that the siderite formed through the reduction of iron oxides under the influence of hydrocarbons (secondary sideritisation). In contrast, they suggest that the iron carbonates formed as a result of the breakdown of iron-rich clay minerals by migrating hydrocarbons in the halo (Yeremin et al., 1986). They noted that the breakdown of the clays is greatest in the immediate vicinity of the hydrocarbon deposits where there has been decolourisation or bleaching due to the loss of iron. In some of the rocks the magnetisation of the rocks can be related to the siderite content but this mostly applies to sediments with susceptibilities in the range χ = 26 to 180 $\times$ 10^{-5} S.I. units while in those rocks with higher magnetisations there is nearly an order of magnitude increase in the remanent magnetisation. The magnetic mineral responsible for this effect could not be identified by optical methods but displayed behaviour on heating that suggested the Curie point was in the range 560-580° C, which is indicative of magnetite (Yeremin et al., 1986). Where the hydrocarbon deposits were small the caprock layers displaying increased magnetisation were only a few metres thick while the altered zones were 60 to 80 m thick in the vicinity of large pools. The authors suggest that it may be possible to detect such alteration haloes by low altitude aeromagnetic surveys but this may prove difficult in the specific cases discussed above because the depth to the reservoirs is between 3100 to 3500 m.

A study of haematite-cemented sandstones (red beds) by Kilgore and Elmore, (1989) suggested that the presence of hydrocarbons caused the removal of haematite from oil-saturated sandstones and the surrounding 'bleached' zone with the result that the susceptibility of the unaffected red beds was around an order of magnitude higher than in the hydrocarbon impregnated and bleached zones. However, work by Benthian and Elmore, (1987) and Elmore et al., (1987) on hydrocarbon-saturated limestones implied an increase in magnetic intensity of approximately an order of magnitude over those carbonate rocks which were hydrocarbon-free. Kilgore and Elmore, (1989) believe that the dissolution of haematite in the red beds was the cause of some local precipitation of magnetite and iron sulphides but the bulk of the iron was transported away to precipitate in other units with an overall reduction in susceptibility and NRM. In the carbonate sediments, it was suggested that the precipitation of authigenic magnetite as a result of hydrocarbon chemical activity was responsible for the increase in

magnetic intensity (Elmore et al., 1987). In other cases, when siderite in carbonate rocks is exposed to oxidising conditions, it can be altered initially to magnetite or maghaemite, causing a substantial increase in magnetic susceptibility (Ellwood et al., 1986). Lowrie and Heller, (1982) and Ellwood et al., (1988) report that marcasite, siderite, pyrite and others can react under diagenetic conditions to produce new magnetic minerals whose properties will dominate those of the sediments. Krs et al., (1992) discuss the magnetic properties of griegite and smythite mineralisation in Miocene claystone layers overlying brown coal seams in the Czech Republic where the mineralisation was strongly associated with fossil micro-organic matter. The most common type of distribution of mineralisation was fine dispersion (1%) throughout the approximately 100 m thick, organic material-rich, clay layers but occasional accumulations in strips along the bedding planes contained as much as 10% wt. of magnetic sulphides while griegite was commonly found in organodetrital material. The magnetic mineralisation was dominated by griegite with smythite ranging from a few percent to around 30 %, while pyrrhotite was only found in small amounts.

Palaeomagnetic studies (Elmore and McCabe, 1991) have revealed the widespread occurrence of *secondary remagnetisations* where the initial magnetisation of sediments, acquired before or during deposition, is altered at a later date by thermal or chemical processes. This has been determined by comparison of the age at which the Natural Remanent Magnetisation (NRM) was acquired and the age of deposition of the sediments which is found by, for example, the use of palaeontological methods. The NRM can be realigned by thermal processes associated with regional metamorphism or, locally, hydrothermal alteration but Elmore and McCabe (1991) refer to a number of cases where the sediments are unmetamorphosed and there is no evidence of elevated temperatures since deposition. In these cases Chemical Remanent Magnetisation (CRM) has been cited as the likely cause of the changes with alteration due to migrating hydrocarbons one of the important examples (Elmore and Crawford, 1990).

The discussion above considers the possibility of post-depositional formation of magnetic minerals by chemical processes in a reducing environment, especially in the vicinity of hydrocarbon accumulations. These chemical processes are likely to proceed quite slowly at low temperatures (< 65° C) but much faster at higher temperatures (100 to 135° C). In contrast, processes mediated by microbial enzymes proceed rapidly at temperatures lower than 65° C but the bacteria are dormant or dead at higher temperatures (Machel and Burton, 1991b).

Bacteria associated with the formation of magnetic minerals can be divided into two groups, the *magnetotactic* bacteria and the *iron-reducing* bacteria. Magnetotactic bacteria form intracellular chains of magnetite (in membrane-enclosed organelles called magnetosomes), with the result that an ultra-fine-grained, single-domain (SD), pure end-member magnetite can be produced in surficial aerobic sediments (Blakemore, 1975; Stolz et al., 1986; Fassbinder et al., 1990, Schwartz et al., 1997) after the death of the organisms. Magnetotactic bacteria have also been found with intracellular chains of fine-grained, SD griegite (and occasionally pyrrhotite) instead of magnetite (Mann et al., 1990; Heywood et al., 1990). The magnetotactic bacteria are widely distributed and are found in shallow and deep marine, lacustrine and soil environments while microfossils have been found ranging in age from Recent to 2 billion years (Chang and Kirschvink, 1989; Chang et al., 1989). There are a number of magnetotactic bacteria that are anaerobic which form iron sulphides but most magnetotactic bacteria live either in water or just below the sediment/water interface in oxic conditions, and the magnetic minerals they contain are deposited in the sediments when they die (Vali et al., 1987). Machel and Burton (1991b) found no references in the literature of magnetotactic bacteria living in hydrocarbon seepage environments so magnetite and other magnetic minerals formed through their activity may not to be associated with hydrocarbon accumulations and it is likely that, under only the most favourable conditions, it may be possible to detect shallow, water-saturated aquifers where these bacteria are present or, at worst, the magnetic minerals deposited after death will only contribute to the background magnetisation of the sediments.

Where oxygen is absent, some sulphate-reducing and *dissimilatory iron-reducing* bacteria break down organic matter in sediments by means of extracellular, enzymatic reactions which reduce Fe(III) from surrounding rocks in order to extract oxygen from sulphates (the oxygen then being used in metabolic processes) or reduce Fe(III) to Fe(II) directly as part of the metabolisation of organic material such as acetates (Lovley et al., 1987, 1993). Some dissimilatory iron-reducing bacteria were found to produce substantial quantities of ultrafine, extracellular magnetite under anaerobic laboratory conditions with one strain (*Geobacter metallireducens*) generating around 5000 times more magnetite by weight than an equivalent biomass of magnetotactic bacteria (Frankel, 1987). The reduction of ferric oxide by the cultured bacteria resulted in the production of magnetite, siderite and soluble Fe(II) when nutrient solutions were buffered with bicarbonate but when bicarbonate was absent, magnetite predominated (Lovley et al., 1990). Magnetite formed either by magnetotactic bacteria

intracellularly or by iron-reducing bacteria extracellularly have been found to be titanium free, usually less than 100 nm in diameter and the crystals are euhedral rather than angular in shape as is the case with detrital magnetite (Maher and Taylor, 1988, Schwartz et al., 1997). McCabe et al., (1987) report the occurrence of magnetite within solid bitumen samples that are most probably the result of microbial attack on crude oil. The magnetite inclusions are present as crystal aggregates in the bitumen, and consist of spherical aggregates of pure magnetite which are occasionally hollow. The authors also suggest that there is evidence of the presence of smaller, single domain grains in some of their samples. McCabe et al., (1987) state that they cannot rule out the possibility that the magnetite was formed after biodegradation but this process must have occurred at temperatures less than 66° C because the rocks have never been buried deeply. They believe that the magnetite is not likely to be older than the bitumen because this would require the transport of the magnetite grains by migrating crude oil.

In their review of deep subsurface microbial processes, Lovley and Chapelle, (1995) report that the energy yield from iron reduction is substantially greater than that from sulphate reduction or methane production, and some organisms which can derive energy from either iron or sulphate reduction will preferentially use iron-reduction if the concentration of Fe(III) in the sediments is great enough. The main physical constraints on the activities of these microorganisms are small pore diameters and the increase in temperature with depth. Lovley et al., (1990) recovered iron-reducing bacteria from Cretaceous aquifers on the Atlantic Coastal Plain, South Carolina, U.S.A., at depths of 52 to around 200 m and these organisms were found to reduce non-magnetic, reddish-brown ferric oxides, which were also recovered from the aquifer, to a black, highly-magnetic precipitate as well as Fe(II) in solution. They report that extensive precautions were taken to avoid contamination by surface-dwelling organisms. In 1993 the recovery of bacteria from basaltic, alkaline, anaerobic aquifers on the Columbia Plateau, Southeast Washington, U.S.A., was reported by Stevens et al., (1993). Bacteria including Fe(III) and sulphate reducers were recovered from two wells at depths of 316 and 1270 m in sedimentary aquifers between impermeable basalt layers.

Lovley and Chapelle, (1995) report that microbial numbers and activity are usually lower in clay-rich layers than sandy aquifers which they attribute to the lower porosity and permeability of clay-rich sediments. They also note that the iron and sulphate reducing bacteria usually cannot metabolise most of the hydrocarbons present in crude oil and must rely on the waste products (long-chain fatty acids, monoaromatics, acetates etc.) of aerobic, fermentation

bacteria which are normally unlikely to be found at depths greater than 600 m. However, these waste products may persist in sediments for long periods of time. Studies of the reduction of structural Fe(III) in smectite by metal-reducing bacteria (Kostka et al, 1996), showed that between 25 % and 41 % of the Fe(III) was reduced to Fe(II) provided the temperature remained between 25° and 37°C and other conditions were typical for anaerobic sediments. The authors found that most of the Fe(II) remained bound to the clay during the reduction process so this is not likely to lead to substantial quantities of Fe(II) being released into solution where it could form magnetic oxides or sulphides. Theoretical studies by Van Cappellen and Wang, (1996) on the cycling of iron and manganese in surface sediments, allowed them to conclude, from their computational model, that 'approximately two thirds of the total rate of iron reduction in the sediment are utilised directly by bacteria to oxidise organic carbon' but only very small amounts of the Fe(II) produced during the early diagenetic processes are incorporated into ferrous minerals in the deeper sediments. Their model suggests that most of the Fe(II) is reoxidised in the surficial sediments or is released into the overlying water.

This discussion of magnetic minerals in sediments demonstrates that there has been considerable controversy over the existence and sources of magnetic minerals, particularly magnetite, in intersedimentary environments, whether those minerals are likely to be stable over geological time, whether there is any association with hydrocarbon accumulations, and the likelihood of magnetic anomalies caused by some of the postulated concentrations of minerals in these environments. The studies of geochemical and biological mechanisms define those circumstances when and where magnetic minerals may form and whether or not there could be any relationship to hydrocarbon concentrations, but literature searches to this date have not revealed any studies which demonstrate that the observed magnetic anomalies can be unequivocally attributed to magnetic minerals generated by hydrocarbons. Some of the studies suggest that, while the relationship between hydrocarbon concentrations and aeromagnetic anomalies is unproven, it is possible to differentiate between sandstone and shale lithologies, and possibly identify hydrocarbon-bearing sediments, by magnetic susceptibility measurements in uncased wells (Bouisset and Augustin, 1993).

The purpose of the preceding discussion has been to present the various arguments that have been advanced on these subjects so that the studies of the author can be seen in context . It is very unlikely that any definitive conclusions on the above subjects could be reached from the studies discussed in this thesis so the analysis will concentrate on what the local evidence

reveals. Theoretical studies in Chapter 5 will concentrate on the magnetic effect of structures revealed from seismic mapping and the magnetic susceptibilities assigned to bodies will be derived from measurements of cores rather than those that might be expected if detrital, authigenic or biogenic processes had produced the concentration of magnetic minerals.

3.2.3 Magnetic Minerals in the Study Area

Most of the mineralogy studies carried out in this area have been for the purpose of identifying hydrocarbon-bearing facies with little attention paid to the occurrence of what are usually considered accessory minerals, such as the iron oxides, which only have a minor effect on those rock properties that are important in petroleum exploration. The exception is the occurrence of ferriginous cements in sandstones and their effect on porosity.

The Little and Phillips (1995) study on the detrital and authigenic mineralogy of the Pretty Hill Formation was the result of the analysis of core samples from seven wells in the Penola Trough. Thin sections prepared from core from Katnook 2, Katnook 3, Ladbroke Grove 1, Laira 1 and Zema 1 were used as well as thin sections of sidewall core samples from Katnook 4 and Haselgrove 1 (fig. 2.2.3.1). The authors found that the main detrital minerals were quartz, feldspars, mica and various silicate accessory minerals. The micas were predominantly the iron-rich varieties, biotite and muscovite, while the accessory minerals include iron-rich garnets with minor amounts of tourmaline and hornblende. There were also lithics (rock fragments) derived from igneous, metamorphic and sedimentary sources which made up around 35 % of the framework grains.

The main authigenic minerals include chlorite, various carbonates, glauconite and illite with laumonite, quartz, feldspar, sphene etc. The dominant authigenic minerals by volume are chlorite, carbonates and laumonite with siderite, calcite, dolomite and ankerite being the main carbonates. The chlorite usually contains between 20 and 30% Fe while the siderite includes a high-Mg variety in some occurrences. The authors believe that the Mg and Fe ions incorporated into the carbonate cement were probably the result of the breakdown of mafic minerals in the volcanic lithics. They feel that alkaline conditions with abundant Fe prevailed during early diagenesis with the result that siderite was the first carbonate to precipitate in the pore spaces. Glauconite usually forms in moderately alkaline conditions, when the Eh is at the oxidation/reduction boundary and if there is sufficient Fe(II) and Fe(III) present. Little and Phillips (1995) believe that the relatively small amount of authigenic sphene and anatase (< 2

%) was formed because of the breakdown of micas, rutile and mafic minerals in the volcanic lithics releasing titanium, but they note that this metal can also be released by the alteration of detrital ilmenite, titanomagnetite and titanohaematite.

In the Little and Phillips (1995) paper, their figure 4 shows the percentages of the important detrital and authigenic minerals and rock types comprising the Pretty Hill Formation, with the most abundant mineral being quartz which comprises 45 to 50 % of the rock volume from all five wells. The volcanic lithics (igneous rock fragments) are typically around 10 % of the total rock volume while chlorite cement comprises between 10 and 15 %, and carbonate ranges between about 2 % up to about 10 % of the rock volume. The authors report that the fragments of volcanic lithics tend to be partially to completely altered, mostly to chlorite, and the very fine groundmass of these fragments is rich in iron and magnesium.

In 1994 Beaumont-Smith, (1994) investigated core material from the Katnook 1, 2 and 4 wells, conducting petrological studies and measuring magnetic susceptibility values (discussed in section 3.3.2) in order to delineate the boundary between the Windermere Sandstone Member at the base of the Eumeralla Formation and the underlying Katnook Sandstone component of the Crayfish Group. The petrological studies of cores from Katnook 4 found a varying composition with quartz naturally dominating the framework grains but with between 5 and 23 % acid volcanic rock fragments, up to 7 % biotite, and around 1 % leucoxene (a breakdown product of ilmenite) and less than 1 % haematite in one core. The amounts of authigenic minerals and cements varied between cores but up to 4 % chlorite was identified as well as trace amounts of pyrite in one core (Beaumont-Smith, 1994). Sedimentological studies of the cores from Katnook 2 and 4 reveal thin haematite-rich layers and red haematite-stained beds which were found to have a strong magnetic response, as well as sideritic cements that have moderate magnetic susceptibility values. There are isolated instances of haematite grains in some layers as well as the much more common haematite staining, but Beaumont-Smith, (1994) found that the haematite-stained layers were a very minor component of the core material.

The only magnetic minerals identified from the Pretty Hill Formation cores were paramagnetic minerals such as siderite and chlorite (with minor pyrite) which occur as authigenic cements. Siderite was sometimes found in a high magnesium variety which could be expected to have a lower susceptibility than minerals that only contain iron. Martin and Baker, (1992) found that siderite is a significant component of the Pretty Hill Formation in the

Ladbroke Grove 1 well only where, for example, it is 10 % of the rock volume at the 2555.57 m level. The fragments of volcanic rock were believed to be derived from trachyte, basalt or andesite (Little and Phillips, 1995), all of which have high susceptibilities. However, as discussed above, the authors have found substantial alteration of these fragments during diagenesis with the probable release of iron into the pore spaces where it was incorporated into the authigenic minerals.

The Eumeralla Formation cores have a higher magnetic mineral content, with the presence of haematite in Katnook wells as well as the volcanic rock fragments and paramagnetic mineral cements (siderite, pyrite and chlorite) found in the Pretty Hill Formation cores, but as discussed above haematite is a minor constituent of the rocks which suggests that it is unlikely to greatly influence the bulk magnetic properties of the rocks (Beaumont-Smith, 1994). In the Sawpit 1 well completion report, Martin (1992) found that pyrite was present in amounts ranging from rare to traces, and as cements, nodules and associated with coaly detritus. There were two main concentrations, near the top of the formation (333 m to 745 m) and in the interval 905 m to 1170 m with the latter group containing occurrences defined as rare (also the presence of nodules) while the upper group contains occurrences defined as rare to traces. Traces of pyrite were also present in the overlying Sherbrook and Wangerrip (Tertiary) Groups (Tabassi and Robbie, 1992). Reeve and Skinner, (1995) also found minor to trace amounts of pyrite in Eumeralla Fm cuttings from the Wynn 1 well, with these traces being found throughout the formation.

In the Katnook 2 well completion report, McClung and Archer, (1989) identified minor glauconite in the Gambier Limestone, occasional pyrite aggregates in the upper part of the Dilwyn Formation and slightly more common pyrite cements in the lower part of the formation, pyrite inclusions, nodules and cement in the Pebble Point Formation (accessory minerals), and occasional pyritic coals in the Sherbrook Group. The trace amounts of pyrite in the Eumeralla Formation were found to be more common in the upper part of the formation while traces of volcanic tuffs were identified in an interval between 1233 m and 1270 m.

The trace amounts of pyrite found as a result of the Beaumont-Smith, (1994) and other studies suggest that the sediments in the vicinity of the wells are not very sulphur-rich, and the likelihood of the formation of magnetic sulphides as a consequence of diagenetic processes at these locations may be low but it is not possible to exclude the possibility of the formation of these minerals completely at all locations. Similarly, there is no reports of

magnetite in cores or cuttings but this does not preclude its presence as a detrital or authigenic component of the sediments.

3.2.4 Palaeomagnetic field direction

The shape of a magnetic anomaly is dependent on the inclination and declination of both the inducing geomagnetic field and the intrinsic remanence. The current geomagnetic inclination angle in the centre of the study area is -69.54° and the declination angle is 9.53° but these angles have varied considerably since the Late Jurassic as Australia has drifted north after the separation with Antarctica. This means that the remanent magnetisation inclination and declination directions will vary with the age at which the remanence was acquired. In a paper on magnetic petrophysics, Clark (1983), published a table of geomagnetic field directions during the Phanerozoic for a reference point in the centre of Australia (**24°S, 134°E**). Also printed was a graph showing the predominance of normal to reversed field polarity during the major periods which shows that the polarity was predominantly normal during the Mesozoic but equally mixed during the Cainozoic. Table 3.2.4.1 reproduces the part of the Clark (1983) table that is relevant for this study but it must be noted that there is a **25.5°** difference in current geomagnetic inclination (and **7.5°** in declination) between the study area and the centre of the continent.

Period	Age (Ma)	Declination (°)	Inclination (°)
Quaternary - Late Tertiary	0 - 4.5	2	-44
Mid - Late Tertiary	20 - 34	11	-55
Early Tertiary	40 - 60	4	-66
Cretaceous - Tertiary boundary	65	27	-73
Middle Cretaceous	100	334	-71
Mid - Late Jurassic	130 -150	278	-74

Table 3.2.4.1 Geomagnetic declination and inclination angles for various geological periods (Clark, 1983)

3.3 Susceptibility Measurements

Magnetic susceptibility values for the major formations from core material were supplied to the author by the South Australian Department of Mines and Energy (MESA).

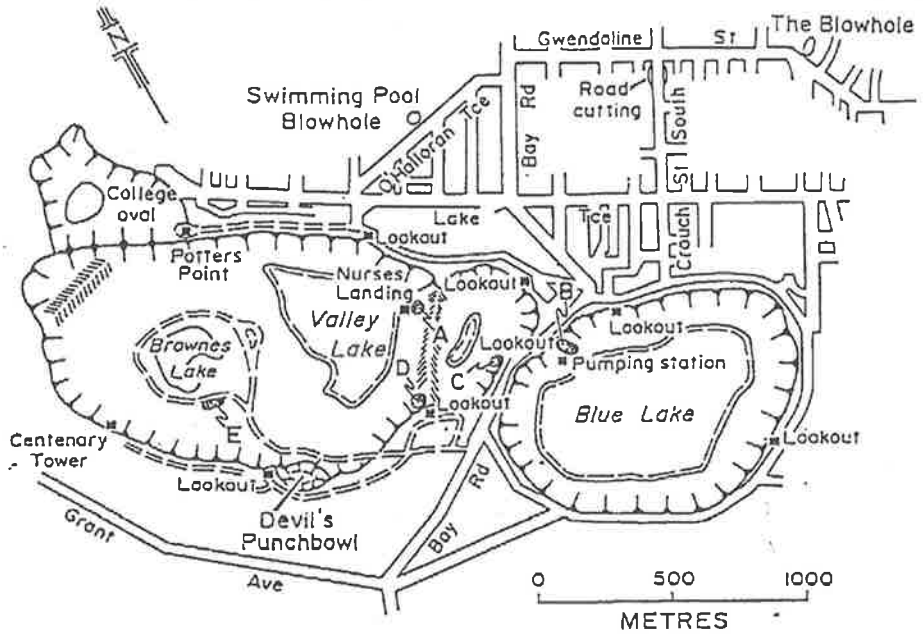

A	A, WA ... 1000 - 8000 Ba, Ma, V 600 - 2500 Ba, RLS .. 400 - 3000 T, M ..... 150 - 400 T, B ..... 40 - 400	Site 2
B	T ..... 1000 - 3000 S, W .... 700 - 900 S, R ..... 500 - 4000 A, Ba .... 900 - 5000 Ba, W ... 5 - 900	Site 1
C	T, M ..... 50 - 250 T, B ..... 4 - 1000	Site 3
D	T, M ..... 50 - 700 T, B ..... 10 - 450	Site 4
E	RLS, M .. 15 - 700 RLS, B ... 0 - 350	Site 5

KEY

A ... Ash
WA . Unsorted tephra
Ba .. Basalt
Ma .. Massive
V ... Vesicular
RLS . Ropey Lava Spatter
T ... Tuff
M ... Matrix
B ... Bomb
S ... Scoria
W .. Weathered
R ... Red
Ba .. Bedded

Fig. 3.3.1.1 Mt. Gambier Volcanic Complex map

Ground Magnetic Susceptibility Ranges (x 10^{-5} SI units)

After Chatfield, (1992), map from Sheard, (1980), SADME 92-1326

Chatfield (1992) measured the magnetic susceptibility of the volcanic units exposed at Mt. Gambier and Mt. Schank, as well as, the Mt. Burr Volcanic Group. Beaumont-Smith, (1994) carried out a series of measurements on cores from the basal Windermere Sandstone member of the Eumeralla Formation, the Eumeralla Formation itself and the Laira Formation from Katnook 1, 2 and 4. Magnetic remanence studies have not been carried out on any of the cores or volcanic material. Tucker and Frears (1995) report that a previous study to the MESA measurements was considered unreliable because cuttings were contaminated with steel particles, and sidewall core material had to be crushed and a poorly-defined correction factor applied to produce a measurement equivalent to a solid slab of rock.

3.3.1 Measurements from Volcanic Extrusions

Chatfield (1992) took measurements from five locations in the Mt. Gambier volcanic cone with readings from a number of different volcanic units at each location. The igneous rock units investigated were, ash, unsorted tephra, massive and vesicular basalt, ropey lava, splatter, tuff and scoria, all of which had relatively high susceptibilities. Similarly, three locations at Mt. Schank were investigated, all of which were in volcanic ash and not near the basalt lava flows. The rock units measured here were, scoria, fresh and weathered, finely-laminated tuff and tephra. The locations and list of values are given in Fig. 3.3.1.1 and Fig. 3.3.1.2.

3.3.2 Measurements from Cores

The core material used to obtain magnetic susceptibility values for this study came from six petroleum wells that are either within the area or are adjacent to it. These wells were, Katnook 2, Katnook 3, Penola 1, Caroline 1, Kalangadoo 1 and Mt. Salt 1. Tucker and Frears (1995) report that the core material was removed from the core store to minimise magnetic background sources and values were acquired with a hand-held susceptibility meter, usually at 0.3 and 0.6 m intervals. These values are raw and uncorrected for the influence of limited core size which Tucker and Frears (1995) suggest could be compensated for by multiplying all values by approximately 1.7. It should be noted that only selected sections of core were extracted from most of the wells and this was usually done in order to define stratigraphic unit boundaries or hydrocarbon-bearing zones. This means that for some wells all the values are clustered around certain levels with the result that no information exists for the rest of the

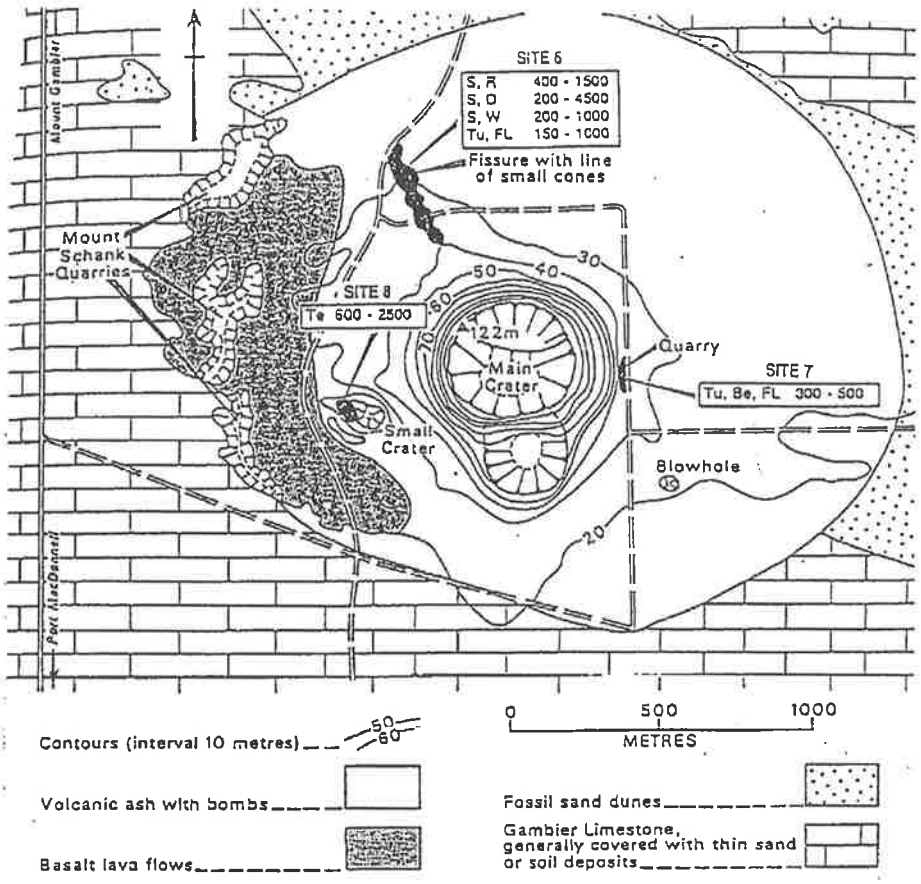

KEY

S scoria	Tu tuff
R red	FL finely laminated
D dark	Be bedded
W weathered	Te tephra

Fig. 3.3.1.2 Mt. Schank Volcanic Complex map

Ground Magnetic Susceptibility Ranges (x 10^{-5} SI units)

After Chattfield, (1992), map from Sheard, (1980), SADME 92-1327

formation. An example of this is the values for the Eumeralla Formation from Katnook 2 where the core consists of the lowermost twenty-two metres of the formation. Figures 3.3.2.1 to 3.3.2.6 show the values for each formation from various wells.

The pre-Mesozoic **Basement** of the area (presumably Kanmantoo Supergroup) was intersected in three wells, Kalangadoo 1, Sawpit 1 and Tilbooroo 1, but magnetic susceptibility readings were only obtained from Kalangadoo 1 cores (2524 to 2753 m). These values were low for meta-sediments, turbidites with minor tuff interbeds (11 to 26 $\times$ 10^{-5} SI raw and *18.7 to 44.2 $\times$ 10^{-5} SI units, corrected*), but this is probably because of the low grade of metamorphism (Morton et al., 1995). No susceptibility values have been obtained from the overlying Casterton Formation. Susceptibility values for the **Crayfish Group** consist of measurements taken from Pretty Hill Formation cores out of Katnook 2 and 3, as well as, Laira Formation cores from Penola 1 and Kalangadoo 1. The Pretty Hill Formation values have the range 11 to 20 $\times$ 10^{-5} SI units (*18.7 to 34 $\times$ 10^{-5} SI, corrected*) from Katnook 2 (2870 to 2876 m) and 9 to 18 $\times$ 10^{-5} SI units (*15.3 to 30.6 $\times$ 10^{-5} SI, corrected*) from Katnook 3 (2852 to 2875 m), while the Laira Formation has a range of 8 to 30 $\times$ 10^{-5} SI units (*13.6 to 51 $\times$ 10^{-5} SI, corrected*) from Penola 1 (1244 to 1455 m) and 7 to 22 $\times$ 10^{-5} SI units (*11.9 to 37.4 $\times$ 10^{-5} SI, corrected*) from Kalangadoo 1 (1865 to 2076 m).

Cores of **Eumeralla Formation** sediments were extracted from Penola 1, Katnook 2, Kalangadoo 1 and Caroline 1, and the magnetic susceptibility measurements from these cores show the highest overall values as well as the greatest range. Values from Katnook 2 (1858 to 1879 m) range from 10 to 82 $\times$ 10^{-5} SI units (*17 to 139.4 $\times$ 10^{-5} SI, corrected*) while those from Kalangadoo 1 (765 to 1720 m) have a range of 8 to 90 $\times$ 10^{-5} SI units (*13.6 to 153 $\times$ 10^{-5} SI, corrected*). The sets of values from Penola 1 and Caroline 1 have the same range of 8 to 45 $\times$ 10^{-5} SI units (*13.6 to 76.5 $\times$ 10^{-5} SI, corrected*) but while those from Penola 1 are reasonably evenly distributed over a depth range of 350 m to 1150 m, those from Caroline 1 are taken from two cores, one from around 3060-3070 m deep and the other at about 3370 m. The **Sherbrook Group** from the Late Cretaceous is represented by cores from Caroline 1, Kalangadoo 1 and Mt. Salt 1, with the Group being undifferentiated in Kalangadoo 1 cores but subdivided into the Timboon Sandstone and Paaratte Formation in Caroline 1 and Mt. Salt 1 cores. The undifferentiated Sherbrook Group from Kalangadoo 1 (around 763 m) has a susceptibility range of 10 to 25 $\times$ 10^{-5} SI units (*17 to 42.5 $\times$ 10^{-5} SI, corrected*) while the

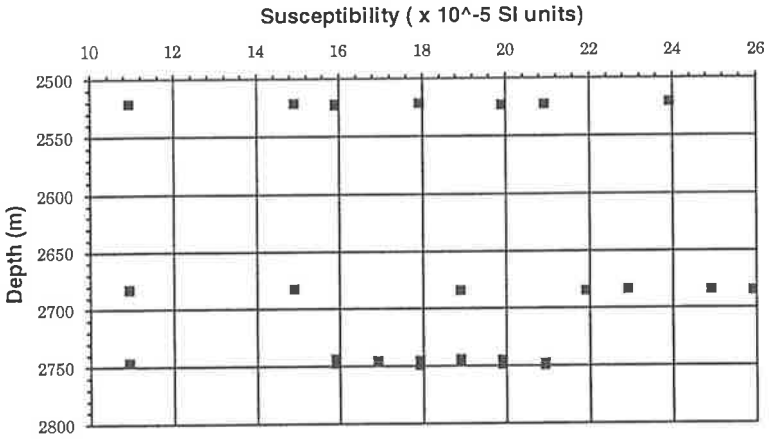

Fig. 3.3.2.1 Basement susceptibility values from Kalangadoo 1

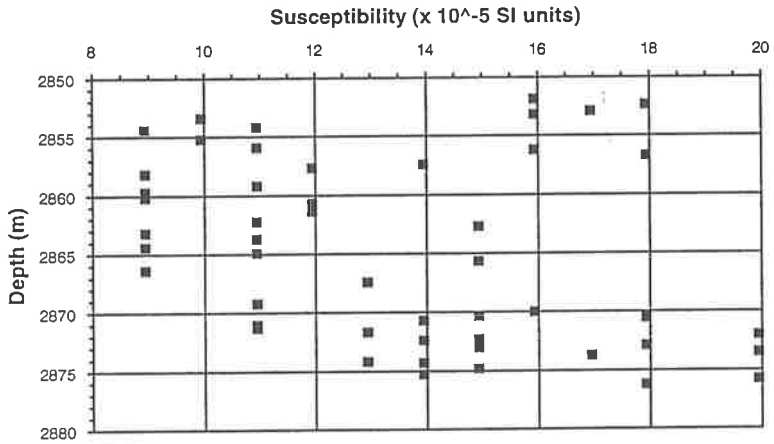

Fig. 3.3.2.2a Crayfish Group (Pretty Hill Fm.) susceptibility values from Katnook 2

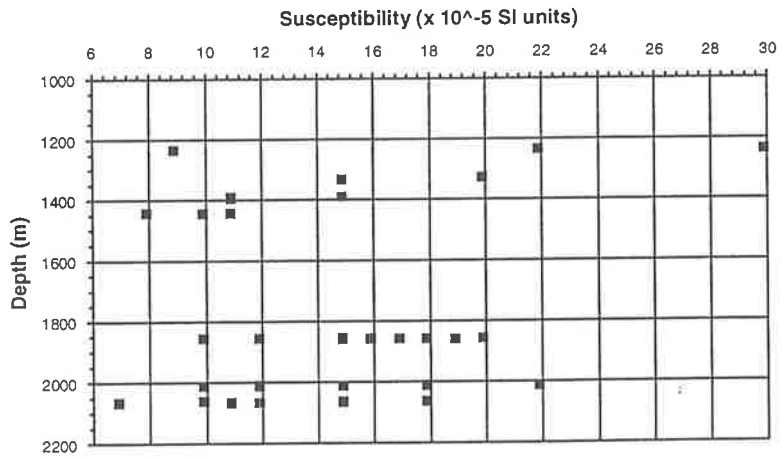

Fig. 3.3.2.2.b Crayfish Group (Laira Fm.) susceptibility values from Kalangadoo 1 and Penola 1

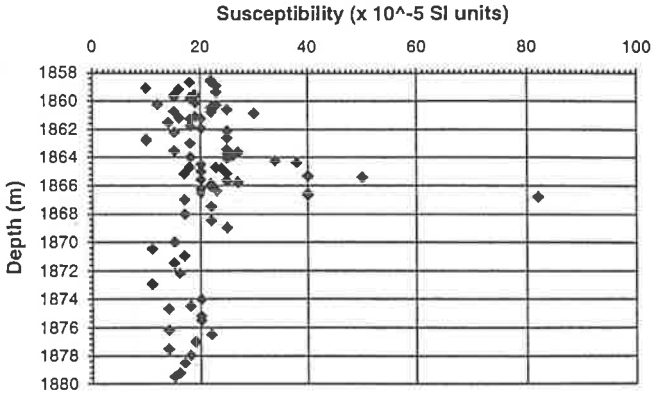

Fig. 3.3.2.3a Eumeralla susceptibility values from Katnook 2

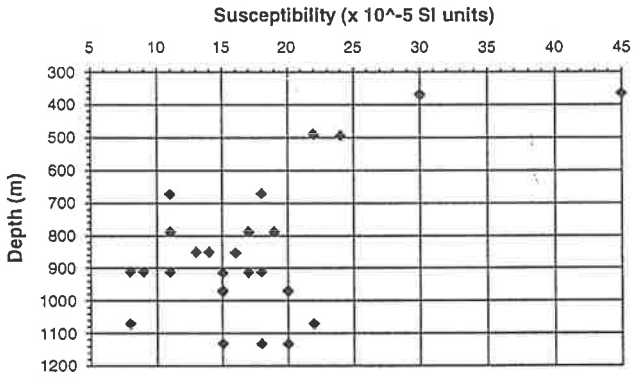

Fig. 3.3.2.3b Eumeralla susceptibility values from Penola 1

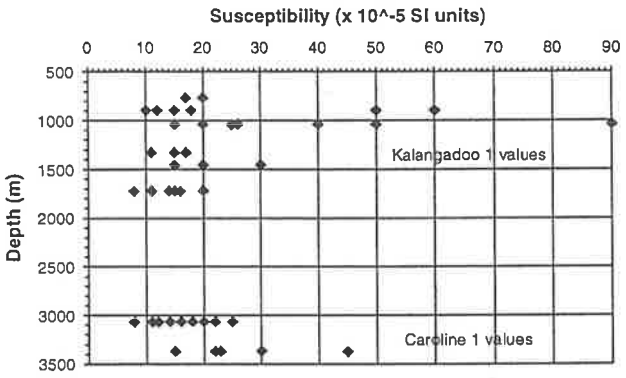

Fig. 3.3.2.3c Eumeralla susceptibility values from Kalangadoo 1 and Caroline 1

Timboon Sst. and Paaratte Fm from Caroline 1 have a susceptibility range of 7 to 10×10^{-5} SI units (*11.9 to 17 $\times$ 10^{-5} SI, corrected*) at around 1250 m and 6 to 19×10^{-5} SI units (*10.2 to 32.3 $\times$ 10^{-5} SI, corrected*) at 1829 to 1835 m, respectively. The Mt. Salt 1 cores yield values with ranges of 5 to 18×10^{-5} SI units (*8.5 to 30.6 $\times$ 10^{-5} SI, corrected*) for the Timboon Sst. (958 to 2136 m) and 4 to 17×10^{-5} SI units (*6.8 to 28.9 $\times$ 10^{-5} SI, corrected*) for the Paaratte Fm (2275 to 3063 m).

Tertiary sediment cores were extracted from Caroline 1 and Mt Salt 1, with susceptibility ranges of 1 to 6×10^{-5} SI units (*1.7 to 10.2 $\times$ 10^{-5} SI, corrected*) for the Gambier Limestone (177 to 182 m) and 7 to 18×10^{-5} SI units (*11.9 to 30.6 $\times$ 10^{-5} SI, corrected*) for the Pember Mudstone (748 to 827 m), both from Caroline 1, while the Dilwyn Formation (304 to 889 m) from Mt Salt 1 has a range of 4 to 10×10^{-5} SI units (*6.8 to 17 $\times$ 10^{-5} SI, corrected*).

The magnetic susceptibility values discussed above are low even for sediments (Clark, 1983) and while it is possible that higher values elsewhere are more representative of the formations as a whole, it would require special circumstances to exist at each well to reduce the measured values. If the measured (raw) values result from the magnetite content of the rocks then a rough estimate of the percentage of magnetite in the total rock volume can be obtained by using the relation published by Balsley and Buddington (1958) where the S.I. susceptibility $k \approx 3.3 \times 10^{-3} \times$ Volume% of $Fe_3 O_4$. Table 3.3.2.1 shows the calculated volume percentages for the ranges of measured values for each formation by well.

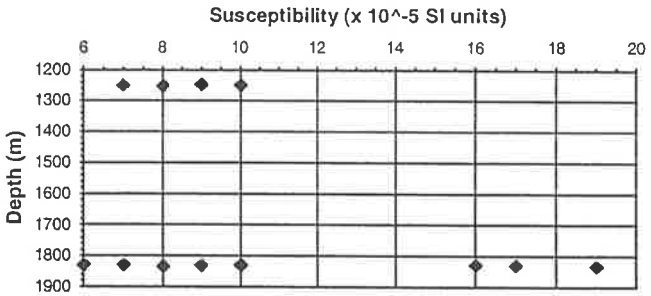

Fig. 3.3.2.4a Sherbrook Group susceptibility values from Caroline 1

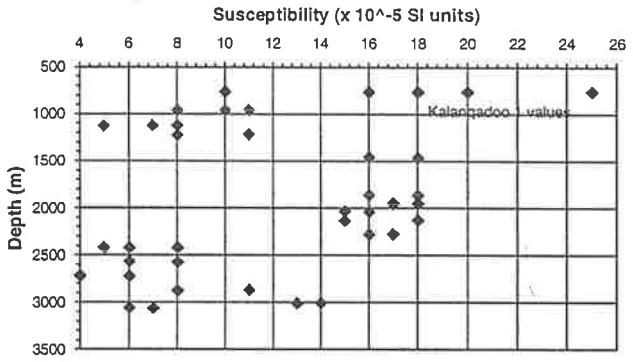

Fig. 3.3.2.4b Sherbrook Group susceptibility values from Kalangadoo 1 and Mt Salt 1

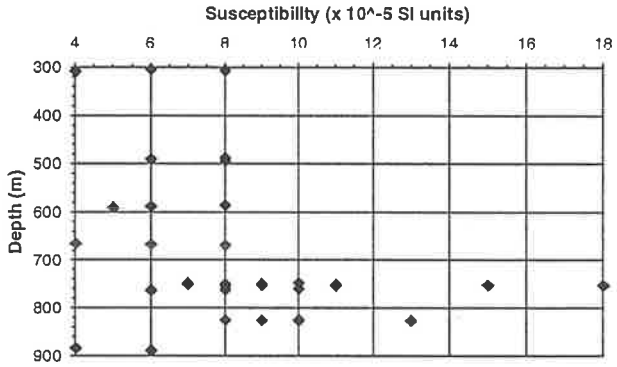

Fig. 3.3.2.5 Dilwyn Formation susceptibility values from Caroline 1 and Mt Salt 1

Formation	Well Name	Susceptibility Range $\times 10^{-5}$ SI	Magnetite Volume %
Basement	Kalangadoo 1	11 to 26	0.033 - 0.079
Pretty Hill Formation	Katnook 2	11 to 20	0.033 - 0.061
	Katnook 3	9 to 18	0.027 - 0.055
Laira Formation	Penola 1	8 to 30	0.024 - 0.091
	Kalangadoo 1	7 to 22	0.021 - 0.067
Eumeralla Formation	Katnook 2	10 to 82	0.03 - 0.248
	Kalangadoo 1	8 to 90	0.024 - 0.273
	Penola 1	8 to 45	0.024 - 0.136
	Caroline 1	8 to 45	0.024 - 0.136
Sherbrook Group undiff.	Kalangadoo 1	10 to 25	0.03 - 0.076
Timboon Sandstone	Caroline 1	7 to 10	0.021 - 0.03
	Mt Salt 1	5 to 18	0.015 - 0.055
Paaratte Formation	Caroline 1	6 to 19	0.018 - 0.058
	Mt Salt 1	4 to 17	0.012 - 0.052
Gambier Limestone	Caroline 1	1 to 6	0.003 - 0.018
Pember Mudstone	Caroline 1	7 to 18	0.021 - 0.055
Dilwyn Formation	Mt Salt1	4 to 10	0.012 - 0.03

Table 3.3.2.1 Magnetic Susceptibility ranges (measured) for specific formations and wells, with possible magnetite content as a percentage of total rock volume.

In addition to this study of magnetic susceptibility, Beaumont-Smith (1994) reports on core studies undertaken in that year which used smaller sampling intervals than previous studies (between 10 and 20 cm). He found that the sandstone units generally had susceptibilities of less than 10×10^{-5} SI units (*17×10^{-5} SI, corrected*) while the siltstone units usually had values greater than 20×10^{-5} SI (*34×10^{-5} SI, corrected*), but the very thin, occasional bands of haematite and/or jarosite discussed in section 3.2.3 (Beaumont-Smith, 1994) were found to have average susceptibility values of around 1300×10^{-5} SI units (*2200×10^{-5} SI, corrected*). For Katnook 2 (1858 to 1877 m), the measurements range from 5 to 1400×10^{-5} SI units (*8.5 to 2380×10^{-5} SI, corrected*) with the vast majority of values between 20 and 30×10^{-5} SI units (*34 to 51×10^{-5} SI, corrected*), while for Katnook 4 (1869 to 1882 m), the range is from 2 to 2000×10^{-5} SI units (*3.4 to 3400×10^{-5} SI, corrected*) with most of the values again between 20 and 30×10^{-5} SI units but with substantial numbers of lower readings, and for Katnook 1

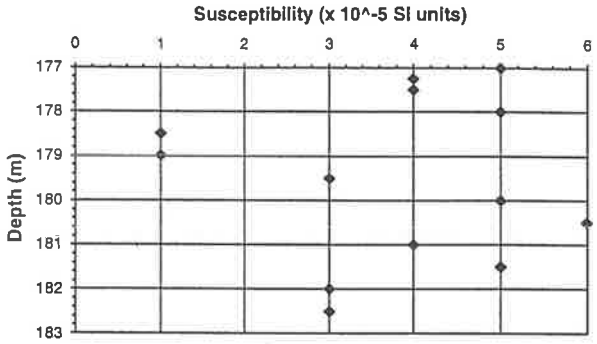

Fig. 3.3.2.6 Gambier Limestone susceptibility values from Caroline 1

(1885 to 1894 m), the range is from 2 to 46 $\times$ 10^{-5} SI units (*3.4 to 78.2 $\times$ 10^{-5} SI, corrected*) with the majority of values less than 10 $\times$ 10^{-5} SI units. The higher susceptibility values of the haematite bands have not been used in this study because they represent only a small fraction of the rock volume compared with the much more representative values from the MESA core study and the lower values of the Beaumont-Smith, (1994) study. The susceptibility of haematite is approximately 0.1% of the susceptibility of magnetite so if haematite comprises 1% of the total rock volume then the overall susceptibility of the rock would be 0.3 $\times$ 10^{-5} SI units (using the Balsley and Buddington relation). This implies that any anomaly produced by haematite concentrations at the base of the Eumeralla Formation will be substantially less than the noise envelope (see section 5.2.2).

The representative susceptibility values used in the simulation study of section 5.2 and in the modelling of intersedimentary magnetic sources in Chapter 8, were obtained by calculating the average of the measured values for each formation from the MESA and Beaumont-Smith core studies. These susceptibility values are, 0.000182 SI units for the metasediment basement, 0.000145 SI units for the Crayfish Group, 0.000201 SI units for the Eumeralla Formation, 0.000118 SI units for the Sherbrook Group, 0.000085 SI units for the Dilwyn Formation and 0.000038 SI units for the Gambier Limestone.

Chapter 4

Previous Studies

4.1 Previous Geophysical Studies

There has been much work completed in the last two decades in the Western Otway Basin. In order to set the framework for the modelling, theoretical studies, depth determination etc. in later chapters, this chapter begins with a discussion of a number of important geophysical (and some geological) papers (section 4.1) before discussing the previous aeromagnetic surveys undertaken in the basin (section 4.2). The review of the 1955 aeromagnetic survey only discusses the interpreted depths of source bodies and reproduces the contour map (section 4.2.1), while the discussion of the AGSO survey is more extensive with the conclusions from their spectral analysis and Euler Deconvolution studies reproduced (sections 4.2.2.& 4.2.3).

The exploration history of the Western Otway Basin was discussed in section 2.1.4 with particular emphasis on the exploration wells and seismic methods used. The overall tectonic history of the basin has been established reasonably well (section 2.1.3), and many researchers have contributed including Wopfner and Douglas, (1971), Cande and Mutter, (1982), Etheridge et al., (1985), Veevers (1986), Veevers and Li (1991), Veevers et al, (1991), Wilcox and Stagg, (1990), etc., with these interpretations being based on the investigation of seafloor magnetic anomalies between Australia and Antarctica, onshore geology and seismic data etc. A number of these studies have focused on the formation of the Southern Rift System that eventually led to the breakup of the two continents (Cande and Mutter, (1982), Veevers (1986), Veevers and Li (1991), Veevers et al, (1991), Wilcox and Stagg, (1990)). This section discusses the recent interpretations of the geological history of the Western Otway Basin based on seismic, magnetic, gravity and other data. Several of the published studies deal primarily with the Victorian part of the Otway Basin but are relevant because the structures in the east of the study area extend into western Victoria. In later sections of this chapter the previous aeromagnetic surveys which covered the study area are discussed and their principal conclusions reviewed. The chronological ages used in this study are based on those published by Harland et al., (1990).

The interpretation presented by Megallaa (1986) is based on previous papers, limited magnetic surveys and well data in addition to seismic mapping, and deals with the whole Otway Basin with a particular emphasis on the Victorian onshore and offshore sections. The geological synthesis presented by Megallaa (1986) accepts previous authors' assertions that the initial rift formed by a wrenching mechanism from a parallel right-lateral strike-slip fault with the deposition of volcanogenic sediments in the developing rift which was followed by basin subsidence caused by the deposition of thick Otway Supergroup sediments (refer to section 2.1.4). The seismic data existing at the time suggested that the Otway Supergroup had been uplifted and folded by the end of the early Cretaceous to form the Merino Uplift (to the east of the Penola Trough) while offshore in the Portland and Voluta Troughs the top of the Otway Supergroup (Eumeralla Formation) is down-thrown by a series of northwesterly trending faults, some of which have throws exceeding 1 km. The seismic sections revealed 'northerly tilted fault blocks with generally down-to-the-south displacement' (Megallaa, 1986) in the Otway Supergroup.

An angular unconformity in the onshore section separates the Eumeralla Formation from the overlying Sherbrook Group, however, the northwesterly trend of Otway Supergroup faults continues in the Sherbrook Group but they are restricted towards the western section of the basin. Megallaa (1986) suggests that 'the occurrence of closely separated faults with much greater throws at the top Sherbrook Group level in the western part of the basin indicates that this area was closer to the actual breakup than the eastern part of the basin'. Basin subsidence and seafloor spreading during the Tertiary resulted in the deposition of extensive marine sediments which were subjected to a period of right-lateral wrench movement in the Middle to Late Eocene which 'produced a reversal of some previously normal faults (Kanawinka Fault) and caused the upward movement of old basement and Early Cretaceous fault blocks' (Megallaa, 1986).

Pettifer et al., (1991) used regional aeromagnetic, gravity and radiometric data as well as older Landsat studies and the Megallaa (1986) seismic data compilation to outline the major structural trends of the Otway Basin. The dominant trend direction on the seismic and radiometric maps is a WNW-ESE trend parallel to the basin margin which is also significant on the gravity maps while the major trend on the published magnetic map (which only covers the Victorian section of the basin and includes Palaeozoic terrain north of the basin) is NNW-SSE. This trend is also found on the Landsat map (covering both S.A. and Vic.) but the most

common trend with this data is more NW-SE. Brown et al., (1988), in a study of aeromagnetic surveys over the Murray Basin, found that the dominant trend of the magnetic anomalies of the Kanmantoo Fold Belt beneath the Padthaway Ridge (north of the study area) is northwest-southeast, which is significant because these metasediments form the basement of the Western Otway Basin. With the exception of the seismic data, all datasets show a significant NE-SW trend, and gravity and Landsat maps also reveal a NS component.

The authors conclude that there are major east-northeast to easterly trends in the basement and basin sections which are orthogonal to the Palaeozoic structural trends that were previously identified and these were reactivated during the Mesozoic. Pettifer et al., (1991) found a linear radiometric anomaly that extends across the Merino Uplift to the Kalangadoo High which the authors speculate may be due to hydrocarbon seepage along a fault (Kalangadoo Fault System or Zone). Pettifer et al., (1991) relate the northeast-southwest structural trends to the orientation of transform faults formed in the basement during the initial rifting process while the previously mentioned east-northeast to easterly trends are related to block faulting in the Lower Cretaceous (Pettifer et al., 1991).

Hill and Durrand, (1993) constructed a number of composite seismic profiles over the Robe and Penola Troughs in the Western Otway Basin, by assembling a number of individual seismic sections that are approximately parallel to the main structural dip direction into five composite seismic profiles. These composite profiles were depth-converted and displayed as line drawings (Hill and Durrand, 1993). The westernmost profile (A) crosses the Robe Trough, Lake Eliza High, Chama Terrace and Voluta Trough offshore while profile B is subparallel to this, crossing the eastern end of the Robe Trough near the Lucindale High, the Kalangadoo High, St. Clair Trough, Beachport High and Voluta Trough. The other three profiles cross the Penola Trough on their northern ends, with profile C extending across the Kalangadoo and Hatherleigh Highs before ending offshore while profile D only crosses the Kalangadoo High before ending onshore west of Mt. Gambier. Profile E begins north of the Penola Trough over the Kanawinka Fault Zone in Victoria, passes east of Mt. Gambier before ending offshore. All profiles have gaps in the section because of permit boundaries and availability of data.

Hill and Durrand, (1993) interpret the structure of the region to be the result of a series of processes beginning with the northern onshore formation of asymmetrical half-grabens, such as the Penola and Robe Troughs, bounded on the south by northerly-dipping

extensional faults. The Early Cretaceous faults were active during the Crayfish Group depositional period and this sequence is rotated and extended (Hill and Durrand, 1993) with a significant change to southerly-dipping faults between profiles D and E which the authors suggest implies the existence of a broad accommodation zone between the profiles rather than a distinct transfer fault or thin fault zone. Hill and Durrand, (1993) note that some 2500 m of the Crayfish Group has been eroded (Kopsen and Scholefield, 1990) which they believe implies that the area underwent considerable uplift around the end of the Neocomian (circa 125 Ma). They find that the Eumeralla Formation is less faulted and subject to much less rotation than the underlying sequence, and fault rejuvenation has been minor onshore (except for the Tartwaup Fault Zone or Hingeline). Hill and Durrand, (1993) believe that the Eumeralla sequence has characteristics that imply it could have been deposited after continental breakup during a thermal subsidence phase as suggested by Stagg and Willcox, (1992), but note that because the Eumeralla sediments are largely non-marine and volcanoclastic, it is more likely that the thick sequence accumulated rapidly with the observed subsidence being caused by the sediment loading.

Hill and Durrand, (1993) found that the Late Cretaceous (Sherbrook Group) and Tertiary sequences show substantial and rapid increases in thickness in the south of the basin, particularly south of the Tartwaup Fault Zone, where the steep, planar Late Cretaceous faults dip to the south with a large degree of offset. They suggest that the faulting style, seaward thickening and margin onlap of the Sherbrook Group sequence is 'consistent with thermally-driven flexural subsidence' which they believe is 'characteristic of an early post-rift section'. Hill and Durrand, (1993) conclude that the initial stages of rift formation occurred between the Tithonian and Barremian (circa 150 Ma to 125 Ma-Crayfish Group) where rifting was controlled by northwestly-dipping faults, which was followed by a period of uplift and erosion, then by the deposition of the Eumeralla Formation (Aptian-Albian, circa 125 Ma to 97 Ma) in the late-stage rift. The subsidence of the rift was caused by the influx of large amounts of volcanoclastic material from the east which buried the Early Cretaceous sediments as well as adjacent basement highs. Continental breakup occurred at the end of the Albian followed by episodic extension (slow drift) in the period from the Cenomanian to the Maastrictian (Sherbrook Group, 97 Ma to 65 Ma). The period from the Eocene to the Quaternary has been characterised by rapid seafloor spreading and thermally-driven subsidence of the basin with the result that carbonate deposition replaced the earlier siliclastic sequences (Hill and Durrand,

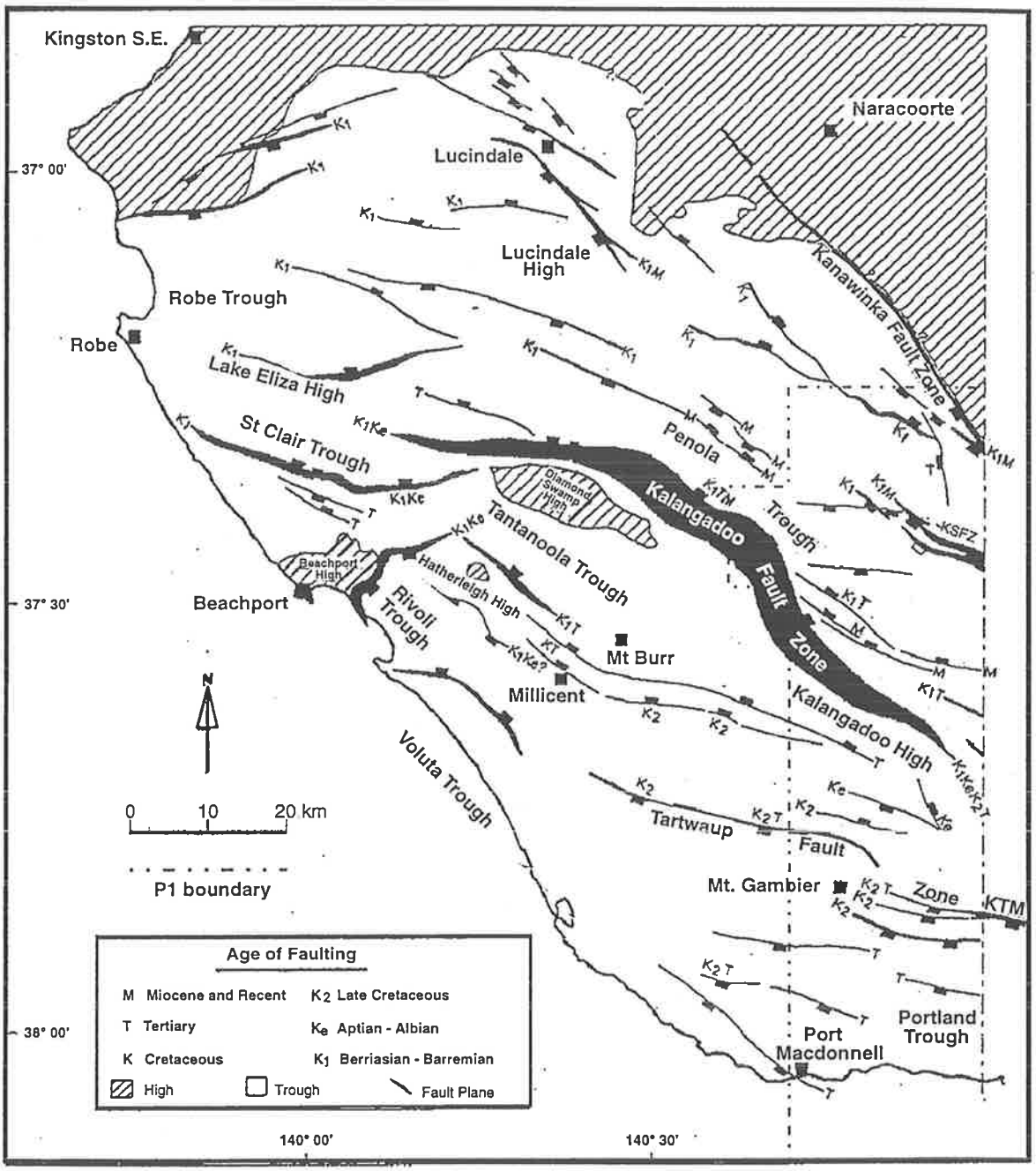

Fig. 4.1.1.1 Structural elements map of the Western Otway Basin showing age of faulting (After Cockshell, Finlayson and Perincek, 1994).

1993). The Quaternary has been characterised by uplift and basic volcanism in the Western Otway Basin.

The study published by Perincek et al., (1994) is based on company and AGSO seismic data with control from wells logs and borehole velocity surveys, and covered the Victorian part of the Western Otway Basin including the section west of the Merino High which contains part of the Penola Trough. The interpretation produced two-way time formation top and thickness images and a structural elements map showing the authors' interpretation of the age of faulting, which were both used to outline the tectonic history of the basin. The structural elements map divides the fault ages into a number of groups, starting with the Early Cretaceous which is either undifferentiated (K) or divided into Berriasian-Barremian (K_1) and Aptian-Albian (K_e). The Late Cretaceous (K_2) is another age group while post-Mesozoic faulting is divided into a Tertiary group (T) or a Miocene-Recent group (M) (fig. 4.1.1.1).

A high amplitude seismic reflector overlying basement has been interpreted as Casterton Formation and Perincek et al., (1994) suggest that there has been minor syndepositional faulting of this basal unit based on the evidence of borehole data. They consider that with the onset of rift formation, the deposition of the Crayfish Group in the Western Otway Basin half-grabens was controlled by the major synrift faulting (K_1), and the northern extent of Crayfish Group deposition was controlled by the southwest-dipping Kanawinka South Fault Zone and Kanawinka Fault with minor faulting occurring at the northeast-dipping Penola South Fault Zone (Perincek et al., 1994). The Kanawinka Fault and the Penola South Fault Zone are called the Kanawinka Fault Zone and the Kalangadoo Fault Zone or System respectively elsewhere in this study. Most of the Crayfish Group faults (K_1) are believed to have been sealed by the deposition of the Eumeralla Formation. Perincek et al., (1994) consider that faulting related to rifting ceased before the Aptian and the Aptian-Albian age faulting (K_e) was syn-depositional with the Eumeralla Formation but the Tartwaup Fault (K) probably continued to be active after the rifting phase. Of the three authors, Perincek favours the interpretation that rifting ceased before the Aptian and breakup occurred with the generation of oceanic crust in the offshore part of the Otway Basin which means that there was a marine incursion during Eumeralla Fm. deposition. The other two interpretations are that rifting stopped onshore but continued during Eumeralla Fm. deposition or that the Eumeralla Fm. was deposited during a post-rift, pre-breakup sag phase.

Perincek et al., (1994) believe that the period from the Late Cretaceous (K_2) to Early Eocene (T) was characterised by major activity on the Tartwaup Fault and reactivation of the faults on the northern margin of the basin which formed shallow grabens in the Penola Trough that were filled by Sherbrook Group and Early Tertiary sediments. The Miocene-Recent (M) period was characterised by a new episode of normal faulting as well as the reactivation of the major bounding fault zones. Perincek et al., (1994) consider that right lateral strike-slip movement occurred at this time, with inversion of the Tartwaup Fault and faults in the Penola Trough occurring post-Oligocene. They believe that the observed strike-slip movement and inversion of faults is related to the predominant northwest-southeast direction of maximum compressive stress which is considered to be caused by the collision of the northern and eastern edges of the Australian plate during this period (Veevers et al., 1991). Perincek et al., (1994) found no evidence in their study area to support the Willcox and Stagg, (1990) hypothesis of a major southeast-northwest extension during the Casterton Formation-Crayfish Group depositional period and believe if this extension occurred, it was prior to the deposition of the Casterton Formation.

An interpretation of seismic, gravity (including Geosat) and aeromagnetic data (Finlayson et al., 1994a) from the Western Otway Basin was used to increase understanding of the regional tectonics of the basin. The seismic data consisted of four of the lines of deep seismic profiling undertaken by AGSO in 1992 as well as mapping of onshore seismic horizons by MESA. The gravity data consisted of the onshore Bouguer gravity data for southeastern Australia which was combined with the U.S. Navy Geosat Geodetic Mission altimetry data by merging the two datasets along the coastline. The authors of this paper refer to several other papers which describe the correlation between altimetry and seafloor geology. The aeromagnetic data was from the AGSO 1:250,000 Penola Sheet Survey, which will be discussed in more detail later in this chapter, and digitised data from the Bass Strait-Encounter Bay (1960-1961) survey which partly overlaps the later AGSO data as well as extending further to the west.

Finlayson et al., (1994a) have used the gravity data to postulate the existence of an Otway-Sorrel microplate which they describe as a triangular region of extended continental crust and lithosphere bounded by the northern margin of the Otway Basin onshore, the eastern edge of the Sorrel Basin offshore to the west of Tasmania, and a prominent lineament on the Geosat map which extends from the Crayfish Platform offshore in S.A. to southern Tasmania.

The microplate's eastern margin passes to the west of King Island and the Otway Ranges, and so does not include the Torquay Sub-basin, the Colac Trough and Gellibrand Trough which most researchers consider part of the Otway Basin. They also discuss the major north-south fracture zones to the south of the microplate and demonstrate that their data shows only two of the postulated systems (the Spencer and Tasman Fracture Systems).

Finlayson et al., (1994a) refer to two of the deep seismic profiles which are oriented approximately north-south across the onshore part of the Western Otway Basin with both seismic lines detecting reflections at up to 16 seconds two-way time (TWT). Line 6 is west of Mt. Gambier, starting to the north of the Tartwaup Fault Zone and ending on the coastline, while line 5 is along the S.A./Vic. border, and starts on the Padthaway Ridge north of the basin and also ends at the coastline. The longer line, line 5, crossed the Kanawinka and Kanawinka South Fault Zones, the Penola Trough, the Kalangadoo Fault System (the Penola South FZ) and the Tartwaup Fault Zone, and they suggest that there is a significant difference between lower crustal reflections beneath the Palaeozoic basement highs which are common while those areas believed to have undergone substantial extension like the Penola Trough or south of the Tartwaup Fault Zone, have lower crustal reflections that are weak or absent. The authors detected reflections interpreted to be from the Moho at around 11 s TWT beneath the Palaeozoic crustal blocks but shallowing substantially on the ocean side of the Tartwaup Fault Zone (around 9 s TWT) which they interpret as implying that the Tartwaup Fault Zone is 'the cratonic boundary for a lower-plate margin during the episode of lithospheric extension which eventually resulted in separation from Antarctica'.

Also published in 1994 was a study of all the 1992 AGSO deep seismic profiles in the Otway Basin which consisted of seven lines over features from the Colac Trough/Otway Ranges in the east to the area west of Mt. Gambier in the west. Finlayson et al., (1994b) interpret the deep seismic data from the whole Otway Basin as showing that the rifting process produced a series of half-grabens separated by basement highs thought to be accommodation zones with complex faulting. They found that the half-graben bounding faults dip predominantly towards the continent soling 'along detachments with ramp and flat geometry at mid-crustal levels'. Finlayson et al., (1994b) interpret reflections on the northern margin of the Penola Trough as implying that the south-dipping Kanawinka and Kanawinka South Fault Zones, which sole at about 7 seconds TWT, are fundamental features controlling early deposition while the Penola South (Kalangadoo Fault System) and Tartwaup Fault

Zones are important structures associated with the later history of the basin. The thickness of the crust in the Port Campbell Embayment, west of the Otway Ranges, was interpreted to be 31 km. (about 10.5 seconds TWT), which is based on the geological control derived from crustal and upper mantle xenoliths brought up to the surface by volcanism. The depth to the Moho south of the Tartwaup Fault Zone is around 9 seconds TWT which corresponds to approximately 25 km.

The results from apatite fission track and vitrinite reflectance analysis (Hill et al., 1994) on samples from wells were used to establish a thermochronology of the Western Otway Basin. The samples were taken from the Robertson 1 well which is close to the northern margin of the basin, Penola 1 in the northern part of the P1 area, Beachport 1 and Geltwood Beach 1 on and adjacent to the Beachport High, Kalangadoo 1 on the Kalangadoo High, and Mt. Salt 1 which is south of the Tartwaup Fault Zone. Hill et al., (1994) conclude from their studies that episodes of Jurassic volcanism occurred in the Western Otway Basin area prior to rifting (Jurassic age trachyte at the base of Robertson 1) but the dominant source of Early Cretaceous sediments was eroded Palaeozoic basement rocks until around 112 Ma when Eumeralla Formation volcanogenic sediments were deposited. Apatite fission track data from Penola 1 suggests a decline in heat flow during the Tertiary and little erosion while data from Robertson 1 implies the sediments have undergone uplift and approximately 1 km. of erosion which the authors believe was in the mid-Cretaceous (Hill et al., 1994).

The fission track results from the wells around the Beachport High suggest that the current temperatures of the sediments (~105°C) are the maximum since they were deposited, while the results from Kalangadoo 1 indicate elevated heat flow during the Early Cretaceous, followed by cooling in the mid-Cretaceous. Hill et al., (1994) found that the basement samples had undergone greater cooling in the Tertiary than the overlying sediments which they suggest follows local heating due to volcanism. Fission track results from Late Cretaceous and Tertiary samples from Mt. Salt 1 imply that the current temperatures (~80°C) are the maximum reached which, they report, conflicts with previous vitrinite reflectance analysis that suggested raised palaeotemperatures (~120°C) and erosion in the range of 2 to 3 km (Hill et al., 1994).

The review and continuing research summary published by Hill et al., (1995) discussed the results of preliminary dip analysis, regional restored and balanced cross-sections,

and apatite fission track and vitrinite reflectance analyses. They report that the dip analysis suggests that the extension direction during the early stages of rifting (Crayfish Group deposition) in the eastern Otway Basin was NNE-SSW (azimuth 193°) but during the Aptian-Albian (Eumeralla Fm. deposition) it was inferred to be NNW-SSE while the extension direction west of the Otway Ranges during this period was inferred to be NNE-SSW. Hill et al., (1995) constructed two balanced and restored cross-sections, in the eastern Otway Basin across the Torquay Sub-Basin and across the Penola Trough, St. Clair Trough and Beachport High in the west. The western cross-section shows progressively shallower detachments to the NNE end of the section which the authors interpret as linking with a SSE-dipping regional detachment horizon. Hill et al., (1995) suggest the section implies that upper plate-lower plate asymmetry could form early in the extension process. An estimate of 10 km. of extension over the section was made for the Crayfish Group depositional period but there was minimal extension during the Aptian-Albian. Apatite fission track and vitrinite reflectance analysis demonstrated regional mid-Cretaceous (post-Albian) uplift and denudation of basement in the eastern basin which is in contrast with the renewed rifting of the Otway-Sorell microplate in the west.

Perincek and Cockshell, (1995) consider the initial extension direction to be NS to NE-SW with local faulting, tilting and erosion in the northwest of the basin before the deposition of the Eumeralla Formation which the authors believe possibly relates to a change in the direction of extension from north-south to NE-SW. Perincek and Cockshell, (1995) compared surface fault lineaments with Late Tertiary volcanic eruption centres and seismic data, and concluded that the Pliocene-Recent volcanic activity in the basin occurred along zones of crustal weakness caused by reactivation of post-Oligocene faults. The paper on the 'Western Otway Crayfish Group Troughs' published by Cockshell et al., (1995) proposed a standard nomenclature for the major structural components of the Western Otway Basin, which is largely the nomenclature used in this study, as well as reporting the results of true dip analysis of Crayfish Group seismic data and sandbox modelling experiments. Cockshell et al., (1995) hoped to reconcile the, sometimes conflicting, tectonic histories presented by different researchers especially the initial extension direction of the rift. The true dip analysis results have been found to yield a consistent azimuth for the extensional direction in the East African Rift but the results from the Western Otway Basin suggest that the tectonic overprint of

Aptian and later events has reduced the usefulness of the method. The results are dominated by those from the Penola Trough which indicate a strong NE-SW dip trend with a secondary NW-SE trend. Cockshell et al., (1995) removed most of the Penola Trough measurements in an attempt to reduce the influence of this feature on the analysis with the result that the NW-SE trend increases in importance. They believe that the true dips of the fault blocks only reflect the tectonics of the structural province they are located in and not necessarily those of the whole basin.

The sandbox modelling experiments used three different directions of extension, NNW, NS and NNE, to investigate the range of directions inferred by most workers (Cockshell et al., 1995). The apparatus used for these experiments consisted of a basal sheet of rubber with a silicone putty layer, a playdough slab (basement) and layers of different coloured sand which represent the initial sediments, with extra sand added during the extensional process to depict sedimentation during rifting. Cuts were made in the playdough layer to represent the faulted northern margin of the Robe Trough, the southwestern margin of the Penola Trough and an approximately north-south vertical basement feature between the two troughs which was inferred from the analysis of the AGSO aeromagnetic data (O'Brien, 1994). The NNW extension direction produced a feature analogous to the Robe Trough but failed to generate any analogue to the Penola Trough which is evidence that this proposed extension direction is less likely than the others. When a north-south extensional regime was applied, the Robe Trough analogue was the first to form, and was bounded by parallel to sub-parallel planar normal faults, while the Penola Trough analogue formed later featuring en échelon bounding faults but is narrower than the actual feature. Cockshell et al., (1995) found that an en échelon step was formed that was similar to the possible NE-trending accommodation zone cutting across the Penola Trough between Penola/Sawpit and the Katnook gas field. The NNE extension direction produced two narrow troughs over the basement feature early in the 'rifting' process while the Penola Trough analogue formed subsequently with only a very shallow feature representing the Robe Trough.

At a later stage the features began to join together with the Penola Trough analogue being a wide extensional graben, the narrow NNW-trending troughs becoming relatively deep but the Robe Trough analogue is narrow and shallow. The authors point out that if the basement feature did not extend past the Robe Trough analogue then only the southern

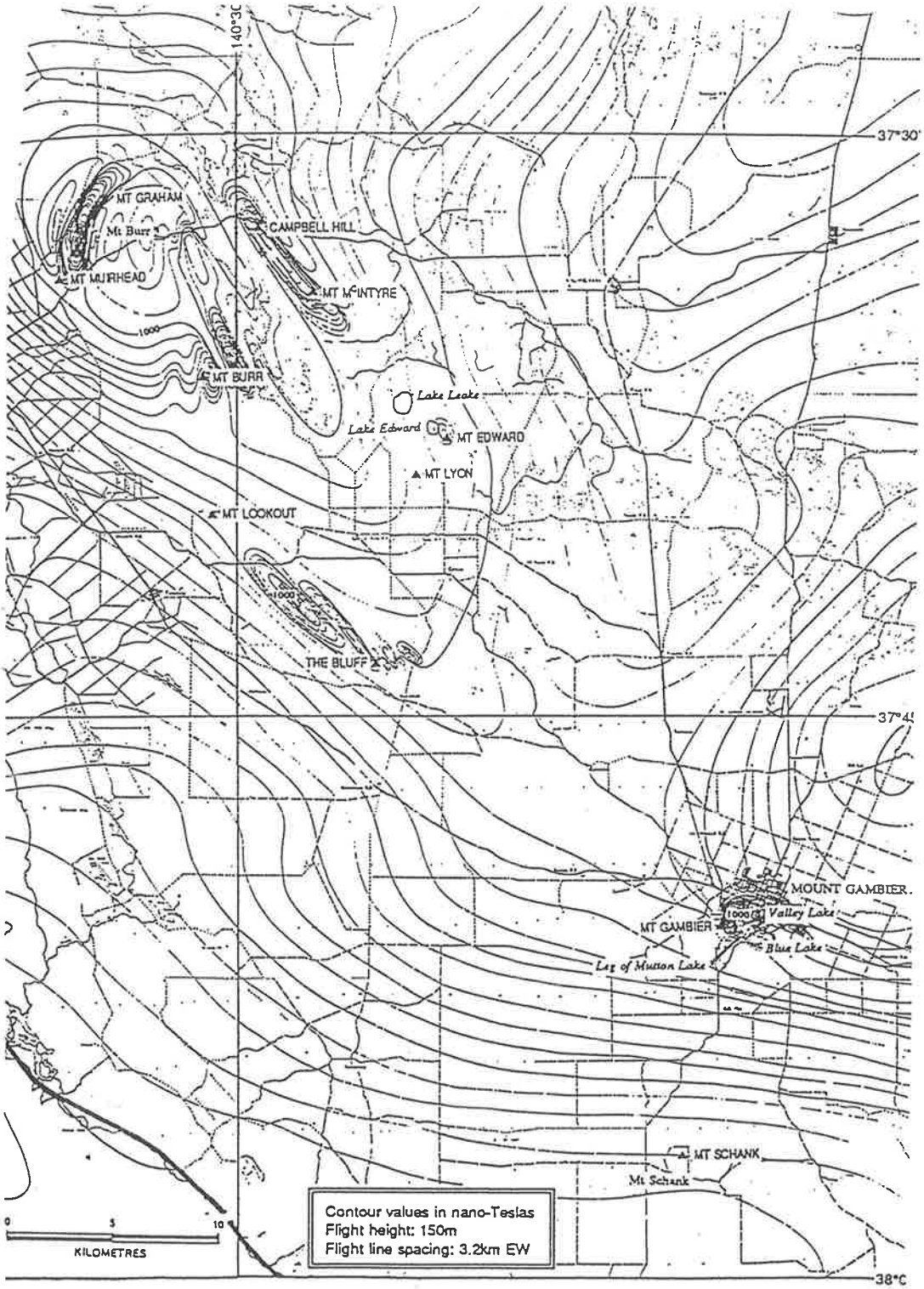

Fig. 4.2.1.1 Aeromagnetic Map of Total Intensity

Section of Penola Sheet 89-277, SADME 92-1323, after Chatfield, (1992)

Adastra Hunting Geophysics for MESA, flown 1955, published 1989

NNW-trending trough would form and the feature would have some resemblance to the Tantanoola Trough. The basement fabric was found to be of particular importance in determining the features generated by the extensional process. However, Cockshell et al., (1995) conclude that the NS extensional model produces results that more closely resemble the geometry of the actual basin with the deepest trough (with the thickest Crayfish Group sediments) being the Robe Trough analogue, with the Robe Trough analogue being wider than the Penola Trough analogue, and the southwestern bounding fault having an en échelon geometry.

4.2 Previous Aeromagnetic Studies in the Western Otway Basin

Prior to the 1993 MESA survey, two surveys had been flown over the Penola 1:250,000 sheet. The first was flown in 1955 by Adastra Hunting Geophysics Ltd and the second by the Australian Geological Survey Organisation (AGSO) in 1992. The 1955 survey was, by current standards, of low accuracy and data quality with a flight line spacing of 3.2 km (east-west) and a flight height of 150m. It is not known what the sample interval for this survey was but, given the level of technology available, it is likely to be much greater than the six to seven metre intervals in both the MESA and AGSO surveys. This section begins with a review of the 1955 and AGSO surveys with a summary of the conclusions in the AGSO report on the survey, as well as, a later paper published in the APEA Journal (O'Brien et al., (1994)). MESA supplied the author with a tape of the AGSO survey data which was used to prepare images and contour maps, and to investigate features that are only partly covered by the MESA survey (Chapter 5 and chapter 7).

4.2.1 The 1955 Adastra Hunting Geophysics/C.G.G. Survey and Interpretation

The 1955 aeromagnetic data was reinterpreted in 1965 by Compagnie Generale de Geophysique (C.G.G., 1965). Mathematical modelling of anomalies and depth estimation allowed the construction of maps with depth contours of magnetic basement and probable intersedimentary horizons (Fig. 4.2.1.1). In the P1 area, aside from the surface volcanics, the authors placed a large body extending to the northeast of Mt. Gambier, at a depth of between 4.8 and 5.5 km (16000 and 18000 ft), as well as, a smaller east-west trending elliptical body

between Mt. Gambier and Tarpeena. This body was interpreted to be between 3.7 and 4.0 km deep (12000 and 13000 ft). The previous two bodies were interpreted to be at or near magnetic basement while three other circular/elliptical anomalies, at a similar depth to the previous elliptical body, were thought to be intersedimentary or 'intermediate' horizons approximately 1000 m thick within the Penola Trough. In the vicinity of Mt. Gambier, C.G.G. (1965) interpreted a sharp anomaly as being caused by the intrusion of magnetic material into the sedimentary section at depths of between 15 to 460 m below the surface.

4.2.2 Summary of the AGSO 'Western Otway Basin 1992 Aeromagnetic Dataset: ' (Record 1993/14)

In November and December 1992 the Australian Geological Survey Organisation (AGSO) conducted an aeromagnetic survey over the western Otway Basin in South Australia. The survey covered the Penola 1:250 000 Sheet and adjacent areas, extending between 37^0S, 139^0 10'E and 141^0E in the north to the 500 m isobath offshore in the south (Reeves et al., (1993)). This survey was flown with a flight line spacing of 1.5 km (north/south direction), tie line spacing of 13 km (east/west direction) and a mean terrain clearance of 80 m with a sampling interval of 0.1 seconds (approx. 7 m), a resolution of 0.01 nT and a noise envelope of approximately 0.1 nT (Brodie, 1993). There were 22 flight lines and 9 tie lines from this survey in the P1 area that has been subsequently covered by the MESA survey.

The interpretation of the results of this survey can be found in the record by Reeves et al., (1993) which incorporates gravity data for the survey area from the AGSO national gravity database as well as Geosat satellite gravity data. The aim of the AGSO survey was to use the aeromagnetic data to provide new insights into the structural architecture, rifting history and petroleum potential of this part of the western Otway Basin (O'Brien et al., (1994)). Reeves et al., (1993) concluded that there have been three distinct structural trends developed during the history of the basin, a north/south trend reflecting basement geology, a northeast-to-east northeast trend originating from the earliest phase of extensional faulting and a northwest-to-west northwest trend defining the 'break-up' normal fault direction. The authors identify three or possibly four northwest-trending volcanic (highly magnetic) provinces which they believe may define the position of major basement or rift-related fault sets. Volcanic rocks may have had a significant effect on the thermal history of the basin and potentially contaminated with carbon dioxide those reservoirs which are adjacent to the

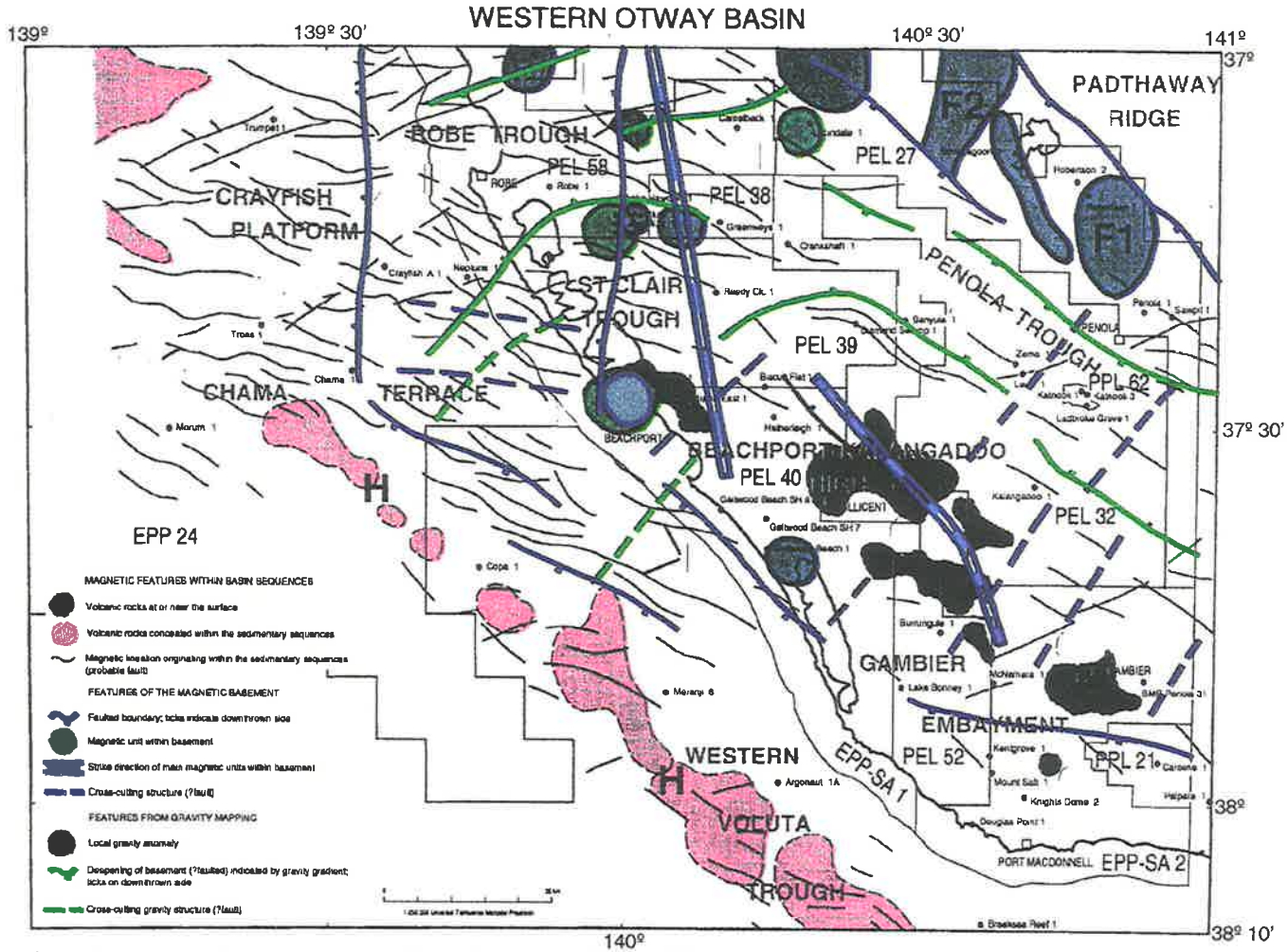

Fig. 4.2.2.1 Structural synthesis map of the Western Otway Basin using the 1992 regional aeromagnetic survey data plus gravity data from AGSO database. After Reeves et al., (1993), AGSO Record 1993/14

volcanic units. Reeves et al., (1993) found 'no obvious spatial or causal relationship between the major/minor basin-forming structures or lineaments defined during the present study and the location of the known hydrocarbon discoveries in the western Otway Basin'. However, they point out that the Katnook and Ladbroke Grove gas fields are bracketed by northeast-trending lineaments which they interpret as either basement faults or Early Cretaceous accommodation zones (fig. 4.2.2.1).

The authors of the AGSO record discuss a number of anomalies revealed in the gravity data. The significant anomalies for the purpose of this study are the Penola Trough and a circular-elliptical anomaly in the vicinity of the Padthaway Ridge. The Penola Trough was found to produce a negative anomaly of approximately 250 μms^{-2} (25 mgal) which they interpret as being caused by an extra 3 km of sediment within the trough, given a density contrast of -0.25 t/m^3. The trough is not delineated by sharp gravity gradients which is attributed by Reeves et al., (1993) to the probability that the denser basement rocks on the flanks of the trough are buried under several kilometres of sediment. In the northeastern corner of the survey area, the authors interpret a local oval-shaped gravity low as a likely granite pluton (F1 on fig. 4.2.2.1). This anomaly is southwest of the Kanawinka Fault Zone and north of the town of Penola in the region O'Brien et al., (1994) refer to as the Northern Penola Terrace.

The Reeves et al., (1993) study found that the magnetic anomalies of their survey area could be divided into several groups (fig. 4.2.2.1). The first group consists of local anomalies associated with cultural features at ground level. The second group consists of high-amplitude, short-wavelength anomalies resulting from the geologically recent volcanic extrusions around Mt Gambier and Mt Schank. The third group are low amplitude anomalies interpreted as intra-sedimentary sources following possible fault lines where a magnetic horizon has been offset by normal faulting. These anomalies generally strike along the same orientation as faulting in this area. The authors report that magnetic forward modelling of a horizon about 50 m thick, 500 m deep and with a susceptibility of 0.063 S.I., when offset 100 m by faulting, could produce anomalies of 5 nT amplitude. This is approximately the amplitude of those anomalies assigned to this group. The fourth group consists of large amplitude, long wavelength anomalies attributed to igneous and metamorphic rocks underlying the sedimentary section. There are several features of this nature in the study area

including those associated with the shallow basement of the Padthaway Ridge, the Mt. Gambier magma chamber, the Kalangadoo High and a series of northeast-trending structures considered to be basement faults. The authors believe a fifth group of anomalies trending NW/SE along the southwestern margin of the survey area (offshore) are associated with intersedimentary volcanic accumulations 200 to 800 m below sea level.

The Reeves et al., (1993) report discusses the results of spectral analysis of the data which was carried out on a 400 × 400 m grid that was generated from line data over the survey area. The radially-averaged power spectrum for the magnetic anomaly field of the grid was calculated (Spector and Grant, 1970), and by fitting straight-line segments to the log power spectrum vs. wavenumber plot (refer to section 5.1.1), the depth to an ensemble of sources can be found. Spectral analysis carried out on the northeast, onshore section of the Penola sheet gave estimates of populations of sources that exist at depths of 9.1, 3.2, 1.1 and 0.4 km.

Various anomalies were modelled by the AGSO staff in order to determine the depth to basement and depth to intra-sedimentary sources. The authors found that the magnetic basement in the Penola sheet was generally between 3.5 and 4.5 km deep but is only a few hundred metres deep on the Padthaway Ridge in the northeast while it plunges to approximately 10 km below sea level offshore. They found that the Penola Trough contains an extra 3 km of sediment resulting in a total depth to basement of up to 7.5 km while the region north of the Kanawinka South Fault Zone and south of the Padthaway Ridge deepens from the northwest to the southeast. Reeves et al., (1993) mention the likelihood of emplacement of intrusives within the sedimentary sequence but do not interpret any anomalies in the P1 area as such. The intra-sedimentary magnetic markers have a low amplitude, as mentioned above, but when modelled as steps, finite-thickness ribbons or tabular bodies have depths in the range of 300 m to 1000 m. The authors present the results of modelling selected anomalies by superimposing the anomaly on a seismic line interpretation with the depth estimate shown. It was found that while some depth estimates were substantially under (below the Tartwaup Fault Zone) or overestimated (offshore), others were more reasonable.

4.2.3 APEA Journal article (O'Brien et al., 1994)

In the article the results of detailed depth-to-basement estimates through Euler Deconvolution are discussed. This paper reports that most of the depths are considered reliable but when they differ from independently-derived estimates it is because they are too shallow due to the presence of shallowly buried volcanics. The authors report that they used Euler Deconvolution software which is part of the GIPSI™ package, finding the position, depth and nature of sources present in the gridded data. These solutions tend to cluster in certain areas with adjacent areas lacking any solutions, with the result that the authors warn that interpolation of data from the clustered solutions to neighbouring regions may be misleading. The O'Brien et al., (1994) article presents the Euler deconvolution data as a depth-to-magnetic basement pseudo-colour image, as a series of dip and strike profiles and as a table of maximum depths for each tectonic subunit along the profiles. The dip and strike profiles are oriented approximately northeast/southwest (7 profiles) and northwest/southeast (2 profiles). In discussing the accuracy of the depth estimates, a comparison is made between the depth-converted seismic profile of Hill and Durrand, (1993) (Fig. 6, profile C) and Line 95 in the article, where the maximum seismically-derived depth for the Penola Trough is 6 km. while the maximum Euler depths are between 6 and 6.5 km. From table (2) in the O'Brien et al., (1994) article it is shown that the maximum depth-to-basement on the Padthaway Ridge is in the range 0.5-0.8 km. in the east to 0.0-0.5 km. in the west. Similarly, the depth estimates for the Penola Trough range from 3.8-4.5 km. in the east to 6.0-7.2 km. in the west. The Kalangadoo High ranges from 0.4 to 2.0 km. while the region south of Mt. Gambier ranges from 5.0 to 6.8 km. and the area between the Penola Trough and the Padthaway Ridge ranges from 1.5 to 3.5 km. deep. The results from spectral analysis and Euler Deconvolution undertaken by AGSO staff that are reported in this chapter, are compared with the spectral analysis results obtained by the author of this study in section 6.1 and with the Euler Deconvolution solutions obtained by Cowan Geodata Services in section 6.2.

Chapter 5

Processing and Interpretation Methods, and Simulation Studies

5.1 Processing and Interpretation Methods

5.1.1 Introduction

The first part of this chapter discusses the processing and interpretation methods used on the MESA aeromagnetic data. The second part discusses a simulation study where a series of models based on seismic horizon mapping are used to calculate theoretical profiles for comparison with real data, and to determine the likely magnetic response of various structures delineated from seismic mapping.

The first section deals with the extraction of the data in its original form from the supplied tape and its use in various software. There is a discussion of the production of images and contour maps of anomalies, and methods used to delineate source bodies and separate magnetic sources that are close together or at different depths. There is also a brief discussion of the limitations of the modelling software.

The simulation study part explains how the models were constructed, how a representative susceptibility value was derived for each of the formations modelled, which major faults were included in the models and how it was necessary to add basement intrusions of substantially higher susceptibility to match the theoretical profiles to the observed data.

5.1.2 Supplied Data and Software

MESA supplied the author with an tape containing the final located data after microleveling had been carried out. This data was in ASCII format and includes flightline numbers, direction, dates, fiducial numbers, time, radar altitude, barometric height, raw compensated and uncompensated values, final TMI, easting, northing, latitude and longitude. The author modified in-house programs to extract the flightline number, easting, northing, final TMI and altitude data for use in proprietary software, in-house

programs written by university staff as well as former and current students, and programs written by the author.

In the initial stages of the project a tape of located data from the AGSO 1992 regional survey was supplied to the author and these data were used to create images and contour maps of the more important anomalies in and around the study area as well as produce profiles for modelling. The profile data that was extracted coincides with the P1 area allowing comparison between the two datasets, as well as including six lines (at 1500 m spacing) on the eastern side of the MESA survey and complete lines where the MESA data has only the western extension of the P1 area.

In the first year of the project the POTENT™ (version 2.12) program by PC Potentials was used to generate models of geological structures. Software was written by the author to convert the original line data into the formats required by POTENT™, ERMapper™ or other imaging and contour generating software. Much of the initial part of the simulation study to be discussed later in this chapter was undertaken using POTENT and a number of complex models were generated. As POTENT is primarily a modelling package and this version is only able to remove linear and planar regional components from observed data, it was necessary to use various in-house programs to process data. Software written by Dr. J. Paine was used to create gridded data from flightline data and to generate contour maps. Amongst the in-house programs available are a number written by Dr. Z. Shi, including one that calculates horizontal and vertical gradients, second derivatives, upward and downward continuation, and horizontal and vertical components of potential field data that is input in gridded form. There is also a program written by Dr. S. Rajagopalan which produces pseudocolour and greyscale images in Postscript™ format. A number of the colour images used in this thesis were produced using this software.

At the beginning of the second year of the project the department acquired a copy of MODELVISION™ (version 1.2 and later upgraded to version 1.3) by Encom Technology which is a forward modelling and data processing package. The MODELVISION™ package includes various convolution and Fourier domain filters for the processing of line (high, low and band pass filters, first and second horizontal and vertical derivatives, upward and downward continuation, averaging and median filters

etc.) and gridded data (sun angle filters, etc.), as well as, algorithms for computing regional surfaces with a polynomial.

The package includes a gridding subroutine as well as a 'compute' function permitting mathematical operations to be carried out on line data or grids such as adding or subtracting a constant, or another data channel. An example of this is calculating a regional component or using a low pass filter and then subtracting the result from the original line or gridded data. While the MODELVISION™ package can directly import data in a number of common line and grid formats, it was necessary to create programs to convert POTENT™ files containing records of models generated using that software into model files that MODELVISION™ can read. The model profiles in section 5.2 of this chapter and Chapter 8 were generated using MODELVISION™ as were the colour contour maps in Chapter 7 and elsewhere.

The author also wrote a program for plotting greyscale or coloured symbols on maps and this was used on diagrams in section 6.2, chapter 8 and appendix A.1.

5.1.3 Source Delineation Techniques

This section discusses various techniques which can be used to define the outline of bodies, and the position of faults and contacts. The upward and downward continuation processes produce data that correspond to that measured at the continuation height above the source, that is, as if it were measured at that altitude, and can be derived from line and gridded data (Peters, 1949, Bhattacharyya, 1965). Upward continuation can be used to suppress noise or the influence of shallow magnetic sources because low amplitude sources are attenuated by increasing the height of the sensor (Williams, 1988). Downward continuation can be used to enhance the signal from shallow sources because the process reduces the effective height of the sensor but care must be taken not to reduce the height below that of the magnetic sources.

The geomagnetic inclination angle for the study area is -69.54° which means that isolated TMI anomalies are bi-polar in shape with positive peaks and negative troughs, and the positive maximum is offset to the north of the centre of the source body. The common method of removing this offset and so simplifying the interpretation procedure, is to apply a Reduction-to Pole (RTP) algorithm to the data which transforms the anomaly to one due to a source body with vertical magnetisation (at the geomagnetic

pole) but the direction of magnetisation either must be known or induced magnetisation only must be assumed. This process is complicated by the presence of remanent magnetisation which causes the transformed anomaly to be severely distorted and is a problem especially where the direction of magnetisation is close to that of the magnetic equator, at which the anomaly disappears. There are various methods sometimes used to correct this problem (e.g. Hansen and Pawlowski, 1989; Mendonca and Silva, 1993; Silva, 1986; Grant and Dodds, 1972, McLeod et al., 1993). It is usually not possible to determine if there is a remanence component present without measurements on rock samples which was not done on the core and outcrop samples from this area (susceptibility values on core and outcrop were measured by MESA staff and Chatfield, (1992) respectively). For this reason Reduction-to Pole was not applied to the data in this study.

High, low and band-pass filters remove undesired components from the frequency spectrum of the data, with the cut-off frequency (or frequencies in the case of band pass filters) defining the point above (low pass) or below (high pass) which the frequency components are attenuated. Low pass filters are used to attenuate high frequency/short wavelength features which result from shallow sources and geological or non-geological noise while high pass filters attenuate the low frequency/long wavelength features associated with deep sources such as intra-basement intrusions. Band pass filters can be used to emphasise a band of frequencies (or wavelengths) between the two cut-off frequencies while attenuating those outside this range. These filters have been used by AGSO staff in their interpretation of the study area to create a kind of 'depth slice' where those frequencies thought to result from sources within a certain depth range are emphasised and those outside removed (Reeves et al., 1993).

First horizontal and vertical derivatives represent the gradient of the magnetic field with respect to x or y (horizontal, $\partial T/\partial x$ or $\partial T/\partial y$) and z (vertical, $\partial T/\partial z$) respectively while the second derivatives represent the change in gradient with respect to the horizontal or vertical parameters ($\partial^2 T/\partial x^2$, $\partial^2 T/\partial y^2$ or $\partial^2 T/\partial z^2$). The first horizontal and vertical derivatives are used because they usually remove the regional component of the TMI data and emphasise the effects of shallow sources over those that are deeper. Narrow dyke-like bodies have maxima of the vertical gradient of RTP anomaly over their centre while bodies such as horizontal plates have their gradient maximum close to

the northern edge (in the southern hemisphere) and a vertical gradient minimum near the southern edge of the body. First vertical derivatives are preferred to the horizontal derivatives because they do not have the directional bias seen in their horizontal equivalents. This directional bias results in features that strike perpendicular to the direction that the derivative is calculated (or sometimes measured) are emphasised, while those at a low angle to this strike direction are attenuated.

The edges of magnetic bodies can be located by determining the maxima of the horizontal gradient of the pseudogravity anomaly which is nearly directly over the top edge of a shallow, near-vertical, fault-like boundary (Grauch and Cordell, 1987; Blakely and Simpson, 1986). The pseudogravity transform is a Fourier domain linear filter which converts the anomaly over a magnetisation distribution $\mathbf{m(x, y, z)}$ into the gravity anomaly measured if density $\mathbf{\rho(x, y, z) = km(x, y, z)}$ where $\mathbf{k}$ is a constant (Blakely and Simpson, 1986). The horizontal gradient maxima can be offset because the boundaries are not vertical, where there are several closely spaced boundaries or where there are gradational boundaries (Grauch and Cordell, 1987).

Second derivatives can be used occasionally to locate the contact between a magnetic source and the country rocks, because the point of zero curvature on the flank of an anomaly approximately defines the edge of a magnetic body. McIntyre, (1981) suggests the use of stacked profiles of the second horizontal derivative (1D) because they preserve more detail than the interpolated values of gridded data and remove the large deviations from the baseline caused by regional gradients in TMI profiles. McIntyre, (1981) prefers second horizontal derivatives to 2nd vertical derivatives because the former can be calculated using simple operators on the profile data rather than using convolution or FFT filters to obtain the latter. The principal problem with the interpretation of all derivatives is that they act in a manner analogous to high pass filters with a subsequent enhancement of geological and non-geological noise which is a considerable problem in this area.

The analytic signal method (Nabighian, 1972, 1974; Nelson, 1988; Roest et al., 1992; McLeod et al., 1993; Qin, 1994) combines the horizontal and vertical derivatives either in 2D (profile) or 3D (grid) form. The absolute value of the 3D Analytic Signal is shown here,

$$|\mathbf{A(x, y, z)}| = ((\partial T/\partial x)^2 + (\partial T/\partial y)^2 + (\partial T/\partial z)^2)^{1/2}$$

Roest et al., (1992) have shown that the shape of the profile of the absolute value of the analytic signal over 2D source bodies is independent of the direction of source body magnetisation and the direction of the Earth's magnetic field. Qin (1994) demonstrates that the response of the absolute value of the 3D analytic signal always produces symmetric anomalies with maxima located over the centres of narrow dyke-like sources.

McLeod et al., (1993) show that a wide prism has analytic signal maxima over the margins with these peaks merging when the width of the body is less than the depth to the top. The amplitude of an analytic signal maxima is proportional to the magnetisation of the edge and so the presence of remanent magnetisation will produce higher analytic signal amplitudes in the direction of the magnetisation vector (McLeod et al., 1993). Roest et al., (1992) in discussing the constraints on interpretation of analytic signal data warn that, in the 3D case, (a) the amplitude of the analytic signal varies with the effective magnetisation which means that it is dependent on the ambient field parameters, (b) magnetisation contrasts that are closely spaced or dipping, or structures that intersect at acute angles produce a much more complex anomaly than that produced by a single contrast, and (c) the enhancement of noise occurs during the calculation of derivatives. Nelson (1988) refers to the analytic signal as the total gradient while Atchuta Rao et al., (1981) discuss the 'complex gradient'.

When there is a strong regional gradient, caused by a large deep source for example, this can have the effect of distorting or masking the lower amplitude anomalies in the vicinity. There are several ways of enhancing the smaller anomalies such as, the calculation of a regional polynomial to represent the deep source contribution and the subtraction of this component from the data (with the residual component remaining), the use of upward continuation or a low pass filter to enhance the regional contribution and then the subtraction of this component from the original data, or the calculation of horizontal and vertical first and second derivatives.

5.1.4 Source Delineation Procedure

The procedure used in preparing models of magnetic sources began with the examination of the TMI images and contour maps to gain a first approximation of the lateral extent and depth of the anomalies, with particular attention on the more subtle features. The examination of the supplied RTP maps enables the location of the centre of

the anomaly to be determined as well as giving some indication of the presence of remanent magnetisation through the distortion of the image or contours. Examination of the vertical derivative maps at this stage enables a preliminary outline to be determined at least for the shallower bodies.

Since the geological maps of this area do not give any indication of the subsurface geology it is necessary to use other geophysical methods to constrain the magnetic models. Seismic horizon maps are most useful in outlining basement topography and help restrict models of intersedimentary sources to structures within particular formations. The amount of seismic data available varies considerably over the area but where it exists it provides a large amount of depth information which is of great importance for constraining the models. Where the magnetic source is beneath the basement-sediment interface even seismic sections can be unreliable sources of information on the depth of the body. Gravity data can be useful in determining depth for deeper sources but its principal use in this study has been in allowing a comparison between magnetic and gravity sources, in particular, where they coincide and where there is a considerable offset between them.

The relatively high population of the study area results in large number of cultural anomalies which represent a major problem in this area. This problem will be discussed in Appendix A but it is important to note that these anomalies can produce lineations on images and contour maps that could be misidentified as being of geological origin. These anomalies are generally of short wavelength (usually much less than a maximum of around 250 m) but can have amplitudes ranging from less than 1 nT to 400 nT. These are major sources of noise contamination especially on first and second derivative maps where they can be very difficult to distinguish from shallow geological sources.

Prior to filtering or calculating derivatives the cultural noise can be suppressed with the use of a moving window median filter on the profile or gridded data followed by a moving average or 'smoothing' filter (Stanley et al., 1992). A median filter replaces the central value within a window with the median value, a process which cuts off the positive and negative peaks of sharp spike-like anomalies with the extent of the reduction in amplitude dependent on the window size. The moving average filter can then be used to remove the abrupt change between filtered and unfiltered data. The

cultural anomalies will still produce detectable features on derivative maps but without the very large gradients produced by them, it is possible to enhance more subtle features, especially on images. TMI data can be processed by a median filter when a stacked profile map is being prepared because in some parts of the study area cultural anomalies obscure features on adjacent lines. Median-filtered data displayed in stacked profiles should not be 'smoothed' with moving average filters because the shape of the median-filtered anomaly is distinctive and allows instant identification of the type of source. This allows the interpreter to ignore these features and concentrate on the more subtle longer wavelength anomalies which are the result of shallow geological sources.

The offshore data was free of cultural anomalies but close examination of the data reveals the presence of oceanic swell noise. This effect is caused by magnetic fields generated by the movement of electrically conductive seawater through the Earth's magnetic field under the influence of oceanic swell (Weaver, 1965; Ochadlick, 1989; Heath et al., 1993). In the preliminary report on the 1994 AGSO Offshore Otway Basin, Victoria aeromagnetic survey (Gunn, 1994), the author discusses the re-examination of data from the 1992 AGSO Penola aeromagnetic survey which also covered the offshore part of the study area for oceanic swell noise.

It was found that their offshore data contain a semi-periodic noise with an amplitude of approximately ± 0.25 nT and a wavelength that averages around 500 m, or is less when the flight direction was towards the oncoming waves (Gunn, 1994). AGSO staff subsequently investigated this phenomenon at the commencement of their offshore survey and found periodic noise with a wavelength of 500 m when flying into the swell and 700 m when flying with the swell. The noise had an amplitude of approximately ± 0.2 nT measured at an altitude of 130 m. This noise level is approximately equal to the effective noise envelope that the surveys were required to remain below. Prior to any processing of the offshore MESA data (which had a flight altitude of 120 m) a low pass filter with a cutoff wavelength of 800 m was used to suppress the swell noise.

Once various types of noise are suppressed or if possible removed altogether the calculation of derivative profiles and maps can proceed. The second derivative maps and profiles were found to be too contaminated with residual noise to be very useful. Vertical gradient images and contour maps of all the major anomalies in the area were

produced with horizontal gradient and analytic signal images of those anomalies that were not clearly delineated on the vertical gradient maps (section 7.2.1).

The vertical derivative images and contours delineate the shallower sources best while the gradient anomalies resulting from deep sources usually require considerable enhancement. In the case of the low amplitude, linear anomalies detected over the Penola Trough and adjacent areas, those of relatively higher amplitude are defined easily by gradient images (or contours) but the smaller anomalies with amplitudes that are closer to the noise envelope (around 0.2 nT) are difficult to delineate from gridded data especially when close to strong noise sources. Stacked profiles of vertical or horizontal derivatives can enhance a linear trend that influences a number of lines but anomalies resulting from noise sources are more difficult to exclude particularly when a median filter has been used on the data prior to calculating the derivative. Removing a regional component from the TMI, RTP or median-filtered data allows the use of residual TMI stacked profiles to trace the path of linear anomalies because there is no offset from the flightline caused by the regional component and the noise sources are relatively easily identified. Residual data has also been gridded and contour maps and images have been produced of both residual TMI and residual derivative data.

The altitude of the survey aircraft can affect the amplitude of an anomaly. Giret (1965) reported modelling results where the magnetic field of the Earth was simulated by a magnetic dipole. It was found that an altitude variation of ± 30.5 m (± 100 ft) produced a field variation of ± 1 nT (or 1 m variation produces a change of 0.033 nT). A theoretical model was created with a source body 3050 m (10000 ft) deep that generated an anomaly of 100 nT. This model produced the same results as that for the magnetic dipole. These results were used to check the residual anomalies modelled in section 8.2 and it was found that the variation in altitude had only a minor influence on their amplitude.

5.1.5 Modelling of Magnetic Sources

The magnetic anomalies of the study area belong to three classes; (1) shallow intersedimentary bodies that are linear-to-curvilinear, (2) circular-to-elliptical shaped anomalies at or close to the basement/sedimentary interface and (3) deep intra-basement. The exceptions are the anomalies associated with the Mt Gambier and Mt Schank

volcanic complexes and the Hungerford anomaly which are at or near the surface (Plate1).

The simulation study commenced using the POTENT™ software package which can create seven body types, (1) Sphere, (2) Dyke, (3) Step, (4) Rectangular Prism, (5) Ellipsoid, (6) 2D Polygonal Prism and (7) 3D Polygonal Prism. In the initial part of the simulation study only 3D polygons and Rectangular Prisms were used. The particular version of POTENT™ that the university possesses has a number of limitations such as, a limit of 100 bodies in a model and a limit of 49 vertices on a 3D polygonal prism. The last limitation is the most problematic because polygons were used to represent sedimentary layers with relatively complex faulting. For these reasons the POTENT™ models were converted to MODELVISION™ format once this software became available.

MODELVISION™ allows the creation of a number of different body types in either a cross-section or plan view. These body types are:- Sphere, Ellipsoid, Horizontal Cylinder, Tabular (i.e. a Rectangular Prism with a horizontal upper surface and parallel sides), a Polygon with arbitrary cross-section (but rectangular in plan view) or a Plunging Prism which has an arbitrary number of vertices in plan view but is rectangular in cross-section. Plunging prisms can have a dipping top surface and plunging sides. In this study only Plunging Prisms, Polygons and Tabular bodies have been used.

In order to represent some of the more complex magnetic sources, it has been necessary to use a number of bodies of different shapes, depths and susceptibilities and assemble them into a model that approximates the geological structures. Where the top of the body is at the basement/sediment interface or at the top of a particular horizon, the seismic data (where available) can be used to map the topography of the body surface (Polygon) but if the body is deeper then a forward modelling approach must be adopted where the shape of the body is determined by fitting the model curve to the observed data.

Some of the bodies used to represent intrusive sources have vertical sides and a rectangular cross-section (Plunging Prism models) but with polygonal top and bottom surfaces. These were constructed by 'drawing' the outline of the body on a contour map or image (usually vertical or horizontal gradient or analytic signal) and then editing the shape and other body parameters to fit the observed data. Other intrusive source bodies were constructed of a number of polygons assembled to represent the complex body which is more

realistic in the case of an igneous source where the susceptibility and other parameters vary within the body. The depth extent of the bodies was largely arbitrary with the large magma chamber beneath Mt Gambier for example, having a base at around 20 km depth while smaller, igneous bodies were considered to be more sill-like. The lower limit of a deep, magnetised body is usually considered to be the depth at which the Curie point (T_c) for magnetite (570°C) is reached, after which the body can no longer be magnetic. If the geothermal gradient in the study area is 30°C/km then the T_c would be reached at around 19 km deep, but if the gradient is 25°/km then the T_c is around 23 km deep.

The igneous complexes at Mt Gambier and Mt Schank were each modelled by assembling a number of polygons and tabular bodies while only polygons were used to model the Hungerford anomaly. Models were created for bodies that are partly or entirely outside the study area because they either influence the regional component of the field of the study area or interfere with the field produced by sources within the area. The shallow linear anomalies were modelled with combinations of polygons.

The modelling software calculates the field due to a tabular body using the formula derived by Vacquier et al., (1951) and extended to bodies with arbitrary polarisation vectors by Bhattacharyya, (1964). The algorithms used for calculating the field of a polygon are based on the 'two-and-a-half dimensional' geometry first developed by Shuey and Pasquale (1973). They took the formulas for 2D bodies of arbitrary cross-section and infinite strike length derived by Talwani and Heirtzler (1964) and incorporated end corrections to account for the finite strike length.

5.2 Simulation Study

5.2.1 Background

The simulation study involved the creation of models of the major sedimentary and basement formations which were based on seismic mapping, and after the assignment of an appropriate susceptibility to each of the formation models, the theoretical anomaly was calculated. The section chosen for the study is part of the Penola Trough and extends along 488000mE (easting) from south of (5852000mN), and substantially to the east of the Ladbroke Grove 1 well, passing slightly to the west of Wynn 1 and ending to the north of, and just to the west of Penola 1 and Sawpit 1 (5868000mN). This part of the Penola Trough

also contains the four Katnook wells, Haselgrove 1 and 2 as well as the recently drilled Tilbooroo 1 well. The aeromagnetic survey was flown prior to the drilling of Wynn 1, Haselgrove 1 and 2, Katnook 4 and Tilbooroo 1. The section was chosen because of the presence of these wells, the number of seismic lines crossing the area and the availability of magnetic susceptibility data acquired from cores taken from the Penola 1 and Katnook 2 and 3 wells (see section 3.3.2).

The major formations (or groups of formations) selected for the study are the basement, the Crayfish Group (which incorporates the Pretty Hill Formation, Laira Formation and Katnook Sandstone), the Eumeralla Formation (which includes the Windermere Sandstone Member) and the Sherbrook Group (which is largely undifferentiated in the Penola Trough). The Tertiary sediments are too thin and shallow and so they are poorly resolved on seismic sections with the result that they were not modelled. Seismic horizon maps supplied to the author by MESA were only for the major groups and for this reason there was no division of bodies into individual formations despite the fact that susceptibility data is available for some of them. While susceptibility data is available for the Crayfish Group members and the Eumeralla Formation from the three wells mentioned above, there are no values for these wells from the Sherbrook Group and basement. The basement values used came from the Kalangadoo 1 well and the Sherbrook Group values came from Kalangadoo 1, Caroline 1 and Mt Salt 1, the latter of which is outside but close to the P1 area (fig. 2.2.3.1). In generating the profiles only induced magnetisation was considered so no remanent magnetisation component needed to be assigned to any of the bodies.

5.2.2 Individual Formations and Multi-layer Models

North-south models were constructed in order to determine the magnetic response of the individual formations or multi-layer models and compare the theoretical profiles with actual flightline data. Each individual model represented the cross-section beneath the flightline but to make the models effectively two-dimensional the individual bodies were made 5 km wide along strike. The individual bodies consisted of, the basement body overlain by the Crayfish Group body, then the Eumeralla Fm. body and finally the Sherbrook Group body at the top. Each body was created by using the corresponding seismic horizon map to locate the major faults and generating a polygon with vertices corresponding to the top and bottom of

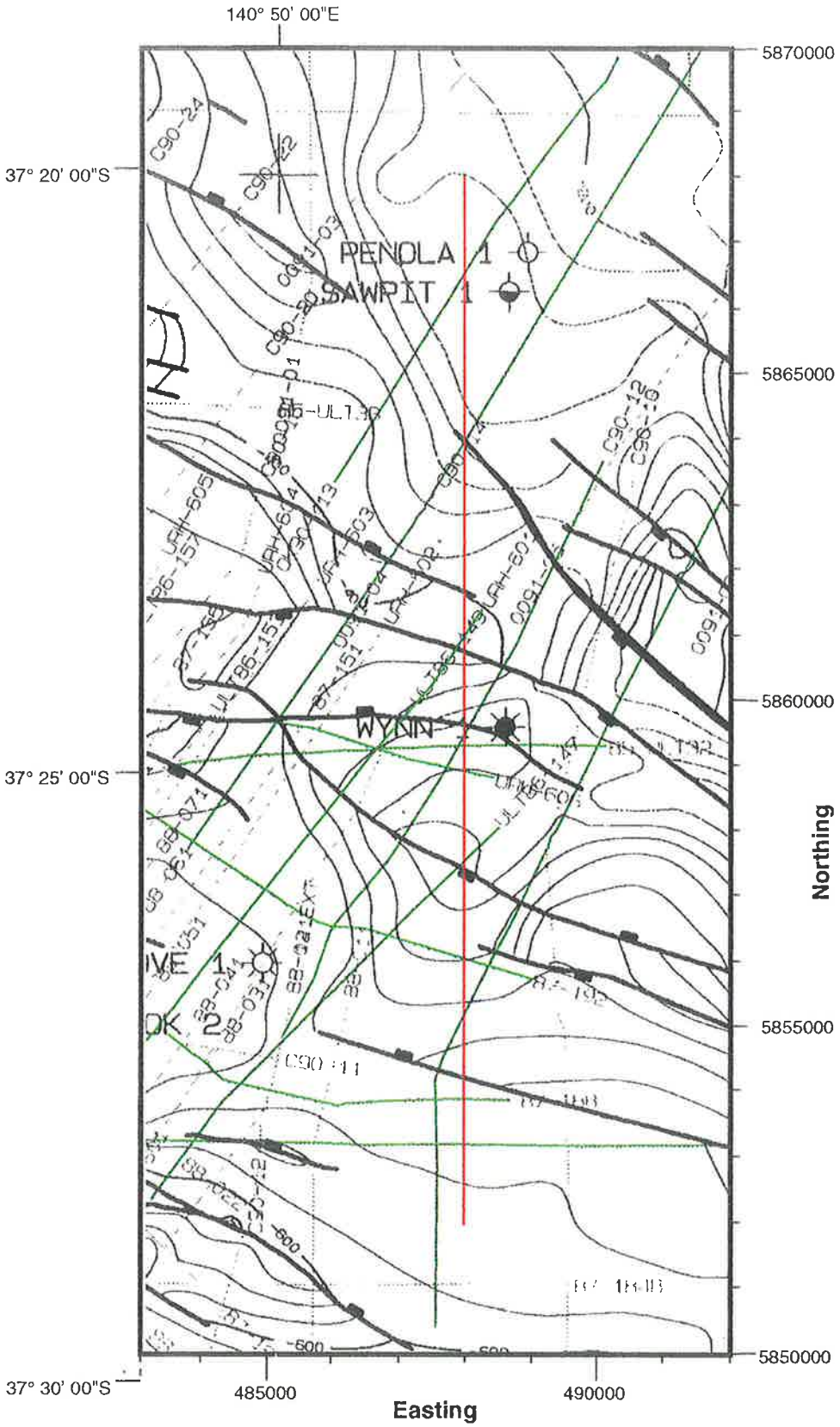

Fig. 5.2.2.1 Depth-Converted contour map of the top of the Eumeralla Fm. The red line shows the location of the cross-section and the green lines show the seismic lines that the cross-section was interpolated from.

the faults (fig. 5.2.2.1). The body representing basement only required fault offsets on the top surface while the other bodies required both sides to be faulted.

The polygon surfaces were created by measuring along a north-south line (approximately corresponding to the flightline) on the appropriate horizon map and assigning a northing and depth value to each vertex (the easting value remaining the same for all vertices). The bodies were extended 4 km to the north and south of the simulation area to eliminate the effect of the edges of the body from the theoretical profiles. The body representing the basement was given a total depth of 20 km although this is not particularly realistic because of the low susceptibility value assigned to the body. It would normally be expected that the basement would become highly magnetic at a depth considerably less than 20 km but the aim was to discover if the change in basement depth over a fault would produce a detectable anomaly. For this reason different susceptibilities were assigned to the basement model to test this.

After constructing the individual bodies using the methods outlined above each body was assigned an initial susceptibility value. The values were, 0.000182 SI for the basement, 0.000145 SI for the Crayfish Group, 0.000201 SI for the Eumeralla Formation, and 0.000118 SI for the Sherbrook Group. These values represent the average for each formation or group over all wells that cores were available from. The theoretical profiles calculated for each of the bodies individually using these susceptibilities are shown in figs. 5.2.2.2, 5.2.2.3, 5.2.2.4, 5.2.2.5 and 5.2.2.6 and show that none of the anomalies caused by the fault offsets has an amplitude greater than 1 nT. The calculated profile for the Sherbrook Group model (fig. 5.2.2.2) shows four very low amplitude, short wavelength anomalies with the largest around 5861000mN (around 0.38 nT) which is the result of the fault offset on the top of the body (125 m) and the offset beneath (75 m) which causes the narrowing of the body to approximately 30 m between the two faults. The second largest anomaly is at approximately 5857500mN (around 0.2 nT) and results from a narrowing of the body (approx. 70 m) with the fault offsets above (50 m) and below (25 m). The southern anomaly (around 5854000mN) is the result of changes in thickness in the formation but this anomaly is not very narrow because the change in thickness occurs at the bottom of the formation. The northern anomaly is narrow because the formation is much shallower at this end of the profile.

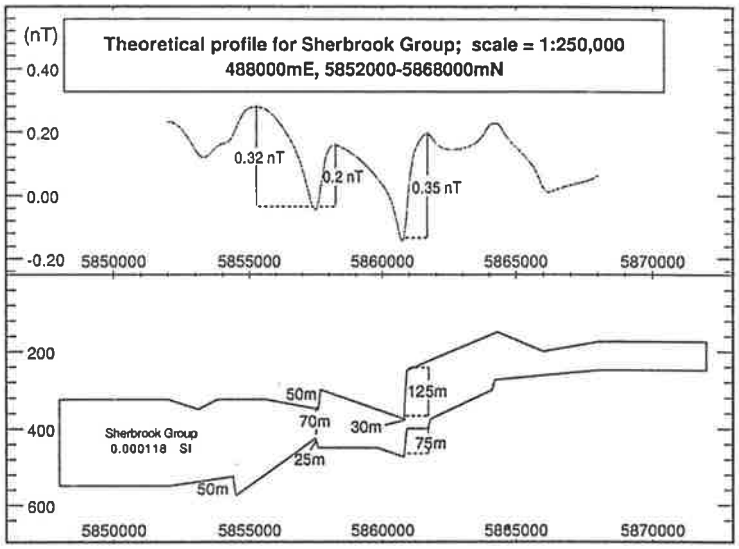

Fig. 5.2.2.2 Sherbrook Group Model

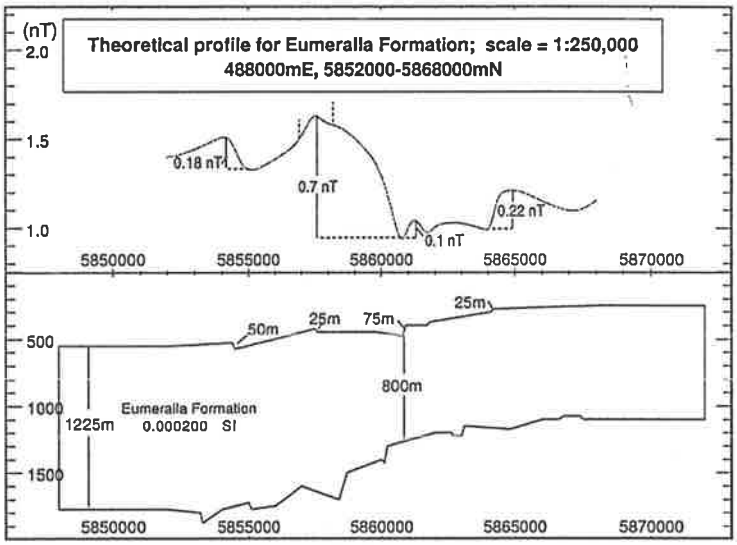

Fig. 5.2.2.3 Eumeralla Formation Model

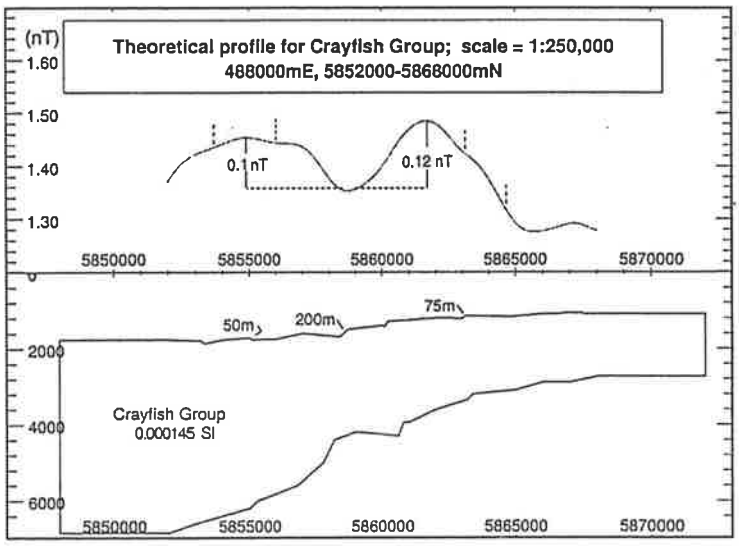

Fig. 5.2.2.4 Crayfish Group model

The calculated profile for the Eumeralla Formation (fig. 5.2.2.3) has a greater overall amplitude because the formation is much thicker and has a greater susceptibility than the Sherbrook Group. The minimum value of the profile occurs around 5860700mN which is the narrowest section of the body where it is approximately 800 m thick compared with 1225 m at the southern end. The overall shape of the anomaly is dependent on the thickness of the body which can be seen by the change in amplitude over the southern part of the body as the thickness changes and the change in amplitude as the thickness increases slightly around 5865000mN. The fault offsets which occur on the top of the body contribute to the anomaly by producing the smaller components such as the one around 5861000mN which is approximately 0.1 nT and is the result of a 75 m fault offset. There is another of these small anomalies around 5857500mN which is superimposed on the larger anomaly and is the result of the 25 m fault offset on the top of the body. The wavelength of the anomalies has increased in comparison to the Sherbrook Group body due to the increasing depth to the source.

The Crayfish Group body (fig. 5.2.2.4) generates a profile that is distinguished by two peaks, the northern one of which is approximately 0.12 nT, with the overall amplitude determined by the thickness of the body. The southern peak is principally the result of the much greater thickness of the body in that part of the profile while the northern peak probably results from the decrease in depth (500 m shallower at the northern end) and the thicker part of the body south of 5863000mN. Superimposed on the southern and northern peaks are two very subtle anomalies which result from, in the southern case, a 50 m fault offset and in the northern case, a 75 m offset. The 200 m fault offset around 5858400mN does not appear to have produced an anomaly on this profile. The subtle anomalies have a relatively long wavelength compared to the wavelength of anomalies generated by the shallower bodies.

The basement profile (fig. 5.2.2.5) is entirely the result of the increase in thickness of the basement body from the south to the north and there are no detectable anomalies due to fault offsets which is most likely to be because of the considerable depth of the body. This is despite an offset of 600 m around 5858000mN and an offset of 350 m around 5860500mN. In fig. 5.2.2.5a the basement susceptibility was increased to 0.01125 SI which is the average susceptibility for basalt extrusions at the Mt Gambier volcanic complex but there was still no anomaly generated by the relatively large fault offsets on the top of the body.

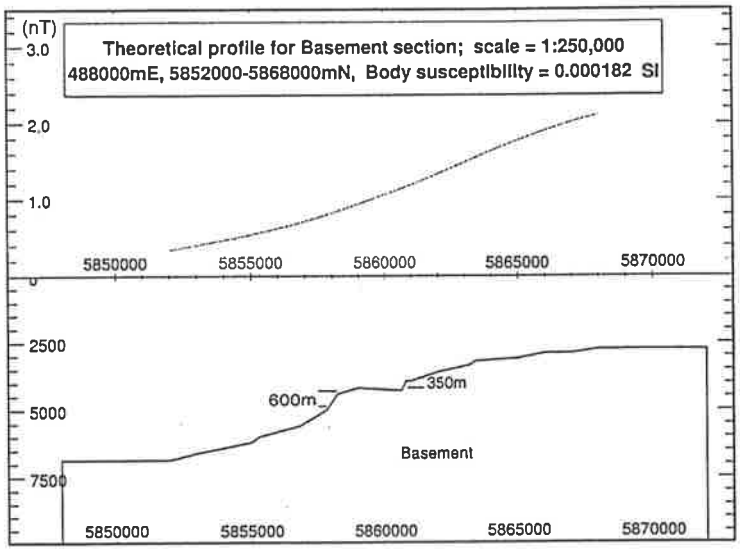

Fig. 5.2.2.5 Basement model (low susceptibility)

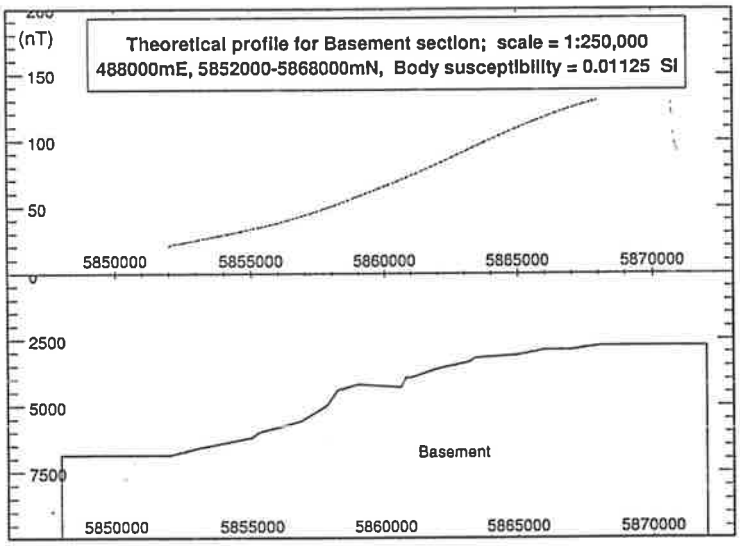

Fig. 5.2.2.5a Basement model (high susceptibility)

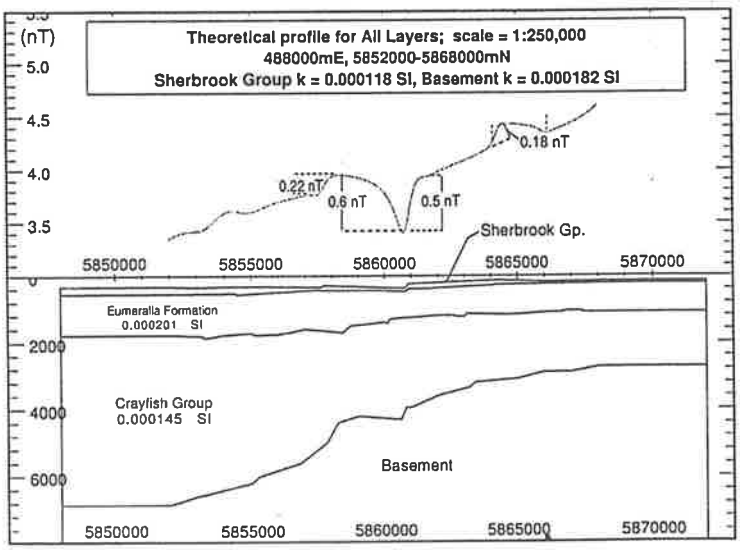

Fig. 5.2.2.6 Combination of all formation models

The profile shown in fig. 5.2.2.6 is generated by a model consisting of all the bodies and shows the contribution of each to the final profile. The overall trend reflects the influence of the basement contribution while the anomalies are the result of the superposition of Sherbrook Group and Eumeralla Formation profiles. The Sherbrook Group is thin compared with the underlying Eumeralla Formation so the fault offsets are effectively on the top of the Eumeralla Formation which has a higher susceptibility. This can be seen from the 0.5 nT anomaly at around 5860700mN while the corresponding Sherbrook Group anomaly is 0.38 nT, and from the shape of the anomaly at around 5865000mN which reflects the overall shape of the Eumeralla Fm. anomaly but with a small component contributed from the Sherbrook Group. There may be a component that results from the Crayfish Group but it appears to be masked by the shallower bodies.

5.2.3 Faulted Models

In the previous section the models treated each formation or group of formations as a homogeneous body with the same susceptibility throughout. Susceptibility data from section 3.2.2 show there can be a considerable variation in susceptibility with depth in a well and with distance between the wells. It is impractical to construct a model consisting of a very large number of layers with each layer having a different susceptibility value assigned to it, because of the limitations of the currently available software. However, the Penola Trough is heavily faulted so a model which divides a formation into several fault-bounded blocks with a change in susceptibility between each block might be realistic geologically. The fault-bounded bodies on the northern side of the simulation area were assigned a susceptibility value that is the average for that formation in the Penola 1 well (where these values exist) while the bodies on the southern side were assigned values that were averages from the Katnook wells with the bodies between them given intermediate values.

There are a series of major faults crossing the simulation area which strike approximately E120°N but because the theoretical profiles only cross these faults at one point there was no attempt to orient the modelled faults in the regional strike direction. These major faults were chosen as the boundaries for the blocks with the result there is a susceptibility contrast between adjacent bodies as well as an offset resulting from the fault throw. This is not as realistic as would be preferable because any change in susceptibility is likely to be more gradational rather than abrupt across a fault, especially as each body is

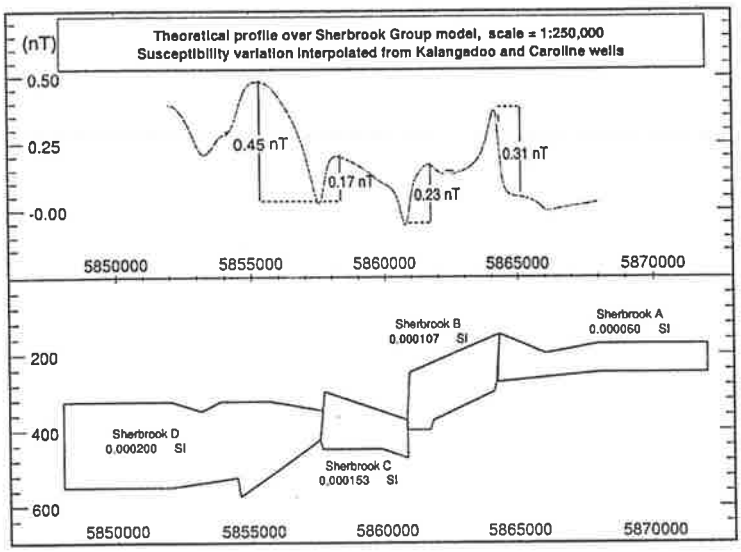

Fig. 5.2.3.1 Faulted Sherbrook Group model

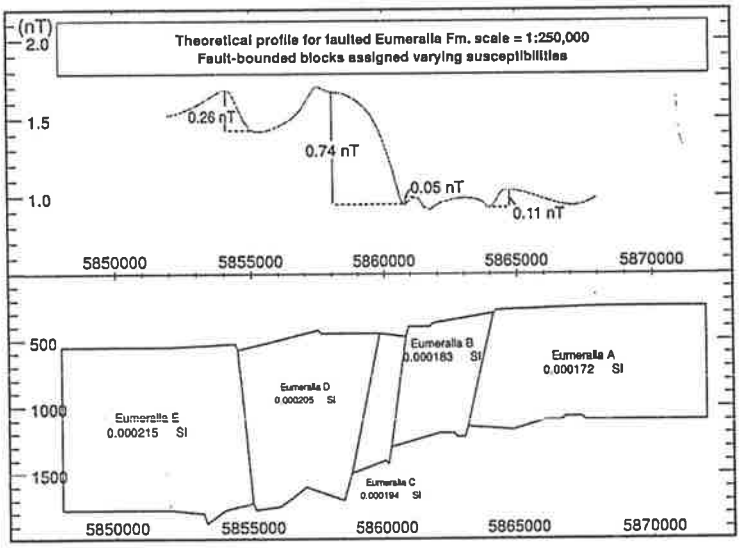

Fig. 5.2.3.2 Faulted Eumeralla Formation model (standard susceptibility range)

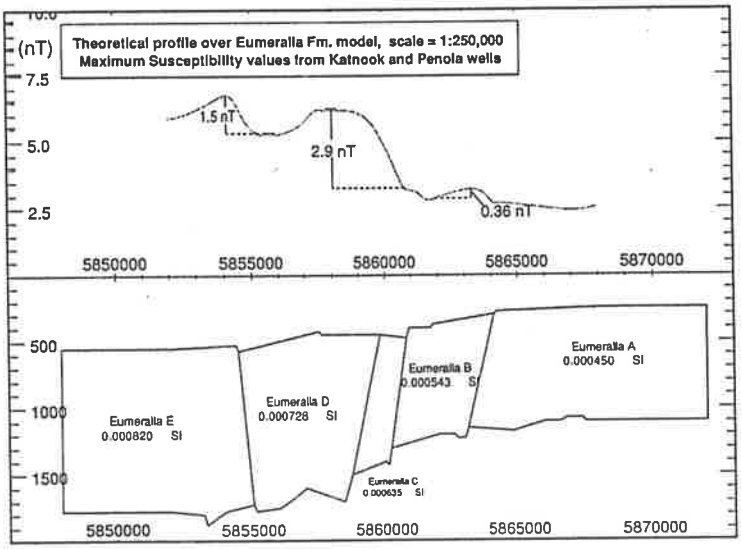

Fig. 5.2.3.3 Eumeralla Fm. model (high susc. range)

considered to be magnetically homogeneous and so there is no offsetting of magnetic horizons by the fault. Each formation was divided into five fault-bounded blocks (four in the case of the Sherbrook Group) which were labelled A to E (or D) from the north to the south. The assigned susceptibilities are listed in table 5.2.3.1.

	A	B	C	D	E
Sherbrook Gp.	0.000060 SI	0.000107 SI	0.000153 SI	0.000200 SI	
Eumeralla Fm.	0.000172 SI	0.000183 SI	0.000194 SI	0.000205 SI	0.000215 SI
Crayfish Gp.	0.000147 SI	0.000150 SI	0.000153 SI	0.000156 SI	0.000159 SI
Basement	0.000223 SI	0.000260 SI	0.000185 SI	0.000148 SI	0.000110 SI

Table 5.2.3.1. Magnetic Susceptibility values assigned to the fault-bounded blocks in the initial models (These values are used for all models unless otherwise stated).

The Sherbrook Group susceptibility values shown in table 5.2.3.1 represent the average range of values from Sherbrook Group cores, that is, the value for Sherbrook A is the average of minimum values while that for Sherbrook D is the average maximum value from Kalangadoo 1, Caroline 1 and Mt Salt 1 while the remaining values were interpolated from them. The basement susceptibility values assigned to Basement B and E represent the maximum and minimum values respectively from cores of basement meta-sediments from the Kalangadoo 1 well with the remaining values being interpolations between these extremes. Basement B was assigned the maximum value solely because there is a magnetic high in the observed data in this part of the profile while Sherbrook A was assigned the minimum value only because the underlying Eumeralla A body was assigned the minimum value (taken from Penola 1).

The faulted Sherbrook Group model (fig. 5.2.3.1) generates a profile similar to that of the unfaulted model (fig. 5.2.2.2) but because Sherbrook D has a higher susceptibility than the original body, the anomaly centred at approximately 5855500mN is larger than its counterpart (0.45 nT compared with 0.32 nT) on the original profile. The anomaly centred around 5857000mN is approximately equal in intensity to its equivalent on the original profile and is the result of the combination of the high susceptibility Sherbrook D and the lower susceptibility Sherbrook C. The anomaly at 5861000mN is smaller than its counterpart (0.23 nT compared with 0.38 nT) which is the result of the susceptibility contrast between

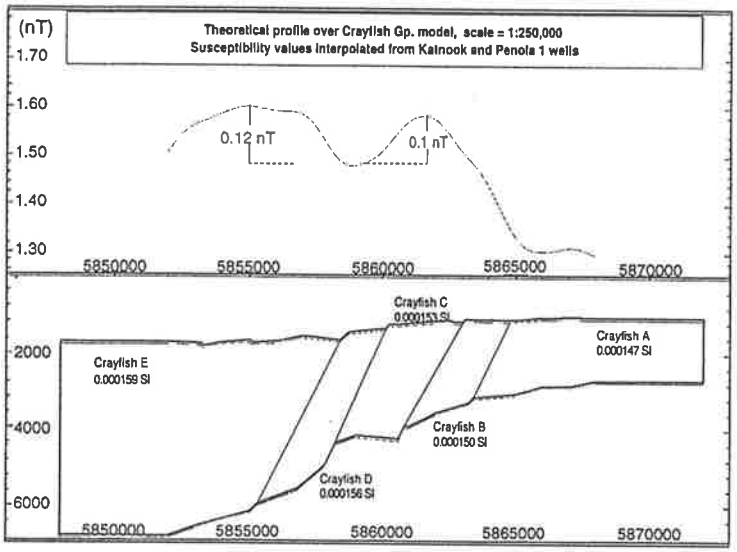

Fig. 5.2.3.4 Faulted Crayfish Group model

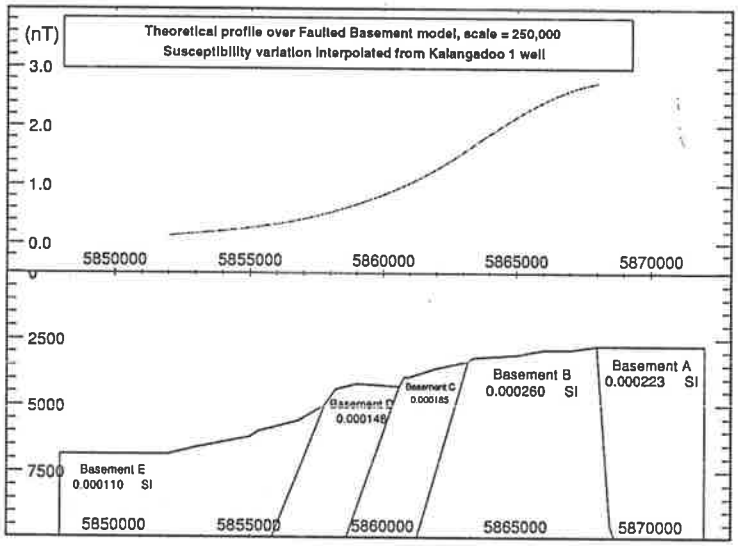

Fig. 5.2.3.5 Faulted Basement model

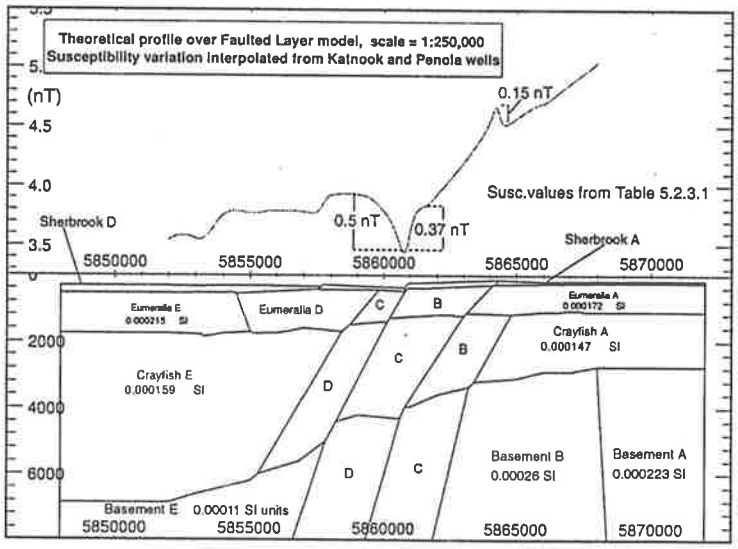

Fig. 5.2.3.6 Combined Faulted Layer model

Sherbrook C and B where Sherbrook B has a lower susceptibility than the original body. Around 5864000mN is an anomaly (0.31 nT) most probably produced by the shallow point at the top of the fault separating Sherbrook B and A.

The faulted Eumeralla Formation model (fig. 5.2.3.2) generates a profile that resembles that of the unfaulted body (fig. 5.2.2.3) especially in the shape of the anomaly south of 5860000mN but the northern part of the profile has a lower amplitude because of the smaller susceptibility of Eumeralla A and B. This lower susceptibility results in the anomalies at around 5861000mN and 5864500mN having 50 % of the intensity of the corresponding anomalies over the unfaulted body while the higher susceptibility of the southern bodies produces larger anomalies at 5854500mN and 5857500mN. Fig. 5.2.3.3 shows the profile generated when Eumeralla E and Eumeralla A are assigned the maximum susceptibility value from Katnook 2 and Penola 1 respectively while the other two bodies were assigned interpolated values. The anomaly at around 5854500mN is now 1.5 nT while the broad high at around 5858000mN is approximately 3 nT, but the smaller anomalies at 5857500mN, 5861000mN and 5864500mN are now much smaller relative to the broader highs.

The faulted and unfaulted models of the Crayfish Group (figs. 5.2.3.4 and 5.2.2.4 respectively) show little difference in the profiles generated except for the reversal in amplitude between the southern and northern anomalies (centred at 5855000mN and 5862000mN respectively). This reversal is due to the higher susceptibility of the southern bodies in the faulted model. The differences between profiles generated by the faulted Basement model (fig. 5.2.3.5) and the original Basement body (fig. 5.2.2.5) are the result of the range of susceptibilities assigned to the fault-bounded bodies. The highest susceptibility is assigned to Basement B which results in the change in curvature in the northern part of the profile but there is no change in the profile at the boundaries of the bodies because of the susceptibility contrast.

When the bodies are assembled into the Faulted Layer model (fig. 5.2.3.6), the resulting profile shows that the basement, Eumeralla Formation and Sherbrook Group are the main influences on the shape and amplitude of the anomaly, in a similar manner to the unfaulted All Layer model (fig. 5.2.2.6). The principal differences between the profiles are, the influence of Basement B which causes the steeper increase in amplitude north of 5861500mN, the small anomaly (0.15 nT) around 5864500mN which results from the

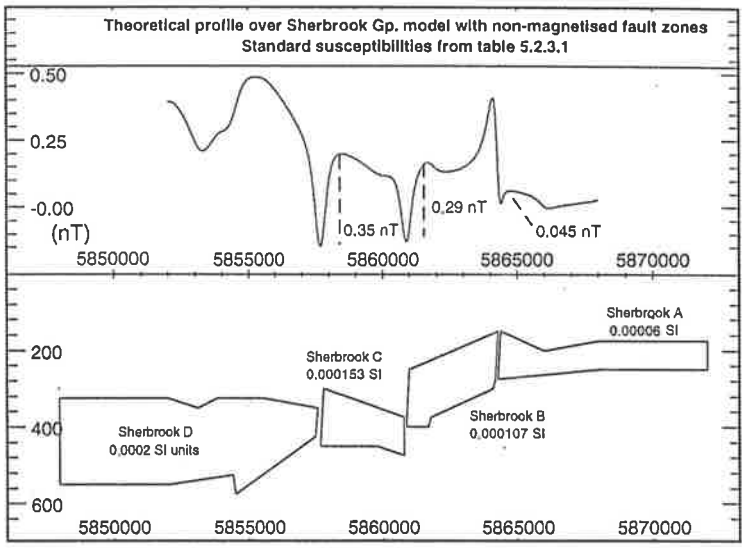

Fig. 5.2.3.7 Sherbrook Gp. model with fault zone demagnetisation (standard susc. range)

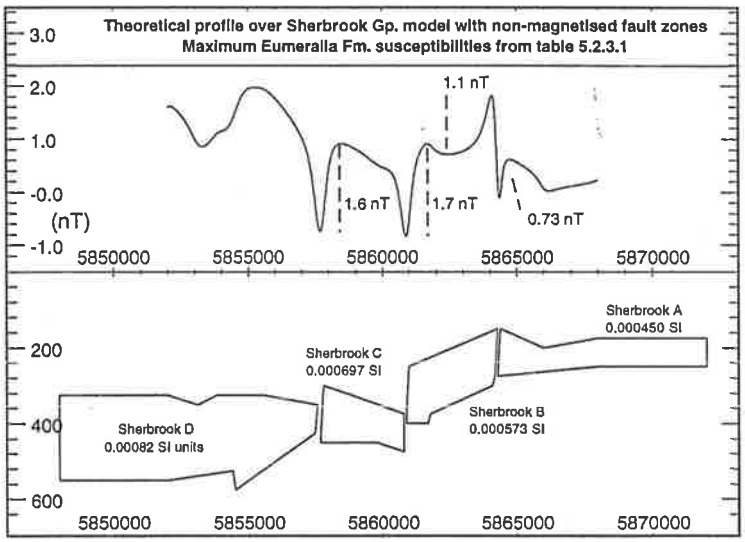

Fig. 5.2.3.8 Sherbrook Gp. model with fault zone demagnetisation (max. susc. range)

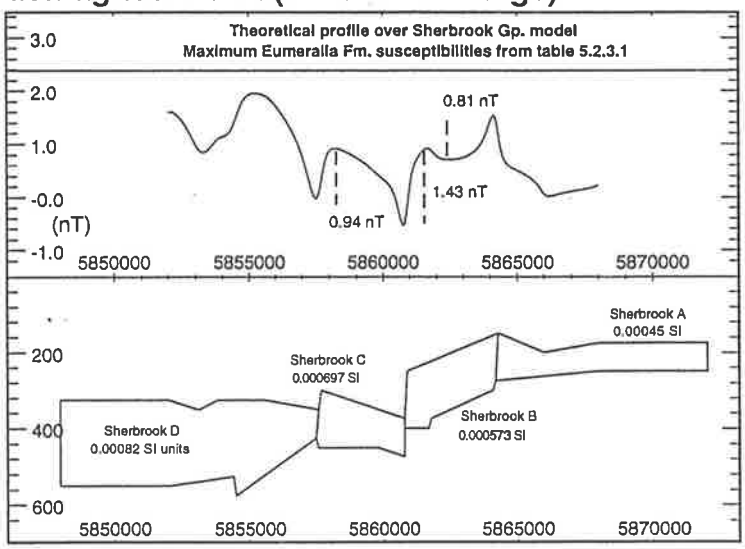

Fig. 5.2.3.9 Faulted Sherbrook Gp. model with max. Eumeralla Fm. susc. range

susceptibility contrast between the shallow Sherbrook Group bodies, and the smaller anomaly (0.37 nT) at 5860700mN which is also because of the influence of Basement B as well as the lower susceptibility north of Eumeralla and Sherbrook C.

Faults in sedimentary basins can facilitate the migration of fluids, particularly water but including hydrocarbons, which can result in the destruction, deposition or perhaps the creation of magnetic minerals along the fault plane. The two latter cases will be dealt with in the next section (5.2.4) but the former situation was modelled using the fault-bounded bodies discussed earlier, by separating each body with a narrow zone that has a susceptibility of zero. This was achieved by moving the vertices of adjacent sides of the bodies apart, with the distance separating the bodies arbitrarily set at approximately 100 m depending on the shape of the body. Each of the offset bodies have the same susceptibility as those in the faulted models.

The profile shown in fig. 5.2.3.7 demonstrates the effect of this offset on the Sherbrook Group model when compared to the faulted model (fig. 5.2.3.1). The offset between Sherbrook C and Sherbrook D produces a negative anomaly (0.35 nT) at around 5857500mN which has nearly twice the amplitude of the corresponding anomaly in fig. 5.2.3.1 while the offset between Sherbrook C and B generates a negative anomaly (0.29 nT) that is only slightly more intense than the corresponding anomaly (0.23 nT) produced by the faulted model. This is probably due to the small distance between the top of Sherbrook C and the bottom of Sherbrook B on both models. A similar situation arises with the anomalies produced by the offset between Sherbrook A and B where there is a positive anomaly similar to that of the faulted model (fig. 5.2.3.1) but with the addition of a very small negative anomaly (0.045 nT) that is caused by the offset.

In order to examine the effect of the offsets on a shallow formation with considerably higher susceptibility, the 'standard' values (from table 5.2.3.1) were replaced by values interpolated from the Eumeralla Formation maxima from the Katnook and Penola 1 wells which are the highest susceptibility values of all the formations. The profile in fig. 5.2.3.8 shows a large increase in amplitude of all the anomalies, with the offset between Sherbrook C and D producing a 1.6 nT anomaly while the offset between Sherbrook C and B generates a 1.7 nT anomaly. The positive and negative anomalies produced by the offset between Sherbrook A and B are 1.1 nT and 0.73 nT respectively. Fig. 5.2.3.9 shows the profile generated when the Eumeralla maxima are assigned to the original faulted model. Note that

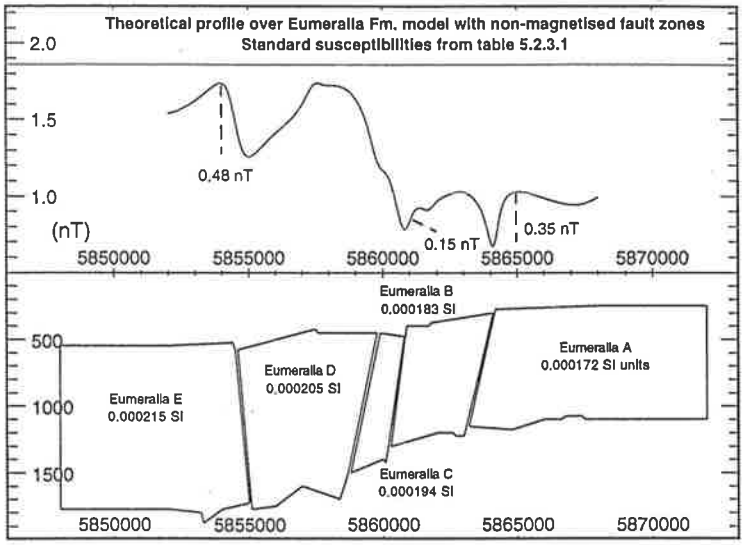

Fig. 5.2.3.10 Eumeralla Fm. model with fault zone demagnetisation (standard Eumeralla susc. range)

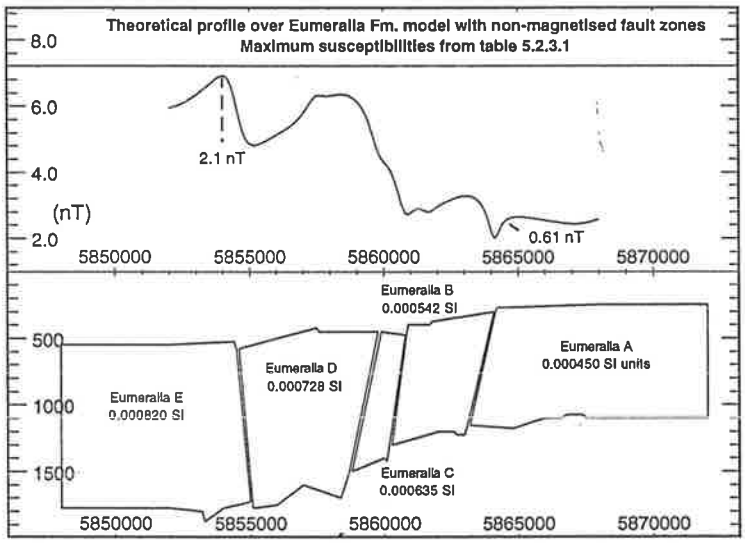

Fig. 5.2.3.11 Eumeralla Fm. model with fault zone demagnetisation (max. Eumeralla susc. range)

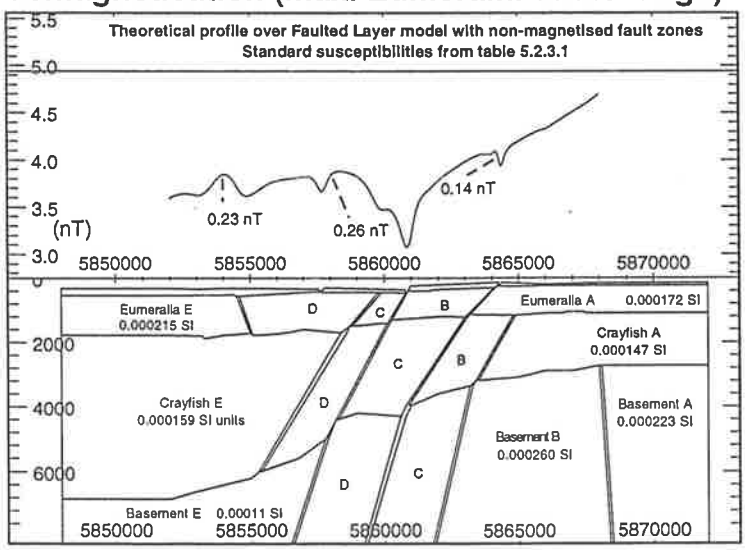

Fig. 5.2.3.12 Faulted Layer model with fault zone demagnetisation (standard susc. range)

the small negative anomaly over the offset between Sherbrook A and B in fig. 5.2.3.8 is missing while the negative anomaly (0.94 nT) at around 5857500mN is approximately 60 % of the previous value. The positive anomaly over the offset between Sherbrook A and B is now 0.81 nT and the anomaly at around 5860700mN has decreased to 1.43 nT (approx. 85 %).

The significant differences between the Eumeralla Formation model with non-magnetised fault zones (fig. 5.2.3.10) and the corresponding fault block model (fig. 5.2.3.2), are the 0.48 nT negative anomaly over the offset between Eumeralla D and E (compared with 0.26 nT), the 0.15 nT anomaly caused by the offset between Eumeralla B and C (compared with 0.049 nT), and the 0.35 nT negative anomaly which results from the offset between Eumeralla B and A (0.11 nT on the original profile). Fig. 5.2.3.11 shows the profile generated when the maximum susceptibility values interpolated from the Katnook 1 and Penola 1 wells are assigned to the Eumeralla offset fault model. Comparison with the profile generated by the corresponding faulted model (fig. 5.2.3.3) shows that the most significant differences are, the negative anomaly (0.61 nT) over the offset between Eumeralla A and B and the increase in intensity of the anomaly at approximately 5854500mN. There is a small change in anomaly shape over the offset between Eumeralla B and C as well as a more subtle anomaly over the Eumeralla C and D fault zone.

From the evidence of previous models the Crayfish Group has a marginal effect on the profiles even when the highest susceptibility values are assigned to the models while the basement only determines the amplitude and regional trend. For these reasons separate Crayfish Group and basement non-magnetised fault zone models were not produced but a composite model was assembled instead (fig. 5.2.3.12). The composite model and the Faulted Layer model (fig. 5.2.3.7) are similar in that the overall trend is controlled by the basement susceptibility variation and the anomalies are a combination of the influences of the Sherbrook Group and Eumeralla Formation bodies. The differences are the 0.26 nT anomaly over the fault zone between Sherbrook C and D, the wider 0.23 nT anomaly over the fault zone between Eumeralla D and E, the anomaly (0.14 nT) over the fault zone separating Sherbrook and Eumeralla A and B, and the small anomaly resulting from the fault zone between Eumeralla C and D. The anomalies that are principally the result of Sherbrook Group fault zones are narrower or have a shorter wavelength than those mainly due to Eumeralla Formation offsets.

5.2.4 Fault-plane Models

The fault plane models assume that the magnetic source responsible for an anomaly is a concentration of magnetic minerals along or near the fault planes with a strong susceptibility contrast between the mineralised fault planes and the surrounding formations. These bodies produce anomalies similar to dipping dykes of finite depth extent and so the bodies were constructed from thin, dyke-like polygons with the surrounding formations having lower susceptibility. The width of these bodies was sometimes determined from the horizon maps used to construct the models but where it was difficult to ascertain this from the maps an arbitrary width of 100 m was used.

The fault plane bodies were initially assigned the susceptibility values for fault-bounded blocks shown in table 5.2.3.1 with the fault plane body 1 given the susceptibility of the fault-bounded body A, body 2 that of body B and so on. Each of the models was created with the fault plane bodies on a background of the original unfaulted formation which was assigned either initially a very low susceptibility (1.0×10^{-6} SI) or later the 'normal' susceptibility of the unfaulted formation (table 5.2.4.1). When the background body is given the normal susceptibility the fault plane bodies are assigned the interpolated maximum Eumeralla Formation values used in the previous sections, in the case of the sedimentary section, or a susceptibility range interpolated from measurements of the Mt. Gambier basalt flows in the case of the basement. Table 5.2.4.1 shows the susceptibility values assigned to the fault plane bodies in the low and normal background situations.

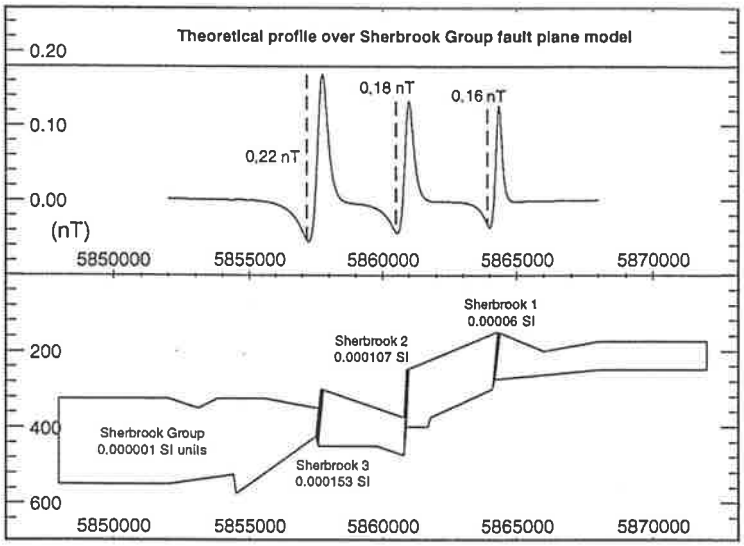

Fig. 5.2.4.1 Sherbrook Gp. model with dyke/fault plane bodies assigned standard susceptibility range with low susceptibility background. [table 5.2.4.1]

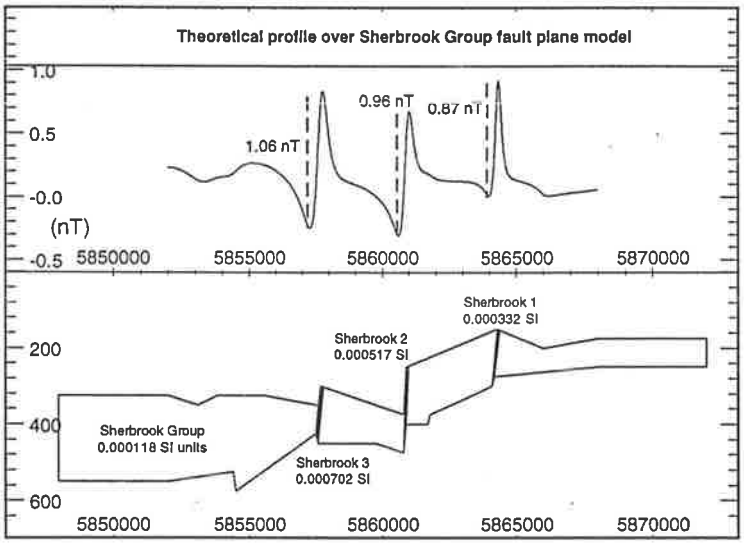

Fig. 5.2.4.2 Sherbrook Gp. model with dyke/fault plane bodies assigned maximum Eumeralla Fm. susceptibility range with standard susceptibility background. [table 5.2.4.1]

Low	Body 1	Body 2	Body 3	Body 4	Background
Sherbrook Gp.	0.00006	0.000107	0.000153		0.000001
Eumeralla Fm.	0.000172	0.000183	0.000194	0.000205	0.000001
Crayfish Gp.	0.000147	0.00015	0.000153	0.000156	0.000001
Basement	0.000225	0.00026	0.000185	0.000148	0.000001
Normal					
Sherbrook Gp.	0.000332	0.000517	0.000702		0.000118
Eumeralla Fm.	0.00025	0.000434	0.000527	0.00062	0.000201
Crayfish Gp.	0.000305	0.000398	0.00049	0.000675	0.000145
Basement	0.0214	0.03	0.0127	0.004	0.000182

Table 5.2.4.1 Susceptibility values (in S.I. units) assigned to the Fault Plane bodies, and the low and normal background bodies.

The profile shown in fig. 5.2.4.1 is essentially that of the three shallow, near-vertical, dyke-like fault plane bodies and shows three narrow anomalies with the most intense caused by Sherbrook 3 (0.22 nT) while Sherbrook 2 (0.18 nT) and Sherbrook 1 (0.16 nT) produce slightly smaller anomalies. Sherbrook 3 produces the most intense anomaly despite being the deepest because it has the highest susceptibility and is slightly thicker than the other two. When the susceptibilities are increased to the maximum values as shown in fig. 5.2.4.2, the resulting profile is a combination of that of the unfaulted body (fig. 5.2.2.2) and the previous figure (fig. 5.2.4.1). Once again the anomaly produced by Sherbrook 3 is the largest (1.06 nT) with Sherbrook 2 less (0.96 nT) and Sherbrook 1 is the smallest (0.87 nT). Note that the anomalies produced by these two models have a relatively narrow wavelength (approximately 2 km. as a result of Sherbrook 1 in fig. 5.2.4.1) which is because of the shallow depth and narrow width of the fault plane bodies.

The Eumeralla Formation fault plane model with low background susceptibility generates a profile (fig. 5.2.4.3) that is almost entirely the result of the fault plane bodies. The anomalies produced have longer wavelengths than those generated by the Sherbrook bodies with the result that there is some interference between the three northern anomalies, particularly between the Eumeralla 2 and 3 anomalies. Eumeralla 1 produces the largest anomaly (0.3 nT), despite having the lowest susceptibility, because the depth to the top of the body is less than for the other bodies. The second largest anomaly is produced by Eumeralla 4 (0.2 nT) which is because this body has the highest susceptibility plus the greatest depth

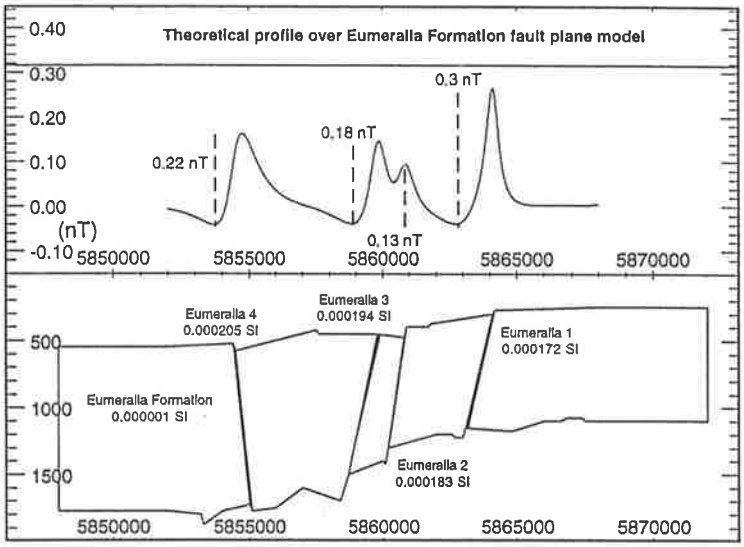

Fig. 5.2.4.3 Eumeralla Fm. model with dyke/fault plane bodies assigned standard susceptibility range with low susceptibility background. [table 5.2.4.1]

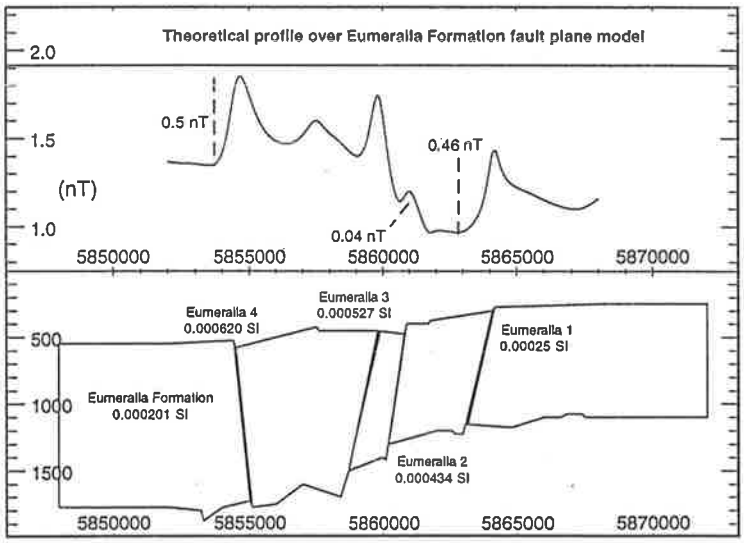

Fig. 5.2.4.4 Eumeralla Fm. model with dyke/fault plane bodies assigned maximum Eumeralla Fm. susceptibility range with standard susceptibility background. [table 5.2.4.1]

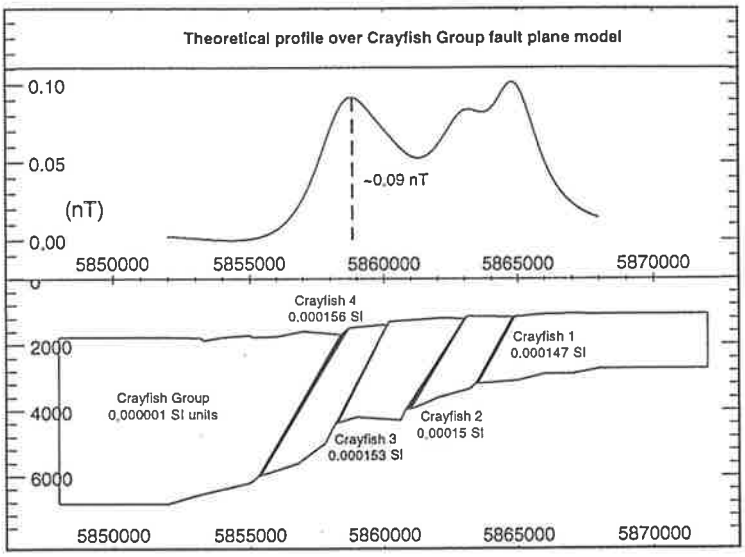

Fig. 5.2.4.5 Crayfish Gp. model with dyke/fault plane bodies assigned standard susceptibility range with low susceptibility background. [table 5.2.4.1]

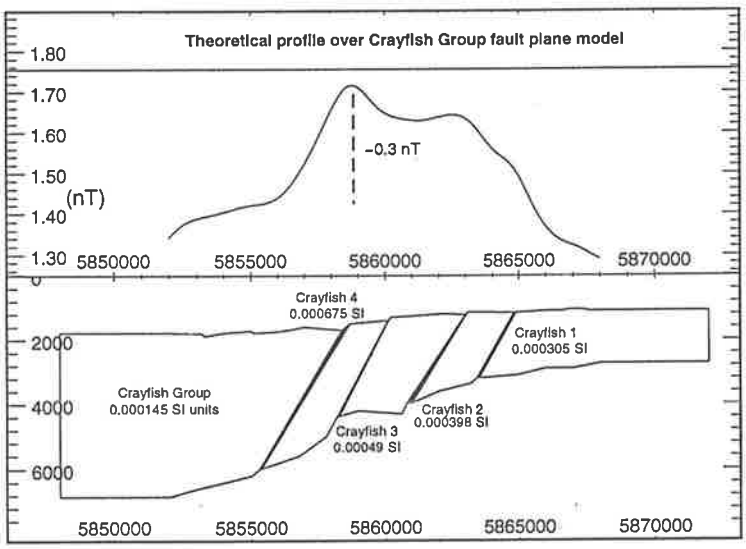

Fig. 5.2.4.6 Crayfish Gp. model with dyke/fault plane bodies assigned maximum Eumeralla Fm. susceptibility range with standard susceptibility background. [table 5.2.4.1]

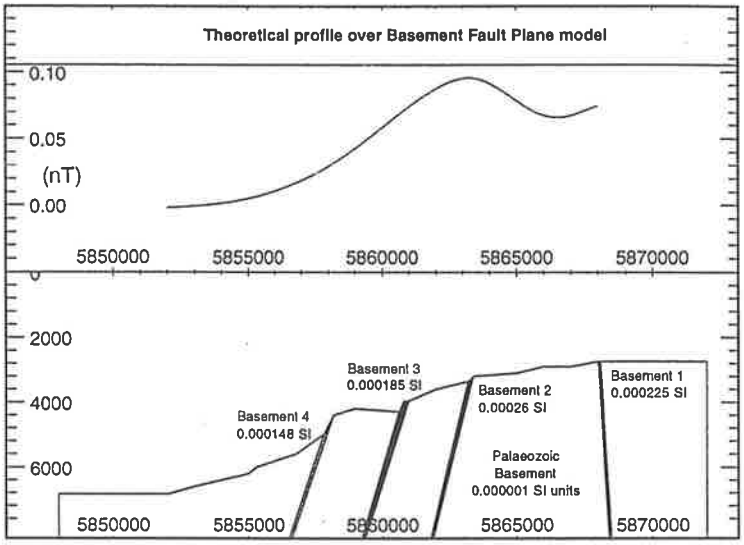

Fig. 5.2.4.7 Basement model with dyke/fault plane bodies assigned standard susceptibility values [table 5.2.4.1] on a low susceptibility background.

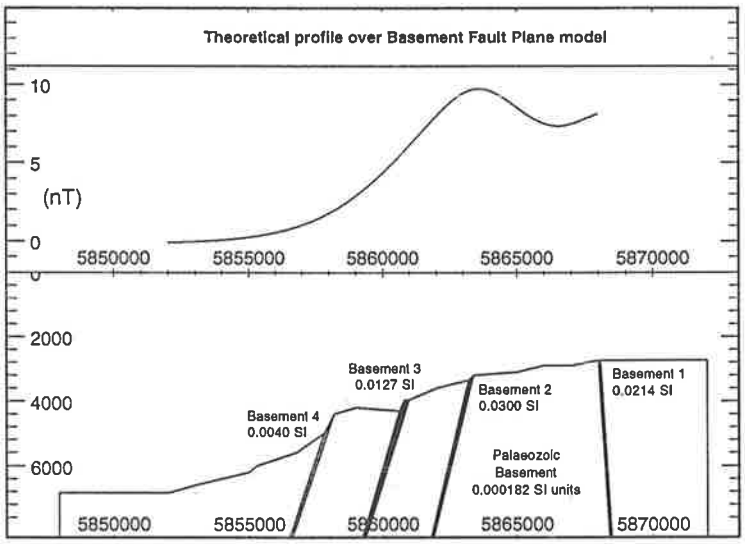

Fig. 5.2.4.8 Basement model with dyke/fault plane bodies assigned susceptibility range derived from Mt. Gambier basalts [table 5.2.4.1] Standard susceptibility background

extent. The two anomalies produced by Eumeralla 2 and 3 have amplitudes of 0.13 and 0.18 nT respectively, the former having the smallest amplitude because it has the narrowest width of all the bodies.

Substitution of the maximum Eumeralla susceptibility values into the Eumeralla fault plane model and normal Eumeralla Fm. background susceptibility produces a profile that is a superposition of the unfaulted model profile (fig. 5.2.2.3) and that of fig. 5.2.4.3. The highest amplitude anomaly is over Eumeralla 4 (0.5 nT) which is the result of the greater susceptibility assigned to this body while the next highest amplitude anomaly is produced by Eumeralla 1 (0.46 nT), a value resulting from the shallow depth and relative width of the body. Eumeralla 2 and 3 produce anomalies that are the result of interference between these two bodies and the background body with Eumeralla 3 having the greatest effect.

The Crayfish Group fault plane model generates a profile (fig. 5.2.4.5) that, like the previous profiles with a low susceptibility background, is completely dominated by the anomalies of the fault plane bodies. Here, the depth of the bodies results in long wavelength, very low amplitude anomalies such as the approximately 0.09 nT anomaly that is the product of Crayfish 4 and the two smaller anomalies produced by Crayfish 1 and 2 while there is no detectable anomaly resulting from Crayfish 3. Note that the wavelengths of these anomalies are so great that all anomalies interfere with each other to some extent. The replacement of the original susceptibilities by the maximum Eumeralla susceptibility values and the normal background value produces the profile shown in fig. 5.2.4.6 where there has been a similar superposition of profiles as was seen with the shallower formations. Comparison of this profile and fig. 5.2.2.4 reveals that Crayfish 4 has the greatest effect on the profile generating an anomaly of approximately 0.3 nT while Crayfish 2 has the next largest effect. Crayfish 1 has only a very subtle effect while Crayfish 3 does not appear to have produced an anomaly which is probably due to its narrow width compared with the other bodies.

The basement model (fig. 5.2.4.7) features dyke-like fault plane bodies extending to considerable depth with what is almost certainly an unrealistic susceptibility value assigned to the background body. The effect of these bodies is to produce a single anomaly with an amplitude of about 0.1 nT with the peak over Basement 2 which has the highest susceptibility. If the profile were extended to the north there would probably be a second anomaly over Basement 1 although it would be likely to have a lower amplitude. Fig. 5.2.4.8 shows the effect of substituting a range of susceptibility values derived from Mt. Gambier

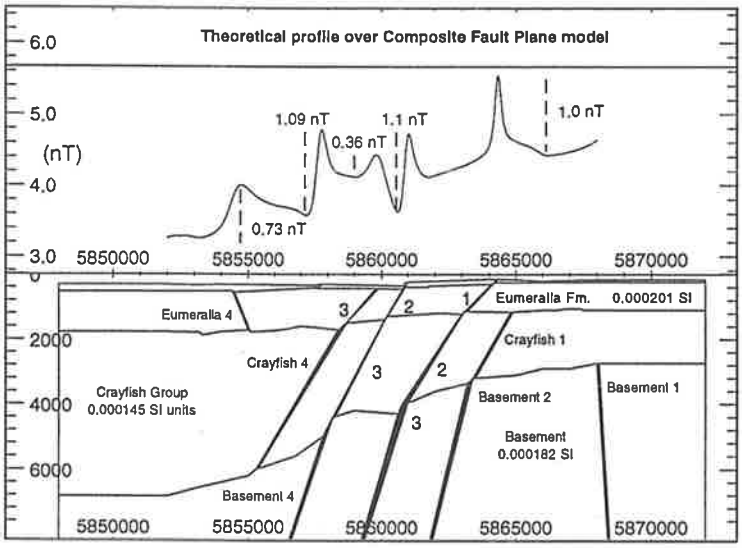

Fig. 5.2.4.9 Composite model with all dyke/fault plane bodies assigned maximum Eumeralla Fm. susceptibility values [table 5.2.4.1], except for basement. Standard susceptibility background

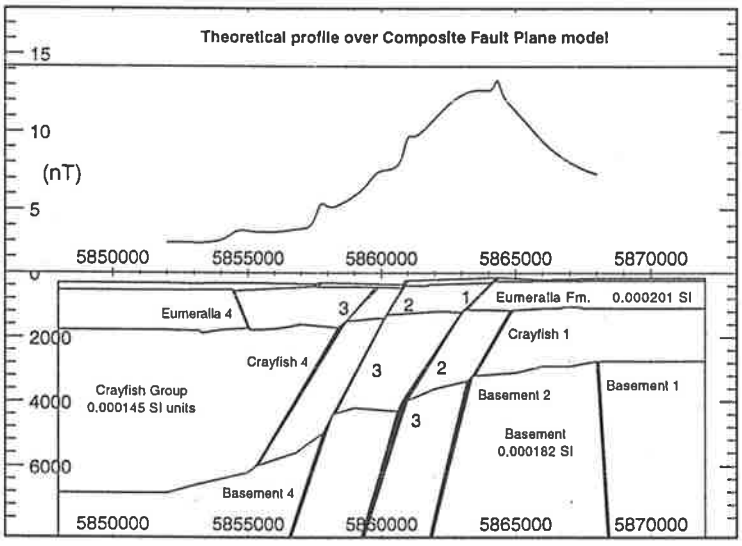

Fig. 5.2.4.10 Composite model with dyke/fault plane bodies assigned maximum Eumeralla Fm. susceptibilities. Basement susceptibility range derived from Mt. Gambier basalts [table 5.2.4.1] Standard susceptibility background

basalt flows on the profile generated by the fault plane bodies. The single anomaly now has an amplitude of approximately 10 nT which is the result of the much higher susceptibilities assigned to these bodies with little contribution from the normal susceptibility of the background body.

The theoretical profile shown in fig. 5.2.4.9 was produced by assembling each of the individual formation models into the final composite model. The sedimentary fault plane bodies were assigned the maximum Eumeralla Formation susceptibility values while the basement bodies remained at similar susceptibilities to the basement background value. The resulting profile shows the dominant effect of the Sherbrook and Eumeralla fault plane bodies with little detectable influence from the Crayfish Group bodies while the basement body contributes predominantly to the overall trend as seen in previous models. Anomalies over the Sherbrook Group bodies or over a body that effectively extends from the top of the Sherbrook Group horizon and through the Eumeralla Formation, have the highest amplitude with the anomaly generated by Sherbrook and Eumeralla 2 (1.1 nT) being the most intense, followed by the anomaly resulting from Sherbrook 3 (1.09 nT) while that generated by Sherbrook and Eumeralla 1 is 1.0 nT. The two anomalies resulting from Eumeralla Formation fault plane bodies have amplitudes of 0.73 nT (Eumeralla 4) and 0.36 nT (Eumeralla 3). Fig. 5.2.4.10 shows the effect of assigning the Mt Gambier basalt flow susceptibility values to the basement fault plane bodies. The simple curve that results from the basement bodies, has anomalies from the shallower fault plane bodies superimposed on it and demonstrates that the shallow bodies will produce subtle anomalies on the large regional trends but only when there is a relatively large susceptibility contrast.

5.2.5 Comparison with Observed Data

The main magnetic features of the study area are the large basement intrusions which determine the regional field. Thus it is necessary to include bodies simulating the effect of these in order to directly compare the observed field with the theoretical profile. This was done with the simple unfaulted layer model, the faulted model, the model with low susceptibility fault zones, and the fault plane model. The observed data is shown in black and calculated profiles are red on all diagrams in this chapter and Chapter 8.

The profiles shown in fig. 5.2.5.1 are the median filtered TMI data and the calculated anomaly resulting from the unfaulted Layer model plus bodies representing basement

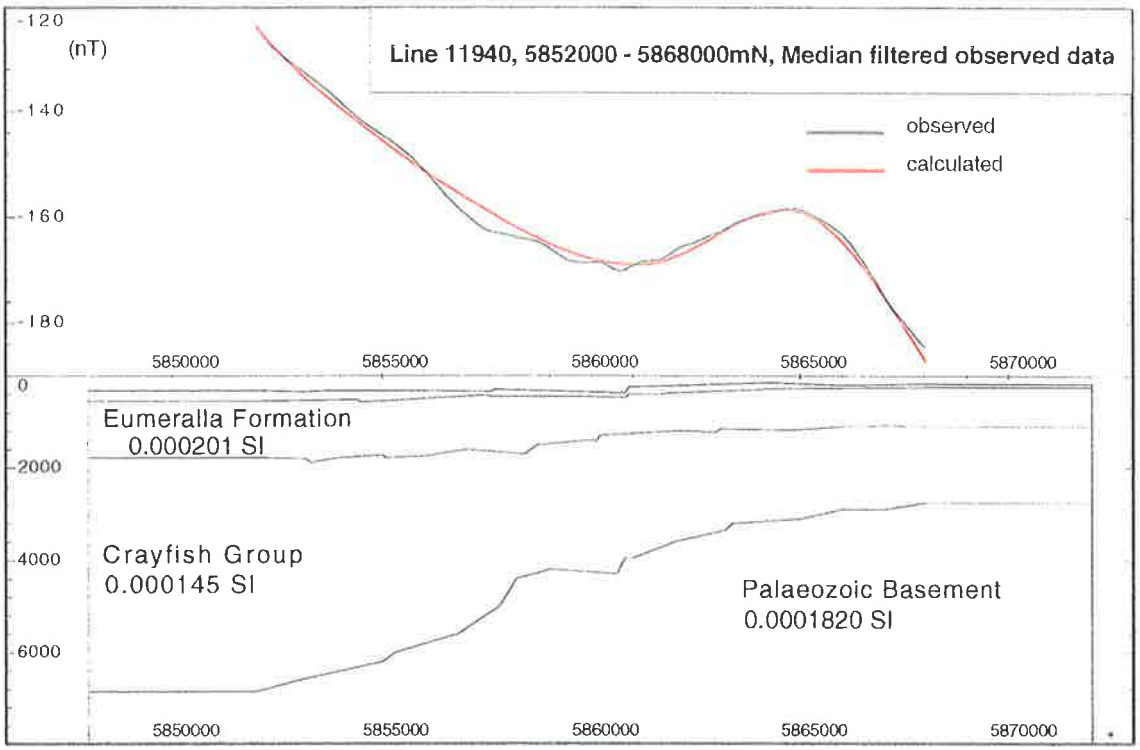

Fig. 5.2.5.1 Comparison of Observed and Theoretical Profiles

Unfaulted Layer model with standard formation susceptibilities

Deep basement bodies added to match regional

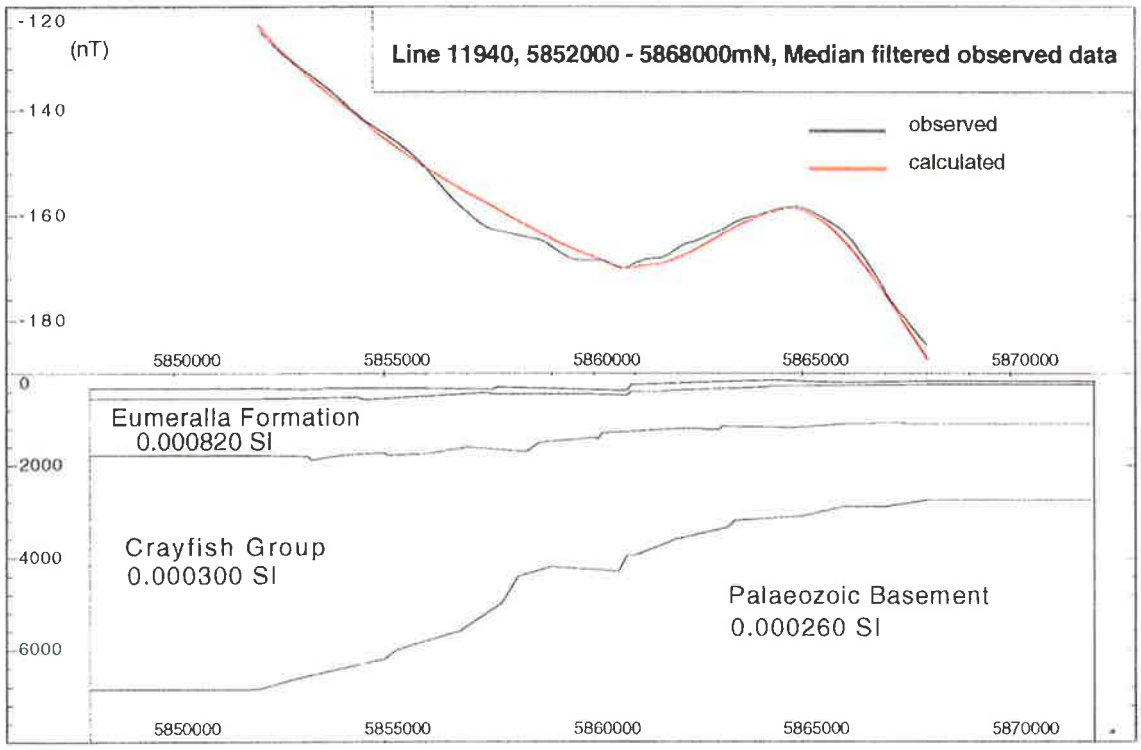

Fig. 5.2.5.2 Comparison of Observed and Theoretical Profiles

Unfaulted Layer model with maximum formation susceptibilities

intrusions. The formation bodies were assigned the susceptibilities used in fig. 5.2.2.6 while the bodies away from the profile that were used to generate the regional component were assigned arbitrary susceptibilities based on the range expected for igneous bodies. The anomaly centred at approximately 5864500mN was simulated by a body near the top of the basement section with a susceptibility of 0.02 S.I. units (not shown to avoid cluttering this and the subsequent figures). The observed profile has a number of shorter wavelength, low amplitude anomalies superimposed on the regional component which might be expected to result from shallow, intersedimentary sources, but it was necessary to use a median filter followed by a moving average filter to eliminate two cultural anomalies from the profile. Close examination of the calculated profile reveals a slight variation in the curvature of the profile around the largest fault offsets in the Sherbrook Group (approx. 5860700mN) but there is little evidence of any other small anomalies resulting from the fault offsets of the model. This is not unexpected because the largest anomaly on the original unfaulted Layer model profile (fig. 5.2.2.6) is 0.5 nT which is extremely subtle and difficult to detect given this regional gradient.

Fig. 5.2.5.2 uses the same unfaulted Layer model as the previous figure but the original susceptibility of each formation has been replaced by the maximum value measured in all wells for that particular formation. The Sherbrook Group body was assigned a susceptibility value of 0.00025 S.I. units while the other values are marked on the figure. Comparison of this figure with the previous one (fig. 5.2.5.1) shows a distinct change in the calculated profile over the fault offset at approximately 5860700mN and a more subtle change in curvature of the calculated profile at around 5861700mN. There also appears to be a very small change in the calculated profile at approximately 5857500mN. In fig. 5.2.5.2a the susceptibilities of the sedimentary formations were all set at the maximum Eumeralla Fm. value, 0.00082 S.I. units, in order to better define the subtle anomalies detected in the previous figure with the result that now the sedimentary section is effectively one large body. The most noticeable change in this figure is the anomaly over the fault offset at approximately 5860700mN which appears to have a greater amplitude and shorter wavelength than the observed anomaly. The subtle anomaly at around 5857500mN is more clearly resolved in this figure but the slight anomaly at approximately 5861700mN shows little change. Taken together, figs. 5.2.5.2 and 5.2.5.2a show that the last anomaly is probably the result of a fault offset in the Eumeralla Formation because in fig. 5.2.5.2 the Eumeralla susceptibility is

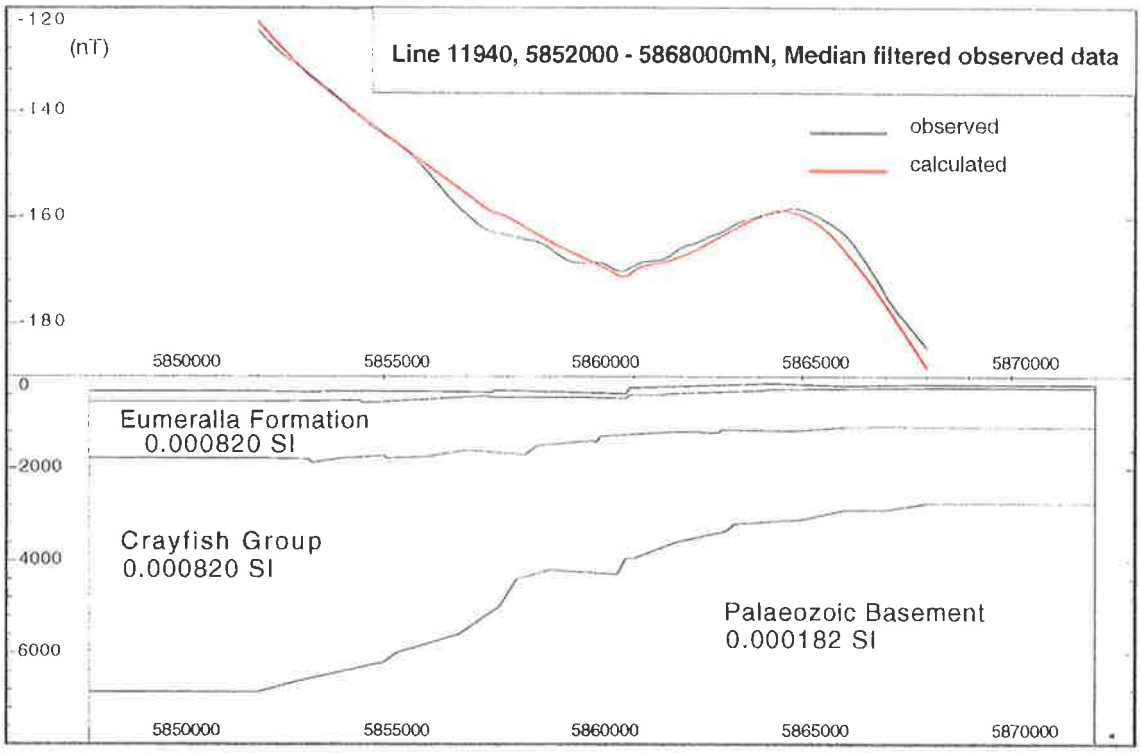

Fig. 5.2.5.2a Comparison of Observed and Theoretical Profiles

Unfaulted Layer model with maximum Eumeralla Fm. susceptibilities

Deep basement bodies added to match regional

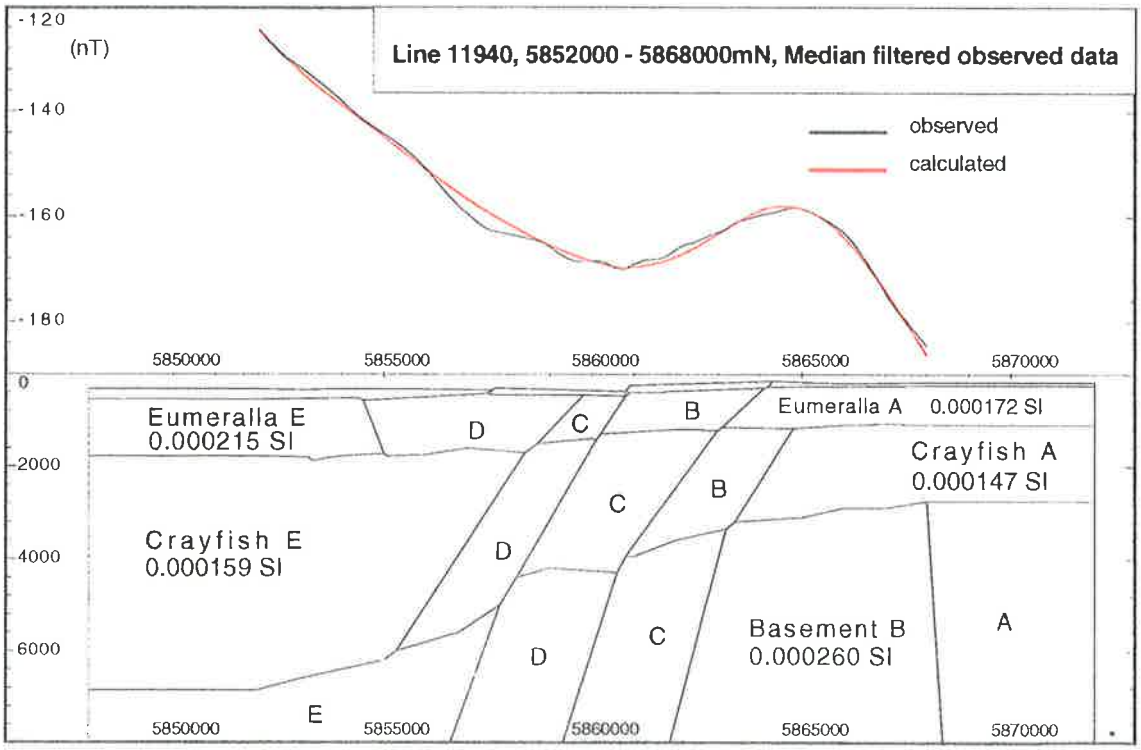

Fig. 5.2.5.3 Comparison of Observed and Theoretical Profiles

Faulted zone model with standard formation susceptibility range

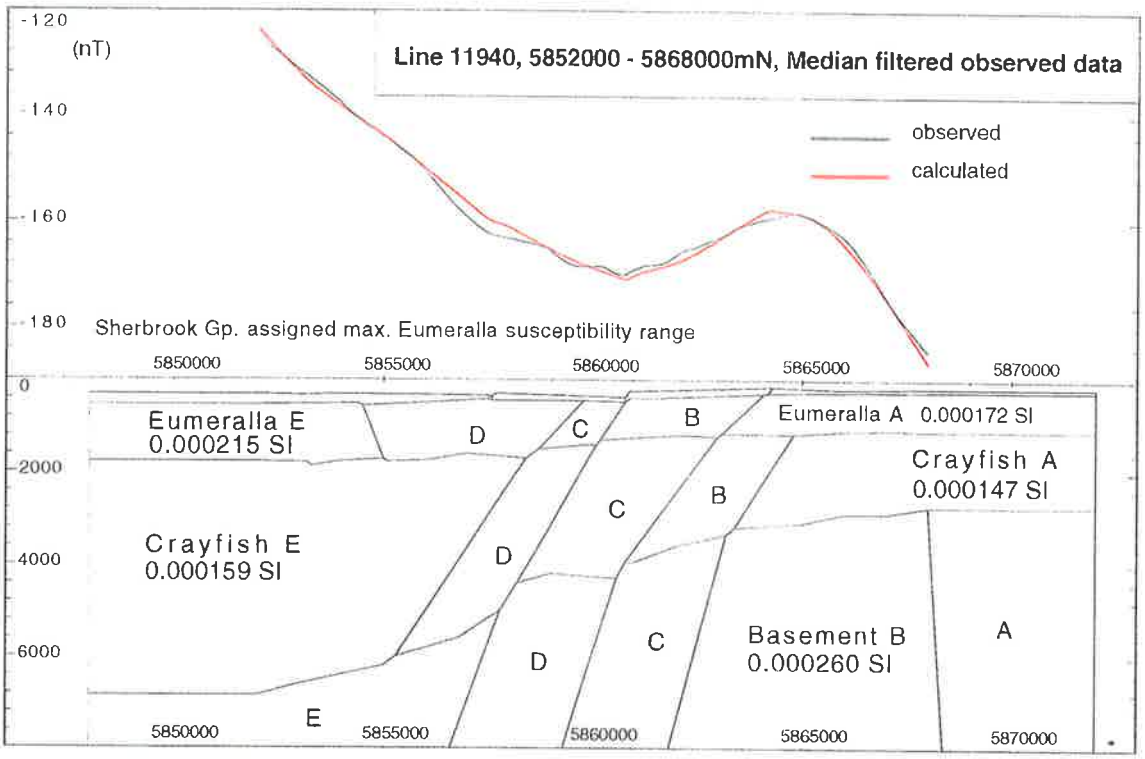

Fig. 5.2.5.3a Comparison of Observed and Theoretical Profiles

Faulted zone model with standard and Eumeralla susceptibility ranges

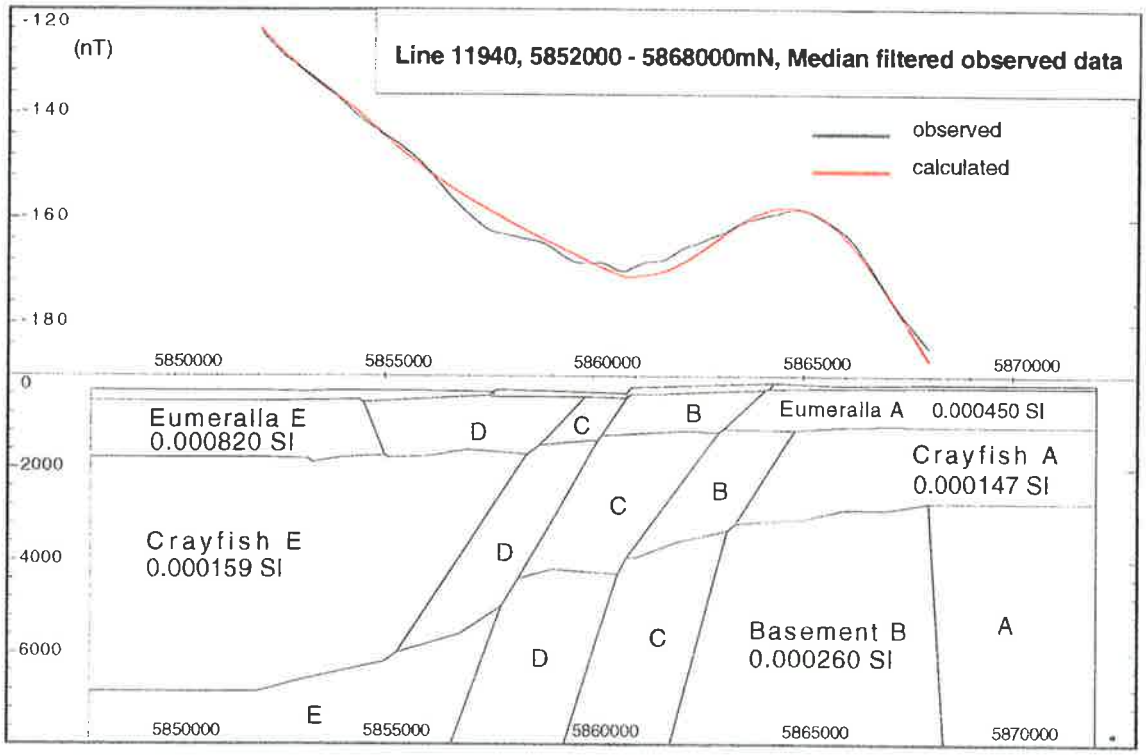

Fig. 5.2.5.3b Comparison of Observed and Theoretical Profiles

Faulted zone model with maximum Eumeralla susceptibility range

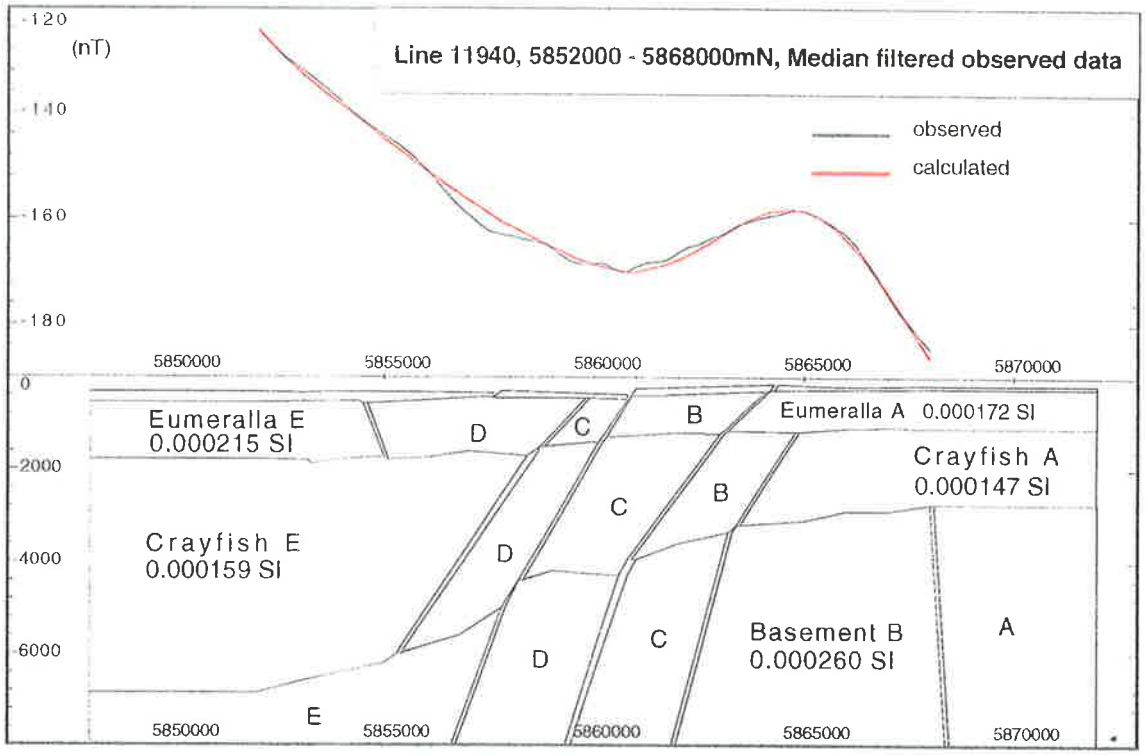

Fig. 5.2.5.4 Comparison of Observed and Theoretical Profiles

Demagnetised fault zone model with standard susceptibility range

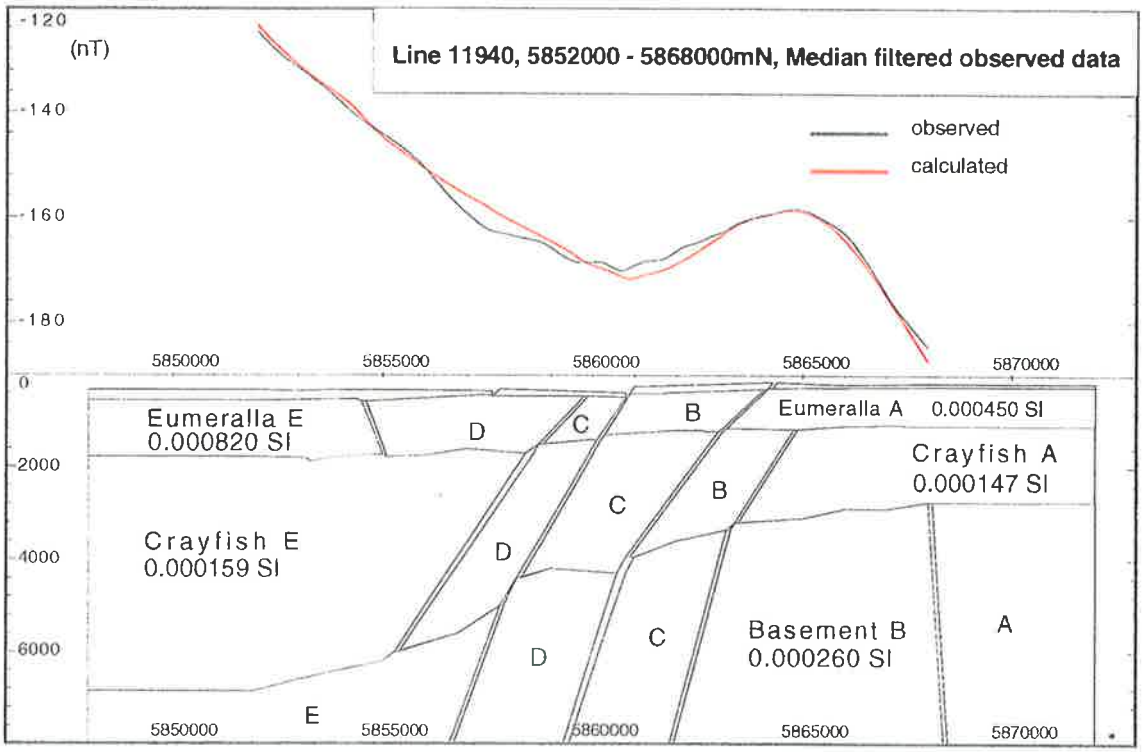

Fig. 5.2.5.4a Comparison of Observed and Theoretical Profiles

Demagnetised zone model with maximum Eumeralla susceptibility range

already set at 0.00082 S.I. units while the values for the other sediments are lower. The other two anomalies discussed are most likely the result of the Sherbrook Group fault offsets because they become more prominent when the susceptibility is increased to the relatively high Eumeralla value. These figures also suggest that the observed anomalies are the result of sources deeper than the Sherbrook Group because of their longer wavelength than anomalies produced by the Sherbrook model.

The calculated profile in fig. 5.2.5.3 is generated by the Faulted Layer model and, apart from the slightly lower amplitude over Eumeralla C and B and slightly higher amplitude over Basement B, the shape of the profile is very similar to that from fig. 5.2.5.1 while the only evidence of any subtle anomalies is a very slight, positive change in curvature over the fault between Sherbrook A and B. The calculated profile has a slightly lower amplitude over Eumeralla C and D because these bodies were assigned lower susceptibilities than the value used in fig. 5.2.5.1 and the amplitude is higher over Basement B again because of the difference between assigned values (see table 5.2.3.1).

Fig. 5.2.5.3a shows the result of assigning the maximum Eumeralla Fm. susceptibility range to the Sherbrook Group bodies. The anomaly over the fault between Sherbrook A and B is more prominent on this profile than in the previous figure (5.2.5.3) as is the fault between Sherbrook B and C while the fault between Sherbrook C and D also produces a small anomaly with a similar amplitude and wavelength to the other susceptibility contrasts. In fig. 5.2.5.3b the maximum Eumeralla Fm. susceptibility range was assigned to the Eumeralla Formation bodies themselves with the result that the small, narrow wavelength anomalies seen in the previous profile have disappeared. The fault between Eumeralla B and C generates a subtle, relatively long wavelength anomaly that appears to have a similar amplitude to the anomaly generated by the Sherbrook fault while the fault between Eumeralla D and E produces an anomaly that is even more subtle and longer in wavelength than that previously discussed, presumably because of the greater depth to the top of the susceptibility contrast. These profiles suggest that if the observed anomalies are the result of fault-induced susceptibility contrasts then the sources should generally be deeper than the Sherbrook Group but the longest wavelength features do not result from Crayfish Group contrasts because their wavelengths are too short. Thus the sources are likely to be within the Eumeralla Formation although not necessarily near the top of the formation.

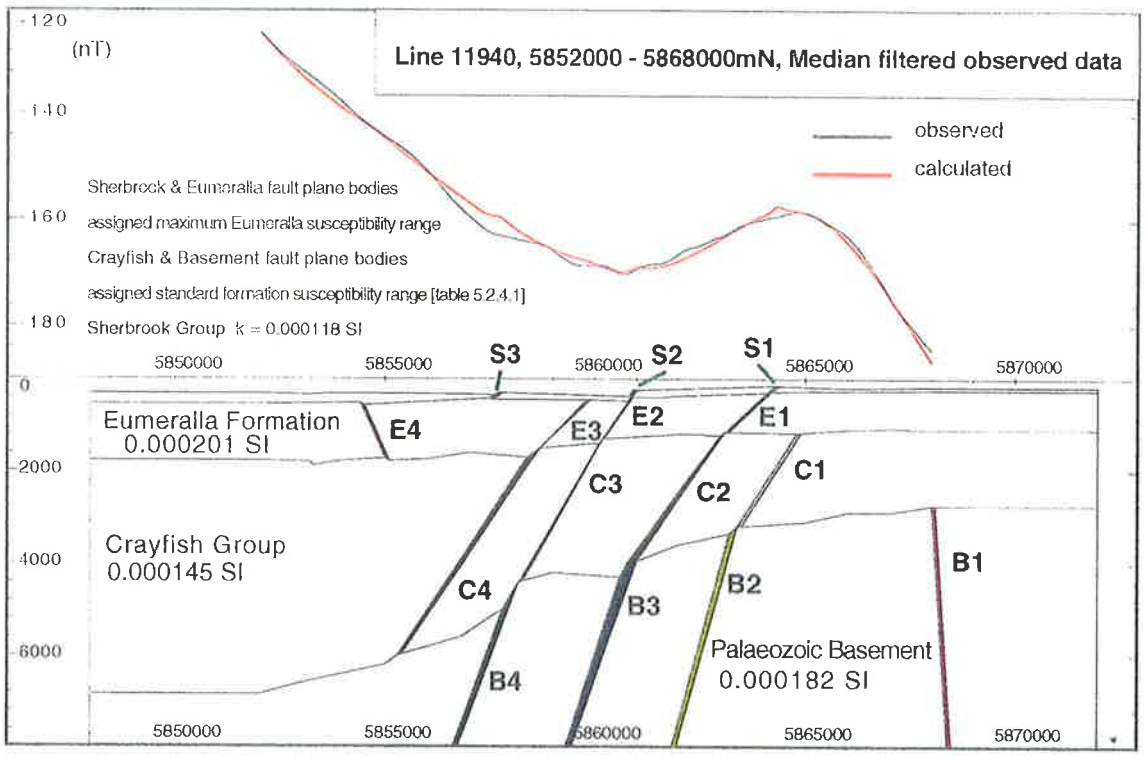

Fig. 5.2.5.5 Comparison of Observed and Theoretical Profiles

Fault plane model with standard and Eumeralla Fm. susceptibility ranges assigned to dyke-like bodies

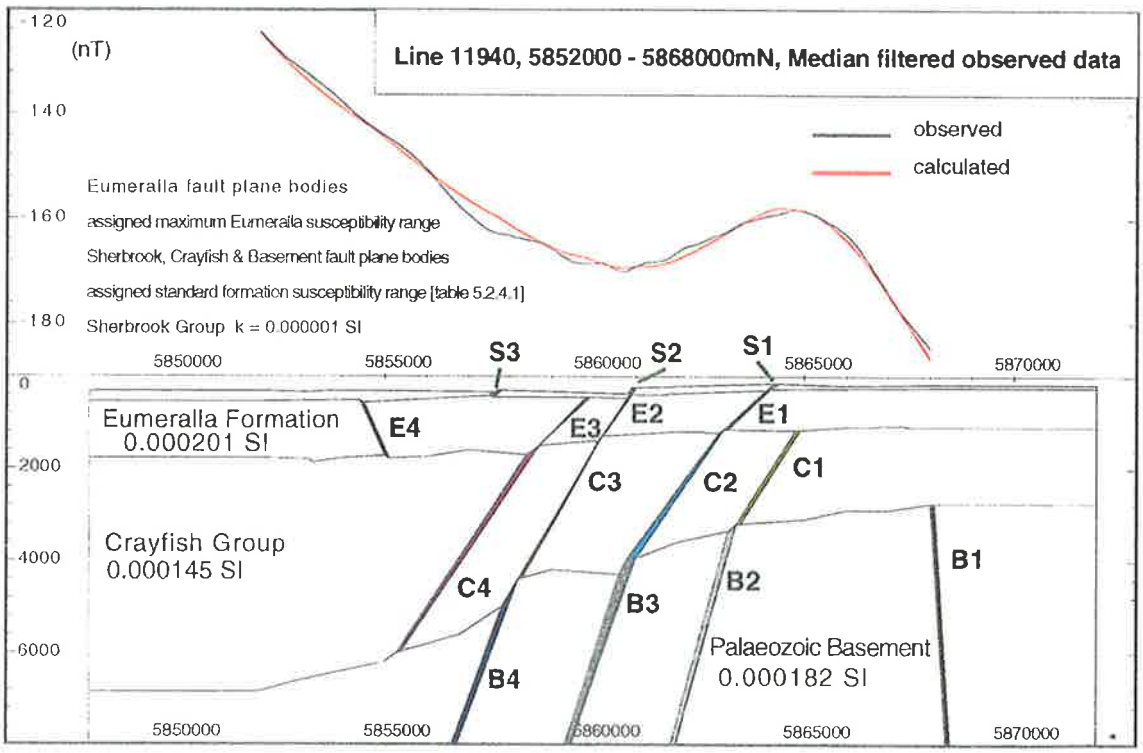

Fig. 5.2.5.5a Comparison of Observed and Theoretical Profiles

Fault plane model with maximum Eumeralla Fm. susceptibility ranges

Comparison of fig. 5.2.5.4 which is generated by the Fault Zone model, with fig. 5.2.5.3 (generated by the Faulted Layer model) reveals the very slight, negative change in curvature that occurs over the fault zone between Sherbrook A and B and a similar subtle feature over the fault zone between Sherbrook and Eumeralla B and C. The calculated profile shown in fig. 5.2.5.4a is similar to that in fig. 5.2.5.3b but with a slightly larger amplitude, negative anomaly over the Eumeralla B and C fault zone and a similar change to the anomaly over the Eumeralla D and E fault zone. In addition, the Eumeralla C and D, and A and B fault zones both generate small anomalies that resemble the observed anomalies, having a similar wavelength but a lower amplitude.

The calculated profile shown in fig. 5.2.5.5 (from the Fault Plane model) has the same overall shape as the calculated profile in fig. 5.2.5.1 because the background bodies have the same susceptibilities. The prominent short wavelength anomalies result from the Sherbrook Group fault plane bodies while the two Eumeralla Formation bodies (3 & 4) appear to have generated longer wavelength, low amplitude features that bear some resemblance to the observed anomalies. Both the Sherbrook Group and Eumeralla Formation fault plane bodies were assigned the maximum Eumeralla susceptibility range in this model and the result is that the shallow bodies produce the short wavelength anomalies shown in the figure. In fig. 5.2.5.5a both the Sherbrook Group background body and the fault plane bodies were given the low background susceptibility values from table 5.2.4.1 in an attempt to isolate the effect of the Eumeralla fault plane bodies. The calculated profile still shows the influence of Eumeralla 3 and 4, as expected, but the short wavelength anomalies over Sherbrook 1 and 2 have disappeared and the anomalies due to Eumeralla 1 and 2 are very subtle with the change in curvature over Eumeralla 1 being the most noticeable.

The comparison of the calculated and observed profiles in this section strongly suggests that, if the faults are involved in generating the observed anomalies, then there are more faults that have a significant influence than just the major ones identified from the seismic horizon maps, because there are more anomalies than can be accounted for from these and also only some of the major faults coincide with observed anomalies. It is also likely that no single mechanism is responsible for all the observed anomalies because some of the anomalies seem to result from a demagnetised fault zone which causes a negative anomaly while others show a more positive response indicative of fault plane bodies or possibly the susceptibility contrast between adjacent fault-bounded blocks.

5.2.6 Discussion

The previous sections of this chapter have shown that the anomalies generated by bodies that have been assigned the average of susceptibilities measured in cores, are all less than 1.0 nT while some anomalies, particularly those of Crayfish Group bodies, are around 0.1 nT in amplitude. The specifications of the aeromagnetic survey required a noise envelope of 0.2 nT which implies that any anomaly 0.2 nT or less could be considered noise. Another factor determining whether an anomaly is likely to be detectable is its wavelength (or alternately the halfwidth) where a body that generates a low amplitude (greater than the noise envelope), short wavelength anomaly is more likely to be detected than a body that produces an anomaly that is larger in amplitude but has a long wavelength. For example, a body generating an anomaly with a wavelength of 10 km and an amplitude of 2 nT would be difficult to detect, especially if there is a substantial regional component due to basement bodies in the observed data, when compared with bodies that generate an anomaly of 1 nT but with a wavelength of 1 km, because the narrower anomaly will be prominent against the regional trend while the long wavelength anomaly will merge with it.

Another important factor to be considered in discussing the detectability of bodies producing these kinds of anomalies is the extent to which similar anomalies occur on adjacent flightlines. Anomalies associated with fault offsets, low susceptibility fault zones or fault plane bodies tend to be linear and can extend across a number of flightlines. For this reason, quite subtle anomalies can be identified because they are part of a noticeable trend of similar features on adjacent lines while an identical anomaly that only occurs on one line is more likely to be considered noise and ignored. Sometimes it will be possible to identify long wavelength anomalies from their influence on the adjacent lines but this will depend on how long the wavelength is and whether this is substantially different from the regional component.

The anomalies produced by fault plane bodies and low susceptibility fault zones are relatively narrow (short wavelength), especially where the bodies or zones are shallow, which causes some difficulty in separating these from cultural anomalies. Where a relatively wide, negative anomaly exists, this implies that the source body is either wide with a low or zero magnetic mineral content compared to the background, or is narrow and comparatively deep with a reversed polarity remanence component (high Koenigsberger ratio). A wide positive

anomaly is either caused by a wide shallow body or a deeper, narrower body so other evidence must be used to constrain any models (although the shape of an isolated anomaly may be indicative of the source geometry).

The results of the theoretical modelling in this chapter were used in Chapter 8 to assist in the construction of the models, especially of the intersedimentary bodies. It was found that the fault plane bodies and low susceptibility fault zones were the most likely sources of the short wavelength anomalies while the offset horizons and varying susceptibility between fault blocks was found to generate too small an anomaly to explain the features in the Penola Trough.

Chapter 6

Introduction

This chapter discusses depth-to-magnetic-source estimates for the study area made by the author and Cowan Geodata Services. The spectral analysis of gridded data and the use of Automag© on line data was undertaken using methods developed by Dr. Irena Kivior and Dr Zhiqun Shi, and using software created by Dr. Shi at the University of Adelaide. Cowan Geodata Services used proprietary software to find Euler Deconvolution solutions on gridded data, and this data was supplied to the author by MESA.

6.1 Spectral Analysis

Spectral analysis of gridded data can be used to obtain estimates of the average depth-to-the-top of various anomalies. The method is based on that developed by Spector and Grant (1970) which utilises the magnetic response of an ensemble of vertical-sided prisms. After transforming gridded data from a specified region to the frequency domain, the natural logarithm of the radial-averaged power spectrum is plotted against wavenumber (in cycles/km). Regression lines are then fitted to the linear segments of the curve and the slopes of the lines are used to calculate an average depth corresponding to the relevant segment by the use of,

$$Depth = -Slope / 4\pi$$

This method yields an estimate for each segment which should be the average depth to the top of the ensemble. By this method the depths of those sources which appear superimposed on the TMI map can be separated, however, the most reliable results can be obtained when the region is restricted to one magnetic province, otherwise the results can yield average depths that are unrelated to any of the provinces (Kivior, 1996).

It has been found that the size of grid used should be at least twice the expected depth to the top of the anomaly and should cover as much of the anomaly as possible. Spectral analysis depth estimates are most accurate for bodies which approximate the

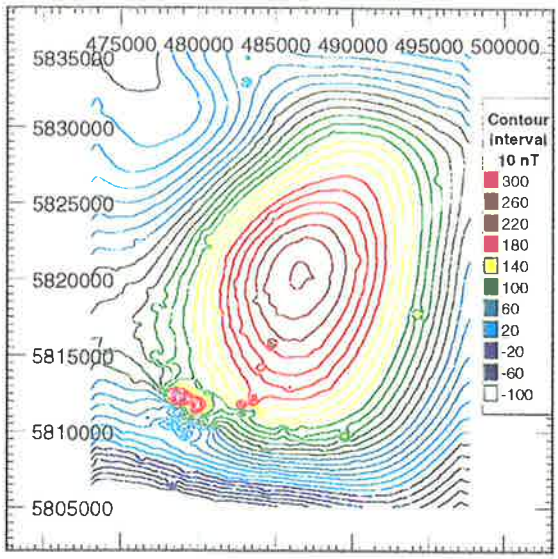

Fig. 6.1.1.1 Mt Gambier Anomaly
473100-497700mE, 5805000-5835000mN
Scale = 1:1,000,000

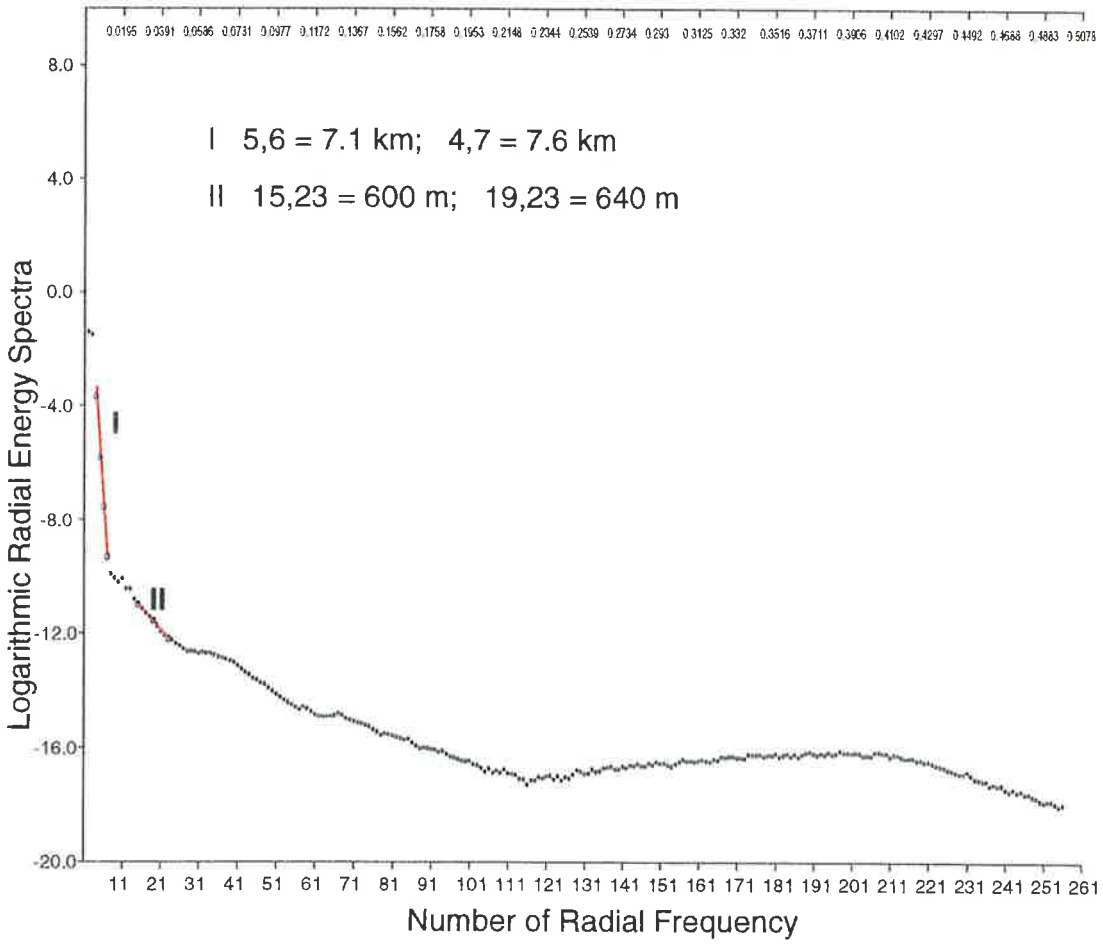

Fig. 6.1.1.2 Mt. Gambier Anomaly Energy Spectra

vertical-sided prisms that the method is based on and are most unreliable for narrow, linear bodies (Kivior, pers. comm., 1996). Dr. Kivior helped select the points on the energy spectra used for the depth calculations in section 6.1.

The grid spacing used on the data from the MESA survey (see Plate 1) was 100 × 100 m and the area was divided into a number of grids, some overlapping and some subsets of larger regions. Most of the regions for which power spectra were calculated were centred on some anomaly discerned from the TMI image and contour maps but with a small number centred on basement highs determined from depth-converted seismic horizon maps. Some of the important anomalies extend outside the study area while there are other nearby anomalies which affect the regional component of the magnetic field in the study area. In order to cover as much of these anomalies as possible, it was necessary to use gridded data generated from the 1992 AGSO Penola 1:250,000 sheet regional aeromagnetic survey. The flight line spacing of the AGSO data was 1.5 km so the grid spacing used on this data was 500 × 500 m.

Anomaly Studies

6.1.1 Mt. Gambier Anomaly

The most important anomaly in the study area, as far as depth estimates are concerned, is the large semi-elliptical anomaly (approximately 400 nT in amplitude) northeast of Mt. Gambier which is interpreted to be caused by the magma chamber that fed the surface volcanics (Plate 1). Depth to basement estimates from seismic sections only exist for the northeastern corner of the anomaly. Seismic resolution over the rest of the anomaly and south to the coast is poor because of the karstic nature of the overlying Mt. Gambier Limestone which outcrops in this area. The seismic data shows that the basement is sloping down from around 2.5 km northwest of the anomaly to over 5.5 km deep east of the centre of the anomaly.

The grid used to calculate depth estimates over this large anomaly was 24 km wide, because this is the width of the study area in the region (from 473100 to 497700 Easting), and 30 km long (5805000-5835000mN). This covers the large anomaly completely and partly covers the smaller anomaly to the northwest (fig. 6.1.1.1). The spectrum shows a discernible linear trend (fig. 6.1.1.2) associated with the long wavelength (and therefore,

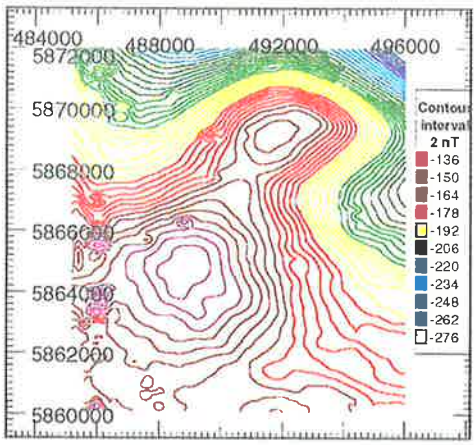

Fig. 6.1.2.1 Northeast Penola Trough Anomalies

485000-496000mE, 5860000-5872000mN

Scale = 1:250,000

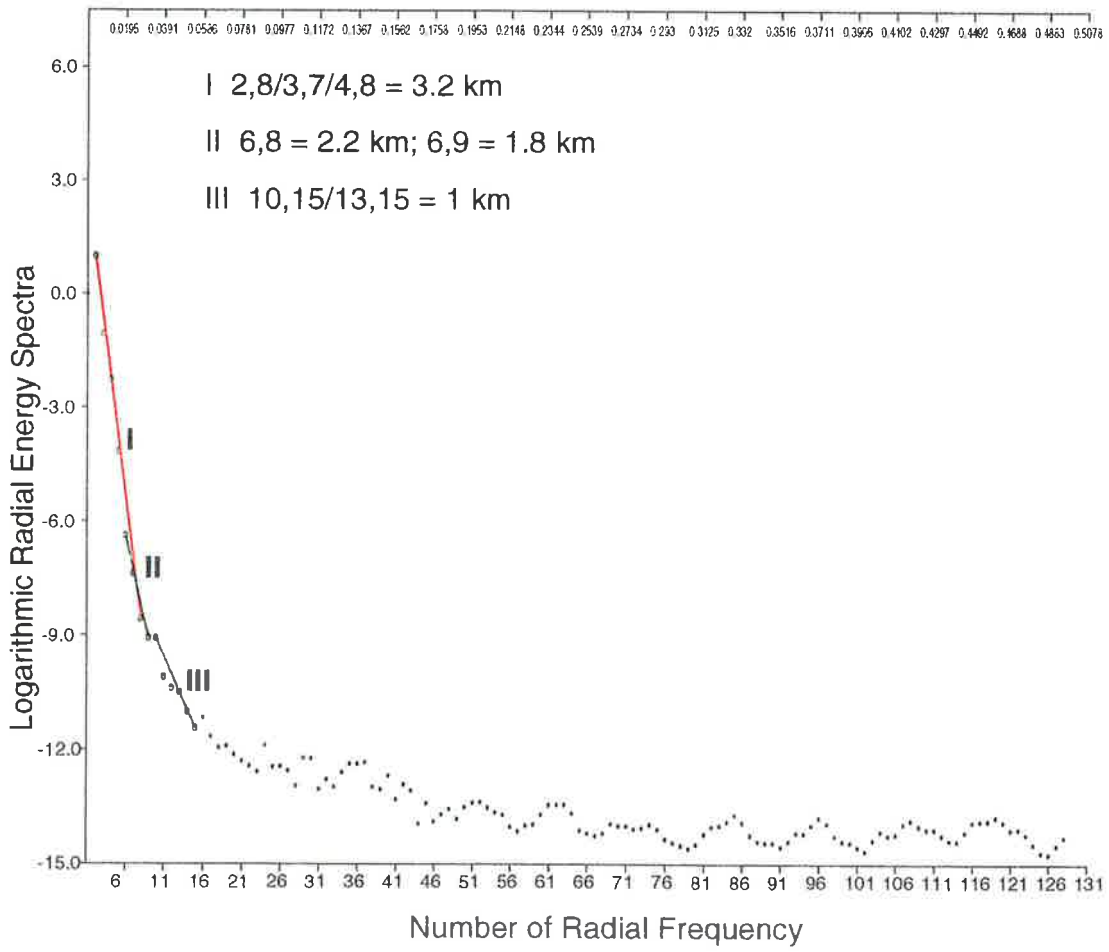

Fig. 6.1.2.2 Northeast Penola Trough Energy Spectra

deepest) anomaly, with depth estimates of 7.1 (points 5 & 6) and 7.6 km (points 4 & 7). These estimates suggest that the probable magma chamber is entirely within basement, however, because there is no seismic control on the southern side of the anomaly, it is not possible to exclude emplacement within the sedimentary section south of the Tartwaup Fault Zone where depth to basement is unknown. Segment II yields depths of 0.61 and 0.64 km (from points 15 & 23 and 19 & 23, respectively) which may represent sources at or near the top of the Late Cretaceous / base of the Tertiary section in the northern part of the grid or, alternatively, represent sources within the feeder system for the Mt Gambier volcanic complex.

6.1.2 Northeast Penola Trough Anomalies

These two anomalies have much lower amplitudes than the Mt Gambier Anomaly (around 30 and 15 nT) and occur in part of the study area that is magnetically low. The southern of the two anomalies (Sawpit Anomaly) is close to the Sawpit basement high while the northeastern anomaly (Penola North Anomaly) does not appear to directly correspond to a major feature mapped by seismic. The grid used for the depth to basement calculation covers the area from 485000 to 496000mE and 5860000 to 5872000mN, producing an 11 × 12 km dataset which includes both anomalies (fig. 6.1.2.1).

The spectrum (fig. 6.1.2.2) shows two or possibly three linear segments (I, II and III) corresponding to depths within and at the top of basement, and possibly within the sedimentary section. Segment I corresponds to a depth of approximately 3.2 km which is calculated using points 2 & 8, 3 & 7, and 4 & 8. Segment II gives a depth of 2.2 or 1.8 km which comes from points 6 & 8 and 6 & 9 respectively. A depth of approximately 1 km is obtained from segment III using points 13 & 15 or alternately 10 & 15.

The seismic coverage of this area is reasonable to excellent because it includes the Penola 3-D seismic survey, as well as 2-D seismic lines spaced approximately 1 km apart in the southern section of the grid. The seismic evidence shows that the basement is deepening generally across the grid with the shallowest at around 2.1 km in the northeast to greater than 4 km in the southwest corner. The southern anomaly does not exactly coincide with the Sawpit High which has been defined from seismic. The centre of the anomaly is offset to the

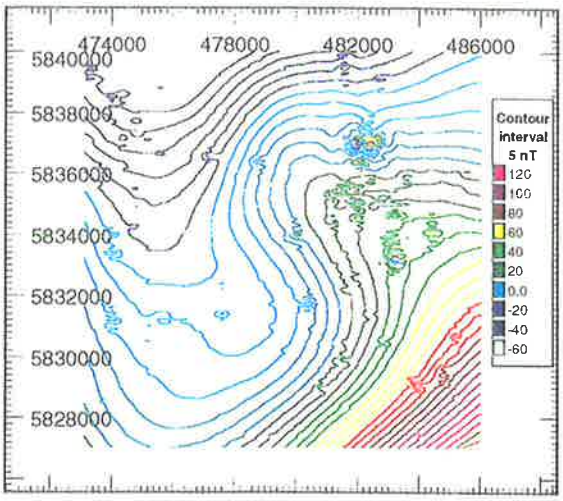

Fig. 6.1.3.1 Kalangadoo High Anomaly

473000-486000mE, 5827000-5840000mN

Scale = 1:250,000

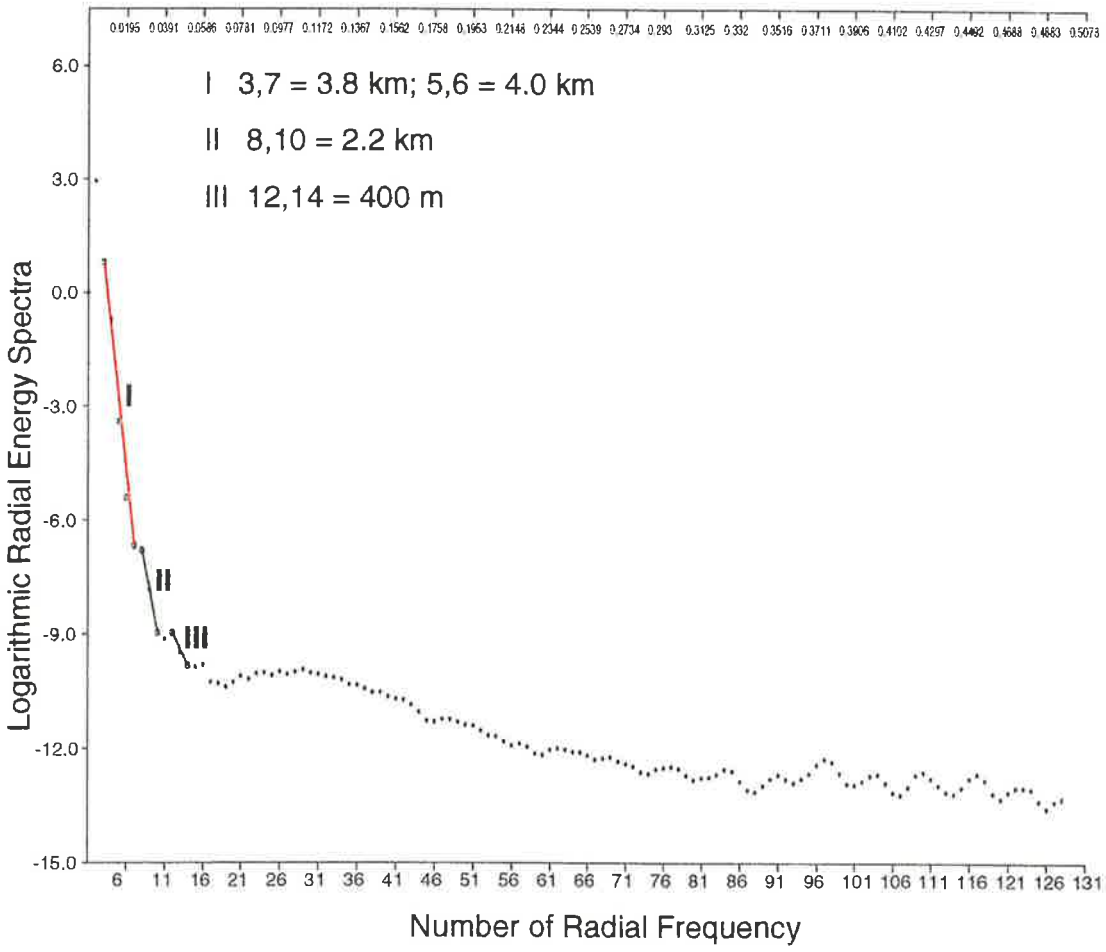

Fig. 6.1.3.2 Kalangadoo High Anomaly Energy Spectra

south and is over a section of basement that is between 3 and 3.2 km deep, which suggests a relationship between this and the depth revealed by segment I.

The northeastern anomaly is over a fault bounded section of basement that ranges from 1.5 to 1.8 km deep. As segment II corresponds to a depth of 2.2 km this suggests that the magnetic source is either below or close to the basement/sedimentary interface. It is possible, although less likely that the source is a highly magnetic sedimentary layer (Casterton Fm) at the base of the sedimentary section. Segment III is based on only a few points so the depth estimate may not be very reliable, but the depth of 1 km could related to sources generating the linear anomalies which strike WNW-ESE across the gridded section. If this depth is to be believed then the source(s) lies near the base of the Eumeralla Formation, however, it has previously been noted that narrow, linear anomalies do not yield very accurate depth estimates.

6.1.3 Kalangadoo High Anomaly

This anomaly is semi-elliptical in shape and is located to the north-northwest of the Mt. Gambier Anomaly. The grid used for the spectral analysis of this anomaly covers the area from 473100 to 486000mE and 5827000 to 5840000mN (fig. 6.1.3.1). The seismic data, while much less closely spaced than over the Penola Trough (four lines), shows that the Kalangadoo Fault Zone crosses the northeastern corner of the grid while the basement slopes down to the southeast from the Kalangadoo High (at Kalangadoo 1) in the northwest corner of the grid, while basement has not been resolved in the southwestern corner.

The spectrum (fig. 6.1.3.2) shows two or possibly three segments, with segment I corresponding to a depth of 3.8 (points 3 & 7) or 4.0 km (points 5 & 6), while segment II gives a depth of 2.2 km (points 8 & 10). If segment III is reliable then the depth calculated for this is 400 m (points 12 & 14). The anomaly partly overlies the Kalangadoo Fault Zone where the seismically determined basement falls from 2.5-3 km down to around 4.5 km which would place the source of the anomaly as determined from segment I below the top of basement south of the fault zone but at the top of basement within the fault zone.

The depth from segment II could represent a source beneath the Kalangadoo High which is around 2.2 km deep in the northwest corner of the grid. Alternatively, it might result from a source at the Crayfish Group / Eumeralla Formation boundary which is approximately 2.2 km deep over the Kalangadoo Fault Zone in the centre of the gridded area. The reliability

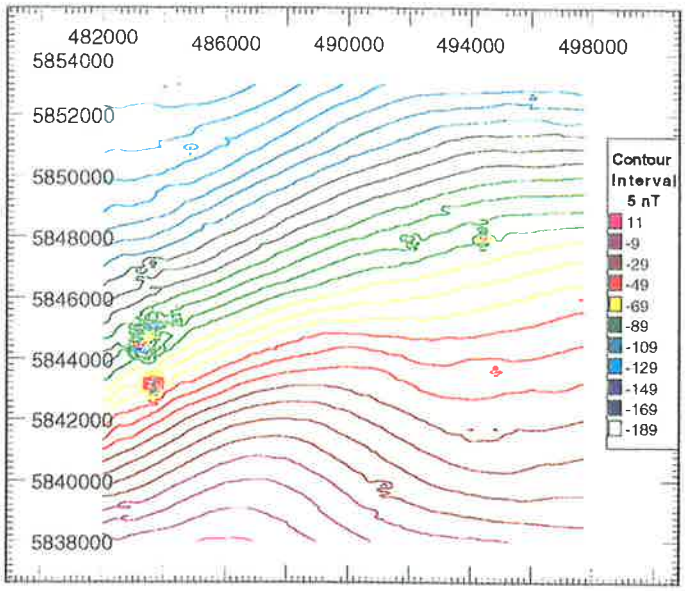

Fig. 6.1.4.1 Mid-Penola Trough Anomaly

482000-497000mE, 5838000-5853000mN

Scale = 1:250,000

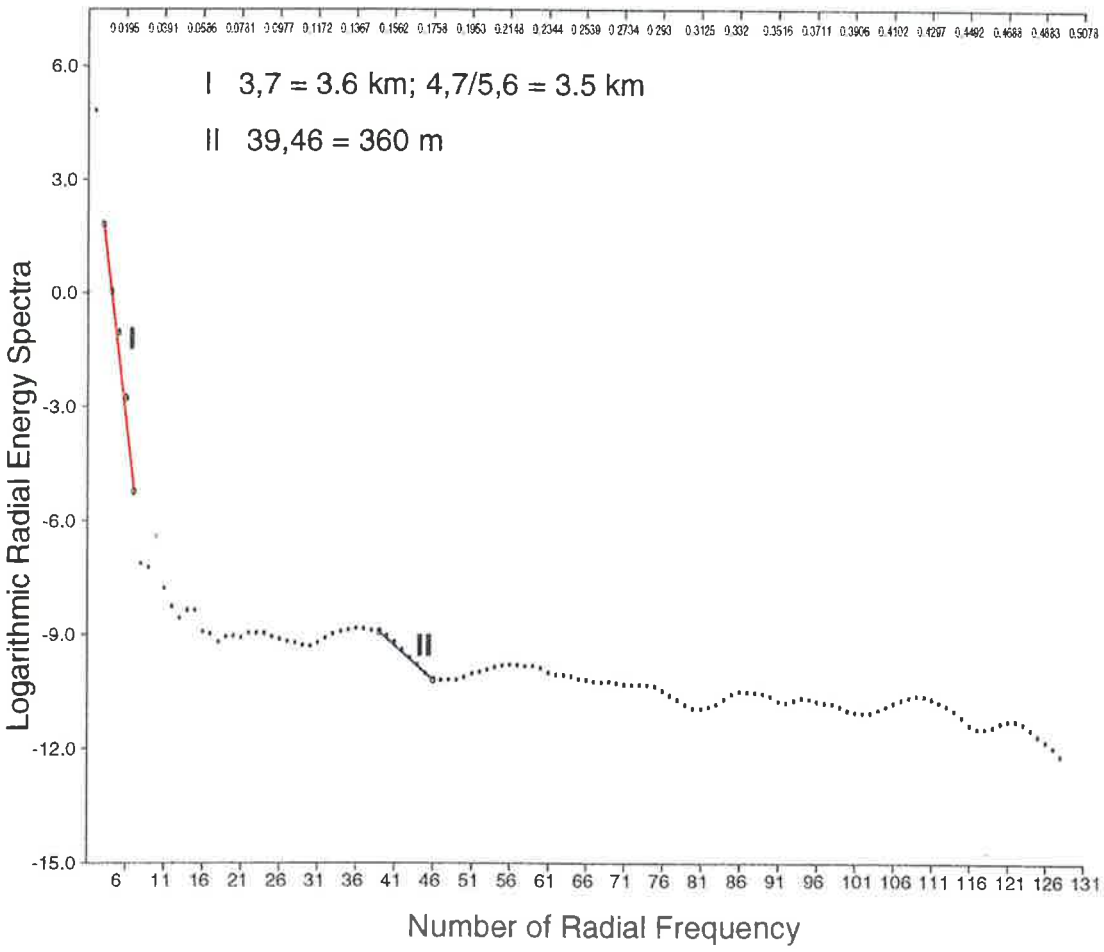

Fig. 6.1.4.2 Mid-Penola Trough Anomaly Energy Spectra

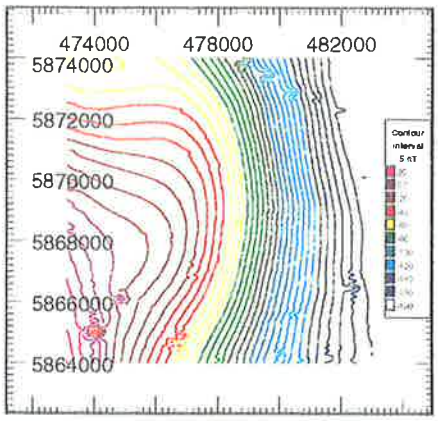

Fig. 6.1.5.1 Northwest Penola Trough Anomaly

473100-483000mE, 5864000-5874000mN

Scale = 1:250,000

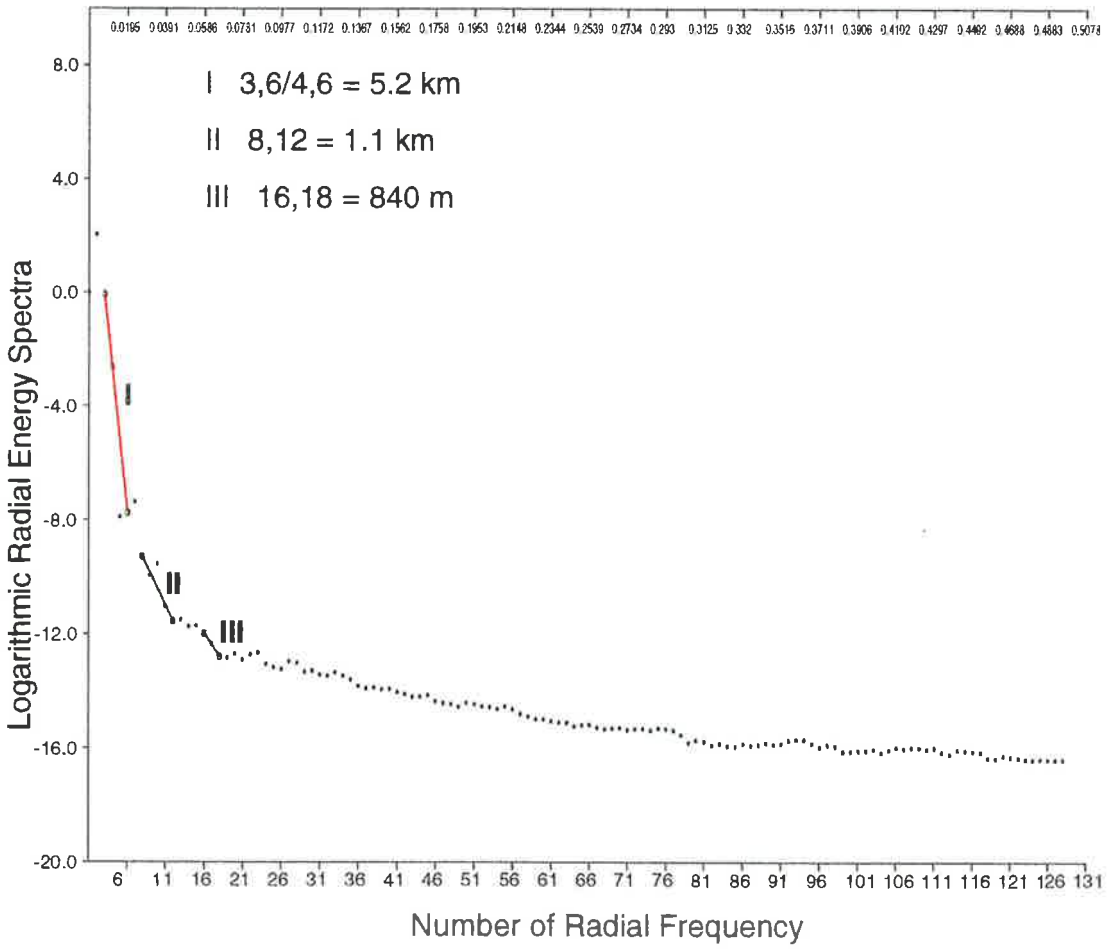

Fig. 6.1.5.2 NW Penola Trough Anomaly Energy Spectra

of the segment III estimate is suspect not only because it is based on three points, but also because four hundred metres is the original line spacing and so a depth of 400 m may represent a processing artifact. If this depth estimate is reliable then it may result from a source at the base of the Tertiary or top of the Late Cretaceous Sherbrook Group.

6.1.4 Mid-Penola Trough Anomaly

This grid is over the area immediately to the northeast of the Kalangadoo High Anomaly but is on the northern side of the Kalangadoo Fault Zone and in the middle of the study area. The anomaly is generally over a basement high on the southern margin of the Penola Trough but the grid used covers the area from 482000 to 497700mE and 5838000 to 5853000mN (fig. 6.1.4.1). The seismic coverage ranges from reasonable in the northwest corner of the grid to very sparse in the east and southeastern margin. The gridded area, from seismic evidence, covers a small part of the Kalangadoo Fault Zone in the southwest corner, the previously mentioned basement high and a deep part of the Penola Trough (approx. 6 km deep).

The spectrum shows a clearly defined long wavelength trend which is designated segment I while a much shorter wavelength trend, segment II, has been tentatively identified (fig. 6.1.4.2). Segment I corresponds to a depth of 3.6 (points 3 & 7) or 3.5 km (points 4 & 7 and 5 & 6) while segment II could represent a depth of 0.36 km The three seismic lines which cross the basement high found the depth to the shallowest part was 3.6 to 3.7 km which is in reasonable agreement with the depth from spectral analysis. In section 6.1.3 there was a discussion of the reliability of depth estimates in the vicinity of 400 m and this may apply to the depth calculated from segment II. However, if this depth is reasonable then the source is within the Tertiary section because the top of the Late Cretaceous Sherbrook Group ranges from 400 m down to 700m deep.

6.1.5 Northwest Penola Trough Anomaly

This anomaly is found on the northwestern edge of the study area (fig. 6.1.5.1) and is northeast of the broad magnetic high that underlies Laira 1 and Zema 1 (the western extension of P1). The grid used covers the anomaly and a small part of the adjacent magnetic low with the boundary coordinates of 473100 to 483000mE and 5864000 to 5874000mN. Seismic coverage is better than the two previous anomalies but not as good as the coverage

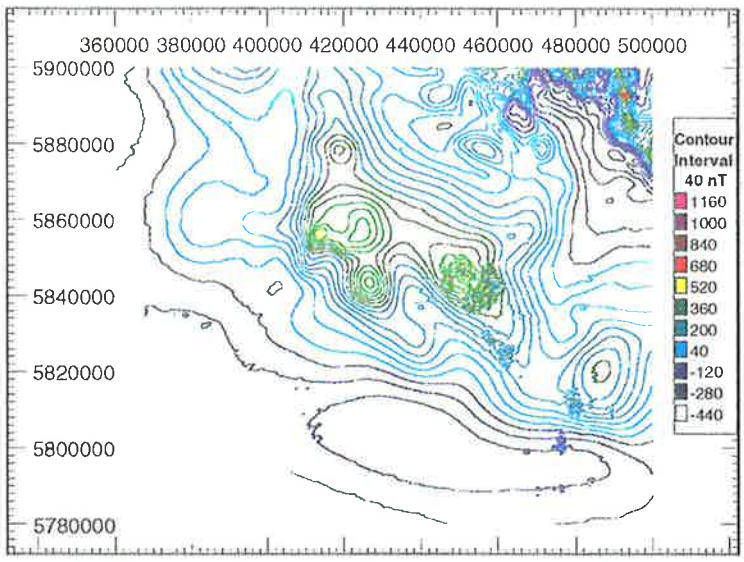

Fig. 6.1.6.1 Penola 1:250,000 sheet, (AGSO data)

360000-500000mE, 5780000-5900000mN

Scale = 1:2,000,000

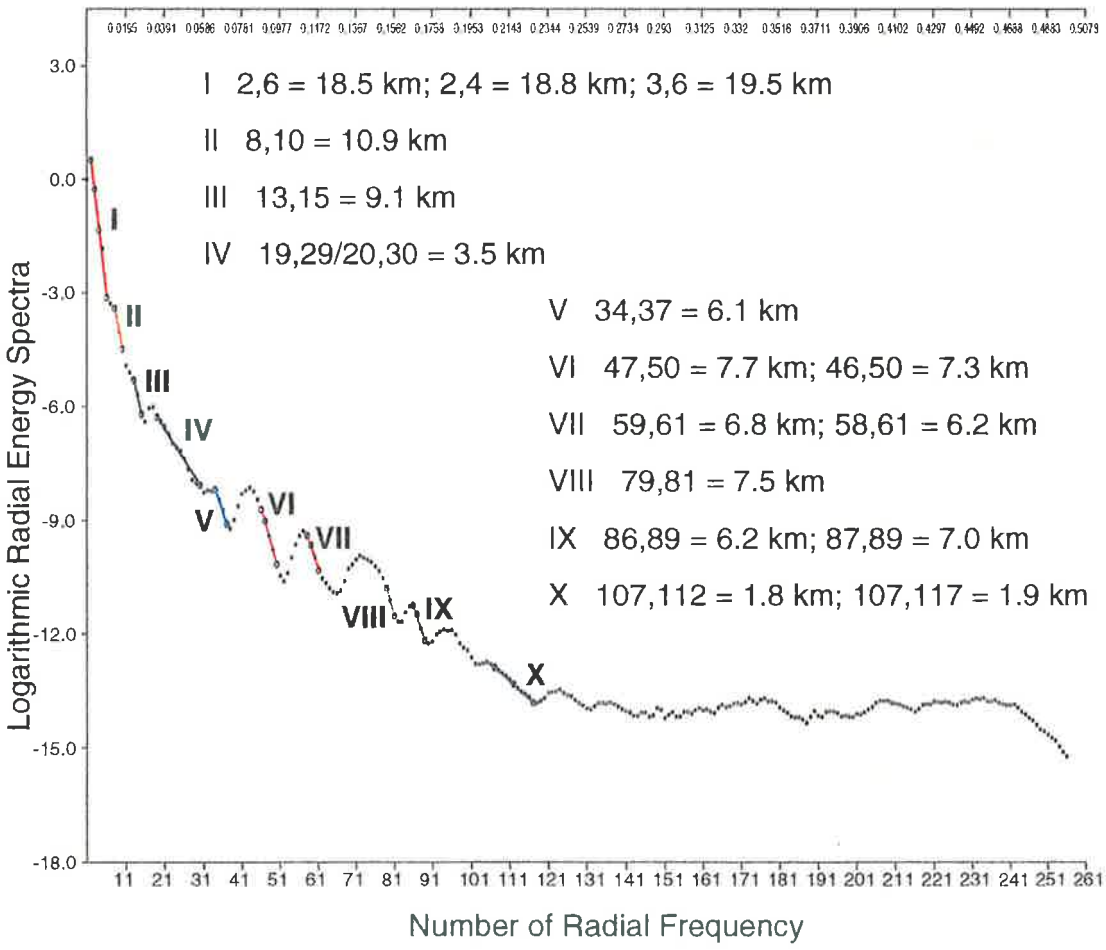

Fig. 6.1.6.2 Penola 1:250,000 sheet Energy Spectra

over the northern Penola Trough anomalies. The basement, from seismic data, is shallowest along the northern margin of the gridded area and increases in depth to the south, reaching the deepest point for this area in the southwestern corner.

The spectrum shows two major trends (fig. 6.1.5.2) with the long wavelength part designated segment I and the shorter wavelength part poorly defined but tentatively divided into segments II and III. Segment I yields a depth of 5.2 km (from points 3 & 6 and 4 & 6) which the seismic evidence suggests is well below top of the basement which ranges from 2.5 to 4.5 km in depth over the gridded section. Segment II yields a depth of 1.1 km (points 8 & 12) while segment III gives a depth of 0.84 km (points 16 & 18). If these estimates are reliable then the likely sources are near the base of the Eumeralla Formation which slopes down from 1.1 to 1.7 km deep within the gridded area.

6.1.6 Penola 1:250,000 sheet, AGSO data

The entire AGSO dataset was gridded at 500 m grid spacing and this used to calculate depth estimates. The boundaries of the grid are 360000 to 500000mE and 5780000 to 5920000mN (fig. 6.1.6.1). The seismic coverage of the Penola sheet ranges from good in parts of the Penola and Robe Troughs, to poor over parts of the Tantanoola Trough/Kalangadoo High and the area around Mt Gambier including the section offshore to the south. The northeast corner of the dataset covers the Kanawinka Fault Zone and the Padthaway Ridge where practically no seismic coverage exists but the pre-Mesozoic basement is very shallow.

The spectrum (fig. 6.1.6.2) shows a number of linear trends, some of which are repeated, which are labelled segments I to X. Segment I yields depths of 18.5 (from points 2 & 6), 18.8 (from points 2 & 4) and 19.5 km (from points 3 & 6) which could represent deep crustal sources amongst the major intrusive bodies which fed the Mt Burr Volcanic Group or alternatively the depth to magnetic basement in parts of the offshore section. Segment II produces a depth of 10.9 km (from points 8 & 10) while segment III gives a depth of 9.1 km (from points 13 & 15) but these depths are similar enough that they might represent a group of sources at around that depth. Segment IV yields a depth estimate of 3.5 km (points 19 & 29 and 20 & 30) which is likely to represent the depth to sources near the top of basement in the shallow parts of the Penola, Robe, Tantanoola and St Clair Troughs and adjacent shelf areas.

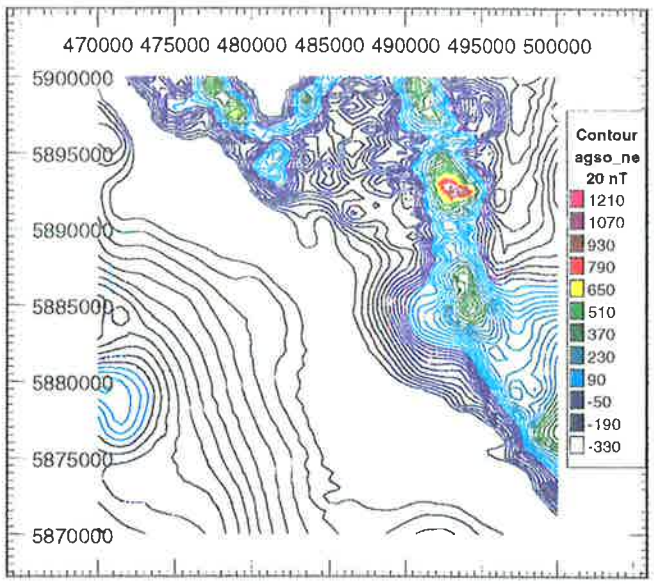

Fig. 6.1.7.1 Northeast Corner (AGSO data)
470000-500000mE, 5870000-5900000mN
Scale = 1:500,000

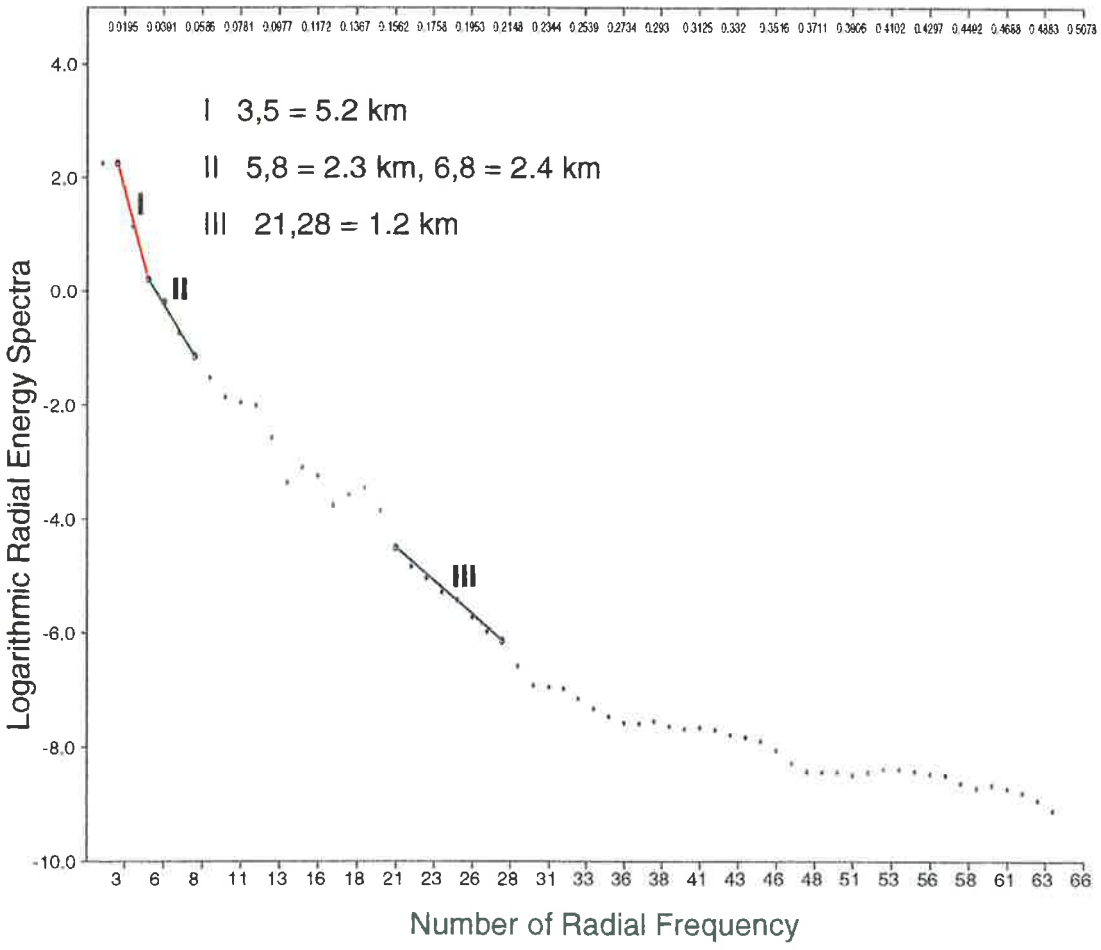

Fig. 6.1.7.2 Northeast Corner Energy Spectra

Segments V to IX are repeated sections and all yield a similar range of depths, with segment V yielding 6.1 km (from points 34 & 37), segment VI 7.7 km (points 47 & 50) and 7.3 km (points 46 & 50), segment VII 6.8 km (points 59 & 61) and 6.2 km (points 58 & 61), segment VIII 7.5 km (points 79 & 81), and segment IX yields 6.2 km (points 86 & 89) and 7.0 km (points 87 & 89). This range of depths is reasonably close to the depth of 7.1 to 7.6 km derived from the grid over the Mt Gambier Anomaly. Segment X yields depths of 1.8 and 1.9 km (points 107 & 112 and points 107 & 117, respectively) which might result from sources at the top of basement in the northeast region or because the line spacing was 1.5 km, it may be an artifact as discussed in section 6.1.3.

6.1.7 Northeast Corner, AGSO data

This is a subset of the original AGSO dataset and covers most of the northeast of the survey area where there are a number of relatively shallow, high amplitude anomalies. The grid used is bounded by 470000 to 500000mE and 5870000 to 5900000mN (fig. 6.1.7.1), which overlaps a portion of the Padthaway Ridge where there is no seismic coverage. Where seismic coverage does exist, depths range from 500 m on the eastern side of the grid adjacent to the Kanawinka Fault Zone, to 3 km along the southern edge, with most of the grid being between 1 and 2.5 km.

The spectrum (fig. 6.1.7.2) can be divided into two or three linear segments, with segment I yielding a depth of 5.2 km (points 3 & 5), while segment II yields 2.3 and 2.4 km (points 5 & 8 and 6 & 8, respectively), and segment III gives a depth of 1.2 km (from points 21 & 28). The 5.2 km depth from segment I seems to result from sources deep within the basement section and most likely south of the Kanawinka Fault Zone rather than the Padthaway Ridge where the sources are relatively shallow. The area in the central part of the grid generally has a depth to basement of 1 to 2.5 km which suggests that the sources that produce the depth of 2.3 km are close to or at the top of basement. The depth of 1.2 km, if it is not an artifact, is most probably related to the shallow sources in the Padthaway Ridge.

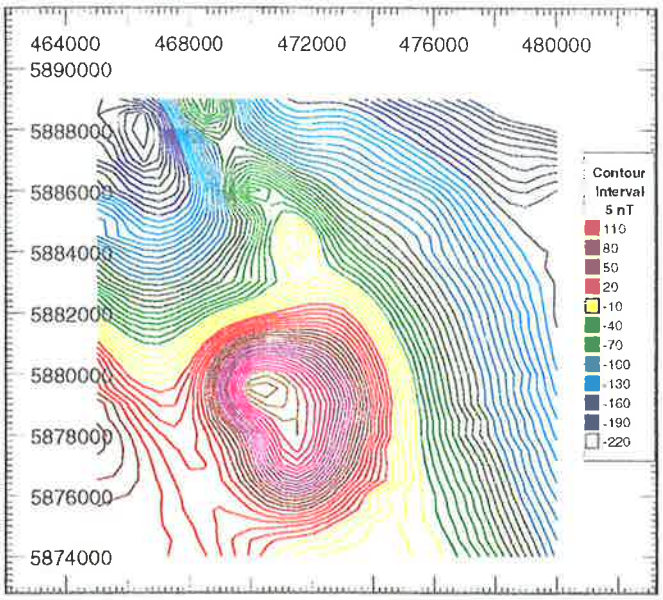

Fig. 6.1.8.1 Northwest Corner, AGSO data 465000-480000mE, 5874000-5889000mN Scale = 1:250,000

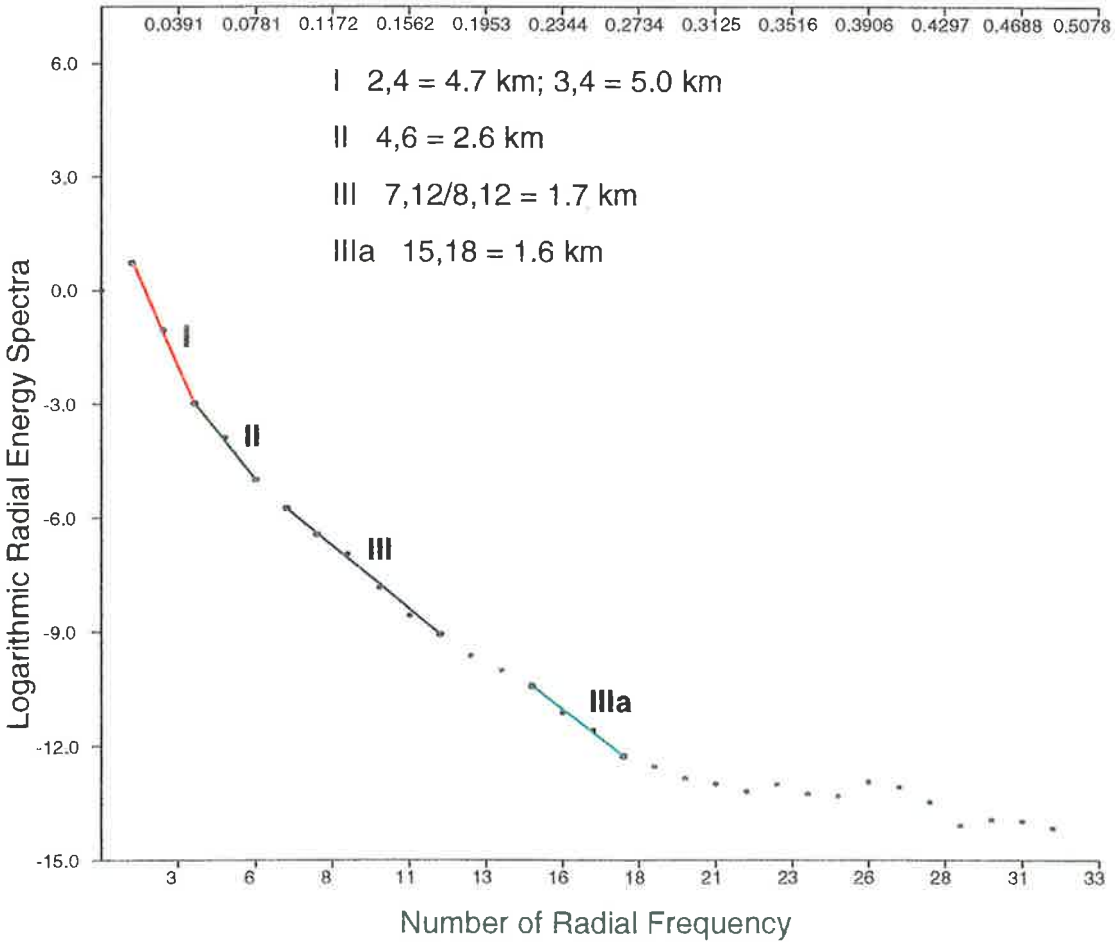

Fig. 6.1.8.2 Northwest Corner Energy Spectra

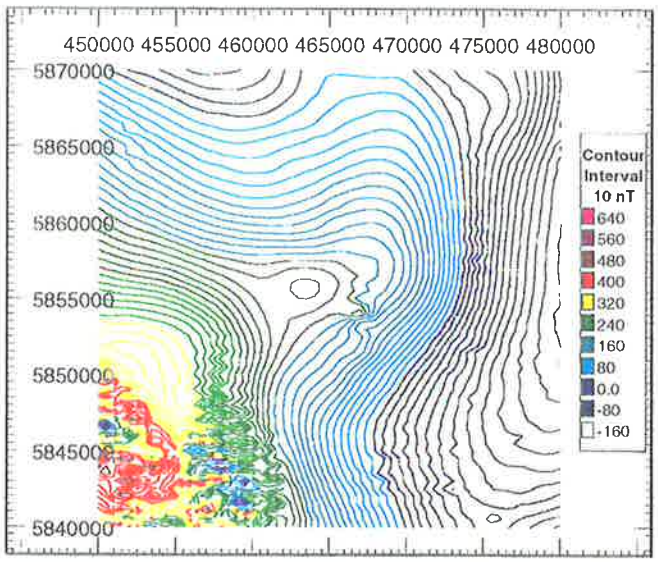

Fig. 6.1.9.1 Western Penola Trough (AGSO data)

450000-480000mE, 5840000-5870000mN

Scale = 1:500,000

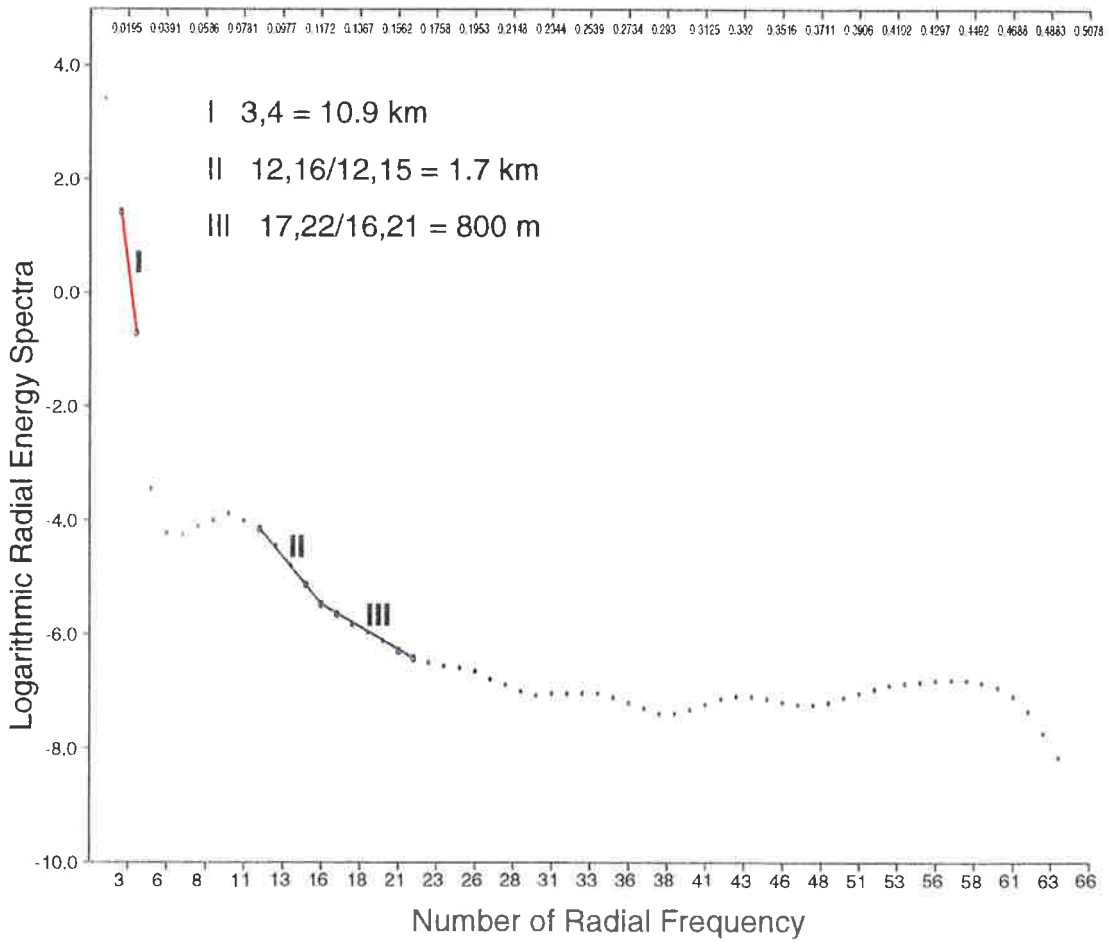

Fig. 6.1.9.2 Western Penola Trough Energy Spectra

6.1.8 Northwestern Corner, AGSO data

This anomaly is outside the study area (fig. 6.1.8.1) but is within the northeast corner AGSO grid discussed in the previous section. The anomaly is southwest of Robertson 1 and 2 and the grid covers the area bounded by 465000 to 480000mE and 5874000 to 5889000mN. The seismic coverage of the gridded area is generally as good as that discussed in section 6.1.5 (which is immediately south), with basement depth increasing from shallowest on the northern edge to deepest in the south.

The spectrum (fig. 6.1.8.2) shows several segments, which have been designated I, II, III and III_a. Segment I yields a depth estimates of 4.7 and 5 km (points 2 & 4 and 3 & 4, respectively), while segment II gives 2.6 km (points 4 & 6), and segments III and III_a yield depths of 1.7 km (points 7 & 12 and 8 & 12) and 1.6 km (points 15 & 18). The depths from segment I are in reasonable agreement with the estimate of 5.2 km from section 6.1.7 which also includes that anomaly (However, this is also the depth to the Northwest Penola Trough Anomaly which is on the edge of that grid). The segment II depth of 2.6 km may represent the depth to basement on the southern margin of the grid or, alternatively, the depth to intra-basement sources in the northern part of the grid. If the segments III and III_a are reliable, then the depths represent the depth to basement southwest of the Robertson wells and southeast of Bool Lagoon 1.

6.1.9 Western Penola Trough, AGSO data

This is another subdivision of the AGSO grid (fig. 6.1.9.1) and covers part of the Mt. Burr Volcanic Group as well as the broad magnetic high along the western margin of the study area. The boundaries are 450000 to 480000mE and 5840000 to 5870000mN, and include parts of the Penola Trough, Kalangadoo High and Kalangadoo Fault Zone where the seismic coverage is good, as well as the southwestern corner where basement has not been resolved on seismic.

The spectrum (fig. 6.1.9.2) shows a long wavelength segment designated I and, probably, two shorter wavelength segments designated II and III, all of which are based on only a few points. Segment I yields a depth of 10.9 km (from points 3 & 4) while segment II gives a depth of 1.7 km (points 12 & 16 and 12 & 15) and segment III a depth of 0.8 km (points 17 & 22 and 16 & 21). The depth of 10.9 km is the same as that for segment II

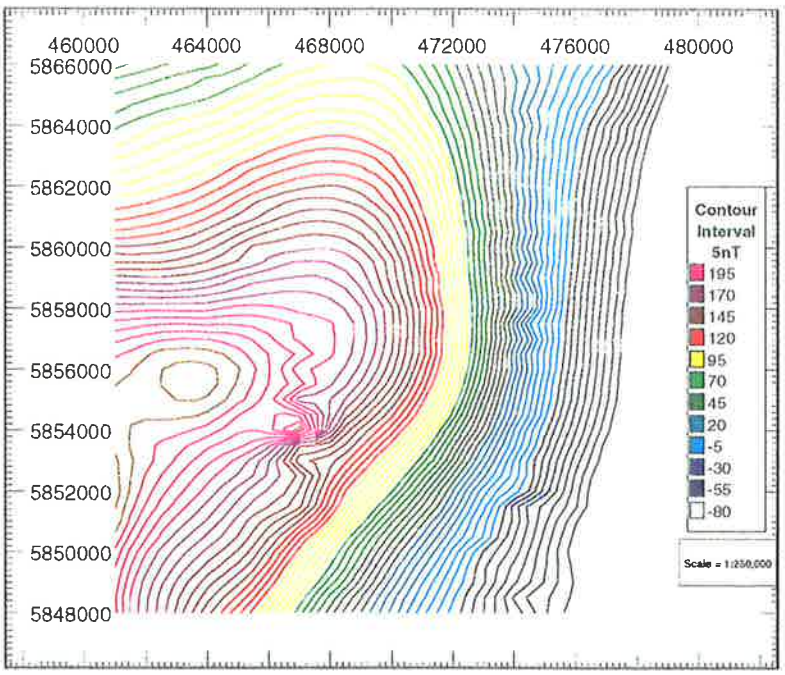

Fig. 6.1.10.1 West Penola Trough, 461000-479000mE, 5848000-5866000mN, AGSO data [subset]

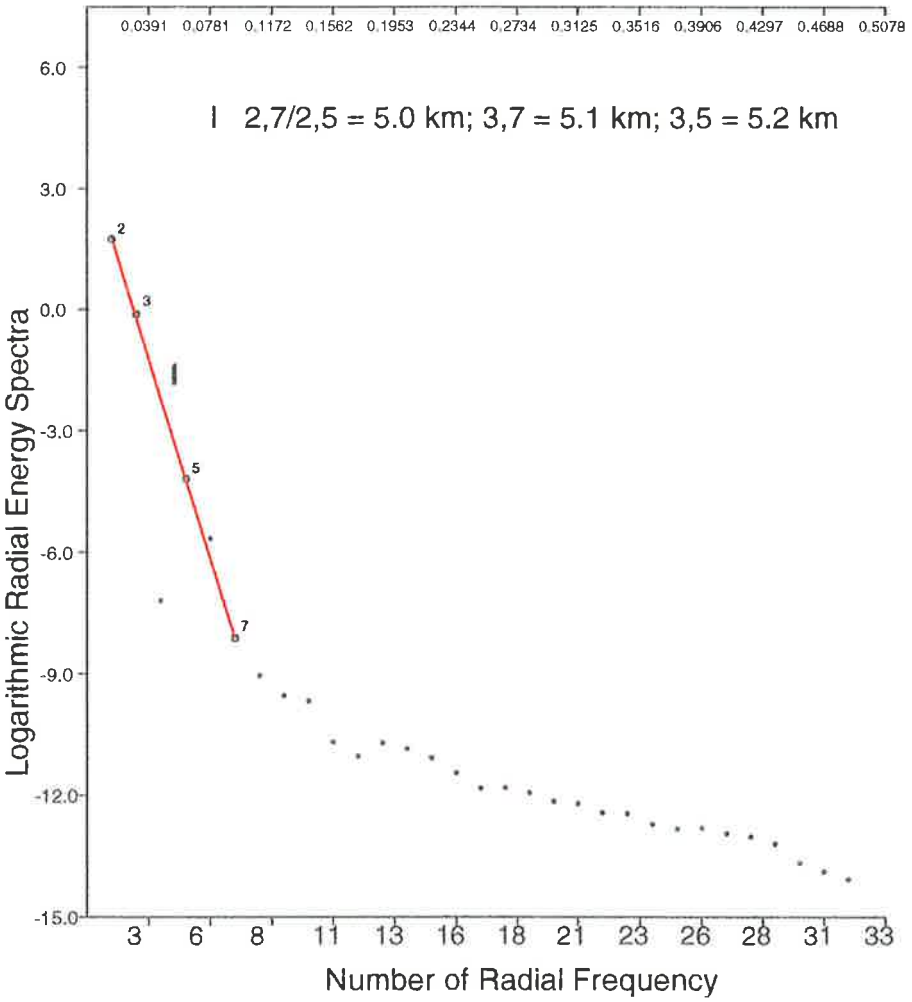

Fig. 6.1.10.2 West Penola Trough Energy Spectra

(section 6.1.6) from the whole AGSO dataset and probably represents a relatively deep source underlying the Mt Burr Volcanic Group.

Segment II gives a similar depth as segment X from the whole dataset which suggests, if it is not an artifact, that it results from the same source. However, the only part of the basement within the gridded area that is this shallow, is a basement high south of the Kalangadoo Fault Zone near the Hungerford 1 well. An alternative explanation for this depth and that from segment III are sources near the base of the Eumeralla Formation in the northern part of the grid (1.7 km), and sources near the top of the Eumeralla Formation near Hungerford 1 for the 0.8 m depth.

6.1.10 Western Penola Trough subset, AGSO data

This grid was generated from the one used in the previous section (fig. 6.1.10.1) in order to obtain an estimate of the depth of the relatively intense anomaly that underlies the western extension of the P1 area. The boundaries are 461000 to 479000mE and 5848000 to 5866000mN, and were applied in an effort to isolate this anomaly from neighbouring ones.

The spectrum (fig. 6.1.10.2) is based on a limited number of points but shows a long wavelength linear trend designated segment I, which yields depth estimates of 5.0 km (points 2 & 7 and 2 & 5), 5.1 km (points 3 & 7) and 5.2 km (points 3 & 5). This depth range is similar to that calculated for the Northwest Penola Trough Anomaly (section 6.1.5) which partly overlaps this area on the northeast side, which suggests sources at a similar depth beneath the Kalangadoo High, Kalangadoo Fault Zone and Penola Trough. The depth to the bottom of the Penola Trough beneath the gridded area is, on average, around 5 km (from seismic interpretations) with a deeper section along the eastern margins of the grid.

6.2 Euler Deconvolution

The Euler deconvolution method produces estimates of the position and depth of a magnetic source and an indication of the source type (dykes, contacts, faults etc.) by finding solutions to *Euler's homogeneity equation*. Following the method established by Thompson (1982), the homogeneity relation is written in the form,

$$(x - x_0)\frac{\partial T}{\partial x} + (y - y_0)\frac{\partial T}{\partial y} + (z - z_0)\frac{\partial T}{\partial z} = N(B - T)$$

where (x_0, y_0, z_0) is the position of the magnetic source, T is the total field at (x, y, z), B is the regional total field and N is the degree of homogeneity which is a measure of the rate of change of a field (Reid et al., 1990). Thompson (1982) designates N as a *structural index* (SI) which is related to the source type. Examples of this are, an index of three for a point dipole (because the magnetic field of a body, such as a sphere for example, falls off as the inverse cube with distance), an index of two for a vertical line source (because the field of a source like a narrow, vertical pipe falls off as the inverse square) and an index of zero for an infinite sheet. Extended bodies can be constructed out of assemblages of dipoles with structural indices of zero to three (Reid et al., 1990).

Reid et al., (1990) outline a procedure to be applied to gridded data where, (1) Each of the three gradients are calculated (or measured) for each grid point, (2) A square window that is at least 3 × 3 grid points or more is generated, (3) All points in the window are used to find a solution of Euler's equation for source position and background field B, (4) Step (3) can be repeated for each desired structural index, (5) Steps (3) and (4) are repeated for all possible window positions in the grid (including overlaps) and (6) Maps of the solutions for each structural index can be plotted with some means of designating the depth.

Reid et al., (1990) use theoretical models to demonstrate that the wrong choice of structural index produces scattered solutions and biased depths, with a low index giving depths that are too shallow while too high an index overestimates the depth. The authors note that depth estimates are more precise for high index sources than for low even when the choice of index is correct. They conclude that a sill edge, dyke or fault with limited throw are best displayed at a structural index of 1.0 while a fault with large throw or irregular contacts are best displayed at a zero index.

The use of a structural index of 0.5 is recommended by Thompson (1982) as generally the best depth estimator for intrusive-type bodies but he points out that the width-to-height ratio of an intrusive body is important in determining the best structural index. If the width-to-height ratio is large as in a wide dyke or sill type body then the response will be like two magnetic contacts and the lower structural index is the best depth estimator. If the width-to-height ratio is small (less than 0.5) as in narrow deep dykes then a structural index of 1 is more appropriate.

Where there is not a significant gradient or there is interference from several sources in a window, the resulting solution has a large uncertainty which may cause some algorithms to reject it in a similar manner to solutions from noisy or poorly gridded data. In order to resolve closely-spaced, interfering anomalies, the window size should be as small as possible but anomalies caused by deep sources will then produce unreliable depth estimates. Reid et al., (1990) conclude that the minimum depths found are approximately the same as the grid interval while the maximum depths calculated are about twice the window size which suggests that the window size should be selected according to the expected depth of the sources of interest.

6.2.1 MESA data

Cowan Geodata Services used proprietary software to calculate position and depth estimates on the whole dataset acquired by World Geoscience Corp. which is larger than the area (P1) that MESA and its co-sponsors commissioned. This area has the same southern and eastern boundaries as P1 but is bounded in the west by 465000mE and includes a section shaped like a right angled triangle extending from the northern margin of P1. This section covers the northern margin of the Otway Basin as well as the Kanawinka Fault Zone and part of the Padthaway Ridge, and overlaps and extends beyond the area covered by the AGSO data. This means that Euler Deconvolution depth estimates exist for anomalies which are adjacent to but outside the P1 area.

The data was gridded at a 135 m grid spacing with a 16 × 16 point window using a 0.5 structural index only. From the Reid et al., (1990) paper, it can be seen that the theoretical minimum depth resolved will be around the grid spacing, 135 m, while the theoretical maximum depth would be approximately 4.3 km. However, the actual minimum is around zero while the maximum is around 5.8 km which spectral analysis suggests is probably an underestimate. The maximum depths calculated for several anomalies seem to be shallower than seismic evidence would suggest, which may be because the bodies possibly have a greater depth extent than expected with the result that the structural index of 0.5 would be too low for the type of body evaluated.

The Euler depth estimates have been plotted on a series of maps (figs. 6.2.1.1 to 6.2.1.3) of the study area where colour corresponds to depth, with blue representing the

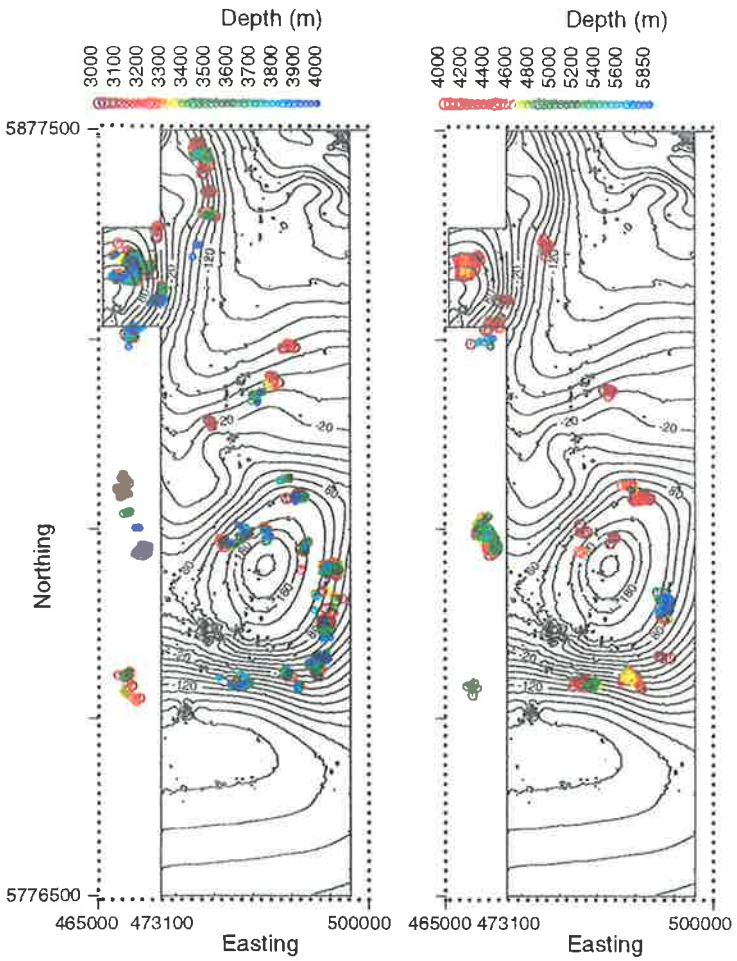

Fig. 6.2.1.1 Euler Deconvolution Depth Estimates, Sources 3 to 6 km. deep

Scale = 1:1,000,000

deepest sources and red the shallowest. Fig. 6.2.1.1 has two plots, the right side showing solutions between 4 and 6 km deep while the left side shows solutions between 3 and 4 km deep. The deepest solutions occur along the eastern side of the Mt Gambier Anomaly (around 495000mE and 5815000mN) which are shown in dark blue on the right side map. This map also shows other, more shallow solutions along the southern side of the large anomaly (near the Caroline Gravity High), scattered solutions around the centre and a closely grouped cluster on the northern side (maximum of about 4.6 km). There are a small group of solutions over the mid-Penola Trough Anomaly which have a maximum depth of 4.2 km while two clusters of solutions, both at a maximum of about 4.4 km deep, are found over the western extension of the P1 area. Those solutions from this group which are on the edge of the survey area, are over the Kanawinka Fault Zone. The north, northeast and area to the south of the Mt Gambier Anomaly have no solutions in this depth range.

The left side of fig. 6.2.1.1 shows many more solutions along the eastern and southern side of the Mt Gambier Anomaly with the whole cluster having the appearance of an arc over the central and southern part of the anomaly. The solutions in this depth range extend to the northeast, from over the mid-Penola Trough Anomaly to a small cluster over the deepest part of the Penola Trough. The solutions over the western extension of P1 have increased in number and the group over the Kalangadoo Fault Zone is more sharply defined. At this depth range there is a group of solutions running generally north-south in the northwestern corner of P1 which are on the eastern margin of the Northwest Penola Trough Anomaly and which are at a maximum of 3.6 km deep and average around 3.0 km below the surface. The deepest solutions for the Kalangadoo High Anomaly occur in this depth range with a maximum of around 3.0 km deep which is marginally shallower than the depths from spectral analysis and seismic mapping.

Fig. 6.2.1.2 shows the mid-range sources with two maps plotted, the right side displaying solutions in the 2 to 3 km depth range while the left side displays solutions in the 1 to 2 km depth range. Compared with the previous figure, there are clusters of solutions along the western side of the Northwest Penola Trough Anomaly in addition to the eastern side. There are still solutions obtained for the western Penola Trough extension but few over that part of the Kalangadoo Fault Zone where the deeper maps show clusters of solutions. There is an increase in solutions at this depth range over the Kalangadoo Anomaly but the solutions

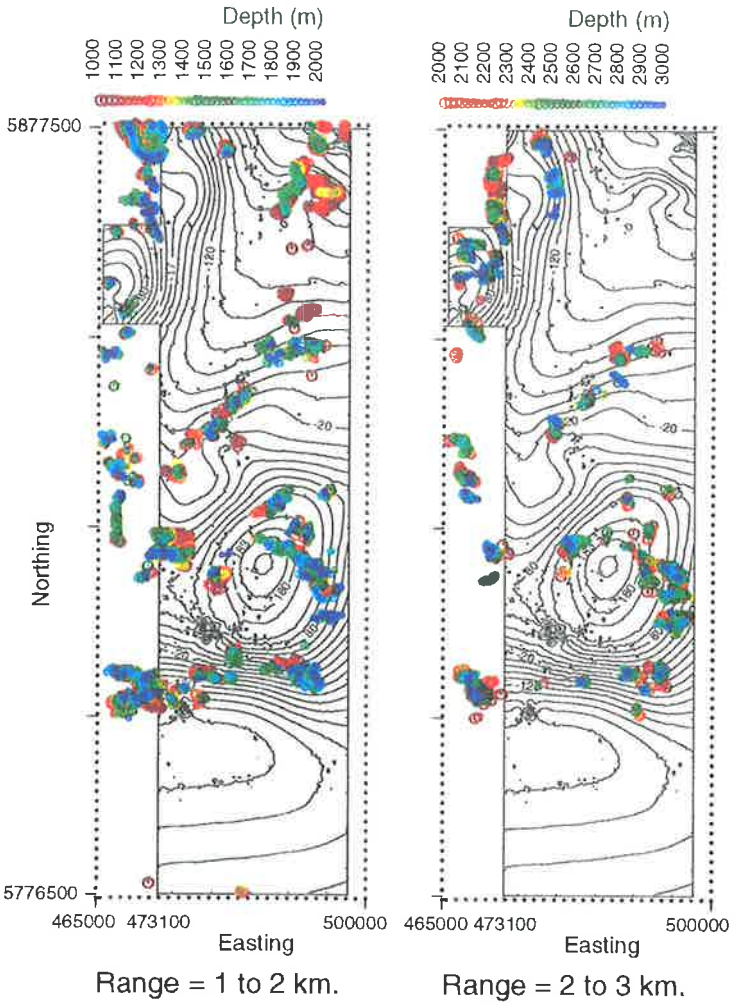

Fig. 6.2.1.2 Euler Deconvolution Depth Estimates, Sources 1 to 3 km. deep

Scale = 1:1,000,000

in the area east of the centre of the Mt Gambier Anomaly have lost the arcuate shape seen on the deeper maps. No solutions have been found for the northeast section of the P1 area.

The left side of fig. 6.2.1.2 (1 to 2 km depth range) shows a small group of solutions in the offshore section where they occur near the southern margin of the study area. This map also shows many solutions over the eastern Penola Trough, as well as over the Kalangadoo High and mid-Penola Trough Anomalies, and a return of the arcuate shape east of the Mt Gambier Anomaly. There is still a small scatter of solutions over the western Penola Trough extension but the eastern side of the Northwest Penola Trough Anomaly shows no solutions at this depth while the western side shows a substantial increase. The northeastern section of the study area has been devoid of solutions at the greater depths plotted on previous maps and it is not until this depth range that solutions appear over the two Northern Penola Trough Anomalies.

The shallow sources have been plotted on fig. 6.2.1.3 where the right side map displays the depth range 500 m to 1 km while the left side displays solutions in the range 100 to 500 m deep. The right side map shows that solutions over the eastern side of the Mt Gambier Anomaly are absent in this depth range with those on the western side more extensive than at greater depths. There are extensive clusters of solutions over the two Northern Penola Trough Anomalies, over the Kalangadoo High Anomaly and over the eastern Penola Trough but very few appear around the Northwestern Penola Trough Anomaly or the western Penola Trough extension. The southern margin of the offshore section shows an increase in solutions at this depth range compared to the 1 to 2 km range and there is also the emergence of scattered solutions along the southeastern corner of the coastline.

The left side map of fig. 6.2.1.3 has been restricted to the range 100 to 500 m because the grid spacing is 135 m and solutions that are substantially less than this may not be valid or alternatively, may represent cultural sources. This map only shows solutions from the western side of the Mt Gambier Anomaly while there are extensive solutions from around the Mt Gambier and Mt Schank volcanic complexes. There are no solutions in this depth range along the southern margin but a large group of solutions are clustered along the southeastern corner of the coastline. The only anomaly that produces a significant number of solutions in the northwest of the area is the shallow Hungerford Anomaly. There are a large number of solutions over the Kalangadoo High Anomaly, the Northern Penola Trough Anomalies and

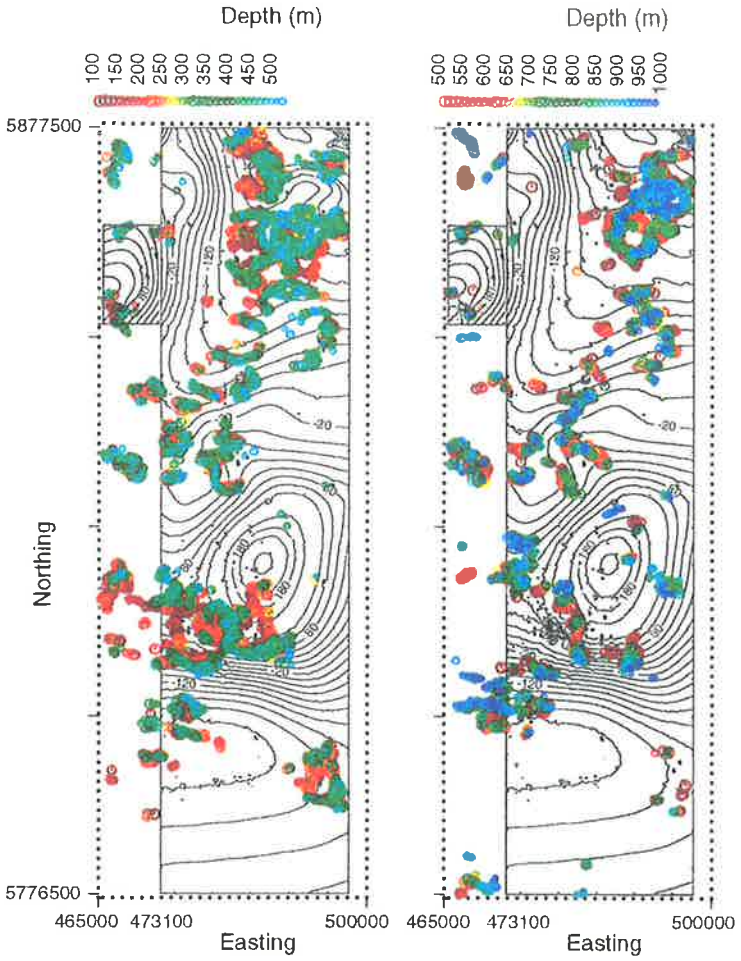

Fig. 6.2.1.3 Euler Deconvolution Depth Estimates, Sources 100 m. to 1 km. deep

Scale = 1:1,000,000

the Eastern Penola Trough Anomalies but the latter solutions do not necessarily coincide with the linear anomalies east of Penola.

A substantial number of solutions can be found running north-south from Coonawarra to Penola, and from Penola to Nangwarry, which are very shallow and are located close to the routes of the high voltage power lines that cross the area. It is likely that these are the result of contamination from the cultural sources and attempting to eliminate the cultural component simply by specifying a cutoff depth does not appear to have been successful. This implies that cultural anomalies on the surface can produce spurious solutions at various depths and locations around the anomalies. This can cause major problems relating the solutions to magnetic sources and geological structures because forward modelling of the linear magnetic anomalies east of Penola suggests that they are in this depth range (100 to 500 m).

6.3 Automag

This method is an improvement of the Naudy technique and was developed by Dr. Zhiqun Shi as part of her PhD. studies at the University of Adelaide. The Naudy technique involves the analysis of the TMI and Reduced-to-the-pole profiles which are both split into symmetrical and antisymmetrical parts (Naudy, 1971). A coefficient of similarity is derived by comparing the symmetrical parts with the profile from a vertically magnetised model, with the locations of the similarity coefficient minima giving the positions of the centre of the anomaly which result from the magnetic sources (Shi, 1991). In approximating geological structures, the Naudy technique uses the simple models of a thin sheet or plate, edge and dyke.

The principal difficulty with the Naudy technique is the precise location of the centre of anomalies on complex profiles, and because the calculation of a reduced-to-the-pole profile involves the assumption that the source structures are two-dimensional and perpendicular to the strike of the profile, the depth estimate must be modified to account for the angle between the strike of the structure and that of the profile. If an anomaly is clearly not two-dimensional then any depth estimate is almost certainly unreliable and has to be rejected (Naudy, 1971).

The method has been improved by using the horizontal and vertical components of the magnetic field for a vertically magnetised model, with the symmetrical parts of the

components used to calculate the similarity coefficient (Shi, 1991). Vertical and horizontal derivatives are used to resolve the problem of obtaining shallow depth estimates. The method has been further refined by replacing the original infinite dyke model by a model where the depth extent of the body is ten times the depth to the top. Error analysis shows that the relative error remains less than 10% for depth extent to depth ratios of greater than 4 to 5, in the case of TMI data and 3 in the case of gradient data (Shi and Boyd, 1993). In most circumstances gradient data produces more precise results but is degraded substantially by strong surface noise, making the results generally unreliable.

The Automag software requires the initialisation of a number of parameters which are, the depth to the top of the source body (h), the half-width of the body (w/2), the sample interval (dx) of the line data, and the type of body (dyke, edge or plate model) as well as the intervals at which the line data is subsampled. The output of the program consists of a plot of the total magnetic intensity (TMI) or gradient profile, plots of the values of the similarity coefficient for each of the sampling intervals, and a plot of the final depth estimates. In addition to these plots, a table of locations and estimates are produced with, the easting and northing value of the centre of the source, the similarity coefficient, sampling interval, depth, half-width, dip and susceptibility of the source. The last three values are probably more of a guide for forward modelling than precise values of these parameters, however, in the case of the dyke model, a depth estimate that coincides with an unrealistically shallow dip angle is probably unreliable. In a similar manner, the half-width and susceptibility parameters can be used to establish the more reliable estimate when adjacent lines yield disparate depth estimates for the same body.

6.3.1 Northern Penola Trough Anomalies

The two prominent anomalies in this area (section 6.1.2), the Sawpit Anomaly and Penola North Anomaly, have been found to lie at basement depth (approx. 2 to 3.2 km) through the use of spectral analysis (also see Plate 1). There are also a number of distinctive low-amplitude linear features which are superimposed over the larger regional anomalies and are in some cases extensions of the linear features in the eastern part of the Penola Trough (section 6.3.3). These linear anomalies were the main subject of the Automag depth analysis with depth estimates not found for the Sawpit Anomaly body or Penola North Anomaly body

which is most probably because of the initial depth and half-width used. Depth estimates for the two previously mentioned bodies were made using spectral analysis (section 6.1).

The depth to the top of the body was initially set at 200 m and the half-width at 100 m with sampling intervals of 2, 3, 5, 7 and 10 on flightlines that were resampled at 20 m intervals. The program was run on segments of flightlines 11900 to 12160 which covers the area from 486300 to 496800mE and 5860000 to 5874000mN. The flightlines only cross the Sawpit Anomaly on the western side of this area (from 11900 to 11970), both anomalies on flightlines 11980 to 12050, and only the Penola North Anomaly on flightlines 12060 to 12160. Some of the sampling intervals on various flightlines, particularly where there is a substantial amount of noise, did not yield a distinct similarity coefficient minima with the result that no reliable depth estimate was produced for these, while on other lines depth estimates coincided with shallow dip angles causing those results to be rejected (The plate model may have produced more realistic depth estimates on these lines but was not used due to time constraints). Seismic evidence suggests that any bodies associated with the fault planes will be near vertical so a depth estimate for a body with a dip angle of less than 60° will be less reliable. There appears to be too high a level of noise for the vertical derivative to yield any useful results. Table 6.3.1.1 collates the estimates with the lowest similarity coefficients and the most realistic dip angles.

Line	Sampling Interval	Easting	Northing	Depth (m)	Coefficient	Dip°
11950	2	488405	5872110	284	92	101
11970	5	489206	5870260	1666	96	60
	7	489207	5870840	806	84	70
11980	3	489605	5871350	362	89	77
11990	2	490013	5871650	1080	69	80
12000	2	490362	5871270	286	24	67
	2	490362	5871550	930	24	74
	3	490362	5871390	557	11	70
12010	2	490808	5872280	267	21	89
12030	2	491593	5872090	698	35	81
12050	3	492420	5871530	398	25	63
12090	3	494006	5871950	850	17	78
12100	3	494408	5871810	745	61	76
12140	3	496007	5871240	717	85	73
12150	2	496406	5870850	291	13	67
	3	496406	5870770	646	86	64
12160	2	496784	5871700	237	43	96

Table 6.3.1.1 Automag Depth Estimates (dyke model) for flightlines crossing the Penola North Anomaly showing location, depth, similarity coefficient and dip.

The depth estimates shown in the above table are all close to or over the Penola North Anomaly source with depths ranging from 237 to 1666 m which place the sources below the top of the Eumeralla Fm. (150 to 225 m), according to seismic evidence, but with two estimates within the Crayfish Group (1080 and 1666 m). The most reliable depth estimates are those where the similarity coefficient is lowest (minima) which in this case should be those between 11 and 25, which correspond to a depth range of 267 to 930 m or entirely within the Eumeralla Fm. but some of the estimated locations do not seem to coincide with the seismically determined faults. Two depth estimates were found for sources whose effects were superimposed on the Sawpit Anomaly and which were 783 and 555 m deep but the dip angles were unrealistically shallow (138° and 140° respectively) for the dyke model.

6.3.2 Hungerford Anomaly

The source of this anomaly is shallow with the Euler Deconvolution solutions mostly less than 400 m deep so the initial dyke model was assigned the parameters of 300 m as the depth to the top and 100 m as the half-width with sampling intervals of 1 to 5. The software interpolated equal spaced points (20 m intervals) from the original flightline data on five lines around the anomaly (11410, 11420, 11430, 11440, and 11450). The TMI map shows that the centre of the anomaly is beneath line 11430 at approximately 467600mE and 5853750mN. The results for these 5 lines are shown in table 6.3.2.1 below.

Line	Sampling interval	Easting	Northing	Depth (m)	Coefficient	Dip°
11410	1	466838	5853530	301	12	35
	2	466837	5853870	508	11	71
	3	466837	5853910	594	35	75
11420	1	467192	5854370	260	11	145
	2	467196	5853570	340	89	42
	3	467195	5853790	416	50	69
11430	1	467587	5853480	188	4	40
	1	467584	5854320	212	4	152
	2	467584	5854260	496	14	144
11440	1	468003	5853650	220	60	51
	2	468003	5853750	403	68	61
11450	2	468399	5853930	753	51	59
	3	468399	5853970	896	25	61
	5	468399	5853910	1007	15	58

Table 6.3.2.1 Automag results (dyke model) for the Hungerford Anomaly showing the location, depth, similarity coefficient and dip for the flightlines at various sampling intervals.

The shallowest estimates are for line 11430 where depths of 188 and 212 m (with a dip angle of 152° which is less likely than 40° for 188 m) were found and these two estimates correspond to the lowest similarity coefficient minima (4) while the deepest estimates are for line 11450 where the depth ranges from 753 to 1007 m with the latter depth having a similarity coefficient minima of 15. Comparison with the Euler Deconvolution solutions

shows that the deeper estimates for line 11410 (508 and 594 with dips of 71° and 75° respectively) are considerably deeper than the deepest Euler solutions (around 400 m) while the Automag estimates for line 11450 are deeper than the thickest cluster of Euler solutions but much shallower than the deepest solution (around 2.7 km). Both methods appear to show a body that is shallowest on the western (line 11410) side but which extends to considerable depth on the eastern side (line 11450). In order for the depth estimates to be within the 10 % error range the body must have a depth extent of between 752 m (for 188 m) and around 4000 to 5000 m (for 1007 m), i.e. around 4 to 5 times the depth to the top of the body.

The shallowest depth estimates place the top of the Hungerford body within the Tertiary sediments and above the Late Cretaceous section with the body probably extending at least to the base of the Eumeralla Formation (around 750 m deep) in this area or probably much less likely, down to the source body of the Western Penola Trough Anomaly which spectral analysis suggests is around 5 km deep. The maximum Euler Deconvolution solution of approximately 2.7 km is close to the depth to basement from seismic sections (2.5 to 3.0 km in this area). The Hungerford Anomaly is located close to the Kalangadoo Fault Zone which may have served as a conduit bringing magma from considerable depth up to the source of the Hungerford Anomaly. The combination of the results from Automag and Euler Deconvolution suggests the possibility that the magma may have risen from basement through the faults overlying the basement fault zone to the Tertiary sediments where it was trapped and so spread to the west of the conduit.

6.3.3 East Penola Trough Anomalies

The Eastern Penola Trough Anomalies (EPTA) are a series of linear features in the study area east of Penola and occur mostly north of 5850000mN (approx. 37° 30') to the northern margin. Segments of the flightlines chosen for the depth analysis are between 5850000 and 5874500mN while the flightlines range from 12000 to 12133 (490400 to 495600mE) which means that there is some overlap between the flightlines used for depth analysis here and those in section 6.3.1. A dyke model was used and the initial parameters for the fourteen flightlines were set at 200 m for the depth to the top of the body (h) and 100 m for the half-width (w/2) with sampling intervals of 1, 2, 3, 4 and 5, and where the initial depth

to the source is a compromise between the seismically determined depth of the top Eumeralla horizon at the southern (400 to 600 m) and northern end (approx. 200 m) of the flightlines. The results of the analysis are shown in Table 6.3.3.1.

Line	Sampling Interval	Easting	Northing	Depth (m)	Coefficient	Dip°
12000	4	490396	5870140	634	77	54
12020	3	491201	5864480	375	96	39
12040	2	492002	5859220	285	31	41
	3	492003	5857560	244	56	26
	4	491992	5873000	621	67	92
12060	2	492777	5867750	385	81	72
12080	3	493607	5867970	862	22	76
	5	493607	5867950	885	22	77
12090	5	493995	5872300	1661	64	86
	4	493995	5872200	1382	64	84
12100	3	494396	5868330	305	37	75
12110	2	494788	5858350	328	74	21
	2	494792	5863030	314	38	46
	2	494798	5870750	283	21	68
12120	3	495192	5873180	318	34	110
	2	495193	5870580	309	25	65
	2	495196	5863840	251	67	47

Table 6.3.3.1 Automag Depth Estimates for flightlines crossing the East Penola Trough Anomalies (dyke model) showing location, depth, similarity coefficient, dip and sampling interval.

The East Penola Trough Anomalies consist of several independent linear features so it is possible to have a number of locations and depth estimates for each flightline and sampling interval. The large number of closely spaced depth estimates for the Northern Penola Trough Anomalies (NPTA) necessitated the use of the calculated dip angle as a means of discriminating between reliable and less reliable estimates (greater and less than 60° respectively) but because the EPTA are isolated it is not necessary to be as discriminating.

Only nine of the flightlines yielded reasonable depth estimates which ranged from 244 to 1661 m and were located at positions from 5857560mN to 5873180mN.

The shallow depth estimates on line 12040, 244 and 285 m, are located at 5857560 and 5859220mN which, according to the seismic horizon maps, places the sources near the base of the Tertiary section and above the top of the Sherbrook Group. The former body (5857560mN) was estimated to have a dip of 26° compared with a dip of 41° for the latter body which suggests that the latter estimate is more reliable. With the exception of the two deep estimates from line 12090 (1661 and 1382 m), the other estimates place the probable sources within the Eumeralla Formation with the sources on lines 12100 to 12120 near the top of the formation while the western group includes deeper sources. Comparison of these depth estimates with those obtained from flightlines over the NPTA reveals that only three coincident lines from each study produced reasonable estimates and on one line, 12100, the location of the sources were widely separated. The depth estimate from line 12000 is close to the average of the depth estimates (286 to 930 m) from the same line in section 6.3.1 but the location is approximately 1 to 1.5 km south of those three location estimates. The similarity coefficients for these are considerably lower than for the EPTA analysis. The two EPTA depth estimates for line 12090 are located within 350 m just as the corresponding estimate from the NPTA analysis. However, the former (1382 and 1661 m) indicate sources within the Crayfish Group while the latter (850 m) indicates a source near the base of the Eumeralla Formation which is more likely given the low similarity coefficient (17) (from table 6.3.1.1).

This chapter has reported the results of three methods of depth determination, of which the results of spectral analysis agree most closely with depths interpreted from seismic surveys. The Automag results appear to be less reliable while the large amount of scatter in the solutions and the underestimated maximum depths substantially reduces the usefulness of the Euler Deconvolution data.

Chapter 7

Geophysical Overview of the Western Otway Basin

7.1 Integrated Regional Overview

7.1.1 Introduction

In previous chapters the history of geophysical exploration in the Western Otway Basin has been outlined. Seismic coverage is very good over the section of the Penola Trough where gas discoveries have been made, with two 3-D seismic surveys completed (the Penola 3D survey over the Sawpit High and the SAGASCO 3D survey over the Katnook and Haselgrove gas fields). Older 2D seismic lines are closely spaced over most of the Penola Trough except for the section near the S.A./Victorian border. The northern margin of the Otway Basin, especially along the Kanawinka Fault Zone, has very little seismic coverage as has the Tantanoola Trough west of the P1 area.

The area around the wells in the Mt Gambier region has good seismic coverage but due to the karstic nature of the Gambier Limestone, the part of the P1 area south of the Tartwaup Fault Zone has few seismic lines (with the exception of the area around Caroline 1). The regions east of Robe and Beachport have seen extensive seismic exploration but little has been done onshore southeast of Geltwood Beach 1 or west of Lake Bonney 1. Offshore the seismic coverage is good over most of the Robe Trough, Chama Terrace and Voluta Trough with only a small section close to the coastline south of Mt Gambier being poor.

As also previously discussed, detailed aeromagnetic coverage exists for the MESA P1 area (Plate 1) and for the regional AGSO Penola 1:250,000 sheet aeromagnetic survey. In 1994 AGSO acquired aeromagnetic data for the offshore Victorian part of the Otway Basin which adjoins the Penola regional survey and MESA survey to the south and extends southeast along the Victorian coast.

AGSO has compiled data from gravity surveys carried out by the Victorian and S.A. Mines Departments, the universities, various mining companies and their own staff into the AGSO National Gravity Database, which was used to create regional scale (1:1,000,000) Bouguer gravity images and contour maps of the Otway Basin. These

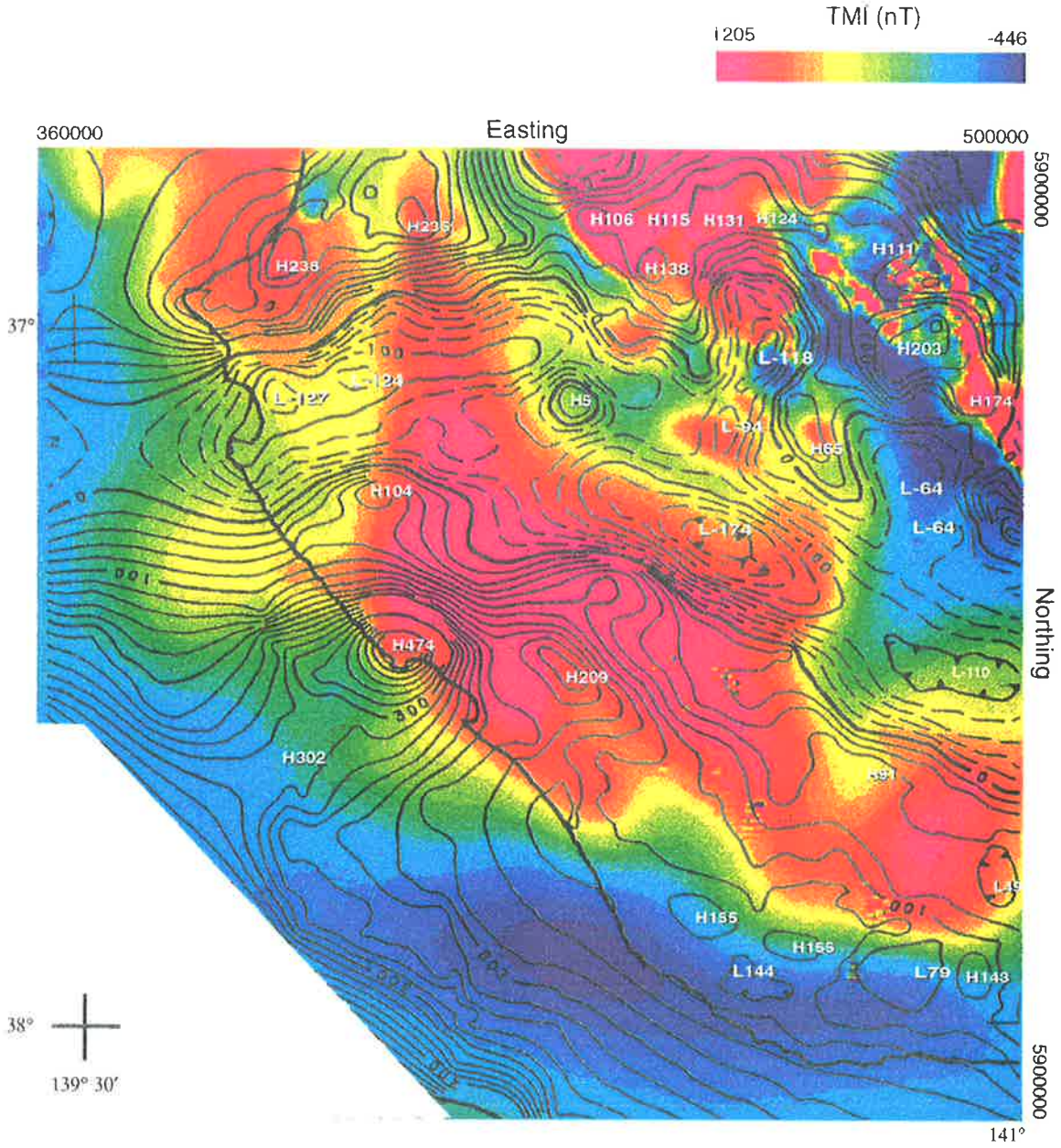

Fig. 7.1.2.1 Regional TMI image of Western Otway Basin (AGSO data) with Bouguer Gravity Contours from AGSO National Gravity Database Scale = 1:1,000,000. Contour Interval = 20 μm/s²

Contours generated from 4 x 4 km. grid with high and low anomalous values shown in white (e.g. H143). Contour map from 21-1/J54+55

contour maps and images were generated from 4 × 4 km grids which were derived from the observations. MESA also supplied the author with maps of gravity traverses containing Bouguer gravity values, colour images and gridded data generated from surveys conducted over the P1 area and adjacent regions.

The area around Mt Gambier and Mt Schank has reasonably good coverage with gravity stations spaced at intervals of 700 m to 1000 m along most of the roads, creating a grid of stations. From this area south to the coastline the coverage is not as good, being limited to the more important roads, but with the same station spacing. There are very few stations along the S.A./Vic. border and the area between Mt Gambier Airport and Nangwarry is limited to five traverses from 4 to 10 km apart. The traverses in the area between Nangwarry and Penola are similarly limited in number and it is only along the main road to Mt Gambier and along the railway line that the stations are spaced at intervals of less than a kilometre. Five hundred metre spacing is used on the traverse heading northeast from Penola to Comaun while the traverse which runs north-south along the S.A./Vic. border from the northern margin of the study area, has a station spacing of 400 m for the first twelve kilometres. The rest of the area is sparsely covered by traverses with what appear to be older station spacings of one mile (1.6 km).

7.1.2 Regional Gravity and Magnetic Features

The most important features (fig. 7.1.2.1) on the regional gravity maps are the prominent gravity low delineating the Penola Trough which extends toward the Robe Trough in the west, the steep gradient and high values offshore, the series of gravity highs along the Kanawinka Fault Zone, and the circular, positive gravity anomalies centred on Beachport and Lucindale, as well as the scattered minor highs and lows which occur in the area around Mt Gambier.

Neither the Penola or Robe Troughs have sharp gravity gradients marking their boundaries, which is not surprising given the evidence from seismic sections and wells that shows metamorphic basement at a depth of 2 to 3 km along the flanks of the troughs, while the deepest part of the Penola Trough is around 7 km deep and the Robe Trough about 6 km. This depth of burial and the small density contrast between the Mesozoic sediments and the Palaeozoic metasediments underlying them contributes to the relatively gentle gradient.

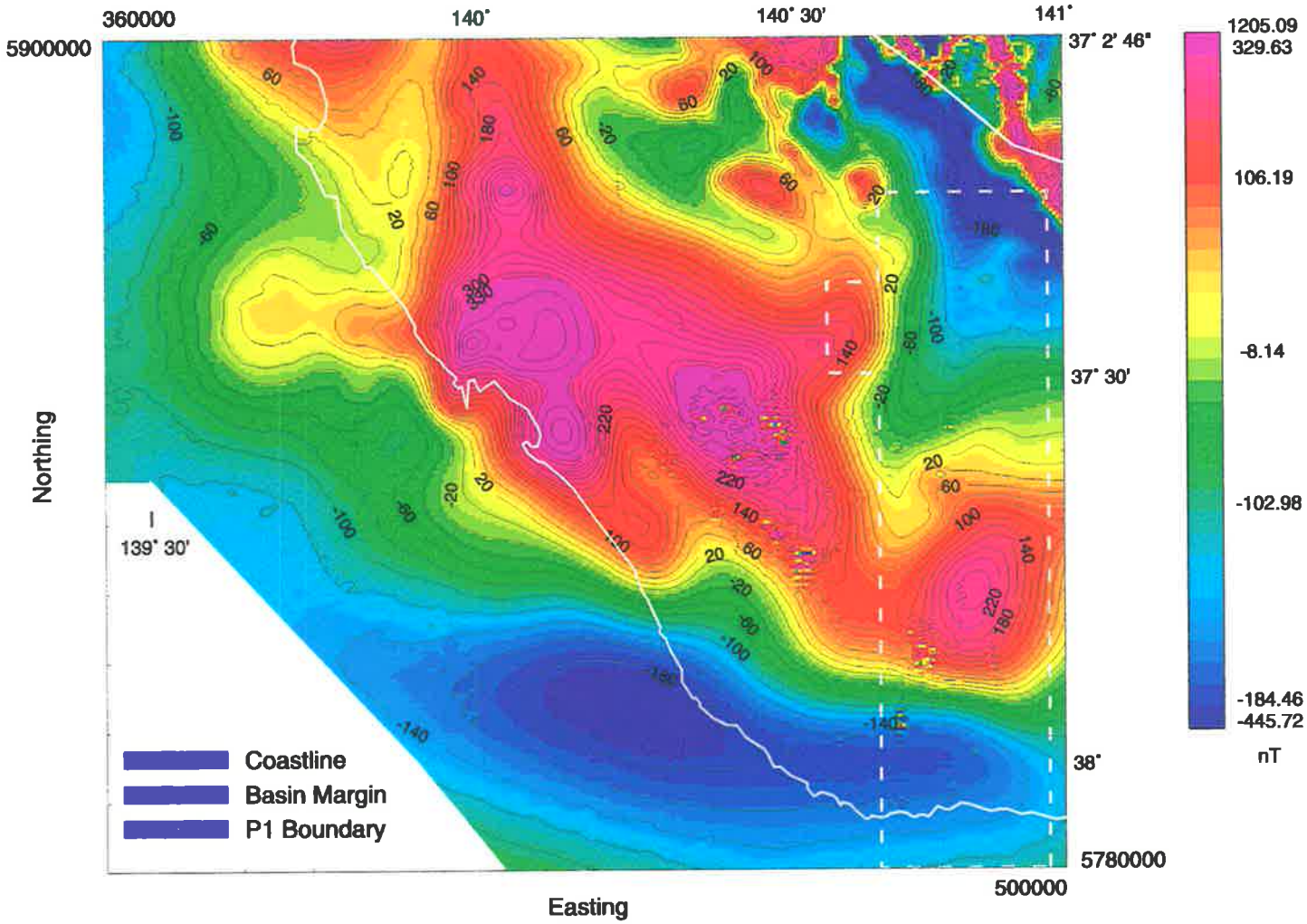

Fig. 7.1.2.2 AGSO 1992 Penola 1:250,000 sheet survey

TMI Image 1:1000,000 scale; Contour Interval = 20 nT

The series of gravity highs along the Kanawinka Fault Zone and the highly variable gravity signature over the Padthaway Ridge, suggests that basement is probably very shallow and there are a number of intrusive bodies close to the surface, some of which are producing positive anomalies while some large bodies, which are less dense than the surrounding basement, are producing negative anomalies. The thickening sediments offshore would normally produce a gravity low but this has probably been cancelled by the proximity to the boundary between oceanic and continental crust which is responsible for the steep positive gradient over the continental slope.

The most important features of the regional magnetic map (fig. 7.1.2.2), which is derived from AGSO data, are the large anomalies that are very likely to be due to either substantial intrusive bodies or the magma chambers which fed the surface volcanics at Mt Gambier, Mt Schank and the Mt Burr volcanic group. On the southeastern side of the region, the Mt Gambier anomaly is a large semi-elliptical anomaly extending approximately 40 km northeast of the Mt Gambier volcanic complex, with two small anomalies to the east and northeast in Victoria which are not shown on the map.

Near the western boundary of the study area, and extending into it in the northwest of the study area, is a very large, irregular shaped group of magnetic highs which underlies the Mt Burr volcanic group on its eastern side and extends to the coast around Beachport. There are three main centres, one northeast of Millicent around Mt Burr, another northeast of Beachport which partly coincides with the Beachport gravity high, and the third which is just to the south of the previous centre and about halfway between Millicent and Beachport. There are a some smaller extensions to the main anomaly, examples of which are the north-south magnetic 'ridge' which starts at a magnetic high east of Lake Eliza 1 and extends north to the basin margin (fig. 7.1.2.2), and the anomalies which underlie the western and northwestern parts of the study area, as well as a large, lower amplitude anomaly offshore to the west of the Beachport magnetic anomaly.

North of the large irregular high are some smaller anomalies including the circular anomaly, southwest of Robertson 1 and 2, which is adjacent to the northwest corner of P1, as well as a larger anomaly due west of it (fig. 7.1.2.2). In this area there is also an intense anomaly northwest of the Bool Lagoon 1 well, which is probably associated with intrusive bodies beneath the Padthaway Ridge. There are a number of

high amplitude, positive anomalies along the Kanawinka Fault Zone in the northeast corner of the regional map, some of which coincide with the gravity anomalies discussed earlier. To the southwest of the positive anomalies is an extended and intense magnetic low, striking northwest-southeast, with a steep gradient between this and the positive anomalies. South of these intense lows is a roughly triangular-shaped magnetic low that is north of the Mt Gambier anomaly and east of the Mt Burr volcanic complex. The Northeast Penola Trough anomalies are situated in this area as are the producing gas wells. The other major regional magnetic low is to the south and offshore from the main regional high discussed earlier, with an extension to the east that has its axis along the south coast of the P1 area (fig. 7.1.2.2), and a probable extension to the west past the survey boundaries.

The relationship between the regional gravity anomalies and the magnetic anomalies is not straightforward because, for example, in the southeast corner of the regional map the magnetic map shows the Mt Gambier anomaly and the eastern part of the anomaly underlying the Mt Burr volcanic complex which are both relatively intense magnetic highs. The gravity map on the other hand shows the area around the Mt Gambier anomaly to have three relatively low amplitude gravity anomalies, while there are no significant gravity anomalies in the region around the Mt Burr volcanic complex or around the magnetic anomaly east of Geltwood Beach 1.

The Beachport High has both a gravity and magnetic expression while a neighbouring gravity high to the east is substantially offset from the magnetic highs in this region. In a similar manner the magnetic anomaly between Lake Eliza 1 and Greenways 1 is offset to the east of the relative gravity high (Lake Eliza High) adjacent to the Robe Trough, and the magnetic ridge extending north from this region has little expression on the gravity map which shows the pronounced low delineating the Robe Trough. There is an offset between the Lucindale gravity high (also delineated on seismic) which is to the west of Lucindale 1 while the small magnetic anomaly is to the east of the well.

The Kanawinka Fault Zone and adjacent Padthaway Ridge host a number of gravity and magnetic anomalies, with a relatively strong magnetic anomaly on the eastern side of the regional map north of where the Kanawinka Fault Zone crosses into Victoria. Immediately to the south of the fault zone is an intense magnetic low which coincides

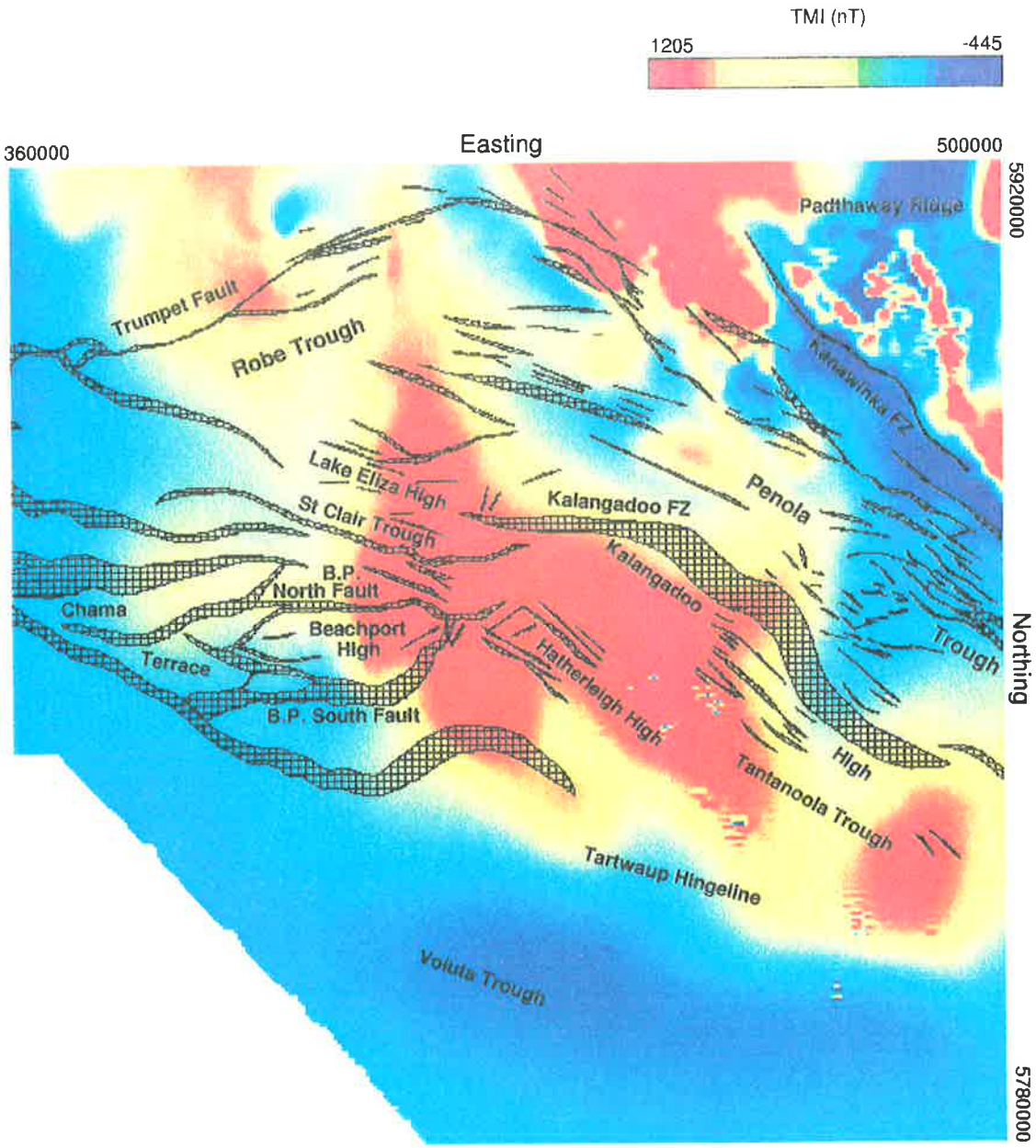

Fig. 7.1.3.1 Regional TMI image of Western Otway Basin (AGSO data) with major Basement faults derived from seismic horizon maps

Scale = 1:1,000,000

with a gravity high which extends to the north and east but is still offset from the magnetic high discussed above. To the north of this region on the Padthaway Ridge, are strong magnetic anomalies which generally coincide with gravity lows.

Near the northwestern corner of the study area (P1) is a gravity ridge that extends southeast from a relative high and it is this ridge that coincides with the circular anomaly just outside the study area. The magnetic anomalies which occur along the western margin of the study area find no expression on the gravity map. Between the circular magnetic anomaly and the Kanawinka Fault Zone anomalies is a region of relatively low magnetic intensity which is associated with a more intense low further north. This whole region coincides with a gravity low but the gravity low does not become more negative over the more intense magnetic low.

7.1.3 Regional structure from seismic data

The data from seismic sections over the Western Otway Basin has been assembled into a series of maps showing the location of faults at the top of the horizon overlying the regional magnetic image, with the horizons represented being the top basement, top Crayfish Group, top Eumeralla Formation and top Sherbrook Group (section 5.2). As discussed in the introduction to this chapter, the basement has not been resolved on seismic sections south of the Kalangadoo High as well as a section stretching from the Kalangadoo Fault Zone, between Hungerford 1 and the Diamond Swamp High (fig. 7.1.3.1), to southeast of Millicent. This area underlies the Mt Burr volcanic group of fifteen Pleistocene eruptive centres.

One of the main features of the basement horizon map is the prominent Kalangadoo Fault Zone (hatched) which is on the southern margin of the Penola Trough and extends from the eastern margin of the study area northwest to the Lake Eliza High and St Clair Trough. South of the fault zone is the Kalangadoo/Diamond Swamp High which is bounded on the southeastern side by a relatively deep low (the southern side is unresolved) and by the St Clair Trough in the west and Tantanoola Trough in the southwest. North of the fault zone is the Penola Trough which the closely spaced seismic sections show is at its deepest south of the Katnook gas fields and more limited data delineates another low southeast of the Haselgrove wells.

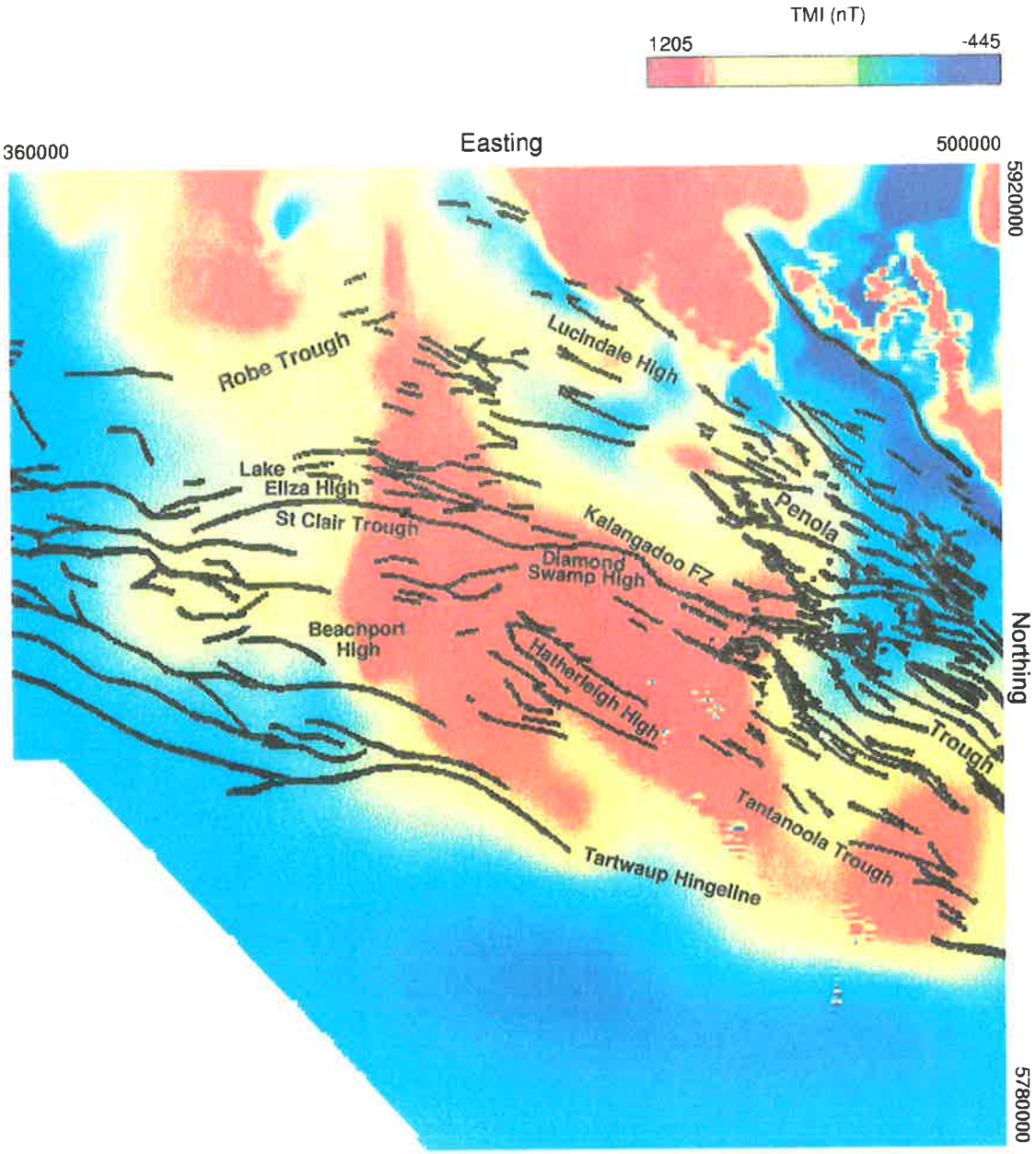

Fig. 7.1.3.2 Regional TMI image of Western Otway Basin (AGSO data) with major Crayfish Group faults (in black) derived from seismic horizon maps. Scale = 1:1,000,000

The western section of the Penola Trough is shallower than the east with the deepest parts being adjacent to and on the northern side of the Kalangadoo Fault Zone. Over most of the Penola Trough and adjacent areas, the dominant trend is the steady increase in depth the further south and southwest from the basin margins the basement depth is mapped (from less than 500 m along the basin margin to between 4 to 6 km in the south), although some faults can locally enhance or reverse this trend.

Seismic evidence shows the Robe Trough is bounded along the northwest margin by the prominent Trumpet Fault while a series of east-west faults separates the Robe Trough from the Chama Terrace and the Beachport High. The latter is bounded by the Beachport North and South Faults, while further to the east is the Hatherleigh High which is bounded on both sides by northwest-southeast trending faults. Basement has not been mapped in the Voluta Trough south of the Tartwaup Hingeline.

The map showing faults at the top of the Crayfish Group horizon (fig. 7.1.3.2) suffers from the same lack of resolution of the horizon in almost the same areas as the top basement horizon map. The exception is the region south of the Kalangadoo Fault Zone, where the horizon has been resolved under the northern part of the Mt Burr volcanic group. In addition, there are three regions where the horizon is absent, one is over the Diamond Swamp High while another is a smaller region north of the Bool Lagoon 1 well. The third region is over the Beachport High and extending a short distance offshore.

The Crayfish Group top horizon undergoes a general increase in depth to the southwest away from the basin margin, with the Kalangadoo Fault Zone causing the top of the horizon to be slightly deeper on the northern side of the fault zone than on the southern side, although the deepening trend continues in areas that have been mapped south of the fault zone. The deepest this horizon has been mapped in the eastern section (P1) of the Western Otway Basin, is 4.6 km deep northeast of Caroline 1 and 4.8 km in a low east of Compton 1, but the depth to the top of the horizon is greater offshore in the Robe Trough. The depth to the top in some cases is influenced by the basement topography, for example, the top of the Crayfish Group is elevated over the Lucindale, Lake Eliza and Hatherleigh Highs, and is depressed over the St. Clair, Tantanoola and eastern Penola Troughs.

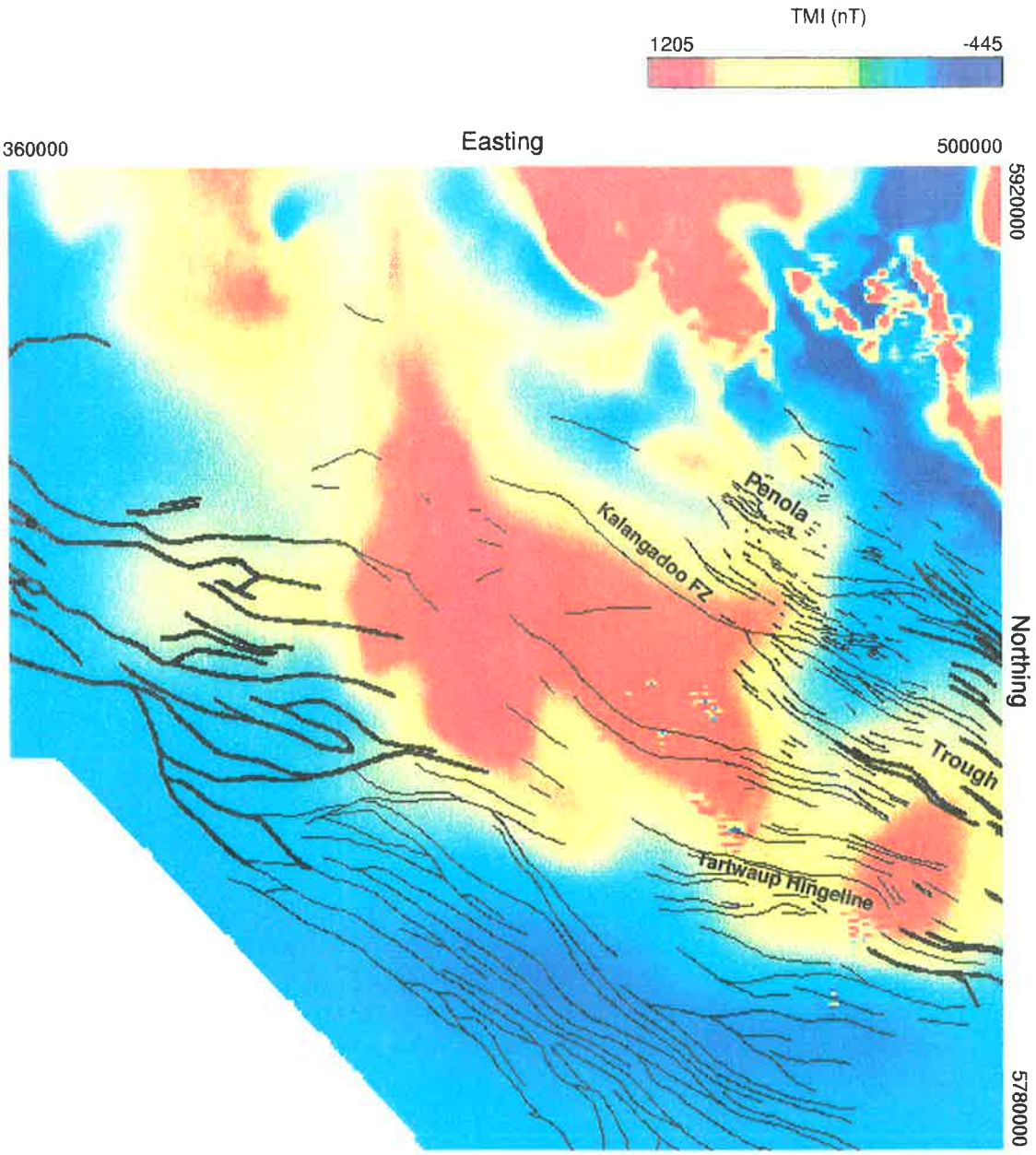

Fig. 7.1.3.3 Regional TMI image of Western Otway Basin (AGSO data) with major Eumeralla Formation faults (in black) derived from seismic horizon maps. Scale = 1:1,000,000

The Eumeralla Formation horizon fault map (fig.7.1.3.3) has only a small section in the southeast corner, south of Caroline 1, where the karstic nature of the overlying Tertiary Gambier Limestone has prevented resolution of the major fault patterns, as well as the northern part of the region where the top of the formation is too shallow to define faults. The formation is absent along parts of the basin margin, but the horizon top ranges from less than 100 m deep near the northern edges of the basin to around 6.8 km deep at the southern extremities offshore. The major structural features evident on the deeper fault maps have not had a significant influence on Eumeralla Formation deposition, with the exception of the Kalangadoo Fault Zone which is complexly faulted along the eastern section of the Penola Trough, and the Tartwaup Hingeline which marks the change in depositional environment.

The Sherbrook Group fault map (fig. 7.1.3.4) shows that the horizon is absent over a considerable part of the northern basin margin. In those northern regions where it exists it is less than 100 m deep, but exceeds 4 km deep offshore. Comparison with the underlying Eumeralla Formation shows that the group ranges in thickness from around 50 m thick at Penola 1 on the margins of the Penola Trough to around 3.3 km at Breaksea Reef 1 offshore from Port MacDonnell (from well intersections). This horizon has been mapped over the same areas as the Eumeralla horizon but this time with the formation top resolved in the karstic terrain south of Mt Gambier. As with the Eumeralla Formation horizon map, the major features of the regional map are the Kalangadoo Fault Zone and the Tartwaup Hingeline, with the former usually resulting in offsets of between 100 and 200 m.

Any comparison between the regional gravity, magnetic and seismic maps shows little correlation between structures delineated on seismic and magnetic maps but a stronger correlation between seismic and gravity maps. This is not surprising because the magnetic maps record the concentration of magnetic minerals which is not necessarily related to the lithology boundaries and other contrasts mapped by seismic methods. Gravity maps on the other hand record the density contrasts between and within lithologies, which in many cases is related to structures delineated from seismic methods. However, gravity anomalies can be produced by bodies deep within basement and well below the depth that most seismic exploration surveys can resolve. This leads to a situation where, for example, seismic mapping can show relatively shallow basement

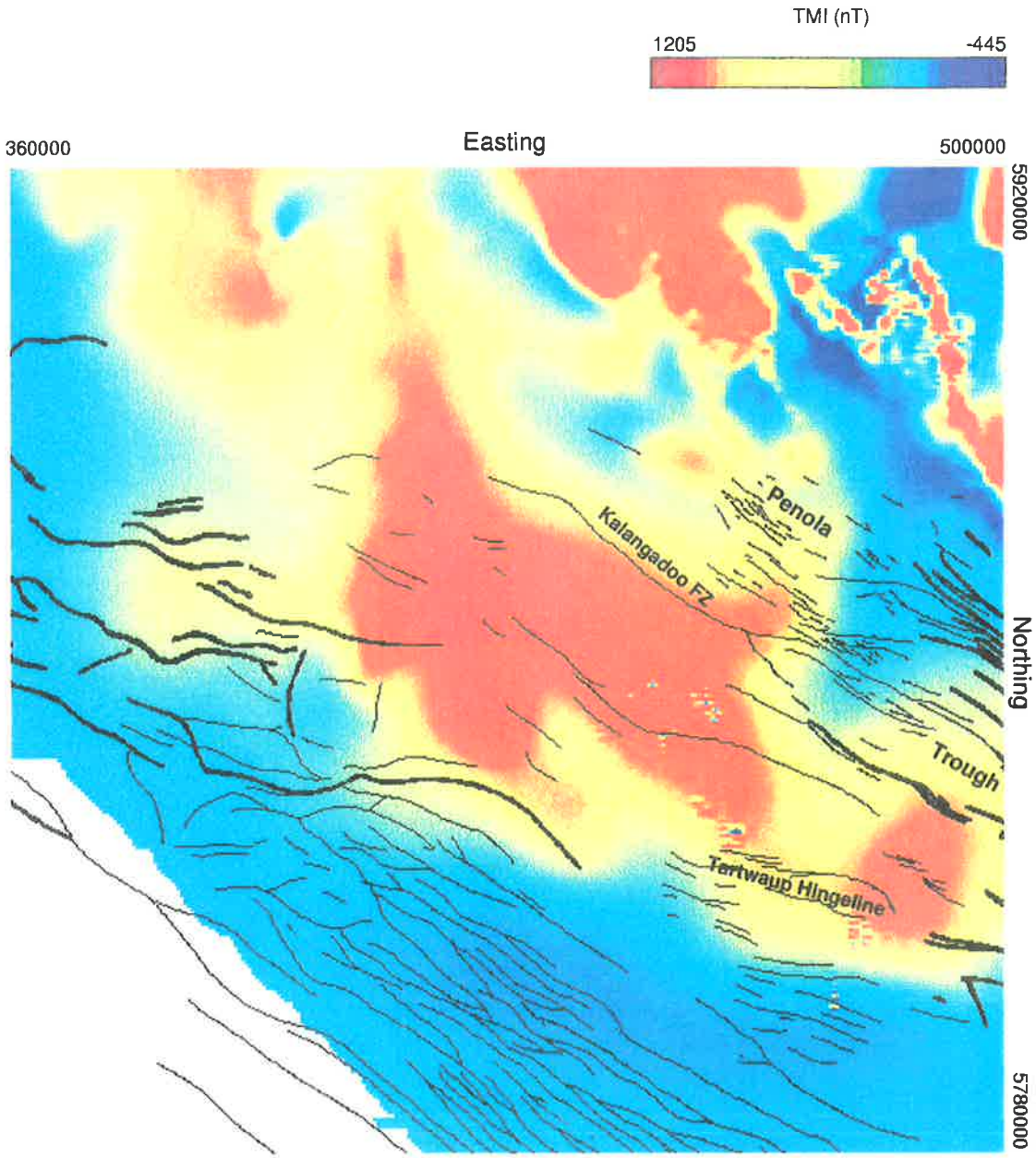

Fig. 7.1.3.4 Regional TMI image of Western Otway Basin (AGSO data) with major Sherbrook Group faults (in black) derived from seismic horizon maps. Scale = 1:1,000,000

while a gravity survey shows an intense low caused by a less dense body at greater depth. Some of the magnetic anomalies in the regional survey can be related to structures delineated by seismic methods. The most important of these are the Beachport and Sawpit Highs, the former having a high amplitude (around 400 nT) on regional magnetic maps and the latter producing a more subtle anomaly (around 14 nT).

Depth estimates using spectral analysis (Chapter 6.1) suggest that most of the sources of the prominent magnetic anomalies on the regional map are within basement and, therefore below the depth that petroleum explorationists would be targeting with seismic surveys. It is unlikely that these deep sources have been resolved on seismic sections and if they do intrude into the sedimentary section (possibly beneath Caroline 1, for example) there have been no clear, unambiguous cases of dykes or other intrusive bodies detected.

The regional magnetic map shows that the major anomaly which underlies the Mt Burr volcanic group, extends past the Kalangadoo Fault Zone into the Penola Trough with a less intense anomaly found to the northeast. This demonstrates that these magnetic sources are not confined to a particular structural province delineated by seismic or gravity methods but in most cases probably reflect basement lithology. In a similar manner the magnetic ridge extending north from a centre east of the Lake Eliza High appears to have little discernible influence on the basement topography of the Robe Trough but seismic coverage of the central part of the Robe Trough is relatively poor compared with the north and south margins.

Most of the other sources of regional anomalies do not appear to have caused the uplift or doming of the basement/sediment interface. The small circular anomaly that is alongside the northwest corner of the study area underlies an region of sloping basement which has been seismically mapped as ranging from 1.5 to 2.5 km deep while spectral analysis suggests the source of the anomaly is at a depth of around 5 km. This makes it unlikely that the source has influenced basement topography.

7.2 Geophysical Overview of the Study Area

7.2.1 Magnetic data

In the introduction the background to the MESA survey was discussed, the specifications for the survey were outlined and a comparison with previous surveys made. This survey covers the same area as the southeastern corner of the AGSO regional survey, so anomalies which are poorly defined in the regional survey are much better resolved by this survey. The small intense anomalies associated with the Mt Gambier and Mt Schank volcanic complexes along with the source of the Hungerford anomaly, were sampled by very few flightlines in the regional survey (1.5 km spacing). Two AGSO flightlines passed on either side of the Hungerford anomaly with the result that, while the anomaly is detectable on the regional map, the amplitude is greatly reduced compared with the high resolution survey where five flightlines crossed it.

The magnetic map is dominated by some large anomalies which are much more intense than other smaller anomalies that in some cases are located close to them. While some of the smaller anomalies, such as the Mt Gambier volcanic complex, are quite distinct from the larger, more regional features due to their high amplitude, there are a number of anomalies which interfere with each other to the extent that it is difficult to separate their effects on TMI images and contour maps.

The contractor, World Geoscience Corporation, supplied MESA with contour maps and images of the first vertical derivative, as well as a series of pseudo depth slice maps where spectral analysis and matched filtering was used to isolate anomalies considered to result from sources at some level in the crust (Chapter 6.1). These maps were used, along with second vertical derivative, horizontal gradient and analytical signal maps produced by the author, to separate anomalies and in some cases outline the source body. All TMI contour maps and images show a large number of small anomalies which are associated with cultural features, which cause significant problems on gradient images by producing large 'spikes' that mask the more subtle geological signal. The pseudo depth slice maps suffer from contamination of the deeper slice maps by cultural anomalies which are, of course, associated with sources on the surface, and can lead to

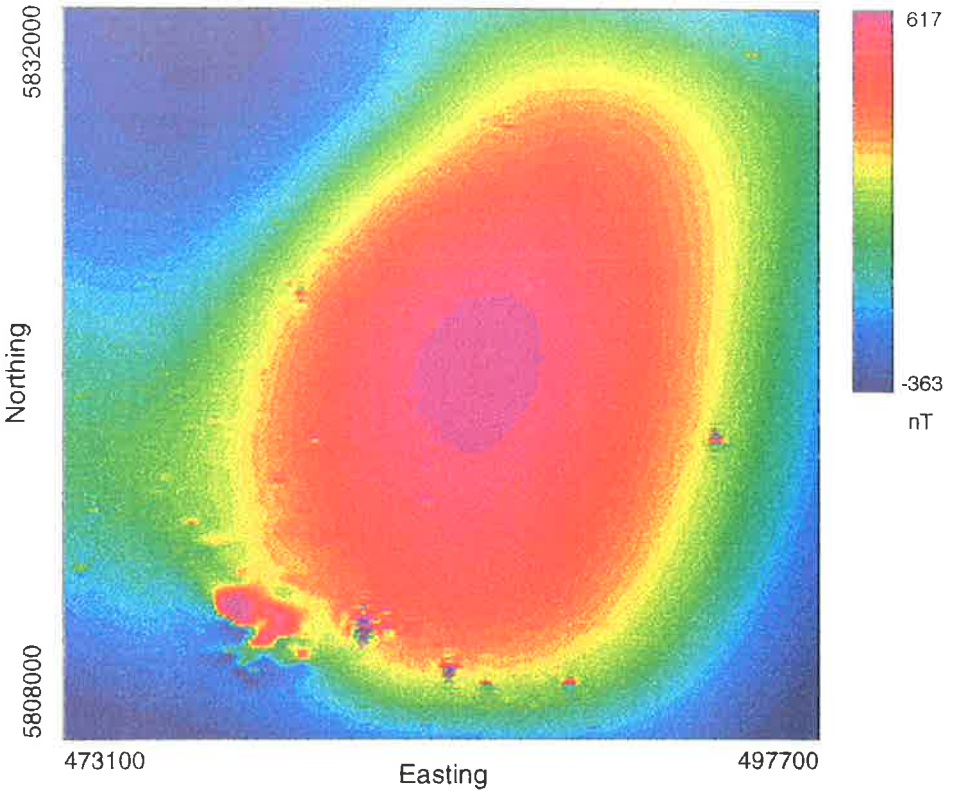

Fig. 7.2.1.1a Mt Gambier Anomaly TMI image with Mt. Gambier volcanic complex at lower left

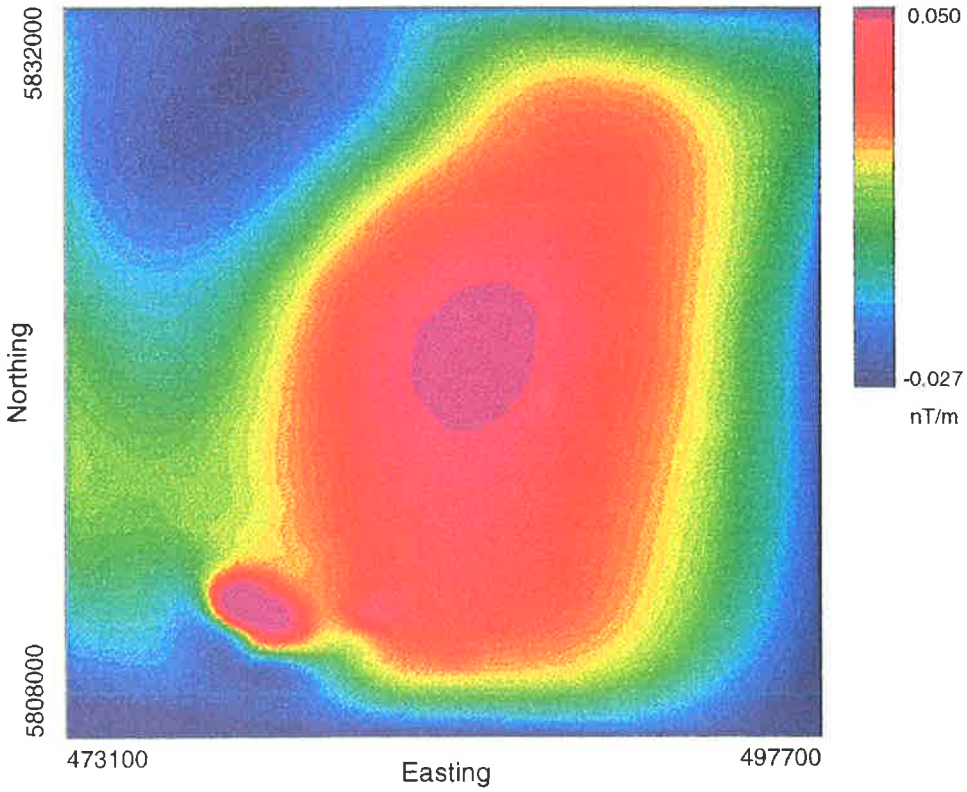

Fig. 7.2.1.1b Mt Gambier Anomaly vertical gradient image (500m. upward continuation)

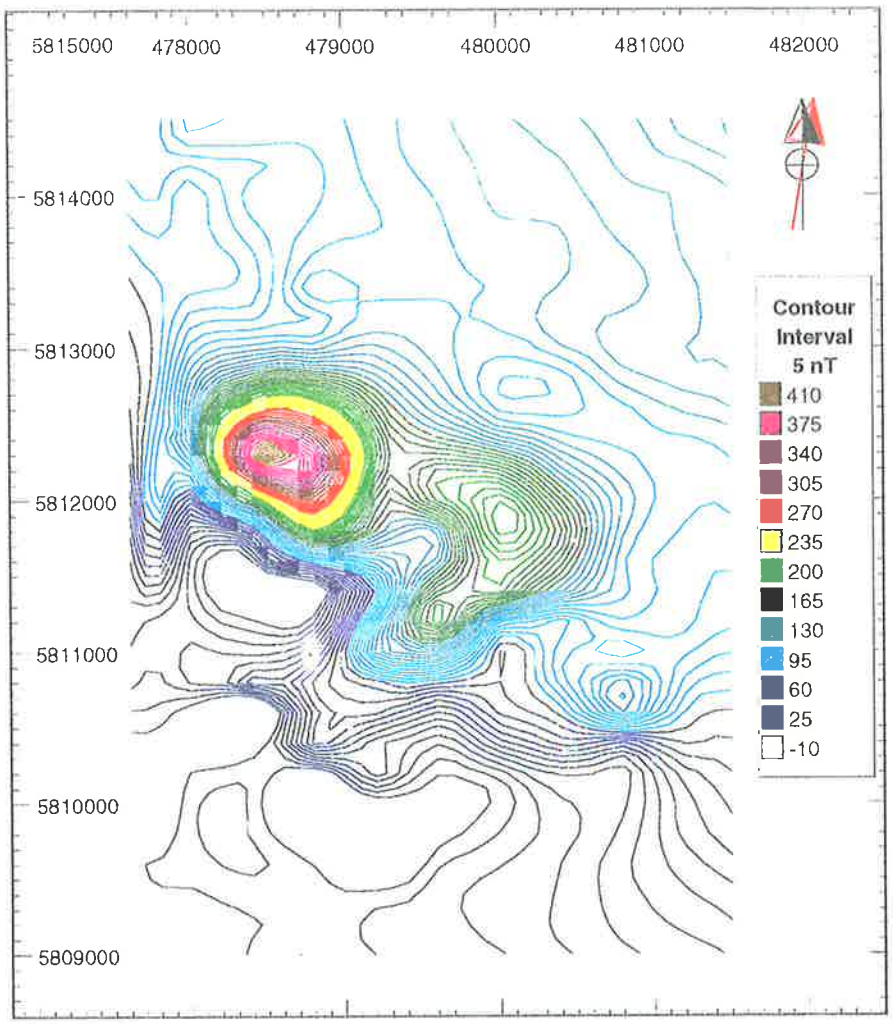

Fig. 7.2.1.2 Mt. Gambier volcanic complex TMI contour map

Scale = 1:50,000

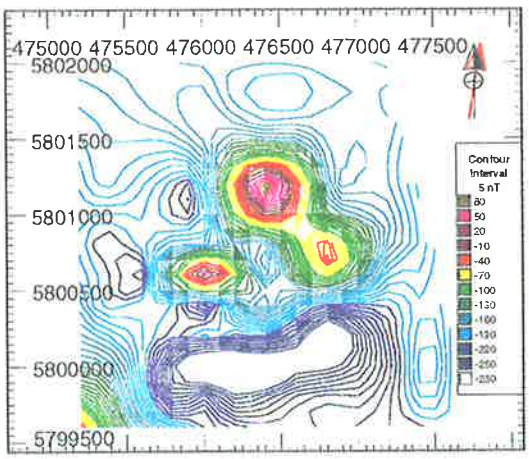

Fig. 7.2.1.3 Mt. Schank volcanic complex TMI contour map

Scale = 1:50,000

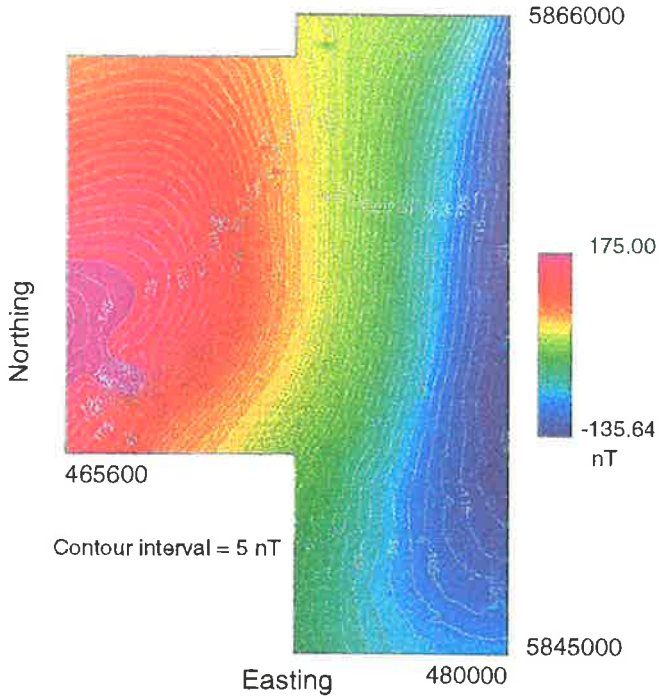

Fig. 7.2.1.4a Western Penola Trough TMI image

Scale = 1:250 000

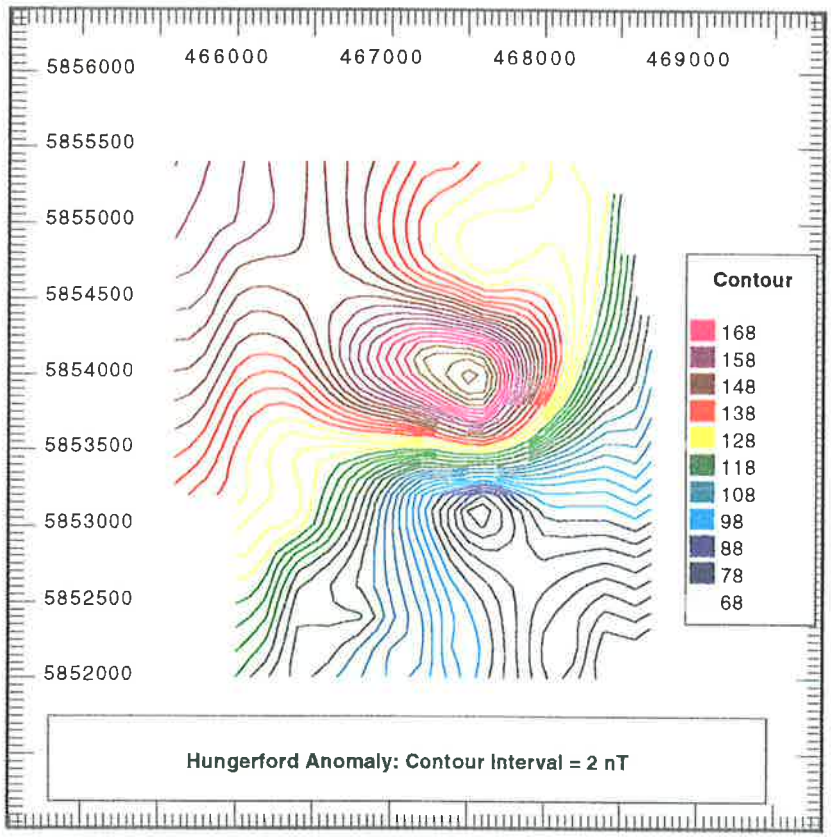

Fig. 7.2.1.4b Hungerford Anomaly contour map

Scale = 1:50 000

the situation where, for example, a sawmill produces an anomaly on a depth slice map representing sources approximately 3 km deep.

The main feature of the P1 survey is the large positive, semi-elliptical anomaly, the Mt Gambier anomaly (figs. 7.2.1.1a and b), that extends to the northeast of the city of Mt Gambier, and is around 35 to 40 km long and 18 to 20 km wide with an overall amplitude of around 400 nT. This anomaly is believed to result from magnetic sources within and associated with the magma chamber that was the source of the Holocene volcanic eruptions at Mt Gambier and Mt Schank. The volcanic complexes are found on the southwestern side of the large anomaly (Mt Gambier), and around 12 km south-southwest of the city (Mt Schank).

The Mt Gambier volcanic complex produces an anomaly which is approximately 3×1.5 km trending east-southeast with three positive peaks (fig. 7.2.1.2). The largest of the peaks is centred over the western side of the complex mostly north of Brownes Lake (fig. 3.3.1.1), while the second peak is centred over the Blue Lake, and the smaller third peak is centred about 500 m southwest of the Blue Lake peak over the edge of the cone. The Mt Schank volcanic complex produces an anomaly around 1.5×1.8 km (fig. 7.2.1.3) which also has three positive peaks that are of lower amplitude than the Mt Gambier complex. The most intense peak is found over a line of small cones that cover a fissure to the northwest of the main crater (fig. 3.3.1.2) while the main crater itself is the source of a less intense, bi-polar anomaly with the positive peak centred over the northern side of the crater. The third component is a smaller, bi-polar anomaly centred to the west of the main crater where a small subsidiary crater has erupted surface basaltic flows. The centre of the anomaly is offset 200 to 250 m to the west of the small crater over an area covered by basalt lava flows.

On the northwestern side of the study area and, particularly in the western extension of the study area, is a broad magnetic high, the Western Penola Trough anomaly (fig. 7.2.1.4a), which is part of the large irregular anomaly around the Mt Burr volcanic group which was discussed in the section on regional magnetic features (section 7.1.2). The source of this magnetic high most probably underlies the Penola Trough and Kalangadoo Fault Zone, with the latter trending southeasterly along the southern margin of the extension. The northeasterly trending margin of the magnetic high has been interpreted as representing basement faulting along which extension occurred (Reeves et

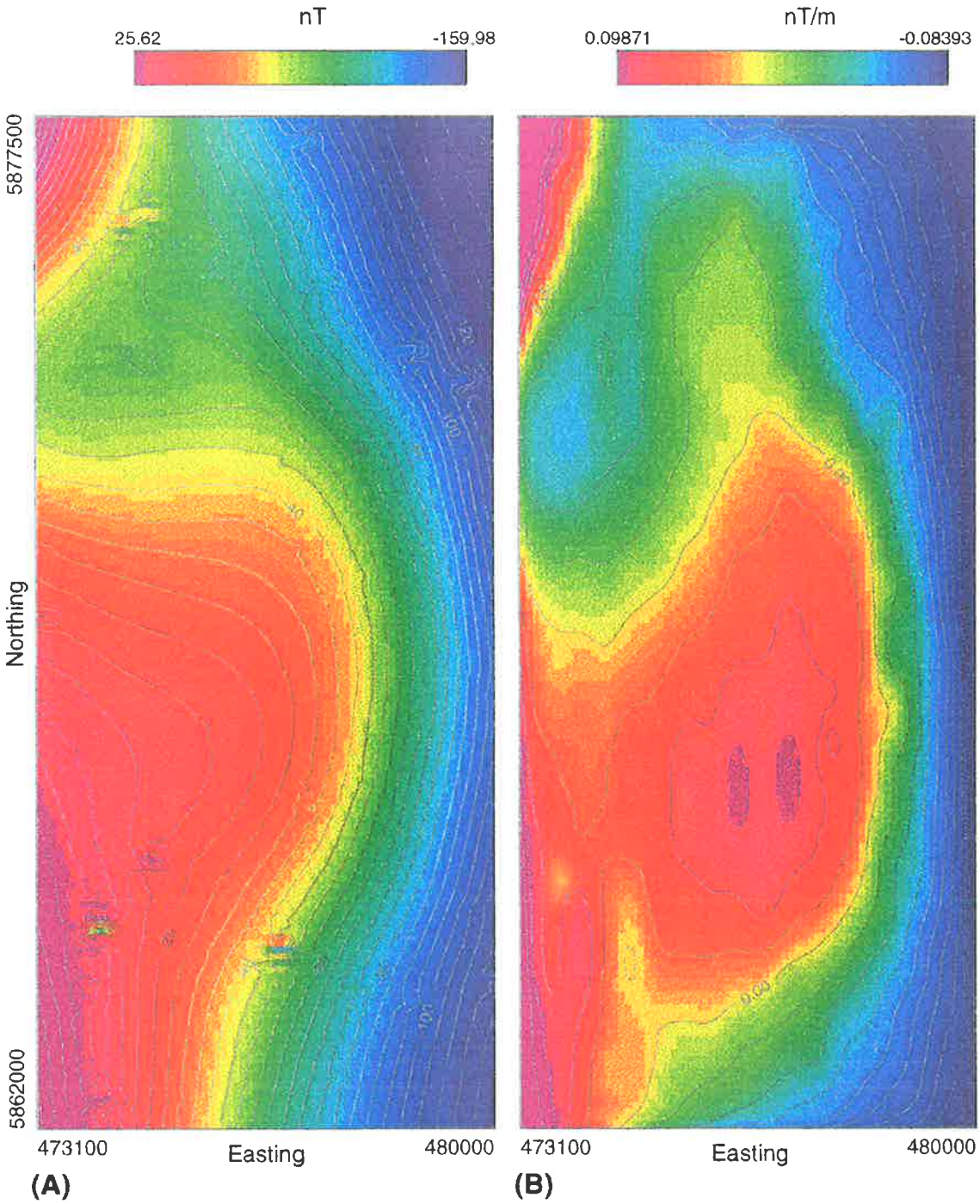

Fig. 7.2.1.5 Northwest Penola Trough contour maps and images

TMI image (A) and Vertical Gradient image (B), Scale = 1:100,000

(A) Contour interval = 10 nT, (B) Contour Interval = 0.02 nT/m

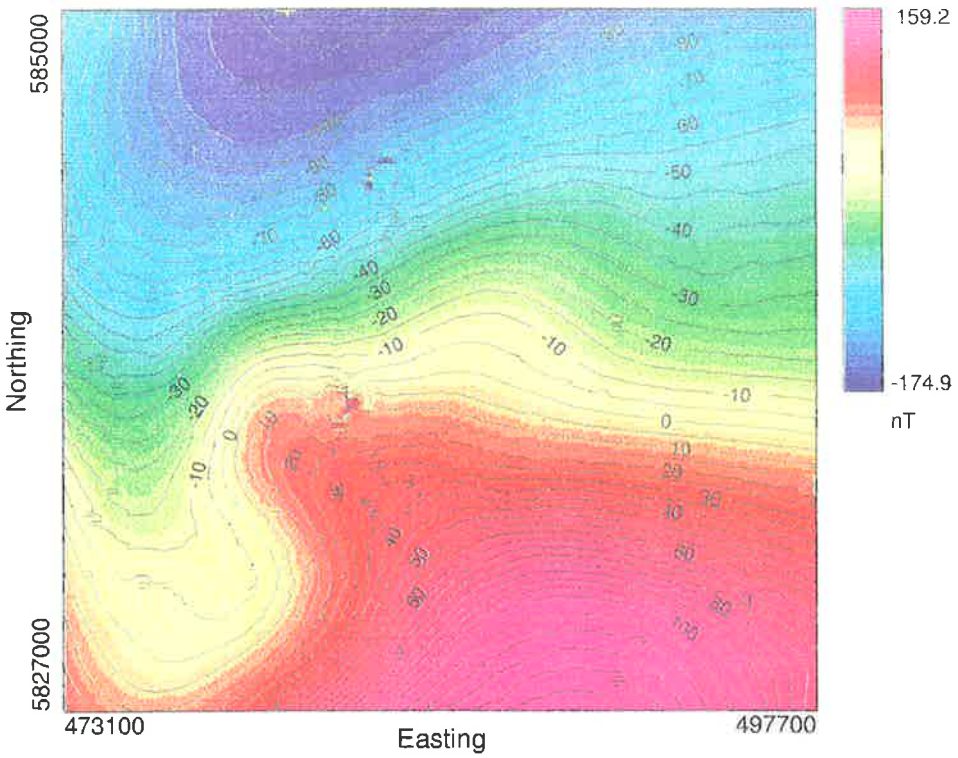

Fig. 7.2.1.6a Kalangadoo Area, TMI image and contour map, Scale = 1:250,000

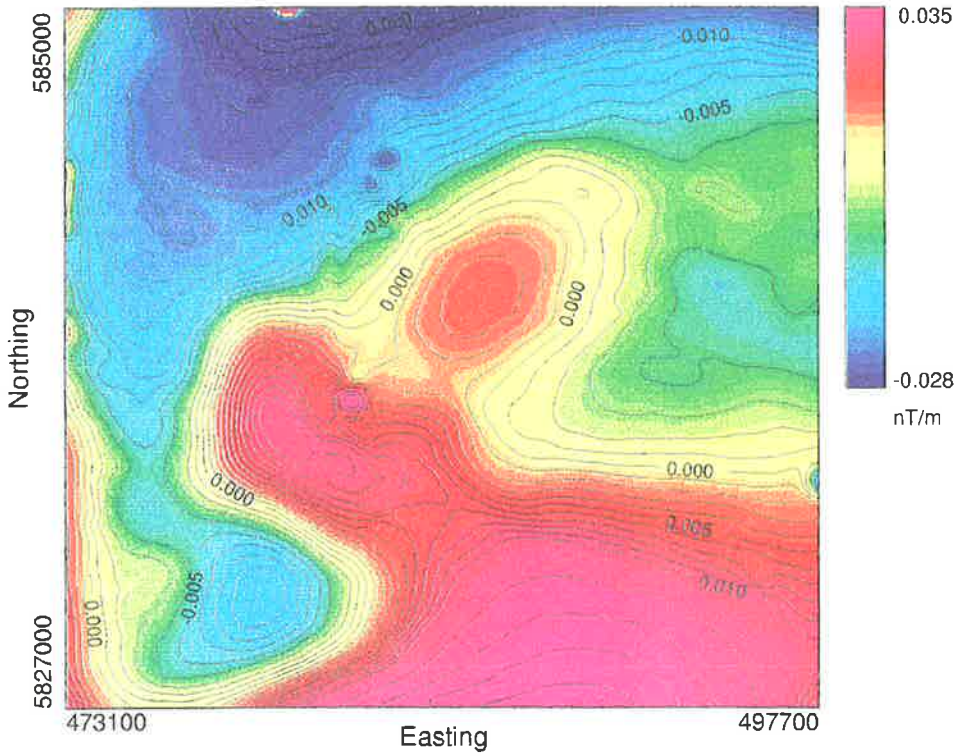

Fig. 7.2.1.6b Kalangadoo Area, image and contour map of upward continuation/vertical gradient, Scale = 1:250,000

al., 1993). The previously mentioned Hungerford anomaly is in the southwestern corner of the extension of the study area and is very likely the result of a basaltic plug or vertical dyke-like feature which has intruded into the sedimentary section but failed to reach the surface (fig. 7.2.1.4b).

Immediately to the northeast of this western extension (fig. 7.2.1.5a) is an elliptical anomaly (Northwest Penola Trough anomaly) trending roughly north-south, approximately 8 by 5 km, which is considerably lower in amplitude than the previously discussed anomaly to the southwest. It is apparent as an eastward 'bulge' in the general north-south trend of the boundary between the western high and the central Penola Trough low and can be seen more clearly on the vertical gradient map (fig. 7.2.1.5b). The boundary extends to the northwest corner where the circular anomaly (Northwest Corner anomaly), discussed in the section on the regional map, produces a steep gradient because of the high intensity compared with adjacent areas.

Northwest of the major Mt Gambier anomaly (fig. 7.2.1.6a) is an relatively small, elliptical anomaly (the Kalangadoo anomaly) trending east-southeast which vertical gradient images suggest is approximately 9 × 6 km, with an amplitude of around 20 nT and located partly over the Kalangadoo High and partly over the Kalangadoo Fault Zone to the north (fig. 7.2.1.6b). To the northeast of the Kalangadoo anomaly is a lower amplitude, more subtle feature, the Mid-Penola Trough anomaly, which is located in the centre of the study area over the Penola Trough and is separated from the Kalangadoo anomaly by the Kalangadoo Fault Zone. This anomaly is reasonably well defined on the southwestern side by the gradient images, less so along the northwest and southeastern sides, but is more difficult to determine the northeastern margin of the source body. The sharp southwestern margin defines the edge of the Kalangadoo Fault Zone while the regional trend along the northwestern margin has been interpreted to outline deep basement faulting (Reeves et al., 1993). The northeast margin is probably difficult to detect because of the substantial increase in depth to basement north of the anomaly (assuming the source is at the top of basement).

In the magnetic low which covers part of the eastern Penola Trough, there are two relatively small anomalies (the Northern Penola Trough anomalies) which are located on the northern flanks of the Penola Trough (fig. 7.2.1.7a). The southern, more circular anomaly, the Sawpit anomaly, is most probably associated with the Sawpit

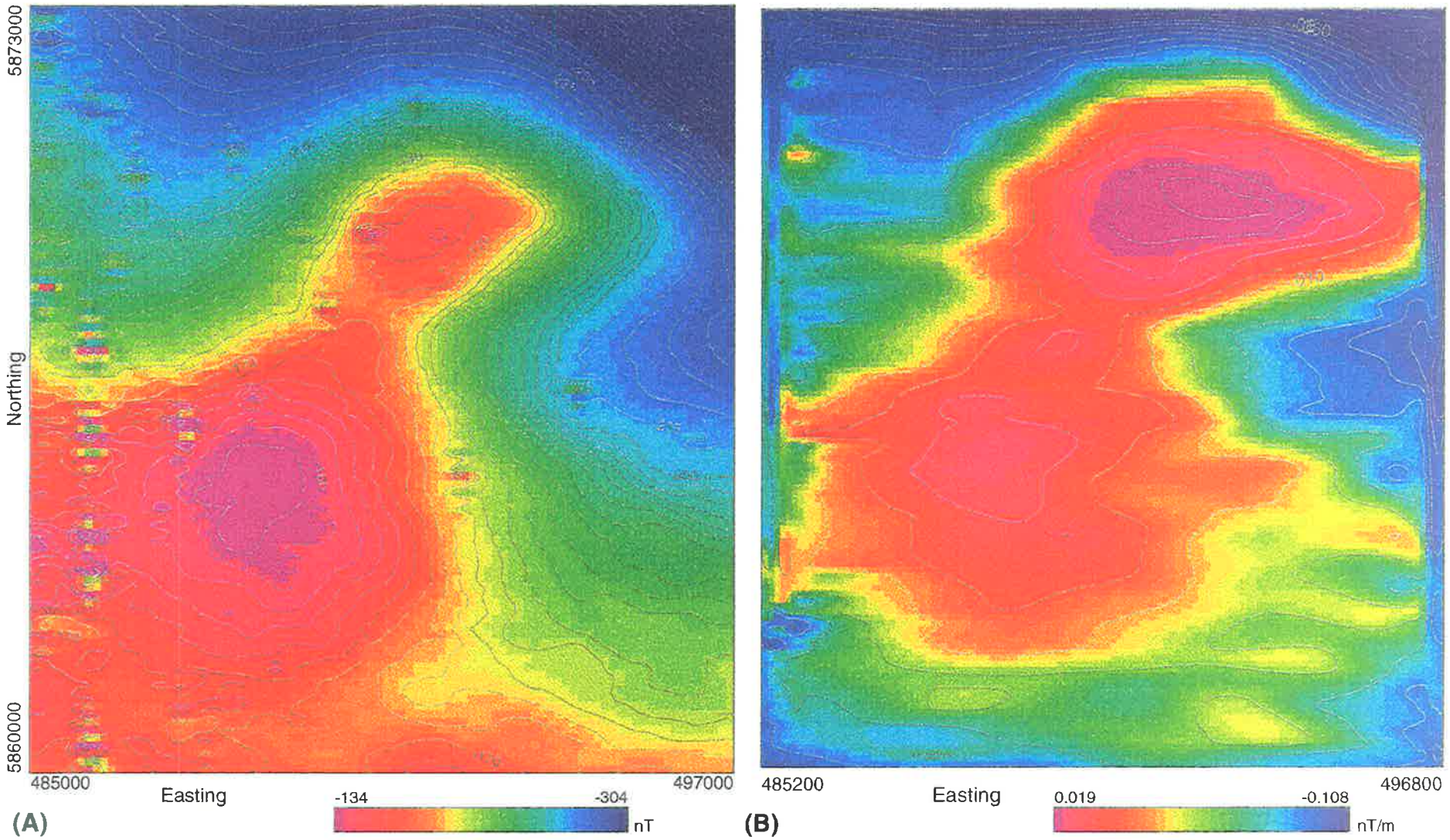

Fig. 7.2.1.7 Northeast Penola Trough images and contour maps. (A) TMI and (B) Vertical Gradient, Scale = 1:100,000

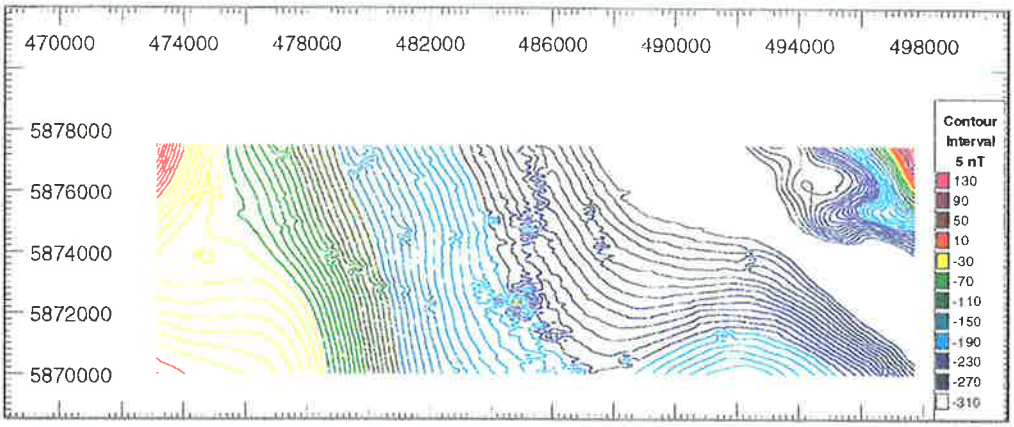

Fig. 7.2.1.8a Northern Margin, TMI contours with culture

Scale = 1:250,000

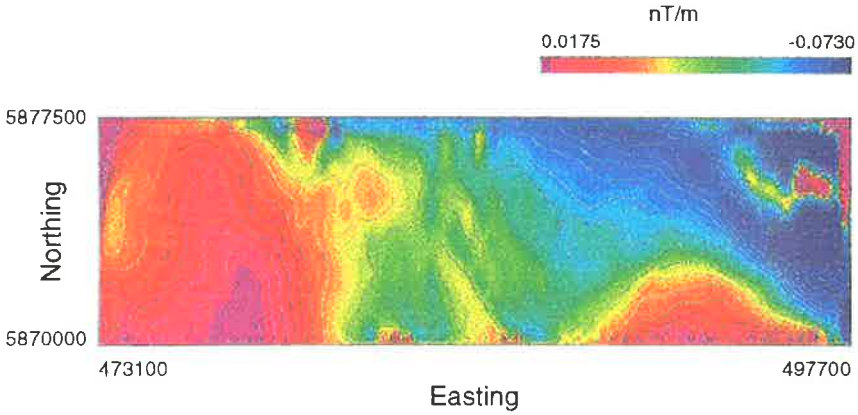

Fig. 7.2.1.8b Northern Margin, vertical gradient image with contours, Scale = 1:250,000

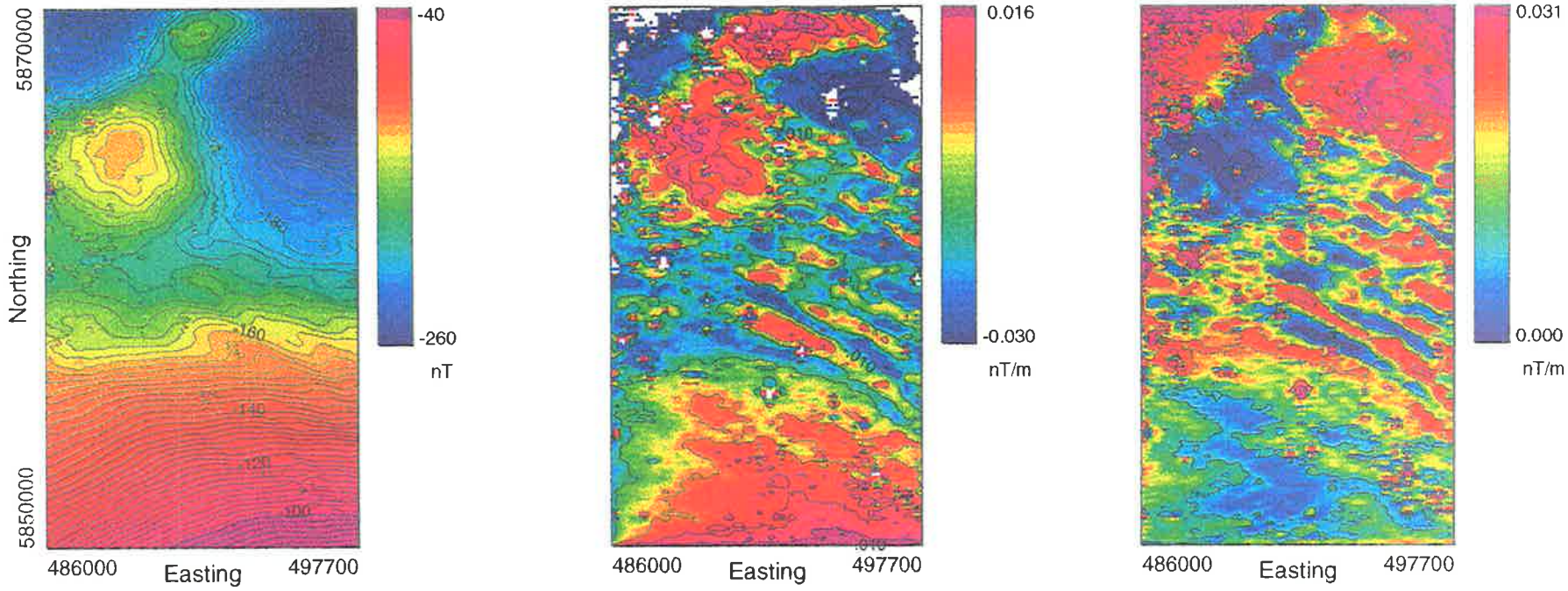

(A) contour interval = 2 nT

(B) contour interval = 0.005 nT/m

(C) contour interval = 0.005 nT/m

Fig. 7.2.1.9 East Penola Trough linear anomalies contour maps and images, (A) TMI, (B) vertical gradient and (C) analytic signal. Scale = 1:250,000

basement high but is offset to the south of that seismically defined feature. This is a broad anomaly with an amplitude of around 15 nT that is poorly defined on the gradient maps but is probably around 5 km in diameter. The elliptical anomaly to the northeast of Sawpit is more intense and is on the flanks of a deep magnetic low but unlike its southern neighbour is not readily associated with any feature located by seismic mapping. The source of the anomaly appears to be around 6 × 3 km and trends approximately east-west according to the evidence of vertical gradient maps (fig. 7.2.1.7b).

The northeast corner of the study area, to the north and northeast of the Northeast Penola Trough anomalies, are two intense elliptical magnetic lows which are displayed in their entirety on the regional map (fig. 7.1.2.2). The northern low has its centre along the northern margin of the study area (around 490000mE) while its northeast counterpart is more elongate and trends around E 140° N along the Kanawinka Fault Zone from just west of the eastern boundary of the study area extending southeast into Victoria (figs. 7.2.1.8a and b).

On the southeastern and eastern side of the two Northeast Penola Trough anomalies are a series of linear magnetic features (figs. 7.2.1.9a, b and c), generally trending around E 120° N, which have a maximum length of around 8 km and a maximum width of around 1 km. The largest two linear anomalies run from the Victorian border (approx. 497700mE, 5855000mN) to the southeastern edge of the Sawpit anomaly (approx. 491000mE, 5859000mN) with an amplitude of between 1 and 3 nT.

These two anomalies are the most prominent of this kind but there are a number of others to the north of these which are emphasised on the vertical gradient and analytic signal maps, and some of this group appear to be superimposed on top of the Sawpit anomaly and its northeastern neighbour. There is another probable linear anomaly around 4 km to the south of the major ones (fig. 7.2.1.9c) with other less likely features to the northeast and east of the Mid-Penola Trough anomaly. Other anomalies of this type can be found over the rest of the Penola Trough but are generally low amplitude, and require substantial image processing to map their extent. A persistent problem in identifying these linear anomalies on gradient maps is the similarity between their appearance and the appearance of anomalies due to power lines.

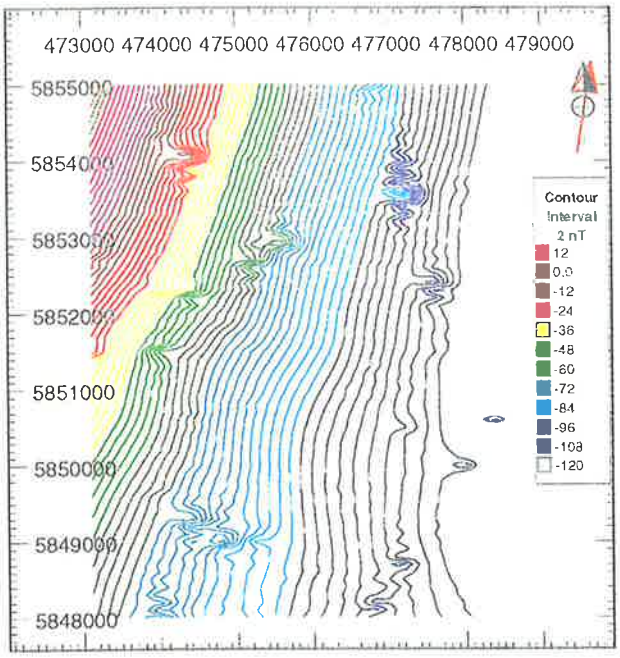

Fig. 7.2.1.10a Northwest Kalangadoo TMI contour map, Scale = 1:100,000

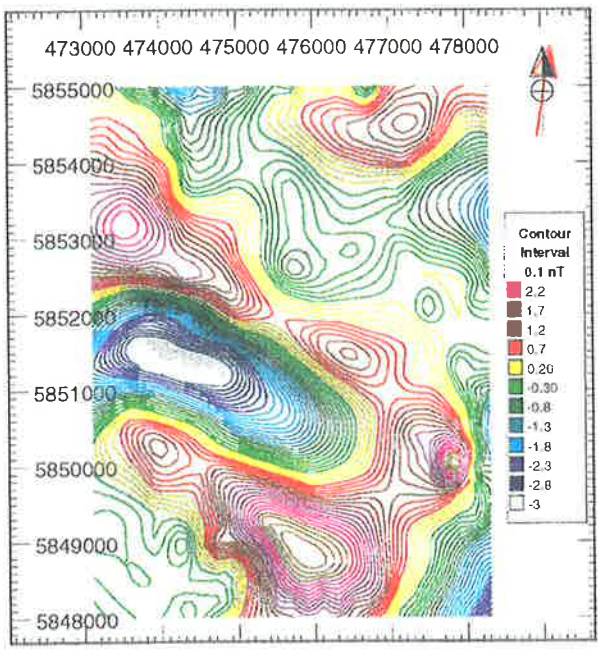

Fig. 7.2.1.10b Residual TMI greyscale image and colour contour map with NE sun angle shading, Scale = 1:100,000

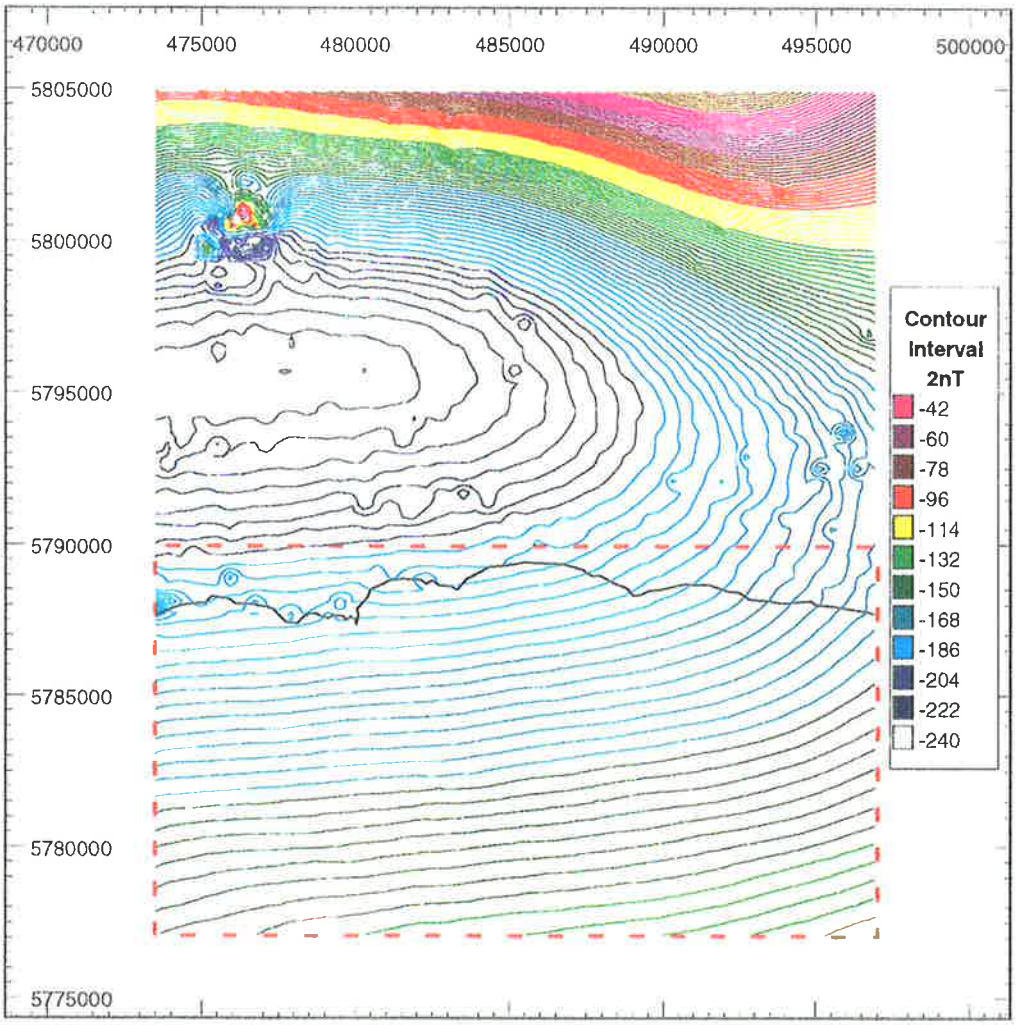

Fig. 7.2.1.11 South coast and Offshore section TMI contour map Scale = 1:250,000, Outline of offshore section vertical gradient map shown in red. Coastline shown in black

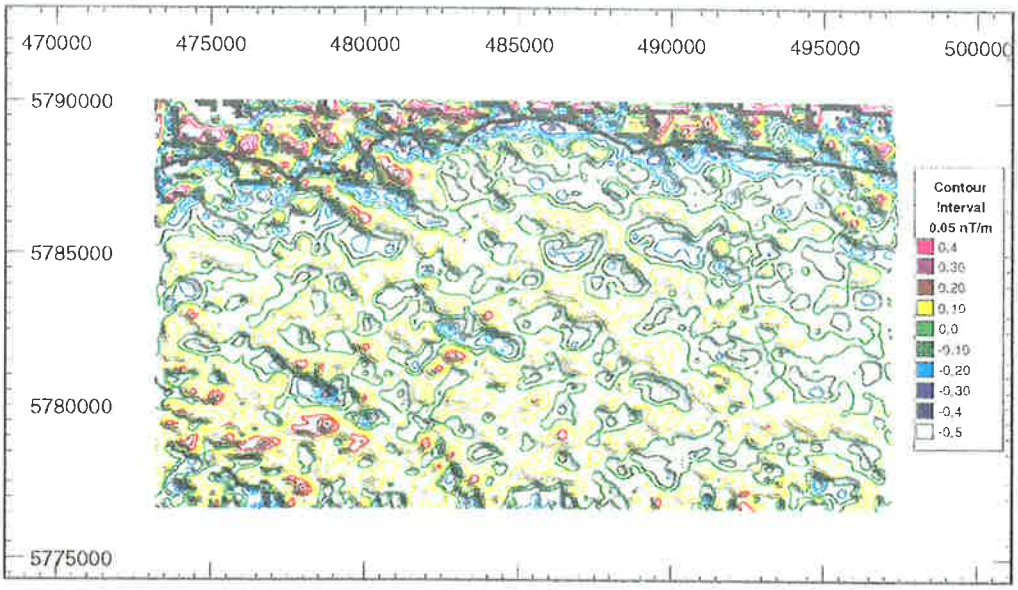

Fig. 7.2.1.12a Offshore vertical gradient image and contour map NE azimuth sunangle applied to image to enhance lineations Coastline shown in black

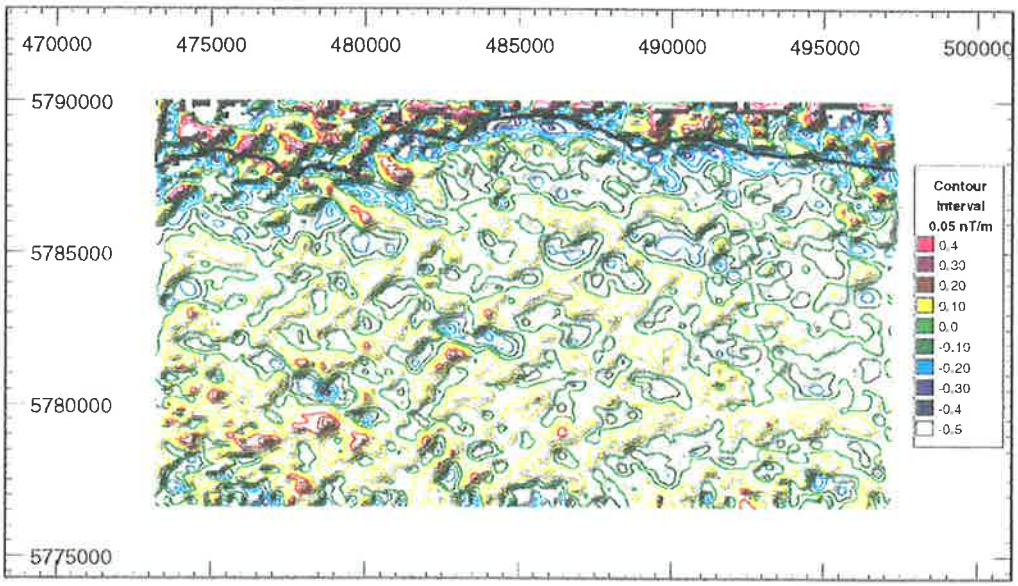

Fig. 7.2.1.12b Offshore vertical gradient image and contour map NW azimuth sunangle applied to image to enhance lineations Coastline shown in black

Possible linear anomalies include two sets oriented similarly to faults near the Haselgrove and Katnook gas fields, and a relatively long wavelength feature about 5 km long trending approximately E 120° N which is aligned with the Hungerford anomaly but begins around 3 to 5 km southeast of it. This last feature is plotted in figs. 7.2.1.10a and b. The use of low-pass filtering to remove the near surface component of the field and emphasise the basement features suggests that these anomalies are due to magnetic sources at shallow depths within the sedimentary section rather than caused by basement faulting which results in offsets of magnetic horizons. There is little evidence of other similar linear features over the western extension of the study area or over the Northwest Penola Trough anomaly.

South of the Mt Gambier anomaly is a large regional magnetic low which was previously discussed as an eastern extension of the major low on the AGSO map (fig. 7.1.2.2). In the study area this is manifested as a semi-elliptical low with an east-west axis that is approximately 5 km south of the Mt Schank volcanic complex. There are a substantial number of small circular anomalies in this area that are very likely to be of cultural origin, which can be seen by their abrupt disappearance to the south where they help delineate the coastline (fig. 7.2.1.11). There are no lineations that might be expected to be the result of magnetic sources in the feeder pipe that brought lava from the magma chamber to the Mt Schank volcanic complex.

The southernmost part of the study area is offshore and because of the problem of oceanic swell noise (Gunn, 1995), was flown at an altitude of 120 m in an attempt to minimise the problem. Images were found to be more useful in defining any linear magnetic features than contour maps because of the very subtle nature of anomalies in this region. Vertical gradient images (with sun angle enhancement at 45° and 315°) were generated in order to emphasise linear features (figs. 7.2.1.12a and b) but cultural features along the coastline at the top of the map created very intense 'spikes' in the gradient maps masking the low amplitude features offshore, which required suppression through filtering. In addition, there were a few individual flightlines which were contaminated by noise of shorter frequency than the swell noise discussed previously which was also suppressed.

The resulting gradient images show what appear to be a series of cross-cutting lineations trending approximately northeast-southwest and northwest-southeast, some of

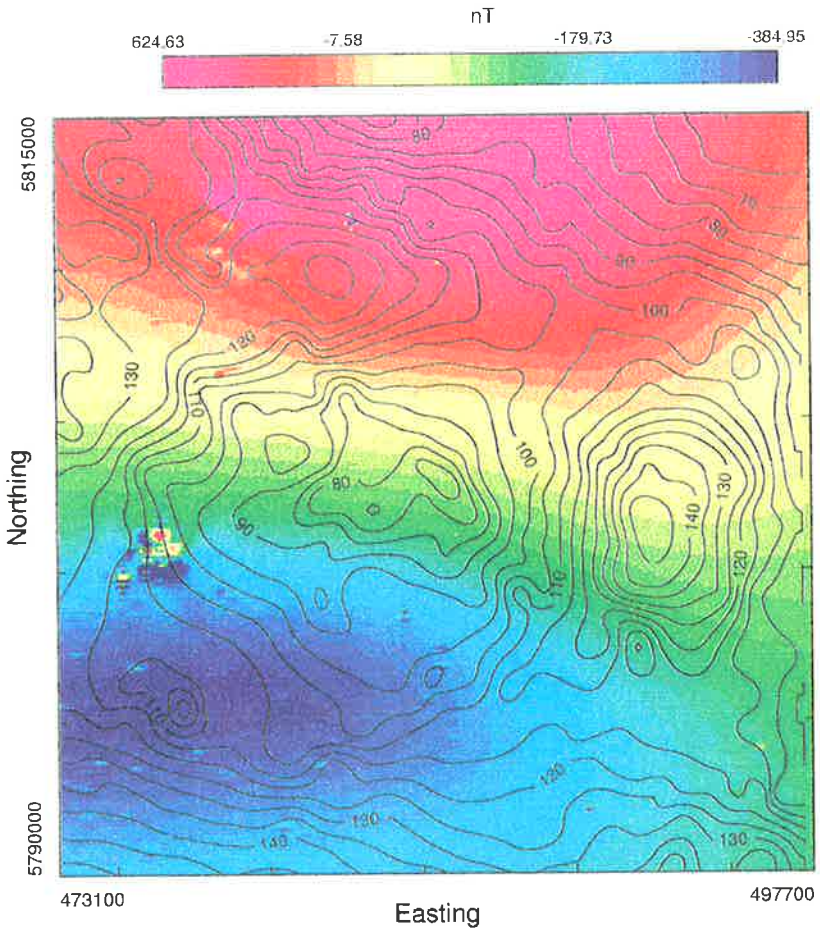

Fig. 7.2.2.1 Southern Mt Gambier area

TMI image + gravity contours

Gravity grid = 200 x 200 m, Gravity contours = 5 micrometres/sec/sec [g.u.]

TMI grid = 100 x 100 m, Scale = 1:250,000

which extend most of the way across the map while others seem to have been offset by lineations with the opposite orientation. The lineations which are oriented northwest-southeast (fig. 7.2.1.12a) follow the regional trend of faults mapped by seismic surveys adjacent to this area and located in the mid to Late Cretaceous section, however, these may be to deep to produce anomalies with the amplitude and wavelength found here. The northeast-southwest anomalies (fig. 7.2.1.12b) could represent sources that are oriented along the direction of main extension or alternatively, could be the result of sources close to the seabed.

7.2.2 Gravity data and its relationship with the magnetic map

The gravity data was supplied in gridded form (in $\mu m.s^{-2}$) by MESA to the author and was taken from the gravity profiles discussed in the introduction to this chapter. This suggests that the gridded values are more reliable in the region around the city of Mt Gambier because of the close spacing of stations while in the section stretching from around Penola south to the Kalangadoo Fault Zone, the gridded data was generated from comparatively few profiles making it less reliable. The section north of Penola has a slightly better coverage of stations than south of Penola, making the gridded data more reliable over this section. The gravity data is presented as contours overlying the corresponding TMI image.

In the southern part of the study area where the magnetic map shows the dominant influence of the Mt Gambier anomaly, the gravity map shows two anomalies, a 40 $\mu m.s^{-2}$ (4 mgal) positive elliptical anomaly about 7 km in diameter on the eastern side near Caroline 1 (Caroline Gravity High), and a 20 $\mu m.s^{-2}$ (2 mgal) irregular-shaped negative anomaly about 12 km across to the east and northeast of Mt Schank (fig. 7.2.2.1). There is also a roughly circular anomaly, approximately 3 km across and 10 $\mu m.s^{-2}$ in amplitude, east-southeast of the Mt Gambier volcanic complex while on the western margin of the study area, southwest of Mt Gambier, is a subtle positive feature. A number of small circular anomalies can be found on this map, including a minor negative anomaly (10 $\mu m.s^{-2}$) over the centre of the regional magnetic low. Some caution is required in interpreting these anomalies as well as what appear to be trends in the gravity contours, because of the incomplete coverage of gravity stations discussed earlier which may mean that these features are artifacts of the gridding process.

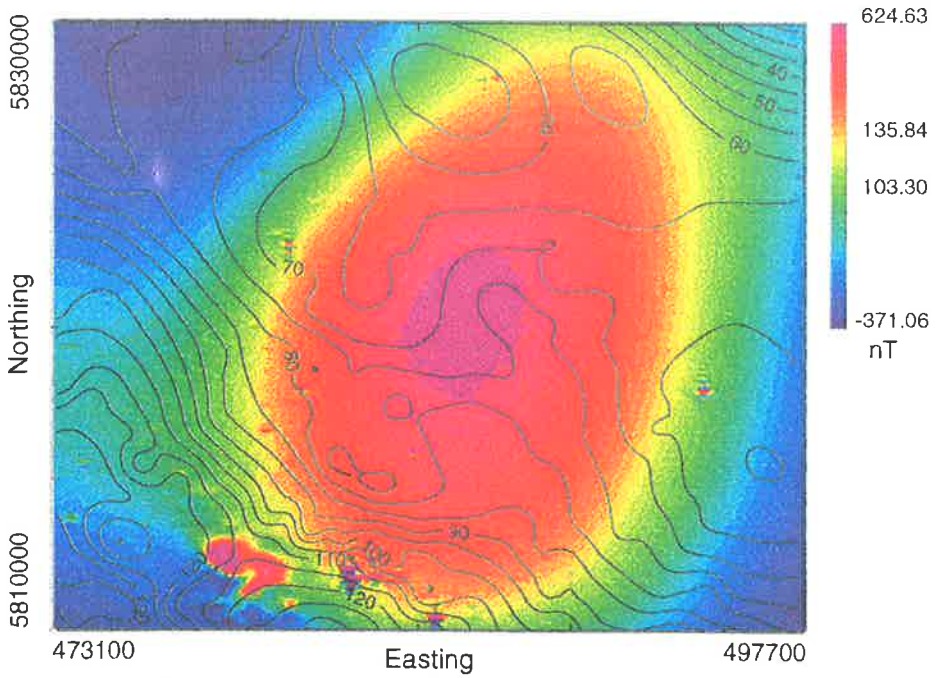

Fig. 7.2.2.2 Northern Mt Gambier area
TMI image + gravity contours

Gravity grid = 200 x 200 m, Gravity contours = 5 g.u.
TMI grid = 100 x 100 m

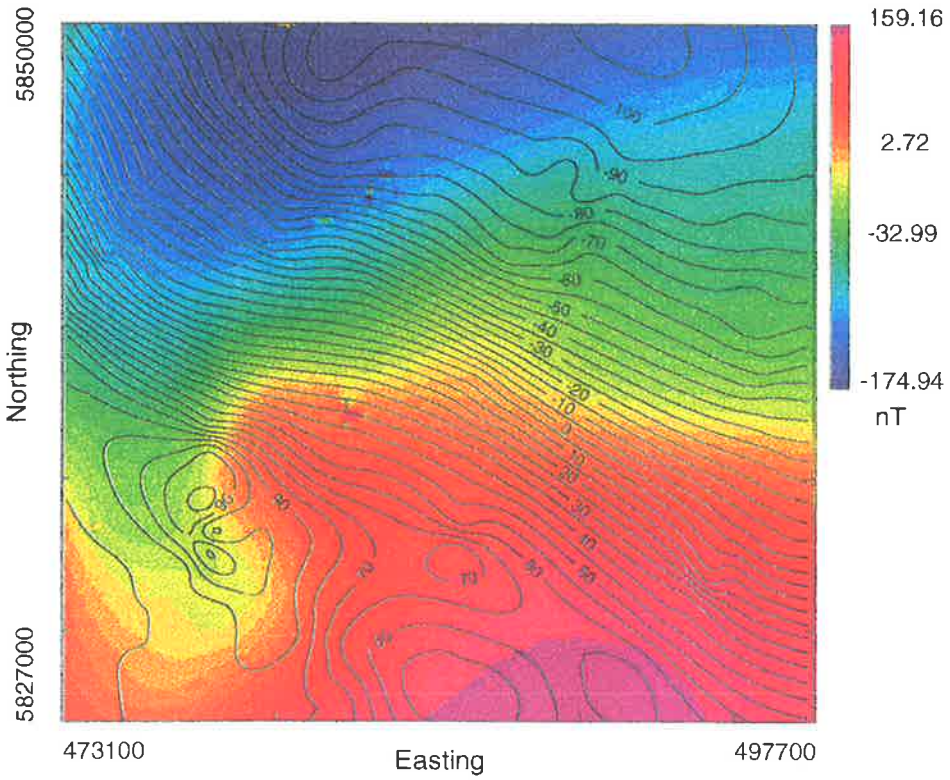

Fig. 7.2.2.3 Kalangadoo & Penola Trough anomalies
TMI image + gravity contours

Gravity grid = 200 x 200 m, Gravity contours = 5 g.u.
TMI grid = 100 x 100 m

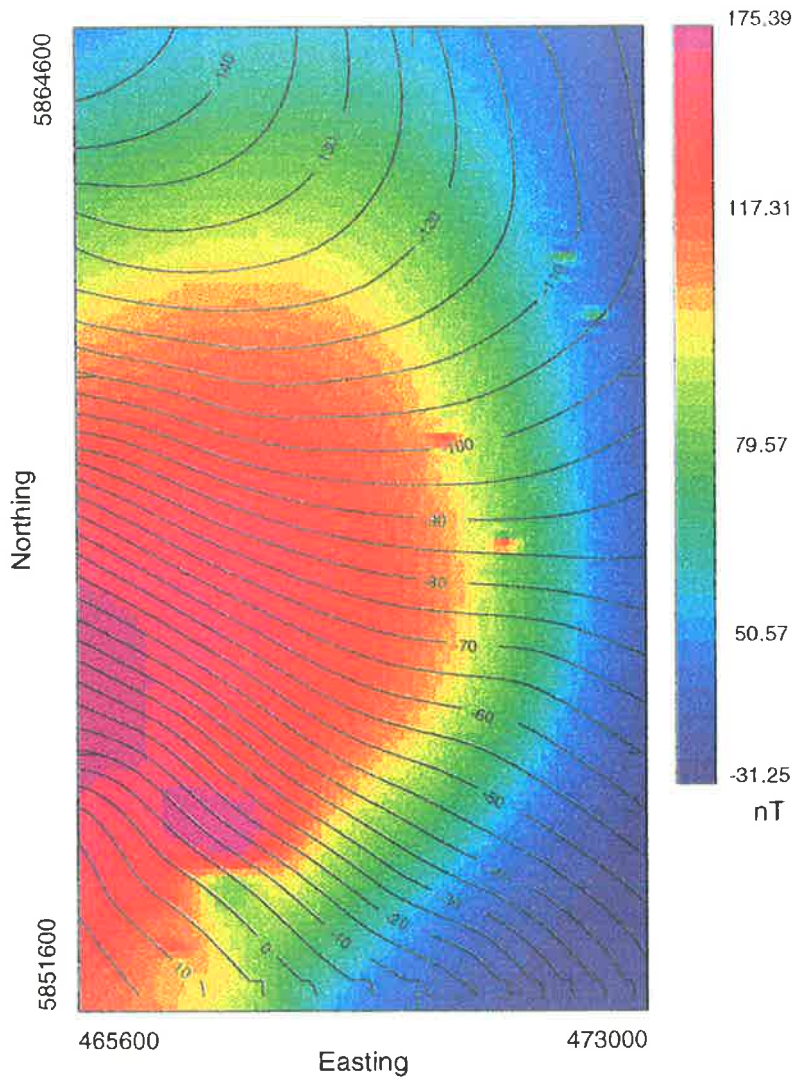

Fig. 7.2.2.4 Western Penola Trough area

TMI image + gravity contours

Gravity grid = 200 x 200 m, Gravity contours = 5 g.u.

TMI grid = 100 x 100 m, Scale = 1:100,000

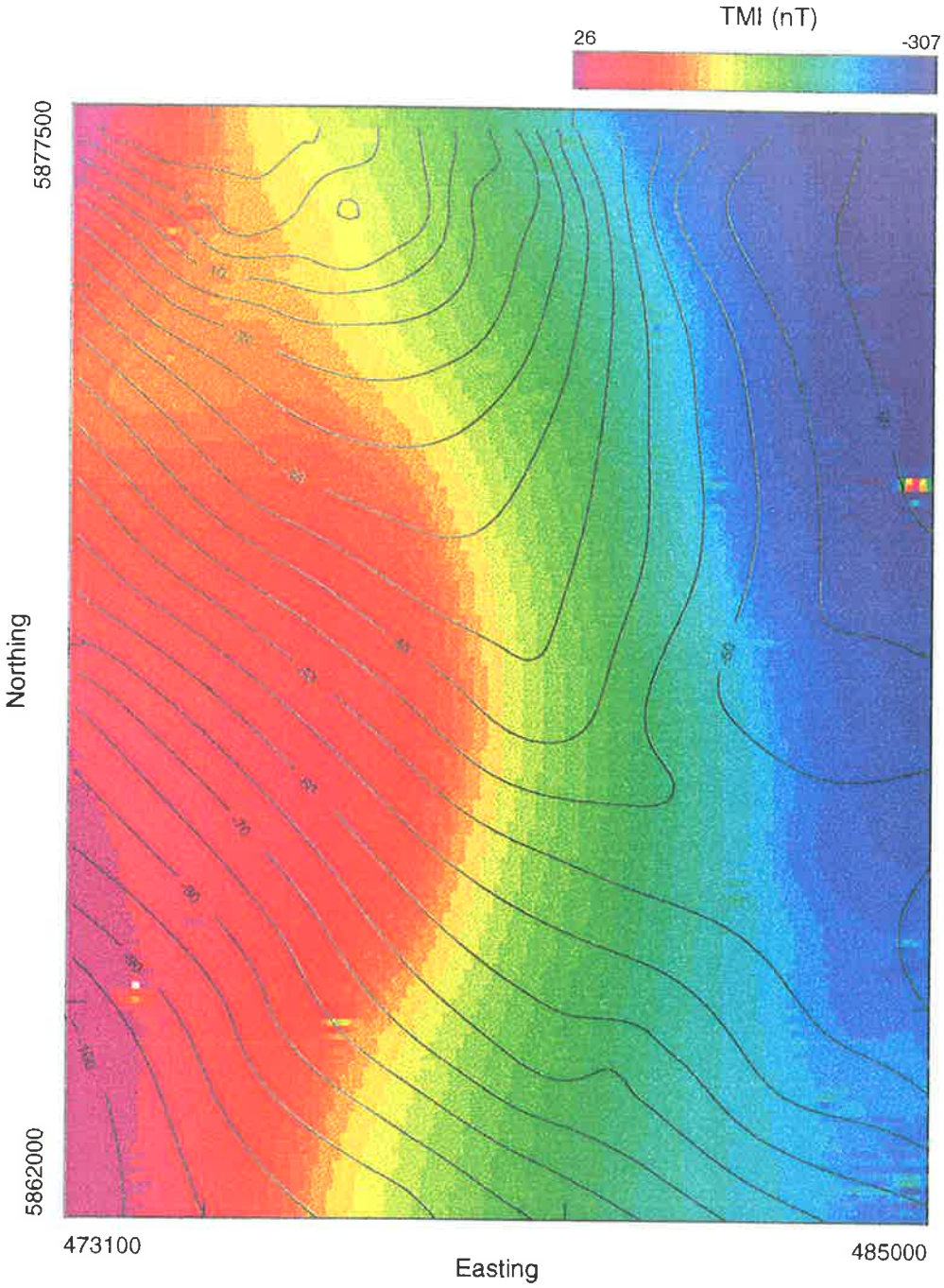

Fig. 7.2.2.5 Northwest Penola Trough area

TMI image + gravity contours

Gravity grid = 200 x 200 m, Gravity contours = 5 g.u.

TMI grid = 100 x 100 m, Scale = 1:100,000

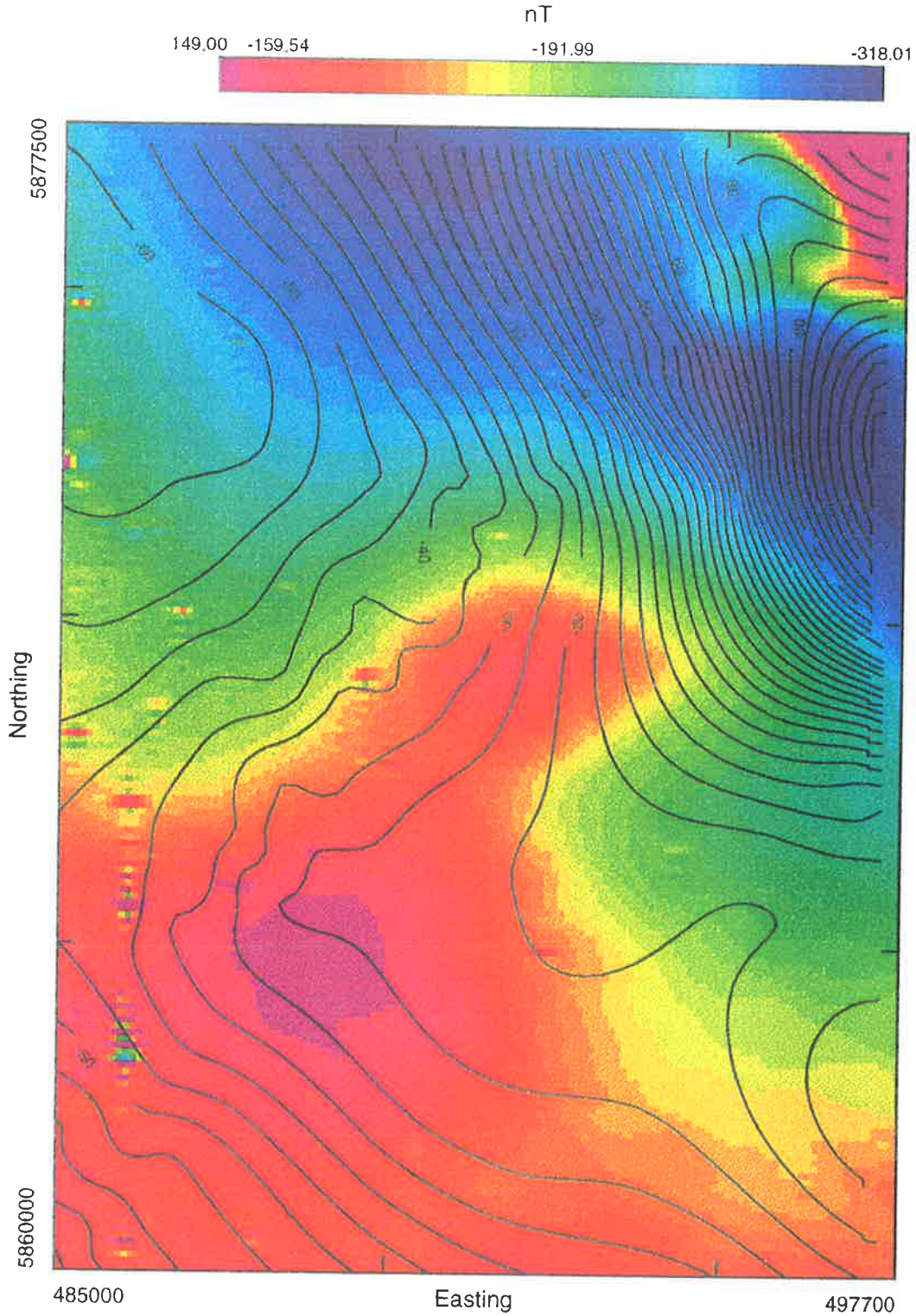

Fig. 7.2.2.6 Northeast Corner

TMI image + gravity contours

Gravity grid = 200 x 200 m, Contour interval = 5 g.u.

TMI grid = 100 x 100 m, Scale = 1:100,000

There is some indication of a subtle positive gravity anomaly centred close to the peak of the Mt Gambier magnetic anomaly while over the northwestern side of this magnetic anomaly is a small, circular, 10 $\mu m.s^{-2}$ negative gravity anomaly around 5 km in diameter (fig. 7.2.2.2). On the eastern side of the map is a broad area that is slightly negative compared with the section further west. To the northwest of the centre of the Mt Gambier magnetic anomaly is another positive 20 $\mu m.s^{-2}$ anomaly (fig. 7.2.2.3) that has two separate peaks and is relatively close to the Kalangadoo magnetic anomaly but offset to the southwest. The Kalangadoo Fault Zone is delineated by a relatively steep gradient which closely follows the seismically defined structure, with the gradient changing from the west-northwest trend on the eastern side of the area to a more northwestly trend around the western extension.

The Penola Trough is represented on the gravity map as two distinct lows in an area of negative Bouguer values. While the number of profiles in this area is lower than might be desirable, the main features of the trough are defined with only the eastern margin ambiguous because of poor coverage. The low which ridges into the western extension has been discussed in the section on regional gravity features (section 7.1.2) but it is notable that while the seismic basement horizon map shows the deepest part of the Penola Trough can be found just to the south of Ladbroke Grove 1 with the Penola Trough shallowing towards the northwest, the gravity map shows the low becoming more intense to the northwest (fig. 7.2.2.4).

The gravity station coverage over the Northwest Penola Trough magnetic anomaly is sparse so only the general trend can be delineated. As can be seen from fig. 7.2.2.5 and the regional map in section 7.1.2, the Northwest Penola Trough anomaly is offset to the southwest of a broad positive gravity ridge while the Northwest Corner magnetic anomaly found on the regional map is offset to the south of the centre of the gravity high.

The northeast corner of the study area has a relatively intense gravity high with the centre adjacent to the Victorian border and a ridge extending towards the northeast. The magnetic map, on the other hand, shows an very intense low in this location while to the southwest the two Northeast Penola Trough anomalies are found in an area where a gravity ridge extends from the main high. The edge of the gravity ridge coincides with

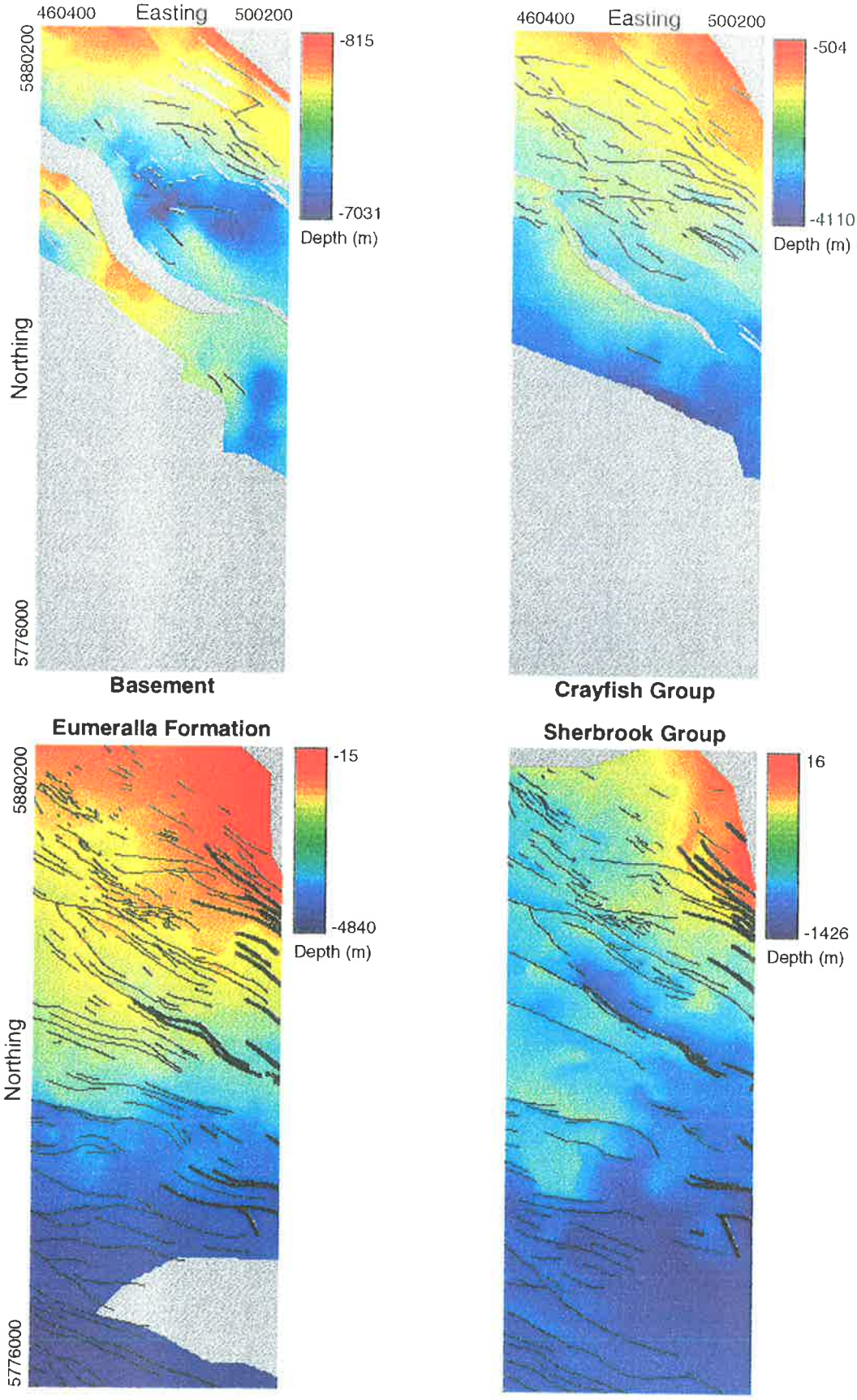

Fig. 7.2.3.1 Images of the four major seismic horizons with faults shown in black, grey represents areas where the horizon has not been resolved. Scale = 1:1,000,000

the Sawpit High (fig. 7.2.2.6) but the northeast magnetic anomaly does not appear to have any expression on the gravity map.

Along the eastern margin of the study area, directly to the east of the Sawpit High, the gravity map shows a minor anomaly which may have some correlation with anomalies on this part of the magnetic map. If the gravity anomaly is the result of a small body at depth then the magnetic influence of this body may be responsible for the change in regional magnetic trend which is found between that of the intense low to the north and that accompanying the linear magnetic anomalies to the south. The large gravity low which extends into the study area from the north (as discussed in section 7.1.2) is offset to the west and southwest of the magnetic low on the northern margin of the magnetic map.

7.2.3 Seismic Horizon Maps and their relationship with the magnetic map

The section on the regional structure (7.1.3) discusses the differences between the AGSO regional magnetic map and the seismic horizon maps, and shows that with a few exceptions the basement topography or that of the sedimentary horizons are not the source of the regional anomalies. Fig. 7.2.3.1 shows the depth to the top of each of the four major horizons.

In the P1 area the seismic basement horizon map shows that only three seismic lines have crossed the Kanawinka Fault Zone and the basin margin in the northeast corner. These lines imply that basement is very shallow to the northeast of the fault zone with a rapid increase in depth to the southwest. The magnetic map shows an intense low oriented along the same trend as the Kanawinka Fault Zone with a small part of a strong magnetic high, displayed in more detail on the regional maps, prominent in the northeastern corner. While this intense low could be part of a bi-polar anomaly centred on or to the north of the fault zone, there is also a positive gravity anomaly over the low.

To southwest of the Kanawinka Fault Zone is the area covered by the Penola/Tilbooroo 3D seismic survey where the Sawpit basement high has been mapped in high resolution. On the northern side of the Sawpit High is a major structural feature named the Sawpit Fault by Moriarty et al., (1995). This is downthrown to the north, which is the reverse of the general regional trend on the eastern side of the study area but is also manifested by the major Woolwash Fault two kilometres to the north as well

as other less prominent faults on the western side of the area. As discussed in the previous section, the magnetic anomaly in the Sawpit area is offset to the south from the basement high. It is centred around 2 km south of the Sawpit 1 well but the source of the magnetic anomaly may be an extensive meta-volcanic succession within the basement that was intersected at the base of Sawpit 1.

The northeastern anomaly of the pair (Northeast Penola Trough anomalies) is not noticeably associated with any seismically delineated feature. The positive peak of the anomaly is near the eastern extension of the Leicester Park Fault as mapped by the 3D seismic survey (Moriarty et al., 1995), but the magnetic map shows that the anomaly extends toward the eastern boundary of the study area where the seismic coverage ranges from sparse to nonexistent.

To the southeast of Penola the series of faults labelled the Kanawinka South Fault Zone (Cockshell et al., 1994) result in a rapid deepening of basement, from around 3.5 to 5 km deep in approximately 3 km distance along the north-south seismic line OK90-414. This fault zone is a more prominent feature in the Victorian part of the Penola Trough but only extends a short distance into South Australia (Perincek et al., 1994). There is some relation between the linear magnetic anomalies southeast of the Sawpit High and the Kanawinka South Fault Zone but the anomalies' sources appear to be considerably shallower than the basement depth found over the fault zone, although the highest amplitude anomalies are almost directly over the sharp increase in basement depth (on the northeastern side of the basement map in fig. 7.2.3.1)

When discussing the regional structure shown on the seismic basement fault map in section 7.1.3, it was noted that the most prominent feature of the seismic map was the Kalangadoo Fault Zone and that there is little indication of this feature on the regional magnetic map. Close examination of the MESA magnetic data from the study area results in a similar conclusion because the TMI map is dominated by the Mt Gambier anomaly and various gradient maps from over the fault zone show lineations that are due, either to much shallower subsurface magnetic sources or to cultural features.

In section 7.2.1 a subtle anomaly on the southern margin of the region that extends to the west of the study area, was identified and its length, orientation and the probable alignment with the Hungerford anomaly was mentioned (Northwest Kalangadoo Linear Anomaly). This anomaly has a wavelength of about 2 km which is

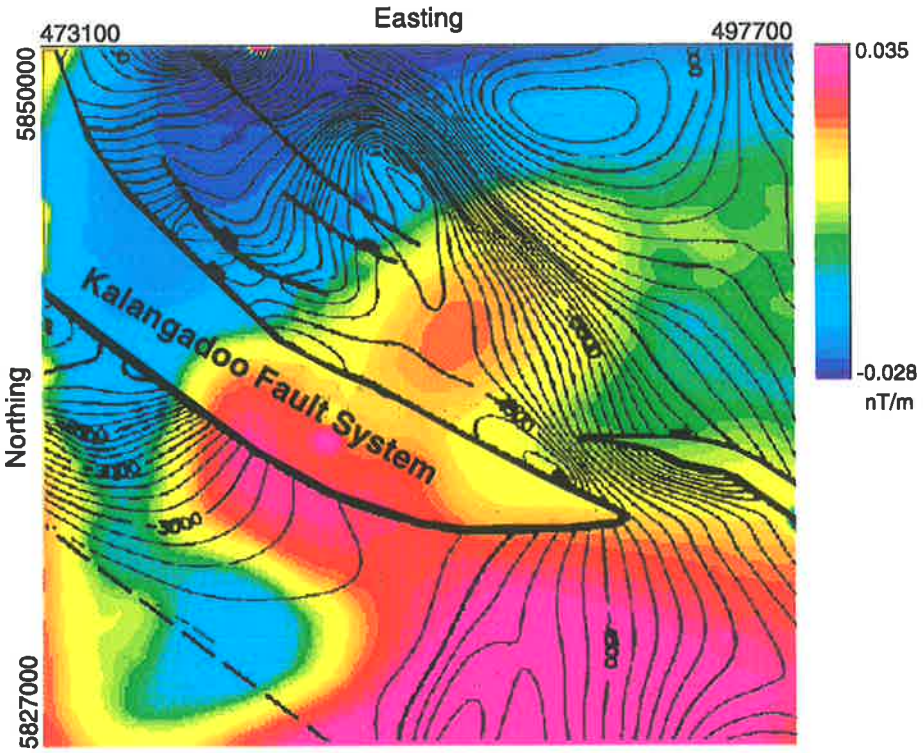

Fig. 7.2.3.2a Kalangadoo Fault System / Mid-Penola Trough area. Seismic basement contour map over vertical gradient magnetic image. Scale = 1:250,000

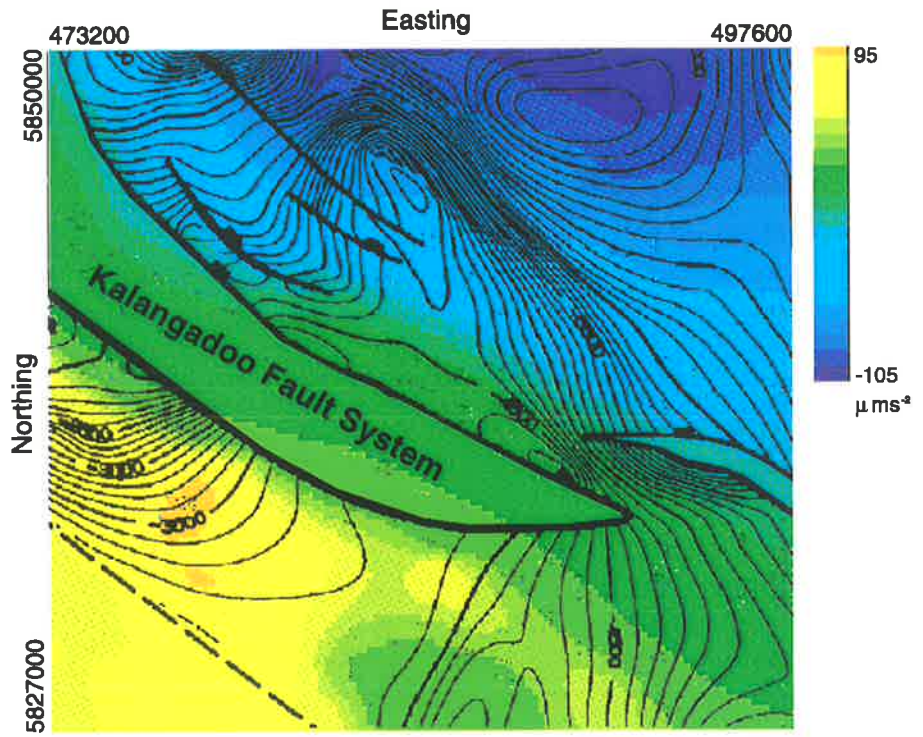

Fig. 7.2.3.2b Kalangadoo Fault System / Mid-Penola Trough area. Seismic basement contour map over gravity image. Scale = 1:250,000

wider than the linear anomalies east of Penola, suggesting that the source is deeper than those features. It is unlikely to be the result of the offset of magnetic horizons at basement level by the Kalangadoo Fault Zone because these would be too deep to produce this type of feature, however, the fault zone extends into the sedimentary section and is close to the anomaly suggesting that the source could have some association with shallower parts of the fault zone.

In the central part of the study area to the north of the Kalangadoo Fault Zone, is an elongate basement feature delineated on seismic sections with a steep gradient on the northeastern and northwestern side (fig. 7.2.3.1, basement map). The feature is separated from the Kalangadoo Fault Zone by a shallow trough on the western side but directly adjoins the fault zone in the southeast. The Mid-Penola Trough magnetic anomaly appears to be closely associated with this seismically delineated feature with the gradient maps showing the western to southwestern margin adjacent to the Kalangadoo Fault Zone as discussed in section 7.2.1 (fig. 7.2.3.2a). There is no indication of this seismically delineated feature on the gravity maps which may be because there is no density contrast between this basement high and the adjacent sediments, or because of poor gravity station coverage (fig. 7.2.3.2b).

The Kalangadoo High is on the southern side of the Kalangadoo Fault Zone with the shallowest part around the Kalangadoo 1 well (2140 m) and deepening to the south and southeast (fig. 7.2.3.2a). The Kalangadoo magnetic anomaly is east-southeast of Kalangadoo 1 with part of the anomaly over the fault zone and the remainder over part of the Kalangadoo High which is between 2.5 to 3 km deep. A depth estimate of 3.8 to 4 km for the deepest source, derived from spectral analysis, would place that source within the basement section rather than close to the basement/sedimentary interface. As discussed in section 7.2.2 there is a gravity feature in this vicinity but it is offset to the southwest of the magnetic anomaly which also means that it does not coincide with the section of the Kalangadoo High around Kalangadoo 1, being to the southeast of that feature (fig. 7.2.3.2b). Seismic sections east-northeast of Mt Gambier delineate a deep basement low along the Victorian border (approx. 5.5 km deep) which has no expression on the magnetic map but corresponds to a broad, low amplitude, negative gravity anomaly (fig. 7.2.3.1, southeast part of basement map).

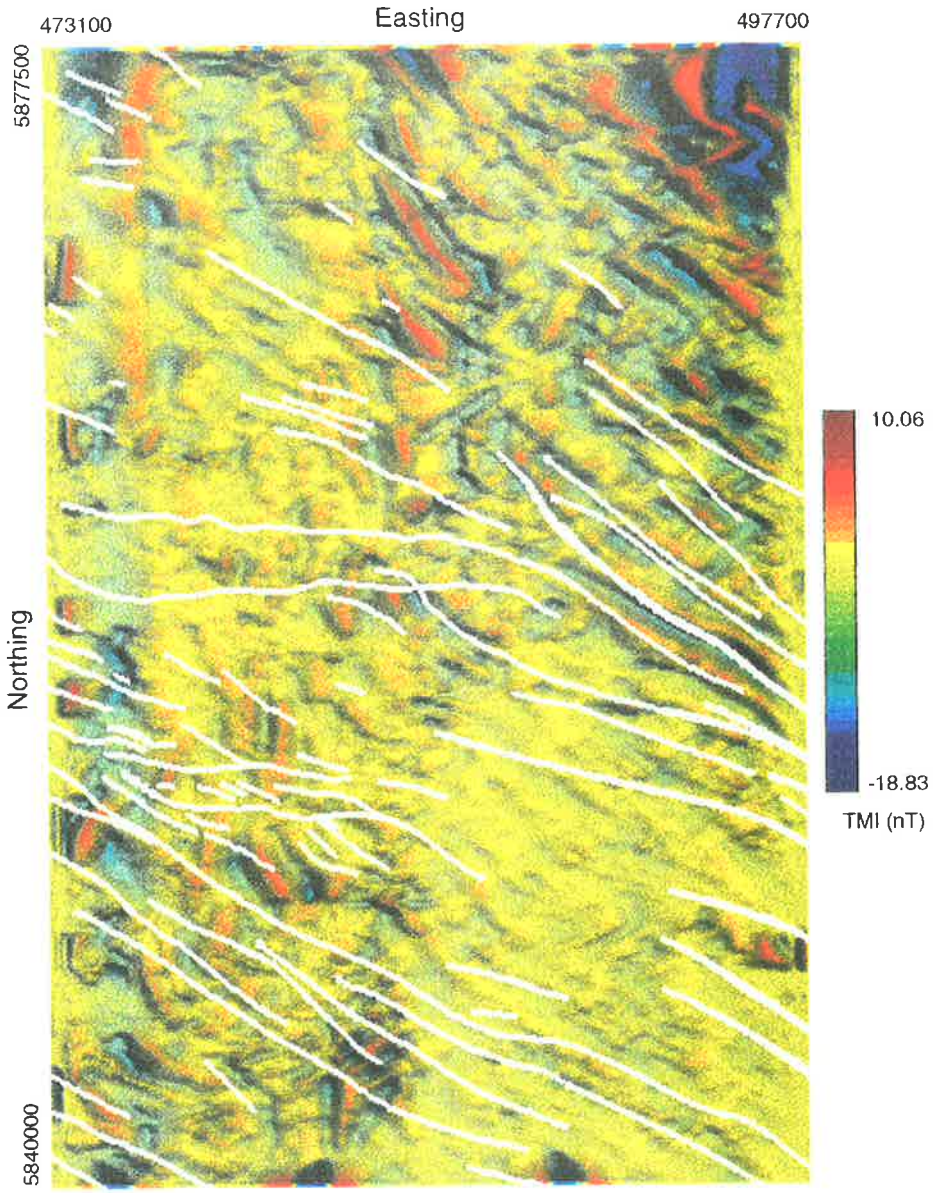

Fig. 7.2.3.3 Residual TMI colourdraped image of the Penola Trough area with major Eumeralla Fm. faults derived from seismic top horizon maps shown as white lines. Residual image dominated by Eumeralla Formation lineations but also contains Sherbrook Group and Tertiary lineations. North-south features are probably cultural noise or processing artifacts. Scale = 1:250,000

Those magnetic anomalies which are unlikely to be the result of basement sources are the linear anomalies (fig. 7.2.3.3) east of Penola (East Penola Trough anomalies), the Hungerford anomaly and the linear feature east of it (Northwest Kalangadoo Linear Anomaly), the anomalies associated with the Mt Gambier and Mt Schank volcanic complexes, the offshore magnetic features and other similar ones in the Penola Trough, and, of course, the cultural anomalies. Various depth estimate methods have been applied to the data (chapter 6.3) in the vicinity of the East Penola Trough anomalies and the Hungerford anomaly with the result that, the East Penola Trough anomalies have been found to be in the range of 400 to 500 m deep which places them within the Eumeralla Formation and partially associated with fault structures (fig. 7.2.3.3), while the Hungerford anomaly should have penetrated through the top of the Sherbrook Group into the Tertiary section. The offshore linear features may be the expression of fault related sources in the Tertiary Gambier Limestone and Dilwyn Formation. The depth to the top of the Late Cretaceous sediments is around 1 km, and the small amplitude and wavelength suggests the sources are shallower than that. The Sherbrook Group seismic horizon map shows a relative high around Caroline 1 with spatial dimensions that approximately coincide with that of the Caroline gravity high, but the effect is significantly less pronounced on the Eumeralla Formation horizon map while the top Crayfish horizon has not been resolved (Fig. 7.2.3.1, Sherbrook Group map).

The following chapter contains models of the magnetic sources in the basement and sedimentary section, along with discussion of geological and geophysical constraints (from this chapter) used to develop the models. Where the geological and geophysical evidence is ambiguous or there is very little evidence to conclude which model is the most likely, a number of models of the same anomaly were produced.

Chapter 8

Magnetic Models

8.1 Models of Igneous Sources

In the first section of this chapter models of the basement and surface igneous or metamorphic sources are presented along with the evidence used to construct the models. In the second section of the chapter the models are of the relatively shallow intersedimentary sources and consist of a number of different models for some anomalies. The methods used to construct the models are those that were outlined in section 5.1 and include seismic mapping, the processing of gravity and magnetic data as well as geological constraints. Most of the models of basement sources are based on the assumption that the source body was originally an intrusion or surface eruption, however, it is probable that there is some pre-rift metamorphic terrain which is highly magnetic and thus able to produce the larger magnetic anomalies. However, where basement has been intersected in wells the rocks have been found to be at a relatively low grade of metamorphism. This does not preclude the possibility that igneous rocks of Palaeozoic age have undergone metamorphism prior to the Late Jurassic (during the Delamerian Orogeny, for example).

The figures in this chapter show the models that have been constructed, the observed (black) and calculated (red) profiles or a calculated grid, and other information such as the major formation boundaries. The profiles usually are of flightline data that have had the regional gradient component removed either by subtracting a calculated polynomial from the original data or using a low-pass filter (wavelengths of 1.5 to 5 km) to emphasise the regional component then subtracting this from the data. Where the strike of the anomaly is not aligned at an angle that is reasonably close to perpendicular to the flightlines (e.g. the Mt. Gambier Anomaly and the two Northeast Penola Trough Anomalies) a traverse has been produced from the observed or residual TMI grid and this line was used for modelling. It is possible that some of the amplitudes and/or shapes of the residual profiles may be incorrect because of difficulties in producing a

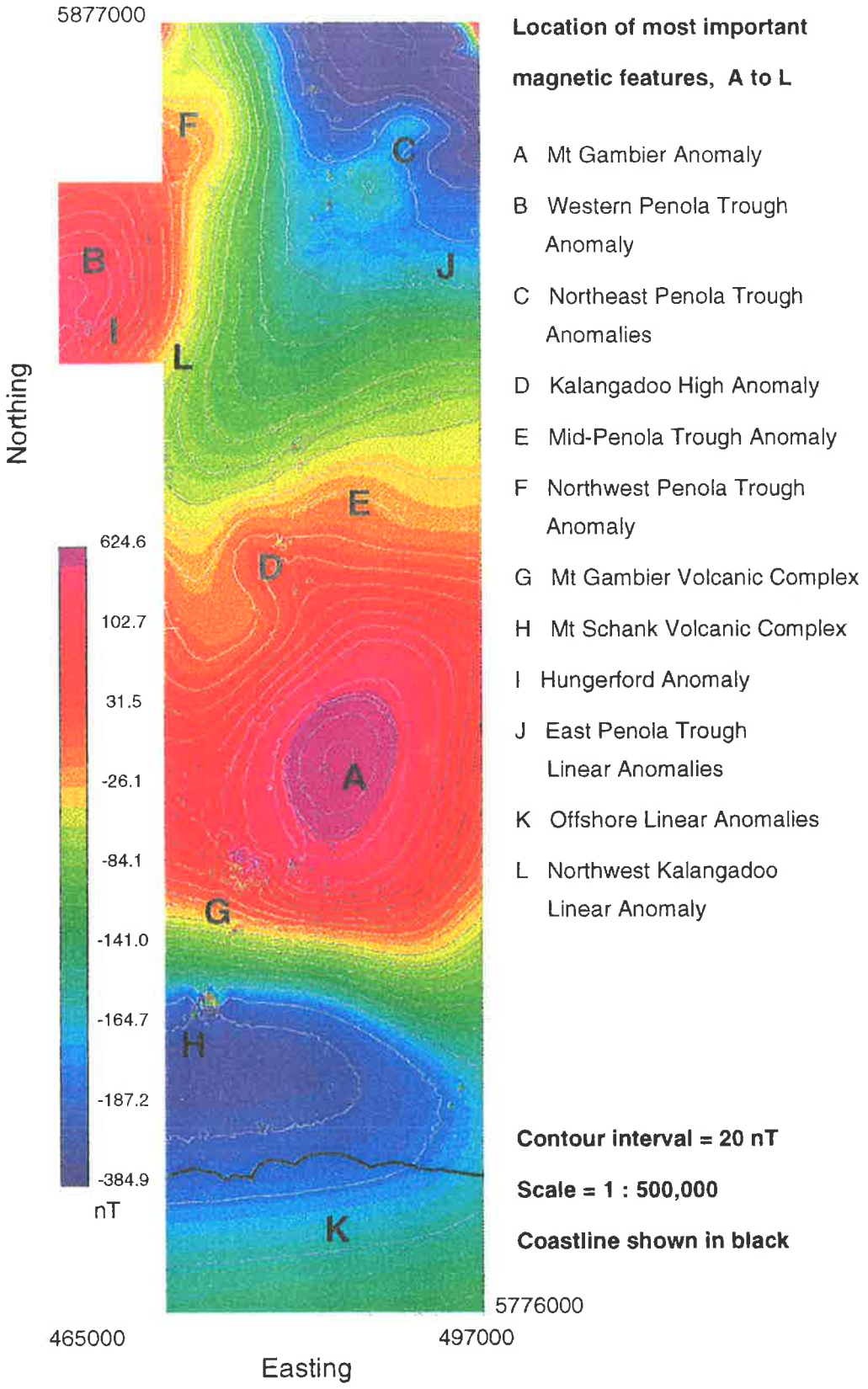

Fig. 8.1.0.1 P1 Area, TMI image & contours showing location of modelled anomalies

representative regional polynomial or because some longer wavelength component remains after the low-pass filtered data is subtracted from the flightline data.

The sources of the higher amplitude magnetic anomalies are three-dimensional so the models must have a finite lateral extent. This can be modelled by calculating the anomaly at every point of a grid over the body and comparing the contours derived from this grid with those created from the observed or residual TMI data. Most of the grids used for this modelling were 100 × 100 m which is the grid spacing used for nearly all of the TMI and gradient contour maps and images, while the gravity data was gridded at a spacing of 200 × 200 m which was also used for TMI data over the Mt. Gambier Anomaly. Fig. 8.1.0.1 shows the location of the anomalies for which models have been constructed in this chapter.

8.1.1 Mt. Gambier Magma Chamber Model

The most prominent magnetic feature in the study area is the Mt. Gambier Anomaly which is believed to result from the magma chamber thought to have been the source of the Mt. Gambier and Mt. Schank volcanic cones. The dimensions of the semi-elliptical anomaly are approximately 35 to 40 km long by 18 to 20 km wide and it has an peak-to-trough amplitude of around 400 nT. Depth studies using spectral analysis (section 6.1.1) have yielded a depth of around 7 km which is the average depth to the top of the body. The assumption that the anomaly is caused by a magma chamber that is the source of the surface basalt flows is reasonable given the proximity of the anomaly to the vents, and the association between surface basalt flows and similar large magnetic anomalies in the Mt. Burr Volcanic Group and in Victoria.

There is a possibility that the anomaly is generated by source rocks that may have intruded as a sill-like body early in the rifting process, and the eruptions at Mt. Gambier and Mt. Schank occurred later when fresh magma was forced up along pre-existing pathways, eventually escaping to the surface. In the study by Irving and Green, (1976) it was found that the absence of high pressure phases such as lherzolite (indicative of upper mantle origin) in the Mt. Schank basalts suggested that the magma had undergone fractionation at relatively shallow, crustal depths like those of the expected magma chamber, while the Mt. Gambier basalts were less fractionated with the retention of lherzolite xenoliths which the authors suggested might result from relatively rapid ascent

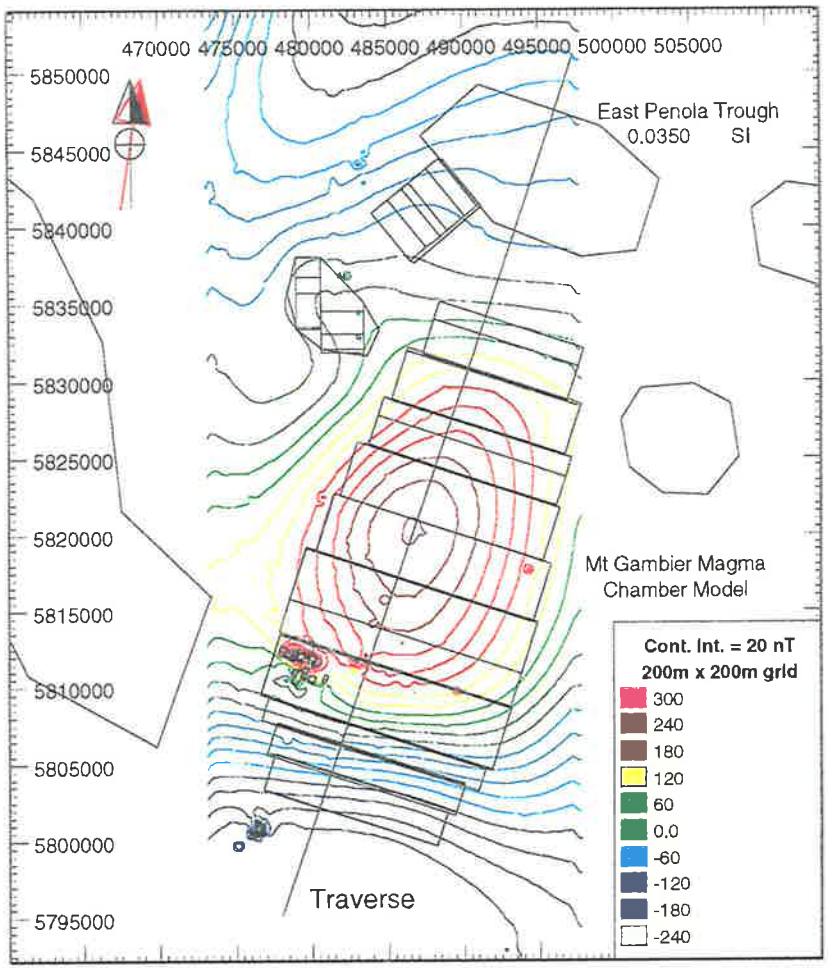

Fig. 8.1.1.1 Mt. Gambier Anomaly TMI contour map showing traverse and modelled bodies. Scale = 1:100,000

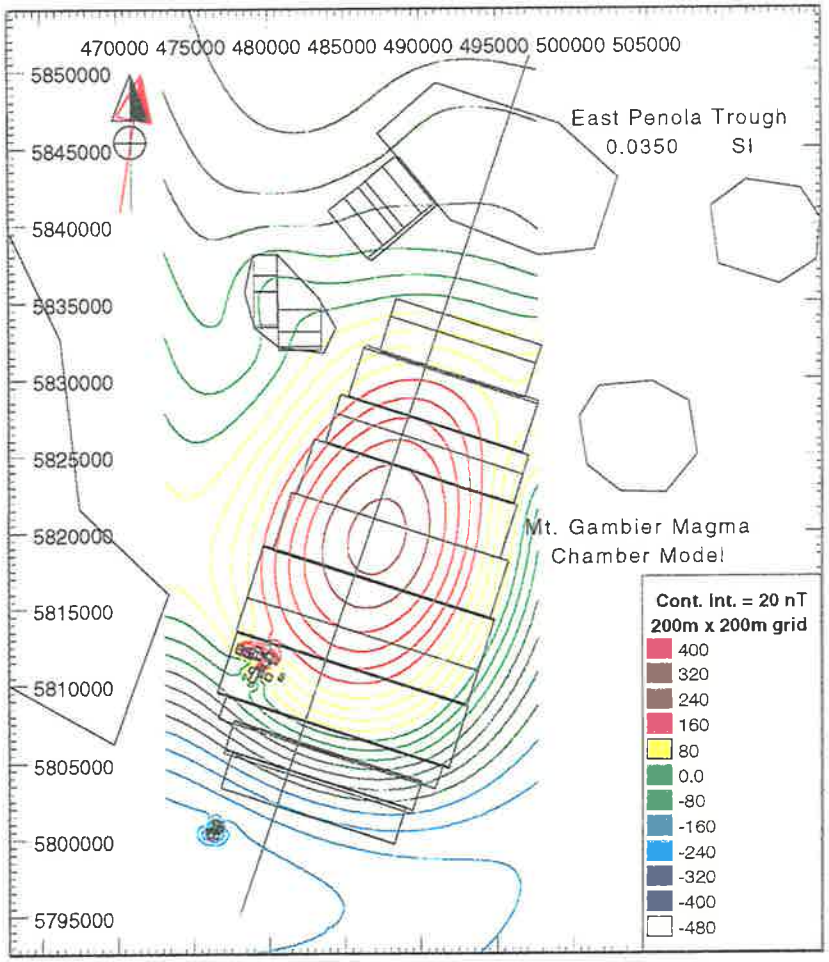

Fig. 8.1.1.2 TMI contour map produced from grid calculated from model. Scale = 1:100,000

from mantle depths. Sheard (1990) reports that the country rock fragments found in tephra at Mt. Gambier include granodiorite which is interpreted as a constituent of the basement at approximately 5.5 km depth (Joyce, 1975).

In a theoretical study of the mechanisms of emplacement of basic intrusions, Petraske et al., (1978) found that, basic intrusions emplaced at depths of less than 10 km where the lithosphere is between 50 and 100 km thick will be laccolithic (dome shaped with a flat floor), while in a lithosphere that is less than 50 km thick these intrusions will be bowl shaped. The authors explain that this occurs because where the underlying lithosphere is thick a forceful intrusion will deflect the overlying strata upwards but have little effect on the underlying strata, but if the lithosphere is relatively thin the underlying strata will be distorted to a greater degree. Where large intrusions (20 km or greater) occur in the upper crust (less than 10 km) they produce a large enough deflection of the overlying strata to generate new or reactivate pre-existing faults. A study of intracontinental intrusive magmatism in Israel (Gvirtzman and Garfunkel, 1997) found that gabbroic intrusions initially produce an uplift of approximately 12% of their thickness with subsequent thermal relaxation reducing this to 9-10%. Maximal uplift occurred while the magma was still liquid while thermal relaxation was a slow process as the magma cooled.

Joyce (1975) found that the upwarping of the area around Mt. Gambier during the Quaternary occurred prior to the eruption of Mts. Gambier and Schank, and probably before the eruption of the Mt. Burr Group, although the time relationship between the upwarping and volcanism was unclear. Joyce (1975) believed that the arching of strata due to upwarping would create favourable conditions for the formation of relatively shallow magma chambers over deep basement faults which would then feed the surface volcanoes. The eruptions would only last as long as the magma chamber contains sufficient magma under enough pressure to reach the surface which then would explain why most volcanic activity in the Otway Basin appears to have had a short duration.

The Mt. Gambier Anomaly source can be represented by a group of polygonal prisms of varying width, which simulates an approximately semi-elliptical shape for the proposed source and when assembled produces a roughly dome-shaped NE-SW cross-section. The use of a series of polygons rather than a single, complex multi-sided body

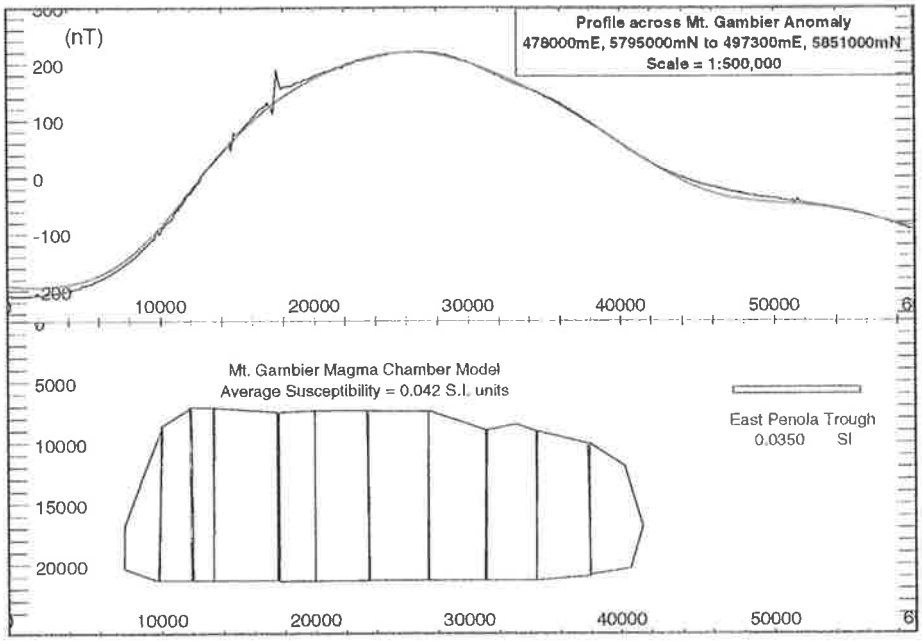

Fig. 8.1.1.3 Mt. Gambier magma chamber model with TMI profiles extracted from grid and calculated from model
Model assembled from eleven bodies, with a small variation in susceptibility across the model
East Penola Trough body represents possible volcanogenic sediments in Casterton Formation

permits a lateral variation of width (and susceptibility) as well as the depth to the top of the body along the profile, which should be more geologically realistic than the assumption of a homogeneous body. The lack of geophysical constraints from seismic mapping or gravity profiles means that the shape of the body must be approximated by forward modelling only, with general restrictions like the depth from spectral analysis, the susceptibilities of the basalt flows measured at the Mt. Gambier volcanic complex, and the evidence of studies of similar bodies in other parts of the world (as discussed above), serving to constrain the model.

The Mt. Gambier Anomaly has a long axis which is oriented N 30° E so the north-south flight lines are not perpendicular to the structure and for this reason a traverse along the long axis was extracted from the gridded data and used to define the shape of the body (fig. 8.1.1.1). This traverse (black) has the same sample spacing as the gridded data rather than the original line data, that is, 100 m instead of 5 to 7 m. The model shown in fig. 8.1.1.3 indicates that the source body is shallowest (7.1 km) at the southern end where a steep slope bounds the body while the top of the body is generally flat in the central part of the body but with some variations in depth on the northern side of the body. These variations in the depth to the top of the body are required for the profile to fit the subtle changes in the extracted traverse.

The eleven bodies used to simulate the magma chamber were initially assigned the same susceptibility (0.042 SI units) and then slightly varied to help fit the profile. This value is greater than that for basalts measured by Chatfield (1992) but is close to that measured for ash and scoria at one location. In addition to the magma chamber model the profile also shows a thin sheet body, East Penola Trough (0.035 SI units), which is used to approximate the slight positive anomaly to the northeast of the magma chamber. This body simulates a 500 m thick volcanogenic Casterton Formation that has been interpreted at the base of the Penola Trough. The calculated grid and contours are shown in fig. 8.1.1.2 along with the profile and models.

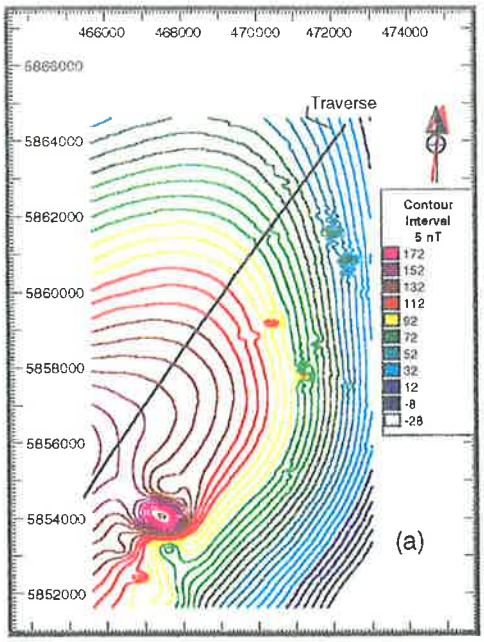

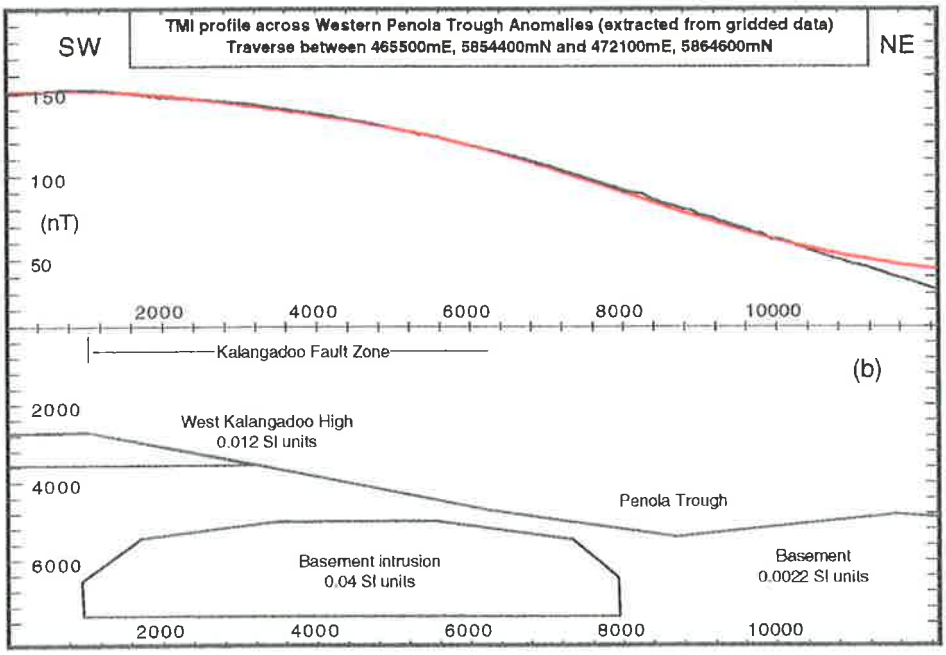

Fig. 8.1.2.1a TMI contour map of Western Penola Trough / P1 extension, showing modelled traverse

Fig. 8.1.2.1b Profile across Penola Trough approximately perpendicular to Kalangadoo Fault Zone.

8.1.2 Western Penola Trough Model

The broad magnetic high intruding into the study area from the west is an extension of the large anomalies associated with the Mt. Burr volcanic complex. The Western Penola Trough Anomaly (section 7.2.1) overlies parts of the Kalangadoo High, Kalangadoo Fault Zone (KFZ) and Penola Trough, which has good seismic coverage over the whole area and allows the construction of models constrained by seismic mapping. The depth estimates from spectral analysis (section 6.1.10) range from 5 to 5.2 km to the top of the source body which is close to the basement depth of 5 km, derived from seismic sections, for the Penola Trough in most of this area.

It can be reasonably assumed that either the source is an igneous body that intruded into the basement section or that there are two sources, one at the base of the Penola Trough and the second, perhaps pre-rift, associated with the Kalangadoo High.. The more intense part of the anomaly is on the southwestern side of the Penola Trough which, from seismic evidence, is the deepest part of the Penola Trough half-graben, and this is where the pre-rift metamorphic terrain would have been down-faulted. Thus if the source was part of the pre-rift terrain the edge of the anomaly would then be expected to define the Kalangadoo Fault Zone (KFZ) rather than extend over the trough. The intrusive model may fit the lateral extent of the anomaly better because the anomaly is found over the northwestern side of the Kalangadoo High as well as the Penola Trough. The body located beneath the Penola Trough could have been emplaced in the basement prior to the formation of the rift but this is less likely than during the extensive volcanism during rifting. The eastern edge of the anomaly has been interpreted as representing the result of pre-rift NS or NNE-SSW basement faulting or a contact (O'Brien et al., 1994, Tucker and Frears, 1995).

The contour map displayed in figure 8.1.2.1a shows the centre of the anomaly, which is located on the western edge of the area, the Hungerford Anomaly (section 8.1.7) and a traverse extracted from gridded data. The model (fig. 8.1.2.1b) constructed to represent the sources of this anomaly consists of a deep body representing basement (0.0022 SI units), a dome-shaped body representing a basement intrusion (0.04 SI) and another body to represent the Kalangadoo High component (0.012 SI), but only the

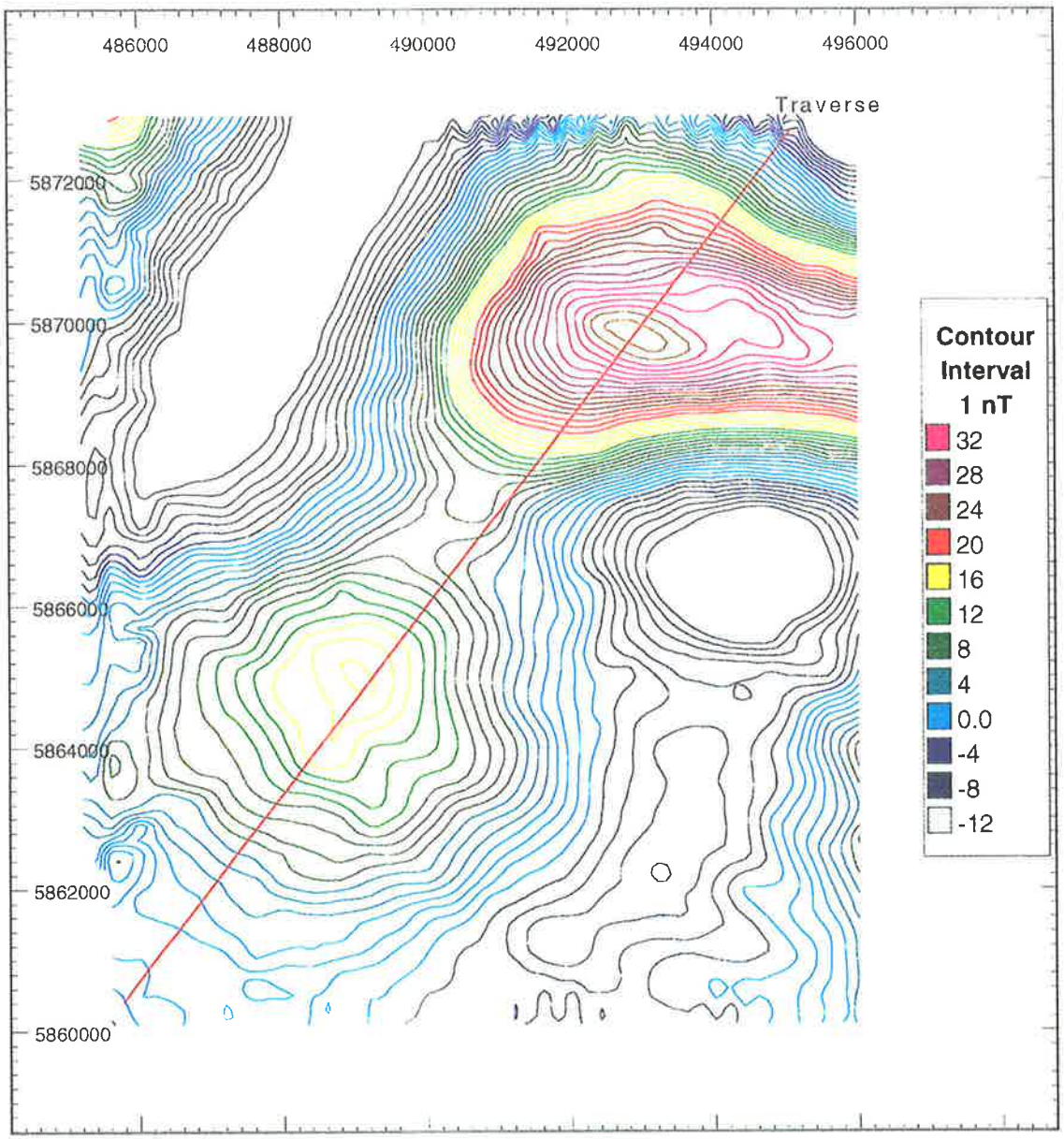

Fig. 8.1.3.1 Residual TMI map of Northeast Penola Trough Anomalies showing modelled traverse. Scale = 1:100,000

shape of the latter body can be constrained by seismic data. The method used to define the basement-sediment boundary (for example) in constructing models, is to find a seismic line on the basement horizon map which is parallel to the traverse or, if none exists with that orientation, find the depth from contours at the points where the traverse intersects the seismic lines.

The profile in figure 8.1.2.1b shows that the Basement Intrusion body is the main source but there is a contribution from the West Kalangadoo High body. The intrusive body is beneath the KFZ but extends under the Penola Trough although not beneath the deepest part determined from seismic. It was not possible to obtain a fit to the profile (black) by constructing a body that extends to the southwest beneath the Kalangadoo High but instead the addition of a relatively shallow body representing the top of the Kalangadoo High improved the fit substantially. The susceptibility assigned to the West Kalangadoo High body was much higher than that measured from the Kalangadoo 1 basement cores which were also recovered from the Kalangadoo High but the well is 10 km to the south and away from the magnetic highs.

8.1.3 Northeast Penola Trough Anomalies Model

The two anomalies (fig. 8.1.3.1), located within the regional magnetic low that dominates the northeast part of the study area, have a much lower amplitude than the anomalies discussed in this section previously, with the southern Sawpit Anomaly having an amplitude of approximately 15 nT while the northeast elliptical anomaly (Penola North Anomaly) is around 32 nT. In section 7.2.1 the difference between the seismically defined Sawpit High and the Sawpit Anomaly was discussed, in particular the offset between the two features where the basement high is approximately 2 km north of the centre of the TMI anomaly. The Penola North Anomaly appears to have only a minor connection with seismically defined features, that were defined either on the 2D profiles or in the 3D Penola survey which partially covered the area. Spectral analysis of a grid (section 6.1.2) covering both of the anomalies yields two depth estimates that correspond to basement depths. These are 3.2 km, which is most likely the depth to the source of the Sawpit Anomaly, and 2.2 km, which is probably the depth to the source of the Penola North Anomaly.

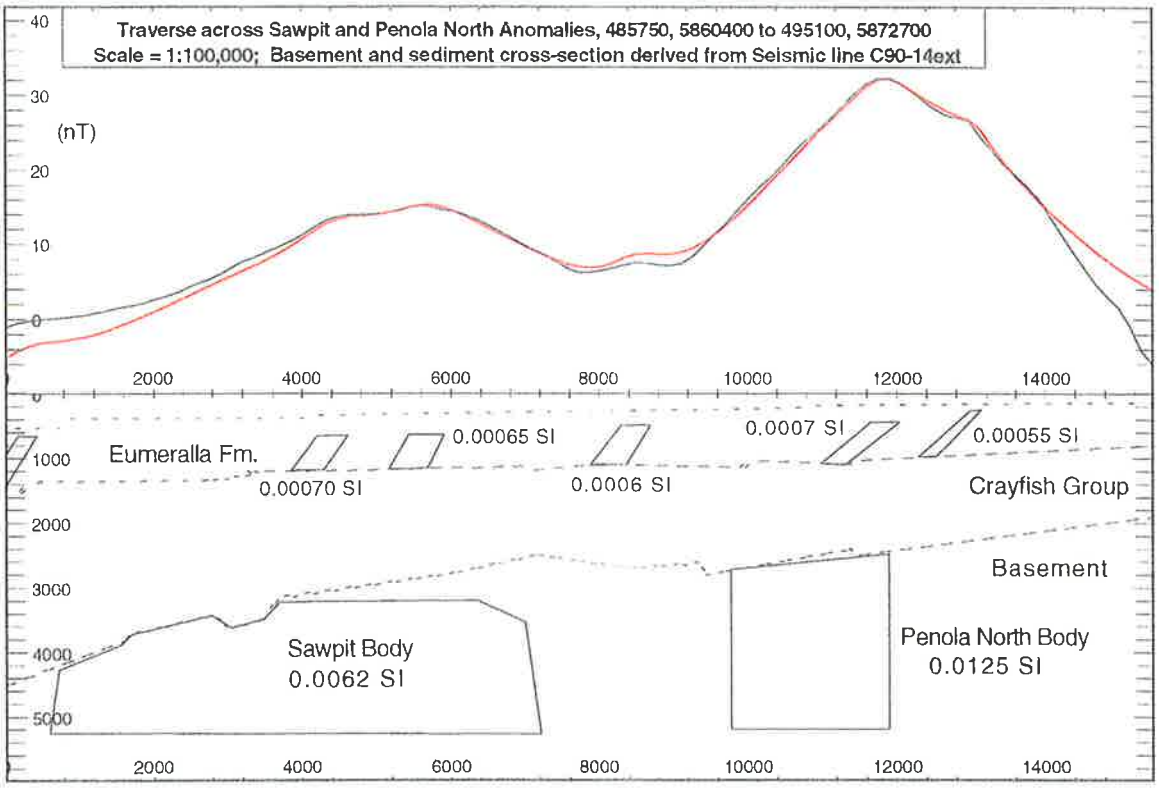

Fig. 8.1.3.2 Northeast Penola Trough traverse, Body model

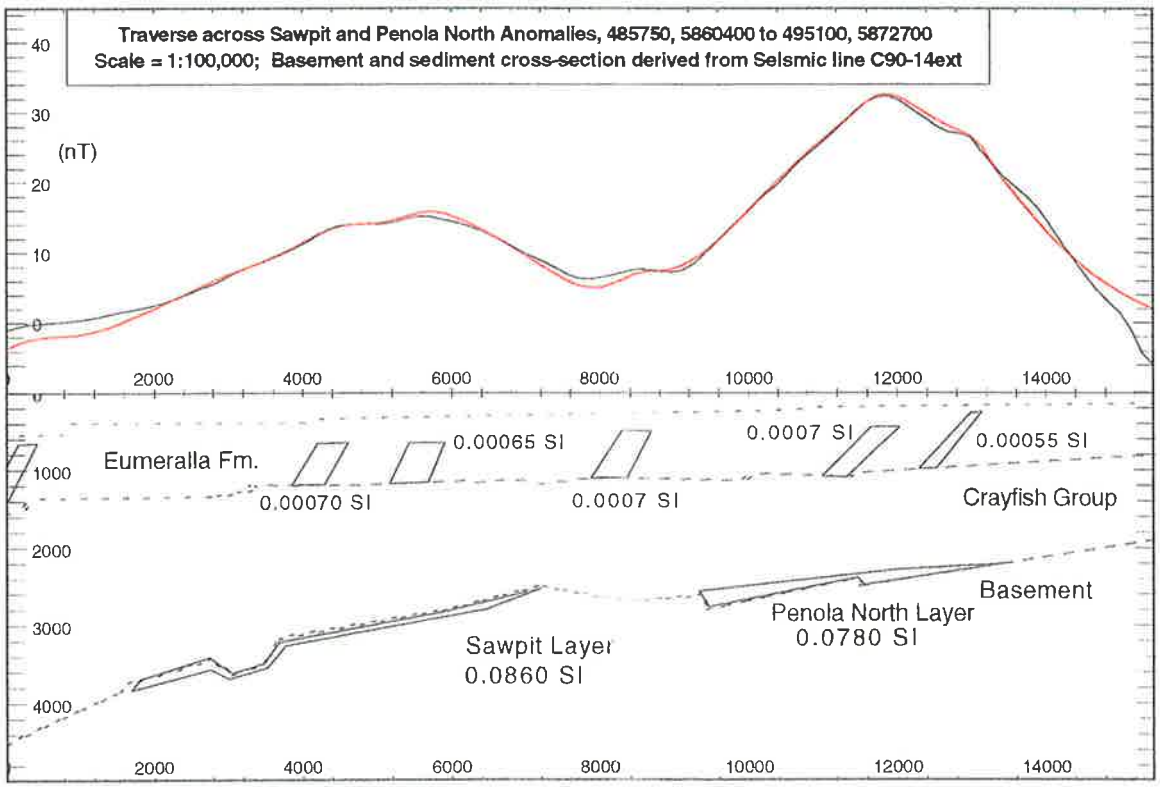

Fig. 8.1.3.3 Northeast Penola Trough traverse, Layer model

The section beneath the Penola North Anomaly has not been drilled so there is no evidence of the lithology of the source although it is reasonable to suggest that it might be similar to the Sawpit Anomaly source. The depth from spectral analysis (2.2 km) places the body either above, at or just below the top of basement which means that if it was originally an extrusive body then it should be relatively thick or have a very high susceptibility in order to produce the measured anomaly. Thick extrusive bodies have been found where lava has filled topographic lows and this could be the case here or there may be a deeper body that is the source.

The profile (black) shown in fig. 8.1.3.2 was produced from a traverse (485750, 5860400 to 495100, 5872700), with the regional trend removed, that passes through the centres of the Sawpit Anomaly and the Penola North Anomaly (fig. 8.1.3.1). The sources, Sawpit Body and Penola North Body, are shown as well as lines delineating the top of basement, Crayfish Group and Eumeralla Formation which were interpolated from the seismic line C90-14ext. as it occurs on the seismic horizon maps. There are also a number of shallow intersedimentary bodies which are required to fit the calculated profile to the subtle anomalies that are superimposed on those due to the deeper sources. The southern end of the traverse coincides with the seismic line C90-14ext. but the traverse diverges to the east of the seismic line as it extends toward the northeastern corner of the study area with the result that the depth to the top of formations, as shown in figure 8.1.3.2, may be too great, especially in the northeast of the profile. The Sawpit Body was placed southwest of the Sawpit basement high with the top of the body at 3.2 km depth and with a susceptibility of 0.0062 SI units while the Penola North body (with a susceptibility of 0.0125 SI units) was placed northeast of the Sawpit high at a depth of 2.2 km (fig. 8.1.3.2). The Sawpit Body is shown at or near the top of basement on the southwestern side of the profile where the basement surface slopes down to greater depth.

The only magnetic anomaly in the study area, attributed to a basement source, where the basement has been intersected by drilling is the Sawpit Anomaly, where the Sawpit 1 well penetrated 190 m into the basement and found a volcanic unit 15 m thick, consisting of andesite, and which is 15 m below the top of basement and overlies metasediments (Moriarty et al., 1995). It is possible to model the Sawpit anomaly (15 nT) by assuming a thin andesite layer at the top of basement (2.5 km) around the Sawpit

High but thickening towards the southwest of the profile, provided the andesite has a susceptibility of around 0.086 SI units. The Sawpit Layer body shown in figure 8.1.3.3 is very thin at its shallowest point at the Sawpit High but increases in thickness relatively rapidly to the southwest of the basement high and is relatively thick (approx. 130 m) southwest of the down-faulted section. The thickness of the body at the southwest end was required for the calculated profile to approximate the residual anomaly, as was the approximately even thickness of the body (approx. 50 m) northeast of the down-faulted section, however, this model conflicts with the most probable depth estimate from spectral analysis. Spectral analysis yields the most accurate depth estimates for bodies which resemble vertical prisms with substantial depth extent. Published well logs do not show a large density contrast or abrupt change on the sonic log (Moriarty et al., 1995, Morton et al., 1995) at the depth of the andesite unit, but the log characteristics may be due to the thinness of the unit at Sawpit 1. It can also be inferred that the andesite layer must be at least Jurassic in age, and very probably older because it is interpreted as being beneath the top of basement and as andesite is an extrusive rock, it must have been buried by the overlying metasediments.

Hill and Durrand, (1993) report that the andesine basalts found at the base of the Casterton 1 well in Victoria have been dated at 153 Ma at the oldest (Late Jurassic) and so were among the earliest rocks deposited in the rift. However, this does not necessarily imply that the andesite layer near the top of basement at Sawpit 1 is related to the andesine basalt at the base of the Casterton Formation in this well although the Casterton 1 well is in a similar tectonic setting. If the andesite layer body shown in figure 8.1.3.3 is not the only body responsible for this magnetic anomaly then the main magnetic body may be an igneous/metamorphic body that was not intersected by drilling but was produced by a series of eruptions separated by periods of sedimentation. The susceptibility assigned to the Sawpit Body in figure 8.1.3.2 is considerably lower than might be expected for a massive andesite body (Telford et al., 1990) but could represent an interlayered volcanic/sediment structure or metamorphic terrain, as the susceptibility is around the average for metamorphic rocks, while the susceptibility assigned to the Sawpit Layer in figure 8.1.3.3 is around half the reported value for andesite (0.16 SI units).

The depth derived from spectral analysis (2.2 km) for the Penola North Anomaly (fig. 8.1.3.2) places the top of the source body or bodies slightly above the top of basement as delineated by the seismic surveys, which suggests possibility that the source body may be volcanic units within the Casterton Formation or that the depth may be the result of the shallower part of the basement body offset to the east of the profile. The Penola North Body in figure 8.1.3.2 was constructed with the top dipping towards the deeper part of the Penola Trough while the shallowest part of the body is on the northeastern side and is not shown on the profile. Volcanic units within the Casterton Formation might have to be thicker than the 43 m section that was intersected at Sawpit 1 (Morton and Drexel, 1995) to produce the observed anomaly. However, there were no Casterton Formation volcanic units intersected at the Sawpit 1 well, unlike wells in Victoria where they are typical of the formation. This implies that these units may have either been removed by erosion during the early history of the rift, were never emplaced or are present beneath the Penola North Anomaly but not at the well which intersects a basement high. If either of the former two possibilities are correct then the anomaly is caused by pre-existing igneous or metamorphic terrain underlying the sediments which implies that either the depth derived from spectral analysis is an underestimate or the depth estimate corresponds to the depth of the top of the body east of the profile. If the latter is true then the source could be a thick extrusive body that filled topographic lows during rift formation or an intrusion that was emplaced after deposition of the Pretty Hill Formation.

Comparison with the basement map produced from the Tilbooroo 3D seismic survey, shows that the magnetic anomaly peak (Penola North Anomaly) is located over the section of basement between the Woolwash and Leicester Park Faults (Moriarty et al., 1995) and extends to the east into an area that has only been mapped relatively sparsely with seismic methods. The Penola North Body shown in figure 8.1.3.2 has been given a substantial depth extent (3000 m) in order to represent an intrusive/metamorphic body and has been assigned a susceptibility of 0.0125 SI units. This value is less than the average for a range of igneous rocks, especially the basic rocks (Telford et al., 1990), but is greater than that of the metamorphic rocks discussed in the previous paragraph. The alternate model is shown in figure 8.1.3.3 where the Penola North Layer is a thick extrusive body which has filled topographic lows in the top basement surface. This body

has its shallowest point at the thin northeastern end where the depth is 2.2 km while the southwestern end is 200 m thick. The susceptibility of this body is 0.078 SI units which is close to the Telford et al., (1990) average value for basalt.

The Penola North Layer could represent a highly magnetic volcanic succession within the Casterton Formation. The formation is thin at Sawpit 1 but has been interpreted from seismic evidence to be up to 500 m thick in undrilled parts of the Penola Trough (Morton et al., 1995). The evidence which supports the thin layer model of the source of the anomaly, is the intersected andesite unit below the top of basement at Sawpit 1 and the possibility that volcanic units which are characteristic of the Casterton Formation in Victorian wells, are the source of the Penola North Anomaly, while the lack of prominent seismic features at or above the top of basement seems to argue against the thin layer model.

The gravity data for this region is based on several profiles which cross major features plus scattered stations filling in the areas between (section 7.2.2). The Sawpit Anomaly appears to have a strong correlation with a secondary gravity anomaly while the Penola North Anomaly does not appear to have any gravity equivalent, which may suggest that the Sawpit Body is the source of the magnetic anomaly rather than a thin layer of andesite that has little density contrast with the surrounding metasediments. The lack of any gravity signature does not preclude the existence of a thick igneous/metamorphic body like the Penola North Body because it is possible there is no density contrast between the body and its surroundings, while a thin layer of basalt which is implied by the Penola North Layer susceptibility, should have a detectable density contrast with the underlying metasediments but the thinness of the layer and the relatively coarse gravity measurements may mean the resultant anomaly is undetectable.

8.1.4 Kalangadoo High and Mid-Penola Trough Anomalies Model

The Kalangadoo High and Mid-Penola Trough anomalies are north of the Mt. Gambier Anomaly and are adjacent to the Kalangadoo Fault Zone. The TMI map of this part of the study area is dominated by the Mt. Gambier Anomaly so the two smaller anomalies are best delineated by vertical gradient or residual TMI maps, where the Kalangadoo High anomaly appears as a semi-elliptical feature trending northwest-southeast while the Mid-Penola Trough anomaly is a more circular-elliptical feature.

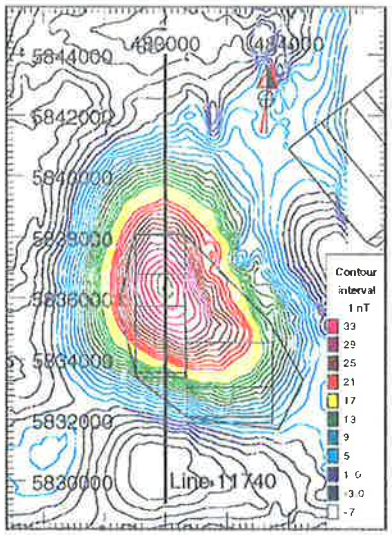

Fig. 8.1.4.1 Residual TMI contour map of Kalangadoo High Anomaly showing part of Line 11740

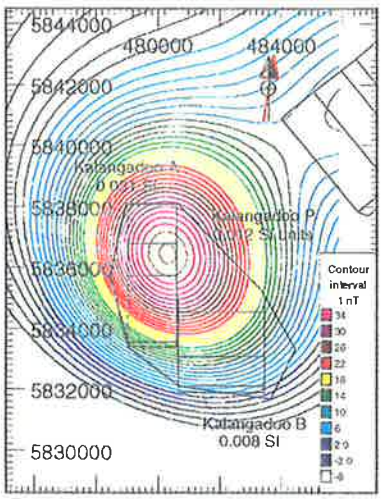

Fig. 8.1.4.2 Calculated TMI contour map of Kalangadoo High model

Scale = 1:250,000

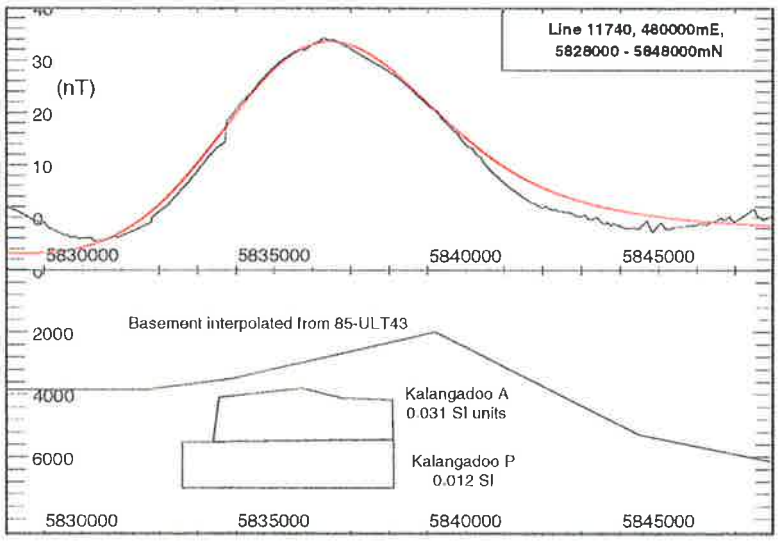

Fig. 8.1.4.3 Residual TMI profile over Kalangadoo High Anomaly showing part of Line 11740

A significant problem with all magnetic maps over the Kalangadoo High anomaly is the cultural noise associated with the town of Tarpeena which is on the eastern side of the anomaly, and the major powerlines (275 kV and 132 kV) that run north towards Nangwarry, south towards Mt. Gambier and east-southeast to the Victorian border. These are strong noise sources which required filtering in an attempt to suppress the effects on maps and profiles, with the result that the residual profile data (after the removal of the regional component), used to model the basement source, is distorted by the effects of filtering on the northeastern side of the anomaly.

The Kalangadoo High anomaly has a peak-to-trough amplitude of approximately 36 nT and is approximately 7.5 × 4 km with the long axis oriented N 155° E (fig. 8.1.4.1). The contour map in figure 8.1.4.2 is produced from a calculated grid generated by the three bodies shown and differs from the residual contour map because of the lack of cultural effects which means that the calculated anomaly is more circular. The three bodies, Kalangadoo A, Kalangadoo B and Kalangadoo P, represent components of the source body of the central anomaly with the first two comprising the upper part and the surface while Kalangadoo P represents the base.

The profile shown in figure 8.1.4.3 is residual data from line 11740 (5828000 - 5848000mN) and displays the upper model component, Kalangadoo A, that was assigned a susceptibility of 0.031 SI units which is near the upper limit of the range of measurements recorded at Mt. Gambier (Chatfield, 1992) while the value assigned to the base (Kalangadoo P) was 0.012 SI units. The top of the body was fixed at 3.8 km deep which was the depth value yielded by spectral analysis and places the body within the pre-rift basement as shown by the top-of-basement horizon plotted on the figure. This line represents the basement/sediment interface as determined from seismic line 85-ULT43 and was extracted from the basement seismic horizon map, however, this seismic line is offset approximately 3 km to the west of the flightline which means that the top of the body is slightly closer to the top of basement than is apparent from the figure. The segment of the basement horizon between approximately 5839000 and 5845000mN represents the fault plane of the Kalangadoo Fault Zone (KFZ) where it slopes down from the shallow parts of the Kalangadoo High on the southern side to much greater depths in the Penola Trough. The calculated profile is not a close fit to the residual profile but approximates the general shape and it is likely that the subtle anomalies

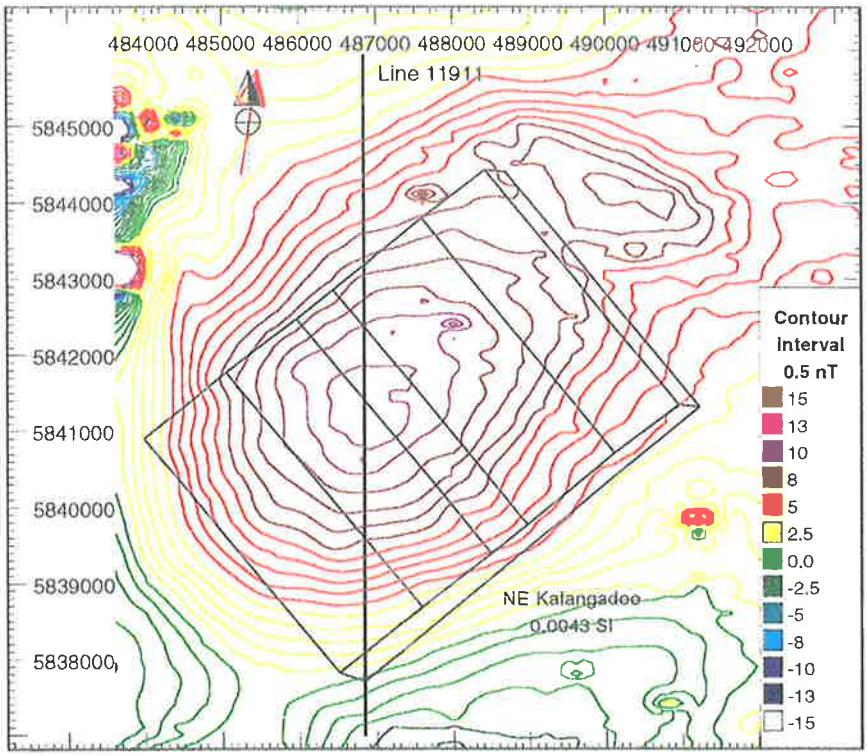

Fig. 8.1.4.4 Residual TMI contour map of Mid-Penola Trough Anomaly showing NE Kalangadoo body and flightline 11911 Scale = 1:100,000

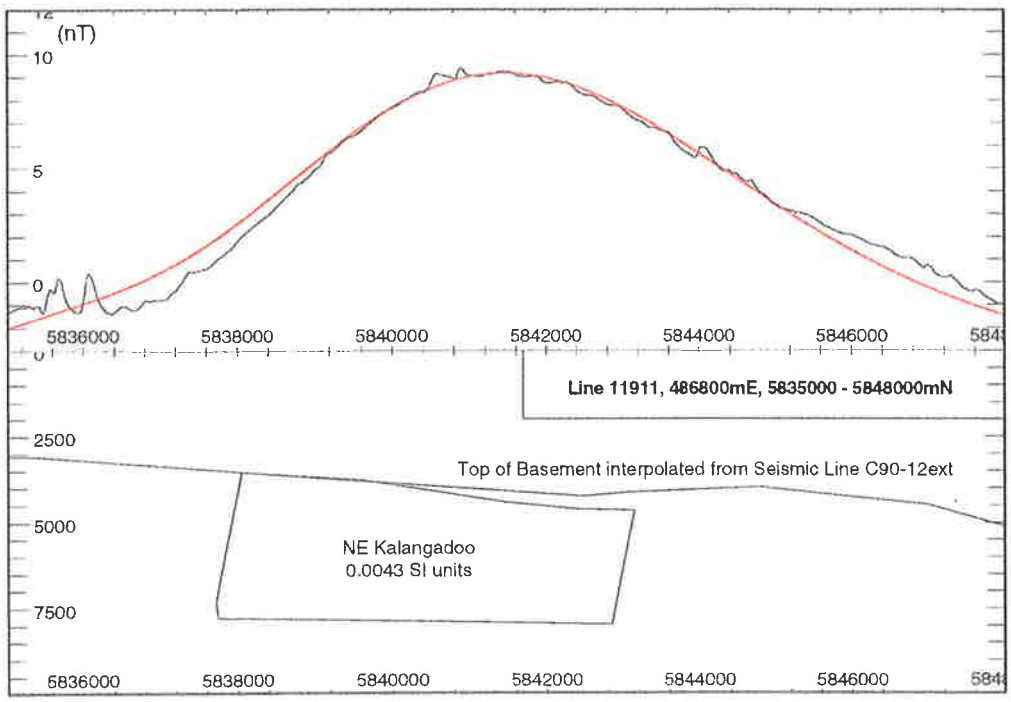

Fig. 8.1.4.5 Residual TMI profile across Mid-Penola Trough Anomaly. Top of Basement derived from seismic horizon map Scale = 1:100,000

superimposed on the larger anomaly are either due to cultural sources that have had their high amplitude reduced during filtering or are due to shallower intersedimentary sources.

The TMI map previously shown in fig. 7.2.1.6a demonstrates that the Mid-Penola Trough Anomaly (MPTA) is a subtle feature on the regional maps and has a much lower amplitude than the Kalangadoo High Anomaly. The removal of the regional component (fig. 8.1.4.4) reveals the MPTA as a broad circular-elliptical anomaly with the longer axis oriented approximately NE-SW. There are also some intense anomalies on the northwest margin of the map which are due to power lines but as these do not interfere with the main anomaly it was not necessary to filter the data. The modelled body is plotted on the map along with the flightline used as a profile.

The residual profile shown in figure 8.1.4.5 is of line 11911 between 5835000 and 5848000mN and has an amplitude of approximately 9 nT with a considerable number of low amplitude, short wavelength anomalies, probably due to culture, superimposed on the long wavelength anomaly. The solid line on the profile represents the top of basement which was interpolated from the seismic line C90-12ext and shows that the top of the body is at the basement/sediment interface (3.5 to 3.6 km as determined by spectral analysis and around 3.6 to 3.7 km from the seismic horizon map). The NE Kalangadoo body was assigned a susceptibility of 0.0043 SI units which is substantially smaller than that assigned to the Kalangadoo High bodies. This value is at the lower extreme of scoria and tuff susceptibilities measured at Mt. Schank and also at the lower end of the susceptibility range for basalts measured at Mt. Gambier (Chatfield, 1992).

NE Kalangadoo partly coincides with a seismically determined basement high adjacent to the KFZ and in the central part of the Penola Trough in the P1 area while the Kalangadoo High bodies are south of the KFZ but with the top of the source at a similar depth. There are a number of possible explanations for the origin of the bodies, their proximity to the Mt. Gambier Anomaly may indicate that they are both igneous bodies that intruded into the basement following the emplacement of the magma chamber, they may be igneous bodies that intruded/extruded during or prior to the formation of the rift, or they may be parts of the metamorphic terrain of the Kanmantoo Fold Belt which were displaced by the formation of the Penola Trough. If they are pre-rift igneous or

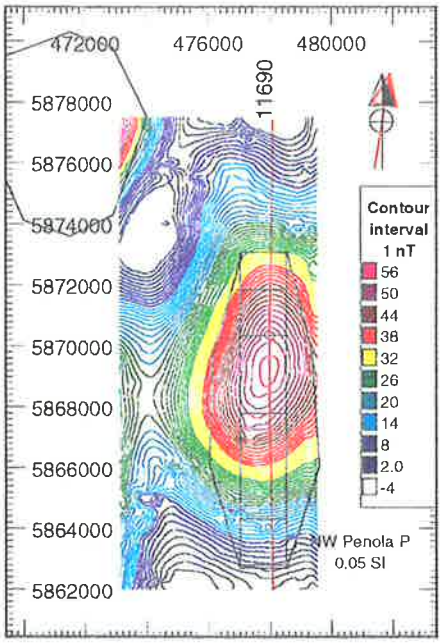

Fig. 8.1.5.1 Residual TMI map showing Northwest Penola Trough Anomaly and Line 11690

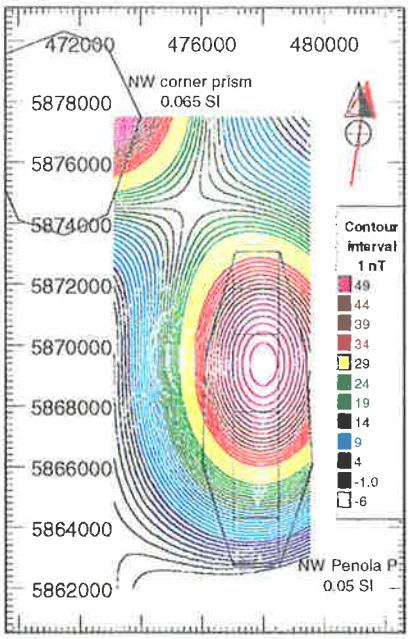

Fig. 8.1.5.2 Calculated TMI contour map showing modelled bodies

Scale = 1:250,000

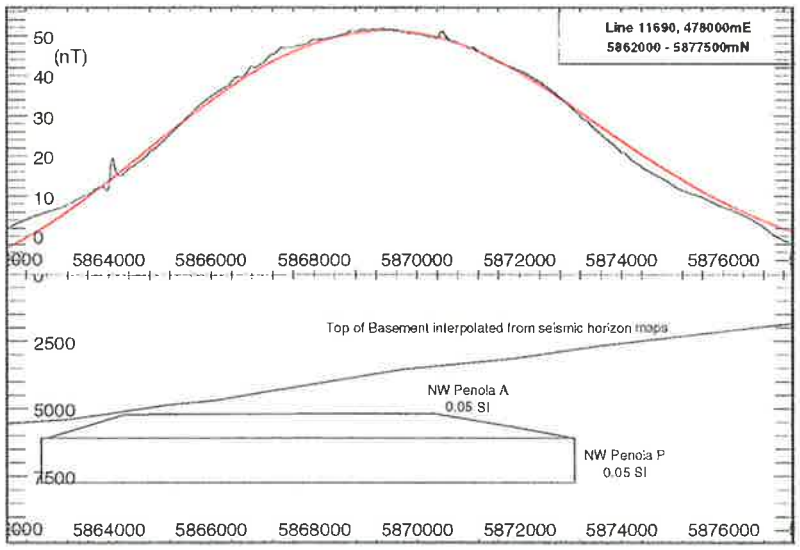

Fig. 8.1.5.3 Residual TMI profile of part of Line 11690 showing model and Basement horizon

metamorphosed bodies it is possible that they were originally connected but were separated later by movement along the KFZ.

8.1.5 Northwest Penola Trough Anomalies Model

This anomaly, while close to the Western Penola Trough Anomaly (WPTA) and Northwest Corner Anomaly (NWCA), has a considerably lower amplitude than these two despite a similar depth to the source body (5.2 km) as determined from spectral analysis. The top of basement horizon increases in depth from around 1.8 km on the northern edge of the study area to over 5.5 km south of the anomaly in the Penola Trough which places the source body well below the sedimentary section except at the southern end. Removal of the regional component reveals an elongated semi-elliptical-shaped anomaly (fig. 8.1.5.1) with the long axis oriented approximately north-south, and another feature in the northwest corner of the map that has only a minor influence on the residual map.

The residual map in figure 8.1.5.1 shows the two components of the elongated elliptical body, NW Penola A and NW Penola P, as well as part of the quasi-circular NW Corner Prism. The Basement Intrusion from section 8.1.2 is not shown. The source body for the Northwest Penola Trough Anomaly (NWPTA) has been assembled from NW Penola P (0.05 SI units) which is a long narrow prism that is rectangular in cross-section and forms the base of the body while NW Penola A (0.05 SI units) is a polygon which rests on top of the base and has a dome-shaped cross-section in profile. Also shown on the residual map is the location of flightline 11690 which is used to model the bodies in profile.

The bodies shown in the plan view were used to calculate a grid using the same grid spacing as the residual map (100 × 100m) with the resulting contour map plotted in figure 8.1.5.2. The differences between the calculated and residual TMI maps are, the calculated anomaly is more circular than the residual anomaly, there is a positive ridge between the NWPTA and the NWCA rather than the magnetic low on the residual map, and there is no positive ridge between the western margin and the NWPTA on the calculated map. Some of these differences may be due to imperfect removal of the regional component which can introduce spurious anomalies into the residual data, or some or all of the bodies may be remanently magnetised whereas only induced

magnetisation has been assumed. When a Reduced-to-the-Pole map was created there was no distortion of the anomalies which is usually indicative of the presence of remanence (section 5.1.4).

The residual TMI profile is of line 11690 that traverses through the centre of the residual anomaly which has an approximate amplitude of 51 nT (Fig. 8.1.5.3). The two component bodies of the model, NW Penola A and NW Penola P, are shown with the depth to the top at 5.2 km below the surface and with the top near the basement/sediment interface at the southern end of the body. The calculated profile is a reasonable fit to the residual data except where high frequency noise occurs, and north of around 5871000mN where there appears to be a relatively short wavelength, low amplitude anomaly superimposed on the profile which is not found on adjacent lines. Also shown as a solid line is the top of the basement body used to illustrate the relationship between the magnetic body and seismically determined basement.

The susceptibilities assigned to the component bodies are greater than most of the measurements taken at Mt. Gambier and Mt. Schank by Chatfield, (1992) and are greater than those expected for metamorphic rocks while being reasonable for basic igneous rocks (Telford et al., 1990). This does not preclude the possibility that the anomaly is produced by pre-Mesozoic metamorphic terrain because if the bodies had a much greater depth extent then the susceptibility would not need to be as high as was assigned. If the bodies had susceptibilities that are near the maximum for gneiss or slate (0.025 and 0.035 SI units respectively, Telford, (1990)) then a depth extent of greater than 10 km may be required to produce the observed anomaly. Since the anomaly is relatively narrow it is more likely that it is the result of a igneous dyke or sill emplaced in the basement section but it is not possible to determine when this occurred.

8.1.6 Mt. Gambier and Mt. Schank Volcanic Complex Models

The two volcanic complexes formed as a result of eruptions from fissures and maars (section 2.2.4) with phases of violent, explosive eruptions in each period of activity in addition to the lava flows and the venting of ash. The explosive eruptions are believed to be caused by the contact between meteoric water and groundwater, and the underlying magma (Sheard, 1978) which is likely to result in fragmented country and igneous rocks being deposited in the vents and surroundings. For this reason it is not

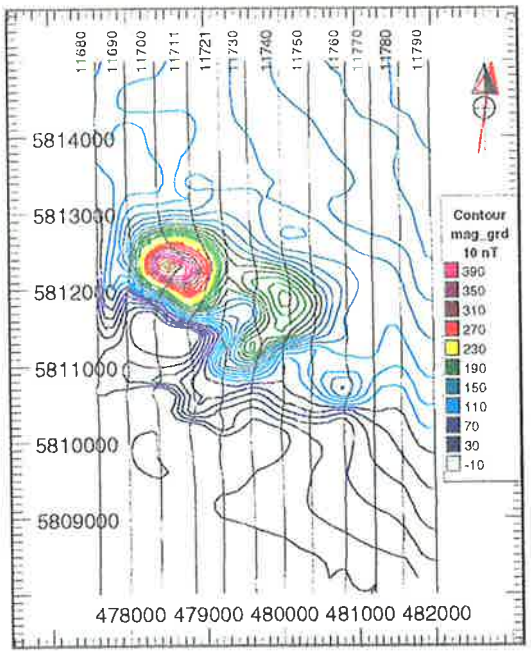

Fig. 8.1.6.1a Residual contours & flightlines over Mt. Gambier volcanic complex

Scale = 1:100,000

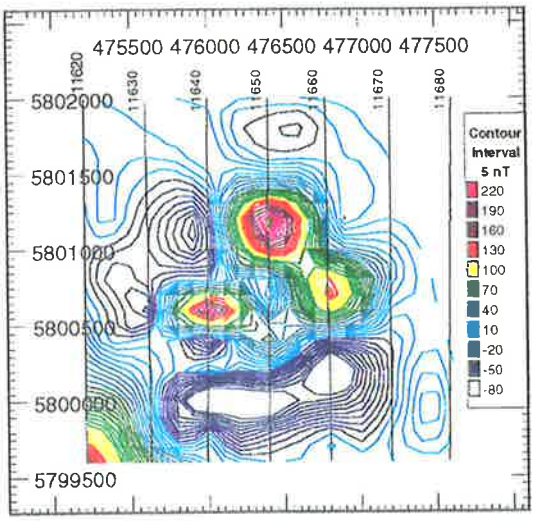

Fig. 8.1.6.1b Residual contours & flightlines over Mt. Schank volcanic complex

Scale = 1:50,000

realistic to create models of each volcanic complex as a single homogeneous body rather than a cluster of bodies representing dykes, sills and subsurface volcanic plugs. The maps and profiles of both volcanic complexes were produced after the removal of the regional component from the original flightline data. Chatfield, (1992) measured susceptibility values at five sites within the Mt Gambier volcanic complex and three sites within the Mt Schank volcanic complex, with values for different deposits such as basalt flows, tuffs, scoria and tephra. These susceptibility values were used as a starting point for forward modelling of the anomalies (figs. 3.3.1.1 and 3.3.1.2).

The Mt. Gambier volcanic complex consists of two main craters that are filled by lakes and the most intense anomaly occurs on a flightline (11700) that passes over the western side of Brownes Lake which is in the northwestern part of the complex, while the second most intense anomaly occurs on flightlines (11730 and 11740) over the Blue and Leg of Mutton Lakes (fig. 8.1.6.1a). This suggests that these anomalies result from the volcanic conduits which brought magma to the surface from depth rather than surface basalt flows, so the models representing these conduits might be constructed as partially cylindrical-shaped at depth, before branching into dykes and sills in the brecciated zone close to the surface.

The city of Mt. Gambier is built mostly on the northern side of the volcanic complex and would normally produce a significant number of cultural anomalies but because of safety considerations the aircraft altitude was increased in the vicinity of the city and volcano to an average of 250 to 300 m (600 m maximum) with the result that the cultural effects were largely suppressed, with some exceptions, and the anomalies are primarily of geologic origin. The flightlines over Mt. Gambier and Mt. Schank (and over Penola) are the only parts of the survey were the altitude of the aircraft was increased to this extent so this is the only section were modelling must allow for the change.

The residual line 11700 (fig. 8.1.6.2) crosses the Mt. Gambier Volcanic Complex west of Brownes Lake with the peak of the anomaly (approx. 380 nT) over the northwestern wall of the crater suggesting that the source body is buried by later ejecta. The body, Mt Gambier volc A, was assigned a susceptibility value of 0.0335 SI units which is considerably higher than the measurement range (15 to 700 $\times$ 10^{-5} SI units for ropey lava splatter) made by Chatfield, (1992) at her site 5 on the southern side of Brownes Lake but the buried source body might be expected to have a higher

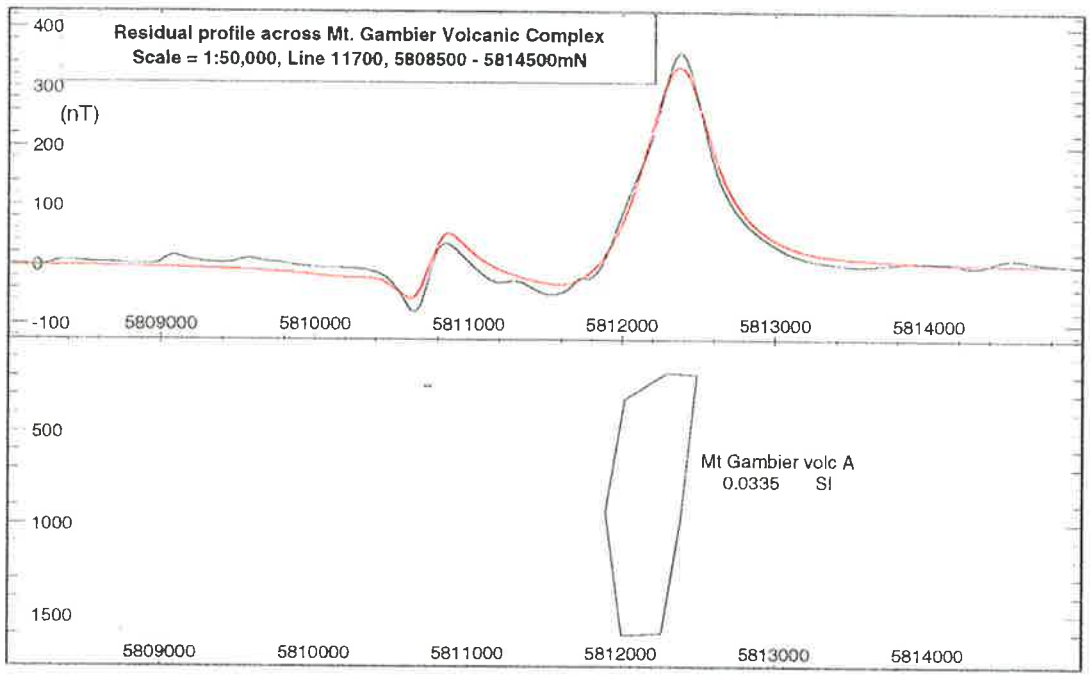

Fig. 8.1.6.2 Mt. Gambier volcanic complex, line 11700 (West of Brownes Lake)

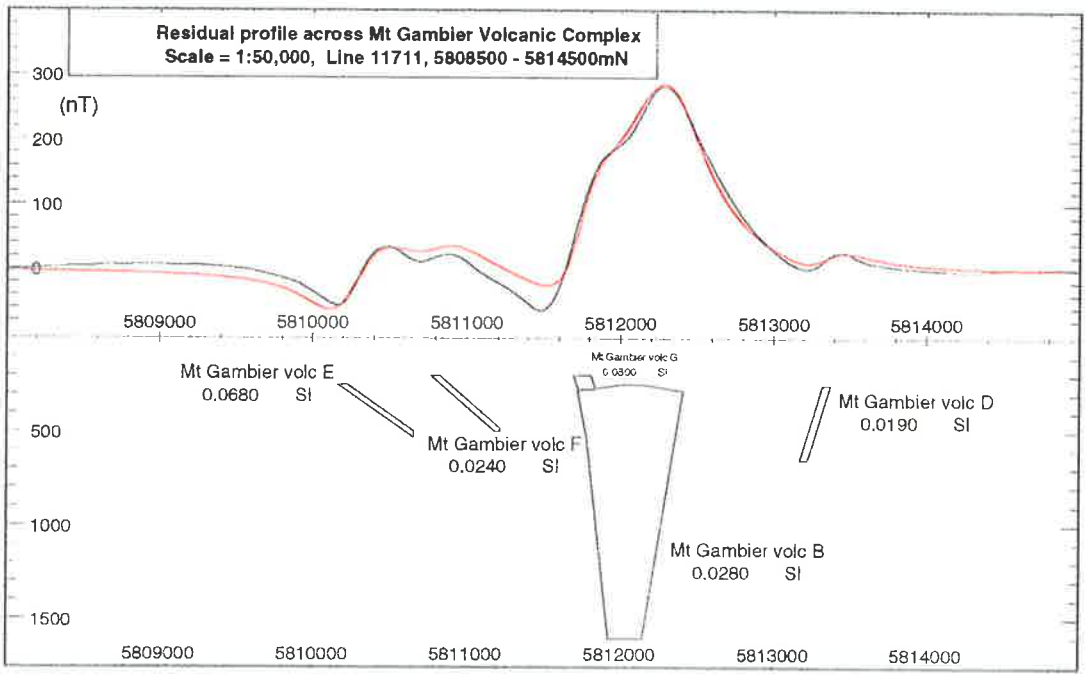

Fig. 8.1.6.2a Mt. Gambier volcanic complex, line 11711

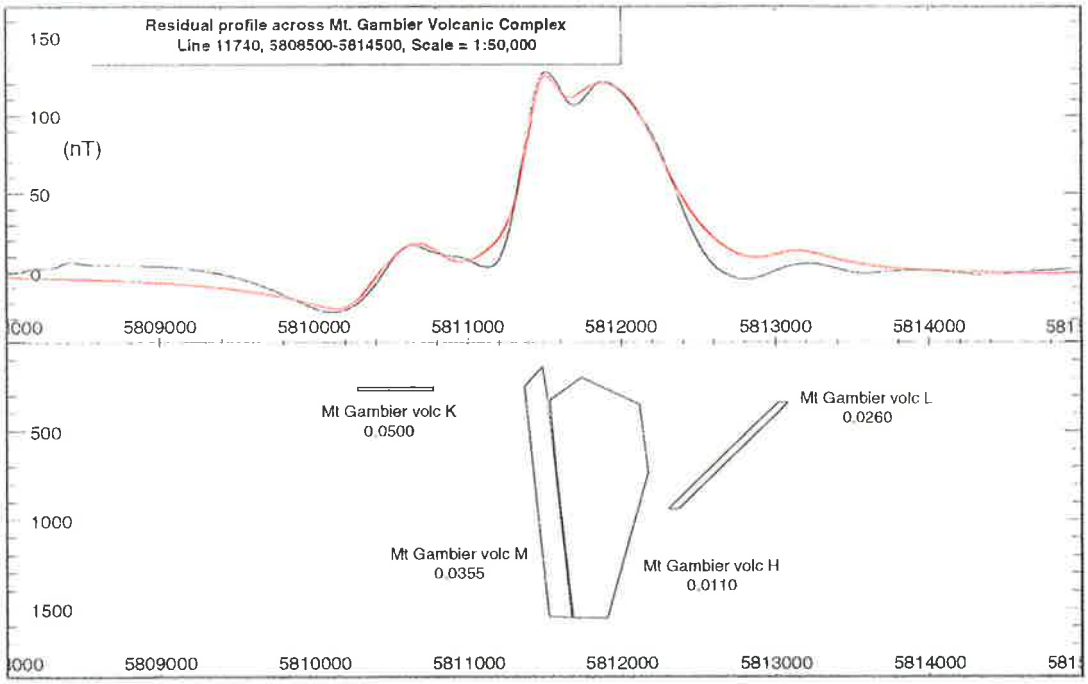

Fig. 8.1.6.3 Mt. Gambier volcanic complex, line 11740

(over Leg of Mutton Lake)

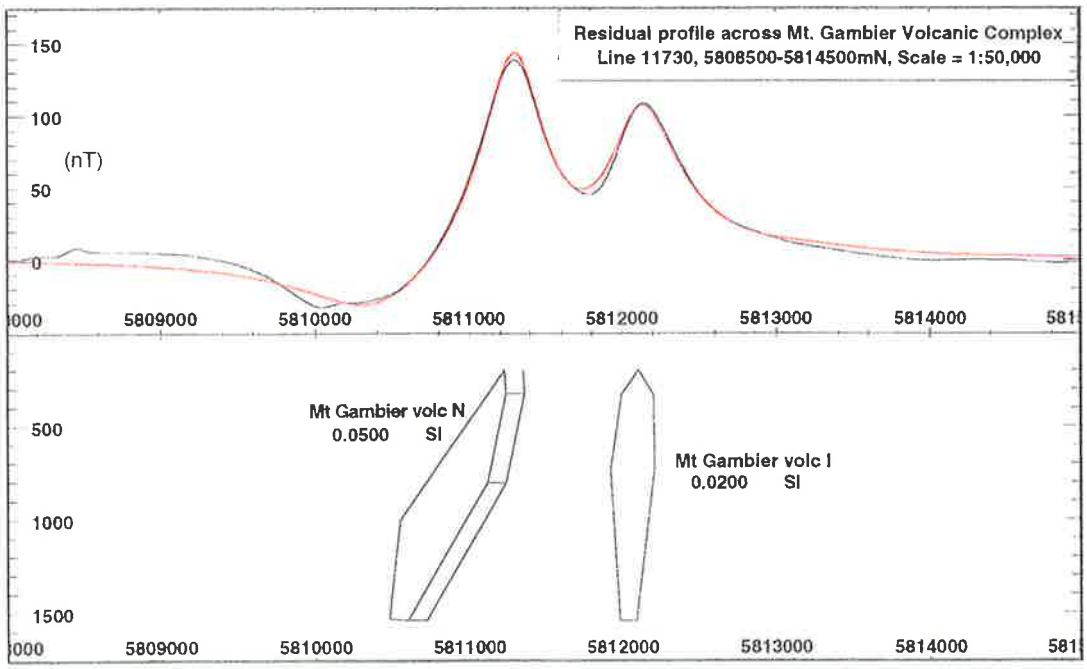

Fig. 8.1.6.3a Mt. Gambier volcanic complex, line 11730

susceptibility than weathered surface rocks. Also on this profile is an anomaly which is located south of the volcanic complex and seems to be produced by cultural features unrelated to the geology. There is a similar feature on the adjacent flightline to the west (11690) which has a lower amplitude, and both features appear to coincide with a major power line although the anomaly has a different shape to those typical of power lines.

The anomaly on line 11711 (fig. 8.1.6.2a) has a slightly lower amplitude than the anomaly on line 11700 and is wider with a different shape, reflecting a probable wider source body (Mt Gambier volc B). In order to fit the calculated anomaly to the residual profile it was necessary to add a small body (Mt Gambier volc G) with a much higher susceptibility (0.08 SI units) to the top of the large body. This may represent a late stage lava flow (Sheard, 1978). The near-vertical dyke-like feature (Mt Gambier volc D) could represent the feeder dyke that brought ejecta to the College Oval crater north of Brownes Lake, while Mt Gambier volc F may be the channel taken by blowhole ejecta erupting from the Devil's Punchbowl blowhole. The remaining dyke-like body, Mt Gambier volc E, is shown with the top near the surface south of the volcanic complex and does not correspond with any mapped geological feature. It is possible that the anomaly may in fact be the result of the cultural features believed to cause anomalies on this part of adjacent lines to the west but this anomaly is further south than those. It also has a shape that does not resemble that of a power line anomaly.

The residual profile (Line 11740) over the Mt. Gambier Volcanic Complex (fig. 8.1.6.3) shows two bodies producing the main anomaly as well as two dyke-like bodies to the north and south which generate the more subtle features. Two main bodies were used rather than one because of the two stages of eruption (Sheard, 1978) with the body, Mt Gambier volc M, that has the highest susceptibility (0.0335 SI units) shown as having forced a path through a pre-existing lava plug (Mt Gambier volc H, 0.011 SI units). The susceptibilities used with these bodies are at the upper extreme of values measured at site 1 (Chatfield, 1992). Both bodies are located below the Leg of Mutton Lake and may represent one of the two initial sites of eruption, and the later stage when the magma supply was dwindling (Sheard, 1990). The dyke-like body on the north side of the main anomaly, Mt Gambier volc L, may represent the feeder dyke that is the source of volcanic gases for a blowhole north of the complex while the southern body,

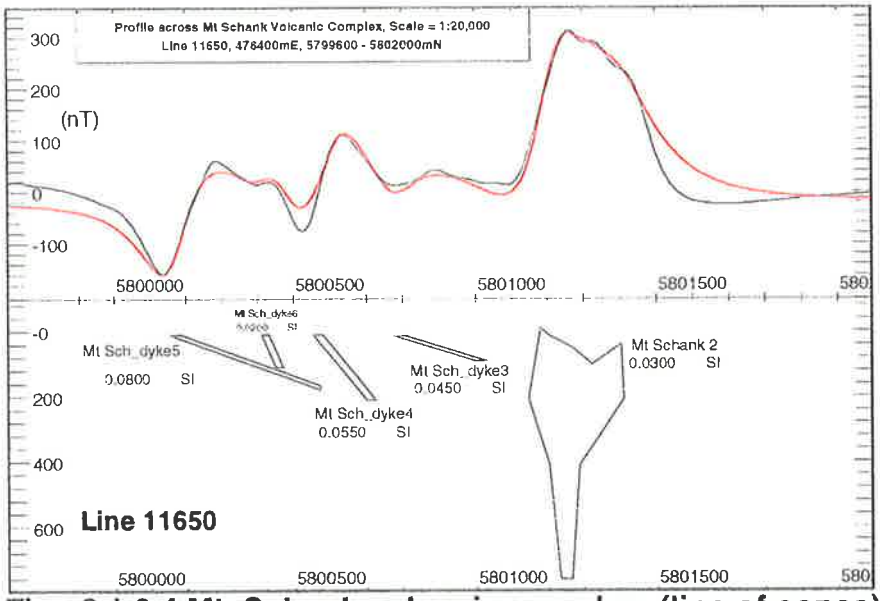

Fig. 8.1.6.4 Mt. Schank volcanic complex, (line of cones)

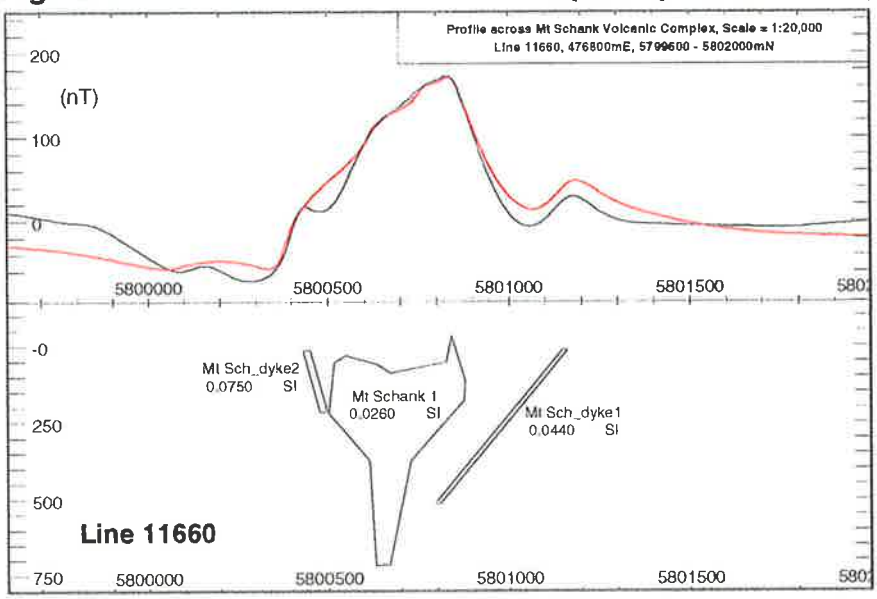

Fig. 8.1.6.5 Mt. Schank volcanic complex, (main cone)

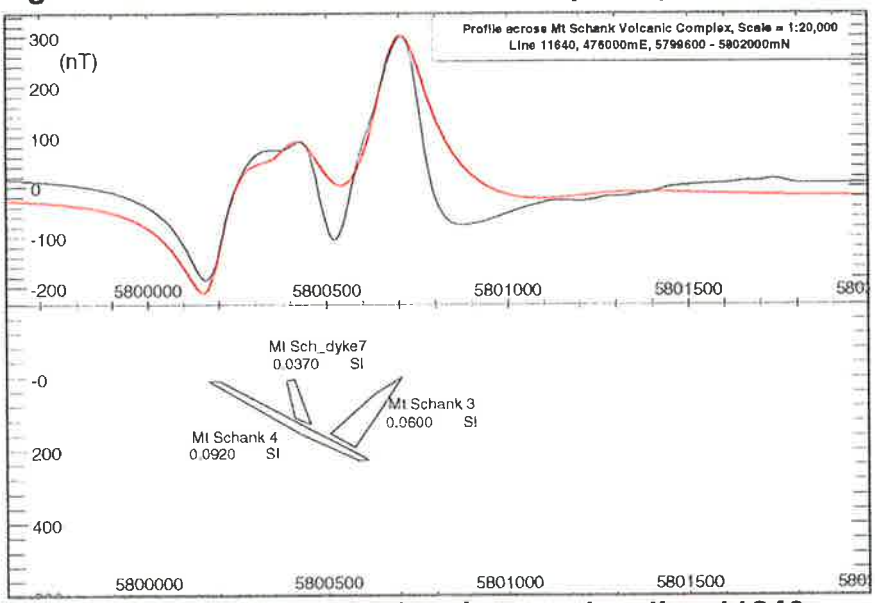

Fig. 8.1.6.6 Mt. Schank volcanic complex, line 11640

Mt Gambier volc K, may be a sill or buried lava flow on the southern side of the Blue Lake.

Line 11730 (fig. 8.1.6.3a) features two peaks, one north of Leg of Mutton Lake beneath the crater walls, and the second on the southern side of the lake. Both of these magnetic sources have been modelled as volcanic pipes which rise from depth and terminate near the surface where they are buried by ejecta. Mt. Gambier volc I was given a susceptibility of 0.02 SI units which is within the range of basalt values measured by Chatfield, (1992) at her site 2 which is close to the anomaly peak at Nurses' Landing, while the value assigned to Mt. Gambier volc N (0.05 SI units) is much higher than the range of tephra values measured at Chatfield's site 4. The strike of Mt. Gambier volc N is at an angle to the flightline so the body has been shown in block form rather than in cross-section as are other bodies. This has been done in order to show the dip of the body at depth in comparison with the near-vertical orientation of the other volcanic plugs.

The anomalies associated with the Mt. Schank volcanic complex are only found on three flightlines, 11640, 11650 and 11660 (between 476000 and 476800mE, and 5799600 and 5802000mN). The most intense anomalies over the Mt Schank volcanic complex occurs, not over the volcanic cone itself, but over a fissure with a line of small cones that is northwest of the main crater, and over a small crater to the west of the main cone (fig. 3.3.1.2 & 8.1.6.1b). The fissure anomaly (approx. 320 nT amplitude) is on line 11650 (fig. 8.1.6.4) and the source has been modelled as a funnel-shaped body (Mt Schank 2) with raised ends that may represent apophyses, and the body was assigned a susceptibility of 0.03 SI units. South of the largest anomaly are four smaller features which have been modelled as mostly shallowly dipping dykes that probably extend from the source of the main cone or the northwest fissure. These dykes (Mt Sch_dyke3 to 6) have been assigned susceptibilities that are, with one exception, greater than the value given to Mt Schank 2, and the bodies generating the largest anomalies, Mt Sch_dyke4 (approx. 180 nT) and Mt Sch_dyke5 (approx. 220 nT), required a remanent magnetisation component in order for the calculated profile to approximate the observed, especially the negative part of the curve.

The main cone, crossed by line 11660, has an anomaly with an amplitude of approximately 260 nT which has been modelled by a complex body, Mt Schank 1 (fig.

8.1.6.5), consisting of a conduit which brought magma to the surface from greater depth, connected to a funnel-shaped feature with a small extension on the top representing a volcanic pipe. This volcanic pipe is inferred to be the source of the buried scoria cone on the northern side of the main crater (Sheard, 1987). In addition, there are two dyke-like bodies which are associated with the complex, one is north of the cone (Mt Sch_dyke1) which is a thin dipping body while the other is south of the main body (Mt Sch_dyke2) and may represent the conduit that fed the southern maar (Sheard, 1987).

The anomaly shown in the residual profile is complex and the calculated profile is a reasonable fit only on the top of the main anomaly while the relatively small anomaly produced by Mt Sch_dyke1 (approx. 25 nT) is the same shape as the corresponding residual anomaly but is offset by interference from the neighbouring anomaly. The calculated anomaly generated by Mt Sch_dyke2 is a poor fit to the residual anomaly. The susceptibilities assigned to the bodies in figure 8.1.6.5 are greater than or at the upper extreme of the measurements acquired at Mt Schank by Chatfield, (1992) but those measurements were of scoria, tuffs and tephra, while the average value reported by Telford et al., (1990) for basalts (0.07 SI units) is close to or greater than the values assigned to the models.

The profile in figure 8.1.6.6 is from line 11640 and shows three approximately dyke-like bodies which produce anomalies that have a similar shape to those of the dyke-like bodies on line 11650 (fig. 8.1.6.4) but with a greater amplitude. This is especially the case with the anomaly produced by Mt Schank 3 (400 nT) while the anomaly generated by Mt Schank 4 (240 nT) is only marginally greater in amplitude than that by Mt Sch_dyke5. These bodies also required a remanence component to approximate the residual profile which may suggest that two of the bodies on this profile may be extensions of those on the adjacent line (11650), in particular, Mt Schank 4 and Mt Sch_dyke7 which have been assigned slightly greater susceptibilities. It was not possible to match the residual profile over Mt Schank 3 with a calculated profile using parameters similar to those of Mt Sch_dyke4 on line 11650. This suggests that the former is a separate body to the latter unlike the other two dykes beneath this flightline.

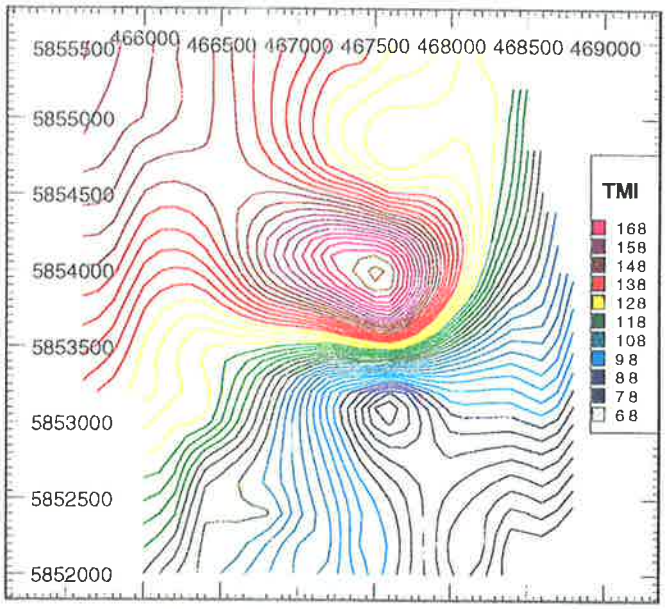

Fig. 8.1.7.1a TMI contour map of Hungerford Anomaly, Scale = 1:50,000

Contour interval = 2 nT

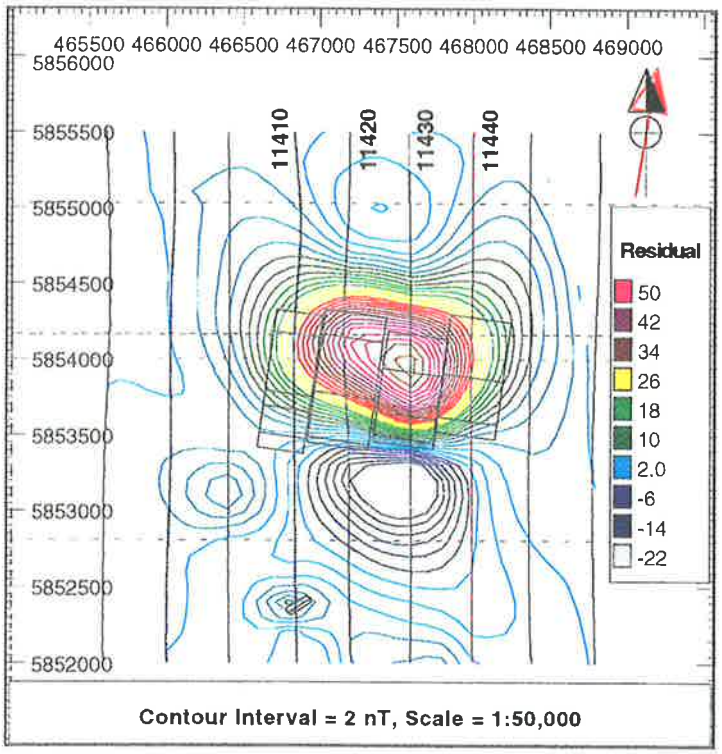

Fig. 8.1.7.1b Residual TMI contour map of Hungerford Anomaly showing flightlines and model bodies

8.1.7 Hungerford Anomaly Model

The Hungerford Anomaly has been interpreted as a blind basaltic plug approximately 300 m deep and 1.5 × 0.9 km which has penetrated through the Cretaceous sediments, stopping above the base of the Tertiary. The anomaly has a peak-to-trough amplitude of around 80 nT (on line 11430) and is elongated on a WNW-ESE axis. Fig. 8.1.7.1a shows the TMI contour map of the anomaly while Fig. 8.1.7.1b shows the contour map produced from residual data extracted from lines 11380 to 11461 (465600 to 468800mE and 5852000 to 5855500mN) with the outline of the four bodies that comprise the model superimposed over the contours.

The residual profile from line 11420 (fig. 8.1.7.2) shows a polygon (Hungerford 1) with a shallower extension on the northern side and with a susceptibility of 0.0082 SI units, while the residual profile from line 11430 (fig. 8.1.7.3) shows a polygon (Hungerford 2) with shallower extensions on both ends of the body and with a susceptibility of 0.012 SI units. Both of the susceptibility values are within the low to mid-range for basalts at some locations in the Mt. Gambier Volcanic Complex and at the higher end of the susceptibility range for basalts at other locations within the complex (Chatfield, 1992).

Residual profiles across Hungerford 4 and 3 are shown in figures 8.1.7.4 and 8.1.7.5 respectively, with line 11410 crossing Hungerford 4 and line 11440 crossing Hungerford 3 (at opposite ends of the model). While Hungerford 3 (fig. 8.1.7.5) is a similar shape and overall depth as the neighbouring body, Hungerford 2, the body at the other end of the model, Hungerford 4 (fig. 8.1.7.4), is more dome-shaped and has a greater depth to the top than the other bodies, a result which is justified by Automag (section 6.3.2). The susceptibilities assigned to the bodies in these two figures are lower than that of the central bodies.

Also shown on figure 8.1.7.4 is the body named 'Shallow Dyke' which is beneath an anomaly centred at approximately 5852400mN which has an amplitude of around 16 nT and a wavelength of approximately 500 m. The anomaly is only apparent on this line (11410) and does not coincide with any power line marked on the utilities map supplied to the author. In addition, the anomaly is not associated with any cultural features such as farm buildings shown on the topographical maps although it is possible that the source was moved or erected there after these maps were compiled (1975). For these reasons

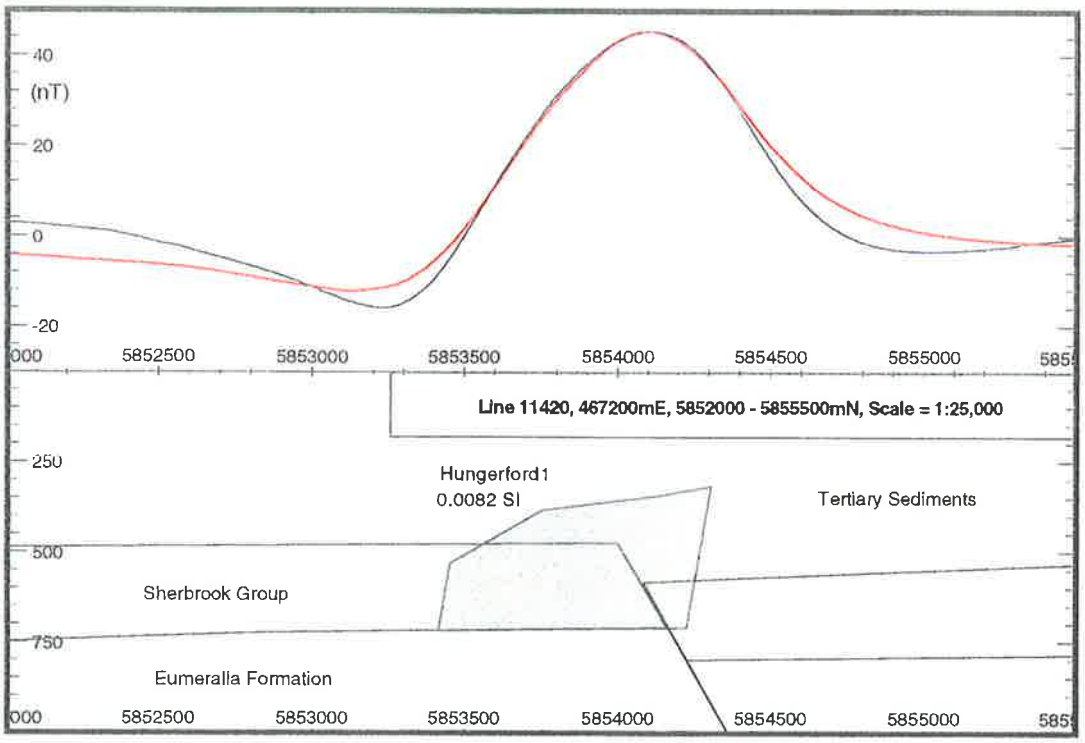

Fig. 8.1.7.2 Residual Profile across Hungerford Anomaly

Line 11420, Scale = 1:25,000

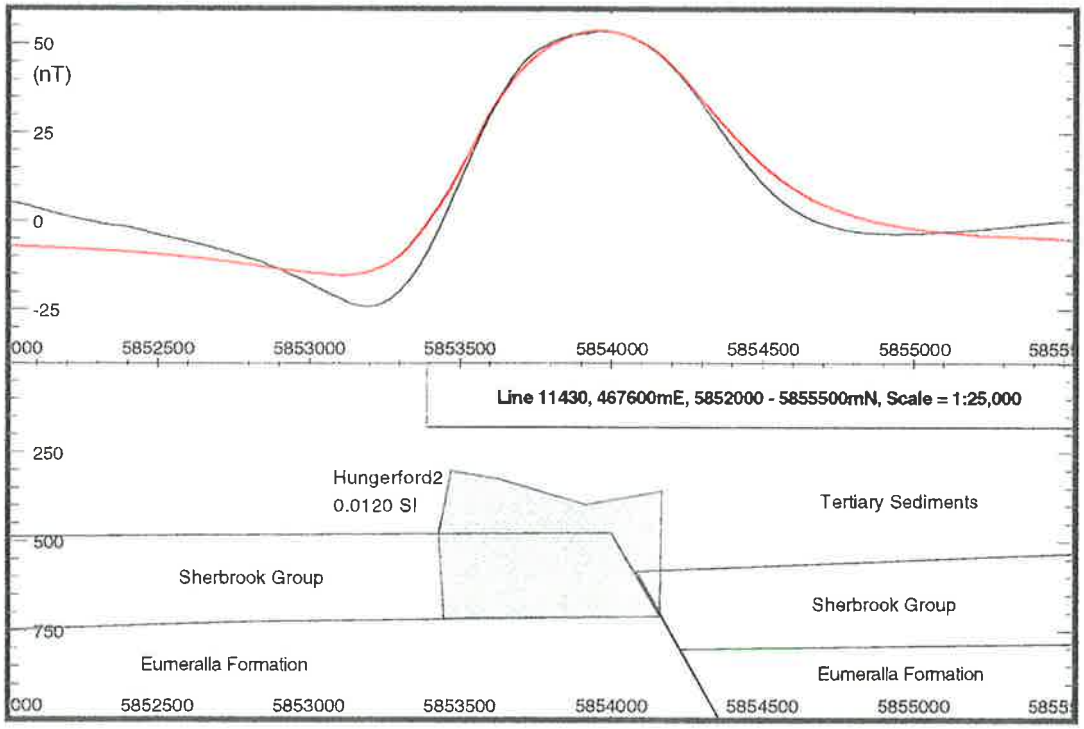

Fig. 8.1.7.3 Residual Profile across Hungerford Anomaly

Line 11430, Scale = 1:25,000

Top of Sherbrook Gp. and Eumeralla Fm. interpolated

from 85-ULT31S and Adjacent Lines

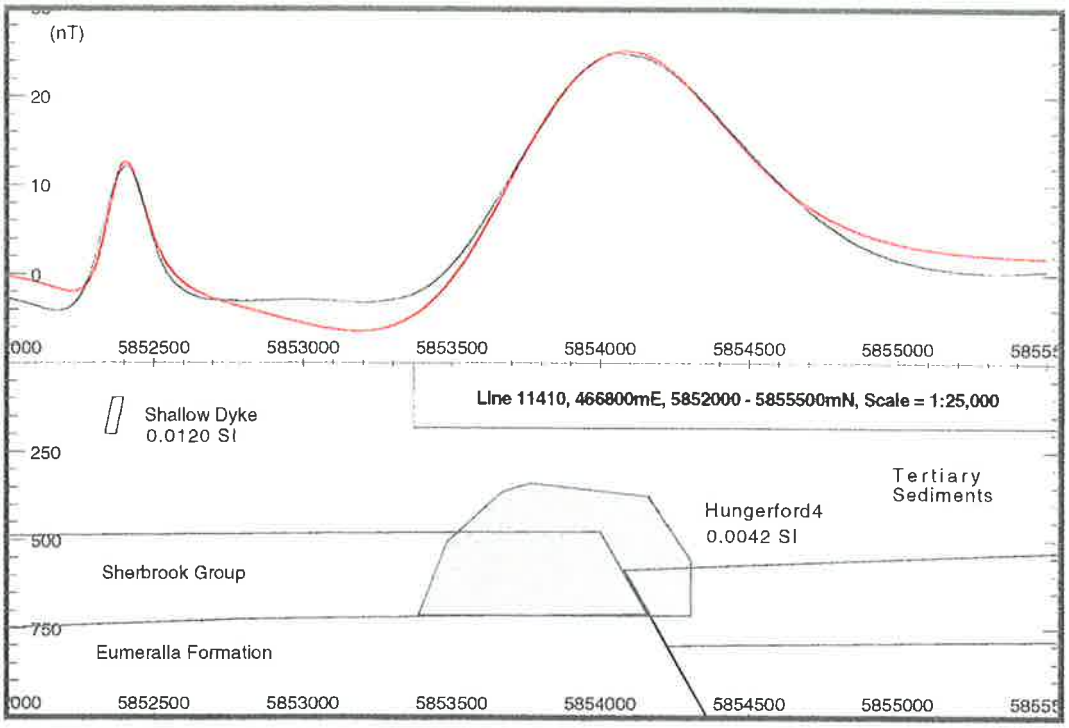

Fig. 8.1.7.4 Residual Profile across Hungerford Anomaly

Line 11410, Scale = 1:25,000

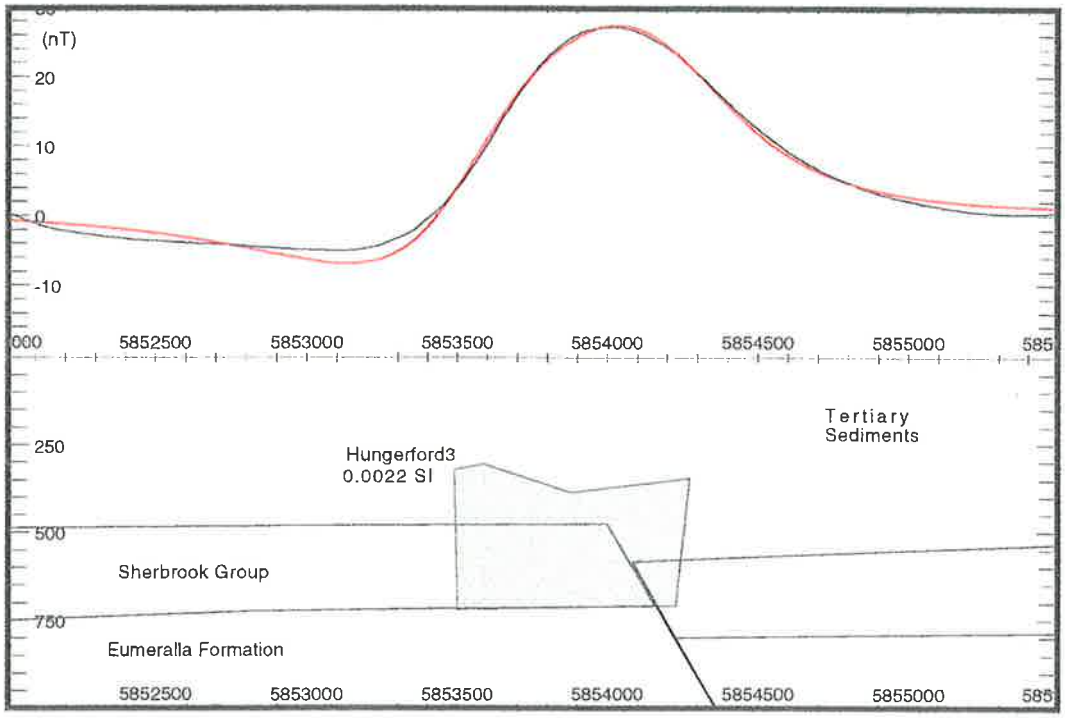

Fig. 8.1.7.5 Residual Profile across Hungerford Anomaly

Line 11440, Scale = 1:25,000

Top of Sherbrook Gp. and Eumeralla Fm. interpolated

from 85-ULT31S and Adjacent Lines

the source has been tentatively identified as a geological feature and a model produced for the anomaly. The Shallow Dyke is approximately 100 m below the sensor (40 m below the surface within the Gambier Limestone) with a thickness of 30 m, a depth extent of around 100 m and a strike length of 160 m with an assigned susceptibility of 0.012 SI units. This body is up to 1 km north of a major fault extending to the top of the Sherbrook Group which is part of the same Kalangadoo Fault Zone that presumably acted as a conduit for the Hungerford Anomaly source, so if the source of the minor anomaly is geological then it may be an intrusive body as well.

The depths to the top of the Hungerford bodies were initially fixed at the Automag-derived depths, and the susceptibility and vertices of each body were subsequently adjusted to fit the profile. The figures also show the top of the Sherbrook Group and Eumeralla Formation as well as the fault that presumably acted as a conduit for the rising magma. The formation tops and the fault orientation were derived by interpolating from seismic lines (including 85-ULT31S and adjacent lines) plotted on the seismic horizon maps, most of which are oriented northeast-southwest rather than the north-south direction of the flightlines. The tops of the bodies are generally below 300 m depth which means that they are within the Dilwyn Formation (as mapped at Laira 1 and Zema 1) which constrains the age of emplacement to be mid-Eocene at the earliest although it is more likely to be the Pleistocene/Recent age of the Mt. Burr Group. The base of the models have not been extended below the top of the Eumeralla Formation (700-750 m deep) although there is no evidence that the bodies do not have a greater depth extent and there has been no attempt to model the magma conduit. If the fault has acted as the conduit, then the conduit is likely to be quite narrow and may not contribute significantly to the profiles unless there has been emplacement of highly magnetic rocks in it.

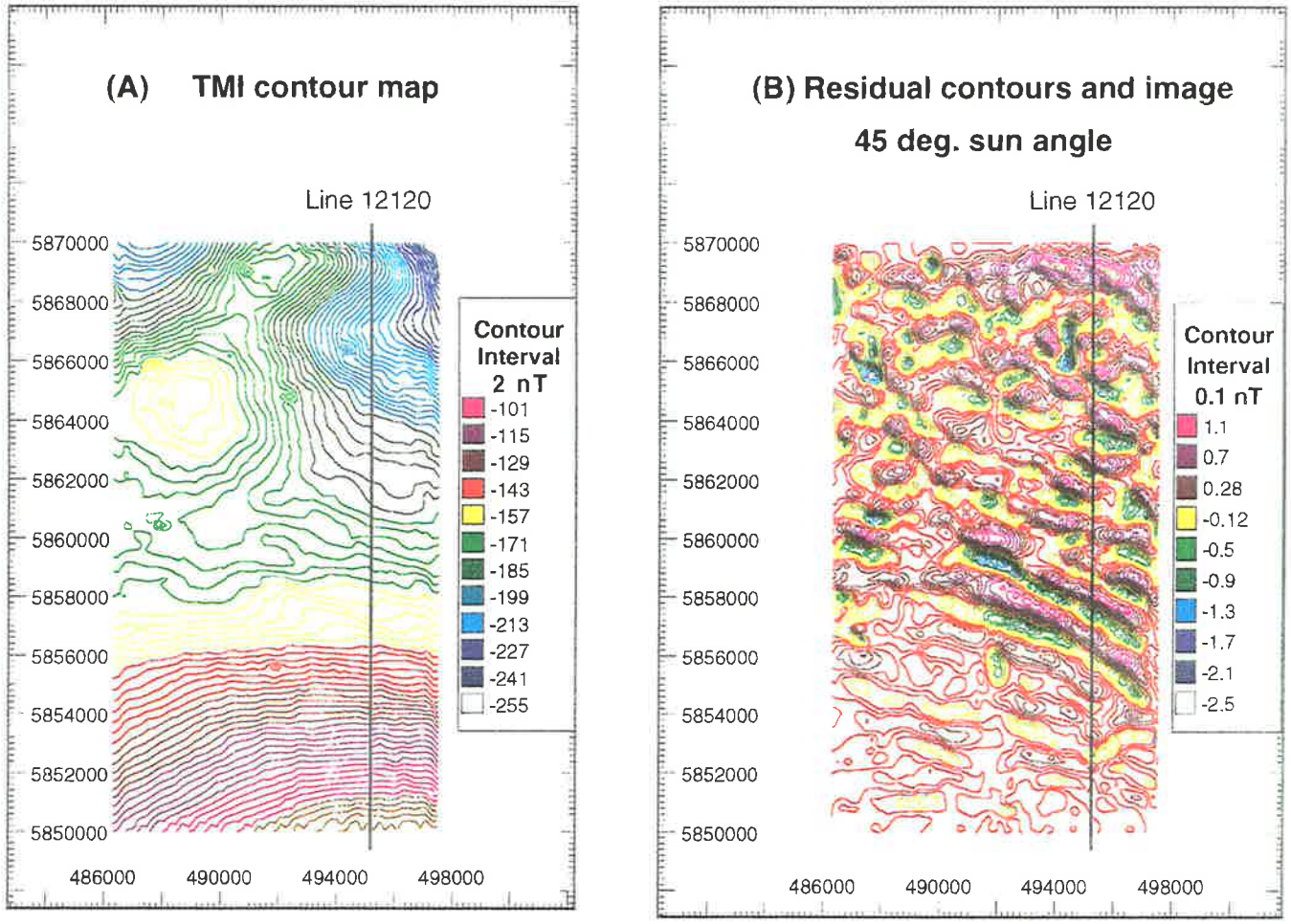

Fig. 8.2.1.1 TMI contour maps and image of East Penola Trough Anomalies showing Line 12120, Scale = 1:100,000

8.2 Models of Intersedimentary Sources

In the previous section the models were of bodies that are most likely to be of igneous origin where magma intruded into the strata or was extruded onto the surface, or alternatively, are of bodies representing pre-existing metamorphic terrain. The intersedimentary anomalies are generally of much lower amplitude than those produced by igneous or metamorphic sources which means that these anomalies are usually only detectable when the source is relatively shallow.

From the theoretical modelling discussed in section 5.2, it is evident that only sources within the Eumeralla Formation (and possibly the Sherbrook Group), in the part of the study area north of the Kalangadoo High, are likely to produce anomalies that are greater than the noise envelope (0.2 nT) when assigned the measured susceptibilities from well cores. In the north of the study area the depth to the top of the Eumeralla Formation horizon ranges from around 300 m at Penola 1 and Sawpit 1, to approximately 600 m at the Katnook and Ladbroke Grove 1 wells, and 765 m at Kalangadoo 1 on the Kalangadoo High. South of the Kalangadoo High the depth to the top of the Eumeralla Formation increases substantially, reaching 2892 m at Caroline 1 and significantly greater than 4468 m at Breaksea Reef 1 offshore where the top of the formation was not intersected. The increasing depth of the formation means that any intersedimentary magnetic sources south of the Kalangadoo High will be within the overlying Sherbrook Group or Tertiary sediments onshore, or only the Tertiary sediments offshore.

8.2.1 East Penola Trough Linear Anomalies Model

These linear anomalies are a series of elongated magnetic features that mostly strike approximately N 120° E and are located in the northeastern section of the study area, mainly in an area bounded by 486000-497700mE and 5850000-5870000mN. The most prominent of these anomalies are two distinct features southeast of Penola and east of Wynn 1 but there are a number of others to the north of these that are delineated more clearly on gradient maps (section 7.2.1) or the residual anomaly map (fig. 8.2.1.1, part B).

The only seismic line through the eastern section of the study area is OK90-414 which is oriented approximately north-south (close to 495200mE or flightline 12120).

This line extends from around 5838000mN at the southern end to approximately 5865000mN at the northern extremity. Examination of the seismic section shows that most of the linear magnetic anomalies occur close to or over prominent faults in the Eumeralla Formation but apart from the faults there is little direct evidence of any discrete bodies or horizons that might be the sources of the magnetic anomalies. There has not been any drilling in this area so it is not possible to unequivocally determine the nature of the sources but the measured susceptibility values of Eumeralla Formation cores from Penola 1 have not revealed the presence of any highly magnetic unit that might generate an anomaly through being offset by faulting (section 3.3.2) or because it is discontinuous. This cannot exclude the possibility, however, because not all the 16 cores recovered from the well had the susceptibility measured and the cores themselves are relatively widely, although evenly, spaced which means that it is possible a highly magnetic unit is present, while in addition, substantial lateral facies variations in the Penola Trough have been found so the measurements at Penola 1 may not be representative.

If the anomalies are not caused by fault-induced offsets in magnetic horizons or by discontinuous magnetic horizons, then it is possible the source bodies are confined to the fault planes or zones. This suggests two possible explanations, either there is a series of igneous dykes of low susceptibility that have intruded into the Eumeralla Fm sediments, or there has been some deposition or destruction of magnetic minerals on or near the fault planes. There does not appear to be any indication of intrusive bodies on the seismic section (Mitchell, pers. com. 1996) but a very thin, near vertical body may escape detection because the width is less than the limit of seismic resolution. Seismic horizontal resolution is limited by the radius of the Fresnel Zone which is approximately 80 m at the location of the most prominent anomalies and igneous dykes can be thinner than this. The anomalies can be modelled by near vertical or steeply dipping bodies that may be either relatively thin (less than 80 m thick) as for an igneous dyke or much wider for a zone around the fault, and which can extend from the top of the formation to near the bottom. The latter source bodies would then represent a zone of elevated (or reduced) magnetisation within the Eumeralla Formation rather than a discrete body like a dyke which is a completely different rock type to its surroundings.

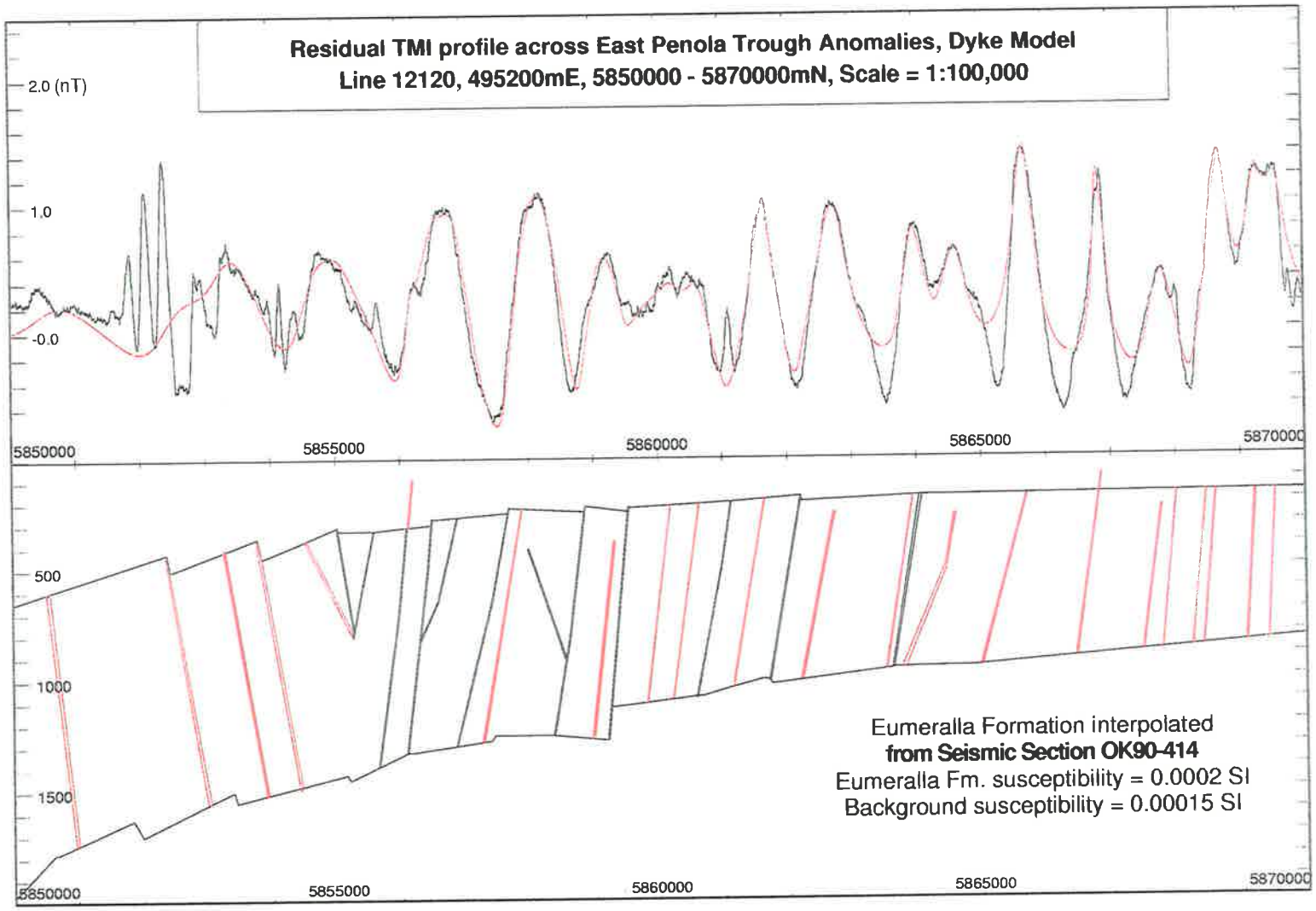

Fig. 8.2.1.2 East Penola Trough section showing igneous dyke model bodies within Eumeralla Fm.

Another possibility discussed by AGSO staff in interpreting an offshore survey in the Victorian section of the Otway Basin (Gunn, 1995) is that the zones discussed above may be deep channels filled with detrital magnetic material. Channel sands overlying meandering fluvial deposits have been interpreted at or near the top of the Eumeralla Formation in the vicinity of the Sawpit 1 well (Martin, 1992, Felton, 1997) but these may possibly be of greater lateral extent and with considerably less depth extent than the channels discussed by the AGSO staff. Morton et al., (1995) used dipmeter data to establish that the predominant palaeocurrent direction for the Penola Trough is E-W to WNW-ESE which suggests that the channels were oriented in the same direction as the main structural strike is at present. Studies of claystone layers overlying brown-coal seams in Bohemia (Krs et al., 1992) have revealed highly magnetic mineralisation due primarily to griegite which probably formed through the alteration of either iron oxides or pyrite. Pyrite is present in trace amounts throughout the Eumeralla Formation as are numerous thin coal beds (Martin, 1992, Felton, 1997) so the presence of magnetic sulphides cannot be excluded. Beds containing such magnetic mineralisation are unlikely to form a continuous layer, not only because of offsetting by faults, but also because the geochemical conditions required for the formation of magnetic minerals are more likely to occur in isolated sections rather than across the whole formation (for example, in coal swamps or at the bottom of shallow lakes). The migration of groundwater through fault zones would be expected to produce oxidising conditions in their vicinity while the migration of hydrocarbons should produce reducing conditions. The former situation could result in magnetic layers separated by non-magnetic fault zones while the latter would result in a magnetic layer centred on the fault with less magnetic sediments between the fault zones. If this has occurred, then it may be difficult to differentiate between the authigenic magnetic mineralisation discussed above and the infill of fluvial/estuarine channels with detrital magnetic minerals which is also likely to produce discontinuous layers.

Since it is not possible to establish the most probable of these different possibilities, models of the different body types have been prepared for comparison, and as well as the output generated by the modelling software, the models have also been superimposed on part of the seismic section. The '*igneous dyke*' model shown in figure 8.2.1.2 was constructed by locating seventeen thin polygon bodies at the positions of the

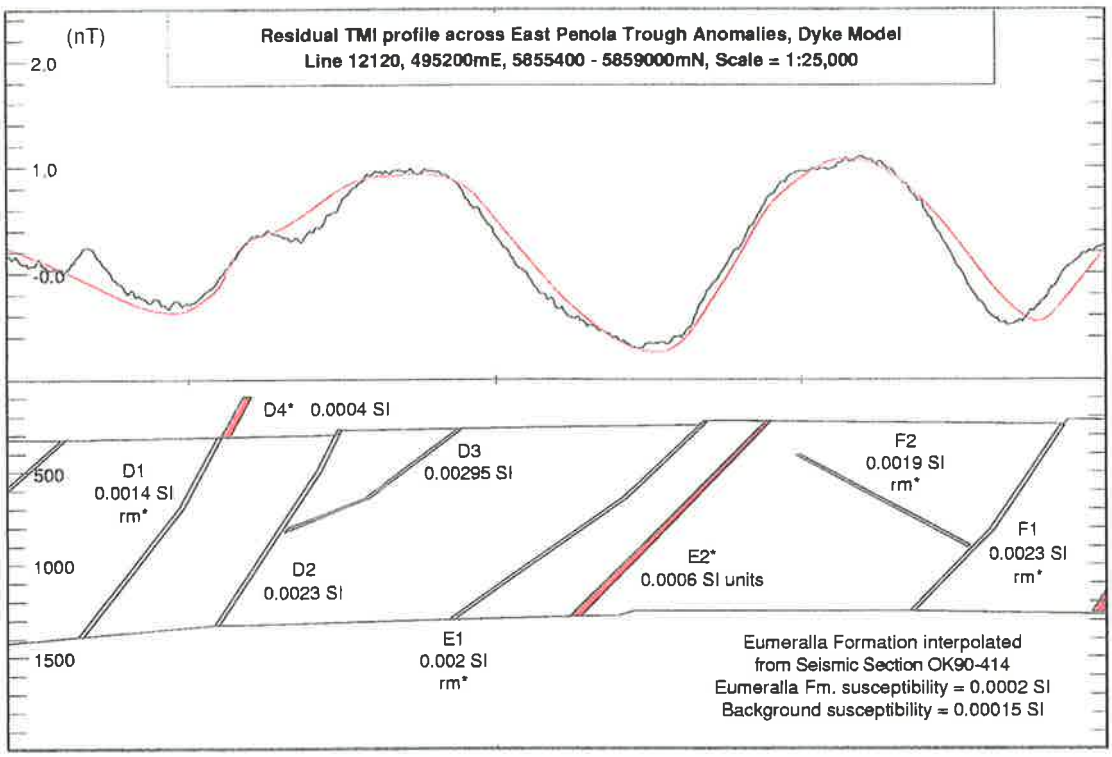

Fig. 8.2.1.3a Part of East Penola Trough section showing dyke model

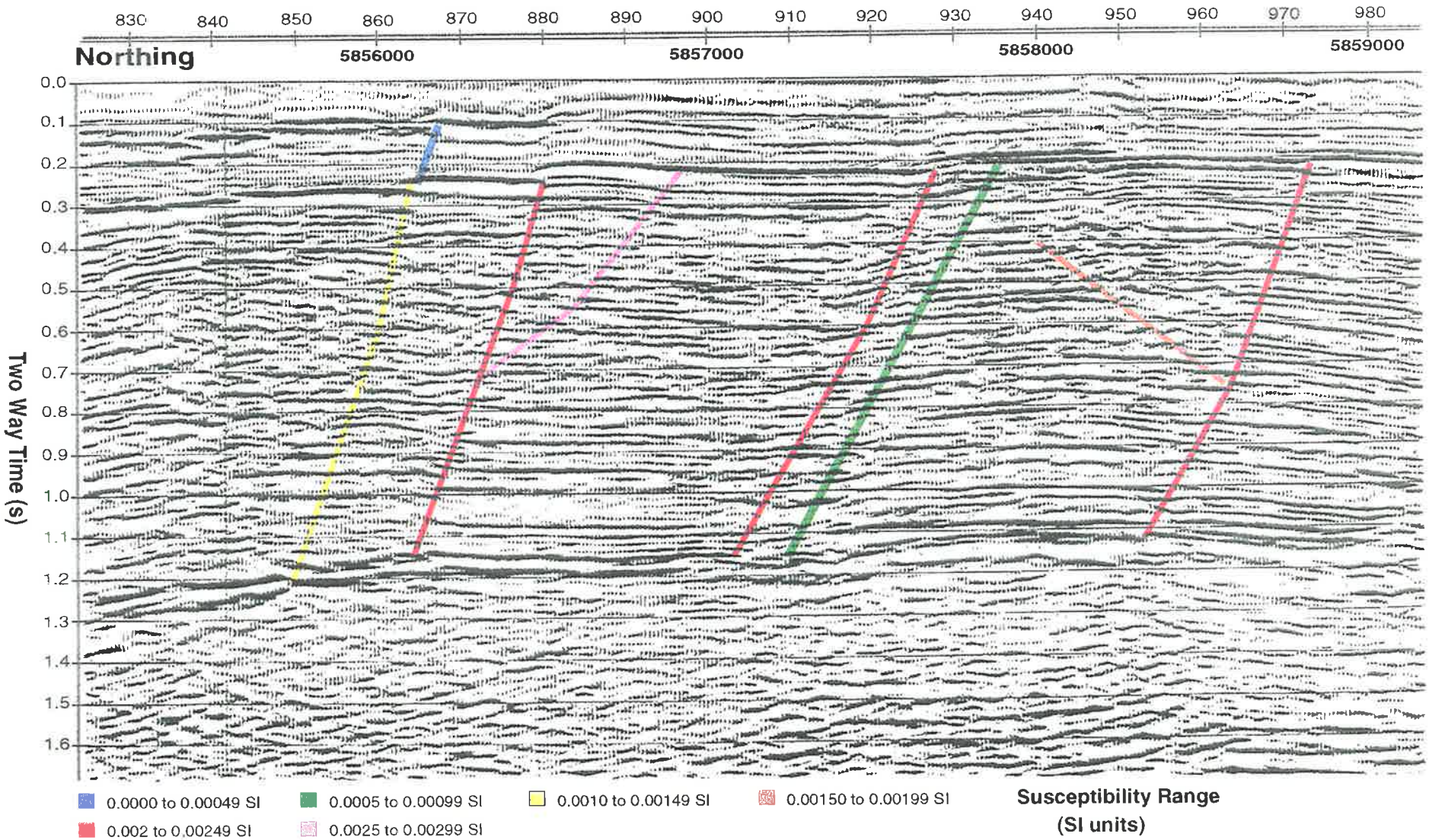

Fig. 8.2.1.3 b Part of Seismic Section OK90 - 414 showing Igneous Dyke Model bodies

prominent faults which were determined from the seismic section OK90-414. The section was also used to construct a body representing the basal and top horizon of the Eumeralla Fm with the formation being assigned an arbitrary susceptibility of 0.0002 S.I. units and the background (above and below the Eumeralla Fm) a susceptibility of 0.00015 S.I. units. The dyke-like bodies are around 10 to 30 m wide, extend from the base of the Eumeralla Fm towards the top and were assigned susceptibilities which are generally at the lower end of the basic igneous rock range with some requiring a reversed polarity remanence component to approximate the profile (Appendix B).

Initial modelling of the residual profile, with bodies only in the positions of the faults prominent on the seismic section, required a number of different remanence inclinations and declinations to approximate the most prominent of the magnetic anomalies and was unsuccessful with some of the other important anomalies. The profile extends past the end of the seismic section so the only information on faults associated with the anomalies in the 5 km to the northern end of the profile comes from the horizon maps. Fault-plane bodies were created for this section and additional bodies (with a * at the end of their name) were created for the seismic section where the fault-plane bodies on the prominent faults are unable to fully simulate the anomalies. These eighteen additional bodies are shown as solid red bodies on the profile rather than the outline of those bodies coinciding with major faults (Fig. 8.2.1.2). Generally, anomalies that have a wavelength of less than about 300 to 400 m are considered likely to be of cultural origin and thus have been ignored. Prominent examples of this are the three short wavelength anomalies around 5852000 to 5853000mN as well as the smaller amplitude anomalies superimposed on the profile between 5853000 and 5856000mN, and between 5859500 and 5861000mN.

The models shown in Figures 8.2.1.3a to 8.2.1.6a are plotted on part of the seismic section to allow comparison between the interpreted bodies and structures on the section, and in particular, between those bodies which appear unrelated to faults (figures 8.2.1.3b to 8.2.1.6b). The fault plane 'dykes' shown in figure 8.2.1.3a approximate the profile only when the bodies, Eumeralla D1, E1 and F1, are assigned a remanence inclination at approximately 180° to the current geomagnetic field inclination (70°, 65° and 65°, respectively) and the body Eumeralla E2* (with induced magnetisation only) is added to the model to help reproduce the width of the anomaly over it and Eumeralla F2

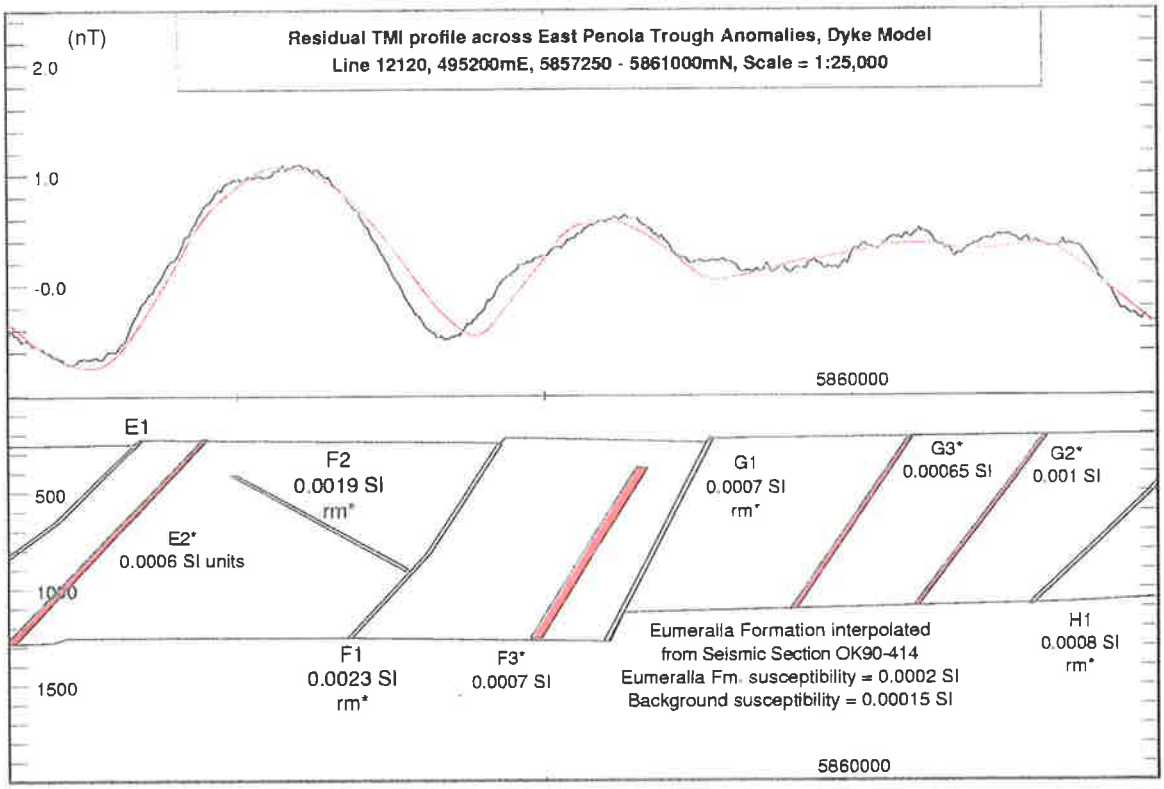

Fig. 8.2.1.4a Part of East Penola Trough section showing dyke model

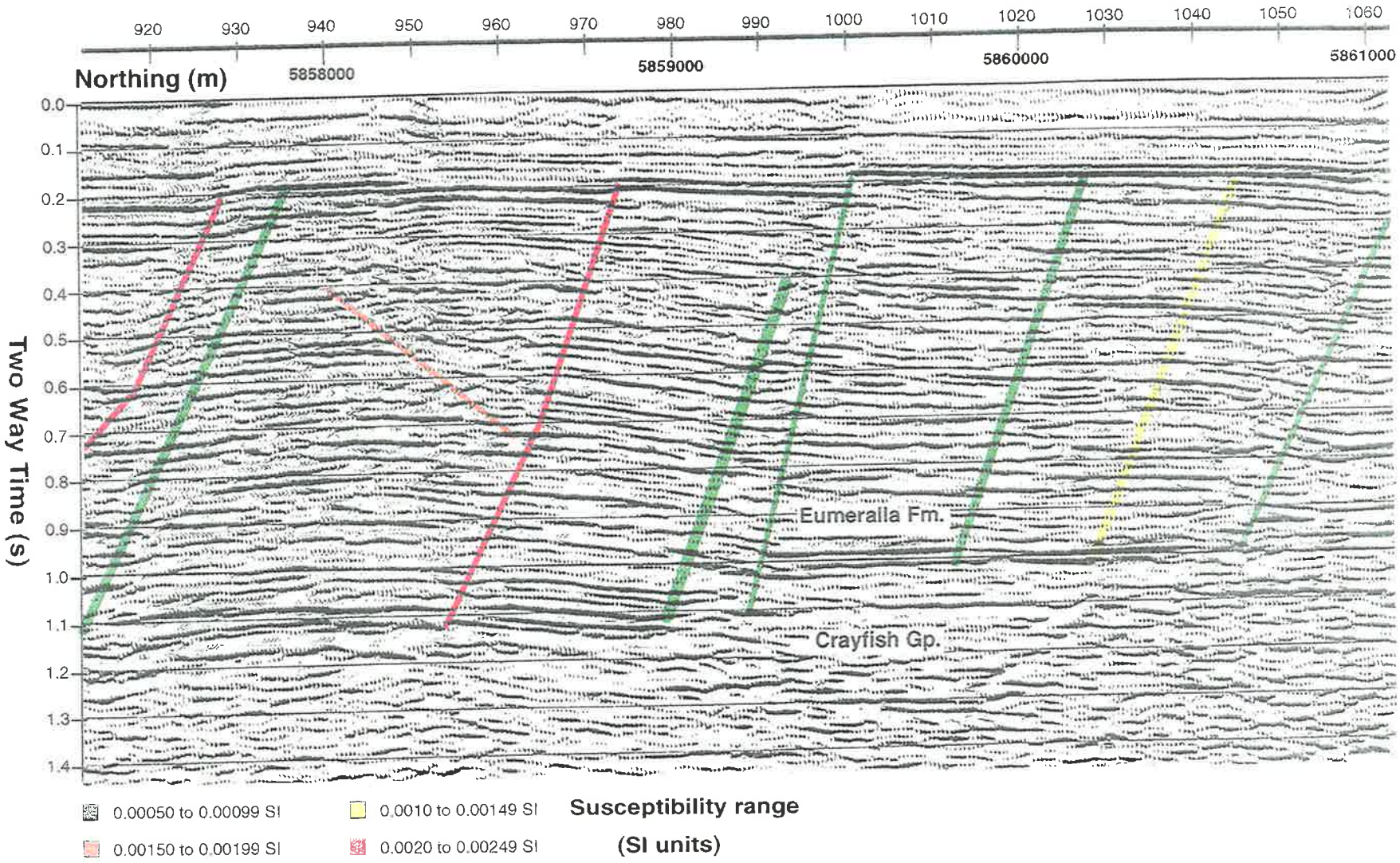

Fig. 8.2.1.4 b Part of Seismic Section OK90 - 414 showing Igneous Dyke Model bodies

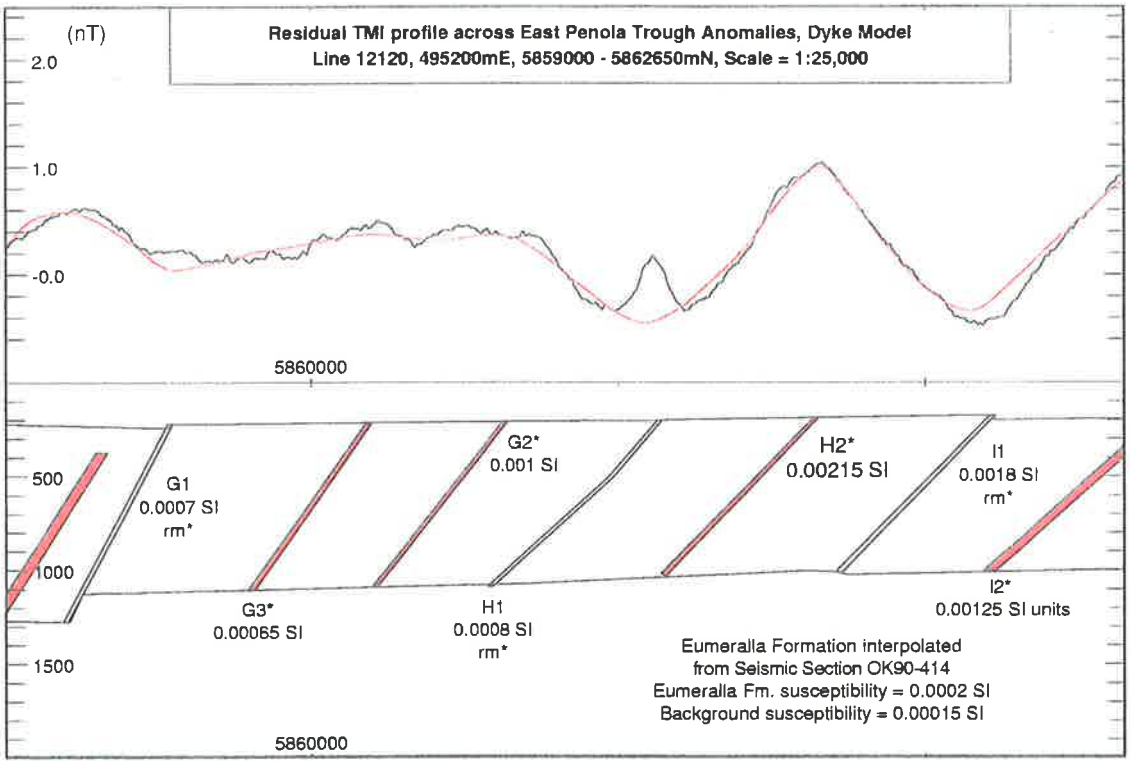

Fig. 8.2.1.5a Part of East Penola Trough section showing dyke model

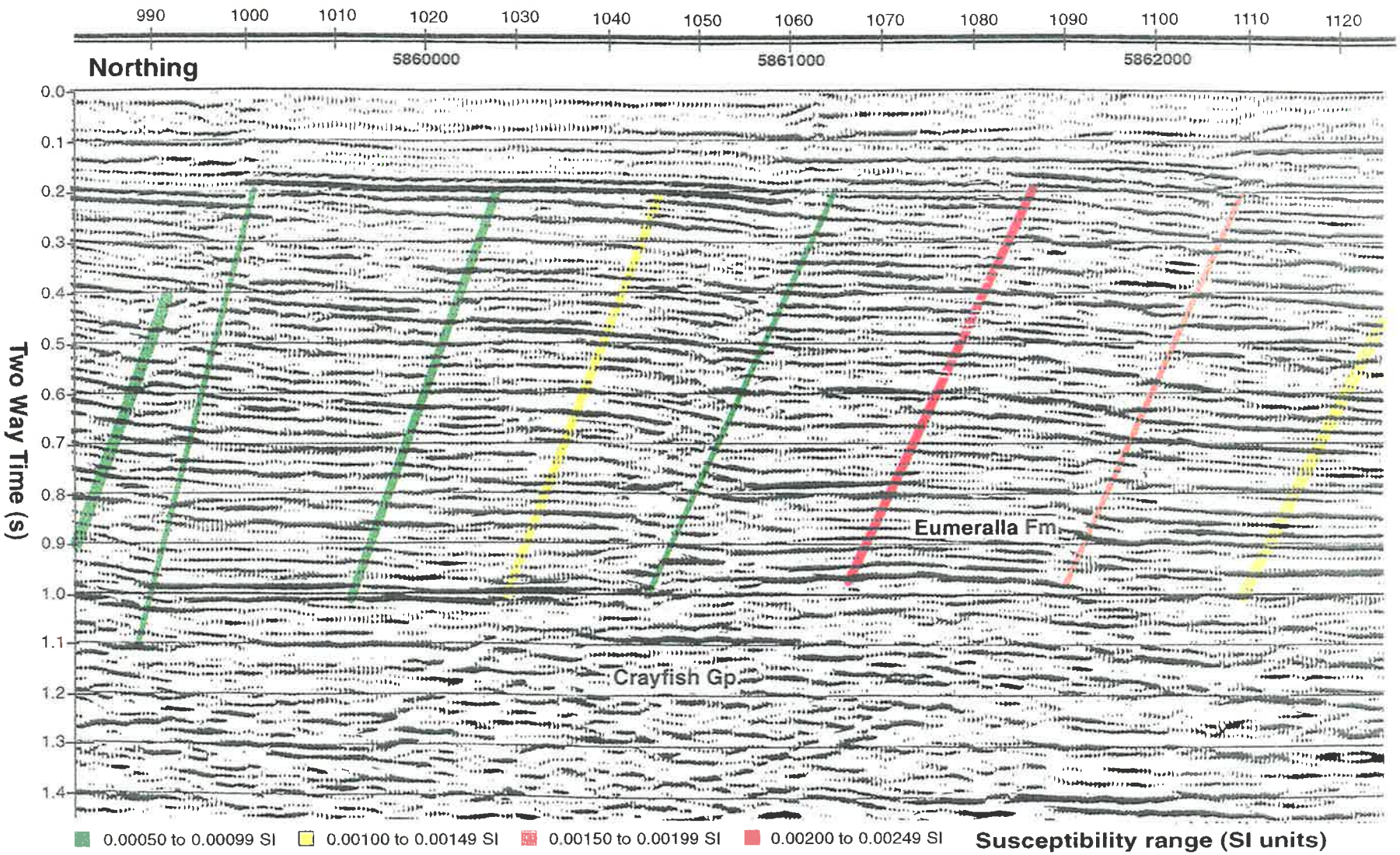

Fig. 8.2.1.5 b Part of Seismic Section OK90 - 414 showing Igneous Dyke Model bodies

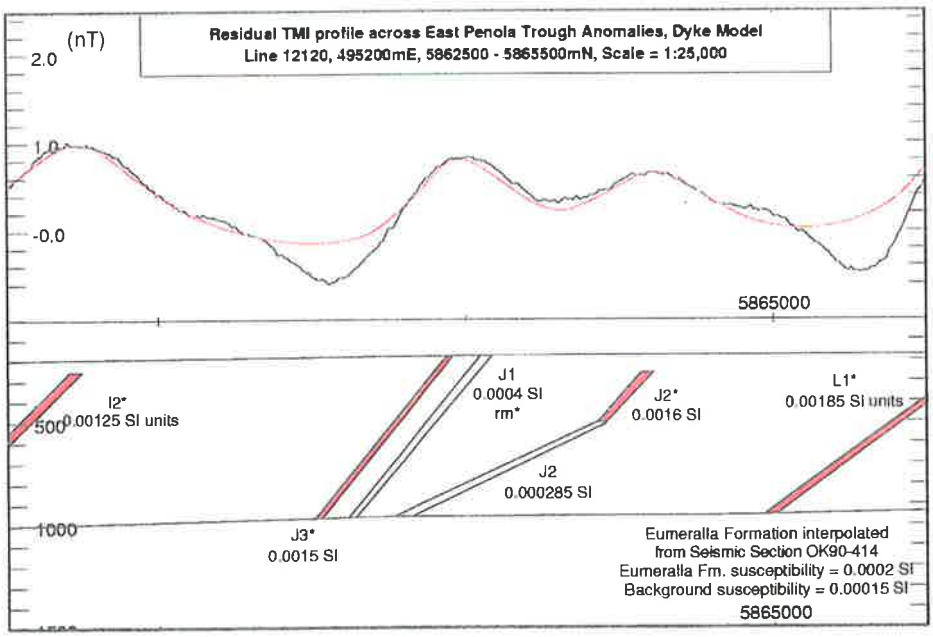

Fig. 8.2.1.6a Part of East Penola Trough section showing dyke model

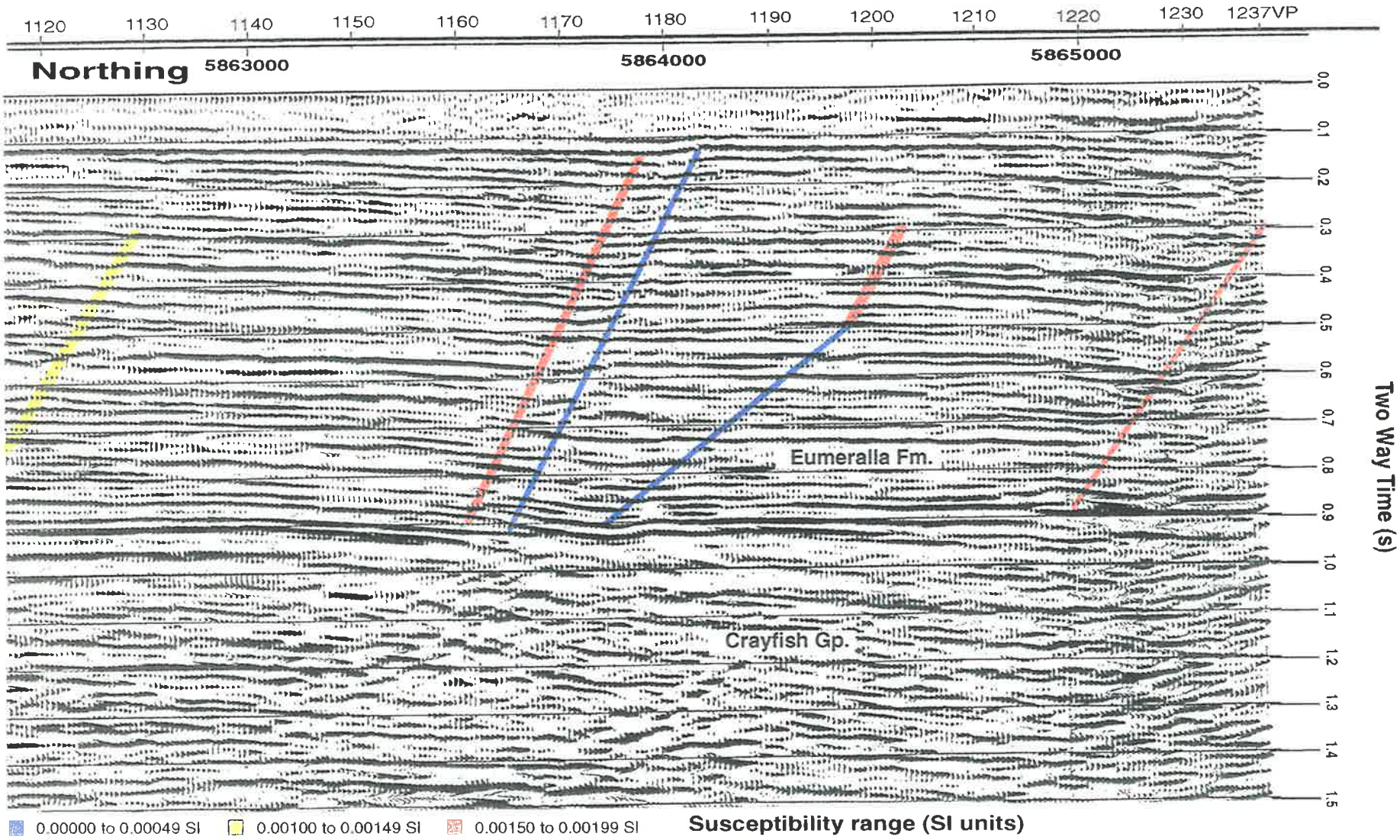

Fig. 8.2.1.6 b Part of Seismic Section OK90 - 414 showing Igneous Dyke Model bodies

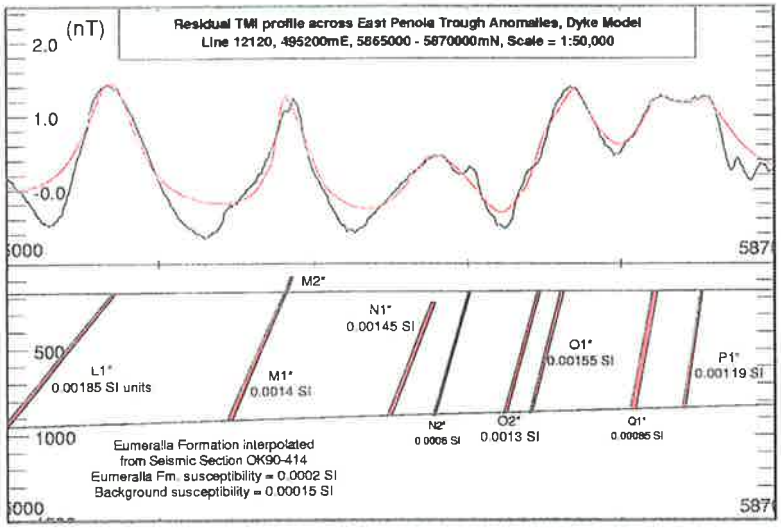

Fig. 8.2.1.7 Part of East Penola Trough section showing igneous dyke model

(which was assigned a remanence parallel to the current field direction). The small anomaly around 5856250mN appears to be a very shallow feature but may not be of cultural origin. The profiles shown in figures 8.2.1.4a and 8.2.1.5a are of overlapping sections and demonstrate that it was necessary to assign a reversed magnetisation remanence component to the bodies Eumeralla G1, H1 and I1 (90°, 85° and 90°, respectively) while adding a number of bodies with a normal magnetisation direction to the bodies placed between them to fit the profile. This procedure was also necessary in the profile shown in figure 8.2.1.6a where the body, Eumeralla J1, was given a reversed magnetisation (30°) while the deep fault plane body Eumeralla J2 and the small extension to this body, Eumeralla J2*, were only assigned a normal magnetisation direction. Eumeralla B and O1* (70° and 30°, respectively) were placed at opposite ends of the profile in order to simulate the negative parts of the respective anomalies (fig. 8.2.1.7).

Where the fault plane bodies have been assigned a remanent magnetisation, it might be expected that the inclination angle of the remanence would be determined by the age of emplacement (or cooling below the Curie temperature) of the dyke. From section 3.2.4 (Clark, 1983), it can be inferred that those dykes with inclination angles of approximately ±70° (-, normal or +, reversed magnetisation) could have been emplaced during the Late Tertiary/Quaternary, once allowance for the 25° difference in inclination between Central Australia and the study area is made. Similarly, an inclination angle of around ±90° suggests emplacement during the Late Cretaceous/Early Tertiary while the two bodies with inclination angles of 30° are anomalous because the geomagnetic field has not had that inclination at any time since the deposition of the sediments (Clark, 1983). It is possible that the inclination angles of 30° represent the vector sum of remanent magnetisations resulting from emplacement at different times.

The *layer* or *channel* model assumes the magnetic anomalies are generated by magnetic minerals in discontinuous layers at the top of the Eumeralla Formation, in the Sherbrook Group or close to the surface in the Tertiary section. There are prominent reflectors at the top of the Eumeralla Formation and within the Sherbrook Group on the seismic section which may be sequences of coal layers. The model shown in figure 8.2.1.8 consists of the Eumeralla body created from seismic section OK90-414, the fault plane bodies inferred from the seismic section, and the layer/channel bodies at or near the top of the Eumeralla Formation, within the Sherbrook Group or overlying Tertiary

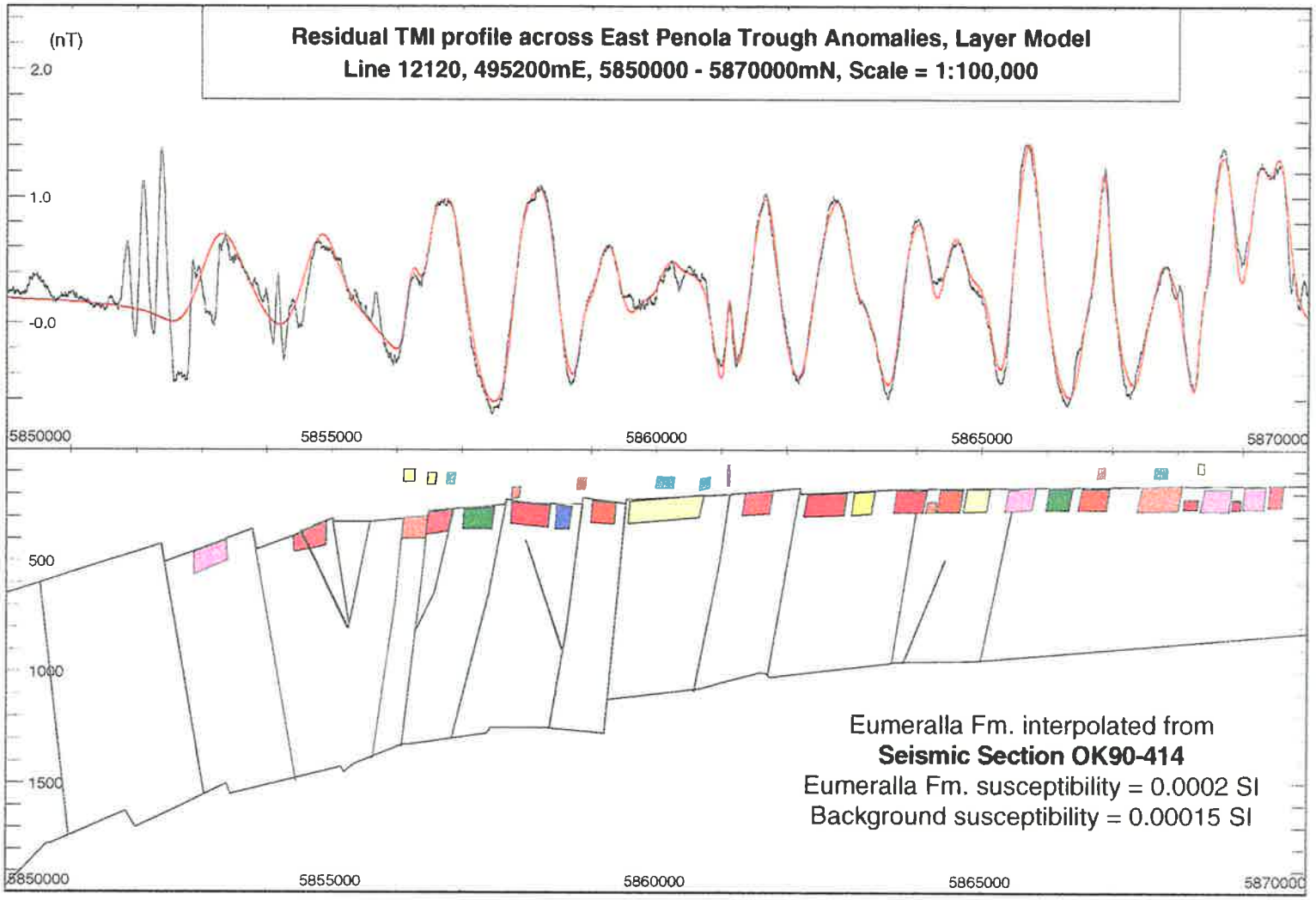

Fig. 8.2.1.8 East Penola Trough section showing layer model bodies within Eumeralla Fm.

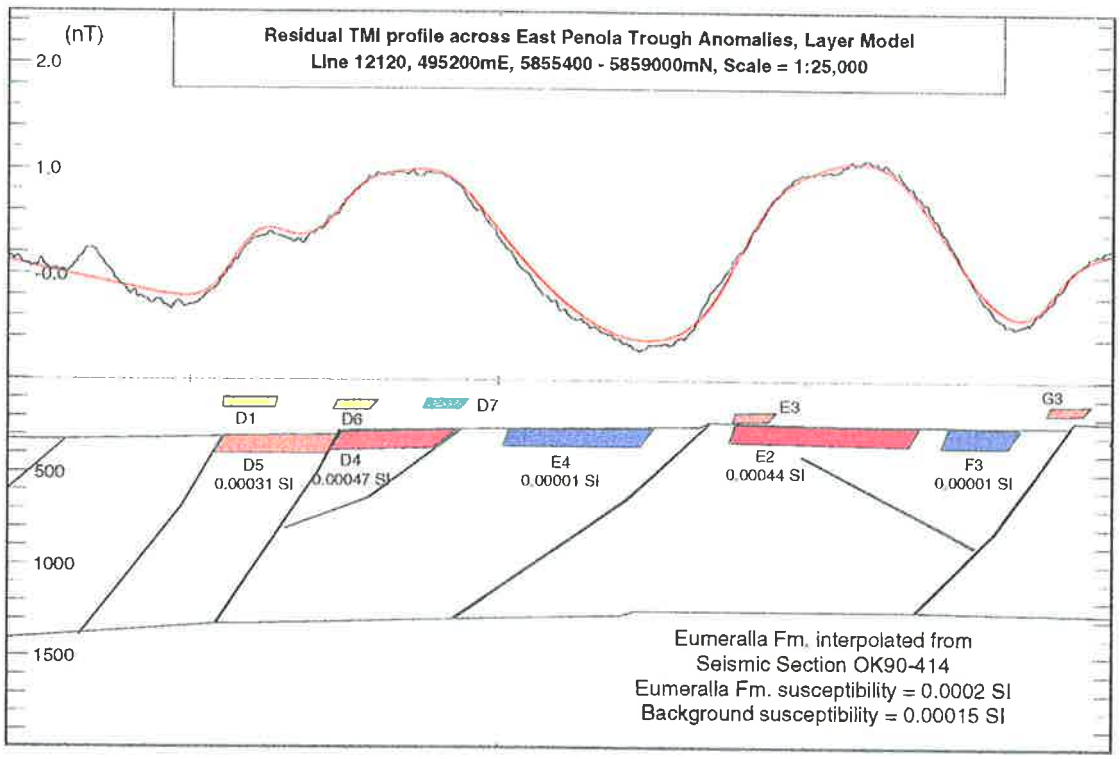

Fig. 8.2.1.9a Part of East Penola Trough section showing layer model

0.0000 - 0.000049 SI	0.00015 - 0.000199 SI
0.00020 - 0.000249 SI	0.00030 - 0.000349 SI
0.00040 - 0.000449 SI	0.00045 - 0.000499 SI

Susceptibility Range (SI units)

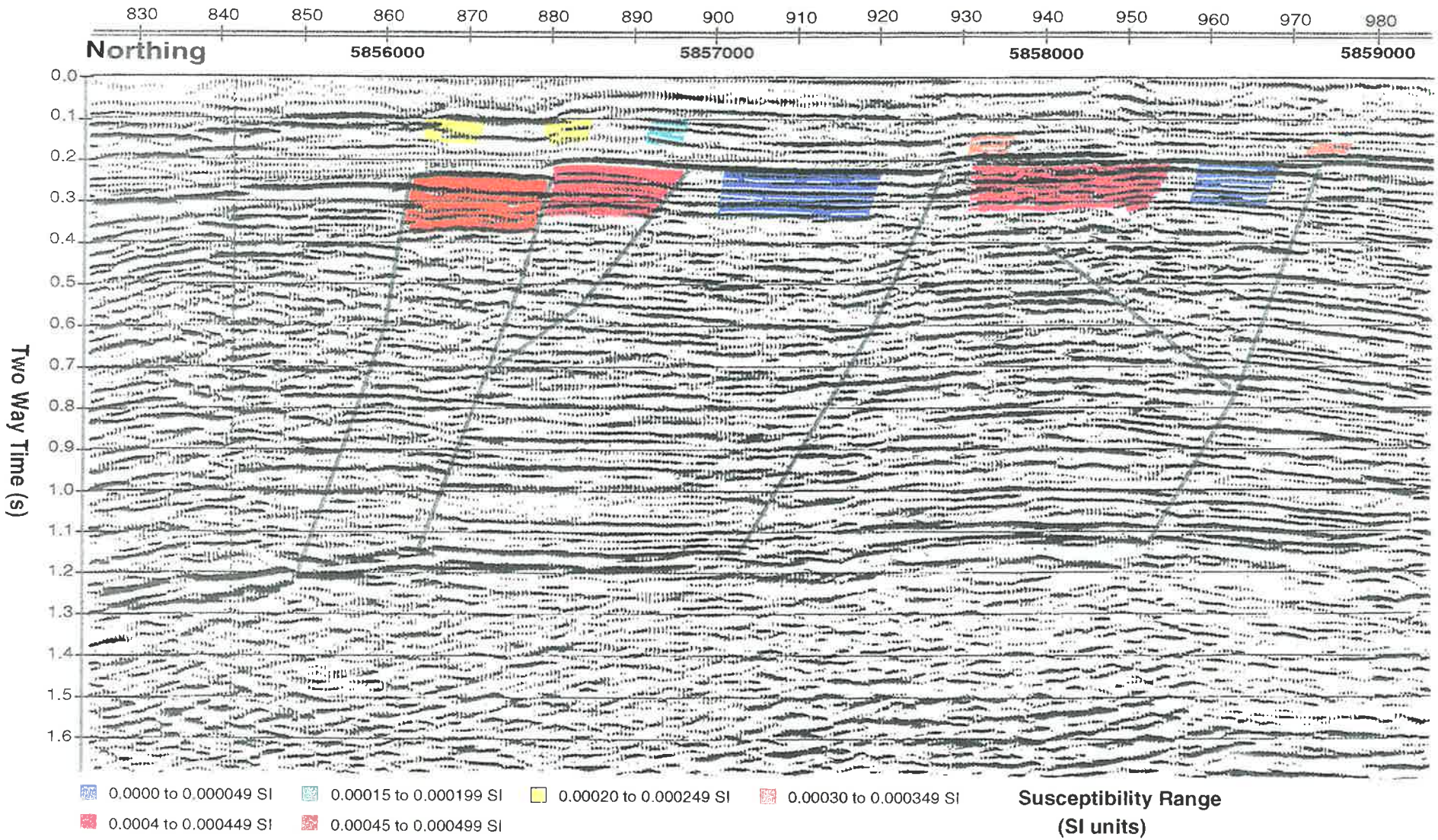

Fig. 8.2.1.9 b Part of Seismic Section OK90 - 414 showing Layer Model bodies

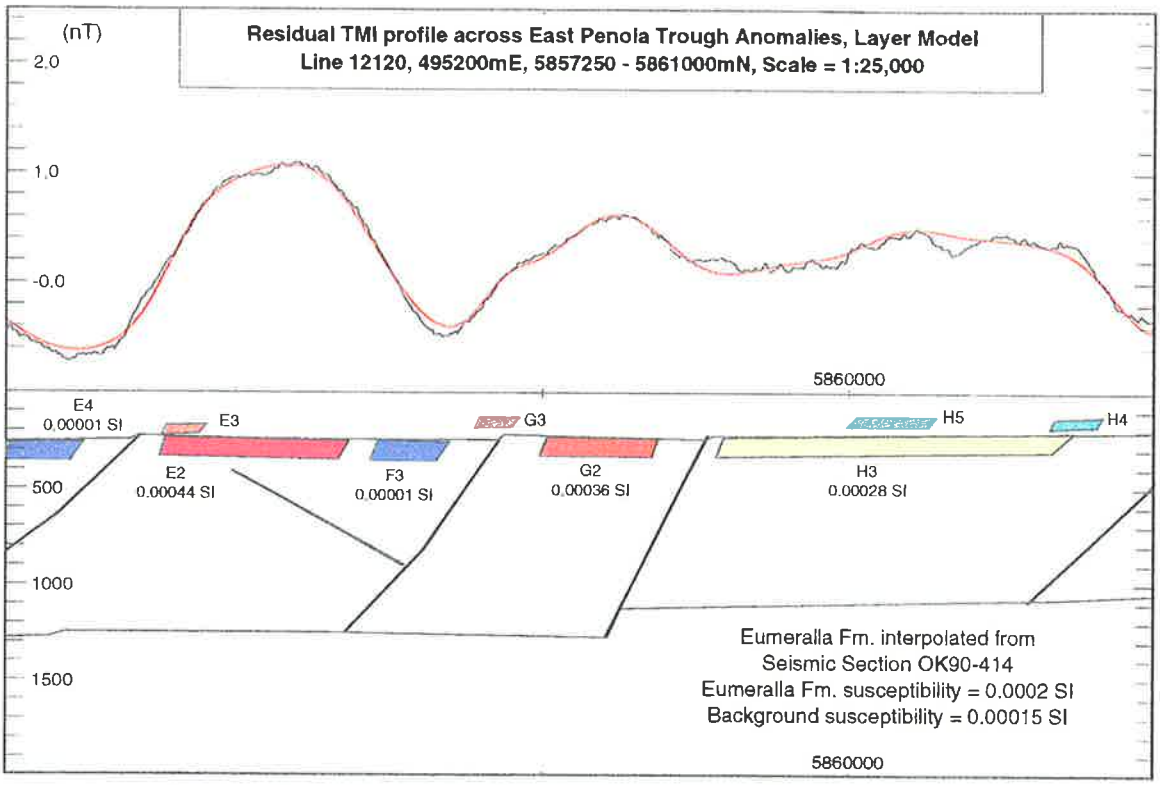

Fig. 8.2.1.10a Part of East Penola Trough section showing layer model

0.0000 - 0.000049 SI	0.00015 - 0.000199 SI
0.00025 - 0.000299 SI	0.00030 - 0.000349 SI
0.00035 - 0.000399 SI	0.00040 - 0.000449 SI

Susceptibility Range (SI units)

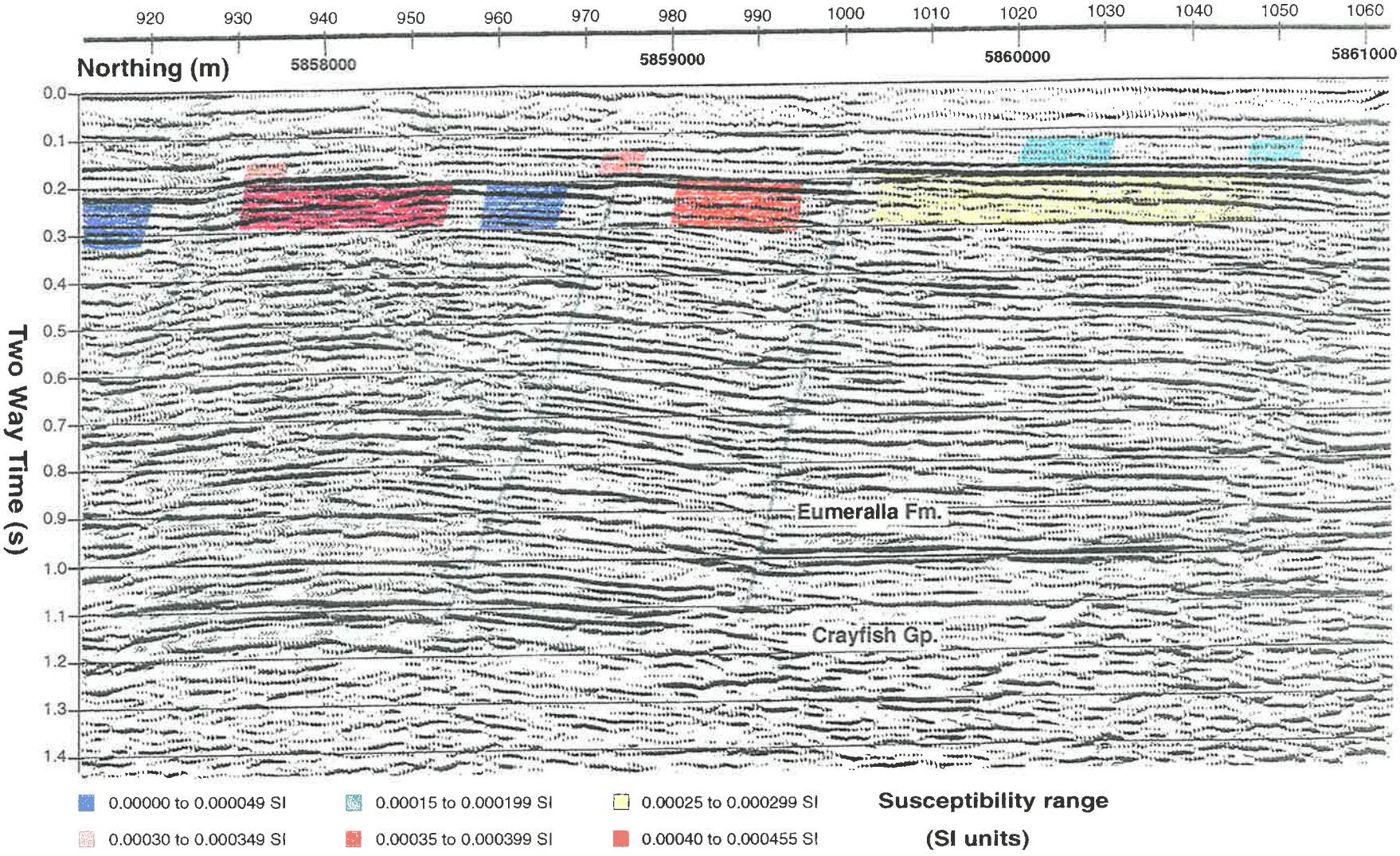

Fig. 8.2.1.10 b Part of Seismic Section OK90 - 414 showing layer or channel model

section. The fault plane bodies have been assigned negligible susceptibilities and serve only to show any correlation between the faults and layer/channel bodies. The layer or channel bodies should be mostly within the Eumeralla IV lithostratigraphic unit of Felton (1997) discussed in section 2.1.1. This unit was found to be predominantly siltstone with subordinate sandstone and coal beds deposited in a meandering fluvial/lacustrine/coal swamp environment.

Those layer bodies in the Sherbrook Group or Tertiary were used to simulate the subtle, sub-nanoTesla anomalies that are superimposed on the longer wavelength anomalies due to Eumeralla Formation sources. Not all the Eumeralla Fm bodies have been placed at the top of the formation (J6, O3 and Q2), because where an anomaly has a relative magnetic low between two positive peaks, the addition of a slightly deeper body between the two adjacent layers will produce this relative low. As with the dyke model the section of the profile between 5850000mN and 5856000mN is too heavily contaminated with cultural noise to obtain a reasonable fit to the profile so two bodies were used to approximate the long wavelength anomalies and the shorter wavelengths were ignored.

The profile was divided into 5 sections corresponding to the parts of the seismic section as with the dyke model and the results are shown in figures 8.2.1.9a to 8.2.1.13. The section of the profile shown in figure 8.2.1.9a has 3 intersedimentary bodies within the Eumeralla Formation (D5, D4 and E2) which are responsible for the basic shapes of the two anomalies while the shallower bodies (D1, D6, D7 and E3) were added to improve the fit. The bodies, D1, D6 and D7, are within the Tertiary section while E3 is within the thin, undifferentiated Sherbrook Group. Figure 8.2.1.10a overlaps the previous figure and has 3 inter-Eumeralla bodies (E2, G2 and H3) of which E2 is repeated while the Sherbrook Group bodies (E3, G3, H5 and H4) were again used to simulate the more subtle anomalies. The reflectors on the seismic section (8.2.1.9b and 8.2.1.10b) indicate that there has been substantial uplift of Eumeralla sediments prior to the deposition of the Sherbrook Group (probably movement on the Kanawinka South Fault Zone which underlies this part of the profile). This may have resulted in the volcaniclastic sediments of the Eumeralla III unit of Felton (1997) being brought closer to the top of the formation.

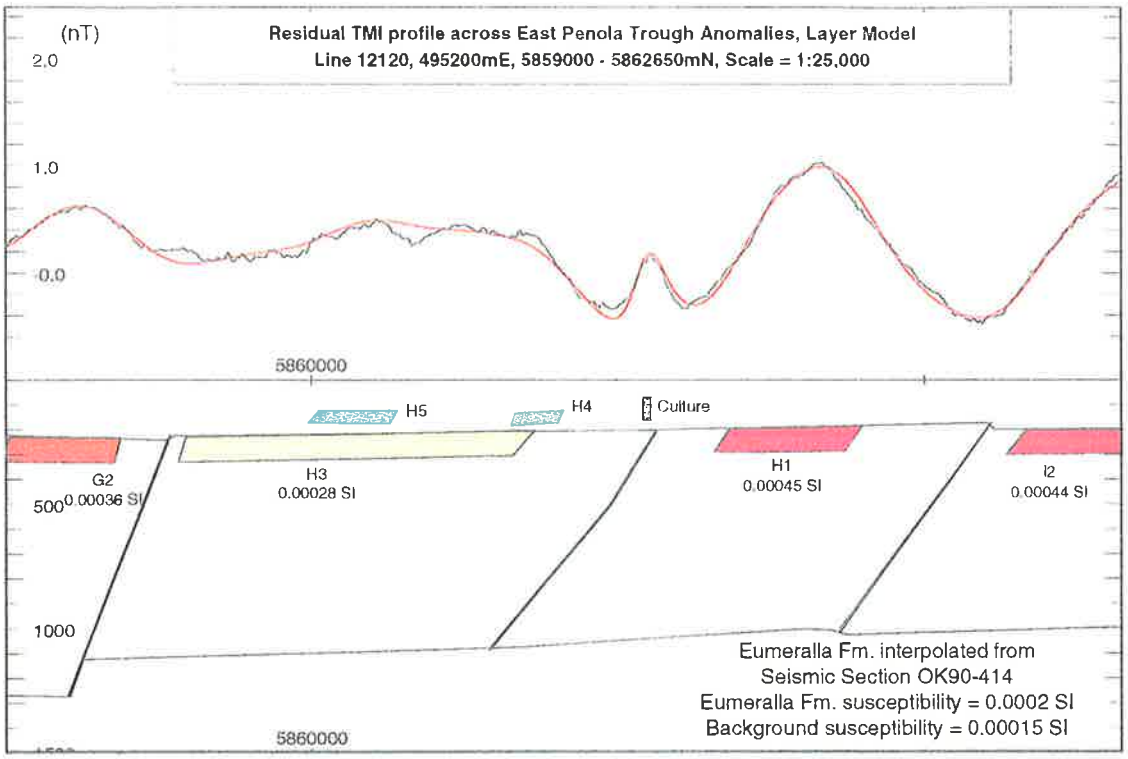

Fig. 8.2.1.11a Part of East Penola Trough section showing layer model

0.00015 - 0.000199 SI

0.00025 - 0.000299 SI

0.00035 - 0.000399 SI

0.00040 - 0.000449 SI

Susceptibility Range (SI units)

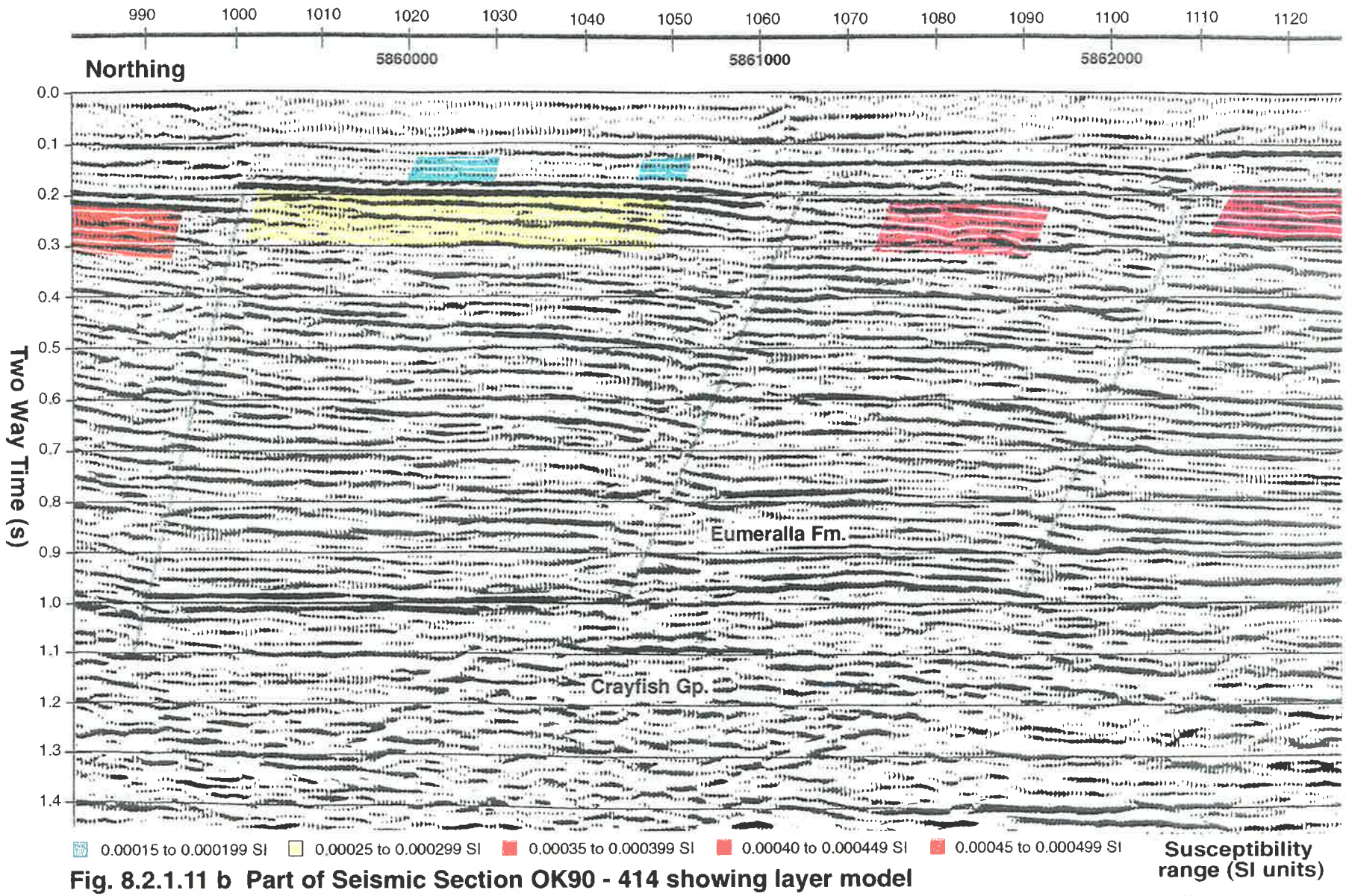

Fig. 8.2.1.11 b Part of Seismic Section OK90 - 414 showing layer model

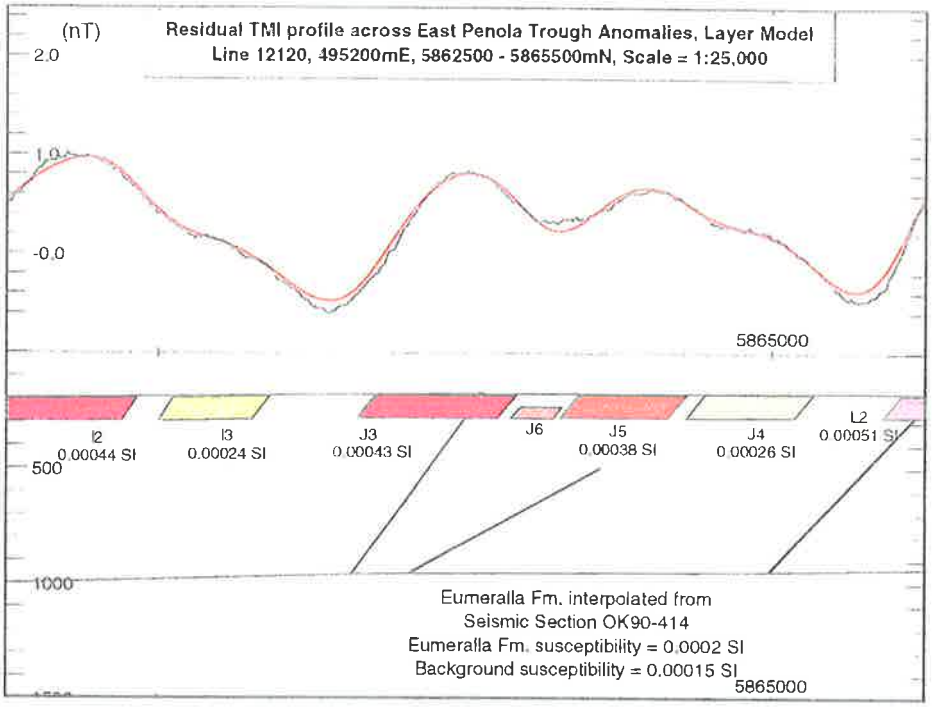

Fig. 8.2.1.12a Part of East Penola Trough section showing layer model

0.00020 - 0.000249 SI	0.00025 - 0.000299 SI
0.00030 - 0.000349 SI	0.00035 - 0.000399 SI
0.00040 - 0.000449 SI	0.00050 - 0.000549 SI

Susceptibility Range (SI units)

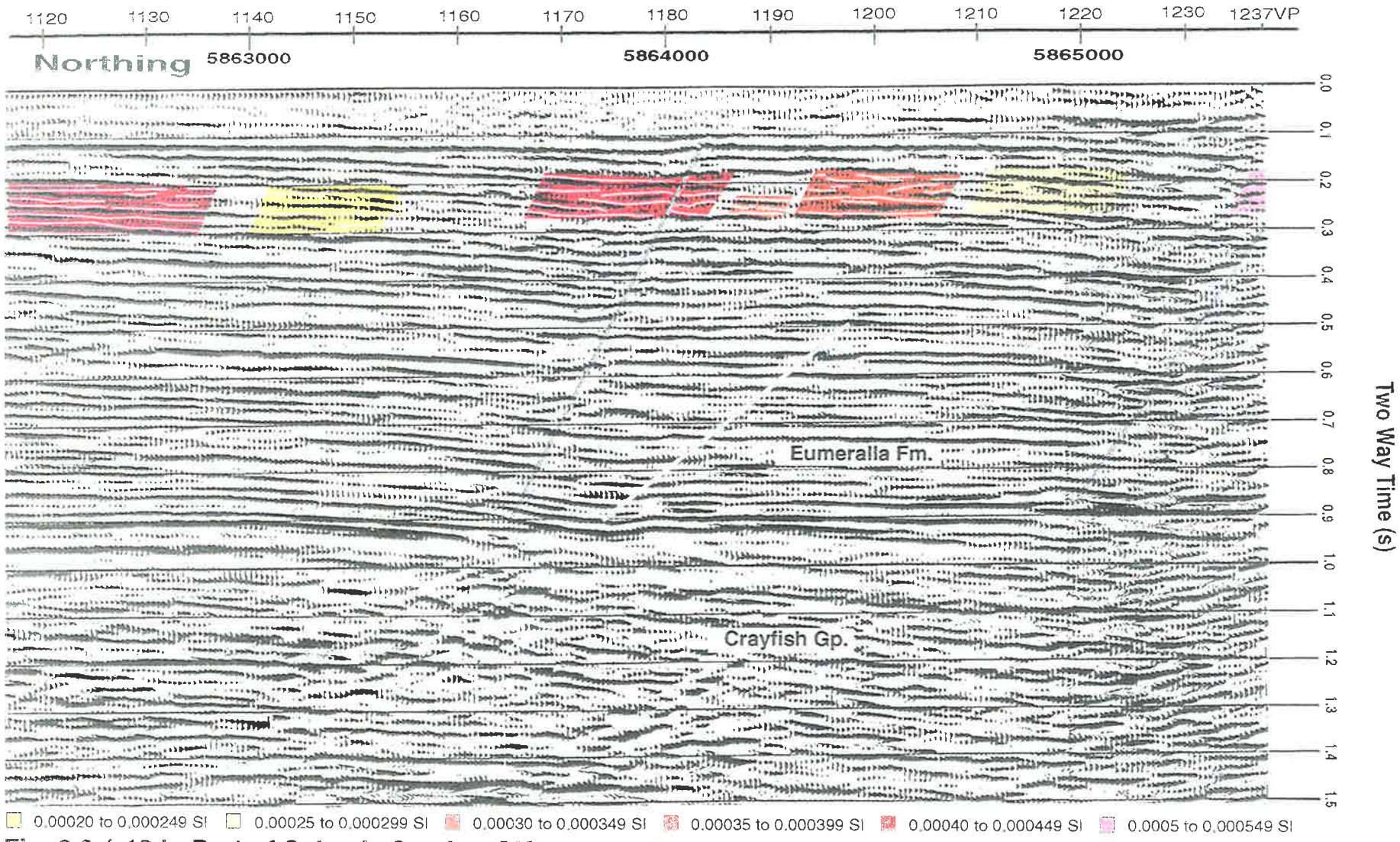

Fig. 8.2.1.12 b Part of Seismic Section OK90 - 414 showing layer model

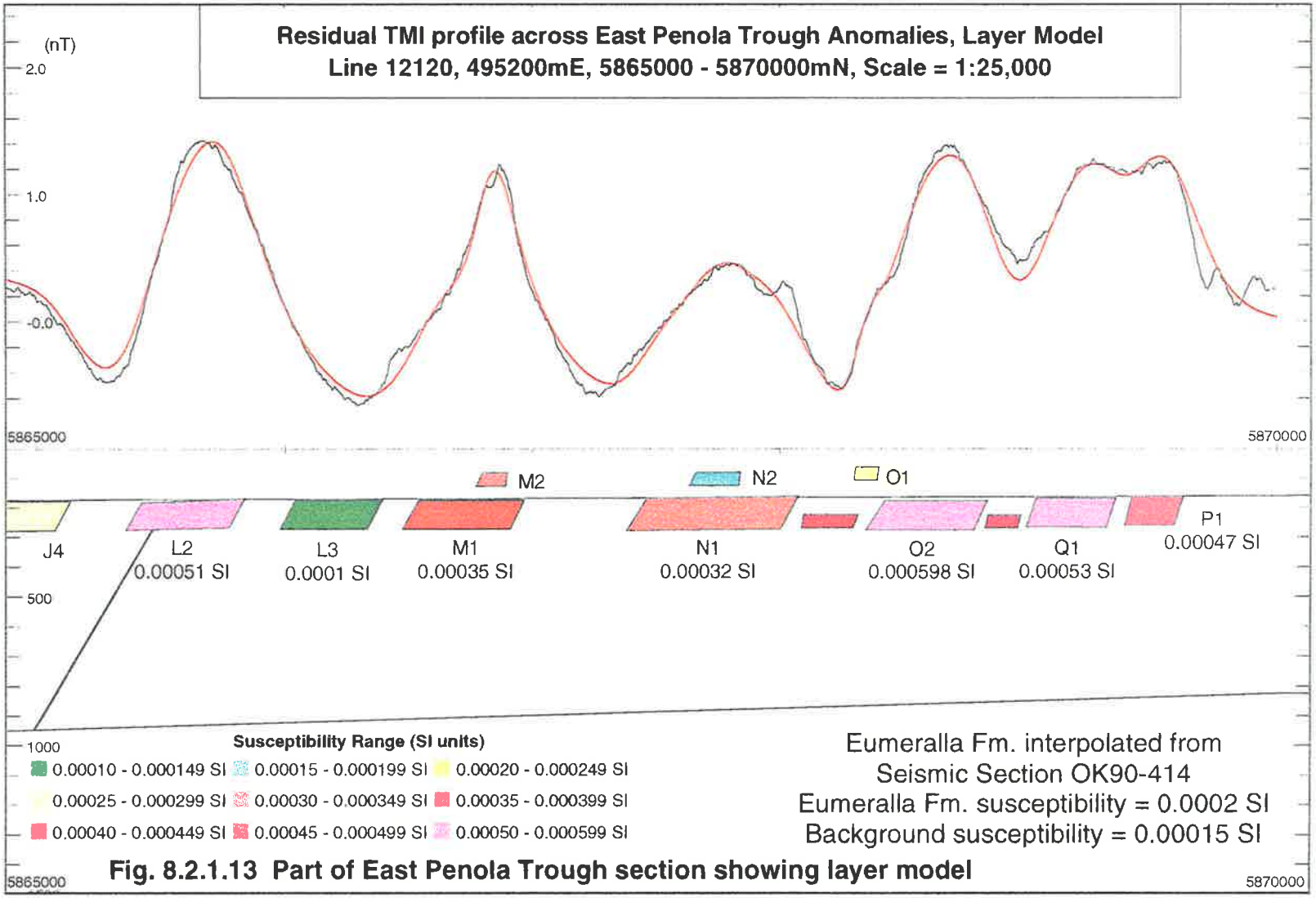

Fig. 8.2.1.13 Part of East Penola Trough section showing layer model

The part of the profile between approximately 5859500mN and 5861200mN is affected by low amplitude, probably surficial noise so the calculated profile generated by the bodies, H3, H5 and H4, is a relatively poor fit especially between around 5860700mN and 5861200mN. In figures 8.2.1.11a and 8.2.1.12a the inter-Eumeralla Fm bodies, H1, I2, I3, J3, J6, J5 and J4, produce a calculated profile that is a reasonable fit to the observed profile without requiring the addition of shallower bodies. The section shown in figure 8.2.1.13 extends beyond the northern extremity of the seismic section so fault plane bodies have not been created for this section, with the exception of the body centred at approximately 5865200mN which is an interpolation of a fault near the base of the Eumeralla Fm on the seismic section. The eight inter-Eumeralla Fm bodies, L2, M1, N1, O3, O2, Q2, Q1 and P1, generate a calculated profile that requires the addition of shallower bodies (M2, N2 and O1) in order to improve the fit, in particular, M2 which produces the narrow peak of that anomaly.

The susceptibilities assigned to these bodies are within the range measured in Eumeralla Fm cores recovered from the gas wells and are rarely more than three times the average value for those cores. The shallowest Eumeralla Fm core recovered from Penola 1, which is the closest well to the profile, was from approximately 50 m below the top of the formation and the highest susceptibility values for the whole formation in that well were measured in this core (0.00045 and 0.0003 SI units). This core would have been recovered from within the Eumeralla IV unit of Felton (1997). The calculated profile was produced without assigning a remanence component to the bodies but this does not mean that remanence is absent, only that it was possible to obtain a reasonable fit without having to create bodies with a reversed polarity of remanence. It is possible to improve the fit in figure 8.2.1.8 by the addition of bodies with a reversed polarity at around 5857500mN, 5858700mN and 5866200mN or alternatively, with use of bodies having a susceptibility lower than that of the Eumeralla Formation body.

The *fault zone* model is similar to the layer or channel model in that there are a number of bodies either associated with a fault zone or between two zones, the difference being that most of these bodies extend to the base of the Eumeralla Fm instead of being confined to a narrow section at the top of the formation. It was found that a reasonable fit to the observed profile could be obtained if the bodies were either assigned a susceptibility greater than the average value for the formation (0.0002 SI

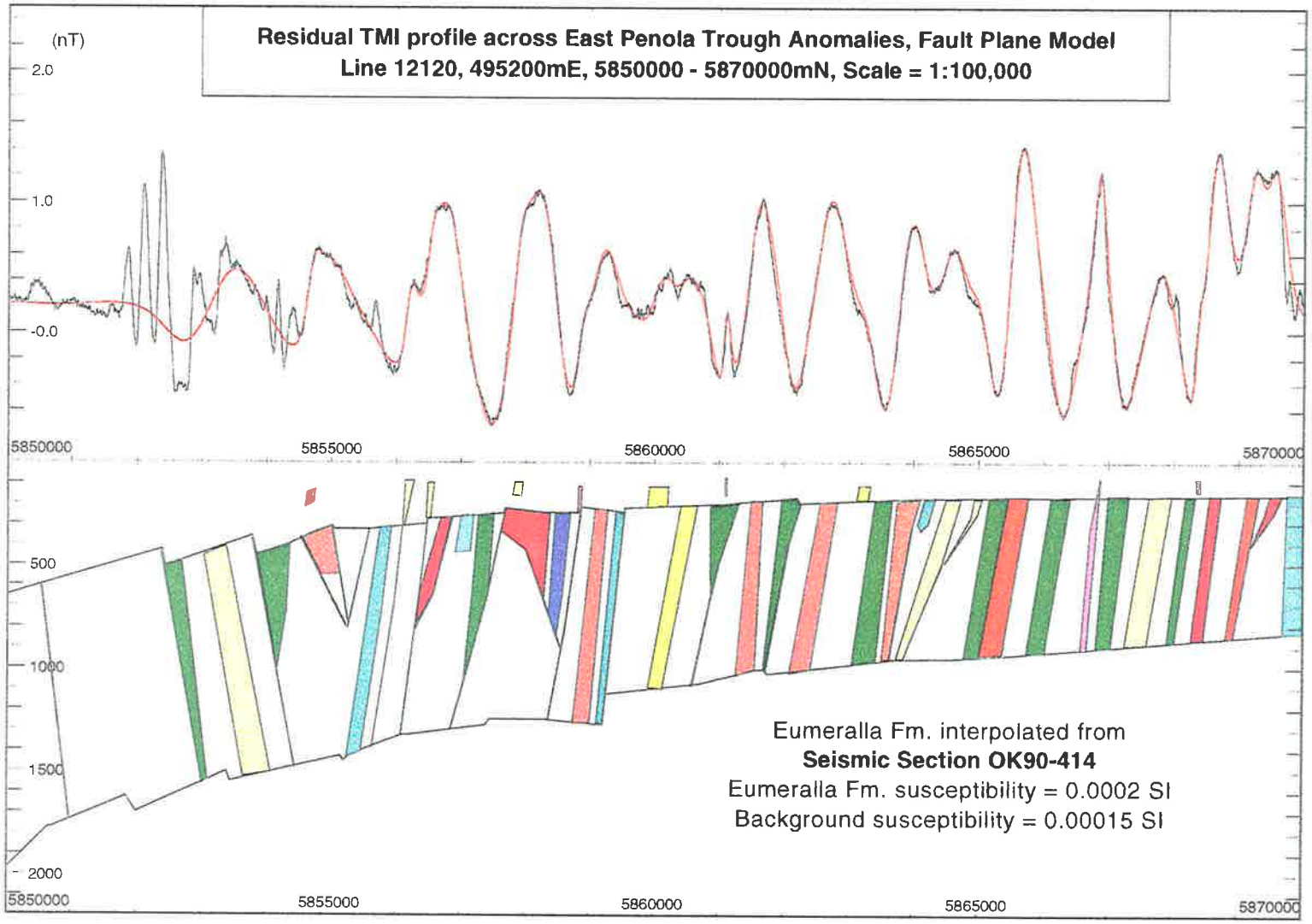

Fig. 8.2.1.14 East Penola Trough section showing Fault zone bodies within Eumeralla Fm.

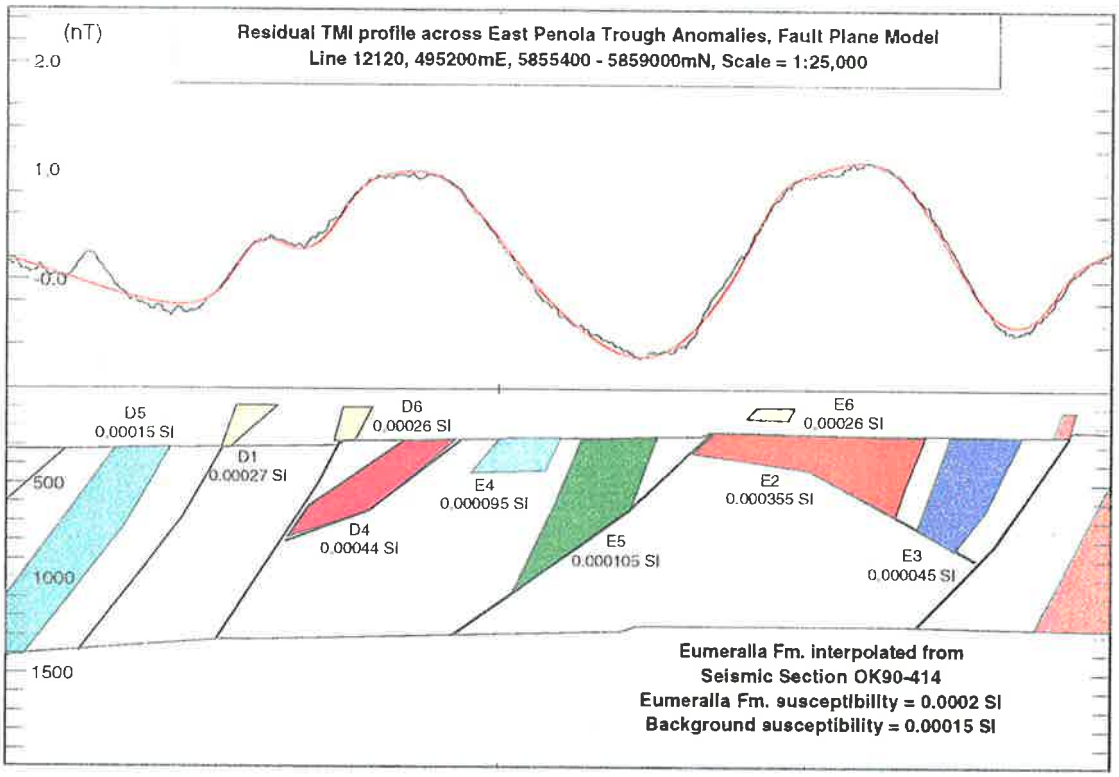

Fig. 8.2.1.15a Part of East Penola Trough section showing zone model

0.0000 - 0.000049 SI	0.00005 - 0.000099 SI
0.00010 - 0.000149 SI	0.00015 - 0.000199 SI
0.00025 - 0.000299 SI	0.00030 - 0.000349 SI
0.00035 - 0.000399 SI	0.00040 - 0.000449 SI

Susceptibility Range (SI units)

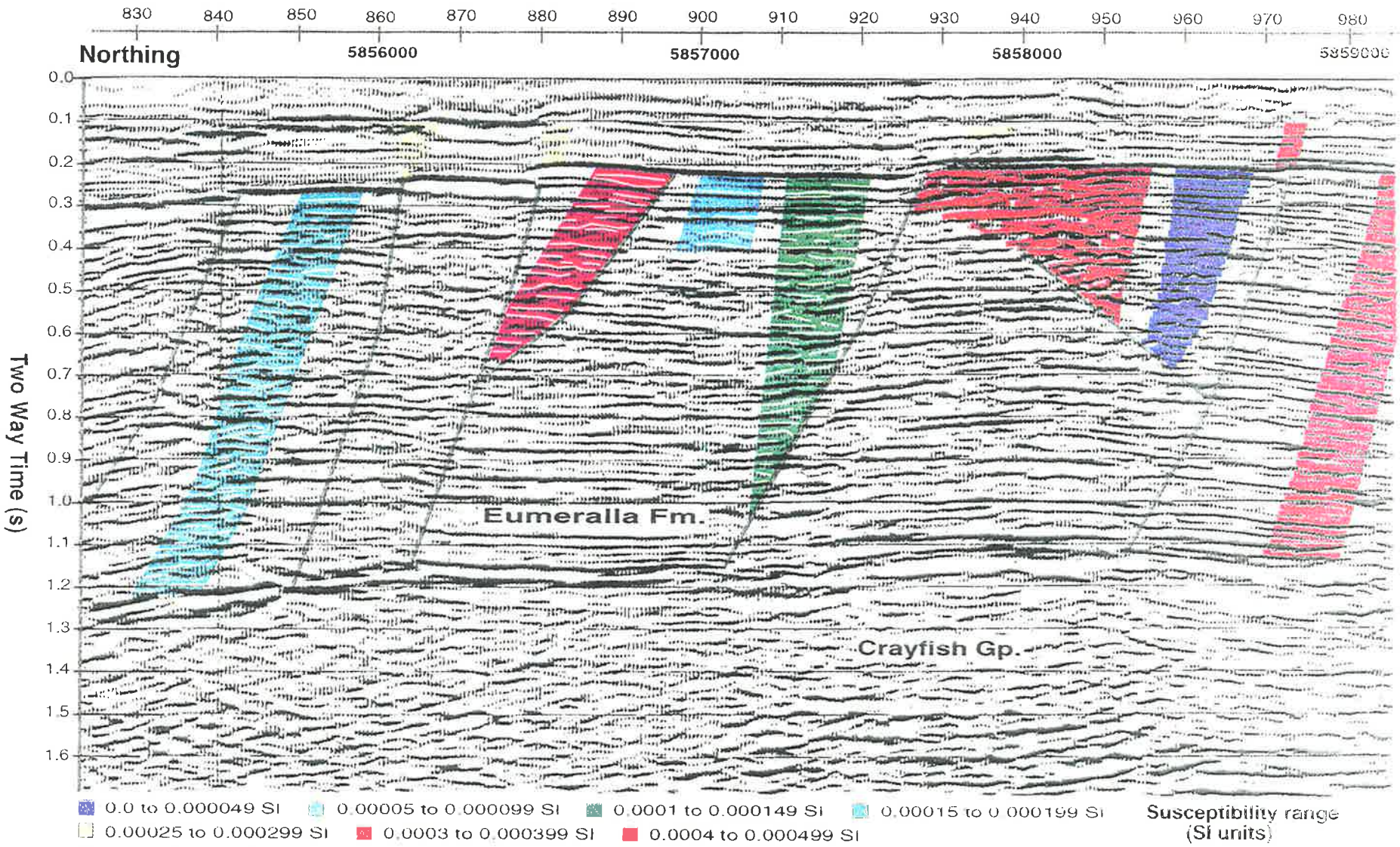

Fig. 8.2.1.15 b Part of Seismic Section OK90 - 414 showing fault zone model bodies

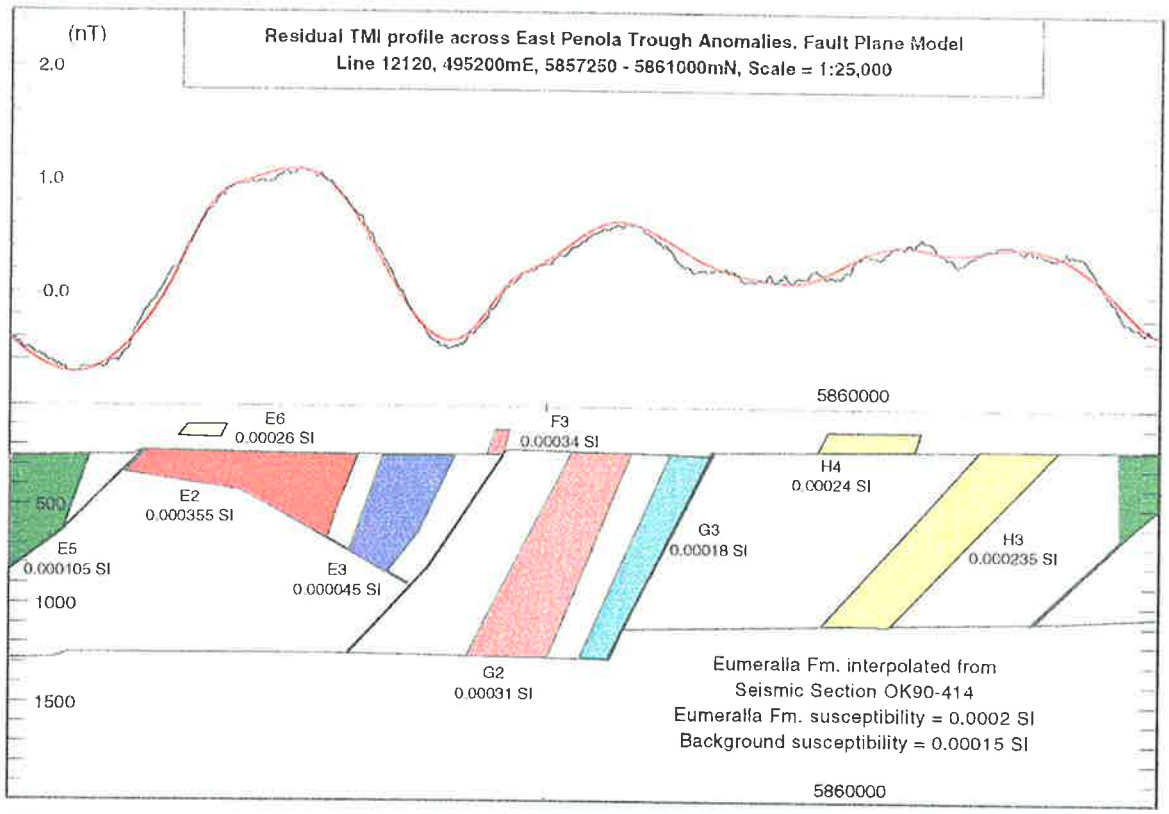

Fig. 8.2.1.16a Part of East Penola Trough section showing zone model

0.0000 - 0.000049 SI	0.00010 - 0.000149 SI
0.00015 - 0.000199 SI	0.00020 - 0.000249 SI
0.00025 - 0.000299 SI	0.00030 - 0.000349 SI
0.00035 - 0.000399 SI	

Susceptibility Range (SI units)

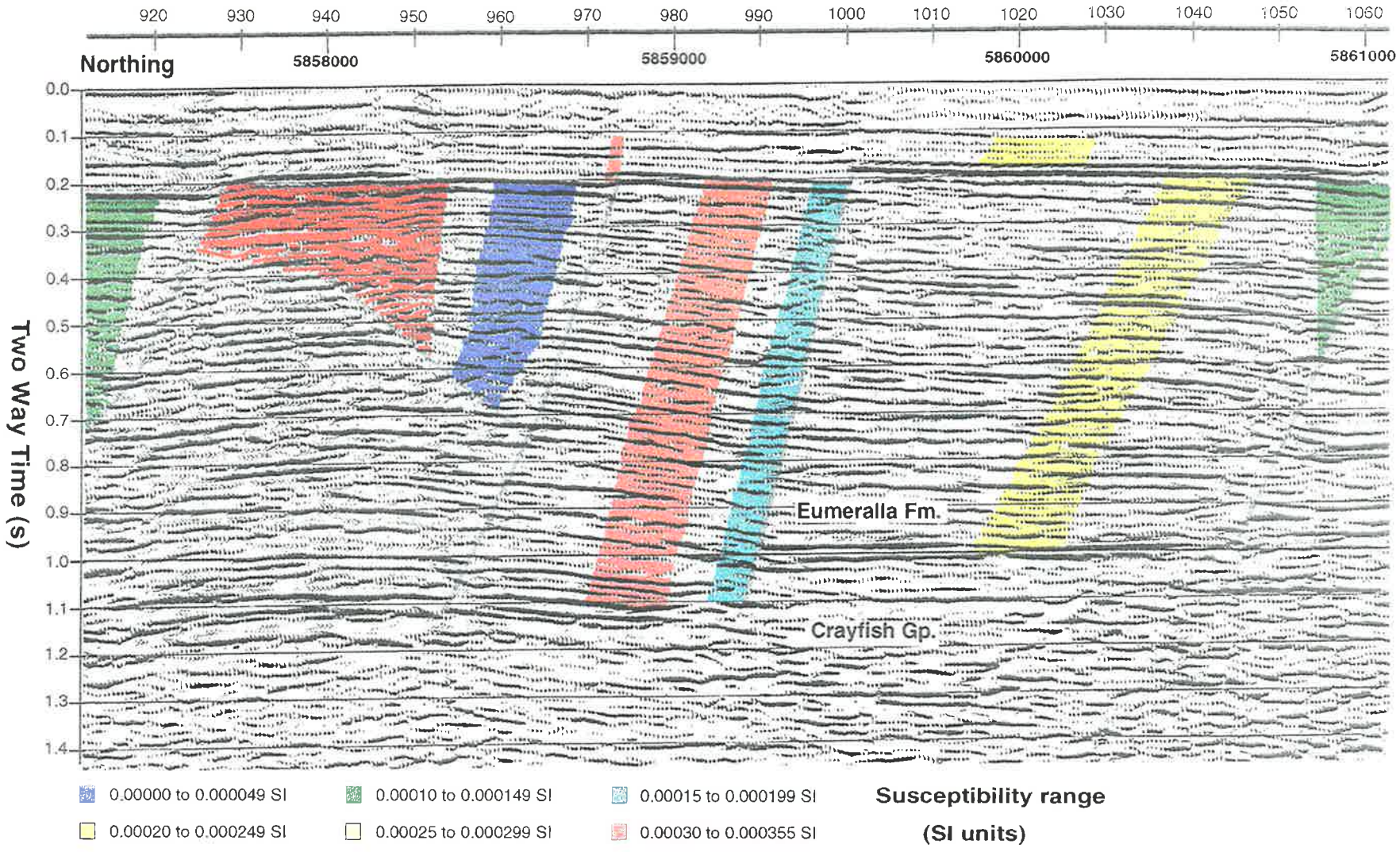

Fig. 8.2.1.16 b Part of Seismic Section OK90 - 414 showing fault zone model

units) or less than the average value. Where a body has been assigned a lower susceptibility than the average, it represents a zone (usually around a fault) where there may have been extensive movement of groundwater with an accompanying destruction of magnetic minerals. Bodies assigned higher than average susceptibilities represent either a zone where detrital minerals were deposited, where authigenic minerals have been created or where the magnetic minerals have been protected from destructive conditions so that the rocks retain a susceptibility that is closer to that at diagenesis. The latter possibility implies that the sections that have average susceptibilities have lost some of their magnetic mineral content since diagenesis.

The model shown in figure 8.2.1.14 is identical to that in figure 8.2.1.8 except that the layer or channel bodies have been replaced by the zone bodies which have been assigned colours to represent their relative susceptibilities. The fault plane bodies used in the other two models have been included here as well as eight intersedimentary bodies in the overlying Sherbrook Group and Tertiary section. In a similar manner to the previous two models (figs. 8.2.1.2 and 8.2.1.8), the portion of the profile between 5850000 and 5855000mN, which is substantially contaminated with short wavelength cultural anomalies, was modelled with a number of bodies in order to simulate the longer wavelength trend.

In figure 8.2.1.15a the bodies responsible for the positive, long wavelength component of the anomalies are Eumeralla D4 and E2 while D1, D6 and E6 are shallower bodies added to the model to simulate the sub-nanoTesla anomalies superimposed on the profile. When the bodies, Eumeralla D5, E4, E5 and E3, were assigned susceptibilities that were less than the 0.0002 SI units given to the Eumeralla Formation body, the calculated profile then fits the negative component of the long wavelength anomalies. The model shows that bodies associated with faults can produce either a positive or negative anomaly, as can be seen from Eumeralla D4 and E2 (positive) and Eumeralla E5 and E3 (negative). These bodies are zones of increased or decreased magnetisation so the distinct boundaries shown in the figures, are unlikely to be geologically realistic and should be more gradational with intertonguing between the adjacent zones.

The overlapping section shown in figure 8.2.1.16a illustrates that the body, G3, associated with a fault, can approximate a relatively negative, long wavelength anomaly

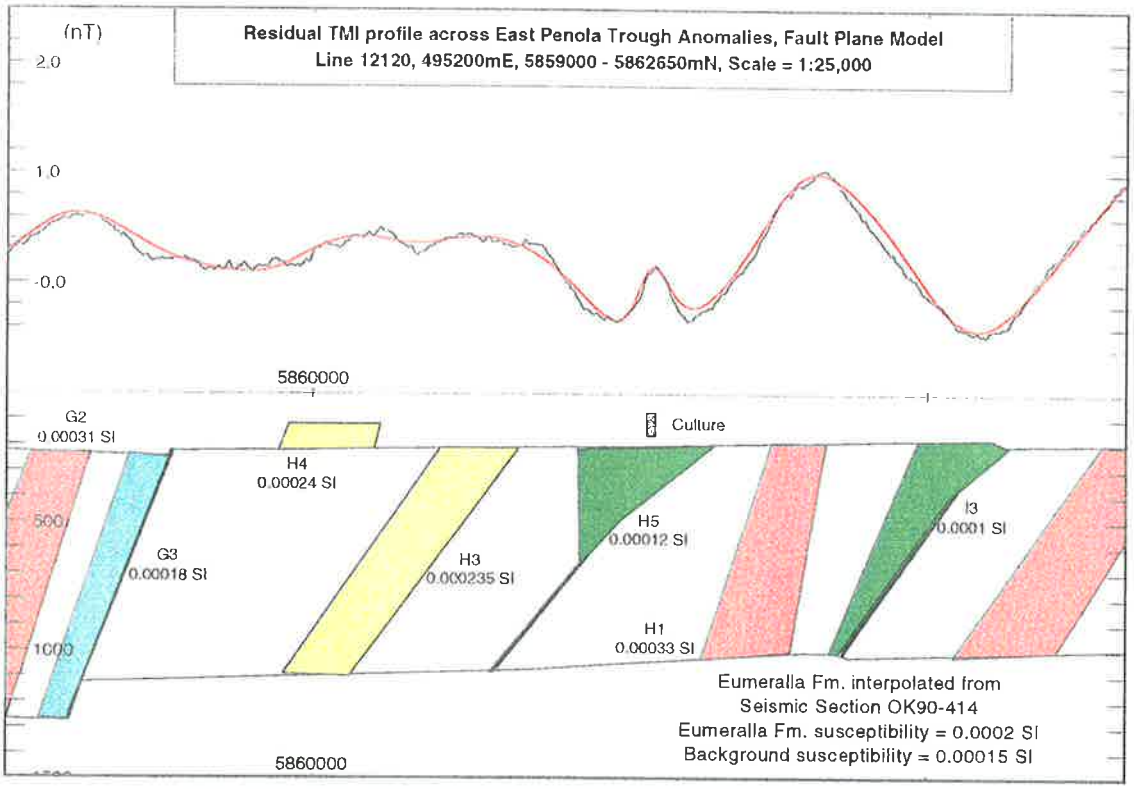

Fig. 8.2.1.17a Part of East Penola Trough section showing zone model

0.00010 - 0.000149 SI

0.00015 - 0.000199 SI

0.00020 - 0.000249 SI

0.00030 - 0.000349 SI

Susceptibility Range (SI units)

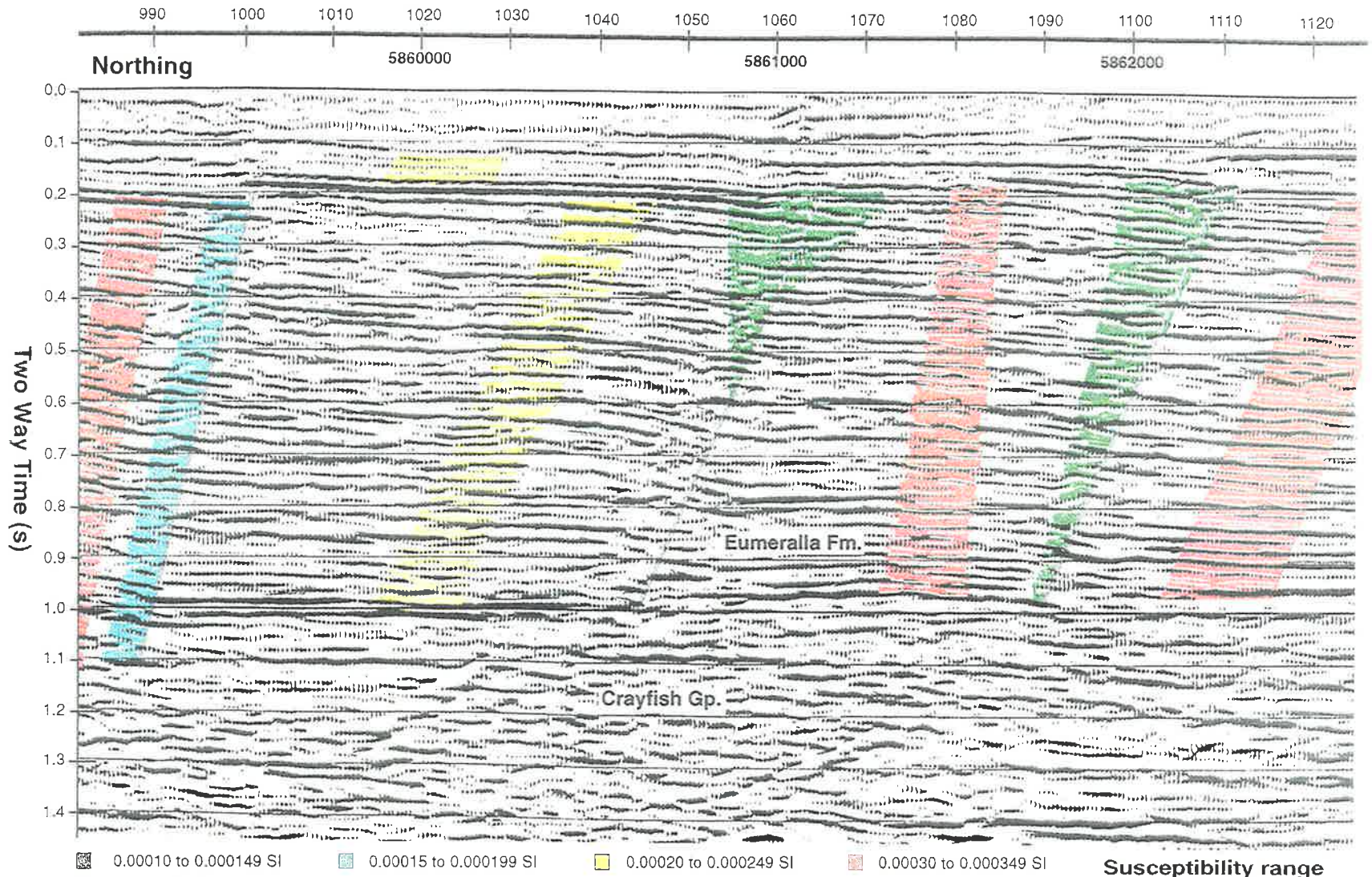

Fig. 8.2.1.17 b Part of Seismic Section OK90 - 414 showing fault zone model

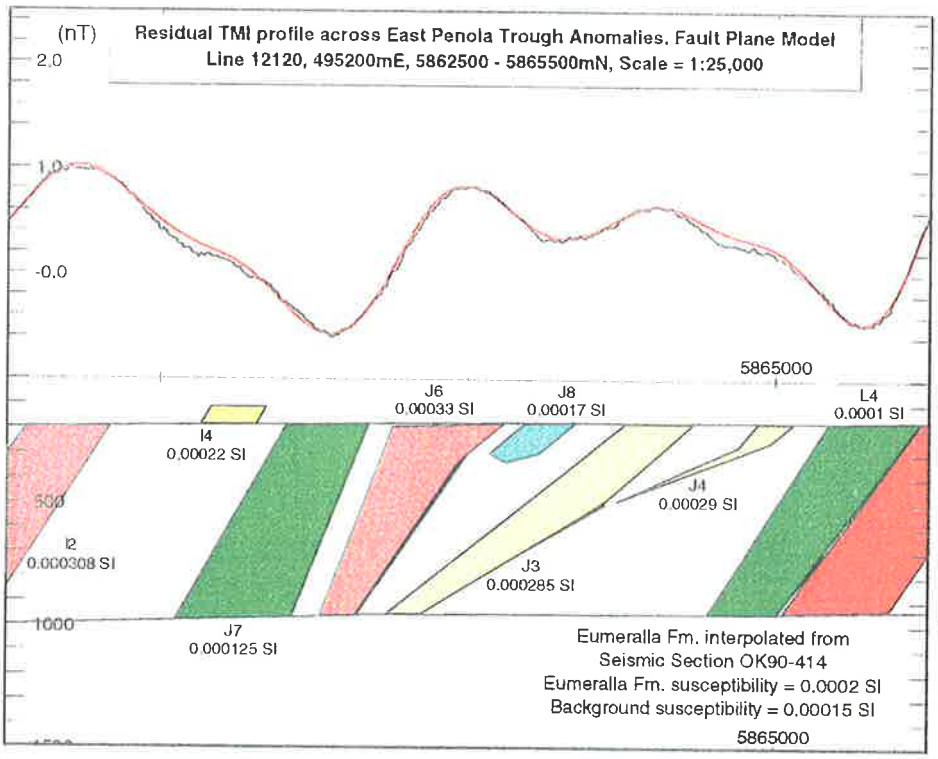

Fig. 8.2.1.18a Part of East Penola Trough section showing zone model

0.00010 - 0.000149 SI	0.00015 - 0.000199 SI
0.00020 - 0.000249 SI	0.00025 - 0.000299 SI
0.00030 - 0.000349 SI	0.00035 - 0.000399 SI

Susceptibility Range (SI units)

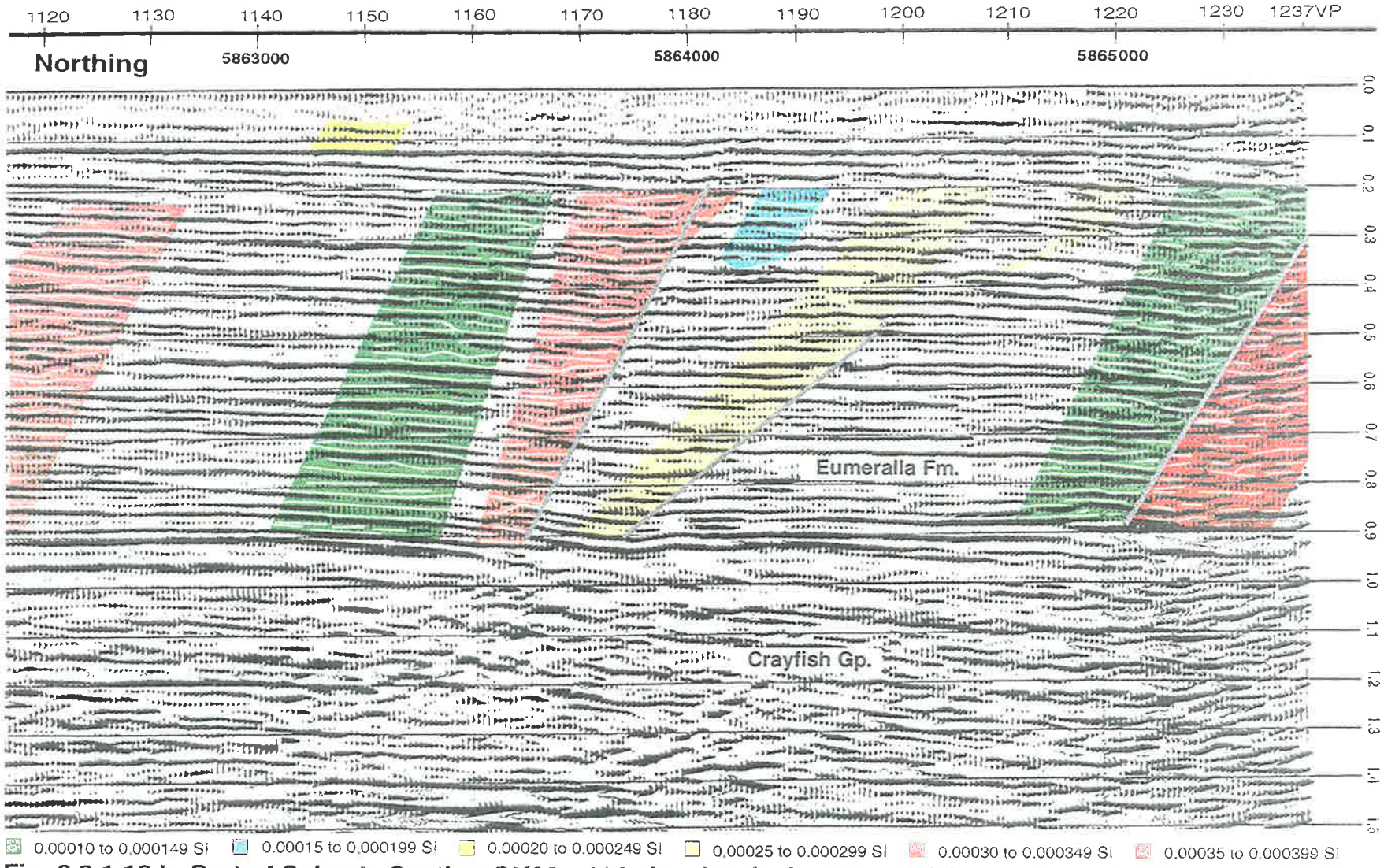

Fig. 8.2.1.18 b Part of Seismic Section OK90 - 414 showing fault zone model

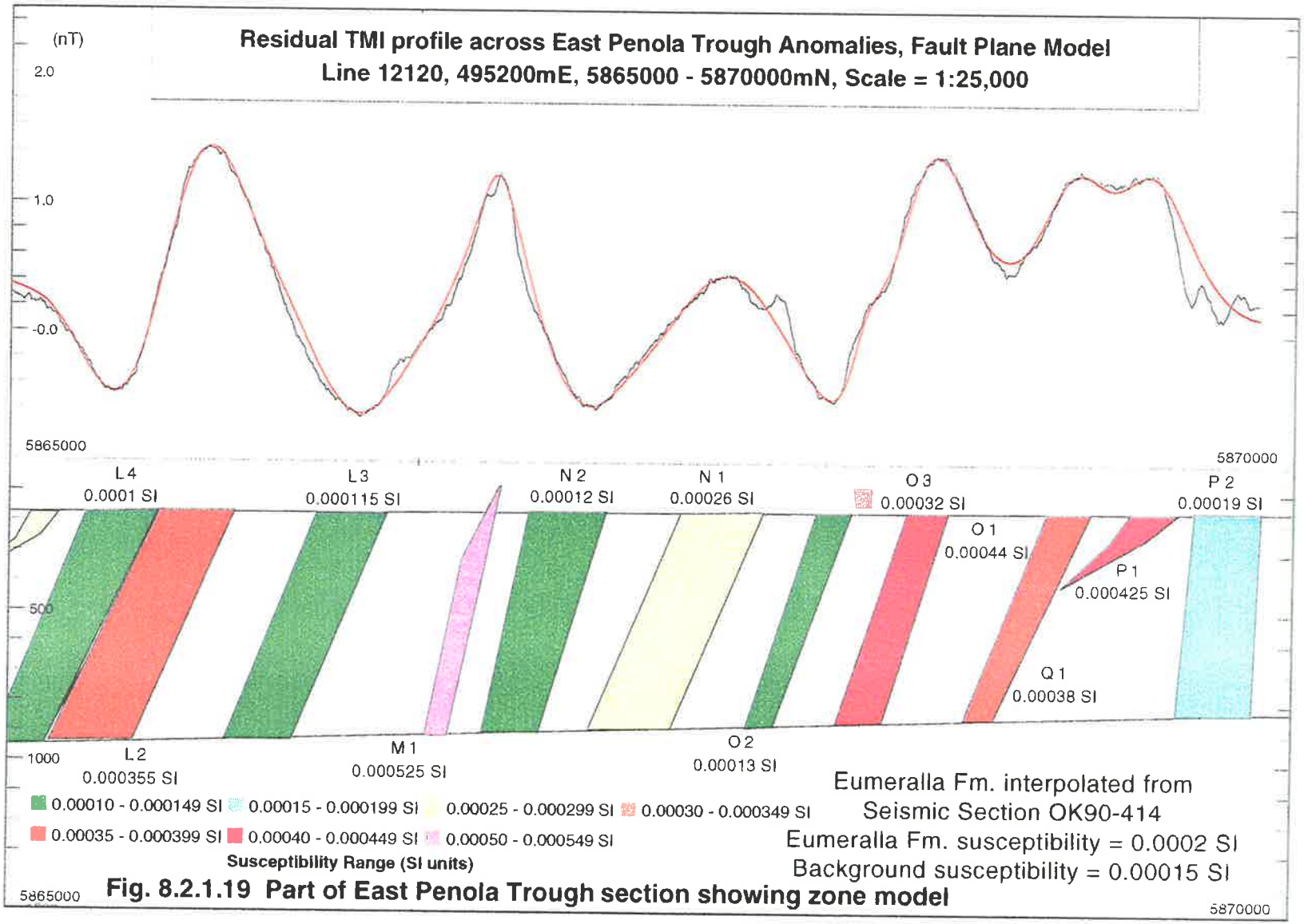

Fig. 8.2.1.19 Part of East Penola Trough section showing zone model

with a small susceptibility contrast (-0.00002 SI), while the bodies G2, H4 and H3 are located between the faults and the bodies, especially H4 and H3, are able to partly simulate the positive anomaly again with only a relatively small (positive) susceptibility contrast. In figure 8.2.1.17a the two bodies, H5 and I3, have low susceptibilities and are associated with the prominent faults while the body between the faults, H1, generates the positive part of the anomaly. The shallow body, Culture, was added to simulate what is probably the effect of a 19 kV power line that crosses the profile at that location. The bodies shown in figure 8.2.1.18a include four that are associated with faults, Eumeralla J6, J3, J4 and L4, with the bodies, J6, J3 and J4, being responsible for the positive components and L4 for the negative part of an anomaly. There are two bodies which are not associated with faults that produce negative components, J7 and J8, while two others generate positive anomalies (I2 and I4). The final figure for this profile, figure 8.2.1.19, shows a series of bodies which alternate between above and below average susceptibilities in order to produce the calculated profile. The body, M1, has been extended above the Eumeralla Fm and assigned a susceptibility of 0.000525 SI units to generate the narrow anomaly over it. The body, O3, was created in order to simulate the subtle anomaly on the flanks of the larger feature produced by O1, however, no attempt was made to model the small anomaly on the profile generated by N1, as this is either very shallow or cultural. The zone bodies in the model are frequently as wide as the layer/channel model bodies but because many extend to the base of the formation the susceptibilities required to fit the observed profile are lower. The width of the bodies, and the angle and direction of dip, was adjusted to simulate the shape of the profile although with many of the bodies that are associated with faults (or shear zones), the edges of the bodies were created parallel to the fault which successfully produced the shape of the anomaly in most cases.

In the absence of information from drilling, it is not possible to conclude which of the three models is correct or even whether some combination of two or all three is responsible for the anomalies. It is certainly possible to model the anomalies, for example, with igneous dykes producing the positive component and wide fault zones with reduced magnetic mineral content producing the negative part of the anomaly or vice versa. However, the igneous dyke model seems to require geologically unlikely circumstances such as the intrusion of a dyke along a fault plane when the geomagnetic field is in one direction followed by the intrusion of another dyke relatively close to the

first, but not associated with the fault, and with a reversed polarity of remanence. While this may occur in one or two occasions it is difficult to imagine circumstances under which this might happen alternately along the profile. The most intense of the linear anomalies terminates close to the Wynn 1 well but the well completion report (Reeve and Skinner, 1995) does not mention the recovery of igneous rock fragments in the cuttings from the well. The reason for this may be that the source of the anomaly terminated before reaching the well so the well did not intersect the postulated dyke or that igneous rock fragments were not recognised or were completely absent.

There is more evidence for the layer or channel model because of the susceptibility measurements from cores recovered from Penola 1 plus features interpreted as channels at the top of the Eumeralla Formation (Martin, 1992, Felton; 1997), however, only two susceptibilities were measured and the Penola 1 well is approximately 6 km west of the profile. The Wynn 1 well is approximately the same distance from the profile as Penola and Sawpit 1 but is closer to the central axis of the Penola Trough, and the upper part of the Eumeralla Formation was found to be a relatively uniform claystone with minor coal beds (Reeve and Skinner, 1995) with little evidence of channels. Both the layer and zone models can be explained by geologically realistic processes and use susceptibilities that are within the measured range. The layer or channel model does not require the formation of authigenic magnetic minerals, which is an alternate, often controversial explanation (section 3.2.2), while the zone model requires that the magnetic highs are over zones where the magnetic minerals from the volcanogenic sediments are less altered than those with close to average susceptibilities. The layer/channel model and the zone model require the alteration/destruction of most of the magnetic mineral content below the magnetic lows and could be regarded as the two extremes of a variation in magnetisation within the sediments It should be noted that the residual anomalies seen in this profile closely match those on a flightline 200 m to the east which was flown as part of AGSO's 1992 regional survey when the same processing is applied to that data.

8.2.2 Central Penola Trough Linear Anomalies Model

There are a number of linear features which either extend from the eastern part of the Penola Trough into this section or are relatively short and are only intersected on a few flightlines. Some of these features extend to the edge of the western basement anomalies but only a few are found over them and in some cases the linear features could

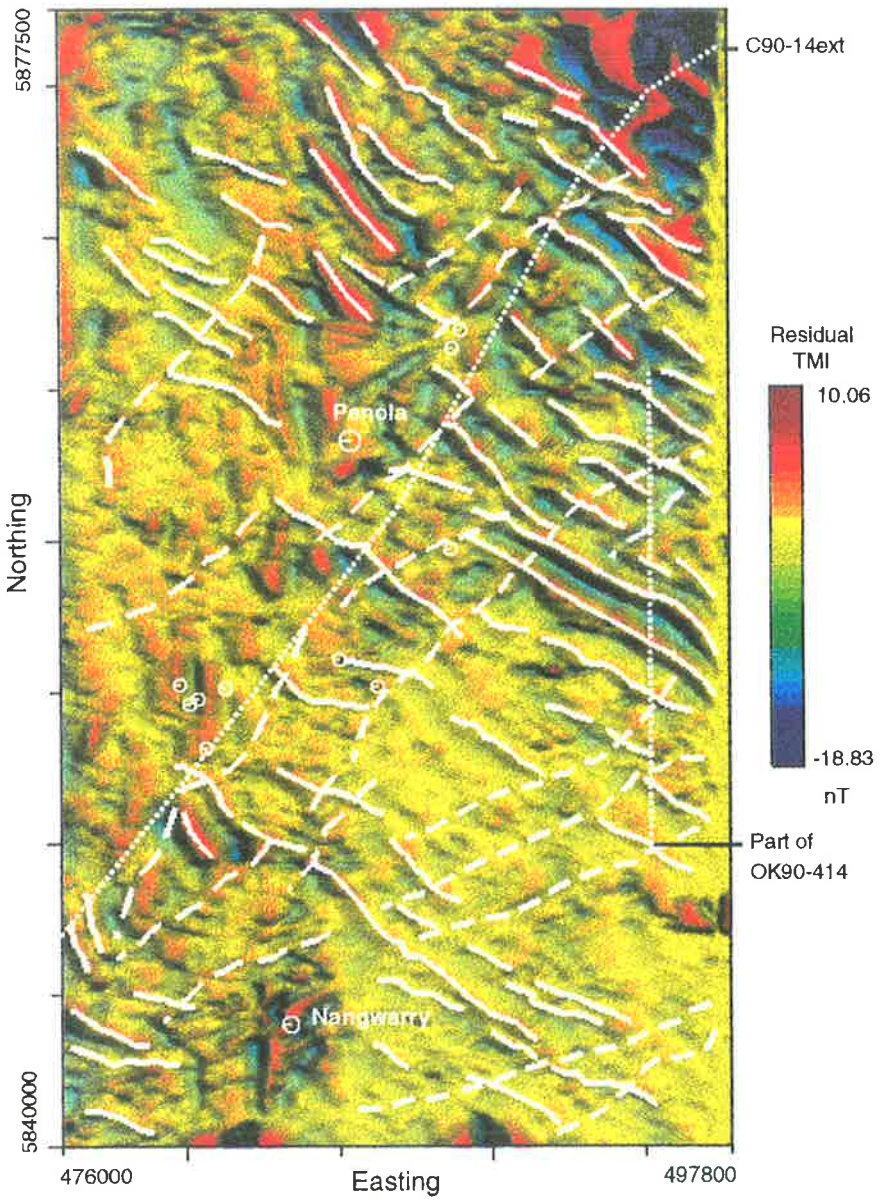

Fig. 8.2.2.1 Colour-draped residual TMI image of northern P1 area with sun-angle enhancement of magnetic lineations [40˚ azimuth, 70˚ elevation]. Interpreted lineations shown in white [solid = NW-SE, dashed = NE-SW]. White circles = wells and towns, dots = interpreted seismic lines

be extensions of the eastern linear anomalies but the cultural noise along the Penola-Nangwarry road, around Penola and to the north around Coonawarra can prevent exact mapping.

The region shown in figure 8.2.2.1 covers the northern third of the study area but excludes the western extension of P1. Figure 8.2.2.1 was produced by subtracting low-pass filtered data (2 km cutoff wavelength) from the original TMI line data, gridding the residual data and then applying a grid-based median filter in an attempt to suppress the substantial cultural noise component. The resulting figure consists of a colour-draped, sun-angle enhanced residual image (40° azimuth, 70° elevation) and also displays the seismic line OK90-414 (partly modelled in the previous section) and the composite line C90-14ext which extends from the northeast corner to the southwest margin near Kalangadoo 1, as well as showing towns and gas wells. The figure shows an interpretation of the shallow magnetic features where the probable magnetic lineations associated with WNW-ESE faults or shear zones are delineated by solid white lines while the features marked with dashed white lines may represent offsets that are aligned in approximately the extension direction (NNE-SSW). There are a number of north-south features that are either cultural noise or artifacts of processing.

The residual profile shown in figure 8.2.2.2a & b follows the composite seismic line C90-14ext and was extracted from the gridded residual data. The anomalies in the southwest section (Fig. 8.2.2.2a) are smaller than 1 nT but increase in amplitude northeast of Ladbroke Grove 1. The locations of the Sawpit 1 and Haselgrove 1 wells marked on the profile (Fig. 8.2.2.2b) are projected along lines perpendicular to the traverse. The formation boundaries used to construct the Eumeralla Formation and Sherbrook and Crayfish Group bodies were taken from the respective top horizon maps as were the locations of the faults. Figure 8.2.2.2a shows that the bodies responsible for the anomalies over the deeper parts of the Penola Trough are primarily within the Tertiary sediments with the deeper sources within the Sherbrook Group while northeast of Ladbroke Grove 1 and in figure 8.2.2.2b the Tertiary sediments and Sherbrook Group thin substantially and the Eumeralla Formation is much shallower so the anomalies are primarily caused by sources within this formation. Figure 8.2.2.3 shows part of the Eumeralla Fm top horizon map that was used to construct the model in figure 8.2.2.2a and b, and has the composite seismic line C90-14ext, as well as OK90-414 marked on it.

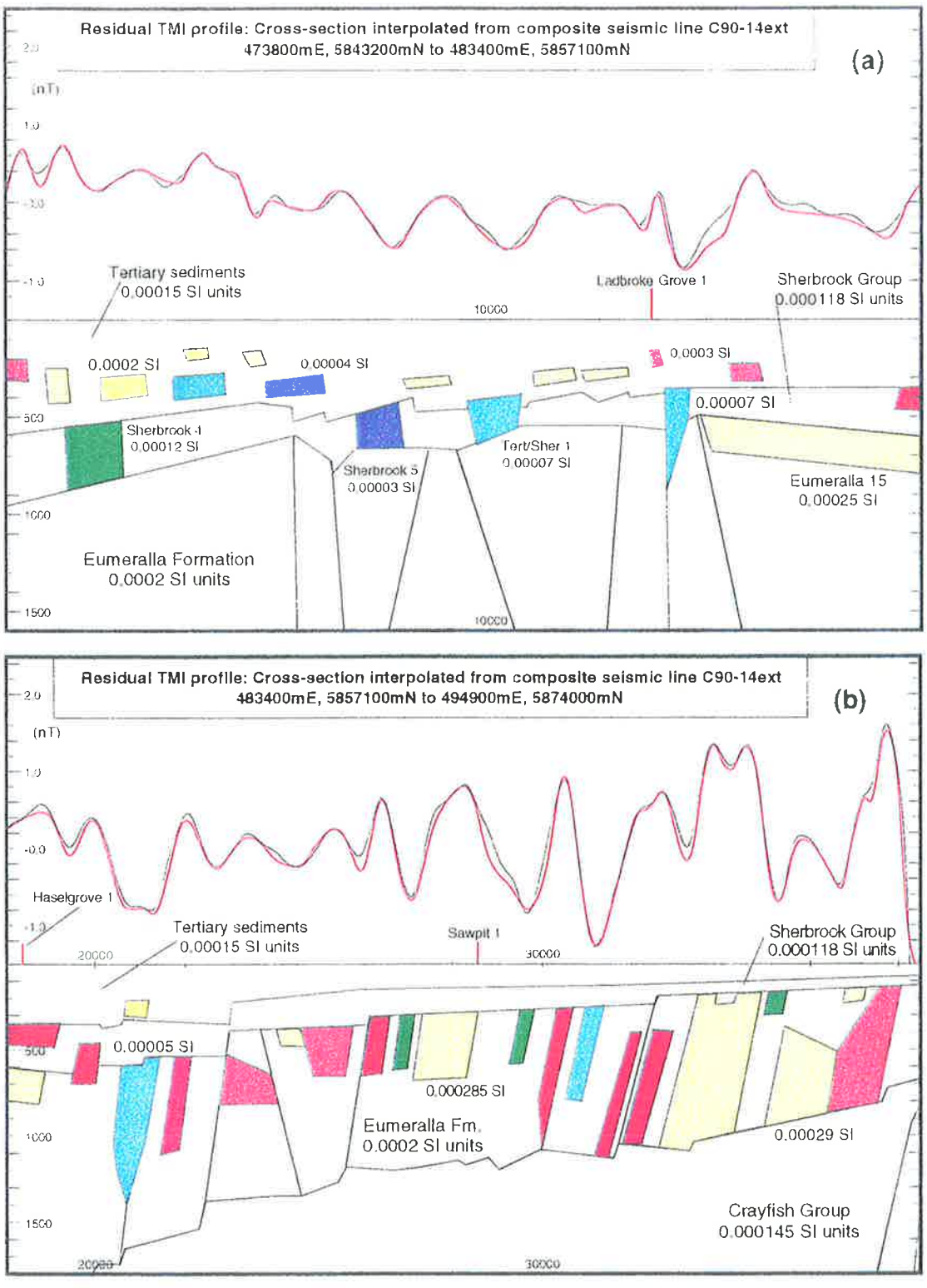

Fig. 8.2.2.2a & b Residual Profile perpendicular to Penola Trough axis

0.00000 - 0.000049 SI	0.00005 - 0.000099 SI
0.00010 - 0.000149 SI	0.00015 - 0.000199 SI
0.00020 - 0.000249 SI	0.00025 - 0.000299 SI
0.00030 - 0.000349 SI	0.00035 - 0.000399 SI
0.00040 - 0.000449 SI	0.00045 - 0.000499 SI

Susceptibility Range (SI units)

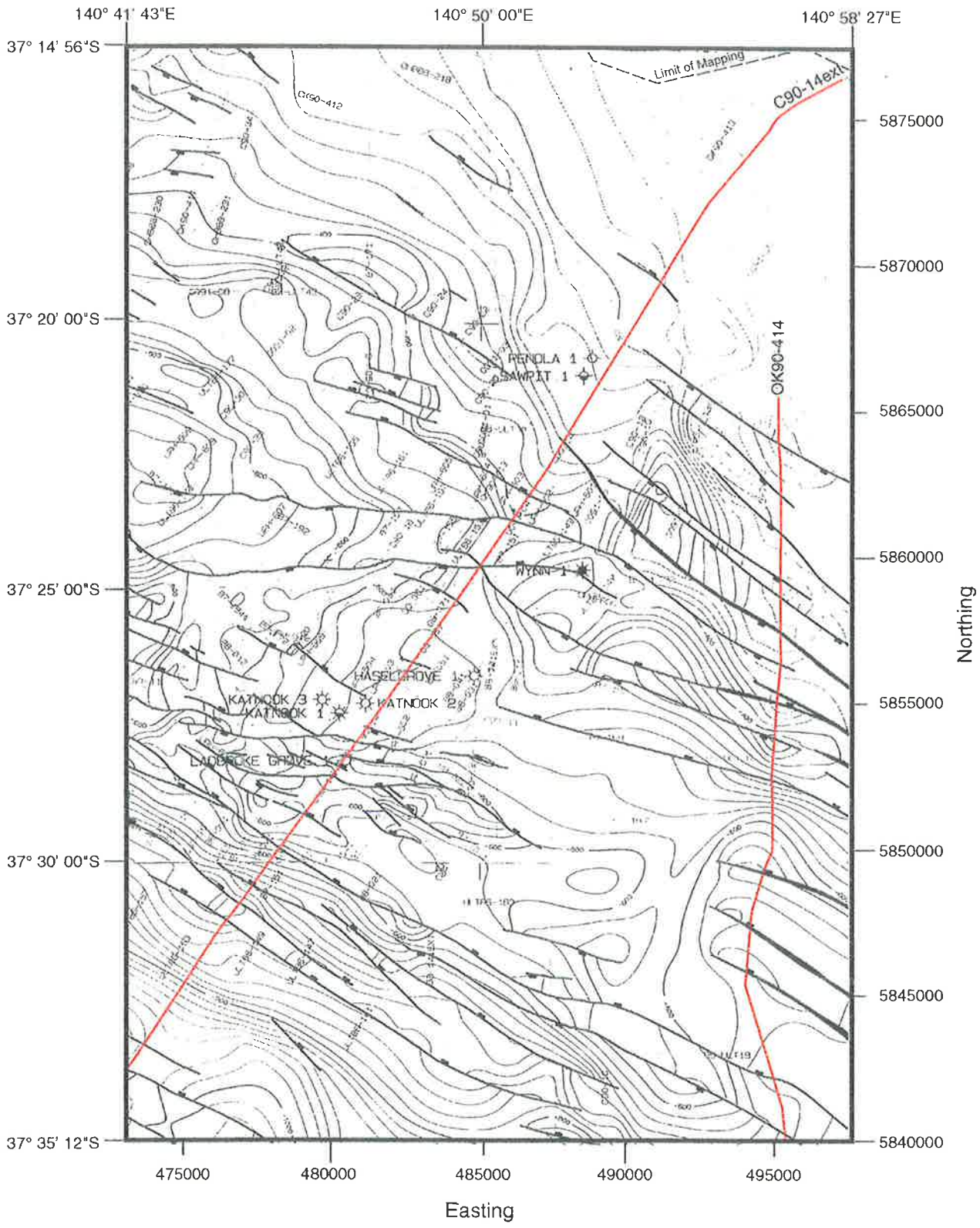

Fig. 8.2.2.3 Top Eumeralla Formation (Depth-Converted contour map)

The susceptibilities assigned to the formation bodies are the averages for the whole formation from several wells while the individual bodies were given values greater or less than the formation average (but within the measured range) depending on the polarity of the anomaly. The shape of the source bodies is largely arbitrary although there has been an attempt to place most bodies within a formation and to make the sides of the bodies parallel to nearby faults. The bodies represent zones within the formations where there has been selective creation, preservation or destruction of magnetic minerals rather than bodies of a distinct rock type. Attempts to model the anomalies as the result of igneous dyke source bodies were deemed unsuccessful. It is likely that any igneous bodies would have to be wide enough to be detectable on seismic sections in order to produce the observed anomalies (width greater than 80 m), and should be intersected by the Sawpit 1 well but no igneous material was recovered from the shallow formations (Martin, 1992).

8.2.3 Offshore Linear Anomalies Model

The offshore linear anomalies are very subtle and can only readily be detected on gradient maps (figs. 7.2.1.12a and 7.2.1.12b) where they form a series of crosscutting lineations oriented NW-SE and NE-SW, the former of which is similar to the regional trend of 'normal' faulting dominant in the Otway Basin while the latter is approximately the direction of extension since the Late Cretaceous (Veevers, 1988). As discussed in the introduction to this section, the anomalies cannot be produced by sources deeper in the section than the Tertiary sediments, the base of which occurs at 1034 m in Breaksea Reef 1 near the southern margin of the study area, and at 1014 m in Douglas Point 1 on the coast. The top of the Gambier Limestone was at 90 m in Breaksea Reef 1 while the sea surface was 22 m below the Kelly Bushing (KB) which means that the sea at the southern extremity of the study area is approximately 70 m deep if the thickness of unconsolidated sediments is ignored. The Early to Mid Eocene Dilwyn Formation underlies the Gambier Limestone at Breaksea Reef 1 and extends from 510 m below KB to the base of the Tertiary.

Figure 8.2.3.1 shows the offshore section on a residual TMI image and contour map with the prominent northwest-southeast lineations enhanced by a NE (45°) sun angle filter which was applied to the underlying image. Line 12000 is also shown. The

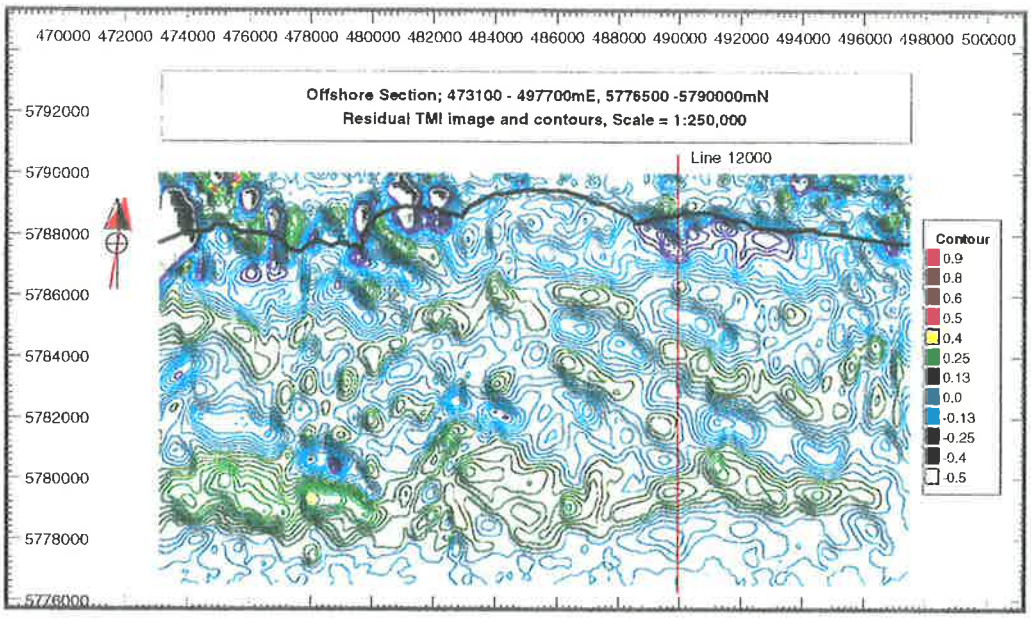

Fig. 8.2.3.1 Offshore Residual TMI image and contours

Line 12000 shown in red, coastline shown in black

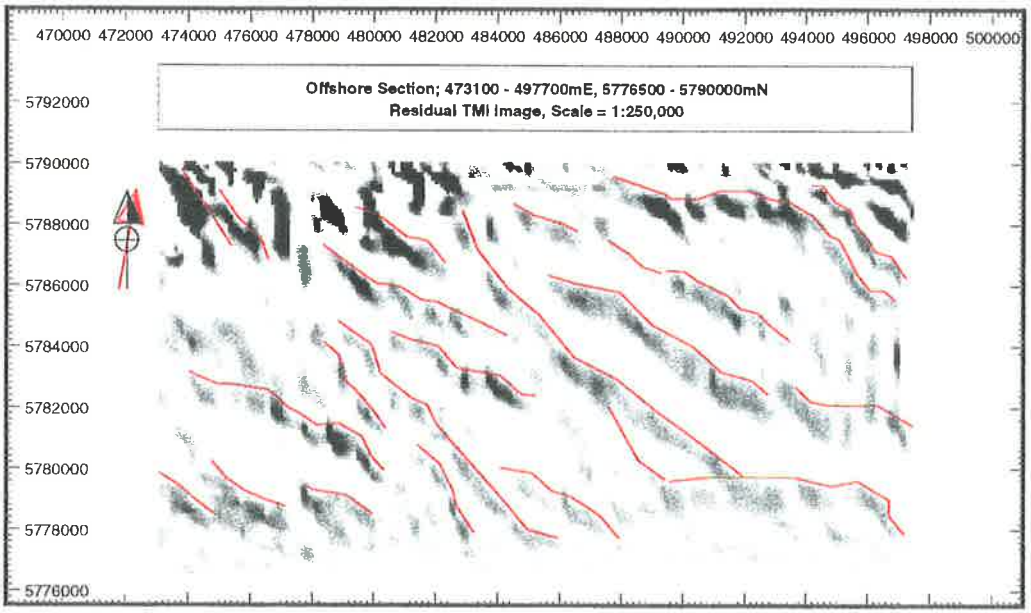

Fig. 8.2.3.2 Offshore Residual TMI image (45 deg. sun angle)

Possible NW-SE magnetic lineations (red)

interpretation shown in red on figure 8.2.3.2 is of the approximately northwest-southeast lineations on the residual TMI image and reveals that the lineations are generally aligned with the regional trend of faults outside this area, especially the trend of the Sherbrook Group faults which are the shallowest that have been mapped. A number of apparent north-south lineations can be seen on the image which are the result of incomplete removal of the swell noise from the line data. The profile shown in figure 8.2.3.3 is of residual TMI data produced from flight line 12000, by the application of a low pass filter with a cutoff wavelength of 5 km to smoothed, median filtered data (which was also used to produce the images). The resulting profile was then subtracted from the median filtered data to produce the residual data shown. This method was again found to produce a closer approximation to the long wavelength anomaly than the calculation of a regional polynomial. The application of a median filter was required to suppress the high amplitude anomalies due to culture along the coastline which would otherwise contaminate the low pass filtered profile.

The amplitude of the residual anomalies averages around 0.1 nT which is much less than the anomalies in the Penola Trough (and below the noise envelope) and is similar to the amplitude (0.1 to 0.2 nT) of the oceanic swell noise reported by AGSO staff (Gunn, 1995) but substantially less than the swell noise encountered by Heath et al., (1993) in the Perth Basin, W.A. (around 0.8 nT). However, the wavelengths of the residual anomalies have a greater wavelength (approx. 2 km) than that of the swell noise (500 to 700 m) and the line chosen for modelling was relatively uncontaminated by this noise. The profile (fig. 8.2.3.3) shows four main anomalies which are centred at approximately 5779600, 5783600, 5786200 and 5788400mE.

The diagram (fig. 8.2.3.3) also shows the approximate location of the seafloor which was produced by adding the offshore flight height (120 m) to the sea depth (70 m) at Breaksea Reef 1 at the southern end of the profile while the northern end was set at the flight height. The top of the Late Cretaceous Sherbrook Group is shown at the base of the figure (approx. 1000 m) while the Tertiary section is divided into the Gambier Limestone and the underlying Dilwyn Formation. The average susceptibility values for the Gambier Limestone (0.000038 SI units) and Dilwyn Formation (0.000085 SI units) were determined from the core measurements from Caroline 1 and Mt. Salt 1, and these were assigned to the background bodies.

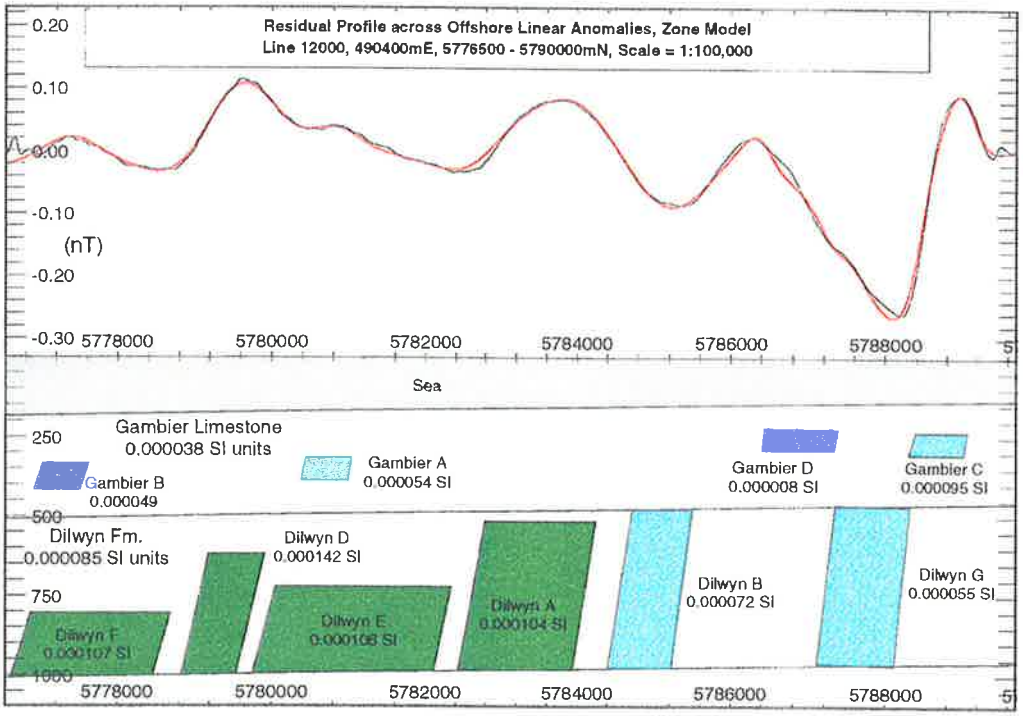

Fig. 8.2.3.3 Offshore section, Residual TMI profile, line 12000

Cross-section shows Gambier Limestone and Dilwyn Formation bodies with top Dilwyn Fm. horizon and seafloor.

Horizons interpolated from Breaksea Reef 1 and Mt. Salt 1 wells

- 0.00000 - 0.000049 SI
- 0.00005 - 0.000099 SI
- 0.00010 - 0.000149 SI

Susceptibility Range (SI units)

The model assumes that the sources of the anomalies are zones of varying magnetisation within the Tertiary sediments that may be associated with faulting (section 8.2.1). The Dilwyn Fm bodies were found to approximate the observed profile reasonably well with the Gambier Limestone bodies only needed in order to simulate the more subtle parts (except for Gambier C). All of the Dilwyn Fm bodies were assigned susceptibilities within the range measured in cores and the susceptibilities of the bodies were either greater or less than the background value depending on whether the anomaly modelled is positive or negative. Three of the Gambier Limestone bodies have susceptibilities that are within the measured range while Gambier C required a higher susceptibility to model the anomaly on the northern side of the profile (approx. 5789000mN). The bodies with higher than background susceptibilities represent zones where a higher proportion of magnetic minerals have remained unaltered while those zones with lower than average susceptibilities have been subject to a larger degree of oxidisation of the magnetic mineral content than the background, possibly due to the migration of groundwater along fault zones.

Comparison of the residual TMI image with the corresponding vertical gradient images (figs. 7.2.1.12 and 7.2.1.13) suggests that some part of the NW-SE lineations seen in the latter images could be due to the effects of swell noise because of the similarity between the wavelengths of the gradient anomalies and that of the noise. However, the residual maps have features corresponding to the higher amplitude gradient anomalies so some of the more prominent NE-SW magnetic lineations are the result of sources other than those generated within the ocean. The residual TMI image (not shown) had a 315° sun angle filter applied to it and the resulting lineations were found to correspond to only a few of the NE-SW lineations on the vertical gradient image, which implies that some of these gradient anomalies are caused by swell noise. As the amplitude of the linear anomalies is less than the accepted noise envelope (0.2 nT), it is not possible to unequivocally conclude whether these anomalies have a geological origin or that they are a combination of oceanic swell noise and other, unidentified noise sources.

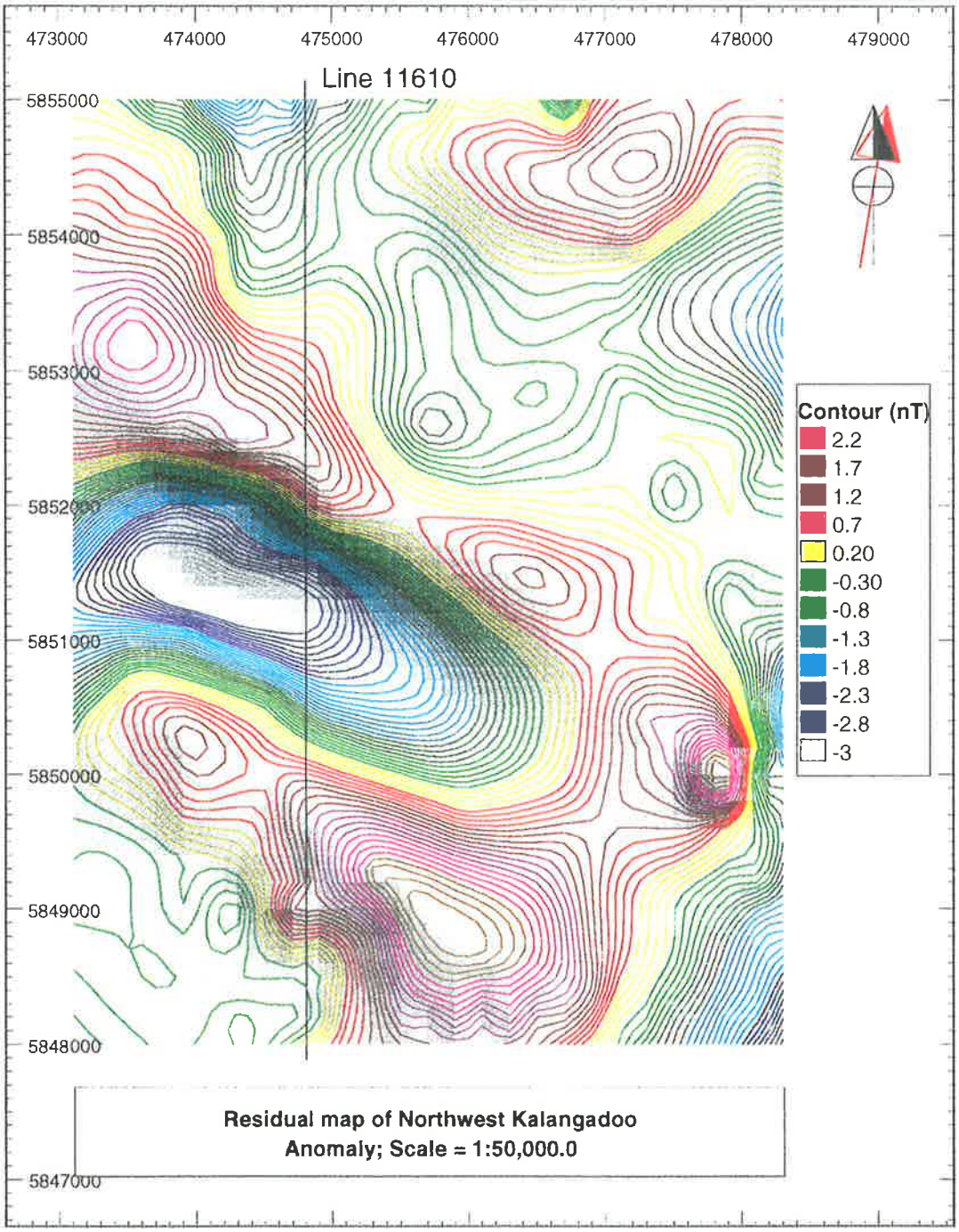

Fig. 8.2.4.1 Residual TMI contours and image of Northwest Kalangadoo Linear Anomaly showing Residual Line 11610 Contour Interval = 0.1 nT

8.2.4 Northwest Kalangadoo Linear Anomaly Model

This feature is composed of subtle anomalies which begin to the east of the Hungerford Anomaly, at approximately the corner of the western extension of the study area (around 473100mE, 5851600mN) and extend approximately 3.5 km ESE. The anomalies consist of a central elongated magnetic low with lower amplitude positive peaks to the north and south along with some linear features to the north which are obscured by cultural noise (fig. 8.2.4.1). Comparison between the magnetic map and the seismic top horizon map for the Eumeralla Formation indicates that the magnetic anomalies are adjacent to two major faults (550 to 600 m deep) which have a similar trend, appear to branch close to the Hungerford Anomaly and seem to be the upper extensions of the basement Kalangadoo Fault Zone (KFZ). The anomalies have a similar trend to faults (400 to 500 m deep) in the Sherbrook Group which are part of the same fault system. Many of the lines are contaminated by high amplitude cultural anomalies which interfere with the longer wavelength features.

The flightline 11610 (fig. 8.2.4.1) was chosen as being reasonably representative of the intersedimentary anomalies despite the presence of some cultural noise because other lines with long wavelength features of greater amplitude are contaminated to a larger extent while the least contaminated lines are on the eastern side of the area but also have the smallest amplitude for longer wavelength features. The closest, approximately north-south, seismic line to the flightline is 85-ULT43 which is around 2.5 km to the east but there are several seismic lines crossing the flightline diagonally, allowing the top horizons of the Sherbrook Group, Eumeralla Formation and Crayfish Group to be interpolated from all of these. Three models were prepared, one consisting of igneous dykes approximately 40 m thick emplaced along fault planes, while the second model consists of discontinuous layers or channels of higher susceptibility sediments at or near the top of the Eumeralla Formation, and the third model has wide zones of varying susceptibility that extend from the top to the base of the Eumeralla Formation. In all models the susceptibility of the Eumeralla Formation was set at 0.0002 SI units, that of the Sherbrook Group at 0.00015 SI units, and the background susceptibility set at 0.00013 SI units.

The residual profile from line 11610 displayed in fig. 8.2.4.2 shows the main negative anomaly with two small positive anomalies on either side and a prominent

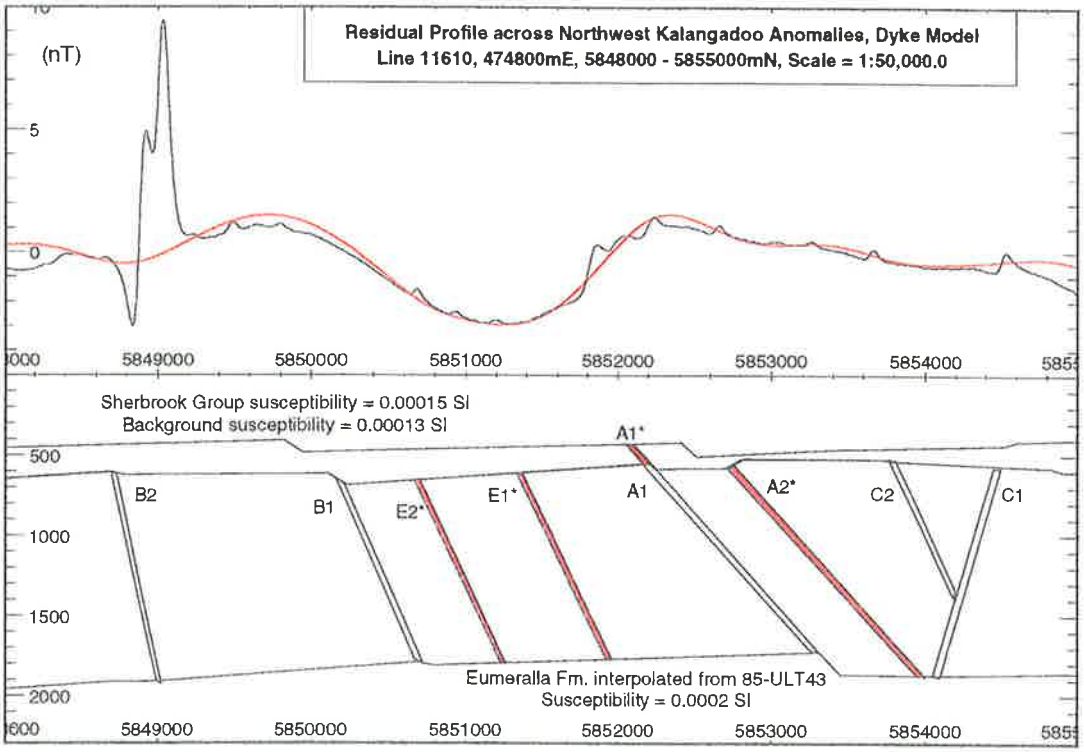

Fig. 8.2.4.2 Northwest Kalangadoo section showing Eumeralla Fm. igneous dyke bodies. Additional bodies shown in red Inclination of remanence = 98 deg.

cultural feature around 5849000mN. There are a number of short wavelength, sub-nanoTesla anomalies along the profile which are most likely caused by surficial/cultural features and so have been ignored. Those dykes thought to have been emplaced along the major faults are shown in outline (A1, B1, B2, C1 and C2) and it was concluded that no reasonable combination of susceptibilities, remanence inclinations and declinations assigned to these bodies would produce an acceptable fit to the observed profile. Four bodies were added to the model (A1*, A2*, E1* and E2*) to produce the calculated profile which fits the negative part of the residual profile reasonably but is a relatively poor fit to the small positive components adjacent to the central negative anomaly. The most significant bodies in influencing the shape of the profile are E1* and E2* which produce the negative anomaly while the effect of the other bodies is minor.

All bodies, except the small dyke crossing the Sherbrook Group (A1*), required a reverse polarity remanence component, in addition to susceptibilities at the lower end of the igneous rock range (Appendix B), to generate the calculated profile so the inclination and declination angles were set to 98° and 340° respectively which is approximately the (reversed-polarity) Mid-Cretaceous geomagnetic field direction (section 3.2.4). If this model is correct then the remanence angle implies that the igneous dykes were emplaced relatively soon after deposition of the formation rather than during the Pleistocene/Recent phase of volcanism. However, E1* and E2*, which have the most influence on the profile, could have been assigned a reversed remanence at 180° to the current geomagnetic direction provided the bodies were relocated and have different dips. Clark and Emerson, (1991) report that remanence is likely to be dominant in basalt dykes and sills with Koenigsberger ratios between 1 and 4 common (section 3.1.1), so the dykes, E1* and E2*, were assigned Koenigsberger (Q_n) ratios of 2.2 and 2.6, respectively.

The layer model shown in figure 8.2.4.3 includes the Sherbrook Group and Eumeralla Formation bodies, the major faults inferred from the horizon maps, and the layer or channel bodies. The bodies were given an arbitrary thickness of 100 to 120 m and all were assigned reversed-polarity remanent magnetisations except the body labelled Tertiary A2* which has a induced magnetisation only. The fault plane bodies were given effectively zero susceptibility because they are only shown for comparison with the previous model. The body that has the most influence on the calculated profile is

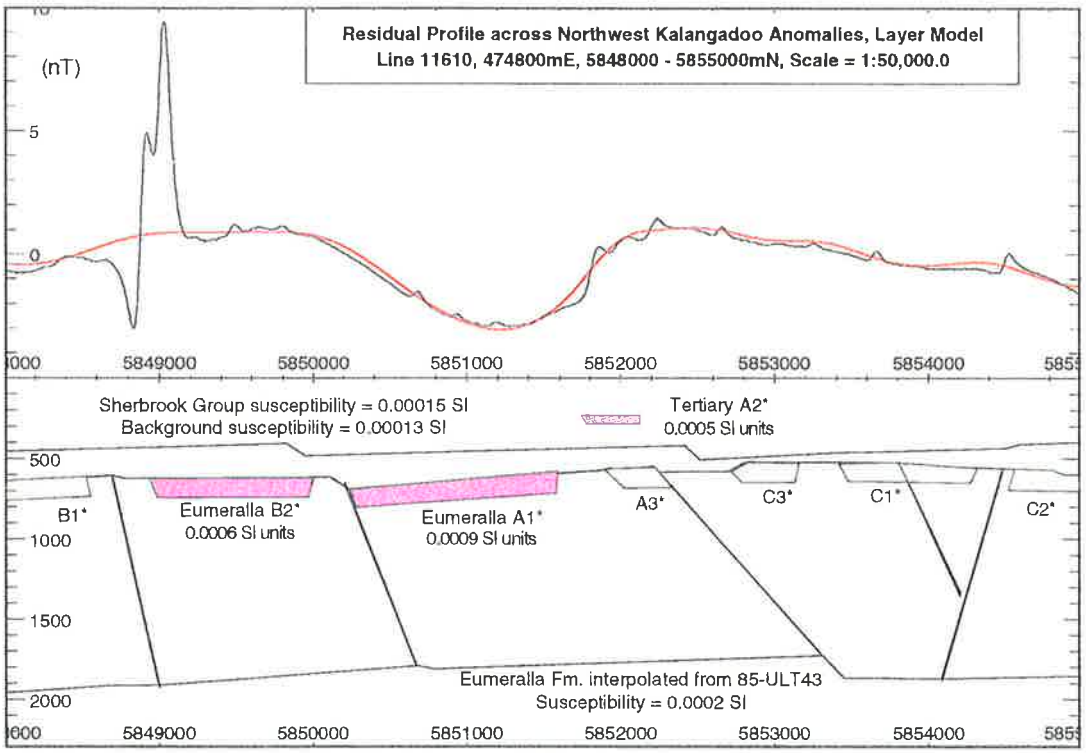

Fig. 8.2.4.3 Northwest Kalangadoo section showing Eumeralla Fm. layer model bodies

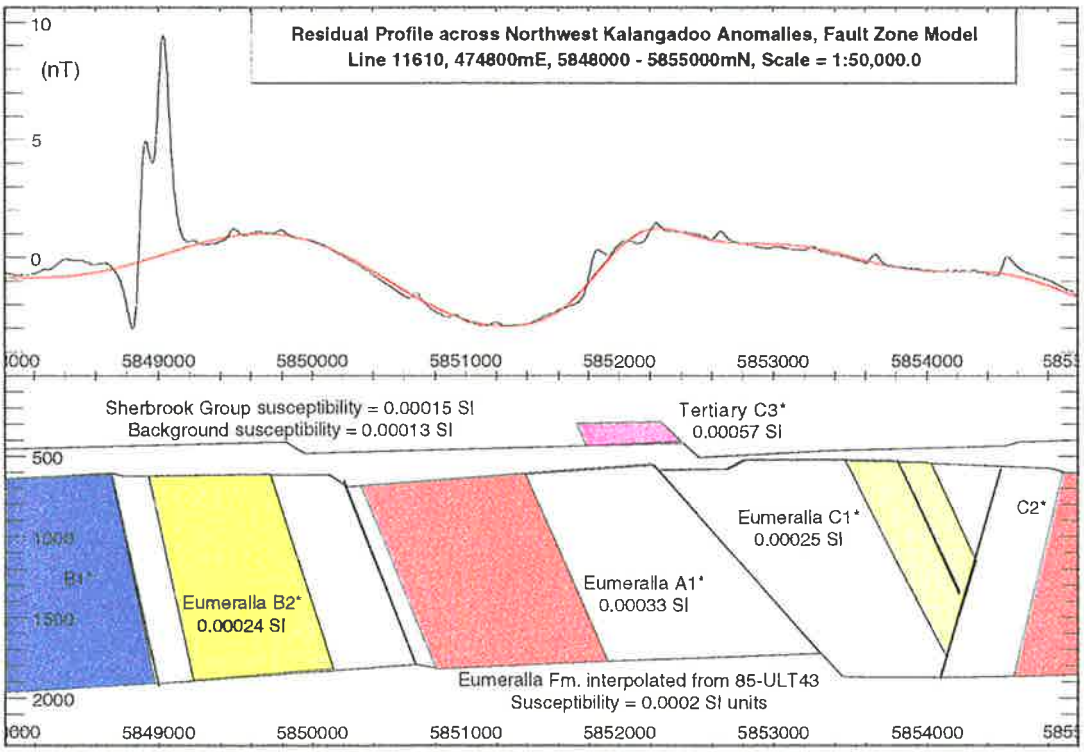

Fig. 8.2.4.4 Northwest Kalangadoo section showing Eumeralla Fm. fault zone bodies

Eumeralla A1* because it has the largest remanence component (Koenigsberger ratio (Q_n) = 4), while most of the other bodies, in a similar manner to the dyke model, have only a minor effect on the profile. Tertiary A2* was added to the model to improve the fit in the noisy section around 5852000mN. Susceptibility measurements from cores recovered from Kalangadoo 1 (the nearest well to the anomalies) show that susceptibility values from a core at the base of the Sherbrook Group have an average of 0.00017 SI units which is only slightly higher than the value assigned to the Group in the model while the core at the top of the Eumeralla Formation has an average susceptibility value (0.000185 SI), slightly less than the value used in the model. The highest values measured in cores from this well, occur at 130 m (0.0006 SI) and 275 m (0.0009 SI) below the top of the Eumeralla Formation.

As with the previous model, the Mid-Cretaceous geomagnetic field direction was assigned to the bodies' remanence, which is reasonable if the magnetisation is considered to be caused by detrital magnetite (Detrital Remanent Magnetisation) in volcanogenic sediments deposited in fluvial channels during the last stage of Eumeralla deposition. If, in contrast, the source of the anomaly is authigenic magnetic sulphides or magnetite then the geomagnetic field direction could vary between that for the Mid-Cretaceous and Recent depending on the circumstances under which the mineralisation occurred (Chemical Remanent Magnetisation). Authigenic magnetic sulphides formed in brown coal basins in Bohemia (Krs et al., 1992), developed during the early stages of diagenesis which would produce a Mid to Late Cretaceous geomagnetic field direction of the remanence if this process had occurred in this area, while the formation of magnetite (or magnetic sulphides) as a result of the migration of hydrocarbons could be expected to have occurred considerably later so the geomagnetic field direction of the remanence would reflect the age of the hydrocarbon migration.

Clark and Emerson, (1991) published data showing that induction is likely to be dominant in magnetite-bearing sediments while remanence is dominant when the sediments are haematite-bearing (max. $Q_n \approx 10$). Pyrrhotite-bearing rocks and ores are almost always remanently magnetised with average Q_n ranging from approximately 2 for massive pyrrhotite to 40 for disseminated pyrrhotite while other magnetic sulphides such as griegite may be expected to show similar properties. If magnetite in channel sediments is the source of the magnetic anomalies it might be expected that the main anomaly

would be positive while sediments dominated by haematite (which has been identified in cores) might produce a positive or negative anomaly depending on the polarity of the geomagnetic field during sedimentation. A similar positive anomaly would result from magnetite formed by migrating hydrocarbons, bacterial action or the oxidation of pyrite/siderite while magnetic sulphides would produce a positive or negative anomaly in the same manner as haematite.

The fault zone model (fig. 8.2.4.4) places the body (Eumeralla A1*) which is primarily responsible for the main negative anomaly, between the two faults in a similar manner to the layer model but the body extends to the base of the formation. Eumeralla A1* is not quite as wide as the equivalent layer model body, has a considerably lower susceptibility and lower Koenigsberger ratio (Q_n = 3), and is not adjacent to the fault zone. The zone bodies all required a reversed polarity remanence component except for Eumeralla B1*, Eumeralla B2* and Tertiary C3* which are the result of induced magnetisation only. Eumeralla B1* was assigned a very low susceptibility while Eumeralla B2* was given a susceptibility that is only slightly greater than the Eumeralla Formation background to produce the southern, positive part of the anomaly. The Tertiary C3* body was added to improve the fit of the calculated profile on the northern side of the anomaly where low amplitude noise contaminates the observed profile and was assigned a comparably high susceptibility because of the limited depth extent of the body. The body, Eumeralla C1*, was created to approximate a very subtle negative anomaly over the fault and required a reversed polarity remanence component but was narrower than the comparable body in the layer model.

All three models show that the source of the negative anomaly is almost certainly located between the two faults which lie under the small positive components on either side of the negative anomaly. Unlike previous models it was not possible to simulate the negative anomaly by creating a zone of very low or zero susceptibility but instead a reversed polarity remanence component must be assigned to the body or bodies. Comparison of the models shows that the dyke model generates an anomaly that is the poorest fit of the three while the calculated profile of the zone model is clearly the best fit. However, the lack of constraint from seismic or other mapping means that the shape and magnetic properties of the bodies are relatively arbitrary and the positions of those

dykes outside the fault zones which have been added to that model are also unconstrained.

One of the reasons for conducting this aeromagnetic survey was to see if it was possible to locate igneous dykes that had intruded along fault planes and acted as conduits for the charging of the sedimentary section with carbon dioxide. It is possible that the proposed igneous bodies responsible for the negative anomaly in the dyke model could act as conduits although they are not emplaced along the major fault planes, and it is equally possible that the other igneous bodies in the model could have served as conduits but this would substantially reduce the usefulness of an aeromagnetic survey in detecting them because of the very low amplitude of the anomalies generated by the bodies. If either of the other two models are correct then the magnetic anomaly is unrelated to the proposed carbon dioxide conduits.

Chapter 9

Conclusions

9.1 Conclusions

The major magnetic features of the study area are possibly the result of post-rift intrusive bodies in or at the top of the basement section but equally the probability that some of the features are produced by pre-rift igneous and metamorphic basement terrain must also be considered. The exceptions to this are the surface volcanic complexes at Mt. Gambier and Mt. Schank as well as the probable basaltic plug, the source of the Hungerford Anomaly, which is about 300 m deep, above the Late Cretaceous section in Early Tertiary sediments.

The most prominent magnetic feature is the semi-elliptical anomaly (35 × 18 km) extending to the northeast from around the Mt. Gambier volcanic complex to the margins of the Penola Trough (section 8.1.1) and is likely to result from a magma chamber approximately 7 km deep (which is most probably below the top of basement). The broad magnetic high on the western side of the study area discussed in sections 7.1.2 & 7.2.1 and modelled in section 8.1.2 is an extension of the magnetic high that covers a large region onshore to the west of the study area. This may be produced by deep intrusions beneath the Mt. Burr Volcanic Group. The Western Penola Trough Anomaly (WPTA) is the result of a source estimated to be approximately 5 km deep which places the top of the source near the basement/sediment interface in the Penola Trough but deeper beneath the Kalangadoo Fault Zone (KFZ) to the southwest. There may be a contribution to this anomaly from the part of the Kalangadoo High (around 2.5 km deep) southwest of the KFZ but this source is most likely pre-rift metamorphic rocks (section 8.1.2).

The circular/elliptical anomaly which is just outside of the study area on the northwest corner (Fig. 7.1.2.2) has the next highest amplitude and is around 5 km deep in an area of relatively shallow basement (1.5 to 2.5 km). Immediately to the north-northeast of the WPTA is another elliptical anomaly (Northwest Penola Trough Anomaly-NWPTA) which is also about 5.2 km deep but has a considerably lower

amplitude than the previously discussed anomalies. The source is beneath a region of deepening basement with the sediments ranging in depth from 2 km in the north to 4.5 km in the south (section 8.1.5) which means that the southern extremity of the source is relatively close to the top of basement in the deeper part of the Penola Trough but, as there is no evidence that the body dips to the south, the source is a considerable depth below the top of basement at its northern end.

The two anomalies north of the Mt. Gambier Anomaly are separated by the Kalangadoo Fault Zone (KFZ), with the Kalangadoo High Anomaly mostly south of the KFZ on the seismically delineated Kalangadoo High, while the Mid-Penola Trough Anomaly (MPTA) is north of the KFZ and coincides with a basement high, mapped by seismic, within the Penola Trough (section 8.1.4). Depth estimates place the tops of these bodies at or near the basement/sediment interface (3.8 and 3.6 km respectively). The Northeast Penola Trough Anomalies (NPTA) are on the northern flank of the Penola Trough with the more southerly feature, the Sawpit Anomaly, being the result of a source around 3.2 km depth and approximately 5 km in diameter which is south of the seismically defined Sawpit High. The source of the northern elliptical anomaly (Penola North Anomaly-PNA) is approximately 2.2 km deep and around 6 by 3 km long (section 8.1.3).

If the sources of the Kalangadoo High Anomaly, MPTA and NPTA are igneous bodies emplaced prior to the commencement of rifting, then these bodies could have been adjacent at that time and have since been moved apart by the formation of the initial rift valley. If this hypothesis is correct then the direction of extension during the Late Jurassic/Early Cretaceous would range from north-south around to northeast-southwest with the northeast-southwest direction of extension being the most likely.

The very small magnetic high in the extreme northeastern corner of the study area is generated by sources in the vicinity of the Kanawinka Fault Zone (KWFZ) which passes through this corner. Those seismic sections that have crossed the KWFZ onto the Padthaway Ridge have found that the basement depth is less than 500 m while to the south and west of the KWFZ the basement deepens rapidly. The two magnetic lows adjacent to the KWFZ coincide with the positive gravity ridge extending from over the Victorian border suggesting the possibility that the source or sources of the anomalies

have a reversed polarity magnetisation and are possibly at considerable depth beneath the fault zone.

The only magnetic anomaly, attributed to a basement source, where the basement has been intersected by drilling is the Sawpit Anomaly. The Sawpit 1 well penetrated 190 m into the basement and found a volcanic unit 15 m thick consisting of andesite, 15 m below the top of basement which overlies metasediments (Moriarty et al., 1995). It is possible to model the Sawpit anomaly (15 nT) by assuming a thin andesite layer (section 8.1.3) at the top of basement (2.5 km) provided the andesite has a susceptibility of around 0.26 SI units which is greater than the value for andesite reported by Telford et al., (1990) but is at the extreme upper end of the range reported by Clark and Emerson, (1991). However, this conclusion conflicts with the most probable depth estimate from spectral analysis but, on the other hand, it is conceivable that the spectral analysis depth may represent an accumulation of volcanic lavas to the south of the Sawpit 1 well. It can be inferred that the andesite layer must be at least Jurassic in age, and very probably older because it has been interpreted as being beneath the top of basement and as andesite is an extrusive rock, it must have been buried by the overlying metasediments. If the andesite layer is not responsible for this magnetic anomaly then the magnetic body should be deeper into the basement and might represent the magma source. The depth from spectral analysis could then represent an average of the andesite layer and the deeper body.

The Penola North Anomaly to the northeast of the Sawpit Anomaly is more intense (31 nT) than the latter and the likely depth of 2.2 km places the anomaly source close to the top of basement. Since there have not been any wells drilled in the vicinity of the anomaly, the source can only be speculated on but comparison with the basement map produced from the Tilbooroo 3D seismic survey, shows that the magnetic anomaly peak is located over the section of basement between the Woolwash and Leicester Park Faults (Moriarty et al., 1995) and extends to the east into an area that has only been mapped relatively sparsely with seismic methods. Possible sources of the anomaly include a strongly magnetic volcanic unit within the Casterton Formation, an andesite extrusive layer within or on top of the basement as at Sawpit 1, an intrusive source below the basement/sediment interface, or pre-existing metamorphic terrain that is strongly magnetic. The Casterton Formation was found to be 60 m thick at Sawpit 1 but

without the volcanic units that are characteristic of the formation in Victoria although it is still possible that these volcanic units are present away from the drillhole. Both a deep intrusion or highly magnetic metamorphic terrain could produce the anomaly but the intrusion would then be too deep to agree with the result from spectral analysis. The types of metamorphic rocks recovered from the Sawpit 1 well are likely to have much too low a susceptibility value to cause the anomaly but the higher end of the metasediment susceptibility range could have resulted in the measured anomaly provided the source layer is thick.

The magnetic features that result from intersedimentary sources are generally linear to curvilinear, extend for several kilometres, and can have amplitudes of up to 3 nT. The depth to the top of the sources is usually about 300 to 500 m on the eastern side of the study area and the depth extent of these sources can be around 1000 to 1200 m. This places them within the Eumeralla Formation when occurring north of the Kalangadoo High. The most prominent of these anomalies are found on the eastern side of the study area (section 8.2.1), east of Wynn 1 and over the series of basement faults that mark the northeast edge of the deepest part of the Penola Trough (the Kanawinka South Fault Zone of Perincek et al, (1994)). Close comparison of the flight line, 12120, with the north-south seismic line, OK90-414, has shown that magnetic lows are generally associated with fault zones but with important exceptions, such as the prominent linear anomaly east of Wynn 1 where the magnetic high is over the fault zone.

Models of fault zone bodies or shallow layers at the top of the Eumeralla Fm produce the best fit to the residual profile but the existence of a series of normally or reversely magnetised dykes cannot be completely excluded. The magnetisation of postulated dykes would have to alternate in polarity along the profile in order to obtain a reasonable fit and this appears unlikely. The zone and layer models may represent the two extremes of a pattern of varying magnetisation but because the depth extent of the bodies is poorly constrained both models have been produced. It has been suggested (Tucker, pers. com., 1996) that the linear anomalies in this part of the study area could be the result of electromagnetic induction effects on the fault zones, however, induction would tend to produce positive anomalies rather than the mostly negative anomalies found in this section. There may be an induction anomaly close to the study area but this

appears to be associated with the Kanawinka Fault Zone along the basin margin (Whellams, pers. com. 1996).

A magnetic profile along the seismic line C90-14ext (where models were constructed from horizon maps) was created and showed that most magnetic lows were associated with fault zones, especially in the northeastern part of the profile where the source bodies are within the Eumeralla Formation. In the southwest the sources are mostly within the Tertiary sediments where the faults have not been mapped and so it is not possible to unequivocally relate the magnetic lows to fault zones. Maps of the shallow magnetic sources reveal a strong correlation between these and the orientation of Eumeralla and Sherbrook faults in the northeast of the Penola Trough, but in the west seismic mapping has shown a more east-west fault orientation which is not readily apparent in the shallow residual map (section 8.2.2). This may be because the dominant intersedimentary magnetic sources are in the Tertiary section which may have a differing orientation to the underlying Cretaceous faults or it may be because the western side of the study area has a larger amount of cultural noise which masks the east-west anomalies.

The linear anomaly northwest of the Kalangadoo Anomaly is over the Kalangadoo Fault Zone and aligned with the Hungerford Anomaly but attempts to model the source as a reversed polarity magnetised igneous dyke or dykes which had intruded along the fault zone from the vicinity of the Hungerford Anomaly were unsuccessful. The three models constructed (zone, layer and dyke) all used reversely magnetised bodies located between the major Sherbrook and Eumeralla faults identified from the horizon maps (section 8.2.4). It was also not possible to obtain a reasonable fit to the profile by assigning susceptibilities to the layer and zone models which are much lower than the average for the formation. This was how magnetic lows on the eastern side of the Penola Trough were modelled but in this case negative susceptibilities would have been required.

The region south of the Mt Gambier Anomaly to the coastline is generally too contaminated with cultural noise to identify any subtle features that result from intersedimentary sources. The offshore section contains a series of cross-cutting features, best identified from gradient maps, which may result from shallow intersedimentary sources, however, these features have amplitudes that are close to the

noise envelope and there is a problem with wave noise that is difficult to completely remove with filters. Assuming these features have a geological origin, then the principal sources of the anomalies are likely to be within the Tertiary Dilwyn Formation (approx. 500 to 1000 m deep) with a few sources within the overlying Gambier Limestone being responsible for the even more subtle features (section 8.2.3). The features that are oriented NW-SE, which can be detected on sun-angle enhanced images, appear to have the same fault orientation as the underlying Late Cretaceous Sherbrook Group while the NE-SW features mentioned above are, with some exceptions, most likely artifacts of processing.

The presence of CO_2 of mantle origin in several wells suggests that the migration of this gas from volcanic or hydrothermal conduits to the gas wells may have occurred since the Pleistocene because the surface eruptions are not older than this. There is little evidence of igneous dykes, detectable on the magnetic maps or profiles, acting as conduits to feed the carbon dioxide to the hydrocarbon wells. This cannot rule out the possibility that igneous dykes either containing very little magnetic material or which are very thin are present and act as feeder tubes for the CO_2 but there do not appear to be any intersedimentary magnetic features that have the correct orientation to supply the contaminated wells. These wells are Caroline 1, Kalangadoo 1 and Ladbroke Grove 1 with the first two producing over 95 % pure CO_2 while the latter produced 54 % CO_2 as well as hydrocarbons and nitrogen. The Caroline 1 well does not appear to have any nearby magnetic lineation or other type of feature that could be interpreted as a feeder conduit, however, there is a subtle positive gravity anomaly adjacent to the well that might be caused by an intrusive body. Kalangadoo 1 is relatively close to Pleistocene surface eruptions but carbon dioxide most probably escaped from the volcanic conduit(s) well below the basement/sediment interface and then migrated through fractures in the basement to the well location where the gas was recovered from basement. There are subtle linear magnetic features that are most probably from sources at intersedimentary depths near Ladbroke Grove 1 but these appear to be significantly shallower than the gas reservoir (250-500 m rather than 2.5 to 3 km deep) as well as being oriented approximately northwest-southeast which is the 'normal' fault direction for the Penola Trough (section 8.2.2). This orientation would mean that CO_2 would be unlikely to be

easily able to migrate from the Kalangadoo Fault Zone to these NW-SE trending features.

Cultural anomalies are a significant problem in this area because the short wavelength, relatively high amplitude noise generated over the more highly populated sections can mask the more subtle longer wavelength, low amplitude features that are the result of intersedimentary sources (Appendix A). The main culture-noise-dominated areas are around the city of Mt. Gambier and the region between there and the coastline, with another significant group around Penola and the Coonawarra area. The highest amplitude cultural anomalies are produced by large industrial facilities such as sawmills but these are not the most significant features compared with the major power lines. There is a large interstate powerline (275 kV) extending from the Victorian border ENE of Mt. Gambier, across the study area to Tarpeena and then north to Nangwarry. The remaining major powerlines range from 133 kV down to 11 kV with ordinary 240 V street lines along most major and minor roads. Close examination of the anomalies generated by these sources reveals that the highest voltage powerlines produce anomalies with wavelengths of around 400 m but 200 m or less is more typical, while the amplitude varies from less than 1 nT up to around 200 nT. There is no typical shape for these kinds of anomalies because the shape varies with the orientation of the powerline with respect to the flightpath as well as the phase of the line when crossed, and there are a number of cases where interference between closely spaced powerlines or other cultural sources has produced complex anomaly shapes. There is little evidence of any detectable anomalies resulting from ordinary street powerlines and anomalies produced by the 11 and 19 kV lines are often sub-nanoTesla in amplitude.

The study has achieved some of its aims but further work is required to resolve other questions. The basement structure in the north of the study area, around the Penola Trough, has been extensively mapped by numerous seismic surveys so the aeromagnetic survey has helped to confirm the previous work. South of the Kalangadoo High, the presence of the Mt. Gambier magma chamber and the lack of magnetic anomalies to the south of the magma chamber and offshore, has not allowed the depth to basement to be determined by modelling or spectral analysis, although the depth estimate for the Mt. Gambier magma chamber (approx. 7 km) suggests a maximum depth for the top of basement in this part of the study area.

The timing of the igneous activity is only known in three locations, the approximately 5000 year old eruptions at Mts. Gambier and Schank, and the Early Palaeozoic basalts intersected by the Hatherleigh 1 well. It can also be inferred that the andesite layer intersected by the Sawpit 1 well erupted prior to the development of the rift. If most of the other magnetic anomalies in the study area are produced by bodies that were emplaced before the formation of the rift then the bodies can have no direct influence on the generation or migration of hydrocarbons. If, however, the source bodies were emplaced in the basement section after the sediments were deposited then there is a possibility that fault reactivation has occurred which could charge the sediments with carbon dioxide or allow trapped hydrocarbons to escape. This could be significant in the case of the Tantanoola Trough which has become the focus of exploration interest. This trough overlies the source of the Mt. Gambier Anomaly which has been modelled as a large, thick magma chamber and could be expected to have produced approximately one kilometre of uplift of the overlying basement and sedimentary section (Gvirtzman and Garfunkel, 1997). If the intrusion occurred prior to rift formation then it will have no implications for petroleum exploration while emplacement at any time from the Late Jurassic to the Early Tertiary may have helped accelerate thermal maturation. Emplacement during the Late Tertiary/Quaternary is more likely to have had adverse effects on the source rocks and, particularly, the reservoirs. Heat flow data compiled by Cull (1982) show higher values at Mt. Gambier and in Western Victoria which is consistent with areas of recent volcanism but well bottom temperatures from the wells drilled near the intrusive body are not significantly different from others at some distance from it. It has been inferred that the source of the Hungerford Anomaly is a basaltic plug, however, this is based on the proximity of the anomaly to the eruptive centres of the Mt. Burr Group rather than any drilling. The source of the anomaly was not apparent on the seismic lines which passed close to the anomaly.

The prominent linear anomalies east of Penola have had three separate models produced for them, based on different interpretations of their sources but without drilling (particularly of the highest amplitude anomalies) these interpretations remain hypotheses. It has been suggested that a closely spaced gravity survey along seismic line OK90-414 may allow the igneous dyke hypothesis to be either confirmed or rejected (Boyd, pers. com., 1996) while the layer model could be investigated by drilling (300 to 400 m deep).

The zone model would be the most difficult to prove or disprove because it is based on small lateral variations in average magnetic susceptibility. The core measurements discussed in section 3.3.2 show that similar variations in susceptibility occur vertically in the wells in the study area but it would require at least two drillholes, one in a relative magnetic low and the other in a relative high, to determine whether the postulated lateral susceptibility variation occurs. This area would be easier to investigate because the sources of the anomalies are likely to be shallower than in the other parts of the Penola Trough or offshore. As mentioned above, the most prominent of the linear anomalies are over the Kanawinka South Fault Zone (KSFZ). If these anomalies are the result of the alteration effects of migrating hydrocarbons then faults associated with the KSFZ may have served as migration pathways.

The linear anomalies have a significance beyond the study area because similar features have been reported in other parts of the onshore Western Otway Basin (Reeves et al., 1993), and in the offshore, Victorian section of the Otway Basin (Gunn, 1994) as well as other sedimentary basins. Establishing the cause or causes of these features would determine whether or under what circumstances magnetic lows delineate fault zones, for example, which would in turn determine whether aeromagnetic surveys can be used to interpolate between seismic lines. If hydrocarbons were to be found in the vicinity of a magnetic anomaly or there was evidence that there had been accumulations in that vicinity in the past then further investigations could assist in resolving the controversy over the authigenic formation of magnetite by hydrocarbons which was discussed in section 3.2.2.

References

Atchuta Rao, D., Ram Babu, H.V., Sanker Narayan, P.V., 1981. Interpretation of magnetic anomalies due to dykes: The complex gradient method. *Geophysics*, 46, 1572-1578.

Balsley jr., J.R., and Buddington, A.F., 1958. Iron-titanium oxide minerals, rocks, and aeromagnetic anomalies of the Adirondack area, New York. *Economic Geology and the Bulletin of the Society of Economic Geologists*, 53 (7), 777-805.

Barbetti, M., and Sheard, M.J., 1981. Paleomagnetic results from Mounts Gambier and Schank, South Australia. *Journal of the Geological Society of Australia*, 28, 385-394.

Beaumont-Smith, N.H., 1994. Definition of the top Crayfish Group unconformity, Western Otway Basin, South Australia. *University of Adelaide (NCPGG). B.Sc. (Hons) thesis* (unpublished).

Benthien, R., and Elmore, R.D., 1987. Origin of magnetization in the Phosphoria Formation at Sheep Mountain, Wyoming: A possible relationship with hydrocarbons. *Geophysical Research Letters*, 14, 323-326.

Bhattacharyya, B.K., 1964. Magnetic anomalies due to prism-shaped bodies with arbitrary polarisation. *Geophysics*, 29, 517-531.

Bhattacharyya, B.K., 1965. Two-dimensional harmonic analysis as a tool for magnetic interpretation. *Geophysics*, 30, 829-857.

Blackburn, G., Allison, G.B., and Leaney, F.W.J., 1982. Further evidence on the age of tuff at Mt. Gambier, South Australia. *Royal Society of South Australia. Transactions*, 106 (4), 163-167.

Blakely, R.J., and Simpson, R.W., 1986. Locating edges of source bodies from magnetic or gravity anomalies. *Geophysics*, 51, 1494-1498.

Blakemore, R.P., 1975. Magnetotactic bacteria. *Science*, 190, 377-379.

Bouisset, P.M., and Augustin, A.M., 1993. Absolute age dating, and correlation of sedimentary rocks, with examples from the Paris Basin, France. *American Association of Petroleum Geologists Bulletin*, 77 (4), 569-587.

Bradshaw, M., 1993. Australian petroleum systems. *Petroleum Exploration Society of Australia Journal*, 21: 43-53.

Brown, C.M., Tucker, D.H., and Anfiloff, V., 1988. An interpretation of the tectonostratigraphic framework of the Murray Basin region of southeastern Australia, based on an examination of airborne magnetic patterns. *Tectonophysics*, 154, 309-333.

Brothers, L.A., Engel, M.H., and Elmore, R.D., 1996. The late diagenetic conversion of pyrite to magnetite by organically-complexed ferric iron. *Chemical Geology*, 130, 1-14.

Busby, J.B., Peart, R.J., Green, C.A., Ogilvy, R.D., and Williamson, J.P., 1991. A search for direct hydrocarbon indicators in the Formby area. *Geophysical Prospecting*, 39, 691-710.

Cande, S.C., and Mutter, J.C., 1982. A revised identification of the oldest sea floor spreading anomalies between Australia and Antarctica. *Earth and Planetary Science Letters*, 58, 151-160.

Canfield, D.E., and Berner, R.A., 1987. Dissolution and pyritization of magnetite in anoxic marine sediments. *Geochimica et Cosmochimica Acta*, 51, 645-659.

Carmichael, R.S., 1989. *Practical Handbook of Physical Properties of Rocks and Minerals*. CRC Press, Bota Raton, Florida.

Chang, S.R., and Kirschvink, J.L., 1989. Magnetofossils, the magnetization of sediments, and the evolution of magnetite biomineralization. *Annual Reviews of Earth and Planetary Sciences*, 17, 169-195.

Chang, S.R., Stolz, J.F., Awramik, S.M., and Kirschvink, J.L., 1989. Biogenic magnetite in stromatolites: Occurrence in ancient sedimentary environments. *Precambrian Research*, 43, 305-315.

Chatfield, K., 1992. The relationship between volcanics, associated intrusives and carbon dioxide within the Otway Basin, South Australia. *University of Adelaide (NCPGG). B.Sc. (Hons) thesis* (unpublished).

Chivas, A.R., Barnes, I., Evans, W.C., Lupton, J.E. and Stone, J.O., 1987. Liquid carbon dioxide of magmatic origin and its role in volcanic eruptions. *Nature*, 326 (6113): 587-589.

Clark, D.A., 1983. Comments on magnetic petrophysics. *Bull. Aust. Soc. Explor. Geophys.*, 14: 49-62.

Clark, D.A., and Emerson, D.W., 1991. Notes on rock magnetisation characteristics in applied geophysical studies. *Exploration Geophysics*, 22, 547-555.

Clark, D.A., French, D.H., Lackie, M.A., and Schmidt, P.W., 1992. Magnetic petrology: Application of integrated rock magnetic and petrological techniques to geological interpretation of magnetic surveys. *Exploration Geophysics*, 23, 65-68.

Cockshell, C.D., O'Brien, G.W., McGee, A., Lovibond, R., Perincek, D. and Higgins, R., 1995. Western Otway Crayfish Group troughs. *Australian Petroleum Exploration Association Journal*, 35: 385-404.

Cockshell, C.D., 1995. Structural and tectonic history. In: Morton, J.G.G., and Drexel, J.F. (Eds.), The petroleum geology of South Australia, Volume 1: Otway Basin (1st. Ed.), *MESA Report Book* 95/12, 15-45.

Compagnie Genérale de Géophysique (C.G.G.), 1965. Gambier-Otway aeromagnetic interpretation, South Australia. Department of National Development, Bureau of Mineral Resources, Geology and Geophysics. *Record No.* 1965/130.

Cull, J.P., 1982. An appraisal of Australian heat-flow data. *BMR Journal of Australian Geology and Geophysics*, 7, 11-21.

Day, R.A., 1989. East Australian volcanic geology, Victoria and South Australia; Older volcanics. In: Johnson, R.W., (compiler and editor), Knutson, J., and Taylor, S.R., (editors), *Intraplate volcanism in eastern Australia and New Zealand*, Cambridge University Press, Cambridge, U.K., 133-137.

Deer, W.A., Howie, R.A., and Zussman, J., 1966. *An introduction to the rock-forming minerals*, Wiley, New York, 528pp.

Donovan, T.J., Forgey, R.L., and Roberts, A.A., 1979. Aeromagnetic detection of diagenetic magnetite over oil fields. *American Association of Petroleum Geologists Bulletin*, 63, 245-248.

Duddy, I.R., 1983. The geology, petrology and geochemistry of the Otway Formation volcanogenic sediments. *University of Melbourne, Ph.D. thesis* (unpublished).

Ellwood, B.B., Balsam, W., Burkart, B., Long, G.J., and Buhl, M.L., 1986. Anomalous magnetic properties in rocks containing the mineral siderite: Palaeomagnetic implications. *Journal of Geophysical Research*, 91, 12,779-12,790.

Ellwood, B.B., Chrzanowski, T.H., Hrouda, F., Long, G.J., and Buhl, M.L., 1988. Siderite formation in anoxic deep-sea sediments: A synergetic bacterially controlled process with important implications in palaeomagnetism. *Geology*, 16, 980-982.

Elmore, R.D., and Crawford, L., 1990. Remanence in authigenic magnetite: Testing the hydrocarbon-magnetite hypothesis. *Journal of Geophysical Research*, 95, 4539-4549.

Elmore, R.D., Engel, M.H., Crawford, L., Nick, K., Imbus, S., and Sofer, Z., 1987. Evidence for a relationship between hydrocarbons and authigenic magnetite. *Nature*, 325, 428-430.

Elmore, R.D., and McCabe, C., 1991. The occurrence and origin of remagnetization in the sedimentary rocks of North America. *Reviews of Geophysics, Supplement*, 377-383.

Etheridge, M.A., Branson, J.C., and Stuart-Smith, P.G., 1985. Extensional basin-forming structures in Bass Strait and their importance for hydrocarbon exploration. *Australian Petroleum Exploration Association Journal*, 25 (1): 344-361.

Fassbinder, J.W.E., Stanjek, H., and Vali, H., 1990. Occurrence of magnetic bacteria in soil. *Nature*, 343, 161-163.

Felton, E. A., 1997. A non-marine Lower Cretaceous rift-related epiclastic volcanic unit in southern Australia: the Eumeralla Formation in the Otway Basin. Part I: Lithostratigraphy and depositional environments. *AGSO Journal of Australian Geology and Geophysics*, 16(5), 717-730.

Finlayson, D.M., Finlayson, B., Reeves, C.V., Milligan, P.R., Cockshell, C.D., Johnstone, D.W. and Morse, M.P., 1993. The western Otway Basin - a tectonic framework from new seismic , gravity and aeromagnetic data. *Exploration Geophysics*, 24 (3/4): 493-500.

Finlayson, D.M., Johnstone, D.W., Owen, A.J., and Wake-Dyster, K.D., 1994. Deep seismic profiling: basement controls on Otway Basin development. In: Finlayson, D.M. (Compiler), NGMA/PESA Otway Basin Symposium, Melbourne, 20th. April 1994: Extended Abstracts, *AGSO Record* 1994/14, 13-18.

Frankel, R.B., 1987. Anaerobes pumping iron. *Nature*, 330, p208.

Frears, R.A., 1995. History of Petroleum Exploration. In: Morton, J.G.G., and Drexel, J.F. (Eds.), The petroleum geology of South Australia, Volume 1: Otway Basin (1st. Ed.), *MESA Report Book* 95/12, 9-14.

Gay, S.P., 1986. The effects of cathodically protected pipelines on aeromagnetic surveys. *Geophysics*, 51 (8), 1671-1684.

Gay, S.P., Jr., 1992. Epigenetic versus syngenetic magnetite as a cause of magnetic anomalies. *Geophysics*, 57 (1), 60-68.

Gerdes, R.A., 1987. Western Otway Basin regional magnetic field study, South Australia. *Geological Survey of South Australia, Quarterly Geological Notes*, 101, 2-8.

Giret, R.I., 1965. Some results of aeromagnetic surveying with a digital cesium-vapor magnetometer. *Geophysics*, 30 (5), 883-890.

Grant, F.S., 1985. Aeromagnetics, geology and ore environments, I. Magnetite in igneous, sedimentary and metamorphic rocks: An overview. *Geoexploration*, 23, 303-333.

Grant, F.S., and Dodds, J., 1972. *MAGMAP FFT processing system development notes*. Paterson, Grant and Watson Limited.

Goldhaber, M.B., Reynolds, R.L., 1991. Relations among hydrocarbon reservoirs, epigenetic sulfidization, and rock magnetization: Examples from the south Texas coastal plain. *Geophysics*, 56 (6), 748-757.

Grauch, V.J.S., and Cordell, L., 1987. Limitations of determining density or magnetic boundaries from the horizontal gradient of gravity or pseudogravity data. *Geophysics*, 52 (1), 118-121.

Gunn, P.J., 1995. Aeromagnetic interpretation, blocks V94-1 and V94-2, Offshore Otway Basin, Victoria. Preliminary report. *Australian Geological Survey Organisation Report.*

Gvirtzman, Z., and Garfunkel, Z., 1997. Vertical movements following intracontinental magmatism: An example from southern Israel. *Journal of Geophysical Research*, Vol. 102, No. B2, 2645-2658.

Hansen, R.O., and Pawlowski, R.S., 1989. Reduction to the pole at low latitudes by Wiener filtering. *Geophysics*, 54 (12), 1607-1613.

Hartland, W.B., Armstrong, R.L., Cox, A.V., Smith, A.G., and Smith, D.G., 1990. *A geological time scale 1989*. Cambridge University Press, Cambridge, 362pp.

Heath, D.H., Clarke, V.S., and Bint, A.N., 1993. High resolution aeromagnetics clarifies structuring in the Vlaming Sub-Basin, Western Australia. *Exploration Geophysics*, 24 (3/4), 535-542.

Heywood, B.R., Bazylinski, D.A., Garratt-Reed, A., Mann, S., and Frankel, R.B., 1990. Controlled biosynthesis of griegite (Fe_3S_4) in magnetotactic bacteria. *Naturwissenschaften*, 77, 536-536.

Hill, K.A., and Durrand, C., 1993. The Western Otway Basin: an overview of the rift and drift history using serial and composite profiles. *Petroleum Exploration Society of Australia Journal*, 21, 67-78.

Hill, K.A., Finlayson, D.M., Hill, K.C., and Cooper, G.T., 1995. Mesozoic tectonics of the Otway Basin region: The legacy of Gondwana and the active Pacific margin - a review and ongoing research. *Australian Petroleum Exploration Association Journal*, 35: 467-493.

Hill, K.C., Cooper, G.T., and Mitchell, M.M., 1994. Burial, heat pulses, inversion and denudation in the Otway Basin. In: Finlayson, D.M. (Compiler), NGMA/PESA Otway Basin Symposium, Melbourne, 20th. April 1994: Extended Abstracts, *AGSO Record* 1994/14, 49-54.

Hounslow, M.W., and Maher, B.A., 1996. Quantitative extraction and analysis of carriers of magnetisation in sediments. *Geophysical Journal International*, 124, 57-74.

Irving, A.J., and Green, D.H., 1976. Geochemistry and petrogenesis of the newer basalts of Victoria and South Australia. *Journal of the Geological Society of Australia*, 23 (1), 45-66.

Joyce, E.B., 1975. Quaternary volcanism and tectonics in southeastern Australia. In: Suggate, R.P., and Cresswell, M.M., (Eds), *Quaternary Studies*, Royal Society of New Zealand, Wellington, 169-176.

Kilgore, B., and Elmore, R.D., 1989. A study of the relationship between hydrocarbon migration and the precipitation of authigenic magnetic minerals in the Triassic Chugwater Formation, southern Montana. *Geological Society of America Bulletin*, 101, 1280-1288.

Kivior, I., 1996. A geophysical study of the structure and crustal environment of the Polda Rift, South Australia. *University of Adelaide, Ph.D. thesis* (unpublished).

Kostka, J.E., Stucki, J.W., Nealson, K.H., and Wu, J., 1996. Reduction of structural Fe(III) in smectite by a pure culture of *Shewanella Putrefaciens* Strain MR-1. *Clays and Clay Minerals*, 44 (4), 522-529.

Krs, M., Novák, F., Krsová, M., Pruner, P., Kouklíková, L., and Jansa, J., 1992. Magnetic properties and metastability of griegite-smythite mineralization in brown-coal basins of the Krušné hory Piedmont, Bohemia. *Physics of the Earth and Planetary Interiors*, 70, 273-287.

Little, B.M., and Philips, S.E., 1995. Detrital and Authigenic mineralogy of the Pretty Hill Formation in the Penola Trough, Otway Basin: Implications for future exploration and production. *Australian Petroleum Exploration Association Journal*, 35: 538-557.

Lovibond, R., Suttill, R.J., Skinner, J.E., and Aburas, A.N., 1995. The hydrocarbon potential of the Penola Trough, Otway Basin. *Australian Petroleum Exploration Association Journal*, 35: 358-370.

Lovley, D.R., and Chapelle, F.H., 1995. Deep subsurface microbial processes. *Reviews of Geophysics*, 33 (3), 365-381.

Lovley, D.R., Chapelle, F.H., and Philips, E.J.P., 1990. Fe(III)-reducing bacteria in deeply buried sediments of the Atlantic Coastal Plain. *Geology*, 18, 954-957.

Lovley, D.R., Roden, E.E., Philips, E.J.P., and Woodward, J.C., 1993. Enzymatic iron and uranium reduction by sulfate-reducing bacteria. In: Parkes, R.J., Westbroek, P., and de Leeuw, J.W., (Eds.), Marine sediments, burial, pore water chemistry, microbiology and diagenesis. *Marine Geology*, 113, 41-53.

Lovley, D.R., Stolz, J.F., Nord, G.L., and Philips, E.J.P., 1987. Anaerobic production of magnetite by a dissimilatory iron-reducing microorganism. *Nature*, 330, 252-254.

Lowrie, W., and Heller, F., 1982. Magnetic properties of marine limestones. *Reviews of Geophysics and Space Physics*, 20, 171-192.

Lu, R., and Banerjee, S.K., 1994. Magnetite dissolution in deep sediments and its hydrologic implication: A detailed study of sediments from site 808, leg 131. *Journal of Geophysical Research*, 99 (B5), 9051-9059.

Machel, H.G., 1987. Some aspects of diagenetic sulphate-hydrocarbon redox reactions. In: Marshall, J.D., (Ed), *Diagenesis of sedimentary sequences*, Geological Society of London Special Publication 36, 15-28.

Machel, H.G., and Burton, E.A., 1991a. Chemical and microbial processes causing anomalous magnetisation in environments affected by hydrocarbon seepage. *Geophysics*, 56 (5), 598-605.

Machel, H.G., and Burton, E.A., 1991b. Causes and spatial distribution of anomalous magnetisation in hydrocarbon seepage environments. *American Association of Petroleum Geologists Bulletin* , 75 (12), 1864-1875.

MacLeod, I.N., Jones, K., and Dai, T.F., 1993. 3D analytic signal in the interpretation of total magnetic field data at low magnetic latitudes. *Exploration Geophysics*, 24 (3/4), 679-688.

Maher, B.A., and Taylor, R.M., 1988. Formation of ultrafine-grained magnetite in soils. *Nature*, 336, 368-370.

Mann, S., Sparks, N.H.C., Frankel, R.B., Bazylinski, D.A., and Jannasch, H.W., 1990. Biomineralization of ferrimagnetic griegite (Fe_3S_4) and iron pyrite (FeS_2) in a magnetotactic bacterium. *Nature*, 343, 258-261.

Martin, K.R., 1992. Petrology of the Eumeralla Formation to basement interval in Sawpit No. 1, South Australia. In: Tabassi, A., and Robbie, S.M., Sawpit No. 1 well completion report, PEL 27, South Australia, for Oil Company of Australia Ltd. *Department of Mines and Energy, South Australia, Open file Envelope*, 7420:223-279 (unpublished).

Martin, K.R., and Baker, J.C., 1992. Petrology, diagenesis and reservoir quality of the Pretty Hill Sandstone, Otway Basin, South Australia. In: Tabassi, A., and Robbie, S.M., Sawpit No. 1 well completion report, PEL 27, South Australia, for Oil Company of Australia Ltd. *Department of Mines and Energy, South Australia, Open file Envelope*, 7420: (unpublished).

McCabe, C., Sassen, R., and Saffer, B., 1987. Occurrence of secondary magnetite within biodegraded oil. *Geology*, 15, 7-10.

McClung, G. and Archer, D.W., 1989. Katnook 2 well completion report, PEL 32, Otway Basin, for Ultramar Australia Inc. *Department of Mines and Energy, South Australia, Open file Envelope*, 7189: (unpublished).

McIntyre, J.I., 1980. Geological significance of magnetic patterns related to magnetite in sediments and metasediments - a review. *Bull. Aust. Soc. Explor. Geophys.*, 11, 19-33.

McIntyre, J.I., 1981. Accurate display of fine detail in aeromagnetic data. *Bull. Aust. Soc. Explor. Geophys*, 12 (4), 82-88.

Megallaa, M., 1986. Tectonic development of Victoria's Otway Basin - a seismic interpretation. In: Glenie, R.C. (Eds), *Second South-Eastern Australia Oil Exploration Symposium*, Petroleum Exploration Society of Australia, 201-218.

Mendonça, C.A., and Silva, J.B.C., 1993. A stable truncated series approximation of the reduced to the pole operator. *Geophysics*, 58, 1084-1090.

Moriarty, N.J., Taylor, R.J., and Daneel, G.J., 1995. The Sawpit structure - evaluation of a fractured basement reservoir play in the Otway Basin. *Australian Petroleum Exploration Association Journal*, 35: 558-577.

Morton, J.G.G., 1990. Revisions to stratigraphic nomenclature of the Otway Basin, South Australia. *Geological Survey of South Australia, Quarterly Geological Notes*, 116, 2-19.

Morton, J.G.G., Alexander, E.M., Hill, A.J., and White, M.R., 1995. Lithostratigraphy and environments of deposition. In: Morton, J.G.G., and Drexel, J.F. (Eds.), The petroleum geology of South Australia, Volume 1: Otway Basin (1st. Ed.), *MESA Report Book* 95/12, 47-93.

Morton, J.G.G., and Drexel, J.F., 1995. Appendix 5.2: Stratigraphic unit tops for South Australian Otway Basin wells. In: Morton, J.G.G., and Drexel, J.F. (Eds.), The petroleum geology of South Australia, Volume 1: Otway Basin (1st. Ed.), *MESA Report Book* 95/12, 192-195.

Morton, J.G.G., Hill, A.J., Parker, G., and Tabassi, A., 1994. Towards a unified stratigraphy for the Otway Basin. In: Finlayson, D.M. (Compiler), NGMA/PESA

Otway Basin Symposium, Melbourne, 20th. April 1994: Extended Abstracts, *AGSO Record* 1994/14, 7-12.

Nabighian, M.N., 1972. The analytic signal of two-dimensional magnetic bodies with polygonal cross-section: Its properties and use for automated anomaly interpretation. *Geophysics*, 37, 507-517.

Nabighian, M.N., 1974. Additional comments on the analytic signal of two-dimensional magnetic bodies with polygonal cross-section. *Geophysics*, 39, 85-92.

Naudy, H., 1971. Automatic determination of depth on aeromagnetic profiles. *Geophysics*, 36, 717-722.

Nelson, J.B., 1988. Comparison of gradient analysis techniques for linear two-dimensional magnetic sources. *Geophysics*, 53 (8), 1088-1095.

Nordstrom, D.K., and Munoz, J.L., 1986. *Geochemical thermodynamics*, Blackwell Scientific Publications.

O'Brien, G.W., Reeves, C.V., Milligan, P.R., Morse, M.P., Alexander, E.M., Willcox, J.B., Yunxuan, Z., Finlayson, D.M., and Brodie, R.C., 1994. New ideas on the rifting history and structural architecture of the Western Otway Basin: evidence from the integration of aeromagnetic, gravity and seismic data. *Australian Petroleum Exploration Association Journal*, 34 (1), 529-554.

Ochadlick, A.R., 1989. Measurements of the magnetic fluctuations associated with ocean swell compared with Weaver's theory. *Journal of Geophysical Research* 94, 16237-16242.

O'Reilly, W., 1984. *Rock and mineral magnetism*. Blackie and Son, Glasgow, 220pp.

Perincek, D., Simons, B., and Pettifer, G.R., 1994. The tectonic framework and associated play types of the Western Otway Basin. *Australian Petroleum Exploration Association Journal*, 34 (1), 460-478.

Perincek, D., Cockshell, C.D., Finlayson, D.M., and Hill, K.A., 1994. The Otway Basin: Early Cretaceous rifting to Miocene strike-slip. In: Finlayson, D.M. (Compiler), NGMA/PESA Otway Basin Symposium, Melbourne, 20th. April 1994: Extended Abstracts, *AGSO Record* 1994/14, 27-33.

Perincek, D., and Cockshell, C.D., 1995. The Otway Basin: Early Cretaceous rifting to Neogene inversion. *Australian Petroleum Exploration Association Journal*, 35: 451-466.

Peters, L.J., 1949. The direct approach to magnetic interpretation and its practical application. *Geophysics*, 14, 290-320.

Petraske, A.K., Hodge, D.S., and Shaw, R., 1978. Mechanisms of emplacement of basic intrusions. *Tectonophysics*, 46, 41-63.

Pettifer, G.R., Tabassi, A., and Simons, B., 1991. A new look at the structural trends in the onshore Otway Basin, Victoria, using image processing of geophysical data. *Australian Petroleum Exploration Association Journal*, 31 (1), 213-228.

Polach, A.H., Head, M.J., and Gower, J.D., 1978. ANU radiocarbon date list VI. *Radiocarbon*, 20 (3), 360-385.

Qin, S., 1994. An analytic signal approach to the interpretation of total field magnetic anomalies. *Geophysical Prospecting*, 42, 665-675.

Reeve, J., and Skinner, J., 1995. Wynn 1 well completion report, PEL 32, Otway Basin, for Sagasco South East Inc., Minora Resources NL, Sagasco Resources, Basin Oil NL, Cultus Petroleum (Aust.) NL, and GFE Resources Ltd. *Department of Mines and Energy, South Australia, Open file Envelope*, 07476/006: (unpublished).

Reeves, C.V., O'Brien, G.W., Finlayson, D.M., Milligan, P.R., Morse, M.P., Brodie, R.C., and Willcox, J.B., 1993. Western Otway Basin Aeromagnetic Dataset: Images and Interpretation. *AGSO Record* 1993/14, 74pp.

Reid, A.B., Allsop, J.M., Granser, H., Millett, A.J., and Somerton, I.W., 1990. Magnetic interpretation in three dimensions using Euler deconvolution. *Geophysics*, 55 (1), 80-91.

Reynolds, R.L., Fishman, N.S., and Hudson, M.R., 1991. Sources of aeromagnetic anomalies over Cement oil field (Oklahoma), Simpson oil field (Alaska), and the Wyoming-Idaho-Utah thrust belt. *Geophysics*, 56 (5), 606-617.

Reynolds, R.L., Fishman, N.S., Wanty, R.B., and Goldhaber, M.B., 1990a. Iron sulfide minerals at Cement oil field, Oklahoma: Implications for magnetic detection of oil fields. *Geological Society of America Bulletin*, 102, 368-380.

Reynolds, R.L., Tuttle, M., Rice, C.A., Fishman, N.S., Karachewski, J.A., and Sherman, D.M., 1994. Magnetisation and geochemistry of griegite-bearing Cretaceous strata, North Slope Basin, Alaska. *American Journal of Science*, 294, 485-528.

Reynolds, R.L., Webring, M., Grauch, V.J.S., and Tuttle, M., 1990b. Magnetic forward models of Cement oil field, Oklahoma, based on rock magnetic, geochemical, and petrologic constraints. *Geophysics*, 55 (3), 344-353.

Roberts, A.P., 1995. Magnetic properties of sedimentary griegite (Fe_3S_4). *Earth and Planetary Science Letters*, 134, 227-236.

Roest, W.R., Verhoef, J., and Pilkington, M., 1992. Magnetic interpretation using the 3D analytic signal. *Geophysics,* 57 (1), 116-125.

Sassen, R., McCabe, C., Kyle, J.R., and Chinn, E.W., 1989. Deposition of magnetic pyrrhotite during microbial oxidation of crude oil hydrocarbons and reduction of sulfate. *Organic Geochemistry*, 14, 381-392.

Schwartz, M., Lund, S.P., Hammond, D.E., Schwartz, R., and Wong, K., 1997. Early sediment diagenesis on the Blake/Bahama Outer Ridge, North Atlantic Ocean, and its effects on sediment magnetism. *Journal of Geophysical Research*, 102 (B4), 7903-7914.

Sheard, M.J., 1978. Geological history of the Mount Gambier volcanic complex, southeast South Australia. *Royal Society of South Australia. Transactions*, 102: 125-139.

Sheard, M.J., 1986. Some volcanological observations at Mount Schank, southeast South Australia. *Geological Survey of South Australia, Quarterly Geological Notes,* 100: 14-20.

Sheard, M.J., 1990. A guide to Quaternary volcanoes in the Lower South-East of South Australia. In: Drexel, J.F., (Ed), *Mines and Energy Review, South Australia*, 157, 40-50.

Sheard, M.J., and Nicholls, I.A., 1989. East Australian volcanic geology, Victoria and South Australia; Mount Gambier sub-province. In: Johnson, R.W., (compiler and editor), Knutson, J., and Taylor, S.R., (editors), *Intraplate volcanism in eastern Australia and New Zealand*, Cambridge University Press, Cambridge, U.K., 141-142.

Shi, Z., 1991. An improved Naudy-based technique for estimating depth from magnetic profiles. *Exploration Geophysics*, 22, 357-362.

Shi, Z., and Boyd, D., 1993. AUTOMAG: An automatic method to estimate thickness of overburden from aeromagnetic profiles. *Exploration Geophysics*, 24 (3/4), 789-794.

Shuey, R.T., and Pasquale, A.S., 1973. End corrections in magnetic profile interpretation. *Geophysics*, 38 (3), 507-512.

Silva, J.B.C., 1986. Reduction to the pole as an inverse problem and its application to low-latitude anomalies. *Geophysics*, 51, 369-382.

Skinner, B.J., Erd, R.C., and Grimaldi, F.S., 1964. Griegite, the thio-spinel of iron: A new mineral. *American Mineralogist*, 49, 543-555.

Smith, B.W., and Prescott, J.R., 1987. Thermoluminescence dating of the eruption at Mt. Schank, South Australia. *Australian Journal of Earth Sciences*, 34, 335-342.

Smith, G.C., 1988. Economic Geology, Oil and gas. In: Douglas, J.G., and Ferguson, J.A., (Eds.), *Geology of Victoria*, Geological Society of Australia, Victorian Division, 514-546.

Spector, A., and Grant, F.S., 1970. Statistical models for interpreting aeromagnetic data. *Geophysics*, 35, 293-302.

Sprigg, R.C., 1986. A history of the search for commercial hydrocarbons in the Otway Basin Complex. In: Glenie, R.C. (Ed), *Second South-Eastern Australia Oil Exploration Symposium, Melbourne, 1985, Technical Papers*. Petroleum Exploration Society of Australia, 173-200.

Stanley, J.M., Sertsrivanit, S., and Clark, P.J., 1992. Magnetic exploration beneath a near-surface magnetic noise source. *Exploration Geophysics*, 23, 323-326.

Stevens, T.O., McKinley, J.P., and Fredrickson, J.K., 1993. Bacteria associated with deep, alkaline, anaerobic groundwaters in southeast Washington. *Microbial Ecology*, 25, 35-50.

Stolz, J.F., Chang, S.R., and Kirschvink, J.L., 1986. Magnetotactic bacteria and single-domain magnetite in hemipelagic sediments. *Nature*, 321, 849-851.

Sutherland, F., L., 1991. Cainozoic volcanism, Eastern Australia: a predictive model based on migration over multiple 'hotspot' magma sources. In: Williams, M., A., J., De Deckker, P. and Kershaw, A., P. (eds.), *The Cainozoic in Australia: A Re-appraisal of the Evidence*, Geological Society of Australia Inc. Special Publication No. 18, 15-43.

Tabassi, A., and Robbie, S.M., 1992. Sawpit No. 1 well completion report, PEL 27, South Australia, for Oil Company of Australia Ltd. *Department of Mines and Energy, South Australia, Open file Envelope*, 7420: (unpublished).

Tarling, D.H., and Hrouda, F., 1993. *The magnetic anisotropy of rocks*. Chapman and Hall, London, 212pp.

Talwani, M., and Heirtzler, J.R., 1964. Computation of magnetic anomalies caused by two-dimensional bodies of arbitrary shape. In: Parks, G.A., (Ed), *Computers in the mineral industries*, Part 1: Stanford Univ. Publ. Geological Sciences, 9, 464-480.

Taylor, R.M., Maher, B.A., and Self, P.G., 1987. Magnetite in soils: I. The synthesis of single-domain and superparamagnetic magnetite. *Clay Minerals*, 22, 411-422.

Telford, W.M., Geldart, L.P., and Sheriff, R.E., 1990. *Applied Geophysics (2nd. Ed.)*. Cambridge University Press, Cambridge, 770pp.

Thompson, D.T., 1982. EULDPH: A new technique for making computer-assisted depth estimates from magnetic data. *Geophysics*, 47, 31-37.

Tucker, D.H., and Frears, R.A., 1995. Otway Basin aeromagnetic/radiometric test survey. *MESA Report Book* 95/40, 23pp.

Vacquier, V., Steenland, N.C., Henderson, R.G., and Zeitz, I., 1951. Interpretation of aeromagnetic maps. *Geological Society of America, Memoir* 47.

Vali, H., Forster, O., Amarantidis, G., and Petersen, N., 1987. Magnetotactic bacteria and their magnetofossils in sediments. *Earth and Planetary Science Letters*, 86, 389-400.

Van Cappellen, P., and Wang, Y.F., 1996. Cycling of iron and manganese in surface sediments: A general theory for the coupled transport and reaction of carbon, oxygen, nitrogen, sulfur, iron, and manganese. *American Journal of Science*, 296, 197-243.

Veevers, J.J., 1986. Breakup of Australia and Antarctica estimated from magnetic and seismic data at the continental margin. *Earth and Planetary Science Letters*, 77, 91-99.

Veevers, J.J., Powell, C. McA., and Roots, S.R., 1991. Review of seafloor spreading around Australia: I. Synthesis of the patterns of spreading. *Australian Journal of Earth Sciences*, 38, 373-389.

Veevers, J.J., and Li, Z.X., 1991. Review of seafloor spreading around Australia: II. Marine magnetic anomaly modelling. *Australian Journal of Earth Sciences*, 38, 391-408.

Weaver, J.T., 1965. Magnetic variations associated with ocean waves and swell. *Journal of Geophysical Research*, 70, 1921-1929.

Willcox, J.B., and Stagg, H.M.J., 1990. Australia's southern margin: a product of oblique extension. *Tectonophysics*, 173, 269-281.

Williams, J.P., 1988. Upward continuation of aeromagnetic profiles. *Exploration Geophysics*, 19, 383-390.

Williamson, P.E., Swift, M.G., O'Brien, G.W., and Falvey, D.A., 1990. Two-stage Early Cretaceous rifting of the Otway Basin margin of southeastern Australia: Implications for rifting of the Australian southern margin. *Geology*, 18, 75-78.

Wopfner, H., and Douglas, J.G., (Eds.), 1971. *The Otway Basin of Southeastern Australia*. Geological Surveys of South Australia and Victoria, Special Bulletin, 464pp.

Yeremin, V.N., Molostovskiy, E.A., Pervushova, Ye.V., and Chernyayeva, A.F., 1986. Magnetic zonation of sedimentary rocks and the spatial distribution of authigenic iron minerals in hydrocarbon haloes. *International Geology Review*, 734-739.

Appendix A

Cultural Anomalies

Introduction

There are many low amplitude anomalies in the study area, some of which are likely to be intersedimentary sources and others, cultural effects. The study area is relatively heavily populated with sawmills, pumping stations, electricity substations, high voltage power lines, railways and a large town (Mt Gambier) as well as a substantial number of farming properties, all of which could introduce anomalies of non-geological origin to the survey data. The anomalies found on farming properties are most likely due to machinery containing electric motors and/or transformers rather than steel sheds and buildings.

A map of the electricity distribution network was obtained by MESA from the electricity supply authorities and was in turn supplied to the author. This map allowed the author and others to eliminate several prominent linear features from the list of possible intersedimentary anomalies. A list of probable power line anomalies was prepared by Alison Bradley while the locations of other isolated anomalies from the study area were identified by the author (section A.1). The author was also supplied with the results of studies conducted by the electricity supply authorities (ETSA) where the electric and magnetic fields of power lines of differing voltages and heights above the ground were measured along traverses perpendicular to the lines (David Johnston, Environment and Technology Department, ETSA, pers. com.). MESA also supplied transparent overlays of the Penola, Gambier and Northumberland 1:100,000 scale topographic maps which were used to identify anomalies associated with farm houses and other buildings as well as other features such as the prominent sand dunes that mark the palaeo-coastlines.

In this study cultural anomalies on profiles have generally been ignored although attempts has been made to select flightlines or traverses that are relatively uncontaminated by cultural noise for figures and diagrams. The worst cases were where the cultural noise had a much greater amplitude than the intersedimentary anomalies, so

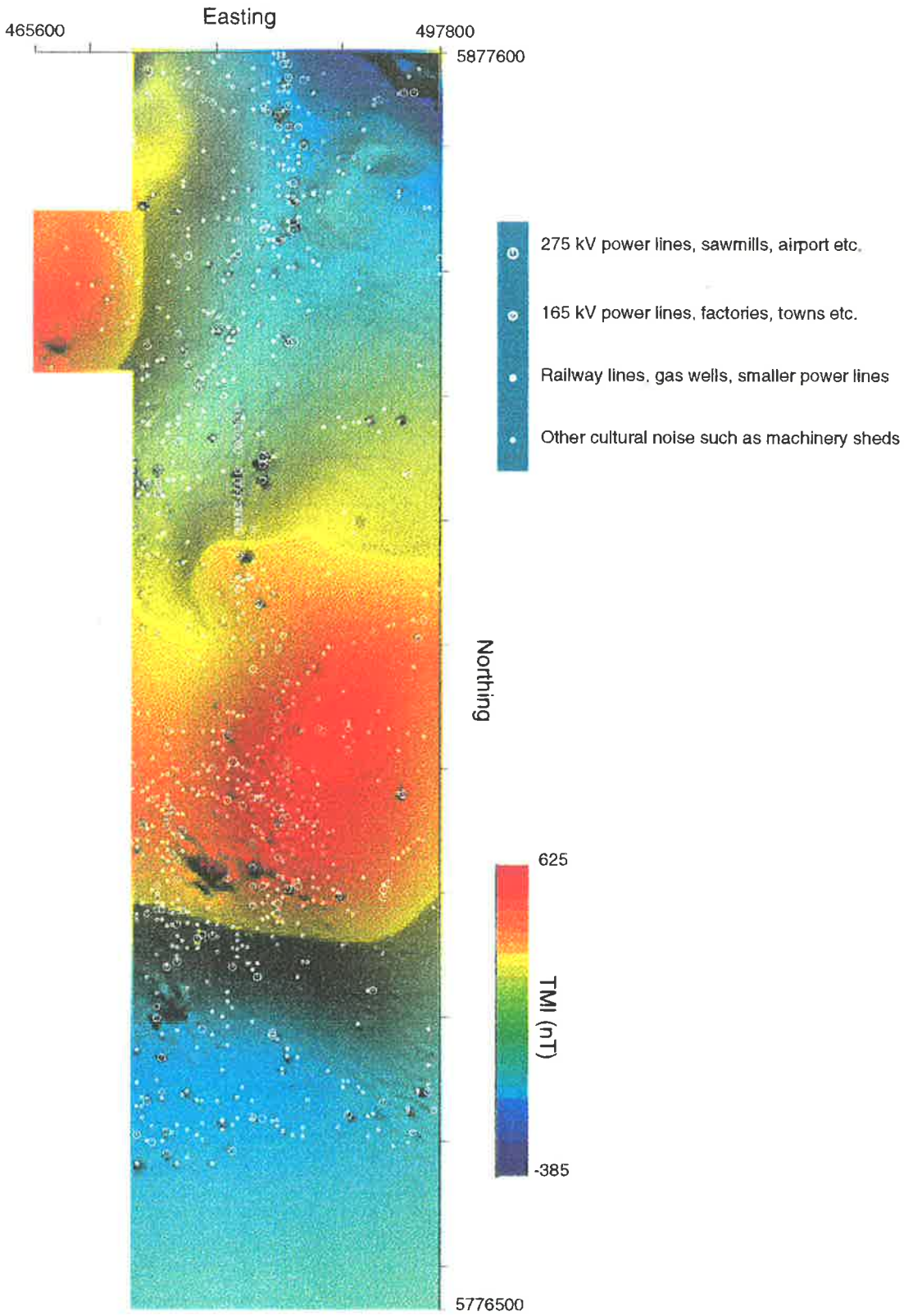

Fig. A.1.1 Colour-draped TMI image of study area with location of cultural features in grey/white circles, Scale = 1:500,000

a moving median filter was used to suppress the noise. The presence of cultural noise in the preparation of images and contour maps is a problem not only because large amplitude spikes cause subtle features to be allocated the same colour/greyscale pixel values or the contour interval to be set too large, but more importantly, distort the gridding process used to produce the grid from the flightline data. Where this was likely to occur, the flightline data was median-filtered prior to gridding with individual lines being assigned different filter window sizes depending on the wavelength of the largest cultural anomalies of that part of the line.

A.1 Identification Methods

Anomalies resulting from cultural sources have been identified by comparison of TMI contour and stacked profile maps with the utilities map, and it was also found that stacked profiles of band-pass filtered data, which were supplied to the author, were sometimes useful in emphasising the short wavelength anomalies associated with culture. Figure A.1.1 shows a map of the study area with the locations of likely cultural anomalies marked. Anomalies are concentrated along major powerlines, railway lines and in the vicinity of the major towns and industries, but with large numbers of isolated anomalies scattered throughout the study area. The peak-to-trough amplitude of cultural anomalies ranges from sub-nanoTesla to over 400 nT but the important difference between cultural anomalies and those of geological origin is that most cultural anomalies have a relatively short wavelength. This can be seen from anomalies associated with farming properties where the low amplitude anomaly has a wavelength typically 50m or less, while anomalies associated with large power lines, for example, usually have wavelengths of 300 to 500m. The largest anomalies are those associated with Mt Gambier airport, sawmills and other large industries, and are presumably the result of radar, high voltage transformers and powerful electric motors. The wavelength of these anomalies is in the order of 0.6 to 1.5 km but the amplitudes can be over 200 nT. In contrast, most geological anomalies found in a sedimentary basin have wavelengths greater than 1 km, for example, the suspected buried volcanic plug (Hungerford anomaly) has a wavelength of 3 km (amplitude approx. 75 nT) while the linear anomalies east of Penola generally have wavelengths of 1.5 km. or greater (amplitude between 1 to 3 nT).

Another distinguishing feature of cultural anomalies are that most usually only occur on one flight-line with no detectable influence on adjacent lines. The exceptions here, are the power line, pipeline and railway line anomalies which occur on neighbouring lines when the flight-lines are not parallel to the sources. On the flight-line closest to the Mt Gambier/Penola road (line 11780), there are a series of anomalies which result from the two power lines (275 kV and 165 kV) along the road. The railway lines cause anomalies where the flight lines cross them but not on every flight line and with varying amplitudes. There are some anomalies apparently associated with the Katnook-to-Mt Gambier gas pipeline but these are small and generally insignificant. Some American authors have published papers showing that pipelines can produce quite significant aeromagnetic anomalies when cathodic protection is used (Gay, 1986). This involves passing a current through the pipe to minimise corrosion due to contact with groundwater.

Power line anomalies vary in shape (and amplitude) depending on the angle that the flightpath of the aircraft crosses the line, as well as the phase and current of the line at the time. The flightpath is well known but the phase and current depend on the load on the grid at that instant and can vary substantially during the day (David Johnston, ETSA, pers. com.). This is likely to preclude any attempt to model the anomaly and then subtract the calculated profile from the data. The anomalies not associated with power lines are just as, or even more variable in shape depending on the type and geometry of the source, but all share the same property of a *relatively* short wavelength compared with other anomalies. It is this short wavelength that is ultimately the only practical distinguishing feature of these anomalies and so close examination of profile data (rather than gridded data) is required in order to become familiar with the different types in an area.

A.2 Distribution of Cultural Anomalies

As seen in figure A.1.1, the cultural anomalies indicate the areas where the population is largest with the result that the area around Mt Gambier has a large number because of the presence of the city and there is also a large number of anomalies to the northwest, west and southwest of the city as well as a large number along the coastline. These anomalies are numerous enough in this part of the study area

to make identification of subtle intersedimentary anomalies extremely difficult because it is necessary to trace the long wavelength features across several flightlines and this is prevented by the presence of the relatively large amplitude anomalies of cultural features that interfere with the more subtle anomalies. Pine forests and reserves to the east and southeast of Mt Gambier (around Caroline 1) have only scattered anomalies that might have cultural sources and the more important of these appear to be on the roads and tracks through the forests.

There are a large number of cultural anomalies north of Mt Gambier, especially around the airport and in the vicinity of the road to Tarpeena and Nangwarry as well as the Kalangadoo/Mt Gambier railway. There are pine forests southwest of Tarpeena and to the east of the Tarpeena to Nangwarry road where the short wavelength anomalies are isolated and restricted to the roads. The area around Kalangadoo and along the Kalangadoo/Penola railway line has a few large cultural anomalies as has the Penola/Nangwarry road with several prominent anomalies over the Katnook and Ladbroke Grove gas fields and over the SAFRIES potato chip factory east of the Katnook field. There are no magnetic anomalies over the Haselgrove or Wynn 1 wells because the survey was flown prior to the wells being drilled.

The eastern side of the area adjacent to the Victorian border is relatively free of cultural anomalies, especially over the deepest part of the Penola Trough, which has allowed the detection of intersedimentary anomalies that may have been masked in other areas. This is particularly important in the eastern section that starts north of the interstate interconnection power line which runs southeast from Tarpeena to the Victorian border. This section continues to the northern margin of the study area and does not have any power lines greater than 19 kV crossing it so the cultural anomalies present are most probably caused by machinery sheds and other farm equipment.

The western side of the study area, north of Kalangadoo and northwest of the railway line, is mostly farmland with a number of isolated, low amplitude anomalies but with the exception of the 275 kV power line which crosses the western extension of P1 from north of Nangwarry diagonally to the northwest corner (around 469000mE, 5864000mN) of the extension, the Laira 1 and Zema 1 wells, and smaller power lines running east-west and north-south. North of Penola there are a substantial number of anomalies along and around the Penola/Coonawarra road and railway line where there

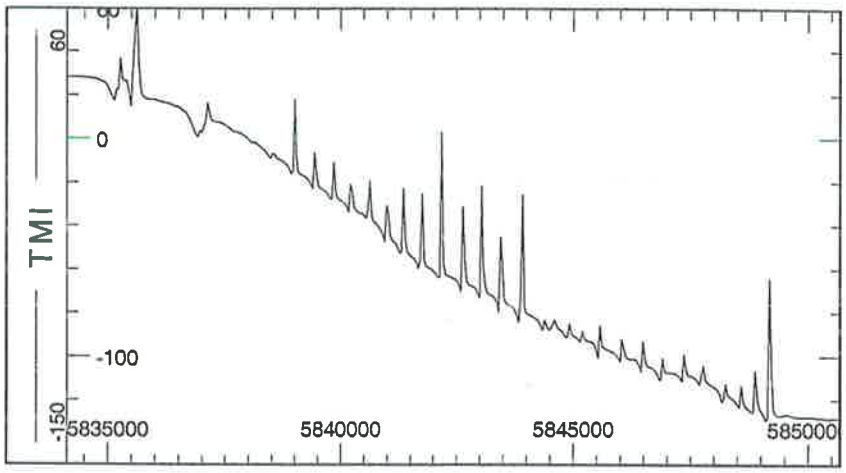

Fig. A.3.1 Section of line 11780 showing power line anomalies along Mt Gambier/Penola road

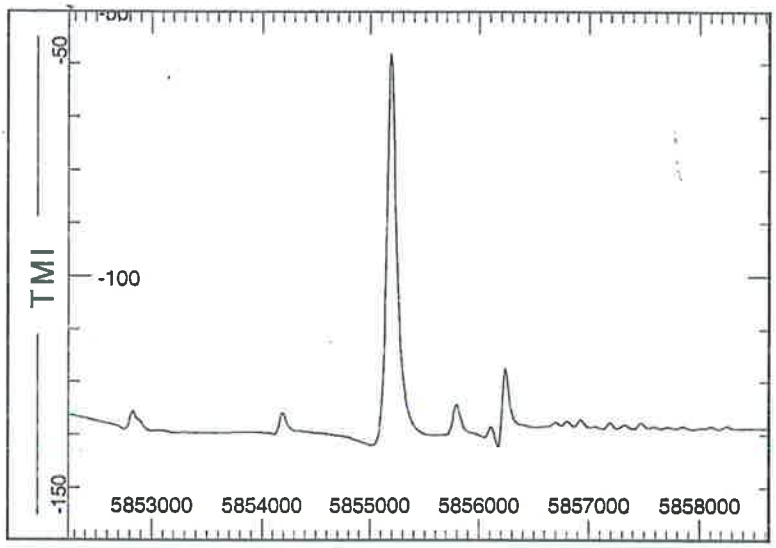

Fig. A.3.2 Section of line 11740 showing anomaly over Katnook 3 gas well

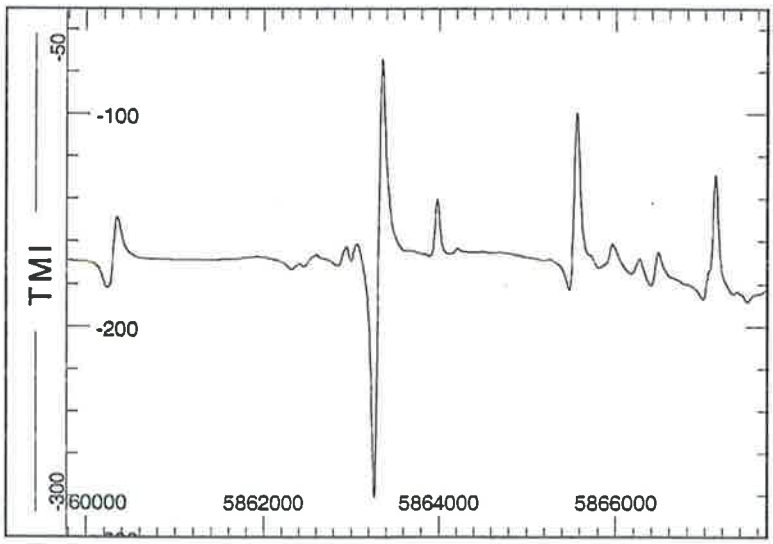

Fig. A.3.3 Section of line 11890 showing cultural anomalies over Penola